# Behaviour of the Sm-Nd isotopie system during metamorphism : Examples from the HT-LP metamorphic terrane of the Limpopo Belt, South Africa and the UHP metamorphic terrane of Dabieshan, Central China.

Valérie Chavagnac

V. CHAVAGNAC

ISSN 1240-1498
ISBN 2-905532-88-2

# Behaviour of the Sm-Nd isotopic system during metamorphism

## EXAMPLES FROM THE HT-LP METAMORPHIC TERRANE OF THE LIMPOPO BELT, SHOUTH AFRICA AND THE UHP METAMORPHIC TERRANE OF DABIESHAN, CENTRAL CHINA

MEMOIRES

1999

Géosciences Rennes

n° 89

MEMOIRE DE GEOSCIENCES - RENNES

N° 89

Valérie CHAVAGNAC

# Behaviour of the Sm-Nd isotopic system during metamorphism : Examples from the HT-LP metamorphic terrane of the Limpopo Belt, South Africa and the UHP metamorphic terrane of Dabieshan, Central China

Thèse de Doctorat de l'Université de Rennes
soutenue le 30 Octobre 1998

Géosciences - Rennes
UPR-CNRS 4661
Université de Rennes I
Campus de Beaulieu
35042 - Rennes Cédex
(France)

1999

ISSN : 1240-1498

ISBN : 2-905532-88-2

1998

GEOSCIENCES-RENNES
UPR-CNRS n°4661
Université de Rennes I - Campus de Beaulieu
F - 35042 - RENNES Cédex (France)

Valérie CHAVAGNAC

Behaviour of the Sm-Nd isotopic system during metamorphism : Examples from the HT-LP metamorphic terrane of the Limpopo Belt, South Africa and the UHP metamorphic terrane of Dabieshan, Central China.

Mémoires de Géosciences Rennes, n° 89, 405 p.

# *AVANT PROPOS*

Ce travail est une co-tutelle de thèse. Les résultats scientifiques de ces trois dernières années, ont été obtenus à l'Université de Rennes 1 et l'Université de Bern (Suisse). Afin de s'affranchir du problème de langue, la thèse a été rédigée en anglais. L'introduction et la conclusion générales sont traduites en français conformément à la convention de co-tutelle de thèse.

## *Acknowledgements - Remerciements - Verdankungen*

Ce travail est l'aboutissement de trois années passées à Géosciences Rennes (Université de Rennes 1) et à l'Isotopengeologie (Universität Bern). Sans le soutien de chaque instant de mes deux Directeurs de Thèse, ce travail n'aurait jamais vu le jour. Je tiens donc à te remercier Toi Bor-ming pour tes conseils très constructifs, pour l'initiation au monde chinois, et pour ta confiance. Many thanks to Jan who encouraged and supported me during these three years, who found the right words when I had "le moral dans les baskets" and who made his possible for the "co-tutelle". Thanks a lot!

Mes remerciements s'adressent aussi aux membres du Jury qui ont accepté de juger ce travail: Robert A. Cliff, Igor M. Villa, Nick T. Arndt, Michel Ballèvre, Bor-ming Jahn and Jan D. Kramers.

Parmi le groupe de Géochimie de Rennes, je suis particulièrement reconnaissante à Raymond Capdevila, Erwan Hallot, Serge Fourcade, Catherine Chauvel, Michel Ballèvre, Nick Arndt pour ces discussions nombreuses et constructives. Jamais je n'aurais eu le goût pour la géochimie et ses isotopes si la "folle" et merveilleuse équipe de techniciens n'était pas là. Mes premiers pas en salle blanche avec Jean Cornichet, les premières manips au spectro avec Joël Macé, les premières mesures à la Fluorescence X avec Martine Le Coz Bouhnik sont de très bons souvenirs. Merci aussi à Nicole Morin, Odile Henin, Marie-Annick Chassonneau et Marie-Hélène Fichet-Delavault pour les moments de détente aux pauses café. Merci à Hugo, P'Tit Panou, Dédelle, Mély, P'tit Fred, Norké Miguel, Maryline, A Ténéné Vali pour ces moments de délires à des heures bien tardives. Merci aux autres thésards et ex-thésards pour leurs encouragements Sidonie Révillon, Philippe Boulvais, Sylvain Gallet, Olivier Bourgeois, Marc Diraison, Richard Morrisseau. Je ne trouve pas de mot pour te remercier Kiki alors je te dirai juste "on n'est pas des tout de même quand même!"

Ich kenne zwei Isotopenlabor: das Erste ist zum arbeiten und das Andere für Späße. Abs Erstes möchte ich der Isotopengeologischen Gruppe für die freundschaftliche Zusamenarbeit danken: Rolf Brunner, Kurt Howald, Börgi Hebeisen, Thomas F. Nägler, Igor M. Villa, Röbi Frei, Freidhelm von Blanckenburg, Jan D. Kramers, Ronny Schönberg, Mathis Passeraub, Oliver Steiner, Ivan Studer, Mirjam Schaller, Lörou Holzer, Katharina Kreissig. Von Thomas F. Nägler habe ich viel gelernt, danke für deine Hilfe im Chemie Labor, für die Korrektur der Diss., für die Diskussionen, die wir in der Kaffepause gehabt haben. Mit Röbi habe ich das erste Kaffe am morgen getrunken und viele schöne Momente mit Pitazios und Tuborg verbracht. Merci viel mal Röbi für deine Spontanität, deinen Enthusiasmus, und die richtigen Worte "tips, remarks, suggestions, conclusions"! Das zweite Labor ist unbedingt in der Gewalt von Elaine, Elena und Regina. The best Partys were always at your houses, many thanks! Die Zeit mit Lörou war immer lustig und abwechstumsreich, entweder im Feld, oder beim Billard, oder mit die 50 Freunden! Vielen Dank! Et Toi Sybille! Ich habe mich über die speziellen Abendessen und Deine Spontanität sehr gefreut, ohne Dich hätte ich nicht des Glück gehabt, den Höhlenforschern (Christian, Bobbob, Marie-Hélène, Carlos, Tom, Pierre-Yves,....) zu begegnen. Merci für alles! Meine Mittwochabende verbrachte ich öftens mit den Schweizerinnen und die Französinnen im downtown Bern. Merci für die wunderbare Zeit, Guillemette, Valérie, Anouchka, Marylaure und Nicole! Werner, Ulli, Lörou, and Valérie were without doubt the best friends for each monday evening that I shared with Celtic music, Egger, Talisker and Lagavullin.

Et vous mes amis, Clairette, Ricoucougne, JYL, Babeth, Manu, Carole, Pierrot, Simon, Nico, Juju, Pierre, Le Lions, Bob, Marie, D'Jo, Magalie, Bertrand, Lolo, Chri-Chri, Moune, Johnny, je ne sais comment vous exprimer ma gratitude. Vous avez été une source infinie d'inspiration, de gaieté, de soutien et de reconfort. Merci à vous!

Les derniers remerciements seront pour mes parents, Christophe et Catherine qui m'ont soutenue et encouragée jusqu'aux dernières minutes. Restez comme vous êtes, vous êtes supers! Je vous dédie ce travail.

## *Abstract*

The aims of this Ph.D. Thesis were to decipher whether the use of Nd model ages are reliable constraints for the crustal evolution on Proterozoic migmatized terrane (example of the Limpopo Belt in South Africa) and to examine the consistency between Sm-Nd garnet and U-Pb zircon ages on eclogites (example of the UHPM Dabieshan in Central China).

The Central Zone of the Limpopo Belt which is mainly composed of orthogneisses and paragneisses underwent granulite facies metamorphism followed by decompression metamorphic conditions (clockwise P-T loop) at 2.0 Ga. We have performed Sm-Nd and U-Pb work associated with major and trace element analyses on three examples of migmatites generated at 2.0 Ga to study the chemical and isotopic fractionation which may occur during migmatization. Partial melting following the Bt dehydration reaction did lead to different behaviour of Sm-Nd systematics for metagreywacke and metapelite. In the first case, chemical equilibrium and full Nd isotope exchanges were not reached due to the incrongruent Pl melting and to the effect of accessory minerals (Mnz and Ap) on the compositions of the partial melt. Monazite entered the melt in prefarence to apatite, either by dissolution or by entrainment, and its unradiogenic Nd isotope signature dominates the leucosome. The Nd model ages on partial melt are up to 400 Ma older than those on paleosomes. The Nd model ages of these rocks cannot be used in a simple way to constrain the evolution of Southern Africa. In the second case, incongruent Pl melting influenced the distribution of major, LILE and also REE between the partial melts and the paleosomes. Full Nd isotope exchange was nearly achieved while Pb-Pb systematics were not fully resetted. Incomplete exchange for both Nd and Pb for two leucosomes is also argued. It appears that the accessory minerals were chemically and isotopically equilibrated with the partial melt and the paleosome. The Nd model ages can be used to constrain the crustal growth of the Limpopo Central Zone. Finally, in migmatites formed by metamorphic segregation at subsolidus conditions on orthogneiss, chemical equilibrium and Nd isotope exchange were not reached during migmatization. The distributions of the elements are related to the proportional amounts of each mineral in the migmatitic components. However, full Pb isotope exchange is reached here as highlighted by a Pb-Pb WR isochron yielding 2.0 Ga. In addition, the geochemical characteristics combined with REE modelling provided arguments for closed system behaviour of the whole rock during migmatization. The isotopic compositions of the protolith obtained via mass balance calculations can be used to constrain crustal evolution.

The UHPM Dabieshan is characterized by the occurrence of coesite and its quartz pseudomorph as inclusions in eclogites of basaltic composition but also of undoubted metasedimentary origin. Sm.-Nd garnet-omphacite-whole rock isochrons on the coesite-

bearing eclogites of the Bixiling Complex gave ages at 210 ± 9 to 218 ± 4 Ma which are similar to 218.4 ± 1.8 Ma and 218.4 ± 2.5 Ma ages obtained by U-Pb zircon data. At the Shuanghe locality, Sm-Nd garnet-kyanite-whole rock isochron on a retrogressed eclogite gave an age at 231 ± 35 Ma in line with the U-Pb zircon data at 233 ± 21 Ma (lower intercept in the concordia diagram). In addition, Ar-Ar and Rb-Sr phengite ages performed on the eclogite host gneisses (Bixilingg locality) yield 198 ± 4 Ma to 212 ± 2 Ma ages, overlapping the previous Sm-Nd and U-Pb zircon ages on the coesite-bearing eclogites. Consequently, the Sm-Nd garnet dating provide ages in agreement with U-Pb zircon ages and the quartzo-feldspathic gneisses underwent an event coeval to UHP on eclogites. Nd isotope equilibration at the UHP metamorphism appears to have been complete.

## *Résumé*

Les buts de cette thèse sont (1) de déterminer si les âges modèles en Nd obtenus sur des terrains protérozoïques migmatisés correspondent réellement à l'âge d'extraction du magma de sa source mantellique (exemple du Limpopo Belt en Afrique du Sud) et (2) de comparer les âges Sm-Nd sur grenat et les âges U-Pb sur zircon déterminés sur des éclogites (exemple du Dabieshan en Chine Centrale).

La Zone Centrale du Limpopo Belt est constituée principalement d'orthogneiss et de paragneiss. Elle a subi un métamorphisme granulitique suivi par des conditions métamorphiques de décompression à 2.0 Ga (trajectoire pression et température dans le sens horaire). Nous avons effectué des analyses isotopiques en Sm-Nd et U-Pb combinées aux analyses en éléments majeurs et traces sur trois examples de migmatites formées 2.0 Ga afin d'étudier le fractionnement chimique et isotopique qui pourrait avoir lieu au cours de la migmatisation. La fusion partielle selon la réaction de déhydratation de la biotite met en exergue des comportements différents du système isotopique Sm-Nd dans les métagreywackes et dans les métapélites. Dans le premier cas, l'équilibre chimique et l'homogénéisation isotopique en Nd n'ont pas été achevés à cause de la fusion incongruente du plagioclase et de l'influence des minéraux accessoires sur la composition chimique des liquides. Il est démontré que la monazite est préférentiellement entrainée dans les leucosomes plutôt que l'apatite, provoquant ainsi la domination de la composition chimique de la monazite sur celles des liquides. De plus, la composition isotopique en Nd non-radiogénique de ce minéral accessoire domine celle du leucosome. Ainsi, les âges modèles en Nd des leucosomes sont jusqu'à 400 Ma plus vieux que ceux obtenus sur les paléosomes. Les âges modèles en Nd obtenus sur ces roches ne peuvent donc pas être utilisés comme âge de formation de la croûte continentale en Afrique du Sud. Dans le cas des métapélites, la fusion incongruente du plagioclase a influencé la distribution des éléments majeurs, des Large Ion Lithophile Elements ainsi que des Rare Earth Elements entre les paléosomes et les leucosomes. L'éechange isotopique en Nd entre les différents composants migmatitiques a été rpatiquement atteint, au contraire du système U-Pb qui ne montre qu'une homogénéisation partielle. Cependant, deux leucsomes à grenat présentent des compositions isotopiques en Sm-Nd et U-Pb supérieures aux autres composants migmatitiques. Ceci suggère qu'en règle générale les minéraux accessoiures ont été chimiquement et isotopiquement équilibrés avec les leucosomes et les paléosomes. De ce fait, les âges modèles en Nd calculés sur les paléosomes et les leucosomes représentent des âges significatifs pour la formation de la croûte continentale dans la Zone centrale du Limpopo Belt. Le dernier exemple est un orthogneiss migmatitique qui s'est formé par ségrégation métamorphique à des conditions subsolidus. La distribution des éléments majeurs et traces est directement proportionnelle à la quantité de chaque minéraux formant les composants migmatitiques. L'échange isotopique

total en Pb a été achevé comme le montre l'isochrone en Pb-Pb sur les roches totales à 2.0 Ga. De plus les caractéristiques géochimiques associées à une modélisation de la distribution des REE indiquent que le système est resté clos à l'échelle de la roche totale durant le processus de migmatisation. Ainsi, la composition isotopique en Nd du protolithe a pu être déterminée grâce à l'équation de conservation de masse et peut être utilisée pour définir l'âge de la formation de la croûte continentale.

Le terrain métamorphique de Ultra-Haute Pression (UHPM) du Dabieshan est caractérisé par la présence de coésite et de quartz pseudomorphe dans les éclogites de composition basaltique mais aussi dans les roches d'origine sédimentaire. Les isochrones en Sm-Nd sur grenat-omphacite-roche totale des éclogites à coésite du Massif de Bixiling donnent des âges variant entre 210 ± 9 Ma et 218 ± 4 Ma, très similaires aux âges U-Pb sur zircon à 218.4 ± 1.8 Ma et 218.4 ± 2.5 Ma (Ames et al., 1995). De plus, une isochrone Sm-Nd sur grenat-disthène-roche totale d'une éclogite rétromorphosée donne un âge à 231 ± 35 Ma en accord avec un âge à 233 ± 21 Ma (intercepte bas dans le diagramme concordia). Nous avons effectué des datations par les méthodes Rb-Sr et Ar-Ar sur des phengites et des biotites de l'encaisssant des éclogites à coésite de Bixiling. Les âges varient entre 198 ± 4 Ma et 212 ± 2 Ma recouvrant les âges précédemment obtenus par Sm-Nd et Rb-Sr sur les éclogites à coésite. Par conséquent, les âges Sm-Nd sur grenat sont en accord avec les âges U-Pb sur zircon et montrent que les gneiss quartzo-feldspathiques ont subi un événement métamorphique à ~210 Ma comme les éclogites. L'homogénéisation isotopique en Nd entre les différents minéraux semblent être atteinte à l'âge du métamorphisme.

# *General Introduction*

In the 19th century, the discoveries of naturally-occurring radioactive elements and their decay products by Becquerel and Curie provided an important tool to geologic researcher who worked on the understanding of the planet formations. One of the samarium isotopes ($^{147}Sm$) is radioactive and it decays by alpha emission to a stable isotope of neodynium ($^{143}Nd$). The decay processes at a very low rate as the decay constant of $^{147}Sm$ is 6.54 $10^{-12}$ $yr^{-1}$, corresponding to a half life approximately 23 times greater than the age of the Earth. As the decay is very long, the variation in $^{143}Nd$ contents compared to the non-radiogenic Nd isotope concentrations varies in the order of 1 per mille. The application of the Sm-Nd system on terrestrial material needs precise measurements of isotopic compositions and further developments in chemical separation and mass spectrometry had to be performed. The first improvement was given by the ion-exchange method for REE separation from other elements in sufficiently pure form (Peppard, 1961; Powell, 1961; Eugster et al., 1970). A few years later, precision of isotopic abundance ratio measurements reached ± 0.1% (the same order as the variation in $^{143}Nd$) by thermal ionization mass spectrometer (Hedge, 1966). Finally, the computer-interfaced mass spectrometer developed by Wasserburg et al. (1969) increased the precison on the isotopic measurements by a factor of 30 arising the feasability of the Sm-Nd method on terrestrial and extraterrestrial materials. In the early seventhies, chemical method of Eugster et al. (1970) combined with computer controlled mass spectrometer allowed Lugmair (1974) and Lugmair et al. (1975a) to apply the Sm-Nd system on meteorite or lunar basalt. Since that, the development of computer-interfaced multi-collector mass spectrometer largely improved the precision on the isotopic ratio measurement at ± 0.005%. As Sm/Nd ratio is not fractionated during intracrustal processes, the Sm-Nd method gives important information on the Earth's interior processes leading to crust formation, mantle composition, or on the evolution of Earth's envelops during geological history. Many geosciences studies may be approached such as igneous, metamorphic, and sedimentary petrology as well as geochemistry, paleoclimatology, oceanography etc...

Sm and Nd belong to the Lanthanide series elements (Fig. 1). They have similar chemical behaviour. However, due to their regularly decreasing ionic radii (assuming all of the valence 3+), their geochemical behaviour is governed by the crystal structures of phases fractionated in magmatic processes. Therefore, most of the variations observed in the Sm/Nd ratio are considered as a result of the Earth's internal processes rather than a result of condensation process at the early stage of Earth formation. From cosmochemical studies, the concentrations of REE and some other refractory elements in the Earth and the Moon were found to be similar to the least differentiated carbonaceaous chondrites (Ganapathy and Anders, 1974; Drake, 1976; Anders, 1977), therefore the term "CHondrite Uniform Reservoir" (CHUR) as being representative of the bulk Earth was defined by De Paolo and Wasserburg (1976a). Sm-Nd isotopic compositions of CHUR at present time are: $^{147}Sm/^{144}Nd = 0.1967$ and $^{143}Nd/^{144}Nd = 0.512638$.

Figure 1:Sm and Nd in the chart of periodic element.

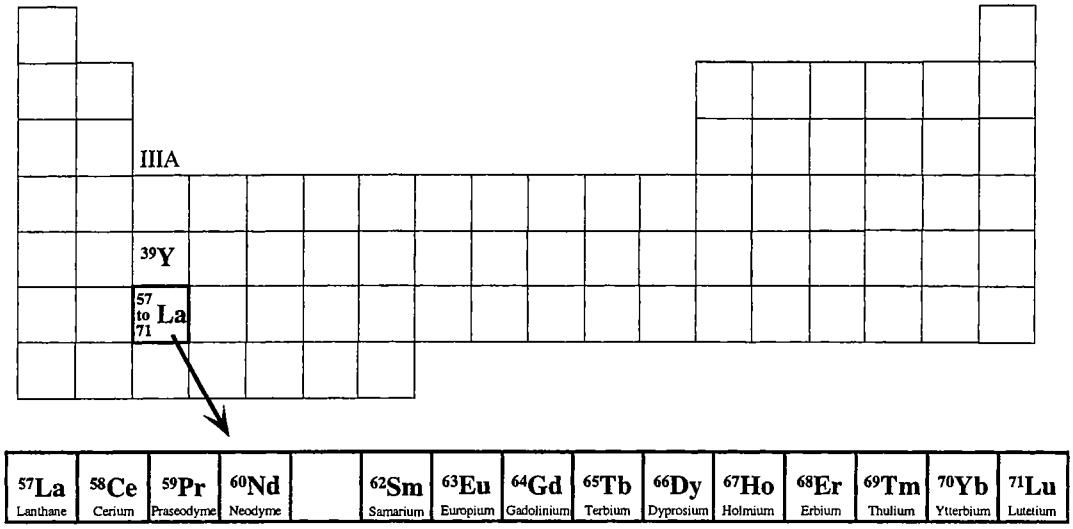


Figure 2: Chondrite-normalized REE patterns of typical mafic and felsic rocks. Mafic rocks present LREE depletion relative to HREE whereas felsic rocks are LREE enriched. The REE are listed by increasing atomic number from left to right. After DePaolo (1988).

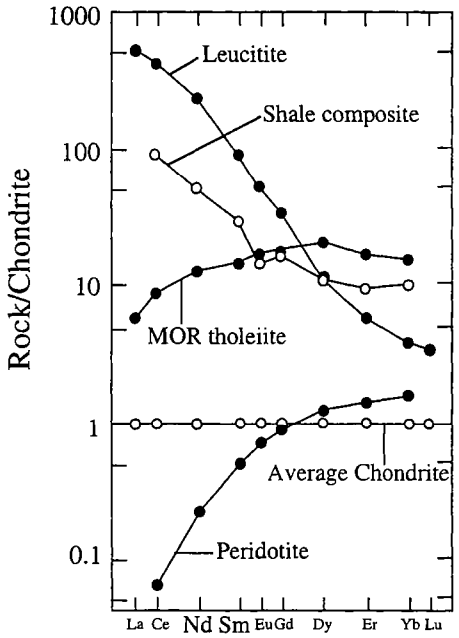

The REE studies of Haskin et al. (1966) and Taylor and McLennan (1985) demonstrated that crustal rocks mainly present LREE enrichment relative to HREE associated with $^{147}Sm/^{144}Nd$ = 0.115-0.118 (Fig. 2). In comparison, mafic rocks such as Mid-Ocean Ridge Basalt (MORB) are characterized by LREE depletion relative to HREE related to $^{147}Sm/^{144}Nd$ up to 0.25. Hofmann (1988) attributed the distinctive Sm/Nd ratios to the differentiation of the continental crust from mantle reservoir. The Sm-Nd system may be used in conjunction with Rb-Sr or U-Pb systems to study the evolution of terrestrial rocks. In contrast to the other systems, the Sm-Nd system is not fractionated during intracrustal processes such as alteration, metamorphism or partial melting. Consequently, geological studies aimed at the understanding of crust formation used intensively the Sm-Nd system. But,"... a detailed understanding of the processes involved and knowledge of the relation mobility of Sm and Nd during metamorphism vis à vis these other elements is still lacking..." (De Paolo, 1988). Some recent studies on high-grade polymetamorphic terranes have provided examples of obvious disturbance of the Sm-Nd system (Arndt et al., 1989; Rosing, 1990; Tourpin et al., 1991; Bernard-Griffiths et al., 1991; Whitehouse et al., 1996; Gruau et al., 1996; Moorbath et al., 1997). Therefore, the knowledge of mechanism leading to Sm/Nd fractionation during metamorphism should be understood. The issue of Sm-Nd systematics on Proterozoic metamorphic rocks as indicator of crustal history constitutes one aim of my Ph.D thesis.

In general, the variation of $^{147}Sm/^{144}Nd$ ratio within a rock suite is quite limited due to the long $^{147}Sm$ decay. However, some minerals may present high Sm/Nd ratio such as garnet which may present a $^{147}Sm/^{144}Nd$ ratio significantly higher than 0.5. Thus, the Sm-Nd system is also a straightforward application for dating metamorphic rocks especially garnet-bearing rocks. Garnet formed during a metamorphic event is not always isotopically equilibrated with the other minerals due to either an open system, or an interaction with a fluid phase, or an additional isotope component (Jagoutz, 1988; Thöni and Jagoutz, 1992). The issue of dating metamorphic minerals by the Sm-Nd system represents the second aim of this Ph.D thesis.

*The Sm-Nd method of dating*

The decay of $^{147}Sm$ and growth of radiogenic $^{143}Nd$ is described by the equation:

$$^{147}Sm \rightarrow ^{143}Nd + \alpha$$

and the age equation is:

$$\left(\frac{^{143}Nd}{^{144}Nd}\right) = \left(\frac{^{143}Nd}{^{144}Nd}\right)_0 + \left(\frac{^{147}Sm}{^{144}Nd}\right) * (e^{\lambda * t} - 1)$$

Figure 3: Sm-Nd isochron diagram. At formation age, the minerals took the same isotopic composition as the whole rock. After, the growth of radiogenic $^{143}Nd$ is related to the decay of $^{147}Sm$.

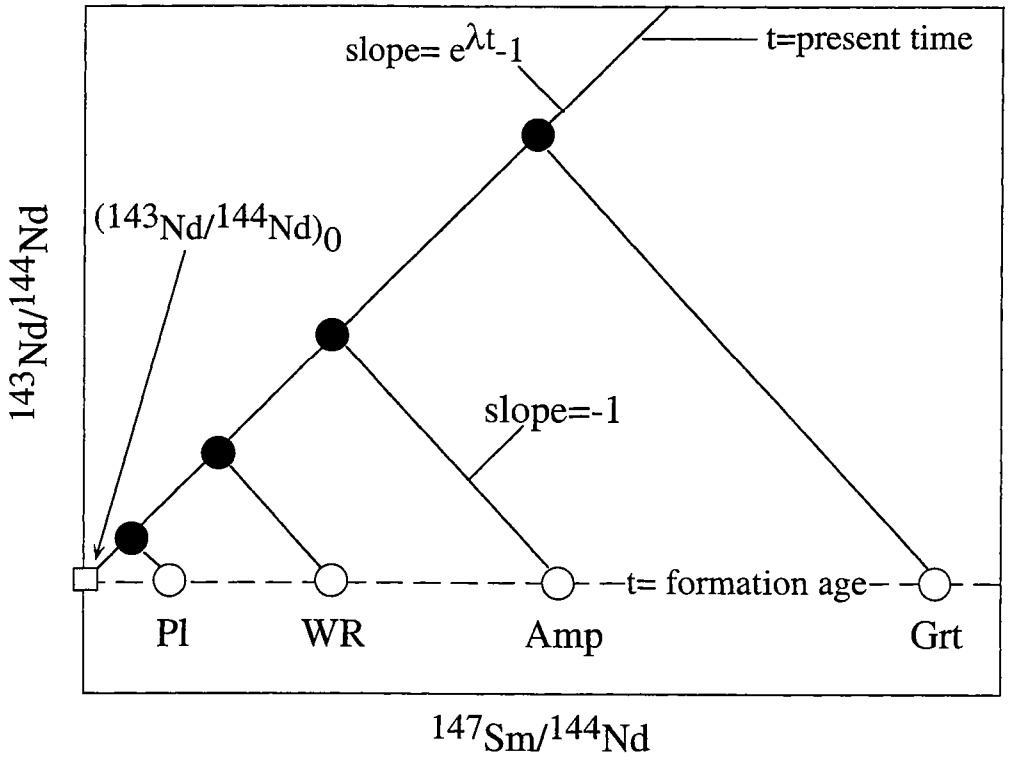

where t is the time and $\lambda$ is the decay constant of $^{147}Sm$ ($\lambda = 0.00654\ Ga^{-1}$). Different minerals or co-genetic whole rocks may have significantly distinctive Sm/Nd ratios. Their $^{143}Nd/^{144}Nd$ ratios plotted as a function of their respective $^{147}Sm/^{144}Nd$ ratios may form a positive correlation as shown in Fig. 3. The best regression line passing through all data points is termed the isochron. The isochron age can then be calculated from the slope (p) according to the following equation:

$$t = \left(\frac{1}{\lambda}\right) * \ln(p+1)$$

The intercept of the isochron at $^{147}Sm/^{144}Nd$ equal to 0 with Nd isotopic composition axis gives the initial Nd isotopic composition $(^{143}Nd/^{144}Nd)_0$ at the rock and minerals were formed. The interpretation of the isochron is based on the assumption that all minerals or all whole rocks have the same initial ratio and that the system remained closed since t = 0, i.e. formation age.

Sm and Nd occur as trace elements in common rock minerals in which they replace major ions. They are highly concentrated in accessory minerals such as monazite, apatite, xenotime or allanite. However, the Sm/Nd ratios in these specific minerals do not differ significantly from those of "common" minerals such as biotite, feldspath, or pyroxene. Sm/Nd ratios vary generally between 0.1 and 0.3. On the contrary, garnet has high Sm/Nd ratio above 0.5 as it preferentially incorporates HREE instead of LREE in its chemical structure. Therefore, garnet is the most useful mineral to obtain a good internal Sm-Nd mineral isochron.

Among garnet-bearing metamorphic rocks, eclogites are of special interest for the evolution of an orogenic belt as they were formed in the highest pressure and temperature (P, T) conditions. Consequently, the eclogitization age determination is an useful indicator on the relationship between the depth reached by eclogitized oceanic or continental crust, the tectono-metamorphic evolution of orogenic belt and the age. Most eclogites are bimineralic rocks composed of garnet and omphacite. $(Sm/Nd)_{Grt}$ ratio is generally higher than 2 (Thöni and Jagoutz, 1992) whereas $(Sm/Nd)_{Omp}$ ratios cluster at 0.7. However available chemical data on garnet and omphacite indicate that garnet presents high and variable Sm/Nd ratios compared to low and constant Sm/Nd ratios of omphacite (Jagoutz, 1988; Thöni and Jagoutz, 1992; Bowtell et al., 1994; Cliff et al.,1998). Jagoutz (1988) and Cliff et al. (1998) suggested that the large variation in Sm/Nd ratios of garnet and omphacite may imply drastic isotopic effects, i.e. an incomplete Nd homogeneisation between these two minerals. An example of incomplete Nd isotope exchange during eclogite facies metamorphism on gabbro is given by Thöni and Jagoutz (1992) as some of their Cpx separats do not lie on the WR-Grts isochron. In addition, accessory minerals which concentrate the REE rock budget may occur as small inclusions within garnet dominating, therefore, the garnet Sm/Nd ratio (Bowtell et al., 1994; Hensen and

Zhou, 1995). The Sm-Nd analyses on these garnet may form either an errorchron or an isochron prodiving a meaningless geological age, due to an isotopic disequilibrium between inclusions and garnet.

From this issue highlighted by Jagoutz (1988), Thöni and Jagoutz (1992) and Bowtell et al. (1994), I performed Sm-Nd analyses on eclogites and their surrounding rocks from the Ultra-High Pressure Metamorphic (UHPM) terrane in the Dabie Shan (Central China) to test the validity of Sm-Nd ages of garnets taken from different rock types and different localities, and compare them with the U-Pb zircon ages. Further, age information derived from other radiochronometers (Rb-Sr, Ar-Ar, U-Pb SIMS and Fission tracks) will allow me to answer the important question concerning the problem whether the eclogites and their surrounding rocks have an "In situ" or a "Foreign" relationship. The results corresponding to this issue represent the Part II of this Ph.D thesis.

*Nd isotopes in studies of Terrestrial crustal evolution*

"... It is in the field of crustal evolutionary studies that Nd isotopes have made the greatest impact. This is because the large and somewhat reproducible fractionation of the Sm/Nd ratios between mantle and upper continental crust allows rudimentary "Chemical crustal ages" to be obtained..." (Patchett, 1992). In addition, "... the close similarity between the Nd isotopic composition and the Sm-Nd ratio of recent upper crustal sediments and those of the most typical anatectic granites which, presumably, sample large crustal regions at depth, confirms that sediment Nd isotopic properties do not deviate drastically from those of the mean crust..." (Albarède and Brouxel, 1987). Three parameters are commonly used: (1) the epsilon Nd value, i.e. $\varepsilon_{Nd}$, (2) Nd model age, i.e. $T_{DM}$ or $T_{CHUR}$, and (3) the Sm/Nd fractionation factor, i.e. $f^{Sm/Nd}$.

Firstly, it is often more senseful to consider variations in the Nd isotopic compositions of sedimentary, igneous or metamorphic rocks relative to the bulk Earth. Thus, the epsilon notation was established and it is calculated by the following equation:

$$\varepsilon_{Nd}(t) = \left[ \left( \frac{\left( \frac{^{143}Nd}{^{144}Nd} \right)_{e,t}}{\left( \frac{^{143}Nd}{^{144}Nd} \right)_{CHUR,t}} \right) - 1 \right] * 10000$$

where the index e indicates the sample and t the age. Due to the small range in the Nd isotopic composition between mafic and felsic rocks, it becomes easier to work with one or two digit number instead of five to six digit one. A negative value of a $\varepsilon_{Nd}(t)$ parameter indicates that the

Figure 4: The formation by melting of reservoirs with high and low Sm/Nd ratios from an initial homogeneous reservoir, and the change of the $^{143}Nd/^{144}Nd$ ratio with time in these reservoirs..

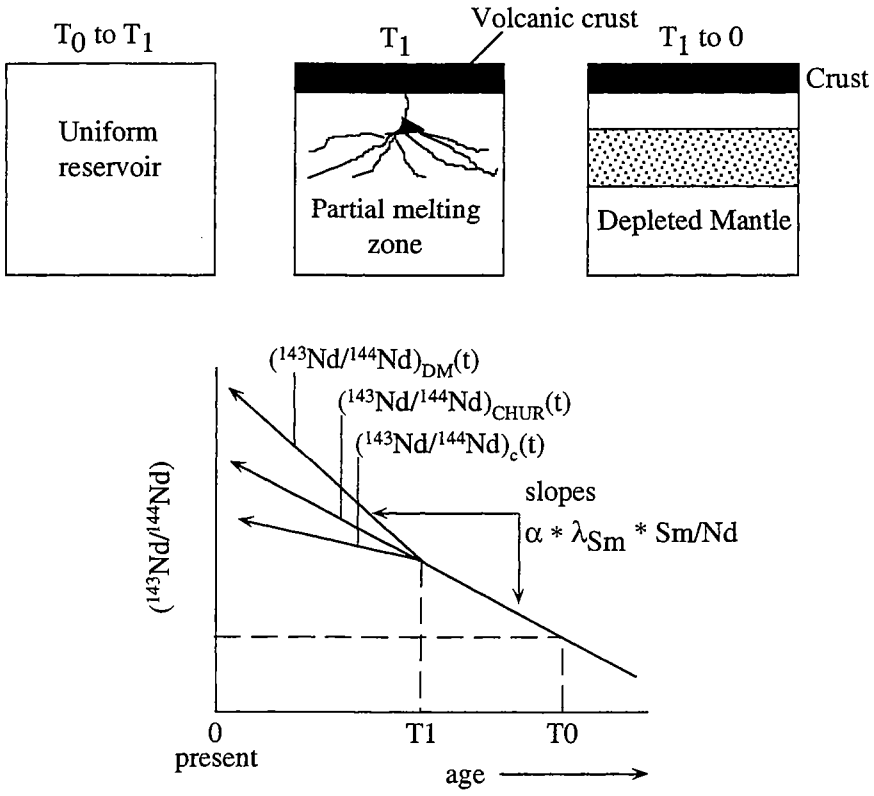


Figure 5: Definition of Nd model ages.

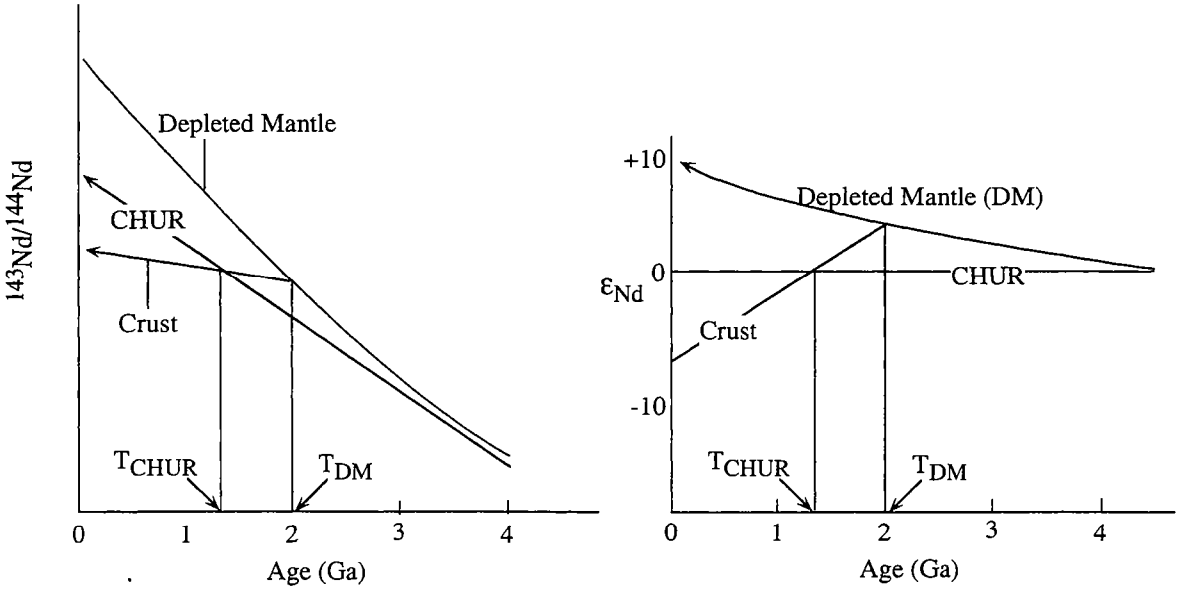

rock protoliths have a lower Sm/Nd ratio than CHUR (for example crustal rocks) whereas a prositive value of that parameter highlights a rock protolith characterized by higher Sm/Nd ratio than CHUR (Fig. 4). For Precambrian crustal rocks, it is useful to calculate the $\varepsilon_{Nd}(t)$ at the age of formation, deposition or metamorphism.

Secondly, a relative large fractionation of Sm and Nd is involved in crust formation. Most crustal rocks have Sm/Nd ratios around 0.18 which tend not to change. Thus, this allows determination of model ages for the crust or crustal residence time. The Nd model age provide the time at which the sample had a Nd isotopic composition equal to that of its mantle source. The following equation gives the age determination:

$$T_m = \left(\frac{1}{\lambda}\right) * \ln\left[1 + \frac{\left(\frac{^{143}Nd}{^{144}Nd}\right)_e - \left(\frac{^{143}Nd}{^{144}Nd}\right)_{ms}}{\left(\frac{^{147}Sm}{^{144}Nd}\right)_e - \left(\frac{^{147}Sm}{^{144}Nd}\right)_{ms}}\right]$$

where $\lambda$ is the contant decay of $^{147}Sm$, and e and ms indications correspond to the sample and the mantle source considered. This age determination is based on the assumption that the Nd mantle evolution through the time is known. Two main mantle reservoirs may be considered: (1) CHUR and (2) the Depleted Mantle (DM). First of all, as mentioned above, CHUR is being representative of the bulk Earth evolution according to De Paolo and Wasserburg (1976) and Hofmann (1984). In that case, $T_{CHUR}$ represents the age at which crustal material is differentiated from a primitive mantle reservoir, which did not vary since the Earth formation (McCullogh and Wasserburg, 1978) (Fig. 5). The Nd characteristics of CHUR at present time are $^{147}Sm/^{144}Nd$ = 0.1967 and $^{143}Nd/^{144}Nd$ = 0.512638 if normalized to $^{146}Nd/^{144}Nd$ = 0.7219 (De Paolo and Wasserburg, 1976). However, Hamilton et al. (1978), Allègre and Ben Othman (1980) and De Paolo (1981) argued that most of the continental crust is differentiated from a depleted mantle reservoir. Consequently, most of Nd model ages are calculated from the Nd model evolution of the Depleted Mantle (Fig. 5). Its Sm-Nd characteristics at present time are much less defined and several values have been proposed by Allègre et al. (1983a), Goldstein et al. (1984), Michard et al. (1985), Peucat et al. (1987), Nägler and Kramers (1998).

The last parameter used in Nd isotopic studies on terrestrial crustal evolution is the Sm/Nd fractionation factor ($f^{Sm/Nd}$). It is the $^{147}Sm/^{144}Nd$ analogue of the Nd epsilon parameter. It corresponds to the Sm/Nd enrichment or depletion of a sample relative to CHUR. It is calculated from the expression:

Figure 6: Model for the interpretation of Nd isotopic compositions of continental igneous rocks. The important assumption is the derivation of continental crust by chemical fractionation processes from the mantle. The portion of crust formed has the Nd isotopic composition of its source at the time of its formation. After that, the Nd isotopic composition of the continent and the mantle diverge sharply as a consequence of different f Sm/Nd values. After De Paolo (1988).

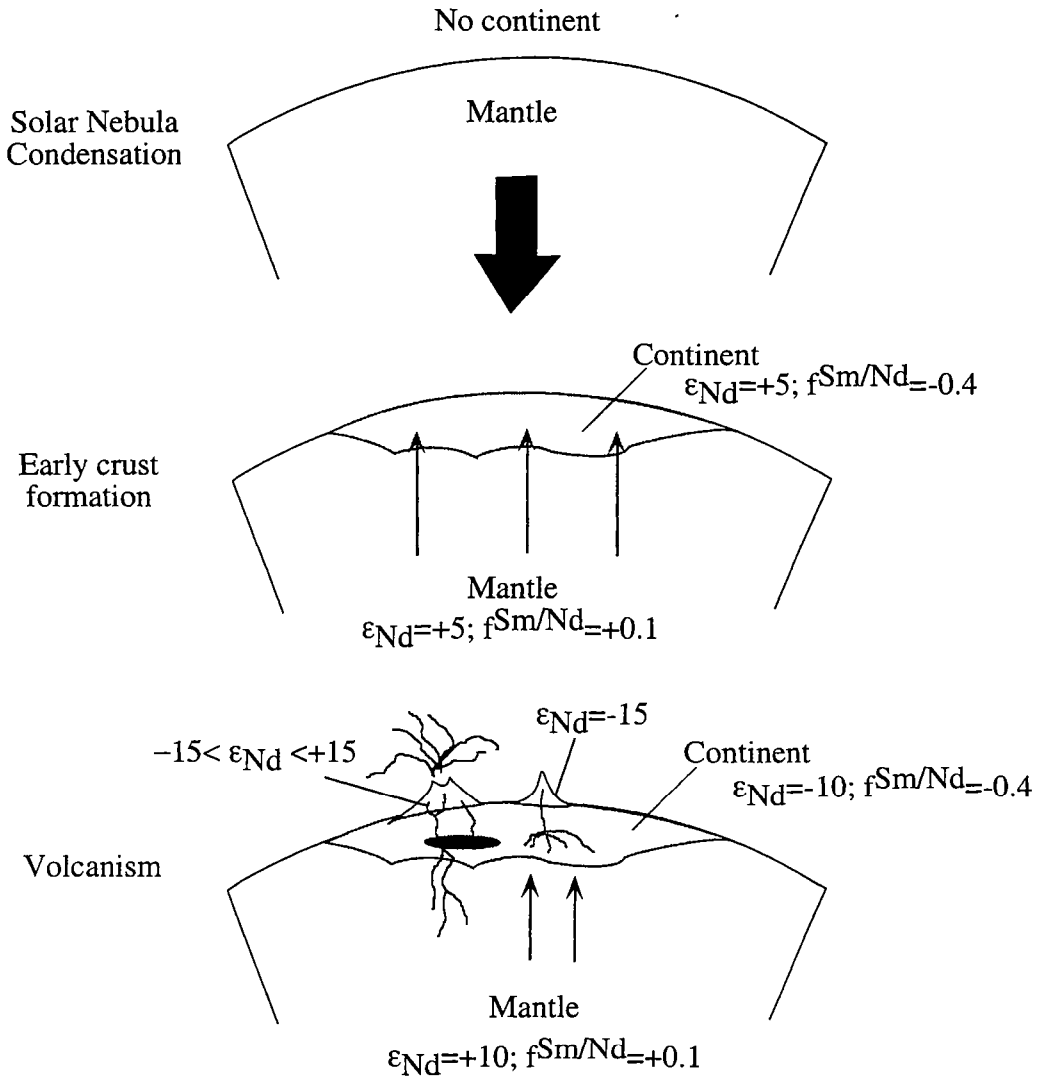

$$f^{Sm/Nd} = \left[ \frac{\left(\frac{^{147}Sm}{^{144}Nd}\right)_e}{\left(\frac{^{147}Sm}{^{144}Nd}\right)_{CHUR}} \right] - 1$$

where e refers to a sample. Considering the terrestrial material, crustal rocks which are characterized by low Sm/Nd ratio compared to CHUR, have a negative $f^{Sm/Nd}$ whereas mafic material (high Sm/Nd ratio compared to CHUR) have a positive value (Fig. 6).

Archean to Proterozoic terranes have been investigated from the isotopic point of view in order to determine "crust-formation" ages. Goldstein et al. (1984) argued that "Sm-Nd isotopic investigation of metamorphosed continental crust ... have provided the general impression that on scale larger than that of local mineral equilibria, metamorphic processe have small effects on Sm-Nd systematics...". However, some recent studies on Archean-Proterozoic terranes provided examples of obvious disturbances of the Sm-Nd system during intracrustal processes. For example, Arndt and Goldstein (1987) suggested that calculated Nd model ages on a granite intrusion may not necessarely correspond to the true age of crust formation event but instead may reflect mixing between a mantle-derived material and an older crustal material (Fig. 7). As a consequence, the Nd model ages may not give the time at which crustal material separated from the mantle but an average age of the crust involved. An example of Sm/Nd fractionation during metasomatism is highlighted by Rosing (1990). In that case, the interaction between a rock and a fluid may altered the initial Sm-Nd characteristics of the sample. The transport of Sm and Nd via a fluid may induce changes in isochron and Nd model ages and in the $\varepsilon_{Nd}(t)$ values. The extend of the disturbance depends on the fluid/rock ratio, on the bulk distribution coefficients for Sm and Nd between rocks and fluids, and also on the time lapse between petrogenesis and second disturbance. Finally, the evolution model of Early Archean mantle and crust is done by the used of initial epsilon Nd values. These models are based on the assumption that the Sm-Nd system remained closed since rock formation. However, Whitehouse et al. (1996), Gruau et al. (1996) and Moorbath et al. (1997) who investigated Archean-Proterozoic crustal rocks in Scotland, Greenland and Canada respectively, suggested that initial Nd isotopic composition on these rocks may not represent reliable constraints to model the Early Earth's history. As a consequence, the initial $\varepsilon_{Nd}(t)$ obtained from poly-tectono-metamorphic Archean provinces should be considered with caution.

Studies on Archean rocks from the last 10 years provided many examples of obvious disturbance of the Sm-Nd system during metamorphism. Therefore, the assumption of closed system with respect to the element of interest during intracrustal processes is no more concivable. From this problematic, my objective is to provide constraints on mechanisms

Figure 7: Example of the evolution of the Nd isotopic composition through the time for a granite. Calculated Nd model ages on a granite intrusion may reflect mixing between a mantle-derived material and an older crustal material. After Arndt and Goldstein (1987).

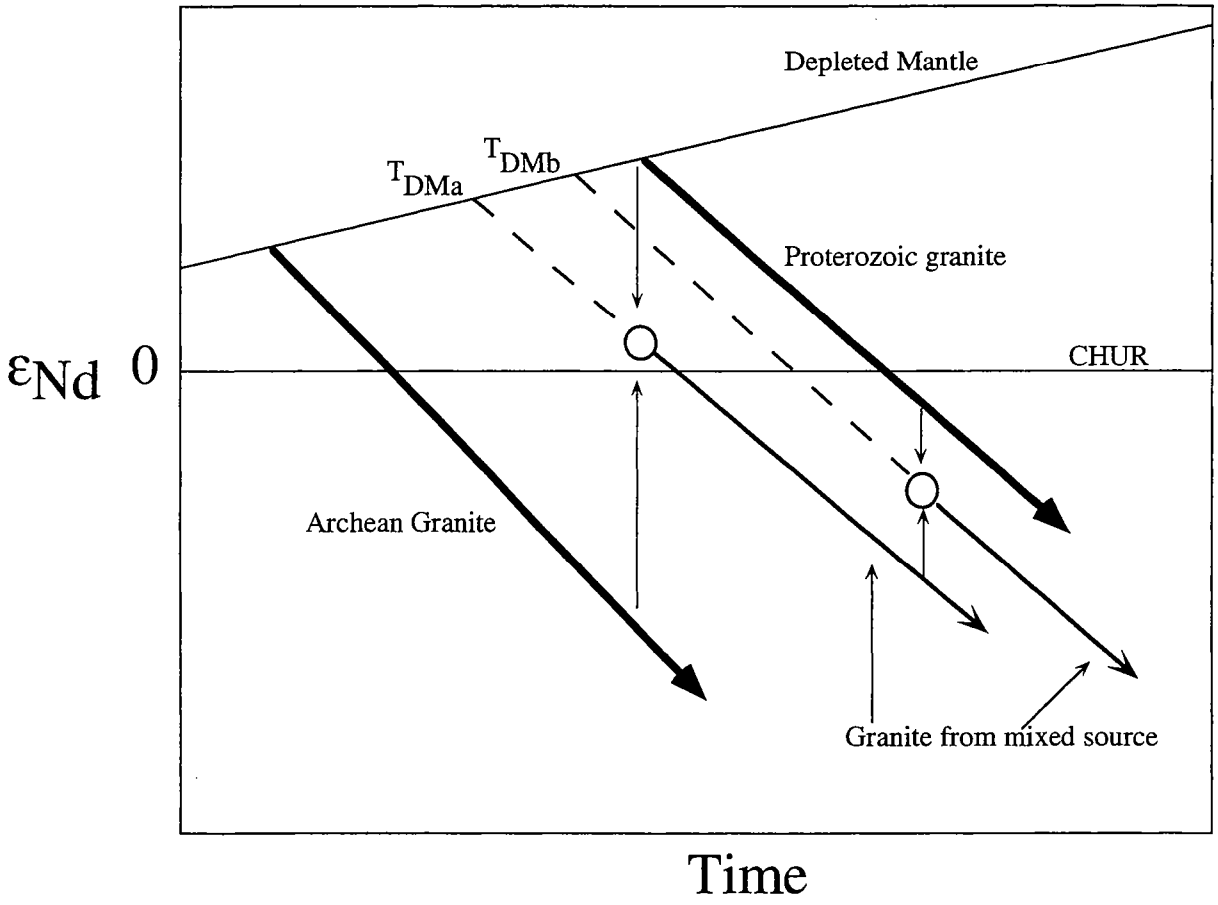

controlling Sm and Nd re-distribution during metamorphism and to assess Nd isotope exchange in that process. The studied area is the Limpopo orogenic belt (Southern Africa) which underwent poly-tectono-metamorphic events in Archean to Proterozoic period. To test whether the initial $\varepsilon_{Nd}(t)$ values may be still used to constrain the crustal evolution in Southern Africa, I have focussed my work on migmatites which give an opportunity to look at the chemical fractionation occurring during partial melting in the crust. I have carried out microprobe analyses on minerals, major and trace elements analyses as well as Nd and Pb isotope measurements on three examples of migmatites in the Central Zone of the Limpopo Belt. The results are reported in the Part I of this Ph.D thesis.

*Nd analytical technique*

Ultramafic rocks and some silicate minerals contain Nd concentration below 0.1 ppm. Substantially better ion efficienties are required and it has been realized that ionization of $NdO^+$ was much more efficient than as $Nd^+$ ion. The Part III of this Ph.D. thesis documents the procedure for $NdO^+$ emission established at the Universität Bern.

The Ph.D. thesis is composed of three parts.

The part I discusses the issue of Sm-Nd systematics on Proterozoic metamorphic rocks from the Limpopo Belt as indicator of crustal history in southern Africa. After a short introduction, I will present the geological setting of the Limpopo Belt and a bibliographic overview on migmatites concerning the protolith lithologies, the petrogenesis and the chemical fractionation occurring during migmatite formation. The behaviour of the Sm-Nd system during migmatization and its effects on crustal growth studies are explained in three articles.

The part II recounts the issue of dating metamorphic minerals by the Sm-Nd system. After a short introduction, the geological setting and the tectono-metamorphic evolution of the Ultra-High Pressure Metamorphic terrane of the Qinling-Dabie orogenic belt are described. The validity of Sm-Nd garnet ages compared to U-Pb zircon ages and the crucial question whether the coesite-bearing eclogites and their currounding rocks have an 'In situ" or a "Foreign" relationship are discussed in two articles.

The part III presents the procedure for $NdO^+$ emission established at the University of Bern. It documents the loading technique, the technical transformation on the mass spectrometer, the determination of oxygen isotopic composition, the mass interferences corrections and finally the Nd standard results.

La découverte des éléments naturels radioactifs par Curie et Becquerel au cours du 19ème siècle a donné la possibilité aux géologues de mieux comprendre l'évolution de la formation des planètes appartenant à notre système solaire. Un des isotopes du samarium ($^{147}Sm$) est radioactif et se désintègre par une émission alpha pour produire un isotope stable du néodyme ($^{143}Nd$). Cette désintégration s'effectue lentement car la constante de désintégration du $^{147}Sm$, égale à 6.54 $10^{-12}$ $an^{-1}$, correspond à un demi temps de vie approximativement 23 fois supérieur à l'âge de la Terre. Dans la mesure où la désintégration du $^{147}Sm$ est très lente, les variations de concentration en $^{143}Nd$ par rapport aux autres isotopes du Nd non radiogéniques sont de l'ordre de 1 pour mille. Par conséquent, l'utilisation du système isotopique Sm-Nd sur des roches terrestres nécessite une mesure très précise des rapports isotopiques du Nd. Ainsi, le perfectionnement des méthodes analytiques soit en spectrométrie de masse soit en chromatographie est indispensable pour l'application de cette méthode. La première amélioration concerne la méthode d'échange ionique pour la purification des fractions des Terres Rares des autres éléments (Peppard, 1961; Powell, 1961; Eugster et al., 1970). Une précision de l'ordre de ± 0.1% (dans la même gamme de variation que la concentration en $^{143}Nd$) a pu être atteinte grâce au spectrometre de masse à ionisation thermique (Hedge, 1966). Finalement, Wasserburg et al. (1969) ont perfectionné le spectrometre de masse par un contrôle à partir d'un ordinateur, ce qui a permis d'augmenter la précision sur la mesure des rapports isotopiques d'un facteur 30. De ce fait, la méthode Sm-Nd peut être utilisée sur des roches terrestres ou extraterrestres. Au début des années 70, l'association des nouvelles méthodes en chromatographie chimique et en spectrométrie de masse donne la possibilité à Lugmair (1974) et Lugmair et al. (1975a) d'étudier les météorites et les basaltes lunaires avec le système Sm-Nd. Dès lors, la précision sur les mesures des rapports isotopiques (jusqu'à ±0.005%) n'a cessé de s'améliorer avec les spectromètres de masse à multi-collecteurs. Du fait que le rapport Sm/Nd n'est pas fractionné durant les processus intra-crustaux, la méthode Sm-Nd est devenue essentielle pour la compréhension des processus intra-terrestres produisant la formation de la croûte, la composition du manteau ainsi que l'évolution des enveloppes terrestres au cours du temps géologique. Plusieurs sciences géologiques peuvent être étudiées telles que la pétrologie magmatique, métamorphique et sédimentaire mais aussi la géochimie, la paléoclimatologie, l'océanographie etc...

Les éléments Sm et Nd appartiennent au groupe des lanthanides (Fig. 1). Ils ont un comportement chimique similaire. Cependant du fait que les rayons ioniques diminuent du $La^{3+}$ à l'$Yb^{3+}$, leurs comportements géochimiques sont controllés par les structures crystallines des phases minéralogiques fractionnées au cours des processus magmatiques. Par voie de fait, les variations observées dans les rapports Sm/Nd sont attribuées aux résultats des processus intra-terrestres plutot qu'aux processus de condensation du début de la formation de la Terre. A partir d'études cosmochimiques, il a été démontré que les concentrations en Terres Rares et en certains éléments réfractaires dans la Terre et la Lune sont similaires à celles des chondrites

Figure 1:Sm and Nd in the chart of periodic element.

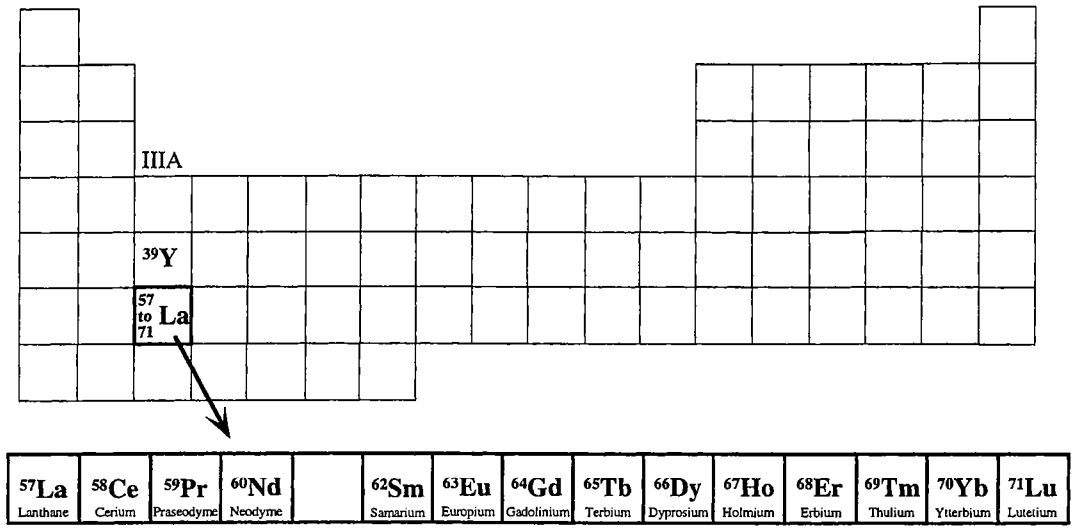


Figure 2: Chondrite-normalized REE patterns of typical mafic and felsic rocks. Mafic rocks present LREE depletion relative to HREE whereas felsic rocks are LREE enriched. The REE are listed by increasing atomic number from left to right. After DePaolo (1988).

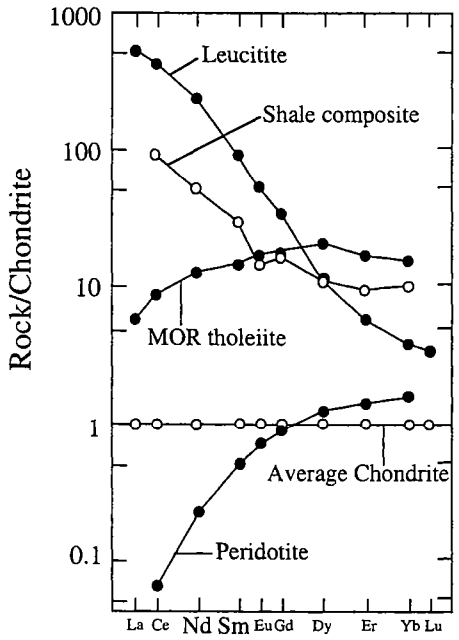

carbonatées les moins différenciées (Ganapathy and Anders, 1974; Drake, 1976; Anders, 1977). Ainsi, le terme "CHondrite Uniform Reservoir" comme représentant de la Terre globale, a été défini par De Paolo and Wasserburg (1976a). Les compositions isotopiques en Sm-Nd du CHUR au temps présent sont: $^{147}Sm/^{144}Nd = 0.1967$ and $^{143}Nd/^{144}Nd = 0.512638$.

L'étude des Terres Rares par Haskin et al. (1966) et Taylor and McLennan (1985) a démontré que les roches crustales sont caractérisées principalement par une enrichissement en Terres Rares légères associé à un rapport $^{147}Sm/^{144}Nd$ autour de 0.115-0.118 (Fig. 2). Au contraire, les roches basiques telles que les Basaltes des Rides Médio Océaniques (MORB) sont, quant à elles, caractérisées par un apprauvrissement en Terres Rares légères par rapport aux Terres Rares lourdes, et un rapport $^{147}Sm/^{144}Nd$ jusqu'à 0.25. Hofmann (1988) attribuent ces rapports Sm/Nd très distincts à la différenciation des roches crustales à partir d'un réservoir mantellique. De plus, le système Sm-Nd peut être associé aux systèmes Rb-Sr et U-Pb afin d'étudier la formation des roches crustales au cours des temps géologiques. Cependant, à l'inverse de ces autres systèmes, le système Sm-Nd n'est pas fractionné lors de processus intra-crustaux tels que l'altération, le métamorphisme ou la fusion partielle. Ainsi, les études géologiques dédiées à la compréhension de la formation de la croûte utilisent préférentiellement le système Sm-Nd. Mais, "... une compréhension détaillée des processus invoqués et la connaissance de la mobilité du Sm et du Nd durant le métamorphisme, vis à vis des autres éléments sont toujours manquants..." (De Paolo, 1988). Par la suite, récentes études sur des terrains métamorphiques de haut-grade ont démontré plusieurs exemples de perturbation du système Sm-Nd (Arndt et al., 1989; Rosing, 1990; Tourpin et al., 1991; Bernard-Griffiths et al., 1991; Whitehouse et al., 1996; Moorbath et al., 1997). Par conséquent, la connaissance des mécanismes induisant le fractionnement du rapport Sm/Nd au cours du métamorphisme doit être comprise ou acquise. L'utilisation du système Sm-Nd sur des roches métamorphiques protérozoïques comme indicateur de l'évolution crustale en Afrique du Sud constitue la première problématique de cette thèse.

En général, la variation des rapports $^{147}Sm/^{144}Nd$ dans une suite de roche est très faible due à la longue constante de désintégration du $^{147}Sm$. Cependant, certains minéraux silicatés peuvent être caractérisés par un rapport Sm/Nd élevé, par exemple le grenat qui peut avoir un rapport Sm/Nd supérieur à 0.5. Par conséquent, le système Sm-Nd peut être aussi utilisé sur des roches métamorphiques à grenat, à des fins géochronologiques. Le grenat qui a été formé lors d'un événement métamorphique n'est pas nécessairement en équilibre isotopique avec les minéraux de la matrice à la suite soit d'une ouverture du système isotopique postérieure à sa formation, soit à son intéraction avec un fluid ou encore à l'incorporation d'une autre source de Nd. La datation des minéraux métamorphiques par le système Sm-Nd est le second sujet abordé dans cette thèse.

Figure 3: Sm-Nd isochron diagram. At formation age, the minerals took the same isotopic composition as the whole rock. After, the growth of radiogenic $^{143}Nd$ is related to the decay of $^{147}Sm$.

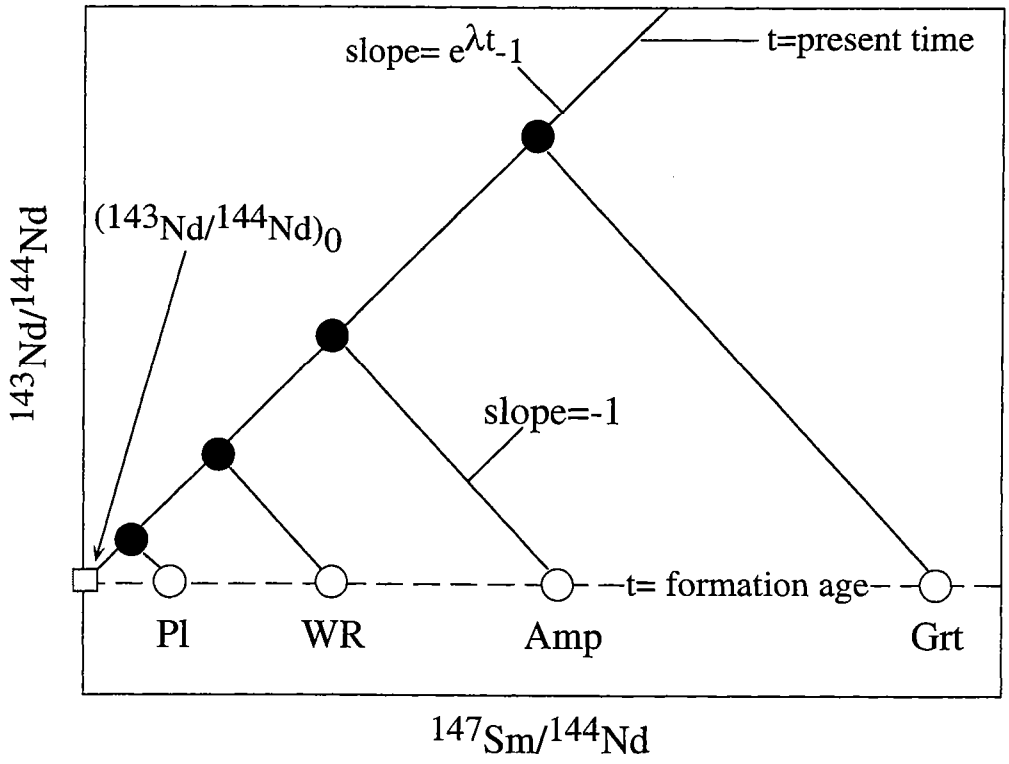

*La datation par la méthode Sm-Nd*

La désintégration du $^{147}Sm$ et la croissance du $^{143}Nd$ radiogénique sont reliées selon l'équation suivante:

$$^{147}Sm \rightarrow ^{143}Nd + \alpha$$

et l'équation de l'âge s'exprime par l'équation suivante:

$$\left(\frac{^{143}Nd}{^{144}Nd}\right) = \left(\frac{^{143}Nd}{^{144}Nd}\right)_0 + \left(\frac{^{147}Sm}{^{144}Nd}\right) * (e^{\lambda * t} - 1)$$

où t représente le temps et $\lambda$ est la constante de désintégration du $^{147}Sm$ ($\lambda$ = 0.00654 $Ga^{-1}$). Différentes fractions minérales ou plusieurs roches totales co-génétiques peuvent avoir une forte variation du rapport Sm/Nd. Leurs rapports $^{143}Nd/^{144}Nd$ reportés en fonction de leurs rapports respectifs en $^{147}Sm/^{144}Nd$ peuvent former une corrélation à pente positive (Fig. 3). La détermination de l'âge dépend de la pente de la droite de régression (isochrone) (p) suivant l'équation:

$$t = \left(\frac{1}{\lambda}\right) * \ln(p + 1)$$

L'interception de la droite isochrone à $^{147}Sm/^{144}Nd$ égal à 0 avec l'axe de la composition isotopique en Nd donne la composition isotopique en Nd $(^{143}Nd/^{144}Nd)_0$ à l'âge de formation. L'interprétation d'une isochrone repose sur le fait que tous les minéraux ou les roches totales ont le même rapport isotopique initial et que le système est resté clos depuis t = 0, à l'âge de formation.

Le Sm et le Nd sont présents comme élément trace dans les minéraux communs, en substitution des ions majeurs. Ces deux éléments sont fortement concentrés dans les minéraux accessoires tels que la monazite, l'apatite, l'allanite ou la xénotime. Cependant, leurs rapports Sm/Nd ne diffèrent pas des autres minéraux communs, par exemple la biotite, le feldspath, le pyroxène. Généralement, les rapports Sm/Nd varient entre 0.1 et 0.3. Á la différence, le grenat peut avoir un rapport Sm/Nd largement supérieur à 0.5 dans la mesure où le grenat incorpore dans sa structure chimique plus les Terres Rares lourdes que les Terres Légères. Ainsi, le grenat est un minéral très favorable pour l'obtention d'une isochrone interne sur minéraux avec le système Sm-Nd.

Parmi les roches métamorphiques à grenat, les éclogites sont de premier intéret dans l'évolution d'une chaine orogénique dans la mesure où elles se sont formées au conditions métamorphiques (P, T) les plus fortes. Par conséquent, la détermination de l'âge de

l'éclogitization permet de relier la profondeur à laquelle la croûte océanique ou continentale a été éclogitisée et l'évolution tectono-métamorphique de la zone orogénique par rapport au temps. La plupart des éclogites sont des roches bi-minérales composées de grenat et d'omphacite. Les rapports $(Sm/Nd)_{Grt}$ sont supérieur à 2 alors que les rapports $(Sm/Nd)_{Omp}$ sont généralement autour de 0.7 (Jagoutz, 1988; Thöni and Jagoutz, 1992; Botwell et al., 1994; Cliff et al., 1998). Cependant, les données sur la composition chimique des grenats et des omphacites suggèrent que le grenat est caractérisé par un rapport Sm/Nd élevé mais très variable alors que celui de l'omphacite est faible mais constant. Ainsi, Jagoutz (1988) and Cliff et al. (1998) démontrent que ces fortes variations peuvent induire de sévères perturbations isotopiques, i.e. une homogénéisation isotopique incomplète entre ces deux minéraux. Un exemple de telle perturbation isotopique en Nd durant le métamorphisme éclogitique est illustré par un "offset" isotopique des omphacites par rapport aux isochrones Grt-WR (Thöni and Jagoutz, 1992). De plus, les minéraux accessoires qui représentent le budget en Terres Rares de la roche totale peuvent être en inclusion dans les grenats, controllant de ce fait le rapport Sm/Nd du grenat (Botwell et al., 1994; Hensen and Zhou, 1995). Les analyses en Sm-Nd sur de tels grenats peuvent produire soit une 'erreurchrone' ou un age géologique irréaliste due au déséquilibre isotopique entre les inclusions et les grenats.

De cette problématique mise en évidence par Jagoutz (1988), Thöni and Jagoutz (1992) et Botwell et al. (1994), j'ai effectué des analyses Sm-Nd sur des éclogites et leurs encaissants provenant du terrain Métamorphique de Ultra-Haute Pression (UHPM) de Dabié Shan (Chine) afin de tester la validité des âges Sm-Nd sur grenat de différent affleurement et de les comparer aux âges U-Pb sur zircon. De plus, les âges obtenus par différents systèmes isotopiques (Rb-Sr, Ar-Ar, U-Pb SIMS, et traces de fission) me permettent de répondre à la question cruciale concernant la coalescense ou la juxtaposition des éclogites et de leurs encaissants durant l'évènement d'UHPM. Les résultats correspondant à cette problématique sont présentés dans la partie II de cette thèse.

*Les isotopes du Nd dans les études de l'évolution de la croûte continentale*

"... C'est dans le domaine de l'évolution de la croûte continentale que les isotopes du Nd ont eu le plus grand impact. Ceci est du au fait que le fractionnement du rapport Sm/Nd entre le manteau et la croûte est reproductible, permettant la détermination de l'âge chimique crustale ..." (Patchett, 1989). De plus, "... les proches similitudes des compositions isotopiques en Nd et les rapports Sm/Nd entre les sédiments de la croûte supérieure et la plupart des granites anatectiques, confirment que les caractéristiques isopiques en Nd des sédiments ne diffèrent pas dramatiquement de celles de la croûte moyenne..." (Albarède et Brouxel, 1987). Trois paramètres sont généralement utilisés: (1) l'epsilon Nd, $\varepsilon_{Nd}$, (2) les âges modèles en Nd, $T_{DM}$ or $T_{CHUR}$, and (3) le facteur de fractionnment du rapport Sm/Nd, $f^{Sm/Nd}$.

Figure 4: The formation by melting of reservoirs with high and low Sm/Nd ratios from an initial homogeneous reservoir, and the change of the $^{143}Nd/^{144}Nd$ ratio with time in these reservoirs..

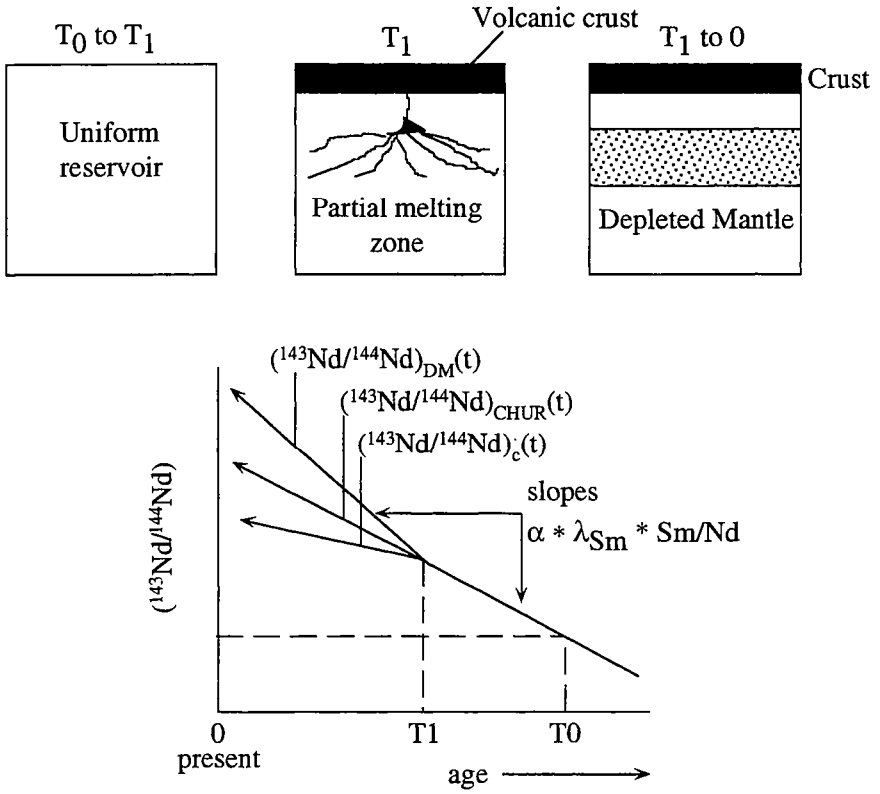


Figure 5: Definition of Nd model ages.

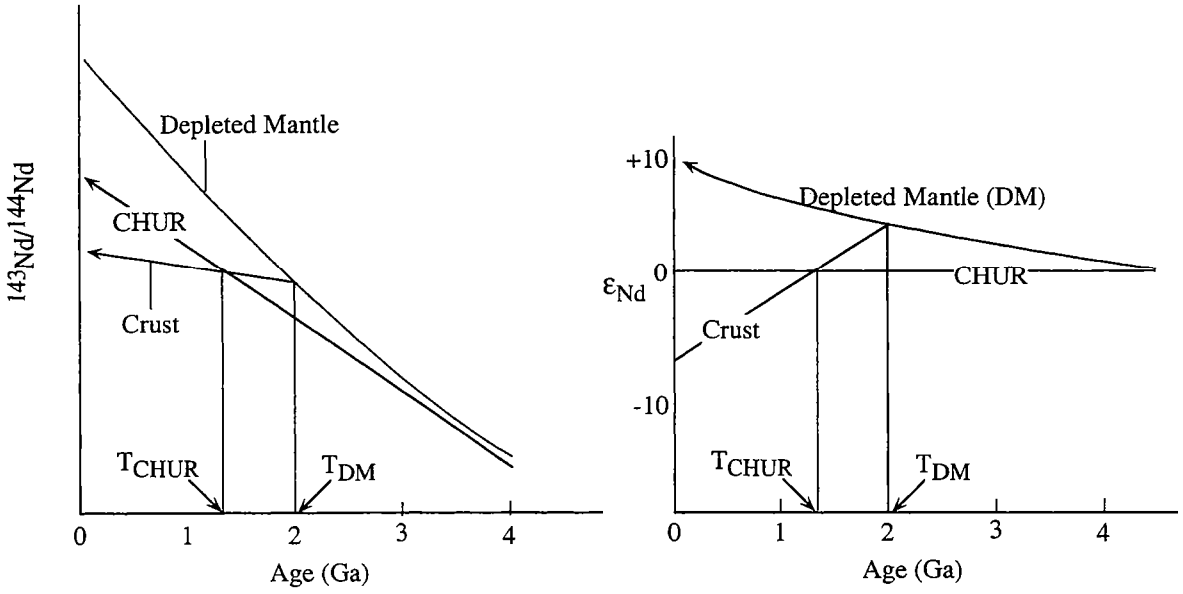

. Premièrement, il est souvent plus sensé de considérer les variations en compositions isotopiques en Nd des roches sédimentaires, ignées ou métamorphiques par rapport à la Terre Silicatée. Ainsi, la notation en epsilon Nd a été établie et la valeur de ce paramètre est calculée suivant l'équation suivante:

$$\varepsilon_{Nd}(t) = \left[ \left( \frac{\left(\frac{^{143}Nd}{^{144}Nd}\right)_{e,t}}{\left(\frac{^{143}Nd}{^{144}Nd}\right)_{CHUR,t}} \right) - 1 \right] * 10000$$

où l'index e réfère à l'échantillon et t à l'âge. Dans la mesure où il existe de faibles variations dans les compositions isotopiques en Nd entre les roches basiques et acides, il est beaucoup facile de travailler avec deux décimales qu'avec cinq ou six. Une valeur négative de l'epsilon Nd indique que le protolith de la roche est caractérisé par un rapport Sm/Nd plus faicle que celui du CHUR (par exemple les roches crustales) alors qu'une valeur positive de ce paramètre correspond à un protolith possédant un rapport Sm/Nd supérieur à celui du CHUR (Fig. 4). Pour les roches précambriennes, il est souvent très utile de calculer la valeur de l'epsilon Nd à l'âge de formation, de sédimentation ou du métamorphisme.

Deuxièmement, un fractionnement du Sm et du Nd est invoqué dans la formation de la croûte. La plupart des roches crustales ont un rapport Sm/Nd autour de 0.18, tendant à rester constant. Ainsi, ceci permet le calcul de l'âge modèle de la croûte ou le temps de résidence crustal. L'âge modèle en Nd indique l'âge auquel la roche possède une composition isotopique en Nd identique à celle du manteau source. L'équation suivante permet le calcul de cet âge:

$$T_m = \left(\frac{1}{\lambda}\right) * \ln\left[ 1 + \left( \frac{\left(\frac{^{143}Nd}{^{144}Nd}\right)_e - \left(\frac{^{143}Nd}{^{144}Nd}\right)_{ms}}{\left(\frac{^{147}Sm}{^{144}Nd}\right)_e - \left(\frac{^{147}Sm}{^{144}Nd}\right)_{ms}} \right) \right]$$

où $\lambda$ est la constante de désintégration du $^{147}Sm$, et les indexes e et ms réfèrent respectivement à l'échantillon et au manteau source considéré. L'âge modèle repose sur l'hypothèse que l'évolution isotopique en Nd du manteau est déjà connue. Deux réservoirs mantelliques peuvent être considérés: (1) CHUR et (2) le manteau appauvri (DM). Tout d'abord, CHUR est considéré comme représentatif de l'évolution de la Terre selon De Paolo and Wasserburg (1976) et Hofmann (1984). Dans ce cas, $T_{CHUR}$ correspond à l'âge auquel le matériel crustal se différencie du manteau primitif qui n'a pas varié depuis la formation de la Terre (McCullogh and Wasserburg, 1978) (Fig. 5). Les caractéristiques en Nd du CHUR au temps présent sont: $^{147}Sm/^{144}Nd$ = 0.1967 et $^{143}Nd/^{144}Nd$ = 0.512638 si on considère une normalization

Figure 6: Model for the interpretation of Nd isotopic compositions of continental igneous rocks. The important assumption is the derivation of continental crust by chemical fractionation processes from the mantle. The portion of crust formed has the Nd isotopic composition of its source at the time of its formation. After that, the Nd isotopic composition of the continent and the mantle diverge sharply as a consequence of different f Sm/Nd values. After De Paolo (1988).

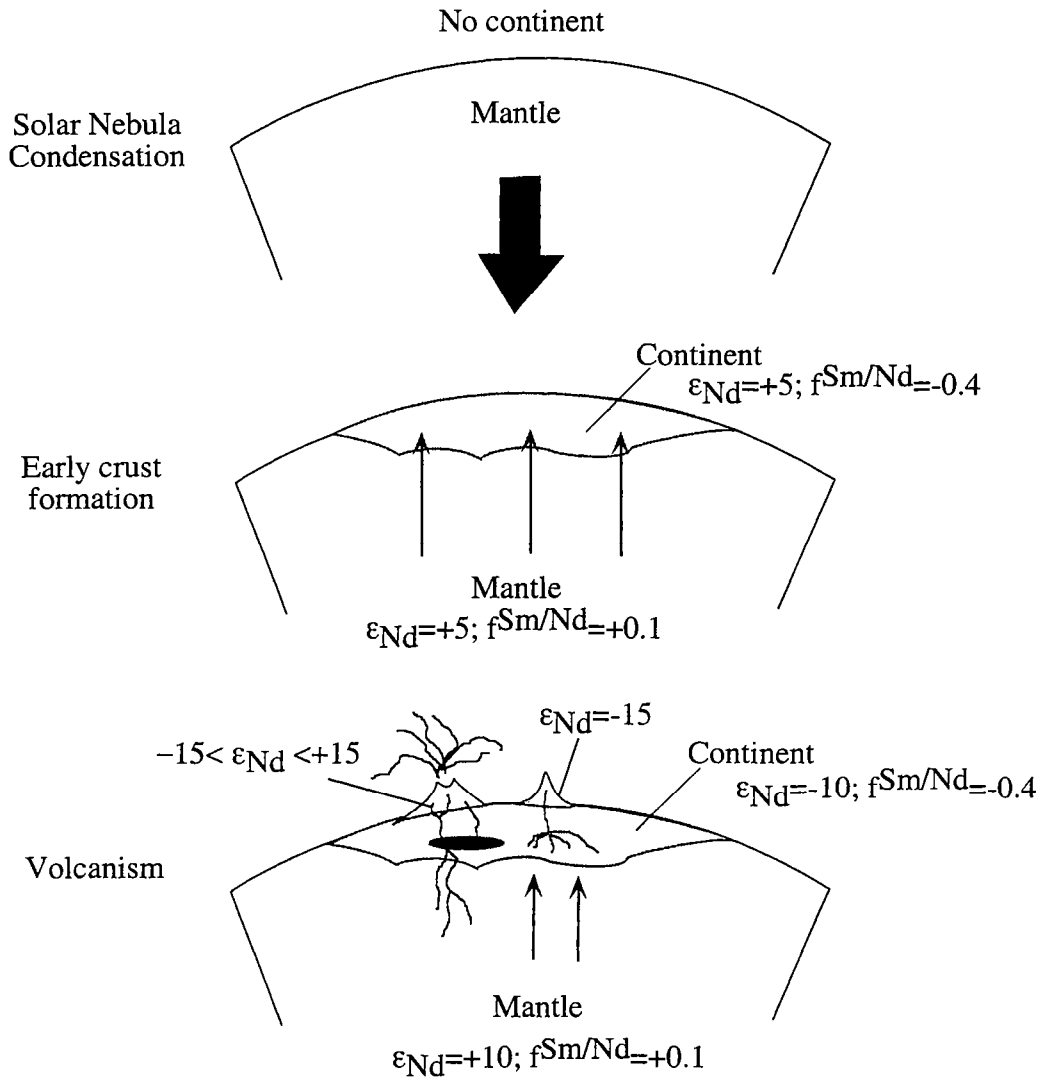

$^{146}Nd/^{144}Nd = 0.7219$ (De Paolo and Wasserburg, 1976). Cependant, Hamilton et al. (1978), Allègre et Ben Othman (1980) et De Paolo (1981) ont démontré qu'une grande partie de la croûte continentale est différenciée du manteau appauvri. Par conséquent, les âges modèles en Nd sont calculés à partir de l'évolution du manteau appauvri (Fig. 5). Ses caractéristiques isotopiques au temps présent sont tout de même beaucoup moins bien définies et plusieurs modèles ont été proposés Allègre et al. (1983a), Goldstein et al. (1984), Michard et al., (1985), Peucat et al. (1987), Nägler and Kramers (1998).

Le dernier paramètre utilisé dans les études de l'évolution de la croûte continentale est le facteur de fractionnement du rapport Sm/Nd ($f^{Sm/Nd}$). Il s'agit de l'analogue $^{147}Sm/^{144}Nd$ à l'espilon Nd. Sa valeur retranscrit l'enrichissement ou l'appauvrissement en Sm/Nd d'un échantillon par rapport au CHUR. Ce facteur est calculé suivant l'expression:

$$f^{Sm/Nd} = \left[ \frac{\left(\frac{^{147}Sm}{^{144}Nd}\right)_e}{\left(\frac{^{147}Sm}{^{144}Nd}\right)_{CHUR}} \right] - 1$$

où e réfère à l'échantillon. Si nous considérons que les roches terrestres, les roches crustales seront caractérisées par un faible rapport Sm/Nd vis à vis du CHUR et donc une valeur négative du $f^{Sm/Nd}$ alors que les roches mantelliques auront un fort rapport Sm/Nd associé à une valeur positive du facteur $f^{Sm/Nd}$ (Fig. 6).

Les terrains archéens à protérozoiques ont été amplement étudiés isotopiquement afin de déterminer l'âge de formation de la croûte. Goldstein et al. (1984) suggèrent que "les études Sm-Nd sur la croûte continentale métamorphique ... donnent l'impression qu'à l'échelle supérieure au minéral, les processus métamorphiques ont peu d'effets sur le système Sm-Nd ...". Cependant, Arndt and Goldstein (1987) démontrent que les âges modèles calculés sur des intrusions granitiques peuvent être tout à fait non-relevant de l'âge véritable de formation crustale mais peuvent plutot refléter un âge mixte entre un matériel juvénile et un matériel ancien (Fig. 7). Par conséquent, les âges modèles en Nd peuvent indiquer un âge erroné pour l'extraction de matériel crustal du manteau, c'est à dire un un âge moyen de la croûte impliquée. Un exemple de fractionnement du rapport Sm/Nd durant le métasomatisme est mis en évidence par Rosing (1990). Dans ce cas, les intéractions fluide/roche peuvent altérer les caractéristiques isotopiques initiales en Sm-Nd de l'échantillon. Le transfert du Sm et du Nd par un fluide peut provoquer des changements dans l'isochrone, dans les âges modèles ainsi que les valeurs de l'espilon Nd à t considéré. L'ampleur de la perturbation isotopique depend du rapport fluide/roche, des coefficients de partage du Sm et du Nd entre le fluide et la roche, ainsi que tu lapse de temps écoulé entre la pétrogénèse et la perturbation. Finallement, le modèle d'évolution

Figure 7: Example of the evolution of the Nd isotopic composition through the time for a granite. Calculated Nd model ages on a granite intrusion may reflect mixing between a mantle-derived material and an older crustal material. After Arndt and Goldstein (1987).

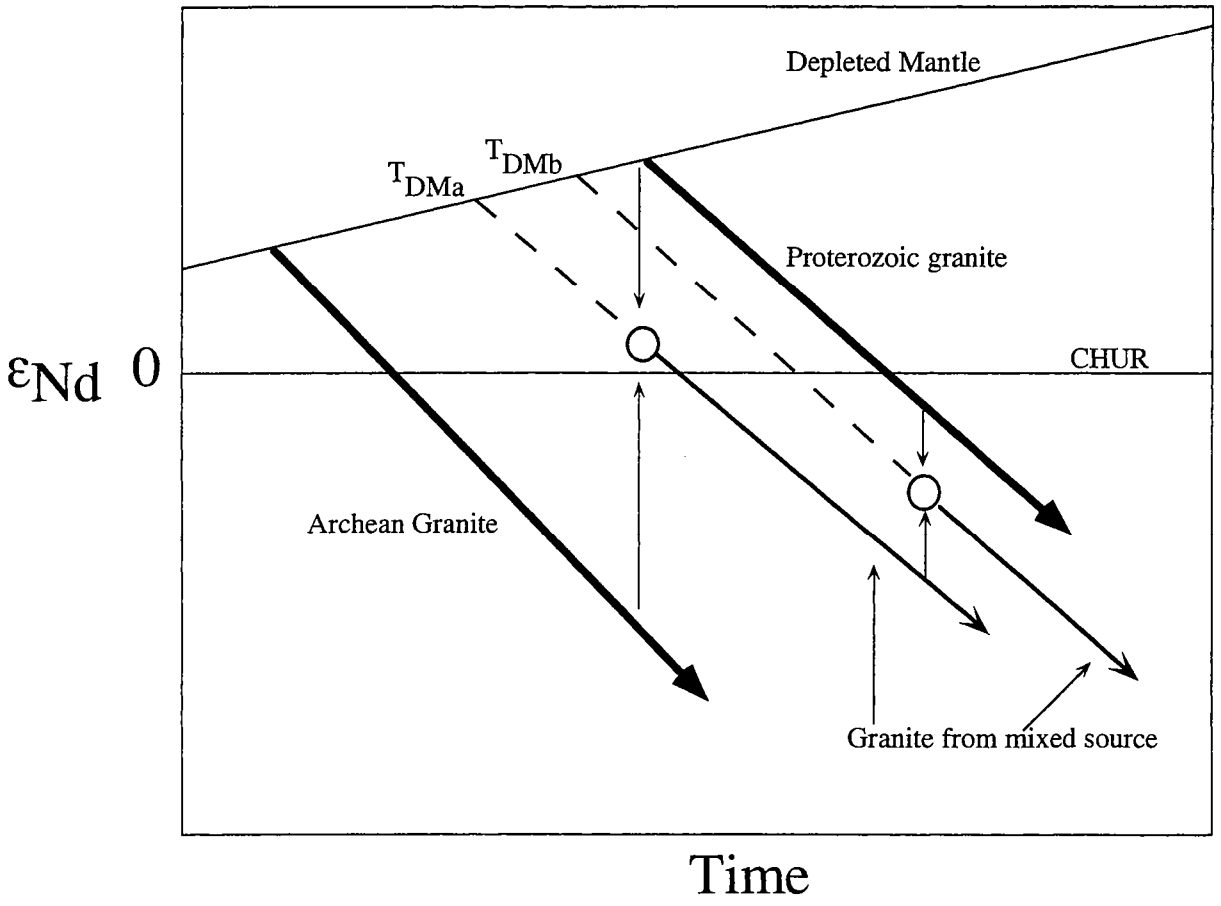

du manteau et de la croûte au début Archéen est basé sur les valeurs intiales en epsilon Nd. Ces modèles reposent sur l'hypothèse que le système reste clos depuis sa formation. Cependant, Whitehouse et al. (1996), Gruau et al. (1996) et Moorbath et al. (1997) qui ont analysé par le système Sm-Nd les roches crustales archéennes et protérozoiques en Ecosse, Groënland et Canada respectivement, démontrent que la composition initiale en Nd de ces roches peuvent être sans aucune signification pour contraindre l'évolution primaire de la Terre. De ce fait, les valeurs en epislon Nd à l'instant t obtenues sur des roches de provinces poly-métamorphiques doivent être considérées avec précaution.

Les études Sm-Nd de ces dix dernières années sur les roches archéennes ont procuré des exemples de perturbations de ce système au cours du métamorphisme. Donc, l'hypothèse d'un système clos durant un processus intracrustal par rapport à l'élément choisi, ne peut plus être considéré comme valide. De cette problématique, mon objectif a été de donner des contraintes sur les mécanismes controllant la re-distribution du Sm-Nd durant le métamorphisme et donc par conséquent d'évaluer l'étendue des échanges isotopiques en Nd durant ce même processus. La région étudiée est le Limpopo Belt (Afrique du Sud) qui a subit plusieurs événements tectono-métamorphiques de l'Archéen au Protérozoïque. Afin de confirmer si les valeurs initiales en Nd peuvent être toujours utilisées pour contraindre l'évolution crustale en Afrique du Sud, j'ai axé mon travail sur les migmatites qui donnent l'opportunité d'étudier le fractionnement en élément chimique durant la fusion partielle dans la croûte. J'ai donc effectué des analyses microsondes sur les minéraux principaux, des analyses en éléments majeurs et traces ainsi que des analyses isotopiques en Nd et en Pb sur trois exemples de migmatites de la Zone Centrale du Limpopo Belt. Les résultats sont reportés dans la partie I de cette thèse.

*Méthode analytique en Nd*

Les roches ultrabasiques ainsi que certains minéraux silicatés peuvent contenir une concentration en Nd inférieure à 0.1 ppm. Une meilleure ionization du Nd est donc indispensable et il a été reconnu que l'ionization du $NdO^+$ est beaucoup plus efficace que l'ionization en $Nd^+$. La partie III de cette thèse décrit la procédure analytique établie à Bern afin de mesurer le Nd comme $NdO^+$.

Cette thèse est divisée en trois parties.

La partie I traite du problème lié à l'utilisation du système Sm-Nd sur des roches métamorphiques protérozoïques du Limpopo Belt afin de contraindre l'histoire crustale en Afrique du Sud. Après une courte introduction, je présenterai le contexte géologique, une synthèse bibliographique sur les migmatites. Je discuterai du comportement du système Sm-Nd

durant la migmatization et ses implications sur l'étude de la croissance crustale sous forme de trois articles.

La partie II relate le problème de la datation des minéraux métamorphiques avec le système Sm-Nd. Après une courte introduction, je décrirai le contexte geologique et l'évolution tectono-métamorphique du terrain à Ultra-Haute Pression de l'orogène Qinling-Dabié. La validité des âges Sm-Nd sur grenats par rapport aux âges U-Pb sur zircon ainsi que le problème sur la juxtaposition ou de la coalescence des éclogites à coésite et leurs encaissants durant le métamorphisme de Ultra-Haute Pression seront ensuite abordés dans deux articles.

La partie III documente la méthode analytique en Nd mise au point à l'Université de Bern pour analyser le Nd sous forme d'oxyde. Elle décrit la procédure de chargement de l'échantillo, les transformations techniques sur le spectromètre de masse, la détermination de la composition isotopique de l'oxygène, les corrections sur les interférences de masse et enfin les résultats obtenus sur les standards internationaux en Nd.

# *Part I: The Limpopo Belt*

# 1. Introduction

The detailed understanding of the origin and mechanisms leading to crust formation is an outstanding geological issue. The growth of the continental crust may be approximated by the geological record coupled with very precise geochronological and isotopic data (Taylor and McLennan, 1985; McCulloch and Bennett, 1995; Bowring and Housh, 1995; Sylvester et al., 1997). From various studies, a consensus on crustal growth is established suggesting an episodic crustal formation throughout the geologic time (Moorbath, 1977, 1978; Taylor and McLennan, 1981, 1985, 1995: Anderson, 1992; Condie, 1993). Although oceans cover about 70% of the Earth, the oldest oceanic lithosphere is 200 Ma years old, whereas the oldest continental crust is dated at 4.0 Ga (Bowring et al., 1990). It has to be noticed that the oldest continental crust occurs only as sparse outcrops corresponding only to small fractions of the mass of the continental crust. However, these portions of the continental crust are of special interest to look at the early stage of internal Earth's differentiation.

The continental crust is composed of two entities, i.e. the upper and lower crusts which are conventionally separated according to P-wave velocities of less and more than 6.5 km/s, the Conrad Discontinuity. The lower continental crust is characterized by higher density than the upper one (Hall, 1986) corresponding to a significantly different chemical composition including depletion in radioactif elements (U, Th, and K: Roy et al., 1968; Jaupart, 1983). Whereas the upper crust is easily accessible to geological sampling, the determination of the physical and chemical features of the lower continental crust, are mainly based on geophysical data as well as geochemical and isotopic analyses on granulites and xenoliths.

Granulites correspond to metamorphic rocks crystallizing at pressure between 3 and 18 kbars and temperature up to 1000°C (Harley, 1989, Thompson, 1990). The (P,T) conditions are significantly higher than those expected for a stable lower continental crust. The large geochemical data set given by Rudnick and Presper (1990) associated with the compilation of (P-T) paths provided by Harley (1989) suggest that (1) granulites following an isothermal decompression (P-T) path during retrograde metamorphism are mainly metasedimentary rocks, (2) mafic granulites essentially occur within granulitic terrain which underwent an isobare cooling, (3) crustal xenoliths are mafic in composition. In addition, geophysical studies argue for a mafic composition for the lower continental crust whereas field observations indicate that the granulitic terrains contain large amounts of metasedimentary rocks. It appears that granulites, in general terms, present highly variable physical and chemical features. The extent to which those metamorphic rock are representative of the lower continental crust is not well established. Their highly variable chemical compositions may, however, result from mechanisms leading to crustal differentiation (Fountain and Salisbury, 1981; Percival and Card,

1983; Newton and Hansen, 1986).

Archean to Proterozoic orogenic belts -mainly located at the junction between two stable cratons- are among the best candidate to look at the evolution of the continental crust and its internal differentiation. They are sufficiantly exhumed to present on the terrain scale large amounts of the mid to lower continental crust, i.e. granulites. The continental crust which was metamorphosed under granulite facies is characterized by layers, pods or veins of granitic material in plastically deformed metamorphosed rocks, forming migmatitic structure (Brown, 1997). Derivation of granitoids by lower crustal anatexis certainly is a major mechanism of intracrustal differentiation. With the intention to constrain the continental crust evolution in the Archean to Proterozoic, geological studies have to deal with migmatites. Considering isotope systematics, the Sm-Nd system has made an important impact in the field of crustal evolution. It is considered to remain relatively unfractionated during intracrustal processes, thus providing a way to determine "crust-formation" ages. Hovewer, no detailed isotopic works have been performed on migmatites to decipher whether the use of the Sm-Nd system produces reliable constraints to model the early Earth's history.

For our study, the Archean-Proterozoic orogenic belt of the Limpopo Belt in southern Africa was choosen for several reasons: (1) detailed mapping of critical areas is provided by intensive field investigations performed by the Geological Surveys of South Africa, Botswana, and Zimbabwe and different universities (among them the University of Bern), (2) the tectonic model elaborated during the Ph.D. thesis of Holzer (1998; University of Bern) presents a totally different view compared to tectonic synthesis presented in several articles written by structural geologists of the Rand Afrikaans University (South Africa). (3) a hudge geochronologic database giving the approximate timing of events that stabilized the crust have been achieved since the early eighties.

In this work, petro-tectonic characteristics of the Limpopo Belt will be correlated with the geochemical features as well as Nd isotopic compositions on three examples of migmatites from the Central Zone of the Limpopo Belt in order to evaluate the significance of Nd model ages in terms of crustal growth. Special attention will be paid to the potential open-system behaviour of Sm-Nd system in the processes of migmatization.

# 2. Geological setting

The Limpopo Belt is a high-grade metamorphic terrane wedged between two low-grade granite-greenstone belts, the Kaapvaal Craton to the south and the Zimbabwe Craton to the north. It covers part of South Africa, Botswana and Zimbabwe (Fig. I.1). It was first

Figure I-1: Geographical location of the Limpopo Belt in South Africa. The Limpopo Belt which covers part of Botswana, South Africa and Zimbabwe, is wedged by the Kaapvaal craton to the south and the Zimbabwe craton to the north. NMZ: Northern Marginal Zone; SMZ: Southern Marginal Zone; CZ: Central Zone.

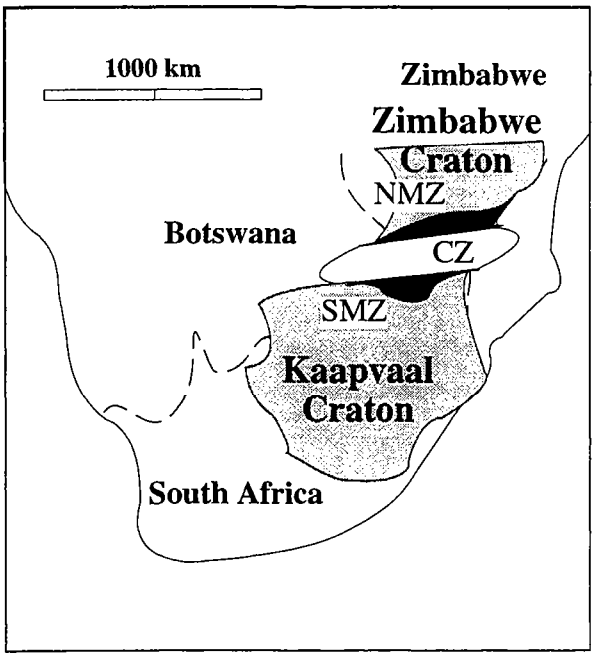


Figure I-2: The Limpopo Belt is composed of a Central Zone (CZ) and two Marginal Zones (SMZ and NMZ). Interconnected shear zones mark the boundaries between the CZ and the adjacent SMZ and NMZ.

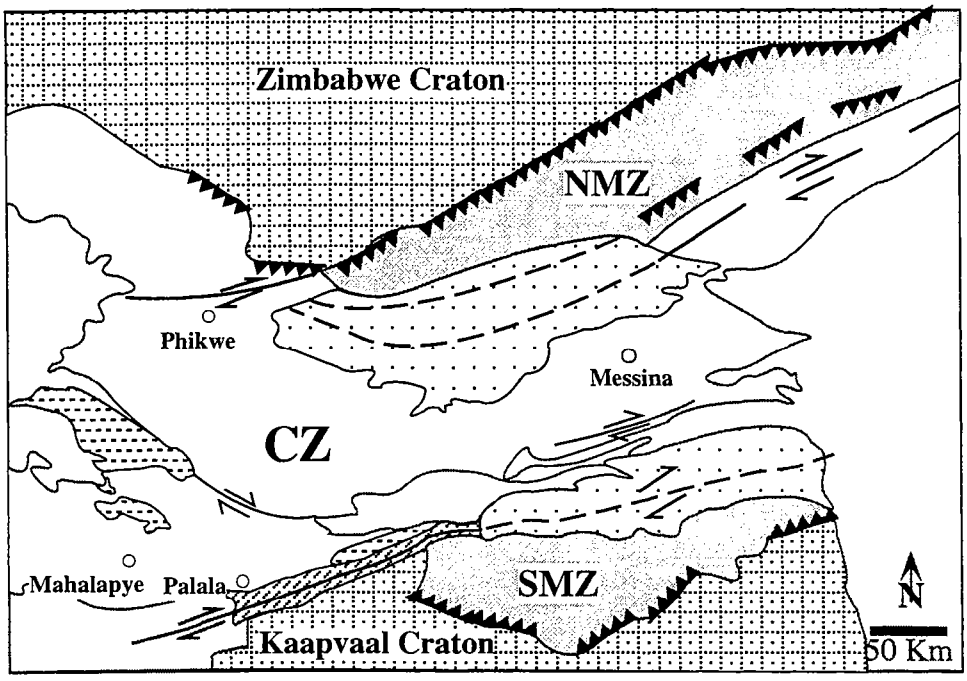

recognized by Mc Gregor (1953) who interpreted this geological entity as the deeply eroded root of a mountain, called the Limpopo Orogeny. A few years later, Holmes and Cahen (1957) obtained isotopic ages on minerals which strongly suggested an Early Proterozoic orogeny. Based on series of works that followed (Cox et al., 1965; Mason, 1973), the Limpopo Belt was subdivided into three subzones which are the Northern and the Southern Marginal Zones (NMZ and SMZ respectively) and the Central Zone (CZ). The boundaries of the CZ are represented by two tectonic lineaments, the Palala Shear Zone (PSZ) to the south and the Triangle Shear Zone (TSZ) to the north. Both lineaments consist of a composite of interconnected shear zones (Fig. I.2).

The three zones were thought to have been amalgamated in a single continental collision at ~2.6 Ga (Corward and Fairhead, 1980; Light, 1982; McCourt and Vearncombe, 1987, 1992; van Reenen et al., 1987; Roering et al., 1992; de Wit et al., 1992; Treloar et al., 1992; Windley, 1993). However, this idea may no longer hold because the Limpopo Belt is now recognized to have undergone a poly-metamorphic evolution. It is characterized by a last transpressional tectono-metamorphic event in Early Proterozoic affecting the Central Zone (van Breemen and Hawkesworth, 1980; Barton et al., 1994; Kamber et al., 1995a, 1995b; Holzer, 1995; Holzer et al., 1996; Jaeckel et al., 1996; Holzer, 1998). The NMZ and the SMZ represent mid to lower Archean crustal sections of their adjacent Cratons, with which they were unified at 2.6 Ga (Kamber et al., 1996; van Reenen et al., 1992).

## 2.1. The Kaapvaal Craton

The Kaapvaal craton covers an area of 1.2 $10^6$ $km^2$ in southern Africa. It is bounded to the north by the SMZ of the Limpopo Belt, to the south and west by Mid-Proterozoic orogenic belts called the Namaqua Belt and the Kahalari Belt, respectively, and to the east by Jurassic volcanics associated with the break-up of Gondwana (McCourt, 1995).

The Kaapvaal craton represents a classic Archean granite-greenstone terrane with Rb-Sr isochron and U-Pb ages between 3.6 and 2.6 Ga (Hawkesworth et al., 1979; Barton and Key, 1983; Kamo and Davies, 1994; de Ronde and de Wit, 1994; Kröner et al., 1996). All the major constituants of the Kaapvaal craton are shown in the Fig. I-3. Archean sequences are characterized by two assemblages of different compositions: (1) a granitoid component (Tonalite-Tronghjemite-Granodiorite suite or TTG suite), and (2) a volcano-sedimentary sequence (greenstone belt). The latter is represented by the Barberton granitoid-greenstone terrane in the Kaapvaal craton (area A on Fig. I-3). De Wit et al. (1992) interpreted this area as the product of 500 Ma of intraoceanic tectonics between 3.7 and 3.2 Ga. They considered the formation of such lithologies as due to a large-scale imbrication of the oceanic lithosphere. Partial melting of the lower parts of the thrust stack produced TTG melts which formed

Figure I-3: Geological map of the Kaapvaal craton showing the major Archean-Proterozoic constituants after McCourt (1995). A: the Baberton granitoid-greenstone terrane; B and C: the Murchison, Pietersburg and Sutherland granitoid-greenstone terranes; D: the Schweizer-Reneke adamellite; E: the Gaborone granite suite; F: the Bushveld Complex; TML: Thabaginbi-Murchison Lineament. The edges of the Archean and Late Archean crustal blocks are also reported.

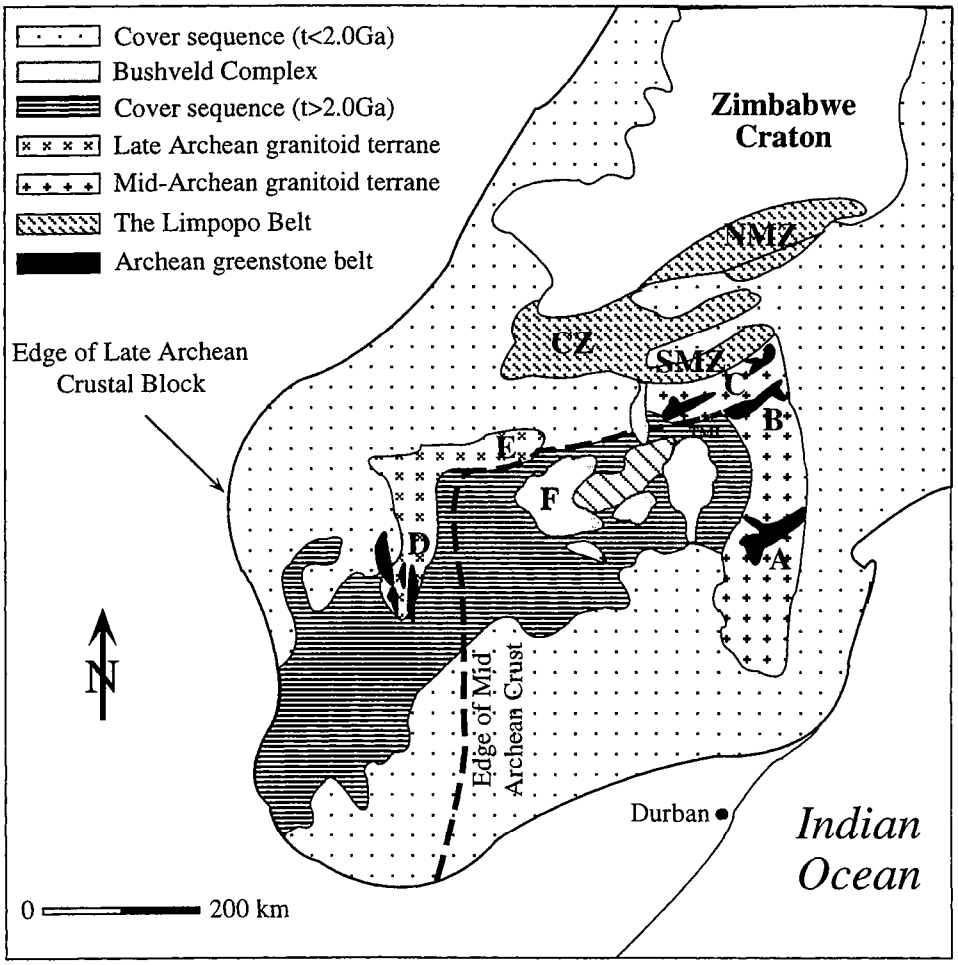

granitoid intrusions and calc-alkaline extrusions. Between 3.1 and 2.0 Ga, major events were related to continental margin tectonics corresponding to collisional orogeny (terrane accretion) around the northern and the western margins of the stable shield. During this period, the intra-continental tectonics as well as the accretion have been recorded in the important Witwatersrand sedimentary basin (Roering et al., 1990).

### 2.1.1. Tectonics of the basement

In the Kaapvaal craton, the principal granitoid-greenstone terranes include the Murchison, Pietersburg and Sutherland in the north (area B and C in Fig. I-3), and the Amalia-Kraaipan terranes in the west (area D in Fig. I-3). They indicate crustal growth related to collisional orogeny between 3.1 and 2.65 Ga (Robb et al., 1991; de Wit et al., 1992) and probably until the Early Proterozoic (Holzer, 1998). The Early Archean Barberton terrane is excluded from the present discussion as it is situated further to the south and sufficiently far away from the Limpopo Belt.

The Murchison greenstone terrane is a mosaic of 5 distinct domains that have been tectonically juxtaposed (Vearncombe, 1988). It corresponds to one part of the Thabaginbi-Murchison Lineament (TML). Vearncombe (1988) supposed that the crustal growth during the Archean could have been accomodated along this ENE-WSW trending TML. He suggested an age of 3.0 Ga for this event which seems to be in agreement with U-Pb zircon ages of 3.1 Ga on tonalitic gneisses adjacent to this greenstone terrane (Brandl and Kröner, 1993).

The Pietersburg greenstone terrane is composed of 2 tectono-stratigraphic units which are separated by an unconformity and locally by a thrust (de Wit, 1991; de Wit et al., 1992). The lower unit is a typical greenstone sequence which has been dated at 3.4 Ga by Pb-Pb method (Byron and Barton, 1990). An arenaceous to rudaceous sequence represents the upper unit which may be correlated with the Central Rand of the Witwatersrand basin (2.9-2.8 Ga; de Wit, 1991). Along the northern margin of the Kaapvaal craton, a northwest verging thrust has been described in the Pietersburg terrane and interpreted as a response to terrane accretion. The accretion of individual tectonic units in the Murchison and Pietersburg terranes was thought to be coeval (Rollision, 1993).

The Sutherland greenstone terrane is exposed at the northern edge of the Kaapvaal craton, immediate south of the Limpopo Belt (McCourt and van Reenen, 1992). Similar to the Pietersburg terrane, the Sutherland terrane is also composed of 2 tectono-stratigraphic units. The lower unit is a greenstone sequence of metavolcanics and metasediments, and the upper unit consists of mainly undeformed clastic sediments including conglomerates (McCourt and van Reenen, 1992). The entire terrane shows a north-dipping thrust with an oblique to reverse movement. This deformation predates the granitic intrusions at 2.65 Ga and is identified in the

tonalitic gneisses of the SMZ of the Limpopo Belt (McCourt and van Reenen, 1992). Moreover, an earlier northward thrust has been observed by de Wit et al. (1992) in the Sutherland terrane. De Wit et al. (1992) correlated this event with the 2.9-2.8 Ga event in the Pietersburg terrane.

The greenstone sequences are associated with numerous tonalitic and granodioritic gneisses which have been dated by U-Pb zircon ages at 3.1 to 2.87 Ga (Barton, 1990; Brandl and Kröner, 1993). These ages are interpreted as the emplacement age of their protoliths. Both greenstone depositions and granitoid plutonism could be correlated with a crustal growth event in the northern part of the Kaapvaal craton prior to the first deformation phase in the Limpopo orogeny. As suggested by Vearncombe (1988), this terrane accretion may be accommodated by the TML in the eastern part of the Kaapvaal craton. Associated with the TTG granitoid plutonism, syn to post-tectonic granites have been dated by the U-Pb zircon and Rb-Sr and Pb-Pb whole rock methods at 2.7 to 2.65 Ga (Barton, 1990). These dates are interpreted as the emplacement ages. These intrusions are associated to the early deformation of the Limpopo orogeny.

The Amalia-Kraaipan terrane is located at the western margin of the Kaapvaal craton. It is composed of a granitoid terrane called the Schwiezer-Reneke adamellite (area D in Fig. I-3), dated at 2.88 Ga by U-Pb zircon method, and the Gaborone granite suite (area E in Fig. I-3) dated at 2.78 Ga (Robb et al., 1990). The Gaborone granite suite consists of A-type rapakivi granite, granophyre microgranite, minor anorthosite and rhyolite. Such granite types are usually post-orogenic in age and are interpreted as the products of high-temperature crustal anatexis (Rollinson, 1993). The second lithology found in the Amalia-Kraaipan terrane is mainly composed of strongly folded banded iron formation (BIF; Vearncombe, 1986). de Wit et al. (1992) interpreted the deformation observed in BIF as due to the late Archean accretion along the line of geophysical lineament (the Colesburg magnetic anomaly of Corner et al., 1990), futher considered this lineament as the boundary between the central and the western segments of the Kaapvaal craton.

### 2.1.2. The sedimentary basins

During the periods of crustal growth as described above, the central and southern part of the Kaapvaal craton underwent crustal extension to form several large sedimentary basins: Pongola, Transvaal, Dominion, Witwatersrand, and Ventersdorp basins (Fig. I-4; Tankard et al., 1982). Even if their tectonothermal origin is not well constrained, two possible tectonic settings for these basins have been proposed: (1) an extensional failed cratonic basin, and (2) a flexural foreland basin.

Figure I-4: Stratigraphic Group forming the sedimentary basins in the Kaapvaal craton after Tankard et al. (1982). The age of each Group is also reported. Age compilation after Jahn and Condie (1995). For explanation see text.

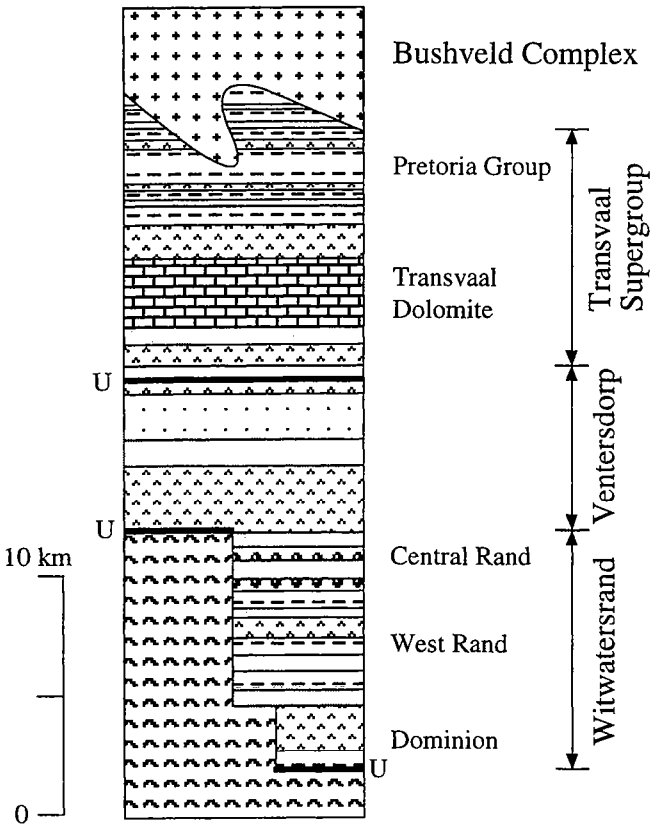


| Age (Ma) | Group | Supergroup | |
|---|---|---|---|
| ~1800 | Soutspanberg Waterberg | | |
| 2200-2400 | Pretoria | Up | **Transvaal** |
| 2600 | Wolkberg | Lo | |
| 2700 | | **Ventersdorp** | |
| 2800-2850 | Central Rand | **Witwatersrand** | |
| 2900-2950 | West Rand | | |
| 3070 | Dominion | | |
| *Relation Unknown* | | | |
| 2920-2940 | Mozaan Nsuze | **Pongola** | |
| 3300-3400 | Moodies Fig Tree | **Swaziland** | |
| 3450 | Onverwacht | | |

The Dominion Group represents the oldest sedimentary basin in the Kaapvaal craton and it accumulated between 3.12 and 3.07 Ga in an extensional failed rift basin (Tankard et al., 1982; Armstrong et al., 1991). This formation is overlain by the Witwatersrand Supergroup ranging in age from 2.98 to 2.71 Ga (Robb et al., 1991; Armstrong et al., 1991). Armstrong et al. (1991) suggested a polyphase structure as reflected by the time break between the deposition of the lower West Rand Group and the upper Central Rand Group (2.84-2.71 Ga; Robb et al., 1991). The lower West Rand Group is considered to be formed in a continental margin setting that was open at the S-SE (Eriksson et al., 1981; Stanistreet and McCarthy, 1991), whereas the upper Central Rand Group in a tectonically margin setting probably linked to a flexural foreland basin (Burke et al., 1991). The Pongola Sequence deposited in Natal is considered as the equivalent of the lower West Rand group (McCourt, 1995). Its age is constrained by the ages of the basal volcanics at 2.94 Ga (U-Pb zircon age) and the younger intrusive Usushwana Complex at 2.87 Ga (Hegner et al., 1984).

The Ventersdorp Supergroup is located in north-central South Africa. It is composed of a large and thick (~8 km) volcanic sequence that was emplaced on rifted basement and Witwatersrand Supergroup supracrustal rocks. Recent U-Pb zircon ages indicate a Late Archean deposition (2.75-2.70 Ga; Myers et al., 1987; Crow and Condie, 1988; Armstrong et al., 1991). The NE-SW oriented structure of the Ventersdorp Sequence is interpreted either as the result in response of a collision tectonic related to the juxtaposition of the Kaapvaal and Zimbabwe cratons during the Limpopo orogeny (Burke et al., 1985), or as the products of a lower mantle diapir unrelated to the Limpopo orogeny (Hatton, pers. com. in McCourt, 1995).

The Transvaal Supergroup is up to 12 km thick in the northeastern Transvaal. It is divided into three Groups: (1) the lower Wolkberg Group of fluvial to shallow marine feldspathic to sub-greywacke, arkose, silstone, pelite and conglomerate, and some basaltic flow, (2) the middle Chuniespoort Group of carbonate rocks and minor clastic sediments, and (3) the upper Pretoria Group of marine tidal quartzite and pelite, with small amount of carbonate and volcanics. The entire Transvaal Sequence is considered to be formed in local rifts to a large cratonic basin (Eriksson and Clendenin, 1990). The age of that sequence is not well constrained. Nevertheless, a Pb-Pb isochron age of 2557 ± 49 Ma is obtained on the Transvaal dolomite and slightly younger than the U-Pb zircon ages on the overlying formation at 2552 ± 11 Ma . The lower age limit is provided by the deposition of the Black Reef formation at 2.7-2.6 Ga and the upper age limit by the upper Pretoria Group at 2224 ± 21 Ma (Rb-Sr whole rock isochron age; Coertze et al., 1980). The Pretoria Group is intruded by the Bushveld Complex at 2 043 ± 11 Ma (Re-Os on chromitite layers, Schönberg et al., 1998).

Figure I-5: The Zimbabwe craton presents an ovoid-shaped granite-gneiss batholiths. The different granite-greenstone belts located close to the Limpopo Belt are reported. 1: Tokwe segment; 2: Masvingo; 3: Belingwe; 4: Buhwa; 5: Mweza; 6: Gwanda; 7: Antelope-Lower Gwanda; 8: Francistown granite-greenstone belt (to the south: Tati, and to the north: Wumba); 9: Mosetze Complex; 10: Bulaya granite-greenstone belt. After Jelsma (1993).

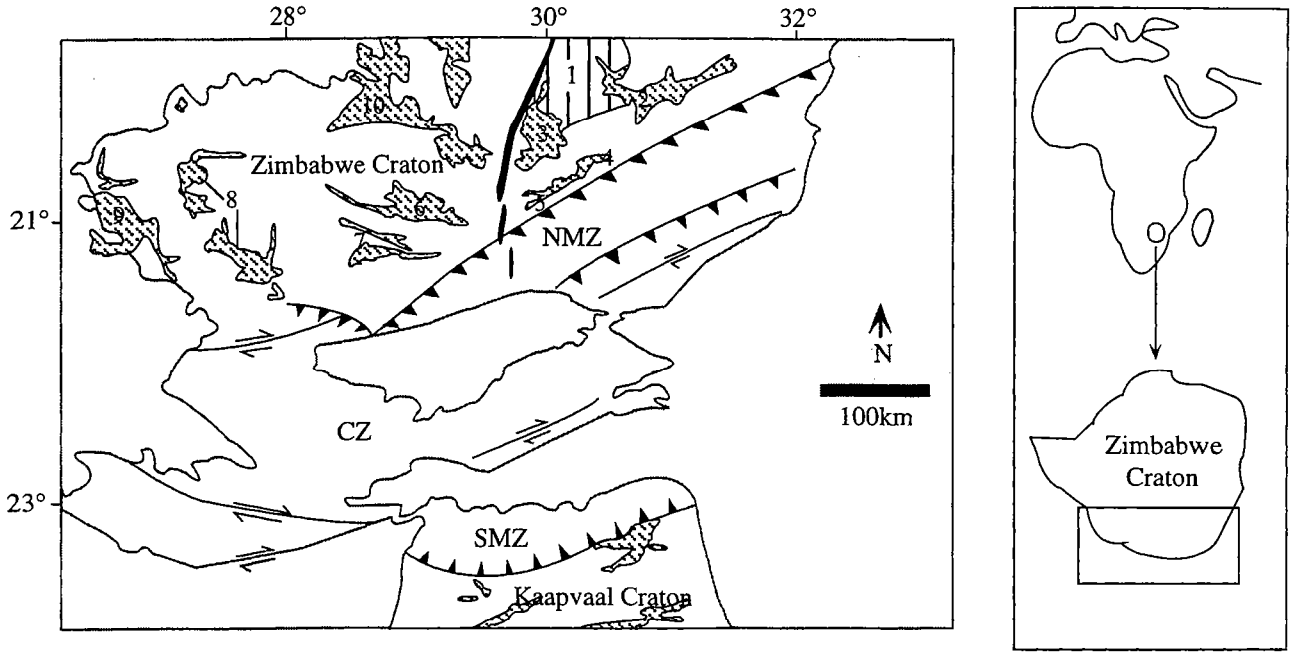


Table I-1: Geological description of the Shabani-Tokwe crust after Martin (1991).

| Tectonic Units | Lithologies | Ages |
|---|---|---|
| **SHABANI GNEISS** | * migmatitic and isoclinally folded gneisses which contain abundant folded cross-cutting aplites and pegmatites, and also foliated tonalitic or granodioritic rocks<br>* greenstone relicts which are intercalated within gneisses (amphibolites, ultramafic rocks, quartz schists and BIF)<br>* gneisses: foliated or banded tonalites, granodiorites and adamellites cut by mafic to felsic dykes | * Rb-Sr whole rock: 3 495 ± 120 Ma (1)<br>* Nd model ages: 3 240 and 3 460 Ma (2)<br>* Pb-Pb whole rock: 3 088 +44, -46 Ma, μ1 = 9 (2) |
| **TOKWE SEGMENT** | * granitic gneisses and greenstone belt | * Rb-Sr whole rock: 3 500 ± 400 Ma (4)<br>* Pb-Pb whole rock: 3 125 +300, - 375 Ma, μ1 = 8.9, (2)<br>* Pb-Pb whole rock: 3 475 +87, - 93 Ma, μ1 = 8.8 (2)<br>* Nd model ages: 3 560 and 3 600 Ma (3) |

(1) Moorbath et al., 1977; (2) Taylor et al., 1991; (3) Moorbath et al., 1986; (4) Hawkesworth et al., 1975;

## 2.2. The Zimbabwe Craton

The Zimbabwe craton shows in plan ovoid-shaped granite-gneiss batholiths, fringed by a linear, arcuate and synformal configuration of greenstone belts (Fig. I-5). the Zimbabwe craton is composed of several major granite-greenstone belts with distinct crustal evolution at 3.5 Ga, 2.9 Ga, and 2.7 Ga. This craton attained its stability at 2.6 Ga after the last widespread emplacement of granites (Jelsma, 1993). The different granite-greenstone belts which are close to the Limpopo Belt are shown in Fig. I-5.

### 2.2.1. The 3.5 Ga terrane

The oldest unit is represented by the Shabani-Tokwe Complex of which the main features are reported in Table I-1. The Tokwe segment called as a mini-craton by Wilson (1979), is a triangular Early Archean crustal block, mainly composed of tonalitic to granodioritic gneisses, dated at 3.5 Ga (Hawkesworth et al., 1975; Moorbath et al., 1977; Taylor et al., 1991) and a few remnants of greenstone belts (Sebakwian Group).

The Shabani gneisses are migmatitic and isoclinally folded (Table I-1). These migmatitic rocks contain several other lithologies: (1) abundant folded and cross-cutting aplites and pegmatites, (2) homogeneous foliated tonalitic and granodioritic gneisses, and (3) greenstone belt composed of amphibolites, ultramafic rocks, quartz schists and banded iron formations. To a lesser extend, the migmatitic gneisses include strongly foliated and banded tonalites, granodiorites and adamellites. They are cut by mafic and felsic dykes.

In the Shurugwi and Mashaba areas occur the the largest greenstone belts. The Mashaba area was intruded by the Mushandike granite which has been dated at 3.45 Ga by the Rb-Sr method (Hickman, 1974). Nd model ages are 3.54 Ga (Taylor et al., 1991). The greenstone amphibolites of the Shurugwi area have been interpreted as a large-scale regional allochtonous fold nappe by Stowe (1984) or as a local parautochtonous syncline by Tsomondo et al: (1992). The Mon d'Or granite intruded the Shurugwi greenstone belt at 3345 ± 55 Ma as defiend by a Pb-Pb whole rock isochron (Taylor et al., 1984) and 3350 ± 120 Ma by a Rb-Sr whole rock isochron (Moorbath et al., 1976). Nd model ages gave 3.67-3.64 Ga (Taylor et al., 1991).

### 2.2.2. The 2.9 Ga terrane

The second episode of crustal growth occurred at 2.9 Ga according to Nd model ages (Chauvel et al., 1983). This tectono-metamorpho-magmatic event is presented by the formation of the Mashaba and Chingezi granitic to gneissic rocks and by the Mtshingwe Unit.

Table I-2: Geological description of the lithologies related to the second episode of crustal growth in the Zimbabwe craton. After Martin (1991).

| Tectonic Unit | Subunit | Lithologies | Ages |
|---|---|---|---|
| **CHINGEZI GNEISS** | Chingezi gneiss | * migmatitic and isoclinally folded gneisses with bounding triking north or northwest, probably a continuation of the Palwan gneiss northwest of the Great Dyke | * Rb-Sr whole rock: 2 810 ± 70 Ma (5) |
| | Chingezi tonalite | * a number of weakly foliated pre-Mashaba-Chibi dyke swarm plutons of diorite, tonalite and adamellite which intruded the Chingezi gneiss | * Rb-Sr whole rock: 2 818 ± 78 Ma (2)<br>* Rb-Sr whole rock: 2 723 ± 102 Ma (2)<br>* Rb-Sr whole rock: 2 684 ± 102 Ma (2)<br>* Nd model ages: 3 050 Ma, 2 950 Ma, 2 980 Ma (2)<br>* Pb-Pb whole rock: 2 800 +72, -76 Ma, $\mu 1 = 8.2$ (2)<br>* Pb-Pb whole rock: 2 874 ±32 Ma, $\mu 1 = 8.4$ (2)<br>* Pb-Pb whole rock: 2 825 +94, -100 Ma, $\mu 1 = 8.1$ (2)<br>* Pb-Pb whole rock: 2 686 +88, -94 Ma, $\mu 1 = 8.1$ (2) |
| **MASHABA TONALITE** | | * body of massive foliated tonalite or more rarely of banded gneiss | * Rb-Sr mineral-whole rock. epidote 2.0 Ga, muscovite 2 910 Ma (5)<br>* Rb-Sr whole rock: 2 860 ± 60 Ma (5) |

(5) Hawkesworth et al., 1979; (2) Taylor et al., 1991

The field observations and chemical characteritics of these units are summarized in Table I-2 and Table I-3.

The 2.9 Ga years old terrane is composed of Late Archean greenstone sequences and TTG gneisses. The Chingezi gneisses are migmatitic, isoclinally folded. They show banding striking to the north or northwest but swinging east-west in the south of the greenstone belt (Orpen, 1978). Martin (1978, 1983) supposed that the Chingezi gneisses may be considered as the continuation of the Palawan gneisses located at the northwestern part of the Great Dyke. Hawkesworth et al. (1979) dated the Chingezi gneisses at 2.81 Ga by a Rb-Sr whole rock isochron. In addition, some plutons of diorite, tonalite and adamellite intruded the Chingezi gneisses. These intrusions have been dated by Pb-Pb and Rb-Sr whole rock isochrons at 2.9-2.7 Ga (Taylor et al., 1991).

In the eastern part of the Zimbabwe craton, the Mashaba tonalite comprises mainly a massive foliated tonalite in association with banded gneisses in some areas. A Rb-Sr whole rock isochron gave an age of 2870± 160 Ma for the tonalitic rocks (Hawkesworth et al., 1979).

Despite the absence of geochronological information, the Mtshingwe Unit may be related with the 2.9-2.8 Ga Chingezi gneisses during the second period of crustal growth from chemical composition and field observations. The Mtshingwe Unit is composed of 4 formations: the Hokonui, Bend, and Koodoovale formations in the west, and the Brooklands formation in the east. The main features of these formations are listed in Table I-3. Its age is constrained by the older intrusive Chingezi tonalite at ~2.8 Ga and by the younger greenstone Ngezi Unit at ~2.7 Ga which overlies unconformably the Mtshingwe Unit. The western part of the Mtshingwe Unit comprises bimodal mafic-felsic volcanic assemblages which were succeeded by an andesite-dominant calc-alkaline volcanic suite. In addtion, the eastern part is constituted of a sedimentary rocks dominated by pelite with intercalated tholeiitic basalts.

### 2.2.3. The 2.7 Ga terrane

The Ngezi Unit represents the younger greenstone belt of the Zimbabwe craton. On the eastern side of the belt, it overlies unconformably the Shabani gneiss and at the western part of the belt, the Mtshingwe Unit. The Ngzi Unit is composed of 4 formations: Manjeri, Reliance, Zeederbergs, and Cheschire. The main characteristics of each formations are summarized in Table I-4. They form a relatively undeformed stratigraphic unit overlying a gneissic basement. The Ngezi Unit represents the central part of the syncline of greenstone belt (Martin, 1991). The Pb-Pb whole rock isochron and Nd model ages give concordant results at 2.69-2.64 Ga for the upper greenstone belt (Chauvel et al., 1983; Hamilton, 1977; Hawkesworth et al., 1975). Jahn and Condie (1976) suggested an age of 2.76-2.73 Ga for the youngest greenstone belt based on a Rb-Sr whole rock isochron.

Table I-3: Geological description of the Mitshingwe Group after Martin (1991).

| Tectonic Unit | Subunit | Lithologies | Age |
|---|---|---|---|
| **MTSHINGWE GROUP** | The Hokonui Formation | * a sequence of andesitic, dacitic and rhyolitic lavas, pyroclastic and re-sedimented volcanic material and similar compotion together with minor amounts of dolerite and fine-grained greenstones<br>* calc-alkaline volcanic rocks in character which probably represent the remains of a large volcanic complex | between 2.9 and 2.8 Ga |
| | The Bend Formation | * dominantly komatiitic<br>* repeated cycles of komatiites, komatiitic basaltes and basaltes, interbedded with ironstone and chert | |
| | The Koodoovale Formation | * dominantly conglomerates and assorted fine-grained sedimentary rocks, with a locally developed unit of felsic agglomerate<br>* unconformably overlain by the Manjeri formation<br>* clasts derived from most of underlying rock types, granitoids clasts including adamellitic and tonalitic from the Hokonui formation or also Bend Formation such as basalts, komatiitic rocks, dolerites and abundant chert and banded ironstone clasts | |
| | The Brooklands Formation | * supracrustal rocks, isolated remnants of greenstone rocks<br>* a conformable set of sedimentary and volcanics rocks, thought to have been laid down on the older gneissic terranes<br>* metamorphosed in the greenschist facies | |

Table I-4: Geological description of the Mitshingwe Group after Martin (1991).

| Tectonic Unit | Subunit | Lithologies | Ages |
|---|---|---|---|
| **Ngezi Formation** | Manjeri Formation | * tonalite, gneiss and eroded older greenstone belt<br>* presence of stromatolite in limestone | |
| | Reliance Formation | * dominantly komatiittes and komatiitic basalts<br>* significant shear are present<br>* very little intercalated sediments, apart from rare chert stringers<br>* low greenschist or sub-greenschist facies metamorphism | |
| | Zeeberbergs Formation | * basaltic lavas overlies the Reliance Group<br>* monotomous sequence of basaltic pillow lavas, flows and possible sills, and brecia, and contains minor intercalation of tuff and hydroclastic debris<br>* up to greenschist facies metamorphism | * Pb-Pb whole rock: 2 690 ± 13 Ma (6)<br>* Nd model ages: 2 640 ± 140 Ma (7) |
| | Cheschire Formation | * sedimentary sequenve with a conglomerate base composed of mafic rocks | * Rb-Sr whole rock: 2 760 ± 70 Ma (8) |

(6) Chauvel et al., 1983; (7) Hamilton et al., 1977; (8) Jahn and Condie, 1976

#### 2.2.4. The late Archean intrusions

During the Proterozoic, magmatic events still occurred until ~1.9 Ga corresponding to the Mashonaland Igneous Event. Among ultramafic intrusions, the most significant are the Shabani Complex, the Vukwe Serpentinite and the Gurumba Tumba Serpentinite (Martin, 1978; Orpen, 1978). The Shabani Complex has been interpreted as the remnants of a large magmatic chamber (Nisbett et al., 1977). During the magmatic fractionation, basalts were formed and are similar to those of the Zeederbergs Formation (Nisbett et al., 1977). The Shabani granite and the Chibi granites represent the younger granitic intrusions which produced a marked metamorphic aureole in the Ngezi Unit and the southern part of the greenstone belt respectively (Catherall, 1973). These rocks have been dated at 2570 ± 25 Ma by a Rb-Sr whole rock isochron (Hickman, 1978). Finally, the latest Proterozoic magmatic activity was expressed by the most important intrusion of the 2.46 Ga old Great dyke and its satellites as well as the dykes and sills intrusions during the 1.9 Ga Mashonaland Igneous Event (Wilson et al., 1987).

## 2.3. The Limpopo Belt

The Limpopo Belt is dominated by an ENE-WSW structural trend with a tripartite internal structure consisting of the Central Zone, flanked by the Northern and Southern Marginal Zones (Fig. I-6; Cox et al., 1965). Both Marginal Zones are interpreted to be mid- to lower crustal sections of the adjacent cratons (van Reenen et al., 1992; Berger et al., 1995; Kreissig and Holzer, 1997).

#### 2.3.1. The Northern Marginal Zone (NMZ)

Based on the latest geochemical, geochronological and petrological studies (Kamber, 1995; Berger, 1995), the NMZ is now known to be autochtonous to the Zimbabwe craton from which it is separated by a thrust zone. Furthermore, on the basis of rock types, metamorphic petrology, structural relations, and isotopic characteristics, the NMZ is subdivided into three units (Fig. I-6; Rollinson and Blenkinsop, 1995; Kamber et al., 1995; Kamber and Biino, 1995): the NMZ sensu-stricto, (2) the Transition Zone, and (3) the Triangle Shear Zone.

##### *2.3.1.a. The Northern Marginal sensu-stricto*

The Northern Marginal sensu-stricto (NMZ s.s.) is separated from the Zimbabwe craton by a major thrust dipping gently to the south. The distinction between them is a rapid transition in metamorphic grade from granulite facies whthin the NMZ s.s. to amphibolite facies in the Zimbabwe craton (Mkweli et al., 1995). The time of the tectonic thrusting was constrained by post and syn-tectonic plutons to about 2.6 Ga (Kamber et al., 1994; Mkweli et al., 1995).

Figure I-6: The Northern Marginal Zone is composed of three entities: NMZs.s., Transition Zone (TZ), and Triangle Shear Zone (TSZ). Modified after Kamber and Biino (1995).

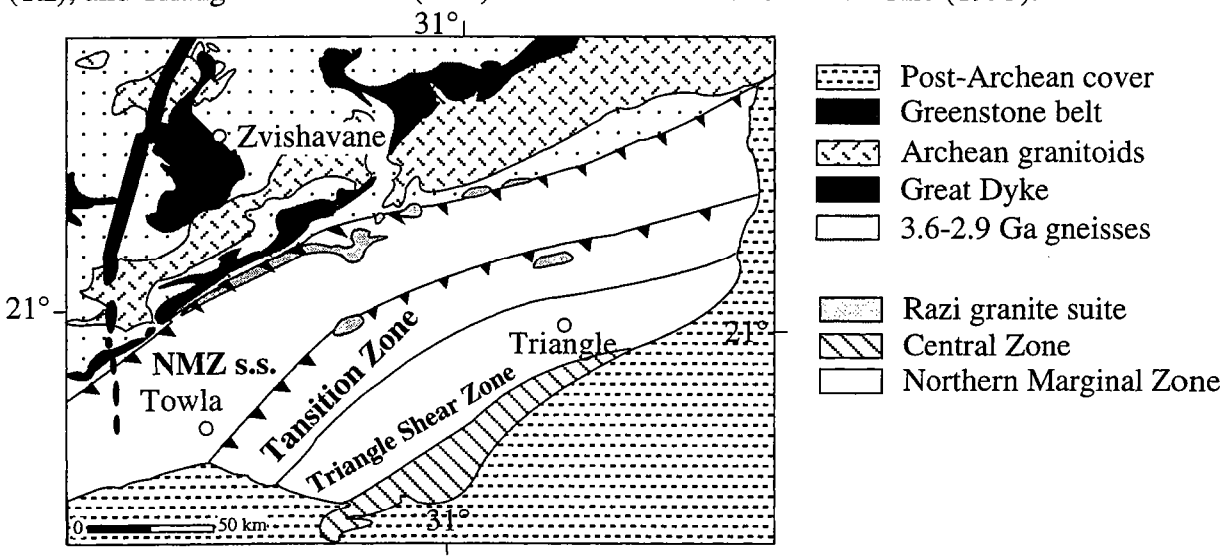


Figure I-7: The 4 stages of deformation and two intrusive episodes in the NMZs.s. are summarized. After Kamber and Biino (1995).

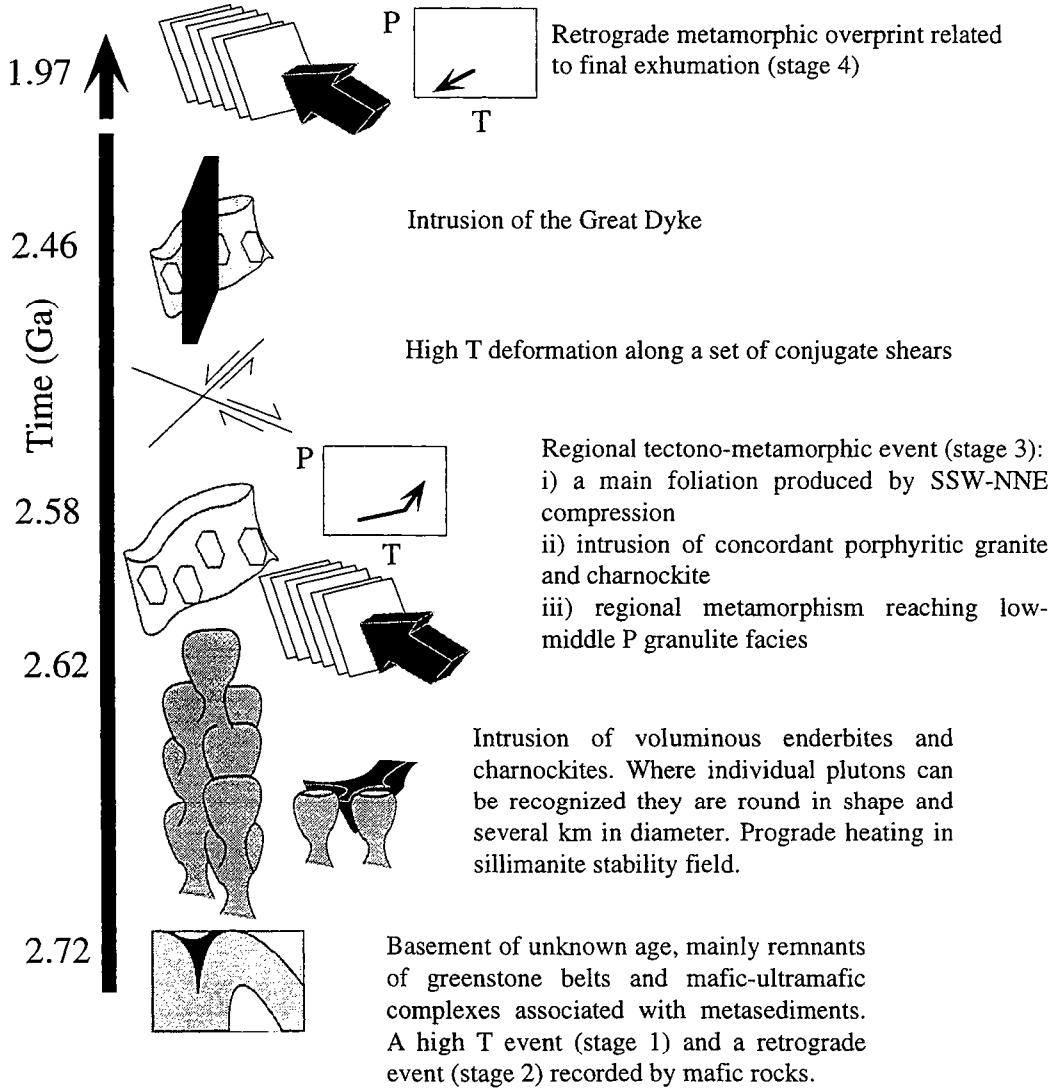

All the Archean basement rocks have been metamorphosed in granulite facies conditions and have shown various degrees of retrogression. The tectono-metamorphic evolution of the NMZ s.s. is characterized by two high-grade metamorphic events associated with 4 stages of deformation and two intrusive episodes (Fig. I-7; Kamber and Biino, 1995). All the charno-enderbites located in the NMZ s.s. are now interpreted as intrusive rocks. Magmatic orthopyroxenes (± clinopyroxene) are present (Ridley, 1992; Berger et al., 1995; Rollinson and Blenkinsop, 1995). The charnockites were previously interpreted as metamorphosed basement gneisses (Worst, 1962; Robertson, 1973, 1974; Odell, 1975).

Remnants of greenstone belts of the Zimbabwe craton consist of pre-intrusive meta-ironstones, metapelites, quartzites, metabasites and subordinates ultramafic rocks (Rollinson and Lowry, 1992; Rollinson and Blenkinsop, 1995). Berger et al. (1995) analysed the oldest enderbitic intrusion. The 2.72 Ga age was interpreted as the minimum age of these relicts (stage 1 in Fig. I-7).

Between 2.72 and 2.62 Ga, charno-enderbites plutons intruded the NMZ s.s. and showing a tonalitic-granodioritic to granitic compositions (stage 2 in Fig. I-7; Berger et al., 1995). The occurrence of magmatic orthopyroxene in these rocks implies an $H_2O$-undersaturated hot melt. Thus, these orthopyroxenes may have crystallized directly from a dry magma at depth under "granulite facies" conditions (Kramers and Ridley, 1989).

Between 2.62 and 2.58 Ga, porphyritic granites and charnockites intruded the NMZ s.s. along the thrust zone during a major phase of NNW-SSE compression under low-pressure granulite facies metamorphism (Mkweli et al., 1995; Kamber, 1995). Subsequent to granulite facies metamorphism, the NMZ s.s. underwent a regional deformation expressed by the formation of conjugate set of ESE-striking dextral and NNW-striking sinistral shears (Treloar and Blenkinsop, 1995). Hamilton (1977) indicated that this predates the intrusion of the Great Dyke at 2.46 Ga. At about 1.9 Ga, $H_2O$-rich fluid circulation implied the retrogression of granulitic rock into greenschist rocks (van Breemen and Dodson, 1972; van Breemen et al., 1986).

Kamber and Biino (1995) determined the P-T conditions for the granulitic metmorphic event related to the NNW-SSE compression. All the observed reactions are consistent with an anticlockwise P-T path in agreement with the P-T loop of Rollinson (1989). The peak metamorphism is characterized by LP and HT conditions ($T > 800°C$ and $P \sim 4$ kbars) and it was followed by a moderate increase in P. Both P-T paths are incompatible with the results of Tsunogae et al. (1992). These metamorphic conditions are the results of the intrusion of charno-enderbites but they are coeval with syn-deformational intrusion of porphyritic granite and charnockite.

### *2.3.1.b. The Transition Zone*

Rollinson and Blenkinsop (1995) identified a 25 km wide Transition Zone (TZ, Fig. I-6). The TZ underwent a major phase of deformation during the 2.0 Ga metamorphic event under the mid-amphibolite facies (Kamber et al., 1995) The foliation and lineation are totally different from those of the NMZ s.s. in the sense that the foliation in this area dips gently to the southeast and carries horizontal to sub-horizontal mineral stretching lineations in spite of steeply dipping foliations.

### *2.3.1.c. The Triangle Shear Zone*

The Triangle Shear Zone (TSZ) extends from the Karoo cover (SW of Triangle) to the overlying Umboko formation (NE of Triangle; Rollinson and Blenkinsop, 1995). Both TZ and TSZ have been interpreted as a continuous entity along the southern edge of the NMZ s.s. in Zimbabwe (Rollinson and Blenkinsop, 1995). The TSZ is largely dominated by proto-mylonitized and mylonitized gneisses. Their protoliths may be divided into three groups: (1) quartzofeldspathic gneisses, (2) re-metamorphised migmatites, and (3) netabasic rocks (Rollinson and Blenkinsop, 1995; Kamber et al., 1995). Furthermore, Rollinson and Blenkinsop (1995) reported the occurrence of quartzitic rocks and Ridley (1992) some calc-silicates and metapelites. The foliation of these lithologies dips gently to the southeast with a strong sub-horizontal linear fabric and they show a consistent dextral sense of shear expressed by $\sigma$ and $\delta$ porphyroclast tails and rolling structures (Rollinson and Blenkinsop, 1995).

Kamber et al. (1995a, 1995b) studied the metamorphic conditions associated with the deformation of the TSZ. The microtextures of these rocks suggest a high-temperature deformation (T>550°C) with the formation of new metamorphic minerals such as garnet, hornblende, sillimanite and cordierite (Kamber et al., 1995a, 1995b). High Al-contents in the coexisting clino- and orthopyroxenes cores imply high temperature and pressure conditions around 700-850°C and 5-9 kbars (Kamber et al., 1995a, 1995b). The variations in pressure may be explained by mineral reactions frozen during different times of uplift (Tsunogae et al., 1992). The retrograde metamorphic reactions, such as examplified by coronitic cordierite and plagioclase rims around garnet or decreasing Al-contents towards the rims of coexisting orthopyroxene and clinopyroxene, characterize an isothermal decompression at about 4-6 kbars. Consequently a clockwise P-T path is deduced for the metamorphic evolution of the TSZ.

Van Breemen and Hawkesworth (1980) obtained 1988 ± 14 Ma and 1974 ± 14 Ma syn-tectonic Sm-Nd garnet ages which were interpreted as a reactivation of the 2.65 Ga structure. However, Kamber te al. (1995a, 1995b) demonstrated a high-grade metamorphism which cannot be related to a reactivation of older structures under low-grade metamorphic conditions. Thus, the TSZ must be associated with a strike-slip movement under granulite

facies metamorphism (Kamber et al., 1995a, 1995b; Rollinson and Blenkinsop, 1995) with an age of ~2.0 Ga (van Breemen and Hawkesworth, 1980; Kamber et al., 1995a, 1995b).

#### *2.3.1.d. Summary*

The NMZ forms a zone about 60 km wide and 450 km long, separated from the granite-greenstone belt of the Zimbabwe craton by a major thrust zone called the Umlali Thrust Zone (James, 1975; Mkweli et al., 1995). The metamorphic grade jump from the greenschist-amphibolite facies in the craton to the granulite facies in this zone. The NMZ has very similar geochemical characteristics to the Zimbabwe craton (Berger et al., 1995) and both entities have also the same crustal thicknesses (Stuart and Zengeni, 1987; Gwavava et al., 1992). Thus, the NMZ is most probably as a mid- to lower crustal section of the adjacent craton. This zone is mainly dominated by charno-enderbitic gneisses and their lower grade equivalents and only a few supracrustal rocks are exposed. The metamorphic grade in the NMZ decreased from low pressure granulite facies in the southeast (TSZ) to upper greenschist facies in the northwest (NMZ s.s.). The NMZ s.s. has an anticlockwise P-T path and the TSZ a clockwise P-T path. These metamorphic conditions are related to the structural features which show a distinct foliation as well as a distinctive stretching lineation. The foliations dips very steeply to the southeast with occasional down-dip lineations (NMZ s.s.) and it dips gently to the southeast with strong subhorizontal stretching lineations which show clearly a dextral sense of shear in the TSZ (Rollinson and Blenkinsop, 1995).

### 2.3.2. The Southern Marginal Zone

The Southern Marginal Zone (SMZ) represents the southernmost unit of the Limpopo Belt and it is separated from the Kaapvaal Craton by the Palala Shear Zone. It has been suggested to be the mid- to lower crustal section of the Kaapvaal craton (du Toit et al., 1983; van Reenen et al., 1990; Smit et al., 1992). The NMZ is now known to be autochtonous to the Kaapvaal craton on the basis of rock types, metamorphic petrology, structural relations, and isotopic characteristics (Kreissig and Holzer, 1997; Kreissig et al., in prep.). The SMZ is separated from its adjacent craton by a thrust zone, i.e. the Hout River Shear Zone.

#### *2.3.2.a. The Hout River Shear Zone*

The Hout River Shear Zone (HRSZ) is a major thrust zone of about 200 km length which separates the WSE-ENE structural trend of the SMZ from the Kaapvaal craton (Fig. I-8). The HRSZ is a reverse fault which dips steeply to the north and carries down-dip lineation. Smit et al. (1992) showed that the HRSZ is a system of frontal and lateral in its central part ramps. The distinction between each side of the HRSZ is a transition in metamorphic grade

Figure I-8: Geological map of the Southern Marginal Zone after Stevens and van Reenen (1992).

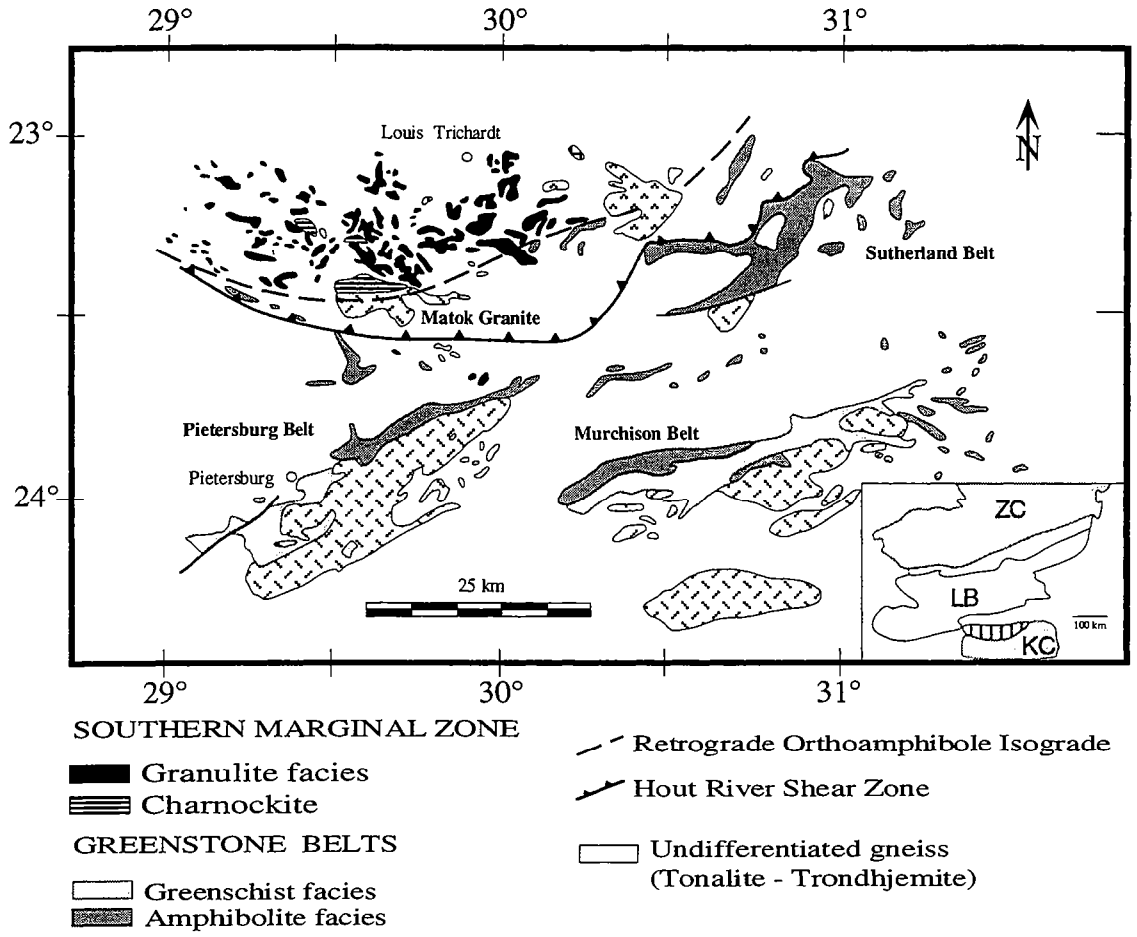


Figure I-9: Poly-metamorphic clockwise P-T evolution of mafic rocks at the Banderlierkop Quarry. After Stevens and van Reenen (1992).

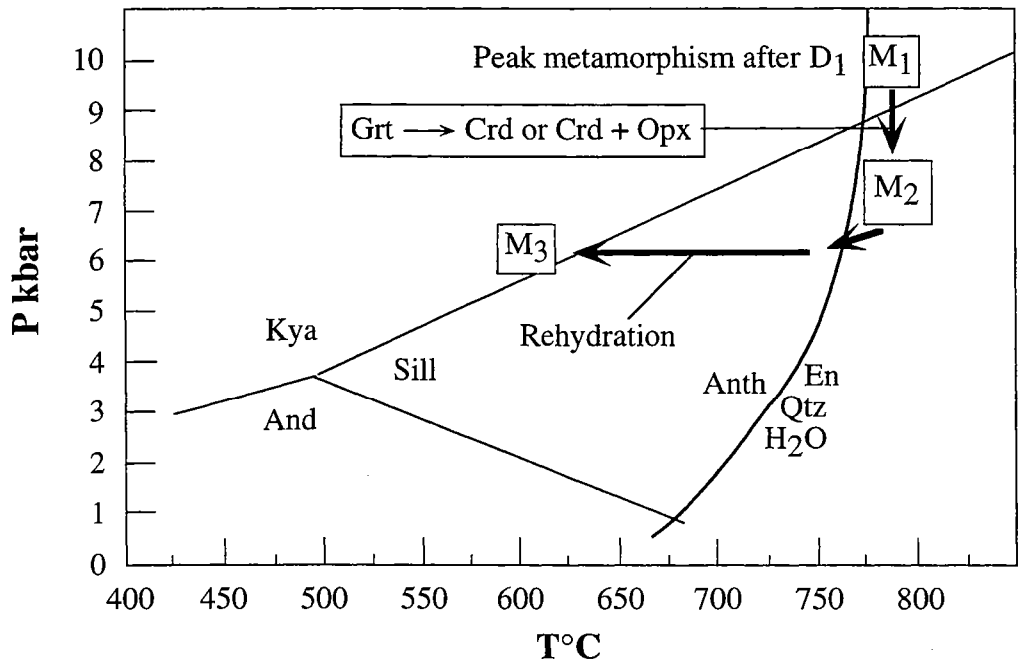

from retrograded granulite facies conditions within the SMZ to greenschist facies metamorphism in the Kaapvaal craton. The thrusting time is constrained by a syn-tectonic granite, i.e. the Matok pluton dated at 2.667 Ga by U-Pb zircon (Barton et al., 1992). A syn-kinematic kyanite in a metapelite was analyzed for its Pb isotopic composition by Pb stepwise leaching (Frei and Kamber, 1995) and the results support the 2.66 Ga thrusting age (Kreissig and Holzer, 1997). The HRSZ represents also the geophysical boundary between the Kaapvaal craton and the Limpopo Belt. From gravity and geoelectrical studies, de Beer and Stettler (1992) showed that a zone of low density rocks underlies the granulites of the SMZ.

*2.3.2.b. The Southern Marginal Zone sensu-stricto*

The basement of the SMZ is represented by the Baviaanskloof gneisses of TTG compositions (du Toit et al., 1983; Barton and van Reenen, 1992). Ultramafic and mafic greenstones, pelitic gneisses and banded iron formations occur as disrupted lenses within the Baviaanskloof gneisses. These TTG were intruded by the granitic Matok pluton and its charnockitic equivalents at 2.67 Ga after a major tectonic event (Barton and van Reenen, 1992). Moreover, the SMZ was intruded at 2.45 Ga by the Palmietfontein granite and by the Schiel alkaline Complex either at 2.05 Ga (Pb-Pb and Rb-Sr whole rock isochrons; Barton et al., 1983; Walraven et al., 1992) or at 1.85 Ga (Barton et al., 1996).

From the metamorphic studies, the SMZ has been subdivided into two distinct zones: (1) the granulite zone to the north, and (2) the rehydrated zone to the south (van Reenen et al., 1992). The limit between these 2 zones is represented by a retrograde orthoamphibole isograd (Fig. I-8; van Reenen et al., 1992). In addition, the remnants of greenstone belts have been transformed into the Banderlierkop Formation (du Toit et al., 1983). From this mafic assemblage, a polymetamorphic clockwise P-T evolution has been determined (Fig. I-9; van Reenen et al., 1992). The granulite facies conditions represent the peak metamorphism ($M_1$) which was attained after the main phase of deformation ($D_1$; van Reenen, 1983). The P-T conditions are determined above P>9kbars and T>780°C, respectively. $M_1$ was followed by an isothermal decompression $M_2$ during which garnet was transformed either in cordierite or cordierite plus orthopyroxene (Stevens and van Reenen, 1992). The last $M_3$ metamorphism is an isobaric cooling during which the zonation of the newly formed $M_2$ minerals have been transformed (Fig. I-9, Stevens and van Reenen, 1992). This P-T loop determined by Stevens and van Reenen (1992) is in agreement with those already published. Stevens and van Reenen (1992) interpreted this metamorphic evolution as a product of rapid tectonic erosion after isostatic rebound ($M_1$ to $M_2$) followed by a re-establishment of the steady state geotherm after the uplift ($M_2$ to $M_3$).

Figure I-10: Geological map of the Limpopo Belt showing the three entities, the mafic to felsic intrusions. 1: the Messina Layered Intrusion; 2: the Bulai Granite Intrusion; 3: the Shiel Complex; 4: the Sutherland greenstone belt; 5: the Matok Granite Intrusion; 6: the Busveld Complex; 7: the Mahalapye Granite; 8: the Mokgware Granite; 9: the Great Dyke.

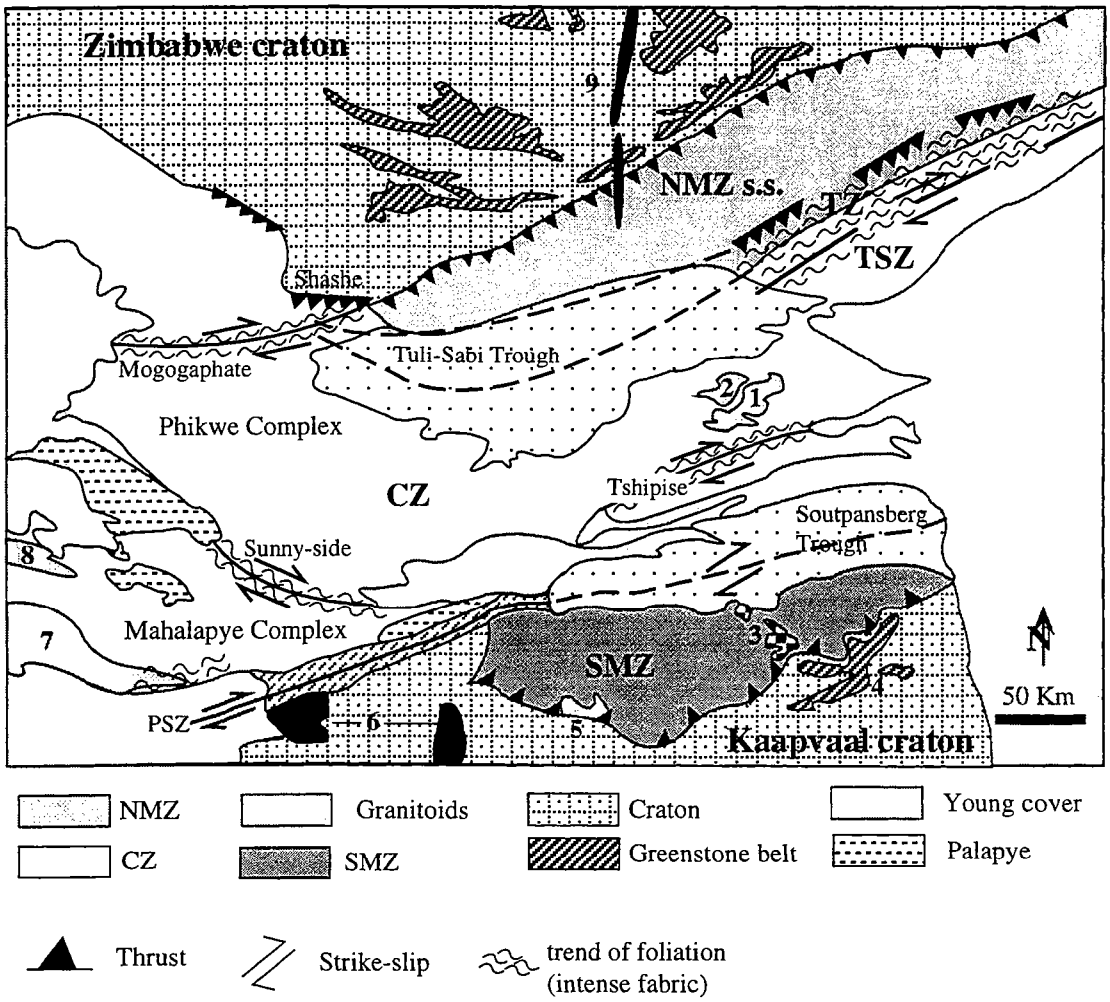

*2.3.2.c. The Palala Shear Zone*

The 10-12 km wide Palala Shear Zone (PSZ) is considered as the boundary between the Central Zone and the SMZ. It is located between the Central Zone to the north and the Bushveld Igneous Complex to the south. It was described by McCourt and Vearncombe (1987, 1992) as a sinistral strike-slip shear zone with several phases of deformation in before and after the Bushveld intrusion. It shows a steep notherly dipping in mylonites with a sub-horizontal mineral stretching lineation. Thus, the movement of this zone was considered as a sinistral strike slip (McCourt and Vearncombe, 1987, 1992). However, Shaller et al. (1997) showed that the PSZ has undergone two major deformation events ($D_1$ and $D_2$) and a minor late brittle deformation ($D_3$). The $D_1$ deformation occurred in high-grade conditions followed by a low-grade $D_2$ phase. Field observations and U-quartz c-axis measurements indicate a dextral shear sense at least for the last stage of the strike-slip motion (Schaller et al., 1997). Schaller et al. (1997) and Holzer et al. (1998) consider the PSZ as an intracontinental tectonic lineament on which the exhumation strain of the CZ was localized after the 2.0 Ga transpression event.

2.3.3. The Central Zone

The Central Zone (CZ; Fig. I-10) is separated from the NMZ by a south -dipping dextral shear zone (TSZ; Watkeys, 1983; Kamber et al., 1995a, 1995b; Rollinson and Blenkinsop, 1995) and from the SMZ by the dextral strike-slip Palala Lineament (PSZ; Schaller et al., 1997; Holzer et al., 1998; Holzer, 1998). On the contrary of the SMZ and the NMZ s.s., the CZ underwent a poly-metamorphic evolution with at least three high grade events at 3.2, 2.6 and 2.0 Ga (Holzer, 1998).

The oldest rocks known in the CZ are the Sand River Gneisses which represent a migmatitic complex of grey diorite and leucocratic granodioritic gneiss. This complex is cut by several generations of mafic dykes (Fripp, 1981). Both U-Pb zircon ages (Retief et al., 1990) and Nd model ages (Harris et al., 1987) give an Archean age between 3.2 and 3.0 Ga. The Messina Layered Intrusion are intensively, heterogeneously deformed and flattened layers and lenses of leucocratic gneisses (Hor et al., 1975; Barton et al., 1979). It consists of variable proportions of white plagioclase and honblende with minor quartz, and also rare layers of chromites and magnetites. The age of this intrusion is poorly constrained. The Rb-Sr, Pb-Pb and Sm-Nd whole rock isochrons on the mafic dykes which cut the Messina Layered Intrusion yield ~3.0 Ga, i.e. as the minimum age of the intrusion (Barton et al., 1977; 1983; 1990). Rb-Sr and Pb-Pb whole rock dating applied on the gneissic layers gave 3157 ± 47 Ma and 3 270 +105,-112 Ma respectively (Barton et al., 1979; Barton, 1983). Barton (1996) suggested that these ages are probably minimum estimations of the time of emplacement of the intrusion due to large isotopic heretogeneity of the Messina Layered Intrusion. The Sand River Gneisses and the Messina Layered Intrusion are related to the first period of magmatic activity in the CZ.

Overlying the Sand River Gneisses if the supracrustal succession of the Beit Bridge Complex. It is mainly composed of quartzo-feldspathic gneisses and paragneisses including metapelitic gneisses, marbles, calc-silicates rocks, quartzites and magnetite quartzites. Eriksson et al. (1988) interpreted the sedimentary end-members as a cratonic-shelf quartz-arenite-carbonate association. The geochemical features of these rocks suggest that they were derived from a variety of mafic and felsic sources (Eriksson et al., 1988). Along the felsic sources, K-rich granite was suggested and it probably represented a product of intracrustal melting in a thick continental lithosphere (Taylor and McLennan, 1985). Nd model ages suggest a 2.9-3.0 Ga mantle source age (Harris et al., 1987).

The second period of crustal growth and tectonic reworking took place between 2.6 and 2.55 Ga. The magmatic event is characterized by a low-pressure granulite facies metamorphism during which voluminous charnockitic plutons intruded the older basement. The best example of thsi plutonism is the cal-alkaline Bulai Pluton which intruded the Beit Bridge Complex (Barton et al., 1990). This pluton consists mainly of enderbitic, charnockitic and granitic orthogneisses. U-Pb zircon ages for this intrusion range from 2.7 to 2.65 Ga which are interpreted as the emplacement time (Robertson and du Toit, 1981; van Reenen et al., 1992, Barton et al., 1979), and from 2.6 to 2.57 Ga which are related to the crystallization time of distinct magmas (Barton and Doig, 1993; Barton et al., 1994; Jaeckel et al., 1997). In some areas, the Bulai melt is mingled with the Singelele granitoid (Holzer et al., 1995), which is thought to have been produced by widespread anatexis and mobilization of leucosome. The 2.57 Ga gives the minimum age for the first granulite facies metamorphism in the CZ of the Limpopo Belt. In addition, structural, petrographic and geochronological studies in the Messina area indicate that this part of the CZ underwent several pulses of thermal disturbance associated with magmatism and tectono-metamorphism characterized by an anticlockwise P-T path between 2.7 and 2.5 Ga (Holzer et al., 1998; Holzer, 1998).

The last high-grade tectono-metamorphic event in the CZ was dated at about 2.0 Ga (Barton et al., 1994; Holzer, 1955; Kamber et al., 1995; Holzer et al., 1998; Holzer et al., in press; Holzer, 1998). This granulite-facies metamorphism is associated with a clockwise P-T path from P-T conditions of P>10 kbars and T>830°C (Chinner ant Sweatman, 1968) through an isothermal decompression at P~5 kbars (Windley et al., 1984; Harris and Holland, 1984; Droop, 1989), to a nearly isobaric cooling. Voluminous migmatitic complex have been formed during the 2.0 Ga metamorphic event (for example the Mahalapye Complex, the Phikwe Complex). This metamorphic event could have been related to crustal thickning by the continental collision between the Kaapvaal and Zimbabwe cratons. The exhumation of these high-grade rocks were controlled by two major strike slip shear zones, i.e. TSZ to the north and the PSZ to the south, both of them showing dextral shear sense (Kamber et al., 1995a, 1995b; Rollinson and Blenkinsop, 1995; Schaller et al., 1997; Schaller et al., in press; Holzer, 1998).

### 2.3.4. The tectono-metamorphic evolution of the Limpopo Belt

The tectono-metamorphic evolution of the Limpopo Belt has long beem explained in a single continent-continent collision in Late Archean and many models have been proposed (Barton and Key, 1981; Light, 1982; Whatkeys, 1983; van Reenen et al., 1987, 1992; Treloar et al., 1992; McCourt and Vearncombe, 1992; Roering et al., 1992; de Wit et al., 1992; Windley, 1993). None of the early models have taken into account the important 2.0 Ga event which was determined for the first time by van Breemen and Hawkesworth (1980). The ideas about the Limpopo Belt evolution have drastically changed since the 2.0 Ga tectono-metamorphic event was firmly established by a series of recent works (Barton et al., 1994; Mkweli et al., 1995; Kamber et al., 1995a, 1995b; Berger et al., 1995; Jaeckel et al., 1997; Holzer et al., 1998; Holzer et al., in press; Schaller et al., in press; Holzer, 1998).

Treloar and Blenkinsop (1995) changed the interpretation of the structural patterns of Treloar et al. (1992). They proposed a double collision model in which the Kaapvaal craton and the CZ collided in the first step and then the amalgamated "continent" collided with the Zimbabwe craton. Nevertheless, this model did not explain all the structural, metamorphic and magmatic features observed in all individual units of the Limpopo Belt.

Berger et al. (1995) studied the geochemical and tectono-metamorphic relationships between the Zimababwe craton and the NMZ. They concluded that the NMZ is autochtonous to the Zimbabwe craton and thus, represents a section of the adjacent craton at middle to lower crustal level. They also concluded that a continent-continent collision model at 2.6 Ga is incompatible with their results because they found a magmatic granulite suite and there is a long time gap between the charnockitic intrusion and the deformation at 2.6 Ga. Therefore, Berger et al. (1995) interpreted that during about 100 Ma, near-solidus conditions occurred in the lower to middle crust which is consistent with the "soft" continent model of Choukroune et al. (1995).

At the same time, Kamber et al. (1995a, 1995b) showed that a high-grade tectono-metamorphic event occurred at 2.0 Ga in the TSZ. While the thrusting time of the SMZ over the Kaapvaal craton, and the NMZ over the Zimbabwe craton clearly occurred at 2.7 and 2.6 Ga, respectively, Kamber et al. (1995a, 1995b) argued that the 2.0 ga event cannot be related to a late reactivation of older structures. They concluded that the 2.0 Ga event should be related to a subvertical extension associated with a dextral sense of shear. The Proterozoic orogeny may be related to a transpressive tectonism during which the CZ rocks were exhumed.

The last tectono-metamorphic model about the Limpopo Belt is proposed by Holzer et al. (1998), Holzer et al. (in press) and Holzer (1998) in yhich they focussed on the last major event at 2.0 Ga. For them, the geological evolution of the high-grade CZ was formed during three distinct high-grade metamorphic events: (1) 3.2-3.0 Ga which is mainly a magmatic

Figure I-11: Cartoon of the continental crust after Wedepohl (1995). Physical, metamorphic, and petrographical features of the lower and upper continental crusts are reported. Orogenic geotherm is calculated by Chapman (1986) and the Vp value of the lower crust is given in Rudnick and Presper (1990). Partial melting of the mafic lower continental crust leads to the formation of tonalitic magma whereas anatexis of the felsic part (one of the migmatization process) provides the formation of granitic melt.

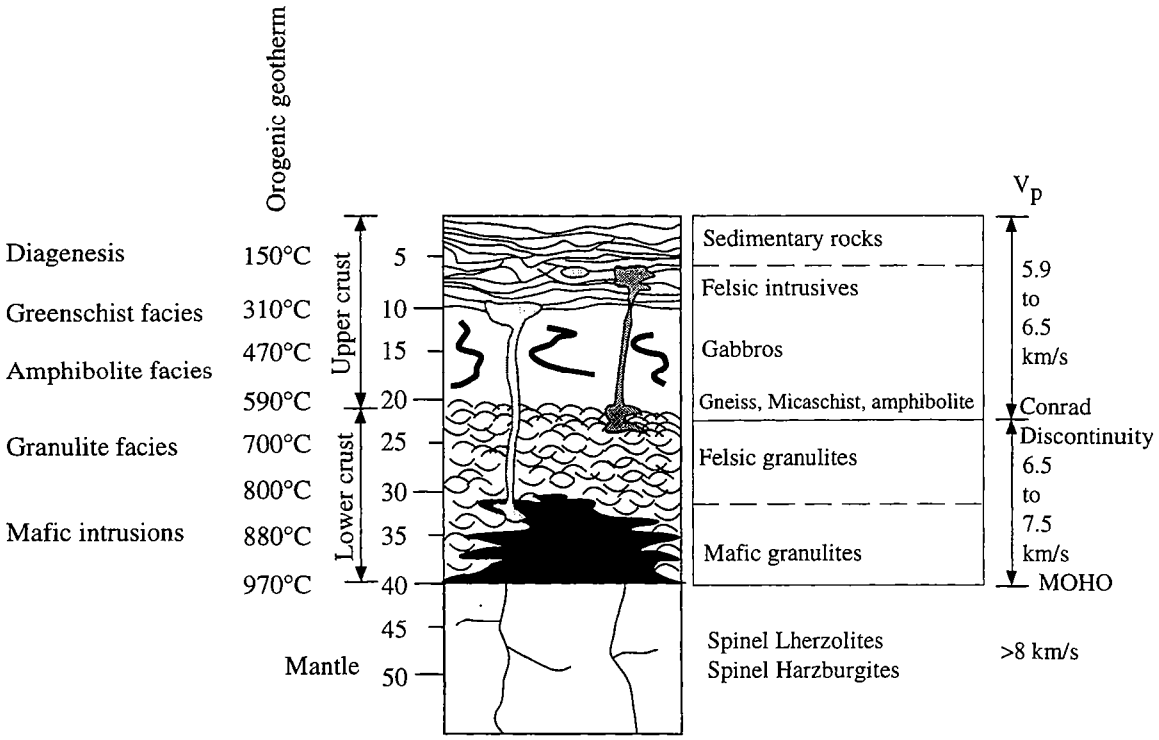

activity (the Sand River Gneisses and the Messina Layered Intrusion for example), (2) 2.6-2.55 Ga which is associated with a low-pressure granulite facies metamorphism and with voluminous granitoid charnockitic plutonism (The Bulai Pluton for example), and (3) 2.0-1.95 Ga which represents a crustal thickening event due to the transpressional orogeny between the CZ and the amalgamated NMZ- Zimbabwe craton and SMZ-Kaapvaal craton. Holzer et al. (1998), Holzer et al. (in press) and Holzer (1998) consider the PSZ and the TSZ as major transcurrent lineament between the Cz and the respective adjacent cratons along which the exhumation strain was localized after the 2.0 Ga tectono-metamorphic event.

It is clearly shown that a single continent-continent model is no longer compatible with the existing data. However, there is still several open questions:

(1) the Proterozoic ophiolite problem: Ophiolites as witnesses of ancient oceanic lithosphere is of crucial importance for the operation of the Wilson Cycle (1968). Their occurrences suggest that geosynclines and orogenic belts evolve as consequence of plate motions by the opening and closing of oceans (Wilson, 1968). The lack of recognized ophiolites as a formation described in the literature does not mean the no-formation of ocean sea-floor in the Proterozoic but only the undefined "ophiolite" in the Proterozoic time. Do the Bushveld Complex or the Great Dyke be referred to the "oceanic lithosphere"?

(2) the subduction problem: A subduction zone for the evolution of the Archean-Proterozoic orogenic belts is still a large domain of controverse. No actual geological studies have convincing arguments for such geodynamic setting in the Early Earth's history.

(3) the tectonic relationship between the dictinct 2.0 Ga orogenic belts in the southern Africa. Do we have to deal with a large amalgamation of different tectonic units at 2.0 Ga (The Limpopo Belt, The Magondi Belt and the Kheis Belt)?

# 3. Migmatite overview

## 3.1. The continental crust

The continental crust is the Earth's envelope located above the Mohorovicic discontinuity at ~40 km in depth (Poldervaart, 1955). It is composed of two entities, i.e. the upper and lower continental crusts separated by the Conrad discontinuity situated approximately 20 km in depth (Fig. I-11). The distinction between the upper and lower continental crust is based on the variations of the P-wave velocities which are significantly higher in the lower part than in the upper one. The upper continental crust has a granodiorite composition (Heinrichs et al., 1980; Wedepohl, 1969-1978) whereas the lower continental crust is composed of felsic and

Table I-5: Terms used for the description of migmatites after Mehnert (1968) and Ashworth (1985).

| | |
|---|---|
| **Migmatite** | A rock, found in medium-grade to high-grade metamorphic areas, that is pervasively inhomogeneous on a macroscopic scale, one part being pale-coloured and consistently of quartzofeldspathic or feldspathic composition. |
| **Bodies within a migmatite** | |
| Leucosome | A body of the pale-coloured, quartzofeldspathic or feldspathic lihtology of a migmatite. |
| Melanosome | A body of the dark-coloured lithology present in some migmatites, rich in mafic minerals, complementary of leucosome. |
| Neosome | Leucosome + melanosome |
| Mesosome or paleosome | A body of that part of a migmatite complex that is not neosome, generally having the appearance of an ordinary metamorphic rock, often immediate in colour between leucosome and melanosome. |
| **Interpretative terms relating to bodies** | |
| Paleosome or protolith | Hypothetical parent rock which developed into the neosomes. |
| Restite | Residual body, from which more mobile material has been extracted. |
| **Structural types of migmatite** | |
| Stromatic | Layered |
| Agmatic | Breccia-like |
| Schollen | Blocks or rafts of non-leucsome in leucosome |
| Schlieren | Streaks of non-leucosome in leucosome |
| **Terms relating to melting** | |
| Anatexis | Partial melting |
| Metatexis | Moderate degree of partial melting; leucosome subordinate to non-leucosome; pre-migmatization structures not disrupted |
| Diatexis | Extensive partial melting; leucosome volumetrically comparable with, or dominant over, non leucosome; pre-migmatization structures disrupted; mafic minerals often prominent in leucosome. |

mafic granulites (Rudnick and Presper, 1990; Rudnick, 1992). From the geochemical point of view, the upper continental crust is enriched in incompatible elements including the radioactif ones U, Th, K and Rb(Roy et al., 1968). The process proposed for this chemical fractionation is the partial melting of the mafic and/or felsic lower crust yielding to the formation of granitic-tonalitic melt (Fig. I-11). In an orogenic setting, intrusions of large mafic material at the interface between the continental crust and the mantle will provide the heat flux (~90mV/$m^2$; Chapman, 1986) necessary to provoke water-undersaturated partial melting of mafic rocks (~1000°C) and of various felsic rocks (~800°C; Johannes and Holtz, 1990; Thompson, 1990; Vielzeuf et al., 1990; Wedepohl, 1995). The products of crustal anatexis are essentially tonalitic to granitic melts leaving the felsic and mafic granulites at the lowest part of the continental crust.

Granulites are characterized by a small amount of hydrated minerals implying that metamorphism occurred at low water activity ($a_{H_2O}$ ~0.2; Valley, 1992). Several possibilities have been proposed to maintain $a_{H_2O}$ close to ~0.2 during metamorphism: (1) dry protolith (Lamb and Valley, 1984), (2) partial melting on hydrated protolith leading to the formation of partial melt which incorporated the water and to the formation of a dry and LILE-depleted residue (Fyfe, 1973; Nesbitt, 1980; Clemens, 1990; Vielzeuf et al., 1990), (3) magmas which incorporated water during their crystallization provoked the dissection of their country rocks during their upward migration (Touret, 1969; Pineau et al., 1981), (4) water dilution with a $CO_2$-rich fluid (Touret, 1971; Newton et al., 1980; Janardhan et al., 1982), (5) brine-rich fluid circulation (Touret, 1985; Aranovitch et al., 1987, Aranovitch and Newton, 1966). In addition, the granulite facies continental crust is also characterized by layers, pods or veins of granitic material in plastically deformed metamorphosed rocks, forming migmatitic structures (Brown, 1997 and references herein).

## 3.2. Terms used to describe migmatites

The term migmatite was used the first time by Sederholm (1907) to describe metamorphic rocks in Finland presenting an interlayering of quartzofeldspathic and mafic zones. The Table I.5 summarized the most common terms used for the description of migmatites (Mehnert, 1968, Ashworth, 1985). Melanosome and leucosome are the products of the migmatization process, and together are termed neosome whereas paleosome refers to the parental rock of neosome prior to migmatization (Mehnert, 1968). The boundary between leucosome and paleosome is sharply defined by a significant coaser grain size within the leucosome than the adjacent foliated lithology (Mehnert, 1968). The melanosome which is mainly composed of a mafic selvage, passes graditionally into mesosome or paleosome (Ashworth, 1976; Dougan, 1979; McLennan, 1983). The grain size within the two latest lithologies is variable (Ashworth and McLennan, 1985). With increasing migmatization process, migmatite textures are stromatic, folded stromatic, agmatic, or nebulitic. Outcrop

Table I-6: Migmatization processes are classified according to an assumed open or closed system and the melt formation. After Ashworth (1985).

| | Open system | Close system |
|---|---|---|
| Melt formation | magmatic injection | anatexis |
| No-melt formation | metasomatism | metamorphic segregation |

photographs presented in the Appendix A show several examples of migmatitic textures observed in the Limpopo Central Zone. These terms will be used for the description of the migmatites studied here.

## 3.3. Petrogenesis of migmatites

The first approach to determine the petrogenesis of migmatite was suggested by Sederholm (1907) who clearly showed that migmatites are a rock formation between metamorphic and igneous ones. In the english version of Sederholm (1907) published in 1967, it is suggested that the fluid linked to the migmatization process came from the granite and not from the originated protolith. However, the modern debate on the origin of migmatizing fluid (Olsen, 1985), favors that the fluid comes from the original protolith and not from the granitic melt produced during migmatization, as already suggested by Holmquist (1921). Several migmatization processes have been proposed (Table I-6; Ashworth, 1985). These processes can be classified according to an assumed open or closed system and the melt formation process. On one hand, a closed system and an isochemical evolution would be expected in cases of partial melting or metamorphic segregation at subsolidus consitions as formation process. On the other hand, an open system would result from metasomatism or magma injection (Olsen, 1985; Ashworth, 1985). It has to be noticed that more than one process can operate simultaneously as emphazised for example by Brown (1973), Olsen (1985) and Whitney et al. (1994). With the intention to assess the behaviour of the Sm-Nd system in a closed system migmatization, I will only explain in detail the anatexis and metamorphic segregation processes.

### 3.3.1. Partial melting

Low water activity (about 0.2; Valley, 1992) predominates at mid- to lower crustal level. However, it was argued that a large quantity of water is needed to enhance crustal anatexis in the deep portion of the continental crust where the temperature is higher than that of water-saturated granite solidus (Tuttle and Bowen, 1958; Lefort, 1981; Wickham and Taylor, 1987). Consequently, vapor-absent dehydration reactions most probably provide the quantity of water necessary to induce crustal anatexis (Brown and Fyfe, 1970; Fyfe, 1973; Clemens, 1990). Considering that most of the igneous rocks do not contain a large amount of hydrated minerals, metasedimentary rocks such as metapelite or metagreywaycke are considered as "fertile" lithologies. The chemical characteristics of the granitic melt formed by such reactions are largly controlled by the modal mineralogy of the source and the hydrous phase assemblage undergoing dehydration melting. Dehydration melting is explained in detail by experimental studies performed on various lithologies (Thompson and Algor, 1977; Thompson and Tracy, 1979; Thompson, 1982; 1988; Grant, 1985; Clemens and Vielzeuf, 1987; Le Breton and Thompson, 1988; Vielzeuf and Holloway, 1988; Patiño Douce and Johnston, 1991; Vielzeuf

Table I-7: Solidus temperature and biotite out temperature are reported from the experimental studies on fluid-absent melting-reactions in metapelite and metagreywacke. The two temperatures vary accroding to the starting material, the bulk-rock $H_2O$ wt%, and the Mg#. VH: Vielzeuf and Holloway (1988); LBT: Le Breton and Thompson (1988); PDJ: Patiño Douce and Johnston (1991); VM: Vielzeuf and Montel (1994); PDB1: Patiño Douce and Beard (1995); PDB2: Patiño Douce and Beard (1996); $SCD_1$: Stevens et al. (1997, in metagreywacke); $SCD_2$: Stevens et al. (1997, in metapelite).

| Ref. | Starting material | Mg# | Solidus | Bulk-rock $H_2O$ wt% | Bt out T°C |
|---|---|---|---|---|---|
| VH | Qtz, Pl, Ms, Bt, Chl, St, Grt | 41 | <750°C | 1.86 | 850-862°C |
| LBT | Qtz, Pl, Bt, Kya | 44 | ~800°C | 1.24 | ? |
| PDJ | Qtz, Pl, Ms, Bt, Als, Il, Grt | 36 | <800°C | 1.69 | 950-1000°C |
| VM | Qtz, Pl, Bt | 47 | ~900°C | 1.43 | 950-1000°C |
| $PDB_1$ | Qtz, Pl, Bt | 55 | ~885°C | 1.4-1.6 | ~940°C |
| $PDB_2$ | Qtz, Pl, Bt | 0.4 | ~840°C | 1.0 | ~920°C |
| $PDB_2$ | Qtz, Pl, Bt | 23 | ~800°C | 1.4 | ~900-925°C |
| $SCD_1$ | Bt + powder (Si, Fe, Mg,Al, Ca, K) | 49-81 | ~775±25°C | 1.1-1.4 | >830°C |
| $SCD_2$ | Bt + powder (Si, Fe, Mg,Al, Ca, K) | 49-81 | ~810±20°C | 0.8-1.0 | >840°C |

and Montel, 1994; Wolf and Wyllie, 1994; Carrington and Harley, 1995; Patiño Douce and Beard, 1995, 1996; Clemens et al., 1997; Stevens et al., 1997). A better understanding of fluid-absent partial melting on "fertile" lithologies has been obtained by the experimental studies of Vielzeuf and Holloway (1988), Le Breton and Thompson (1988) and Patiño Douce and Johnston (1991) in metapelites, and Vielzeuf and Montel (1994), Patiño Douce and Beard (1995, 1996) and Stevens et al. (1997) in metagreywaykes. Two examples of migmatites studied in this work concerns fluid-absent partial melting of metapelite and metagreywacke respectively, and therefore I will focus the following overview on biotite dehydration reactions in those lithologies.

The experimental works performed by Stevens et al. (1997) in comparison with the previous studies provide important constraints on the mechanism of melt formation during granulite-facies anatexis. All details concerning the starting materials, the apparatus and the control of redox state are decribed in Stevens et al. (1997). A summary of the results obtained by the experimental studies are listed in Table 1-7. Two generalised melting reactions are responsible for biotite breakdown:

$$Bt + Qtz + Pl_1 + Sil = Kfs \pm Grt \pm Crd + melt + Pl_2 \text{ (in metapelite)}$$

$$Bt + Qtz + Pl_1 = Kfs \pm Grt \pm Crd + Opx + melt + Pl_2 \text{ (in metagreywacke)}$$

The reactions are very similar to those obtained on metasediments by Vielzeuf and Holloway (1988), Le Breton and Thompson (1988), Patiño Douce and Johnston (1991), Vielzeuf and Montel (1994). The results related to the reactions are reported in Fig. I-12 which illustrates the location in the P-T space of the fluid-absent metapelite and metagreywacke solidi and the upper temperature of biotite-melt coexistence. Several important points have to be noticed: (1) biotite breadown in metapelite occurs at lower temperature compared to that in metagreywacke, i.e. 750° ± 50°C compared to 800° ± 50 °C at 0.4 GPa pressure, whereas the solidus temperatures of the two systems are quite similar at 1 GPa; (2) bulk-rock Mg# of metapelite and metagreywacke appears to raise slightly the solidus temperature; (3) $TiO_2$ content within biotite does not influence the position of the solidus but enhances the upper limit of biotite-melt coexistence; (4) biotite is not stable at temperature above 950°C; (5) a steep positive dP/dT slope for biotite dehydration reaction in metapelite is suggested while a steep negative dP/dT slope for metagreywacke is observed, (6) biotite out curves have steep positive dP/dT slopes in both lithologies. The main difference between these experiments on those performed by Patiño Douce and Beard (1995, 1996) is the occurrence of Opx as a main product of biotite breadown. Patiño Douce and Beard (1995, 1996) only observed the Opx product at high temperature and pressure experiments. In addition, the amount of melt produced by biotite dehydration reactions significantly increases at the critical temperature interval of 800 to 900°C. Fig. I-13 shows the amount of melt produced by fluid-absent partial melting process on

Figure I-12: Examples of experimental studies on fluid-absent melting reaction. Results of biotite breakdown reactions are reported in the P-T space for metapelite in a) and for metagreywacke in b) (Stevens et al., 1997). Explanation see Text. AS, BS, CS and NBS correspond to different starting metapelitic material. A, B, C and NB correspond to different starting metagreywacke material.

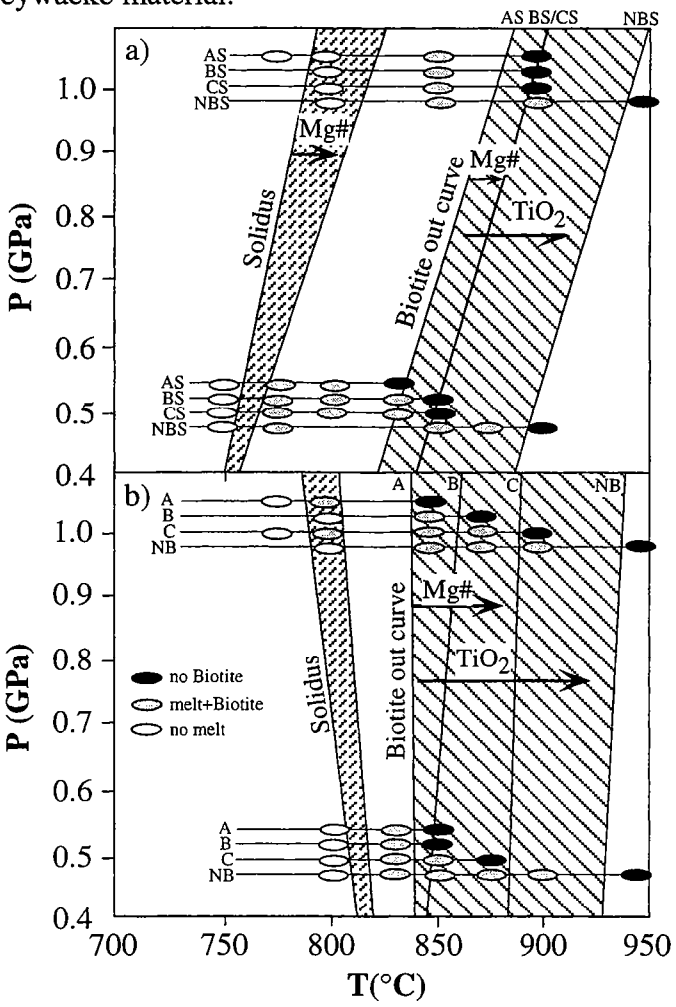


Figure I-13: Evolution of the melt fraction in vol% is reported as a function of the temperature according to the Mg# and Ti contents in biotite. After Stevens et al. (1997).

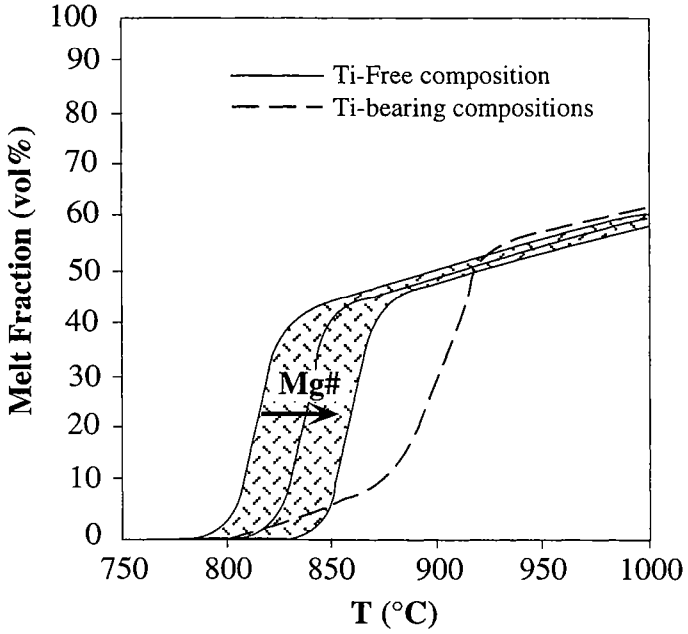

metagreywacke at temperature increasing and pressure equal to 5 GPa. It arises that the melt fraction in vol% depends on the behaviour of biotite, the Ti content of biotite and on the bulk-rock Mg#. As soon as biotite starts to breakdown, water which is incorporated in the melt, enhances crustal anatexis which will continue as far as water is available. It is not surprising that a large quantity of melt is formed in a short temperature interval. In addition, the concentrations of Ti in biotite or Mg in the bulk-rock dominate the temperature at which partial melting begins but do not influence the amount of melt produced by biotite breakdown.

The biotite breakdown leading to partial melt formation was largelly invoked as migmatization process in many high-grade metamorphic terranes (e.g. Mehnert, 1968; Johannes and Gupta, 1982; Olsen, 1985; Grant, 1985; Weber and Barbey, 1986; Vernon and Collins, 1988; Maaløe, 1992; Whitney and Irving, 1994; Johannes et al., 1995).

### 3.3.2. Metamorphic differentiation at subsolidus condition

The second migmatization process evolving as a closed system is the metamorphic segregation at subsolidus condition (Robin, 1979; Lindh and Wahlgren, 1985; van der Molen, 1985; Sawyer and Robin, 1986; Blom, 1988; Whitney and Irving, 1994). This process was invoked for the formation of stromatic migmatite which presents on outcrop scale a well defined layering of leucocratic and mafic bands. The mass tranfert that leads to the differentiation is attributed to the combination of stress and a static metamorphic fluid (Robin, 1978, 1979; van der Molen, 1985; Sawyer and Robin, 1986). The experimental work in the quartz-albite-$H_20$ system demonstrated that the porosity becomes connected at temperature increasing some tens of degree below the solidus (Holness, 1995). Consequently, the formation of quartz-feldspath veins as leucosomes is driven within the rock where the local variations gradients are the highest, i.e. bedding, dilatent fissures and tectonic layering (Lindh and Wahlgren, 1985; Robin, 1979). The pressure gradients are enhanced by the variable orientations of grain boundaries within a rock. In fact, mineralogic variations between layers lead to constrasts in competency which in turn produce pressure gradients during deformation. Mass transfert will occur down to the pressure gradients, from the less viscous to the more viscous layer (Robin, 1979; Brown et al., 1995 for the filter-pressure model). It has to be noticed that the quartz-feldspathic bands in the migmatites do not correspond to a "true leucosome" and do not represent more than 10-15 volume % of the entire migmatite.

### 3.3.3. Open or close system during migmatization

Even if partial melting and metamorphic segregation at subsolidus conditions are suggested to evolve as close system, the assumption should be confirmed. Mass balance calculations can be done in different manner to demonstrate that no foreign material came into the migmatite or that no melt escaped from the site of migmatization (Gresens, 1967; MacRae

Figure I-14: Example of isocon diagram based on the Gresens' equation (Gresens, 1967) and used for the graphical representation of Grant (1986). This example shows a complete dehydration reaction and a K metsomatism undergone by the original rock. The $\Delta C_0$ represents the $C_0$ enrichment in the altered rock compared to the original one.

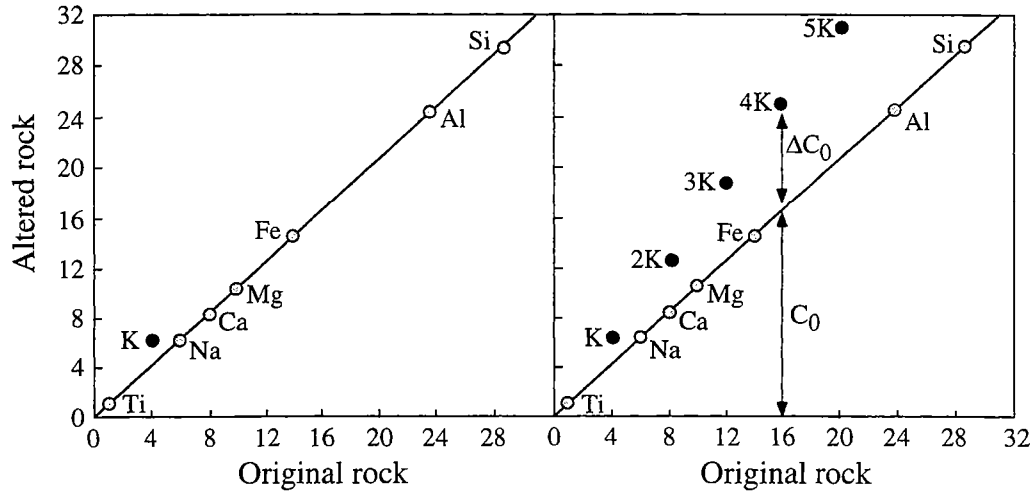

and Nesbitt, 1980; Olsen, 1982, 1984, 1985; Grant, 1986; Olsen and Grant, 1991; Baumgartner and Olsen, 1995).

Gresens (1967) focussed on the composition and volume changes occurring during metasomatic alterations. The study provides a general set of equations which allow the calculation of gains and losses of elements. At the first stage, the given equations were used only to assess the behaviour of elements during the alteration process and to examine if the gains and losses of certain elements might be related to mineralogic transformation. Considering that migmatite studies were confronted to the issue of close or open system to evaluate the chemical composition of partial melts, Grant (1986) provided a simple graphical method based on the Gresens's equations for both volume (or mass) change and concentration changes. The main assumption in the Gresens's equation is that some elements are immobile, or conserved, during the metasomatism process. The ratios of concentrations of immobile elements are similar in both altered and original rock and therefore the ratios are independent of mass or volume changes during the process. They are used to calculate the mass or volume loss of the mobile elements (Gresens, 1967). The main advantage of the Grant's method is the graphical representation of compositional variations by plotting the chemical composition of the altered rock against that of the original rock. Grant (1986) gives the mathematical basis for the diagram and discusses the assumptions involved. The Fig. I-14 illustrates the case of a rock which underwent complete dehydration reaction followed by K-metasomatism (Olsen and Grant, 1991). The concentrations of all immobile elements lie on a straight line through the origin. This line is called isocon and its slope gives the volume or mass changes. The deviation of chemical species concentration above or below the isocon gives the gain or loss of these species relative to the amounts in the original rock. The Grant's diagram is used for the major and trace element concentration (Olsen and Grant, 1991). However, caution should be paid on the use of trace elements in the determination of the isocon: (1) their referred concentration uncertainties are significantly highly variable, (2) the behaviour of accessory minerals which are the main REE, U and Th carriers, is not well understood, and the use of these trace elements for the isocon may deviated from the reality, (3) the behaviour of the different trace elements cannot be explained in a simple and unique manner.

A different approach for the issue of open or close system during migmatization may be used via the mixing equations given in Albarède (1995). If all migmatitic components are present in a rock, the volume % of each may be estimated. Consequently, mixing calculations using the chemical composition and the volume % of the respective leucosome and melanosome should match the chemical composition of the paleosome in a closed system. The estimated volume proportion of leucosome should be below 50% otherwise neither fluid-absent partial melting nor metamorphic segregation can be assumed as migmatization process (as demonstrated by the experimental studies, see §3.3.1.). In the same way, the chemical

composition of each mineral forming a migmatitic layer can be used instead of the chemical composition. The minerals which participated to the formation of the leucosome will be considered in the mixing-model calculations (Bea, 1989).

Depending on the available data, there are several mass balance models which allow the confirmation of open or closed system during migmatization.

### 3.3.4. REE modeling

In order to decipher whether leucosome is formed by partial melting or metamorphic segregation at subsolidus condition processes, REE modeling may be applied. REE concentrations in melts give informations on the melting conditions, the mineralogical and chemical composition of the source during melting and the modification in melt composition by differentiation and fractionation (Hanson, 1980). REE modeling can be performed using (1) batch, (2) fractional, and (3) disequilibrium melting equations. The two first equations refer to partial melting whereas the third is related to metamorphic segregation at subsolidus condition.

Equilibrium melting or batch melting implies that thermodynamic equilibrium is attained between the melt and the solid and thus that equilibrium partition coefficients can be used (Allègre and Minster, 1978). The trace element concentrations in the leucosome (Qtz-fs layer of our study) are given by the following equation:

$$C_l^i = \frac{C_0^i}{\left(D_0^i + F \times \left(1 - D_0^i\right)\right)} \qquad (1)$$

$C_l^i$ is the concentration of trace element *i* in the leucosome, $C_0^i$ is the concentration of trace element *i* in the source rock, $D_0^i$ is the total partition coefficient of element i in the source rock and F is the degree of partial melting.

Fractional melting relates to the immediate migration of melt from the source, so that equilibrium is limited to the site of melting at infinitesimal melt batches (Allègre and Minster, 1978). The leucosome trace element concentrations are given by the following equation:

$$C_l^i = C_0^i \times \left(\frac{1}{D_0}\right) \times (1 - F)^{\left(\left(\frac{1}{D_0}\right) - 1\right)} \qquad (2)$$

In disequilibrium melting, no trace element equilibration takes place between the residue and melt, and chemical compositions of leucosome depend only on the concentration of trace element in different minerals which enter the melt. Therefore, the same treatment applies to

Table I-8: Chemical compositions of minerals which may be found in granulite rock. Mineral abbreviations according to Kretz (1983). Data on Pl, K-fs, Bt, Crd, Grt, Mnz, Ap and Zrn are given in Bea et al. (1994). Hbl and Ttn major element concentrations are given by Gromet and Silver (1983). Trace element concentrations in Hbl, Ttn, Xnt, and Cpx are provided by Bea (1996).

| | Pl | K-fs | Bt | Crd | Grt | Mnz | Ap | Zrn | Hbl | Aln | Xnt | Ttn | Cpx |
|---|---|---|---|---|---|---|---|---|---|---|---|---|---|
| **Major elements in wt%** | | | | | | | | | | | | | |
| **SiO2** | 63.17 | 64.80 | 35.27 | 47.29 | 37.08 | - | 0.21 | 31.98 | 42.1 | 34.15 | 0.31 | 29.82 | - |
| **TiO2** | 0.00 | 0.01 | 3.85 | 0.00 | 0.02 | - | 0.00 | 0.02 | 1.37 | 0 | 0 | 36.48 | - |
| **Al2O3** | 22.83 | 18.43 | 9.66 | 31.82 | 20.68 | - | 0.00 | 0.39 | 11.66 | 16.16 | 0 | 1.44 | - |
| **FeOtot** | 0.04 | 0.04 | 21.08 | 11.53 | 35.92 | - | 0.58 | 0.19 | 20.39 | 17.5 | 0.13 | 0.98 | - |
| **MgO** | 0.00 | 0.01 | 7.13 | 5.54 | 2.56 | - | 0.00 | 0.02 | 8.12 | 0.75 | 0 | 0.01 | - |
| **MnO** | 0.03 | 0.01 | 0.16 | 0.25 | 3.75 | - | 0.10 | 0.09 | 0.42 | 0 | 0 | 0.17 | - |
| **CaO** | 4.11 | 0.03 | 0.00 | 0.01 | 0.74 | - | 54.36 | 0.17 | 11.96 | 9.86 | 0.14 | 27.31 | - |
| **Na2O** | 8.93 | 0.91 | 0.18 | 0.41 | 0.01 | - | 0.06 | 0 | 1.56 | 0.14 | 0.05 | - | - |
| **K2O** | 0.17 | 14.94 | 9.63 | 0.00 | 0.00 | - | 0.06 | 0 | 1.55 | 0 | 0 | - | - |
| **P2O5** | 0.20 | 0.21 | 0.00 | 0.01 | 0.00 | - | 42.91 | 0 | - | 0.04 | 33.01 | - | - |
| **ZrO2** | - | - | - | - | - | - | - | 65.65 | - | 0.02 | 0.11 | - | - |
| **Trace elements in ppm** | | | | | | | | | | | | | |
| **Rb** | 8.40 | 316.20 | 718.00 | 6.63 | 1.01 | - | - | - | - | - | - | - | - |
| **Sr** | 277.00 | 217.00 | 3.52 | 63.20 | 2.49 | - | - | - | - | - | - | - | - |
| **Ba** | 122.00 | 3075.00 | 270.00 | 13.20 | 2.86 | - | - | - | - | - | - | - | - |
| **Y** | 0.77 | 0.86 | 0.03 | 0.66 | 21.00 | 3996 | 192.00 | 77.80 | 17.90 | 1456.87 | 197149.72 | 245 | 2.71 |
| **Nb** | 0.02 | 0.35 | 47.30 | 0.02 | 0.02 | - | - | - | - | - | - | - | - |
| **Ta** | 0.06 | 0.09 | 6.29 | 0.01 | 0.00 | - | - | - | - | - | - | - | - |
| **Th** | 0.10 | 0.30 | 0.02 | 0.08 | 0.03 | 162665 | 21.8 | 12.10 | 0.25 | 4921.53 | 1581.92 | 46.9 | 0.04 |
| **U** | 0.41 | 1.39 | 0.16 | 1.01 | 0.05 | 12772 | 19.3 | 159.00 | 1.76 | 0.00 | 0.00 | 32.3 | 0.09 |
| **La** | 7.31 | 2.53 | 0.040 | 0.12 | 0.06 | 92898 | 1162.0 | 2.58 | 8.7 | 20251.16 | 127.90 | 281 | 0.2 |
| **Ce** | 15.00 | 4.28 | 0.120 | 0.33 | 0.21 | 232144 | 2898.0 | 7.75 | 39.4 | 41920.12 | 640.33 | 987 | 0.96 |
| **Pr** | 1.52 | 0.47 | 0.010 | 0.04 | 0.03 | 32657 | 403.0 | 0.97 | 8 | 5037.13 | 170.75 | 182 | 0.2 |
| **Nd** | 2.68 | 1.04 | 0.040 | 0.10 | 0.14 | 104781 | 1827.0 | 5.10 | 39.9 | 10502.55 | 1628.97 | 831 | 1.29 |
| **Sm** | 0.30 | 0.23 | 0.010 | 0.04 | 0.03 | 26589 | 589.0 | 1.40 | 11.5 | 1854.14 | 2716.53 | 185 | 0.47 |
| **Eu** | 1.75 | 1.84 | 0.020 | 0.01 | 0.00 | 330 | 16.0 | 0.32 | 1.44 | 0.00 | 0.00 | 57.5 | 0.21 |
| **Gd** | 0.31 | 0.18 | 0.010 | 0.06 | 0.31 | 19737 | 639.0 | 1.93 | 9.48 | 390.42 | 8285.49 | 140 | 0.56 |
| **Tb** | 0.04 | 0.02 | 0.001 | 0.01 | 0.15 | 2152 | 104.0 | 0.50 | 1.52 | 0.00 | - | 19.7 | 0.09 |
| **Dy** | 0.24 | 0.14 | 0.008 | 0.15 | 2.64 | 6153 | 645.0 | 5.43 | 7.23 | 130.70 | 23133.49 | 102 | 0.53 |
| **Ho** | 0.05 | 0.04 | 0.002 | 0.04 | 1.13 | 870 | 131.0 | 2.24 | 1.43 | 0.00 | - | 19.3 | 0.11 |
| **Er** | 0.12 | 0.10 | 0.007 | 0.14 | 5.87 | 1648 | 356.0 | 9.93 | 3.7 | 43.73 | 18889.64 | 57.8 | 0.27 |
| **Tm** | 0.02 | 0.02 | 0.002 | 0.02 | 1.22 | 184 | 52.0 | 2.82 | 0.51 | 0.00 | - | 8.46 | 0.04 |
| **Yb** | 0.10 | 0.10 | 0.008 | 0.15 | 10.50 | 522 | 316.0 | 27.80 | 2.9 | 43.91 | 11899.63 | 57 | 0.23 |
| **Lu** | 0.02 | 0.01 | 0.002 | 0.05 | 1.87 | 64 | 40.0 | 9.24 | 0.45 | 0.00 | 1275.11 | 7.9 | 0.03 |

subsolidus metamorphic differentiation (Whitney and Irving, 1994). The leucosome trace element concentrations are given by the following equation (Prinzhofer and Allègre, 1985; Barbey et al., 1989; Sawyer, 1991):

$$C_l^i = C_0^i \times \left( \frac{x_1 + \left( \frac{\sum_{j=2}^{n} x_j \times D_j}{D_l} \right)}{X_1 + \left( \frac{\sum_{j=2}^{n} X_j \times D_j}{D_l} \right)} \right) \qquad (3)$$

In Eq. (3), the variables are the same as in Eq. (1) plus $X_j$ which corresponds to the weight proportion of mineral j in the source rock and $x_j$ to the weight proportion of mineral j entering the leucosome.

## 3.4. Distribution of trace elements during migmatization

### 3.4.1. Major and trace element concentrations in minerals

In Table I-8 the chemical composition of minerals which can be found in metamorphic rocks are reported. Their chondrite-normalized REE patterns are illustrated in Fig. I-15 and I-16. It has to be noticed that the concentrations of trace elements in minerals may vary significantly from those listed in Table I-8 according to the lithology, the metamorphic grade and the fluid activity. Therefore, the Table I-8 provides only one example among a large data set. Nevertheless, several conclusions can be drawn: (1) major and Large Ion Lithophile elements are concentrated within the main minerals such as Pl or Bt; (2) LREE are concentrated in accessory minerals such as Mnz, Ap or Ttn, (3) HREE are mainly concentrated in Grt and Zrn, (4) the REE concentrations within accessory minerals are significantly higher (up to a factor of 1000) than those in main minerals, and (5) Nb and Ta HFS elements are concentrated within Bt whereas Th, U, Zr, Hf HFS elements are concentrated within accessory minerals.

The behaviour of minerals during migmatization controls the concentrations of LIL, HFS and RE elements in the melt. For example, Bt breakdown will induce Nb, Rb and Ta enrichments in the melt as these elements are highly incompatible whereas the participation of Pl or K-fs in the chemical composition of the melt may be highlighted by Sr and/or Ba concentrations. In addition, the REE concentrations in the melt will depend on the behaviour of accessory minerals during migmatization as they represent the most important REE carrier. Therefore, the association of U, Th and REE concentrations may provide arguments for the

Figure I-15: Chondrite-normalized REE patterns of minerals after Gromet and Silver (1983).

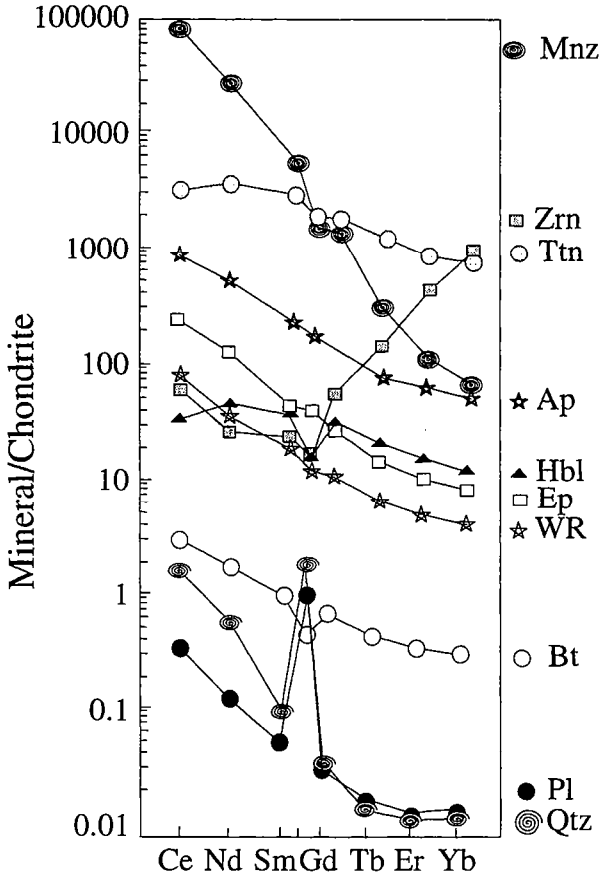


Figure I-16: Chondrite-normalized REE patterns of garnet after Bea et al. (1994).

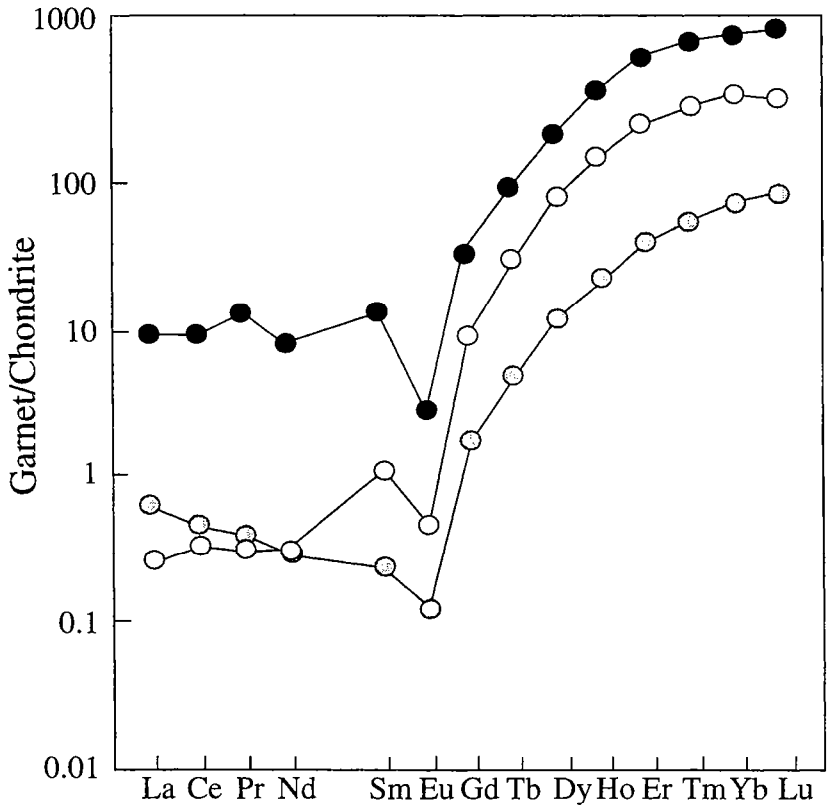

effect of accessory minerals on the chemical composition of the leucosome.

### 3.4.2. Metamorphic segregation at subsolidus condition

Fig. I-17 shows a hypothetical stromatic migmatite which was formed by metamorphic segregation at subsolidus condition. The sample presents a very well defined layering of all migmatitic components. The organization of minerals under deformation leads to the formation of leucosome and melanosome. Their respective mineralogic composition is Pl + Qtz ± Bt and Bt + Pl ± Ap ± Zrn ± Mnz. The paleosome is considered as the protolith prior to migmatization and it contains higher amounts of accessory minerals compared to the melanosome. If the system remained closed during migmatization, the distribution of trace elements should follow their best host mineral. Therefore, it is expected that the leucosome is depleted in Rb, Ba and Th whereas the melanosome should show the highest Rb and Ba concentrations. The unmigmatized rock should have a chemical composition between these two extremes as shown in Fig. I-17. However if the system did not remain close during migmatization, the distribution of trace elements cannot be related to the mineralogic association. As a consequence, the chemical composition of the paleosome will not be an intermediate between those of leucosome and melanosome and the mass conservation is not be respected.

In the case that mass conservation is maintained, i.e. the system remained closed, the Chondrite-normalized REE patterns of all migmatitic components should highlighted the mineralogic association of which they are composed. An example is illustrated in Fig. I-18 (Sawyer and Robin, 1986). The leucosome which is mainly composed of Pl and Qtz presents LREE depletion, strong positive Eu anomaly and low REE contents whereas the melanosome is characterized by LREE enrichment and high REE contents. Consequently, the distribution of major and trace elements reflect only a mixing of variable mineral proportions in the respective layers.

### 3.4.3. Partial melting

Migmatites which are formed by partial melting are recognized as the precursor of granite formation. The Bt breakdown yields to the formation of partial melts which are generally of granitic to granodioritic compositions. Their mineralogic association is essentially composed of Pl, K-fs, Qtz and Bt with small amounts of accessory minerals such as Ap, Ttn or Zrn.

#### *3.4.3.a. Major element distribution*

The field of leucosome chemical composition produced by anatexis are represented in the haplogranitic system Qtz-Ab-Or±$H_2O$ in Fig. I-19. The minimum melt compositions are

Figure I-17: Theorotical example of the distribution of major and trace element in a migmatite which was formed by metamorphic segregation at subsolidus condition. Explanation see text.

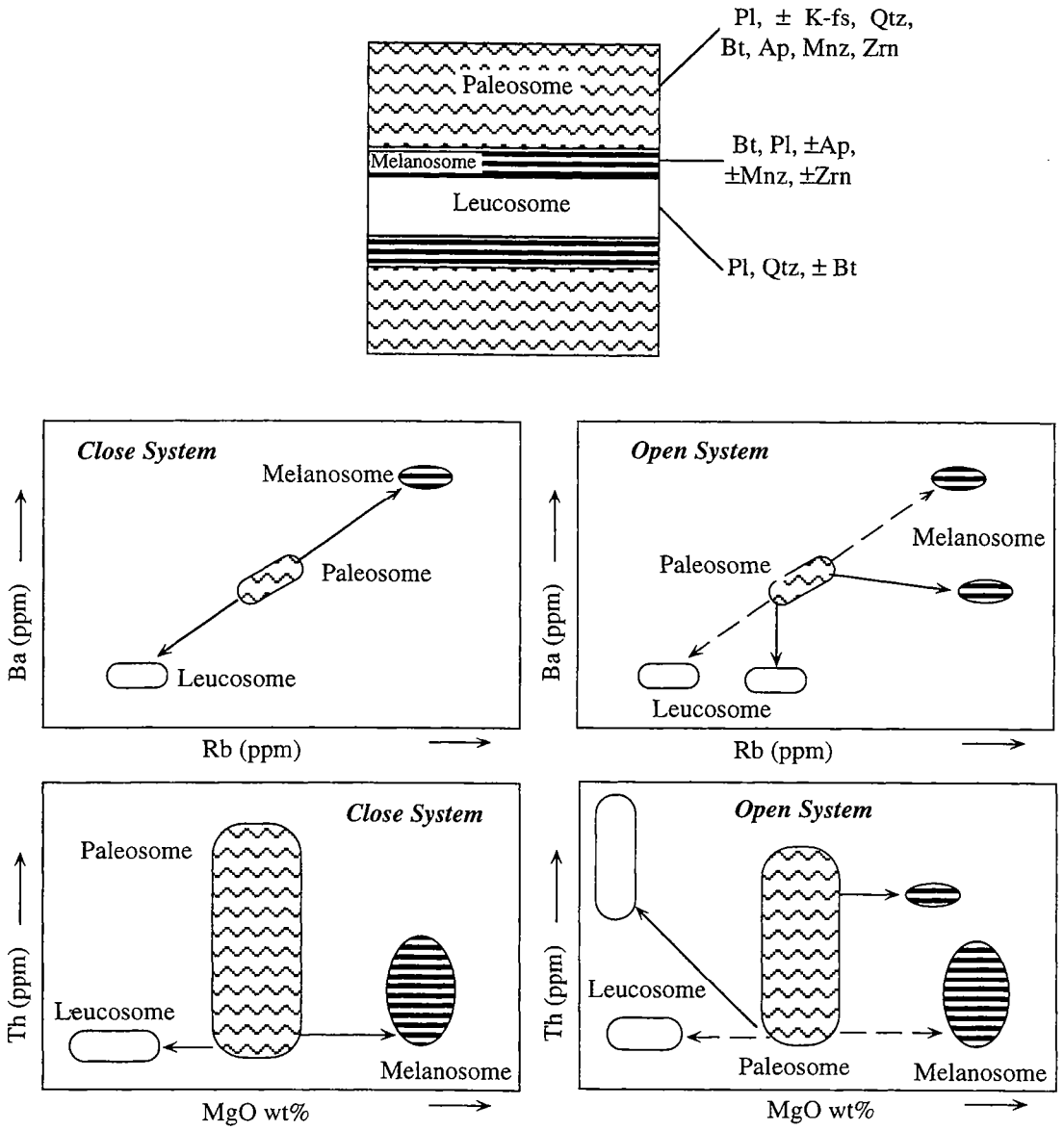

Figure I-18: REE patterns normalized to Chondrite for all migmatitic components in the case of metamorphic segregation at subsolidus condition is the migmatization process. After Sawyer and Robin (1986).

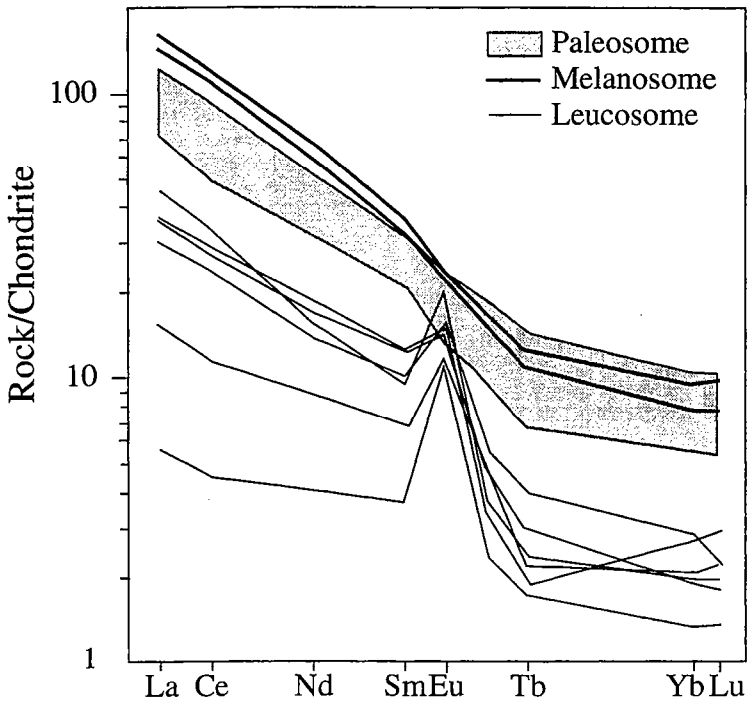


Figure I-19:.Chemical composition fo migmatitic components are ploted in a haplogranitic triangle using the CIPW normative composition. Eutectic melt composition is indicated for variable water activity (open square: $a_{H2O}$ = 1; + : $a_{H2O}$ = 0.5) and pressure 1, 2, 5 and 10 kbar. Modified after Inger and Harris (1993). Shaded area corresponds to the eutectic melt field. Dashed arrows represents the expected trend of a restitic melt. Bold arrows present two possible trend for a melt formed by fractional melting.

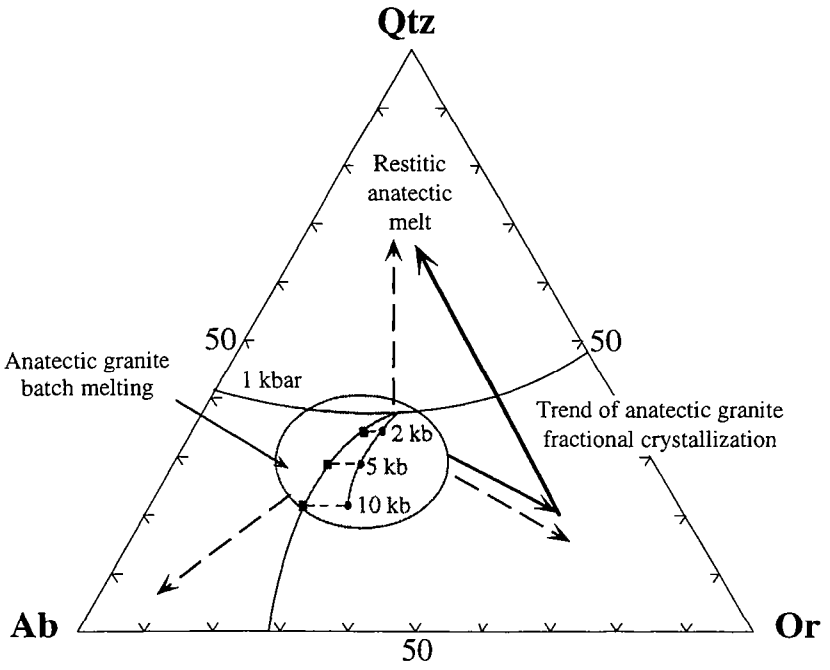

shown as function of different water activity and pressure values.

If we consider that a closed system is maintained during migmatization, therefore the chemical composition of the leucosome should cluster around the minimum melt composition corresponding to pressure and water activity values at the site of migmatization.

However, fractional melting relates to the immediate migration of melt from the source, so that equilibrium is limited to the site of melting at infinitesimal melt batches. Mass balance relations of mica-dehydration-melting reactions suggested the following proportions of each mineral for the bulk composition of leucosome (Patiño Douce and Johnston, 1991): 41% Bt, 23% Pl, 31% Qtz, and 6% Als. Consequently, the melt which migrates immediately after is formation is enriched in K compared to Na or Ca. The chemical compositions of the fractional melt defines a trend in the triangle closer to the Or pole as shown in Fig. I-19.

The last case to consider is the restitic melt. Fluid absent dehydration reactions continue as far as hydrated minerals are present. At temperature increasing, the participation of Bt and Pl in the chemical composition of leucosome is reduced whereas those of Qtz and Als increase. Consequently, the chemical composition of partial melt tends to be more and more enriched in Qtz compared to the Ab or Or components as illustrated in Fig. I-19.

### *3.4.3.b. Trace element distribution*

Hanson and Langmuir (1978) define a trace element as an element (1) which has such a low abundance in a system that changing its abundance does not affect the stability of any phase in the system, (2) which folows Henry's Law in all phases in the system, and (3) its distribution between any two phases in the system can be calculated using a mineral-melt or mineral-mineral distribution coefficient ($K_{di}$) without consideration of the element's abundance in any other phase of the system.

For batch melting, the abundance of a given element in the melt relative to its abundance in the protolith for a certain degree of partial melting is given by the following equation (Schilling, 1966):

$$C_l^i = \frac{C_0^i}{\left(D_0^i + F \times \left(1 - D_0^i\right)\right)}$$

In Fig. I-20 are reported the variations of the $C_l/C_o$ ratio of a given element i as function of the degree of partial melting. It arises that trace elements which are characterized by very low $D_i$ ($D_i < 1$) entered the melt immediately after the beginning of melting where as those which are characterized by high $D_i$ ($D_i > 1$) tend to stay within the protolith.

Figure I-20: Variation of Cl/C0 ratio is reported as a function of the degree of partial melting (F) and the bulk partition coefficient of the element of interest ($D_i$ = 0 to 9). After Hanson (1989). Explanation see text.

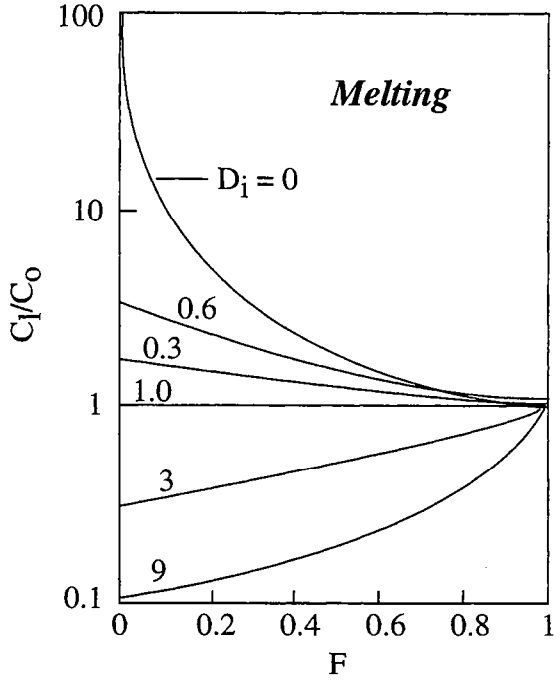


Figure I-21: Variation of Cl/C0 ratio is reported as a function of the degree of partial melting (F) and the bulk partition coefficient of the element of interest ($D_i$ = 0.01to 10) according to batch melting anf fractional melting. Explanation see text

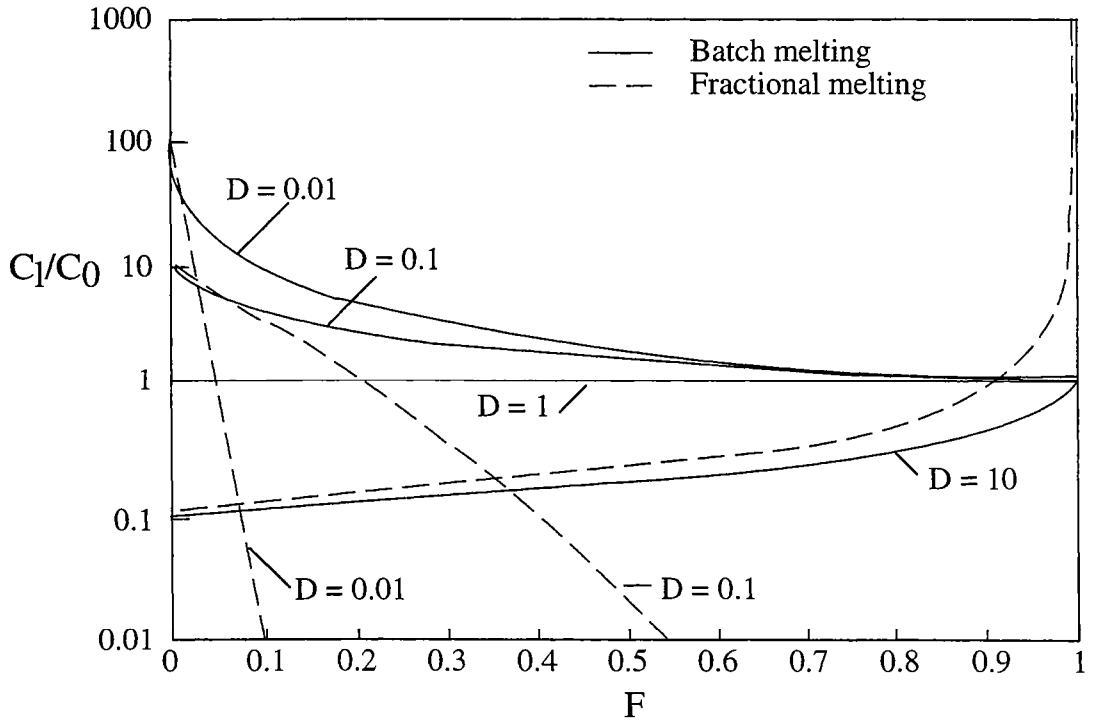

The behaviour of trace element during fractional melting is difficult to predict. Nonetheless, the first increment of melt will be strongly enriched in all incompatible elements whereas as the farctional melting is going on, the melt will tend to incorporate more and more compatible elements. An attempt to represent the variation of $C_l/C_o$ ratio of a given element i is presented in Fig. I-21.

In the Fig. I-22 are reported the Rb/Sr ratio versus Ba concentration for all migmatitic components. If the system evolves as a closed system, the leucosome should be characterized by high Rb/Sr ratio and low Ba concentration as a result of Bt dehydration reaction and as Bt is the main reactant compared to Pl, Qtz or Als. However, if the leucosome is a restitic partial melt, the main minerals which influence the chemical composition of the partial melt should be Pl or K-fs implying lower Rb/Sr ratio and high Ba content.

Special attention should be paid on the behaviour of ESC (Essential Structural Constituents) within the accessory minerals. It is for example Zr for Zrn or P for Ap or LREE-Th for Mnz. The concentration of an ESC in the melt is not dependent on the bulk distribution coefficient because the ESC is one major element of the considered mineral. Therefore, the concentration of an ESC in the melt depends only on the mineral-melt distribution coefficient for the mineral which has its site filled with the ESC. In Fig. I-23 is reported the path for Zr in a melt with zircon-melt $K_d = 2500$ (Example from Hanson, 1989) assuming that all other mineral-melt $K_{dZr} = 0.1$. In that case, it is considered that Zr concentration in Zrn is approximately 500000 ppm. The concentration of Zr in the melt is deduced by the following equation:

$$C_l^{Zr} = \frac{C_{Zrn}^{Zr}}{K_{d_{Zrn}}^{Zr}} = 200 \text{ ppm}$$

For melting with 100 ppm of Zr in the protolith, Zrn is present in the residue and the melt will have 200 ppm Zr until the last infinitesimal amount of Zrn is molten. The fraction of melt at which the last Zrn melts is given from the equation:

$$C_l^{Zr} = \frac{C_0^{Zr}}{\left(D^{Zr} + F \times \left(1 - D^{Zr}\right)\right)}$$

which suggests a degree of partial melting of 44.4%. After Zrn is no longer a phase in the residue, the melt has less than 200 ppm Zr. If the melt did have 200 ppm of Zr, Zrn is not stable.

### *3.4.3.c. REE patterns*

Batch melting implies that equilibrium partition coefficients between melt and solid

Figure I-22: Rb/Sr ratio versus Ba diagram used for the discrimination between restitic partial melt and eutectic melt composition. Explanation see text.

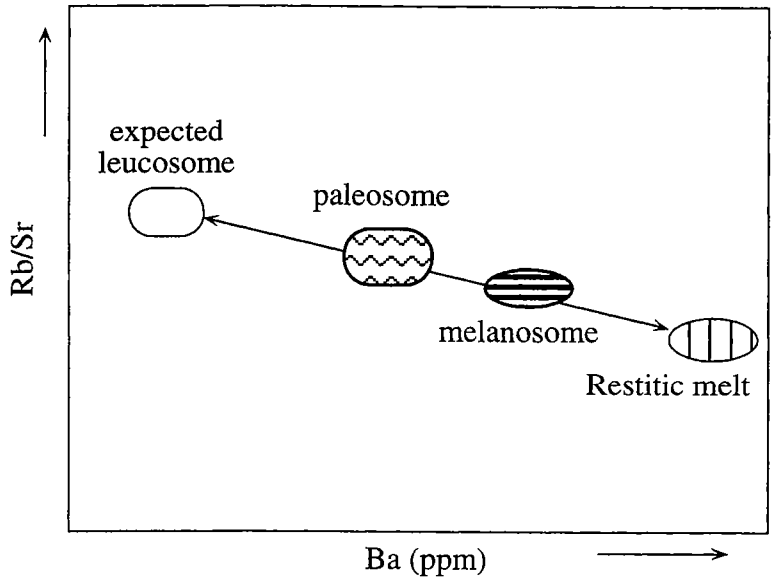


Figure I-23:. Path for Zr in a melt formed by batch melting assuming that zircon - melt Kd = 2500. After Hanson (1989). Explanation see text.

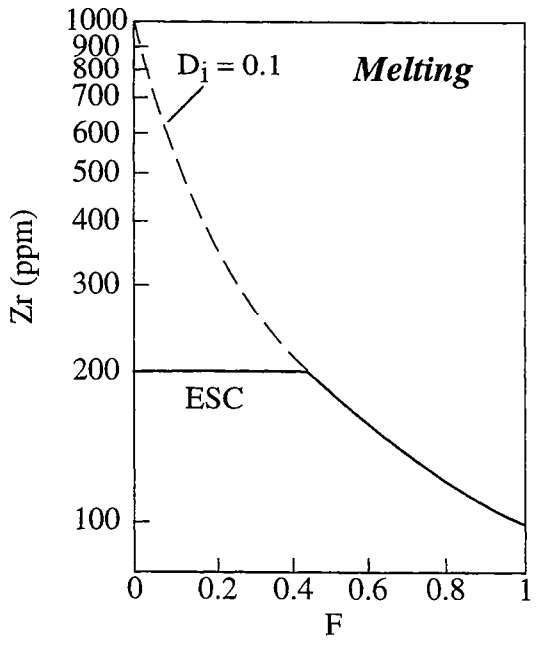

Figure I-24:Condrite-normalized REE patterns calculated for modal batch partial melting of a primitive mantle source with ca. 2.15 chondrite concentration of REE and with the mineralogy olivine 55%, orthopyroxene 25%, clinopyroxene 11% and garnet 9% . Curves are shown for 0.1 to 10 % partial melting. After Rollinson (1993, p.167).

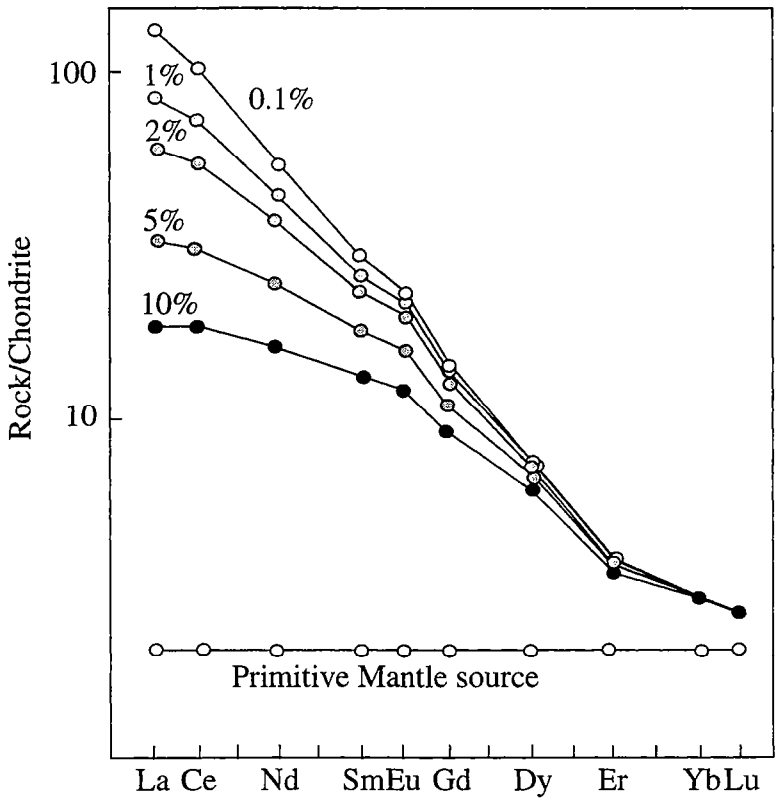


Figure I-25: Model chondrite-normalized REE diagrams for the equilibrium crystallization of leucosome. A illustrates the range of cumulate and fractionated melt compositions possible by varying the degree of crystallization from 0.1 to 0.5; B shows the range of compositions possible at a fixed degree of crystallization (0.44) obtained by varying the weight fraction (0 to 0.5) of trapped fractionated melt in the cumulate. After Sawyer (1987, p.465).

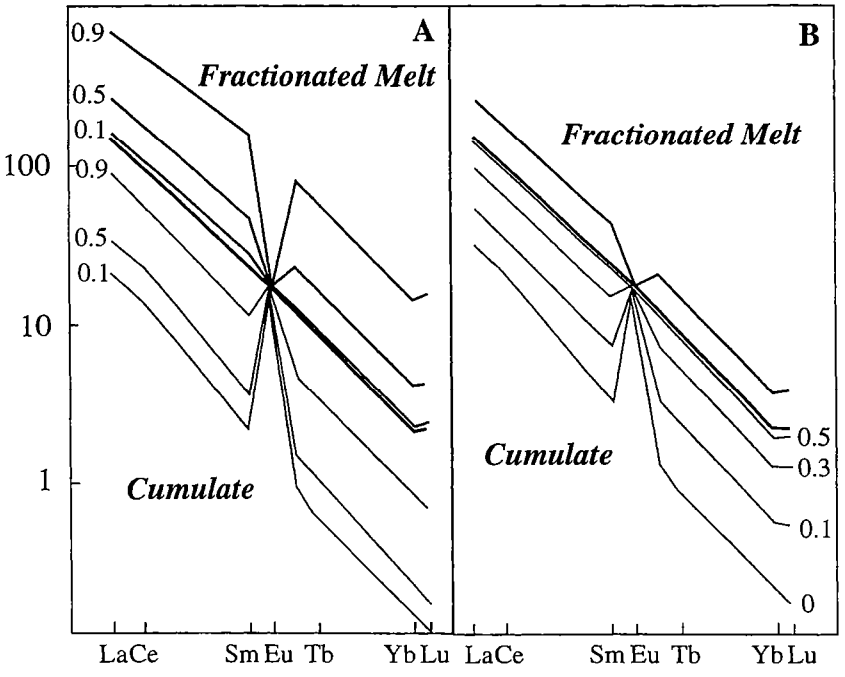

can be used (Allègre and Minster, 1978). In Fig. I-24 are reported the chondrite-normalized REE patterns of a primitive source and its related partial melts at various degree of melting. It shows that the partial melts are enriched in LREE compared to HREE and that the LREE concentrations in the partial melts decrease as the degree of partial melting increases. For the migmatization process, we expect therefore that fluid-absent dehydration reaction on a "fertile" lithology will give partial melts which are characterized by a LREE enrichement. However for fractional melting, the REE patterns of the leucosome depend on the proportions of minerals which are involved in the dehydration reaction at each steps of partial melt formation due to migration of partial melts immediately after their formation.

### 3.4.4. Possible problems

Several chemical, physical and geological processes may induce variable changes in the chemical composition of partial melts syn to post migmatization. I will describe the effects of these processes on the chemical features of the leucosome .

#### *3.4.4.a. Fractional crystallization*

The partial melt of a batch melting process may undergo fractional crystallization after its formation, i.e. crystallized phases may segregate from the melt. Therefore, the "total" partial melt is composed of a cumulate and a fractionated melt. The REE patterns of fractionated melt, cumulate and the "total" are reported in Fig. I-25 (from Sawyer, 1987). This example illustrates the fractionation of plagioclase and/or K-fs as the cumulate shows LREE depletion, positive Eu anomaly and high Sr contents. It arises that the fractionated melt should be LREE enriched compared to the "total" melt with a negative Eu anomaly. However, if the crystallized phases contain monazite, the cumulate should be LREE enriched relative to the fractionated melt. In order to decipher whether accessory minerals are segregated crystallized phases, a positive correlation between REE contents and concentrations in HFSE is a strong argument (Nabaleck and Glascok, 1995).

#### *3.4.4.b. Chemical re-equilibration during cooling*

An example of chemical exchange during cooling is provided by Fourcade et al. (1992). They demonstrated that the sum of leucosome and melanosome match the paleosome arguing for a closed system during migmatization. However, the chemical composition of the leucosome and the melanosome do not picture those of partial melts and refractory residues. They argued that chemical diffusion transport for Rb, Sr and REE in the melt is faster by at least one order of magnitude than in the minerals considered. Consequently, they interpreted the unexpected chemical composition of leucosome and melanosome as the effect of chemical re-equilibration of the system during cooling.

*3.4.4.c. Effect of accessory minerals*

Accessory minerals are recognized as the main carrier of HFS and RE elements. Therefore, their behaviour during migmatization is critical for the interpretation of geochemical and isotopic data. 4 factors will affect the concentration of ESC in the anatectic melt: (1) the extend to which the accessory minerals are in contact with the melt, (2) the solubility of accessory minerals, (3) the rate at which the accessory minerals dissolve in the melt, and (4) the initial ESC concentrations of the protolith (Watt and Harley, 1993).

The first factor is essential as armouring accessory minerals within main minerals such as Bt, prevents chemical exchange between them and the partial melt (Watson et al., 1989). This will imply drastic effects on the isotope exchanges. In addition, if the partial melt escaped the site of partial melting shortly after its formation, no chemical equilibrium and full isotope exchange may be expected (Watt et al., 1996).

The second factor has been investigated experimentally by Rapp and Watson (1986) and Montel (1993). Montel (1993) describes monazite solubility in Ca-poor partial melts by the following equation:

$$\ln \frac{REE_t}{X_{REEPO_4}} = 9.5 + 2.34 \times D + 0.3879 \times \sqrt{H_2O} - \frac{13318}{T}$$

$$REE_t = \sum \frac{REE_i\ (ppm)}{at.weight\ (gmol^{-1})}$$

$$D = \frac{(Na + K + Li + 2Ca)}{(Al \times (Al + Si))}$$

where Na, K, Si, Al, Li and Ca are in atomic%, $H_2O$ in wt% and T is the absolute temperature. Sawyer (1991), Rapp et al. (1987) and Wickham (1987) suggested that the solubility of monazite is very low in peraluminous granite and it increases as melt composition becomes more and more metaluminous.

Zircon solubility can be described by the relationship:

$$LnD_{Zr}^{Zm/melt} = (-3.8 - 0.85 \times (M - 1)) + \frac{12900}{T}$$

$$M = \frac{Na + K + Li + 2Ca}{Al \times Si}$$

This equation is valid for peraluminous and metaluminous granitic melt containing > 2wt% $H_2O$ (Harrison and Watson, 1983; Watson and Harrison, 1983).

Pichavant et al. (1992) describes apatite solubility in peraluminous felsic melts as follows:

$$P_2O_5^{PMR} = P_2O_5^{HW} + P_2O_5^{Per}$$

$$P_2O_5^{HW} = \ln D_P^{Ap/melt} = \frac{8400 - 10000 \times 2.64 \times (SiO_2 - 0.5)}{T} - [3.1 + 12.4 \times (SiO_2 - 0.5)]$$

$$P_2O_5^{Per} = \left(\frac{A}{CNK} - 1\right) \times e^{\left(\frac{-5900}{T} - 3.22 \times SiO_2 + 9.31\right)}$$

which is a combination of Harrison and Watson (1983) studies and those of Pichavant et al. (1992). All these equations which relates the solubility of accessory minerals during anatexis are based on several assumption such the $H_2O$wt%, the value of A/CNK, and the empirical parameters. In addition, the rate at which the accessory minerals are dissolved in the melt are not yet well understood.

The last factor which concerns the concentration of ESC in the protolith is important as it controls in part the crystallization of accessory minerals in the melt or the residual occurrence of the accessory minerals in the refractory residue.

### *3.4.4.d. Lanthanide Tetrad effect*

The geochemical behaviour of trace element is controlled by their CHARAC (CHarge RAdius Controlled) features indicating that elements of similar charge and radius should display coherent behaviour, e.g. Zr anf Hf, or Y and Ho, or Nb and Ta. In magmatic system, highly evolved silicate melts ($SiO_2$ > 70 wt%) are rich in components such as $H_2O$, Li, B, F, P and Cl (Bau and Dulski, 1995). These rocks are also characterized by non-chondritic Zr/Hf ratios and irregular REE patterns which are subdivided into 4 concave-upward segments "Tetrad" (Bau, 1996). The non-CHARAC behaviour may be explained by chemical complexation of REE with a wide variety of ligants (F or Cl for example), leading to changed mineral/melt partition. Therefore, the Zr/Hf or Y/Ho ratios give constraints on whether or not the trace elements behave according to their CHARAC characteristics during magmatic process.

### *3.4.4.e. REE complexations*

It has been demonstrated that the occurrence of fluids is necessary to induce partial melting of the lower crustal section. The most probable fluid at mid to lower crustal level are $CO_2$, $H_2O$ and brine. During high-grade metamorphism, REE are considered as immobile elements (see Reference list in Grauch, 1989, p. 152). However, Stähle et al. (1987) suggested that the $[REE\ (CO_3)_3]^{3-}$ complex may transport REE during granulite facies metamorphism. The thermodynamic data for REE indicated that carbonate complexes predominate under low

temperature whereas at increased temperature, fluoride complexes become more and more important. Moreover, fluorine is a common major constituents in rock forming minerals of many granulite terranes (Valley et al., 1990; van der Auwera, 1993). Fluorine due to its affinity to the melt will be enriched in the late hydrated minerals. Consequently, fluorine which affects the phase equilibria and partial melting (Peterson et al., 1991; Zhu and Sverjensky, 1992), may play an important role in granulite facies metamorphism with respect of the transport of REE (Fleet and Pan, 1995; Pan and Fleet, 1996). Furthermore, Fyfe (1977) suggested that chlorine has a strong affinity with aqueous phases of a magma and it will tend to be concentrated in early formed hydrous minerals in a melt. Therefore, chlorine may affect the REE concentration during the retrograde metamorphism.

## 3.5. Migmatization effects on the isotopic systems

The behaviour of isotopic system during migmatization is of crucial importance for studies aimed at the understanding of crustal evolution through the geologic time. In Fig. I-26 are reported the isotopic geochemistry of typical, bulk crust and mantle reservoirs (after Moorbath and Taylor, 1986). The Fig. I-26 have been etablished from an isotopic compilation on several high-grade gneisses from cratonic areas bordering the N Atlantic (NW Scotland, N Norway, W-E Greenland). Granulites are known to be depleted in LIL elements and U (Rudnick and Presper, 1990). Rb-Sr and U-Pb isotopic studies on Archean-Proterozoic crustal and mantle-derived rocks demonstrated that (1) the lower continental crust and most upper mantle magma have similar Rb/Sr ratios but very different average U/Pb ratios; (2) Sr isotopes cannot discriminate, in the whole, between magmatic region in the lower crust and upper mantle; (3) Pb isotopes may help to decipher lower mafic granulites from the upper mantle source, (4) Rb/Sr and U/Pb ratios are highly variable within the continental crust according to the depth, the metamorphic grade and the lithology; (5) the upper continental crust as the product of partial melting of the lower continental crust is characterized by high Rb/Sr, Th/Pb and U/Pb ratios relative to the lower continental crust. The concentrations of incompatible elements in the lower mafic-felsic crustal sections are determined by Rudnick and Presper (1990), Rudnick (1992), Rudnick and Fountain (1995). If we consider a suite of low U/Pb granulites formed at $t_1$ which underwent a second metamorphic event at $t_2$ leading to U-addition (Fig. I-27), two main possibilities may be propossed for the evolution of the radiogenic lead isotopes: homogeneization at $t_2$ or incomplete homogeneization at $t_2$. In both cases, the primary Pb isotopic signatures of the suite of granulite were erased during the second metamorphic event. The erradication of the primary Sr isotopic features during metamorphism is also well demonstrated. As Sm and Nd are considered as immobile during metamorphism (Fig. I-26), the crustal evolution is best constrained by the use of the Sm-Nd system.

Figure I-26: Isotopic geochemistry of typical, bulk crust and mantle reservoirs. After Moorbath and Taylor (1986).

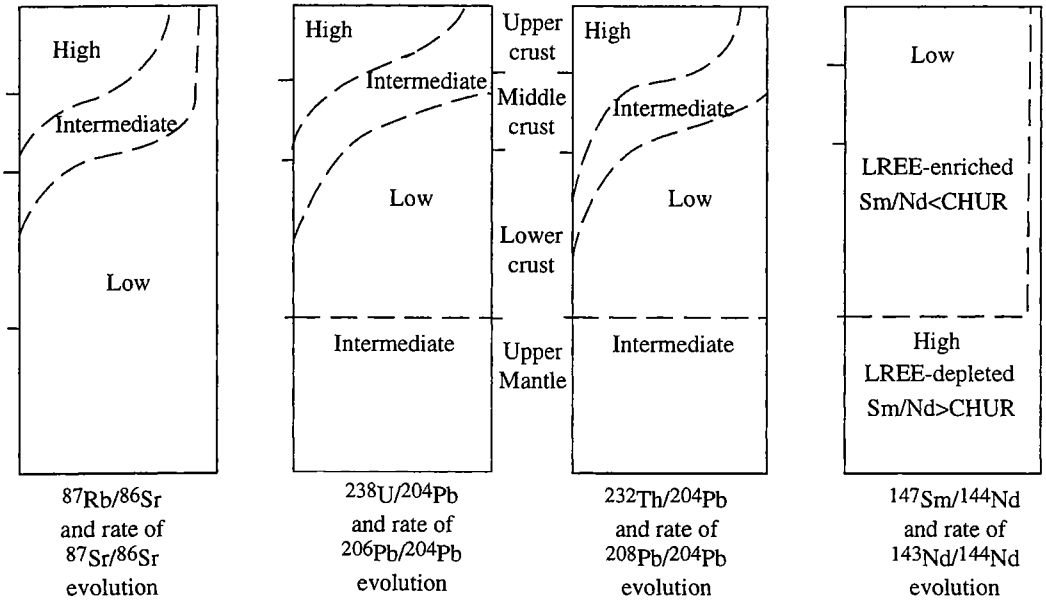


Figure I-27: A: Effect of U-addition at time $t_2$ to a suite of low U/Pb granulites, formed at time $t_1$, with Pb-isotopic homogenization at $t_2$ during crustal anatexis. B: ditto, but without Pb-isotopic homogenization at t2 during metamorphic retrogression. After Moorbath and Taylor (1986).

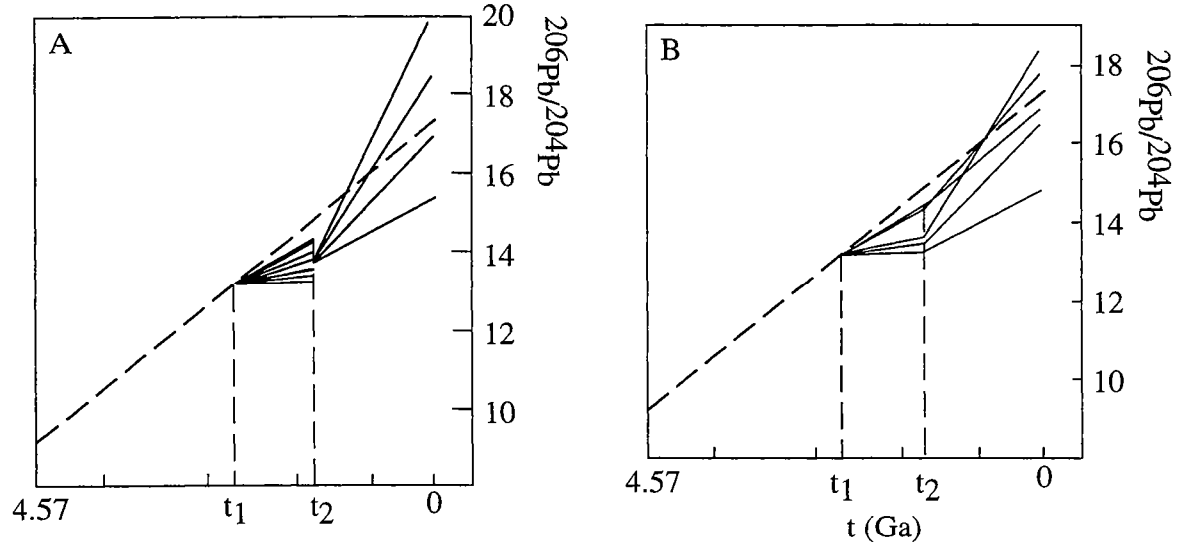

If the high-grade metamorphic event is characterized by a migmatization process, partial melts of granitic composition will be formed. The accuracy of Nd model ages on those melts depends on the non-fractionation of Sm/Nd ratio during partial melting. Additionally, contamination of the partial melts by the older surrounding rocks may occur (Fig. I-28; Arndt and Goldstein, 1987). Then, the Sm/Nd ratio of the melt corresponds to a mixing between that of its source and that of the incorporated rocks. Consequently, the initial Nd isotopic composition is meaningless in terms of crustal history. The effect on Sm/Nd ratios of mixing between partial melts and surrounding rock on the interpretation of crustal evolution may be avoided by considering only migmatized rocks which have $^{147}Sm/^{144}Nd$ ~0.12, the average value of the whole continental crust. However, the Nd isotopic composition would still be a mixture. $T_{DM}$, therefore, represent average crust ages, and do not date geologic events. Three main possibilites on the behaviour of the Sm-Nd system and its implications that follow on crust-formation ages are discussed: (1) no perturbation (Fig. I-29), (2) resetting (Fig. I-30), and (3) incomplete isotope exchange (Fig. I-31). These diagrams correspond to theoritical disturbation of the Sm-Nd system, and even more complicated perturbation may occur in nature.

A crustal rock suite is formed at $t_1$ from the mantle and its Sm/Nd ratio scattering within the suite is significantly lower than that of the mantle. At $t_2$ the suite undergoes a high-grade metamorphic event but their Sm/Nd ratio are not affected by the changement of environmental conditions. Consequently, Nd model ages on each rock of the suite will give the age at which the magma is separated from the mantle. The $T_{DM}$ obtained are useful indicator for crustal growth studies.

The second case illustrated in Fig. I-30 highlighted the record of the metamorphic event by the rock suite. At $t_2$ the variation in Sm/Nd ratio of the rock suite is changed and each sample took the same average Nd isotopic composition. Therefore, the primary Nd isotopic features of the protolith are erased but the similar epsilon Nd values of each sample at $t_2$ suggested either an age formation at $t_2$ or a full Sm-Nd resetting of the whole rock suite at $t_2$. Furthermore, the whole rock isochron will never give the true formation age but the metamorphic age in agreement with the Sm-Nd mineral isochron age. From the point of view of Nd model ages, they are meaningless in terms of crustal history. Nonetheless, $T_{DM}$ scater around the true formation age and provide consequently a time interval for crust formation (shaded area).

Incomplete Nd isotope exchange during metamorphism is certainly the worst case for Sm-Nd systematics on crustal rocks. At $t_2$ the rock suite undergoes a metamorphic event which changes the Sm/Nd ratio in each sample but no full Nd isotope homogeneization is attained (Fig. I-31). For example, a partial melt formed at $t_2$ by migmatization allowed the

Figure I-28: Theoritical example of how Sm/Nd ratio and Nd model ages on partial melts can be unrelated to crust-formation event. The Sm/Nd ratio of partial melt may represent a mixing between that of its source and that of the incorporated rocks. After Arndt and Goldstein (1987).

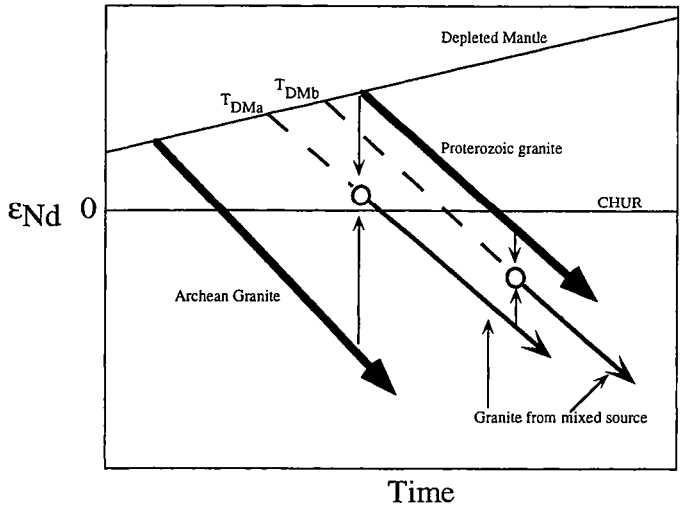


Figure I-29: Ideal case of the behaviour of Sm-Nd system during migmatization. The Sm/Nd ratio of each rock is not fractionated during the high-grade metamorphic event at $t_2$.

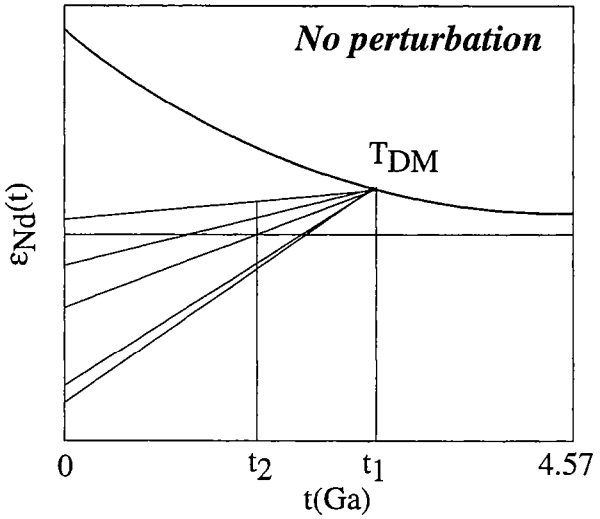


Figure I-30: Theoritical case of the behaviour of the Sm-Nd system during migmatization illustrating the record of the metamorphic event by the rock suite at t2. Primary Nd isotopic features are erased but full Nd isotopic exchange took place at $t_2$.

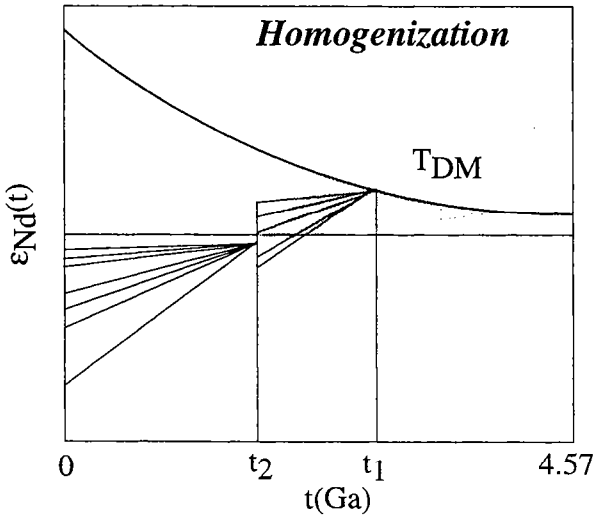

crystallization of newly formed minerals. However, due to melt migration or partial dissolution or entrainment of accessory minerals, the partial melt did not reach chemical equilibrium with the refractory residue. Therefore, the partial melt will acquire Sm-Nd isotope features decoupled from its original rock. Samples enriched in old and high Sm/Nd ratio minerals at t2 (such as Grt for example) attain a higher Nd isotopic composition than samples containing relectic low Sm/Nd minerals (such as Mnz) In both cases, the Sm/Nd ratios of the partial melts are changed. Under such circumstances, no mineral Sm-Nd isochron can be obtained and the TDM of each samples are meaningless.

By analogy to the diagram proposed by Arndt and Goldstein (1987) who demonstrated that a granite pluton may be a mixing between a mantle-derived granite and an older granite, I suggest a similar Sm-Nd diagram which shows that, from an unique mantle-derived rock, two different rocks may be formed. In both cases, "use and abuse crust-formation ages" are critical for the understanding of crustal growth with the Sm-Nd system.

Figure I-30: Theoritical example of incomplete Nd isotope exchange during metamorphism. Fractionation of the Sm/Nd ratio may be related to the behaviour of minerals.

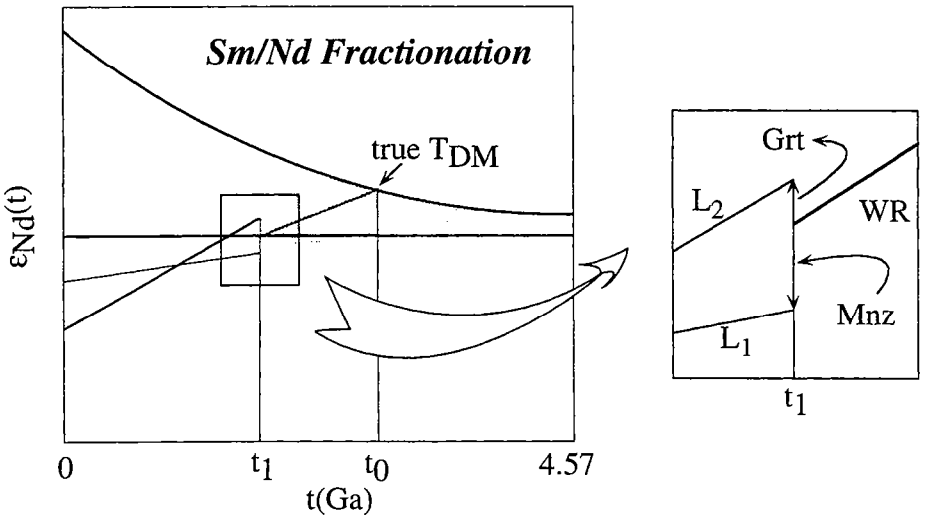


Figure I-31: By analogy to Arndt and Goldstein (1987), the bebaviour of the Sm-Nd system may be also fractionated and the Nd model ages are unrelated to geological event.

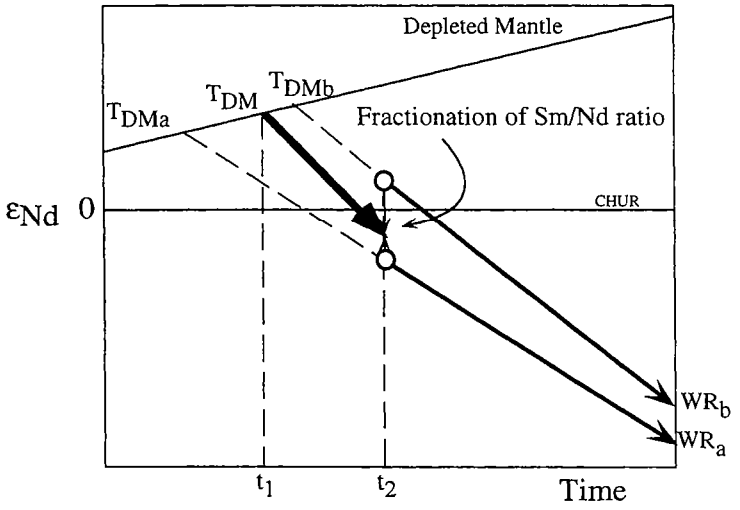

# 4.Migmatization at 2.0 Ga in the Mahalapye Complex, Limpopo Belt, Botswana: Implications on Nd model ages

Valérie Chavagnac[1], Jan D. Kramers[1], Lorenz Holzer[1],

Thomas F. Nägler[1], Boikobo K. Paya[2]

1: Universität Bern, Min. Pet. Inst., Gruppe Isotopengeologie, Erlachstrasse 9a, 3012 Bern, Switzerland. e-mail address of the corresponding author: chava@mpi.unibe.ch

2: Department Geological Survey of Botswana, P/BAG 14, Lobatse, Botswana.

**submitted to Contributions to Mineralogy and Petrology**

## Abstract

We have carried out major and trace element analyses as well as Nd isotope measurements on different components of a migmatite outcrop in the Mahalapye Complex (Botswana) in order to assess the effect of migmatization during a high grade metamorphic event on Sm-Nd systematics and Nd model ages.

The Mahalapye Migmatite unit is situated in the westernmost part of the Central Zone of the Limpopo Belt. At the studied locality (Lose Quarry) Leucosomes of a granitic and peraluminous composition formed by incongruent biotite melting in a Fe-rich metagreywacke. Monazite U-Pb and garnet Sm-Nd ages yield close to 2.0 Ga for the high grade event, confirming other recent work in the CZ. The chemical compositions of the main mineral phases (Pl, Bt and Grt) indicate minimum melt formation at T>750°C and P<7 kbars. The partial melts are enriched in Rb/Sr, K/Na, and Ba and contain equal K/Ba or Na/Sr ratios compared to paleosomes, indicating that the nascent melt did not equilibrate extensively with the residual feldspars and biotite in the paleosomes. Moreover, the distribution of Th, U, La and Ce between these migmatitic components show that monazite influenced the bulk REE, Th and U budget and was entrained or dissolved in partial melt in leucosomes in preference to apatite. Sm-Nd results on whole rocks do not form an isochron. When calculated back to 2.0 Ga, the paleosomes fall in a narrow range of $^{143}Nd/^{144}Nd$ around $\varepsilon_{Nd}$ = -4. The $\varepsilon_{Nd}$ values of leucosomes are on average 4 units lower, causing them to have apparent $T_{DM}$ ages in the mean 250 Ma older than those of the paleosomes. We conclude that metasedimentary rocks can retain primary Nd isotope heterogeneities during migmatization, and REE-bearing minerals within them may escape full Nd isotope exchange. Rather than defining the protolith crustal age as a weighted average of the $T_{DM}$ ages derived from a migmatite outcrop, the true spread in mantle derivation ages for the sediment source region probably exceeds the range of $T_{DM}$ ages found in the outcrop.

# 1. Introduction

Sm-Nd systematics have been used extensively to study the growth of continental crust through the history of the Earth. Approaches making use of initial $\varepsilon_{Nd}$ values and Nd model ages are based on the assumption that there is little or no fractionation of Sm/Nd ratios during intracrustal processes such as metamorphism, fractional crystallization and even partial melting (McCulloch and Wasserburg, 1978). However, some recent studies have provided examples of obvious disturbance of the Sm-Nd system during these processes (Moorbath et al., 1997; Whitehouse et al., 1996; Gruau et al., 1996; Bock et al., 1994; Bernard-Griffiths et al., 1991). It has become apparent that not only isotopic resetting of the Sm-Nd system in whole rock suites can occur, but also, that some fractionation of the Sm/Nd ratio can take place during migmatization. These observations potentially put many wide ranging conclusions from crustal Sm-Nd work into question.

Migmatites provide an opportunity to study the chemical fractionation which occurs during partial melting in the crust. The mass balance of major and trace elements during the anatectic process can often be quantitatively evaluated (Olsen, 1986; Bea, 1996). Thereby, recent geochemical studies suggest that major and particularly trace element equilibrium between melt and residue is not always attained. From studies based on structural and petrological observations combined with geochemical and trace element modelling, several mechanisms have been proposed to explain such chemical disequilibrium, particularly with regard to Th, U and the REE. Apatite, monazite and zircon mainly control the REE as well as Th and U budget of a rock, and equilibration of nascent melt with these accessory minerals could be poor (Sawyer, 1991; Watt and Harley, 1993) whereby armoring within residual phases would be an important, but not necessary, contributing factor (Johannes et al., 1995; Nabelek and Glascock, 1995; Wolf and London, 1994; Watt and Harley, 1993; Montel, 1993; Watson and Harrison, 1983; Green and Watson, 1982). This would be particularly important in rapid melt extraction (Watt et al., 1996). Alternatively, Fourcade et al. (1992) suggest that trace element features of migmatites may be altered by chemical exchange during cooling. Whatever the underlying cause for chemical disequilibrium between the different domains of a migmatite, it is clear that full isotope exchange of Nd ("resetting" of the Sm-Nd isotope system) cannot be assumed to have taken place while it persists.

This paper is aimed at gaining some understanding of mechanisms controlling Sm/Nd ratio fractionation during migmatization, and at assessing Nd isotope exchange. The motivation for this is the need to strengthen the basis for the interpretation of Sm-Nd data in terms of crustal history. The study focusses on the REE distribution and Nd isotopic composition in partial melts and restitic components within the Mahalapye Migmatite Complex, Botswana, in the Central Zone of the Limpopo Belt. This complex shows well exposed

Figure I-32: Geological map of the southwestern part of the Limpopo Belt, in Botswana, map modified after Geological Survey of Botswana, South Africa and Zimbabwe (1981). MoSZ: Mogagaphate Shear Zone, MSZ: Molabe Shear Zone, LSZ: Lepokole Shear Zone.

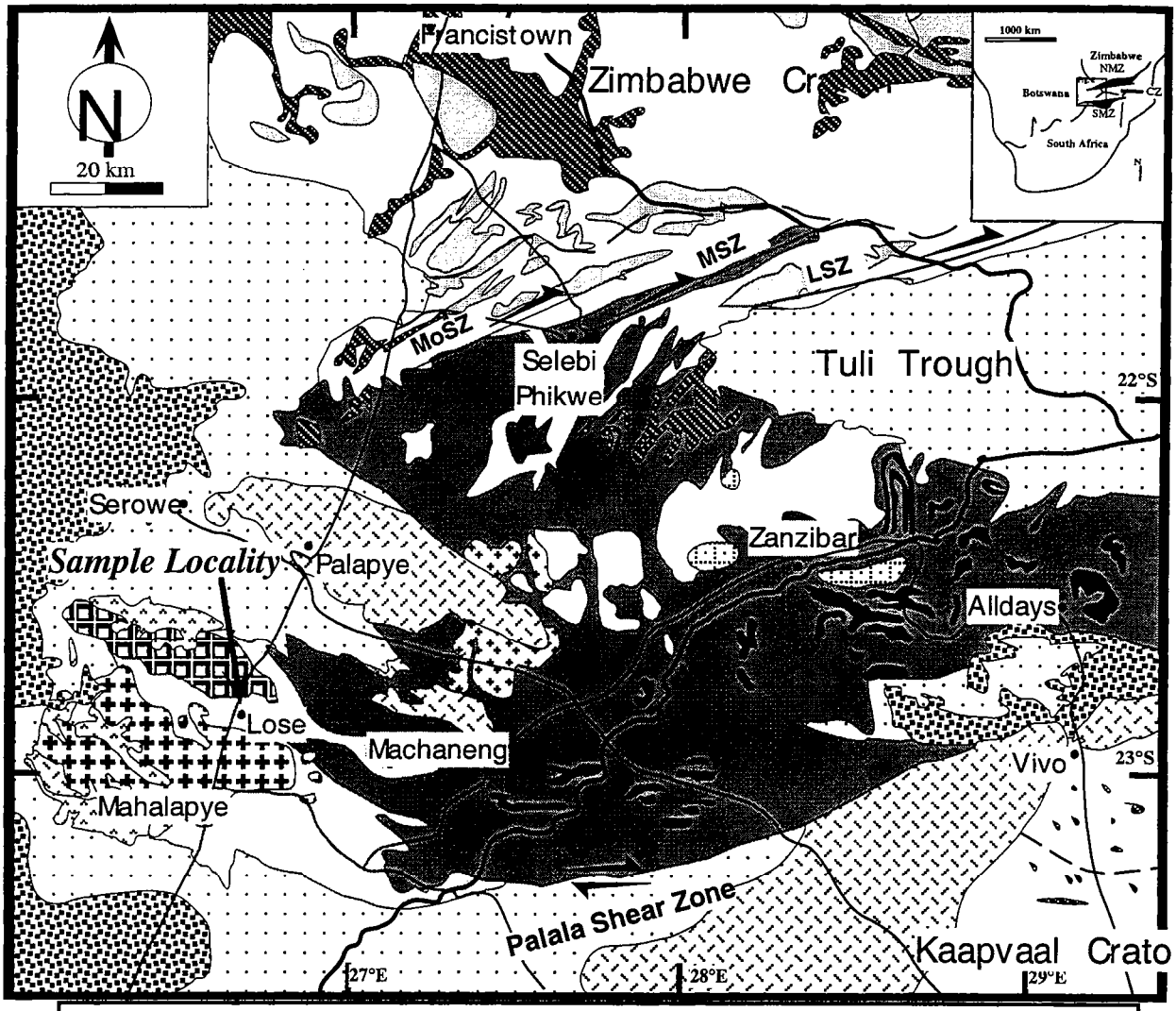


Craton : Tonalite Gneisses

Granodiorite gneisses

Greenstone Belts

Porphyritic granites

Bulaï Gneiss : pophyroblastic adamellitic and charnoenderbitic gniesses

**Kalahari** sediments

**Karoo** : sediments overlain by volcanics

**Palapye Group** : dolerite

**Soutpansberg trough** : clastic sediments with intercalated volcanics

**Central Zone granulites** : metasediments, paragneisses and intercalated orthogneisses

**Mafics to ultramafics rocks, Messina Suite** : meta-anorthosites, metagabbros, hornblendites, and Qtz-Hbl gneisses

**Mahalapye Complex**

Mahalapye Granite

Mahalapye Migmatite

Mokgware Granite

Boundary limits

Limit between Kaapvaal Craton to the South with the Southern Mariginal Zone to the North

Limit between Zimbabwe Craton to the North with the Northern Mariginal Zone to the South

Roads

Towns

migmatitic components from cm to outcrop (~10m) scale. Our scope is fourfold. First, mineral ages (Sm-Nd on garnet, monazite and apatite; U-Pb on monazite) are used to constrain the timing of high grade metamorphism and associated migmatization in this part of the Central Zone. Second, the trace element chemistry and Sm-Nd systematics of leucosomes are compared with paleosomes in order to assess the trace element fractionation and degree of equilibrium between parts of the suite. Third, the amount of Nd isotope exchange ("resetting" of the Sm-Nd system) during the high grade metamorphism and associated migmatisation is examined, and fourth, the Sm-Nd systematics are (with the caution learnt from the previous three steps) evaluated in terms of the regional crustal history.

## 2. Geological setting

The Limpopo Belt is a high-grade metamorphic province wedged between the Archean Kaapvaal and Zimbabwe Cratons to the North. It is subdivided into three subzones: the Northern and Southern Marginal Zones (NMZ and SMZ), and the voluminous Central Zone (CZ). Two Proterozoic strike slip shear belts mark the suture zones between the CZ and the marginal zones (e.g. Holzer et al., 1997).

The granulite facies metamorphism in all three subzones has previously been explained as the product of a late Archean continental collision; the "Limpopo Orogeny" (e.g. Van Reenen et al., 1992; Barton and Van Reenen, 1992; Light, 1982). However, recent combined petrological, structural, geochemical and geochronological work has indicated important tectonic reworking and high grade metamorphism in the CZ and part of the NMZ at 2.0 Ga (Jaeckel et al., 1997; Kamber et al., 1995, 1996; Barton et al., 1994). Holzer et al. (1997 and submitted) conclude that each of the subzones is characterized by a distinct Archean tectono-metamorphic history and that the final juxtaposition of the CZ with the SMZ and NMZ occurred during this 2.0 Ga old event, which they describe as a transpressive orogeny. Furthermore Holzer et al. (1997) suggest a direct tectonic relationship between the transpressive orogeny in the Limpopo Belt and two Proterozoic thrust-fold belts at the western rims of the Kaapvaal and Zimbabwe Cratons (Kheis and Magondi belts).

The Mahalapye Complex (MC) is situated close to the junction of the Limpopo CZ with these Proterozoic belts and defines the westernmost extension of the CZ into Botswana (Fig. I-32). It consists of three distinct lithological units: the Mahalapye Migmatites, the late-tectonic Mokgware granite and the post-tectonic Mahalapye granite (Ermanovics, 1980; Key, 1979; Skinner, 1978). The northern and southern boundaries of the MC are both defined by shear zones that were active in variable tectonic regimes and at different metamorphic grades. However, no structural discontinuity has been found between the CZ further to the east (Beit Bridge area) and the Mahalapye Migmatites (Holzer et al., 1998). Assuming contemporaneous

Figure I-33: Spatial relationship between leucosomes and paleosomes are drawn in broad outline.

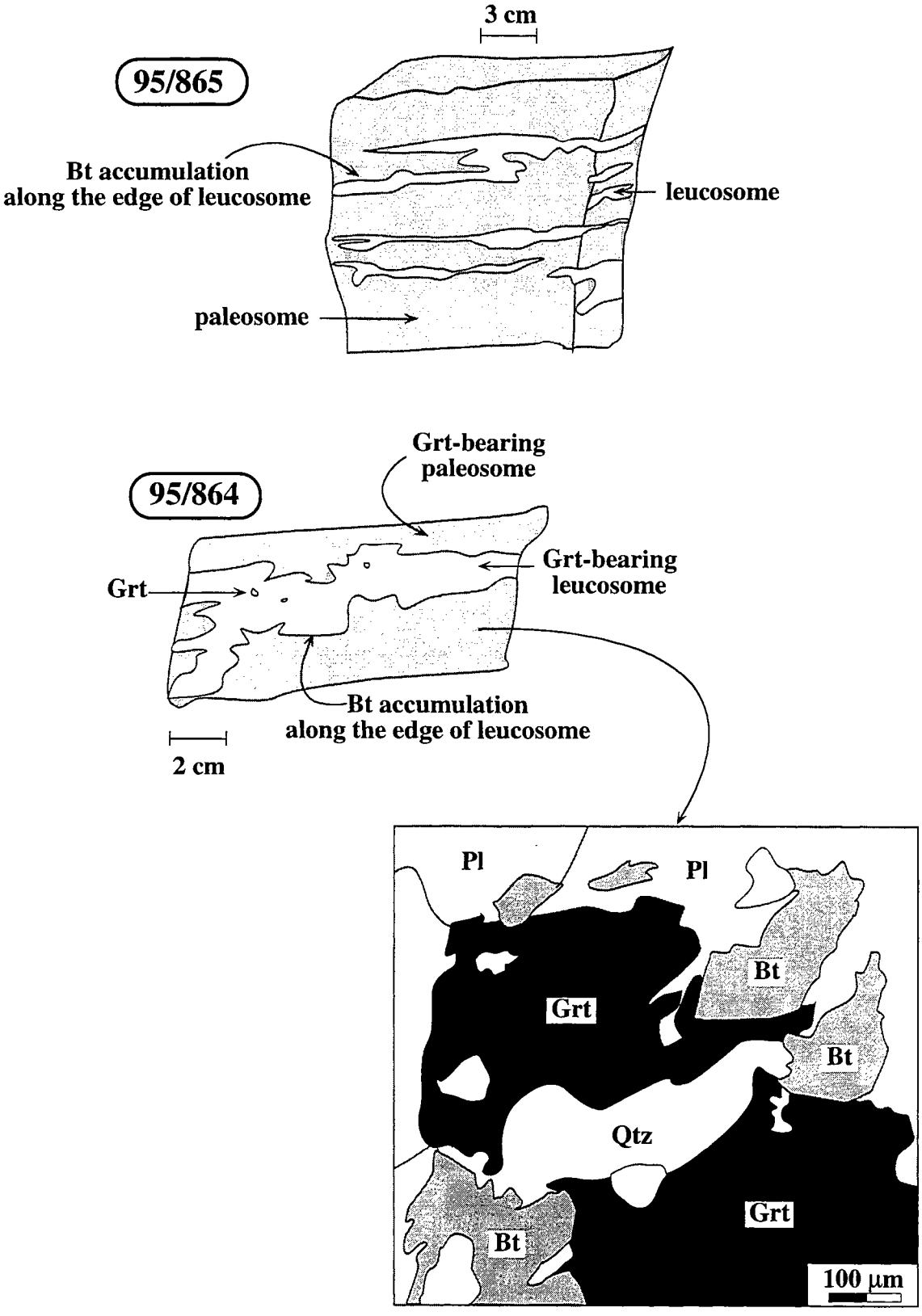

metamorphism, this supports a continuous transition from high pressure granulites in the Beit Bridge area (Droop, 1989) to higher crustal levels with medium pressure and high temperature metamorphism in the Mahalapye Complex (Hisada and Paya, 1997). Within the MC, an overall continuous increase of melt fraction occurs from east (CZ) to west (MC). The migmatites grade into massive plutonic bodies and therefore on a map scale no sharp contact between the Mahalapye Migmatites and the Mokgware and Mahalapye granites can be drawn. Field observations thus do not support a scenario in which a tectono-metamorphic event (producing migmatites) was followed by the intrusion of granites at shallow crustal levels. Instead, voluminous granitic melts appear to have been mobilized during widespread syn-tectonic migmatization. The sources of these melts may partly be in situ, and partly at lower crustal levels.

## 3. Sample locality and description

All samples for this study were taken from Lose Quarry which is situated north of Mahalapye town in the center of the Mahalapye Migmatite Complex. The Lose gneisses represent a relatively small portion (few %) of the entire migmatite complex. They are strongly foliated and migmatized gneisses, containing more plagioclase than alkali-feldspar and ranging from meso- to melanocratic (restitic) biotite-rich in composition. Garnet, orthopyroxene or amphiboles may occur in minor and variable amounts.

Geochemical characteristics (see below) indicate greywacke as a potential protolith Metagreywackes are a fertile lithology for the production of granitic melt during regional anatexis (Clemens and Vielzeuf, 1987; Patiño Douce and Beard, 1996). At Lose Quarry, migmatization is observed on different scales. Within the mesocratic 'palaeosome', cm-size garnetiferous Qtz-Fs patches occur. Such leucosome patches may grade into concordant stringers and veinlets, and further into veins on m-scale, with a partly garnetiferous leucogranitic composition. A clear biotite accumulation is seen along the edge of leucosomes either on a centimeter scale (Fig. I-33), or on the outcrop scale. Theses textures are interpreted as the result of in situ melting with garnet formation, followed by progressive mobilization. While the migmatites are folded, leucogranite veins show little to no deformation. Thus migmatization appears to have occurred mainly syntectonically, while late mobilization of in situ produced leucosome postdated the last high grade deformation.

The samples taken for this study include four meso- to melanocratic, broadly homogeneous metagreywackes (95/864, 95/865, 95/866, and 95/868) as well as four leucosomes (95/860, 95/861, 95/862, and 95/863) which are spatially associated with migmatitic metagreywackes and are interpreted as having been produced locally. The metagreywackes are hereafter referred to as paleosomes. On the basis of the relationship

Figure I-34: Isocon diagram according to the graphical representation of Grant (1986). We used as parental protolith a paleosome (95/865) and as a result of migmatization a garnet-bearing leucosome. The best fit isocon is represented by Al, Na, Mn, P, and Sm and it is distinct from the isocons corresponding to either mass conservation or volume conservation isocons. Melt escape may be suggested.

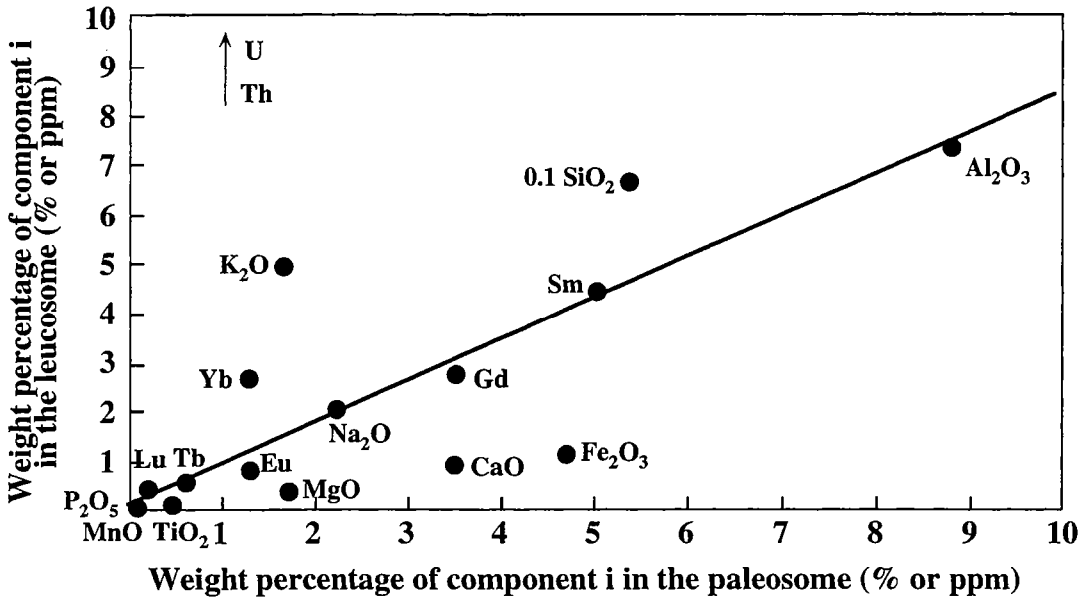


Table I-9: Modal analyses of leucosomes and paleosomes (in vol% with 1500 point counts on each thin section).

| sample number | type | Qtz | Pl | Mc | Bt | Cum | Grt | Ap | Mnz | Zrc | Ores |
|---|---|---|---|---|---|---|---|---|---|---|---|
| **95/860** | leucosome | 28.8 | 18.5 | 46.1 | 6.4 | - | - | - | x | x | <1 |
| **95/861** | leucosome | 36.6 | 18.6 | 33 | 5.8 | - | 5.8 | - | x | x | <1 |
| **95/862** | leucosome | 24.3 | 18.8 | 55.3 | | - | 1.6 | - | x | x | - |
| **95/863** | leucosome | 32.6 | 39.1 | 21 | 7.3 | - | | 1.3 | x | x | - |
| **95/864** | paleosome | 27.7 | 45 | 5.1 | 21.8 | - | 0.4 | x | x | x | <1 |
| **95/864L** | leucosome | 19.04 | 15 | 15 | - | - | 50 | 0.05 | 0.01 | - | - |
| **95/865** | paleosome | 33.9 | 18.6 | 6 | 21.5 | 15 | 1 | 2 | 0.01 | 0.01 | <1 |
| **95/866** | paleosome | 24.5 | 39.4 | 20.4 | 14.7 | - | 1 | - | 0.01 | 0.01 | <1 |
| **95/868** | paleosome | 30.6 | 12 | 13.6 | 30.6 | - | 2 | 2 | x | x | <1 |
| **95/868L** | leucosome | 19.04 | 15 | 15 | - | - | 50 | 0.05 | 0.01 | - | - |

Mineral abbreviations according to Kretz (1983)
xx: occurrence; x: few occurrence

between minor leucocratic and foliated melanocratic domains within them, three kinds of paleosome can be distinguished. Those of the first, exemplified by samples 95/864 and 95/868, contain garnet-bearing leucocratic pods (analyzed separately as leucosome parts 95/864L and 95/868L) which postdate the deformation. The second type (95/865) contains very thin bands of leucosome concordant with the foliation. In the third type (95/866) thin slightly deformed quartzo-feldspathic veins occur. Leucosomes can likewise be heterogeneous and samples 95/861 and 95/863 were split into two parts: from 95/861 a biotite free, garnet rich part (95/861L) and from 95/863 a biotite rich, restitic layer or melanosome (95/863B) were separated.

In order to test further the cogenetic relation between partial melts and paleosomes we used a graphical Gresens' method (Olsen and Grant, 1991) to assess variations in the concentrations of elements during migmatization. Fig. I-34 shows results, using as a parental rock before migmatization a paleosome and as result of migmatization a garnet-bearing partial melt. The best fit isocon is defined by Al, Na, Mn, P, and Sm and it is distinct from the isocons corresponding either to constant mass or constant volume. As a consequence, the transformation of paleosome (for example 95/865) into the leucosome (for example 95/861) according to migmatization process, implies 1) a mass decrease of 5 percent of the paleosome, 2) K and Si gains for the leucosome, and 3) gains of Mg, Ca and Fe for the paleosome. The distribution of major elements are in agreement with the participation of Bt and Pl in the leucosome formation, and local derivation of melt during migmatization on the outcrop scale as well as on the centimeter scale is suggested.

*Sample description*

The modal mineralogical composition of the studied samples is given in Table I-9. All partial melts have granitic to alkaligranitic compositions with a few vol% of either biotite (Bt) or garnet (Grt) or both. The leucosomes are characterized by heterogranular and granoblastic textures. Lobate grain boundaries between feldspar (Fs) and quartz (Qtz) and myrmekite formation at plagioclase (Pl) - K-feldspar (K-Fs) boundaries indicate high temperature subsolidus recristallization. Grt can occur as small idiomorphic grains but mainly forms aggregates with coarse, irregularly shaped grains, intergrown with lobate Fs and Qtz. Fs and Qtz also occur as kidney shaped inclusions within Grt. Apatite (Ap), zircon (Zrn), monazite (Mnz), and magnetite (Mag) are important accessory phases. Ap and Mnz occur interstitially at grain boundaries, and Zrn mainly as inclusions in Bt, Pl or even K-Fs. Ap is found as hypidiomorphic grains whereas Zrn and larger Mnz (100-300μm) mostly consist of rounded cores, rimmed by an idiomorphic overgrowth. Minute grains of Mnz found at grain boundaries are not zoned.

The meso- to melanocratic metagreywackes (95/864 and 95/868) consist mainly of Qtz, Pl, Bt, with small amounts of K-fs and Grt. These minerals form a grano-lepidoblastic texture with a well defined foliation. Accessory minerals are Ap, Zrn, Mnz and Mag. Zrn has rounded cores overgrown by subhedral rims. Small Zrn occurs as inclusions in Bt. Mnz is confined to grain boundaries. Adjacent to the leucocratic pods the paleosomes are enriched in Bt (up to 50%). Grt in these leucosomes may form 2-3 cm big aggregates consisting of sinoidal grains, intergrown with lobate and kidney shaped Qtz and Pl. Fracturing is frequent in Grt. A second generation of green Bt has formed at the rims of Grt and within fractures. Sample 95/865 is characterized by the occurence of cummingtonite (Cum) together with Pl, Qtz and Bt. The foliation is defined by the perfect alignment of Cum, Bt and elongated Pl. No Opx or Grt were identified. Accessory minerals are Ap, Zrn, Mnz and Mag. Ap occurs in two varieties: As euhedral grains (up to 200 μm) which are mainly located within Bt and Pl, and as rounded ones (up to 300 μm) with an internal zonation, which occur at grain boundaries. Sample 95/866 is a garnetiferous Pl-Qtz-K fs-Bt gneiss. The grano-lepidoblastic matrix is well foliated. The foliation is also observed within the concordant leucocratic bands which consist of Qtz, Pl, K-fs and minor Bt.

In all these samples minor retrograde reactions have been observed. Bt has locally grown at the expense of garnet, and has then be replaced by chlorite or prehnite. Muscovite and associated calcite formed in fractures during late hydrothermal overprint.

In order to define the relationships between the rock types and provide a framework for the isotope studies, all samples were analysed for major and some trace element concentrations. Microprobe analyses were carried out on samples 95/864 and 95/866 and also on 95/861.

## 4. Analytical techniques

Major and trace elements were determined by X-ray fluorescence spectrometry (XRF) using a Philips spectrometer at the University of Rennes 1. Relative analytical uncertainties range from ±1% to ±3% for major elements, around ±5% for trace elements with concentrations around 20 ppm and around ±10% for those < 20 ppm. Nb was determined with long counting time so that the precision was maintained at ~±10% even for concentration less than 5 ppm. Some trace elements and REE were determined by INAA at ACTLABS, Canada. The detection limits are shown in brackets in Table 3.

Mineral compositions were analyzed with a Cameca SX50 electron microprobe at Microsonde Ouest in Brest (France), operating at 15 kV high voltage and 20 nA beam current.

For Sm-Nd analysis, about 100 mg of powdered rock samples or 50 mg of different size fractions of garnet (samples 95/864 and 95/868) were spiked with a $^{150}Nd$-$^{149}Sm$ tracer before dissolution. Sample dissolution was carried out in two steps. First, the samples were dissolved with a 1:3 mixture of ($HNO_3$ + 40% HF 1× dist) in a sealed savillex beaker at room temperature for one day. In order to break down any fluorite complexes and facilitate the dissolution, the Savillex beaker was repeatedly placed in an ultrasonic bath for 20 minutes. After one day, the solution was evaporated to dryness. The same acid mix was added a second time and was heated at 150°C for seven days. During this time the Savillex beaker was placed in an ultrasonic bath for 20 minutes twice a day. After evaporating to dryness, any remaining fluorites were eliminated by treating the samples with 6N HCl on a hot plate during several hours. Apatite was spiked with a $^{150}Nd$-$^{149}Sm$ tracer and attacked with 6N HCl at 150°C for two hours. Monazite was dissolved in $HNO_3$ + 40% HF 2xdist (for U-Pb) or $HNO_3$ + HCl (for Sm-Nd) in a Teflon bomb at 200°C for several days together with a mixed tracer ($^{205}Pb$-$^{235}U$ or $^{150}Nd$-$^{149}Sm$). Separation of Sm and Nd was done by a group separation of REE through a cation exchange column, followed by a separation of Nd from Sm through a second column packed with Kel-F Teflon coated with HDEPH, conditioned and eluted with dilute HCl. U and Pb were separated using standard anion exchange. Mineral and chemical separations have been done at the University of Bern.

Whole rock and apatite Nd isotope analyses were done at the University of Rennes 1 using double Re filament ($Nd^+$ emission) in a seven-collector Finnigan MAT 262 mass spectrometer in semi-dynamic mode. $^{143}Nd/^{144}Nd$ ratios were normalized against $^{146}Nd/^{144}Nd = 0.7219$. During the period of data acquisition, the AMES standard gave $^{143}Nd/^{144}Nd = 0.511967 \pm 0.000007$ (2 standard deviation; n=20) and the La Jolla standard gave $0.511856 \pm 0.000006$ (2 standard deviation; n=15). Nd isotopic compositions of garnet fractions were analysed using single Re filament ($NdO^+$ emission) in a modified VG Sector mass spectrometer at the University of Bern in single collector mode. The oxygen composition used for isotopic corrections was determined by analysing pure $^{150}Nd$ spike as described by Wasserburg et al. (1981) and the average compositions gave $^{18}O/^{16}O = 2.024\ 10^{-3} \pm 0.23\ 10^{-3}$ and $^{17}O/^{16}O = 3.83\ 10^{-4} \pm 0.03\ 10^{-4}$ which are close to the Nier (1950) value $^{18}O/^{16}O = 2.045\ 10^{-3}$. Mass interference and oxygen corrections as well as fractionation and spike corrections are done on-line during the measurement. La Jolla standard gave $0.511840 \pm 0.000029$ (2 standard deviation; n=6). In order to confirm the Nd isotopic compositions, we duplicated one sample for which we used different spikes. The results indicate that the reproductibility for Sm/Nd using different spike concentrations are within the errors and confirm the Nd isotopic compositions obtained. Pb isotopic compositions were measured on Re single filament on the VG Sector in static multi-collector mode; fractionation correction was done empirically using measurements of the NIST SRM 981 Pb standard, and amount to 0.08 ± 0.02 % per mass unit. All Sm and U isotopic compositions were analysed from triple Ta-Re-

Ta filaments on an AVCO, single collector mass spectrometer at the University of Bern. The uncertainty on Sm/Nd ratios is less than ±0.3%. Chemical procedural blanks are Sm ~50pg and Nd ~150 pg and Pb ~50pg.

Sm-Nd model ages were calculated relative to depleted mantle evolution. The Nd evolution of the Depleted Mantle is approximated by a third order polynomial fit:

$$\varepsilon_{Nd}\,(T)_{sample} = 0.164T^3 - 0.566T^2 - 2.79T + 10.4 \text{ (Nägler and Kramers, 1998)}$$

## 5. Mineral compositions and metamorphic conditions

Representative microprobe analyses of Bt, Pl and Grt from samples 95/864 and 95/866 are shown in Table I-10. The stochiometric formulas are calculated on the basis of 8 (Pl), 16 (Grt) and 22 oxygen atoms and 4(OH, F, Cl) ions (Bt).

Bt in these rocks is always associated with Fe-Ti oxides, so that the Ti versus $Al_{VI}$ diagram (Schreurs, 1985) can be used to estimate the metamorphic grade (Fig. I-35a for 95/864 and 35b for 95/866). Most Bt are characterized by high Ti-contents and plot into the high temperature field (T°>750°C) or close to the boundary of this field. Bt which are texturally associated with resorbed Grt have lower Ti contents and variable $Al_{VI}$ contents, which indicates retrograde growth of Bt at the expense of Grt.

Pl compositions are plotted in an Or-Ab-An triangular diagram (Fig. I-36a for sample 95/864 and Fig. I-36b for sample 95/866). Two main features can be noted: 1) Compositions range between andesine and oligoclase; 2) Some plagioclases have a high Or content (up to 20%) which is related to the antiperthite formation.

In Grt from samples 95/864 and 95/866, slight compositional variations are visible in microprobe scan profiles (Fig. I-37 and I-38). The zonations are restricted to a thin rim (up to 70 μm) at the contact with Bt as well as Fs either in the matrix, or occurring as inclusions. At joint boundaries with Bt, smooth Fe and Mn enrichment correlates with Mg depletion whereas Ca contents are quite constant. In contrast, at joint boundaries with plagioclase, Ca contents of garnets increase sharply whereas the other elements remain virtually constant. All data from the sections are shown in Fig. I-39 for sample 95/864 and Fig. I-40 for sample 95/866. The garnets of 95/866 have more restricted end-member mole proportions ($Prp_{8-14}Alm_{70-74}Grs_{4-6}Sps_{9-14}$) than the garnets of 95/864 ($Prp_{7-17}Alm_{72-78}Grs_{4-6}Sps_{3-8}$). Garnets from sample 95/866 have an almandine-rich composition and the Prs and Sps end-members vary in the same order (Fig. I-39). Moreover, the chemical compositions, from core to rim on garnet 95/864 form a linear trend.

Table I-10: Representative chemical analyses and cation proportions of biotite, plagioclase and garnet of samples 95/864 and 95/866.

sample 95/864

| biotite | | | plagioclase | | | | garnet | rim | core |
|---|---|---|---|---|---|---|---|---|---|
| SiO2 | 34.40 | 35.38 | SiO2 | 61.54 | 62.51 | 59.95 | SiO2 | 37.54 | 37.76 |
| TiO2 | 2.43 | 2.74 | Al2O3 | 24.46 | 23.98 | 25.24 | Al2O3 | 21.24 | 21.24 |
| Al2O3 | 17.14 | 16.57 | Fe2O3 | 0 | 0.08 | 0.16 | MgO | 3.94 | 4.26 |
| Cr2O3 | 0.00 | 0.00 | CaO | 6.18 | 5.57 | 6.91 | FeO | 32.97 | 33.18 |
| FeO | 23.87 | 22.94 | Na2O | 7.97 | 8.51 | 7.74 | MnO | 2.82 | 2.65 |
| MnO | 0.03 | 0.17 | K2O | 0.2 | 0.09 | 0.1 | Cr2O3 | 0.00 | 0.03 |
| MgO | 8.93 | 8.56 | -> | 100.35 | 100.74 | 100.1 | TiO2 | 0.00 | 0.02 |
| CaO | 0.00 | 0.04 | | | | | NiO | 0.00 | 0.05 |
| Na2O | 0.05 | 0.05 | Si | 2.723 | 2.75 | 2.669 | CaO | 1.71 | 1.64 |
| K2O | 9.09 | 9.30 | Al | 1.276 | 1.244 | 1.325 | Na2O | 0.04 | 0.00 |
| -> | 95.94 | 95.75 | Fe3 | 0 | 0.003 | 0.005 | K2O | 0.00 | 0.00 |
| | | | Na | 0.684 | 0.726 | 0.668 | Σ oxydes | 100.26 | 100.84 |
| Si | 2.67 | 2.74 | Ca | 0.293 | 0.263 | 0.33 | Si | 5.99 | 5.98 |
| Aliv | 1.33 | 1.27 | K | 0.012 | 0.005 | 0.006 | Al IV | 0.01 | 0.02 |
| Alvi | 0.23 | 0.25 | -> | 4.988 | 4.991 | 5.003 | Al VI | 3.98 | 3.95 |
| Cr | 0.00 | 0.00 | OR | 0.012 | 0.005 | 0.006 | Cr | 0.00 | 0.00 |
| Ti | 0.14 | 0.16 | AB | 0.684 | 0.726 | 0.668 | Ti | 0.00 | 0.00 |
| Fe2 | 1.55 | 1.48 | AN | 0.293 | 0.263 | 0.33 | Mg | 0.94 | 1.01 |
| Mn | 0.00 | 0.01 | | | | | Fe | 4.40 | 4.40 |
| Mg | 1.03 | 0.99 | | | | | Mn | 0.38 | 0.36 |
| Ca | 0.00 | 0.00 | | | | | Ni | 0.00 | 0.01 |
| Na | 0.01 | 0.01 | | | | | Ca | 0.29 | 0.28 |
| K | 0.90 | 0.92 | | | | | Na | 0.01 | 0.00 |
| -> | 7.86 | 7.81 | | | | | K | 0.00 | 0.00 |
| XMg | 0.40 | 0.40 | | | | | % Alm | 73.22 | 72.81 |
| XFe | 0.60 | 0.60 | | | | | % Grs | 4.86 | 4.62 |
| | | | | | | | % Prp | 15.59 | 16.67 |
| | | | | | | | % Sps | 6.34 | 5.90 |

Sample 95/866

| biotite | | | plagioclase | | | | garnet | rim | core |
|---|---|---|---|---|---|---|---|---|---|
| SiO2 | 35.01 | 35.26 | SiO2 | 60.71 | 60.90 | 60.85 | SiO2 | 36.77 | 37.24 |
| TiO2 | 3.08 | 2.77 | Al2O3 | 24.67 | 24.57 | 24.51 | Al2O3 | 21.01 | 21.16 |
| Al2O3 | 16.11 | 16.03 | Fe2O3 | 0.30 | 0.14 | 0.05 | MgO | 3.38 | 3.55 |
| Cr2O3 | 0.00 | 0.07 | CaO | 6.52 | 5.95 | 6.37 | FeO | 33.05 | 32.17 |
| FeO | 23.13 | 23.83 | Na2O | 7.84 | 8.34 | 8.11 | MnO | 4.98 | 4.95 |
| MnO | 0.13 | 0.21 | K2O | 0.16 | 0.26 | 0.22 | Cr2O3 | 0.00 | 0.05 |
| MgO | 8.71 | 8.71 | -> | 100.23 | 100.20 | 100.15 | TiO2 | 0.00 | 0.00 |
| CaO | 0.00 | 0.02 | | | | | NiO | 0.00 | 0.00 |
| Na2O | 0.08 | 0.10 | Si | 2.70 | 2.71 | 2.71 | CaO | 1.58 | 1.77 |
| K2O | 9.91 | 10.38 | Al | 1.29 | 1.29 | 1.28 | Na2O | 0.00 | 0.01 |
| -> | 96.16 | 97.38 | Fe3 | 0.01 | 0.01 | 0.00 | K2O | 0.00 | 0.01 |
| | | | Na | 0.68 | 0.72 | 0.70 | Σ oxydes | 100.78 | 100.91 |
| Si | 2.71 | 2.71 | Ca | 0.31 | 0.28 | 0.30 | Si | 5.87 | 5.93 |
| Aliv | 1.29 | 1.29 | K | 4.99 | 5.02 | 5.01 | Al IV | 0.13 | 0.07 |
| Alvi | 0.18 | 0.17 | OR | 0.01 | 0.02 | 0.01 | Al VI | 3.83 | 3.90 |
| Cr | 0.00 | 0.00 | AB | 0.68 | 0.71 | 0.69 | Cr | 0.00 | 0.01 |
| Ti | 0.18 | 0.16 | AN | 0.31 | 0.28 | 0.30 | Ti | 0.00 | 0.00 |
| Fe2 | 1.50 | 1.53 | | | | | Mg | 0.81 | 0.84 |
| Mn | 0.01 | 0.01 | | | | | Fe | 4.42 | 4.28 |
| Mg | 1.01 | 1.00 | | | | | Mn | 0.67 | 0.67 |
| Ca | 0.00 | 0.00 | | | | | Ni | 0.00 | 0.00 |
| Na | 0.01 | 0.02 | | | | | Ca | 0.27 | 0.30 |
| K | 0.98 | 1.02 | | | | | Na | 0.00 | 0.00 |
| -> | 7.87 | 7.92 | | | | | K | 0.00 | 0.00 |
| XMg | 0.40 | 0.39 | | | | | % Alm | 71.61 | 70.27 |
| XFe | 0.60 | 0.61 | | | | | % Grs | 4.40 | 4.97 |
| | | | | | | | % Prp | 13.06 | 13.80 |
| | | | | | | | % Sps | 10.93 | 10.96 |

Figure I-35: Ti versus AlVI diagram for the same biotite chemical compositions used in the phyllosilicate diagram after Schreurs (1985) for samples 95/864 in a) and 95/866 in b). Biotite compositions indicate a temperature of at least 750°C for the peak metamorphism.

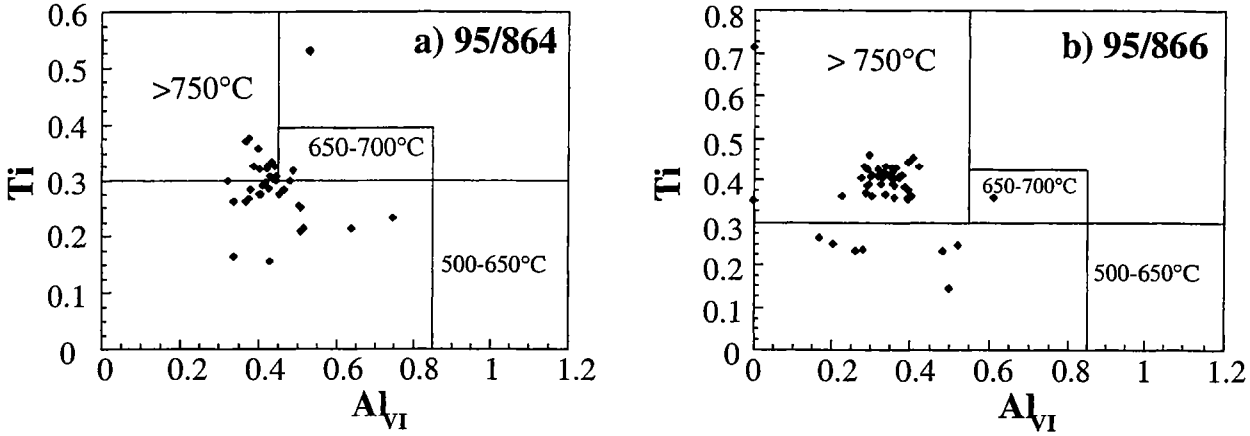


Figure I-36: Chemical compositions of plagioclase plotted in an Or-Ab-An triangle, (a) for sample 95/864 and (b) for sample 95/866. Most plagioclases have an andesine to oligoclase composition. Some of them have Or contents up to 20% related to the antiperthite formation and also to their albitisation during retrograde metamorphism. The different symbols used in this diagram are related to different groups of analyses.

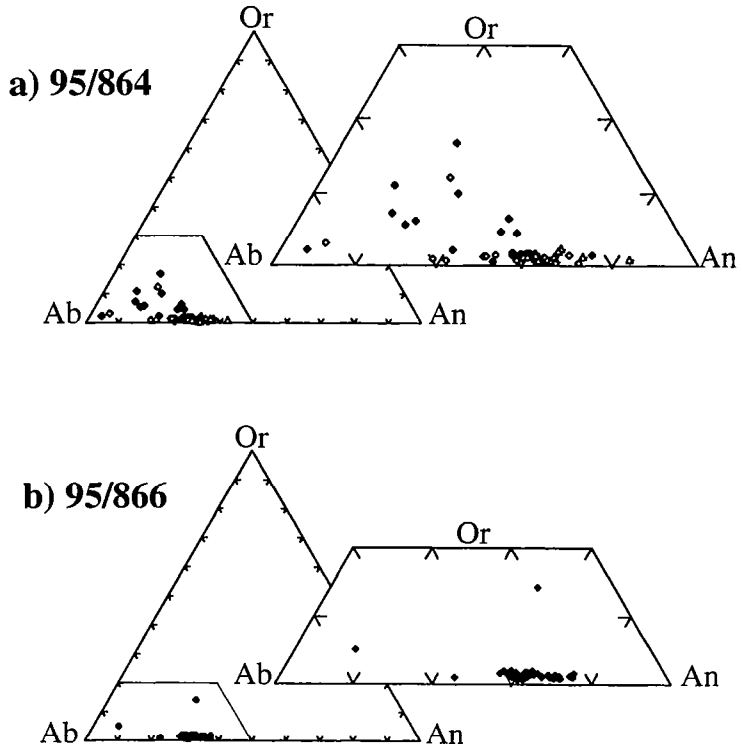

Figure I-37: Chemical compositions versus distance plot along garnet profile from sample 95/864, showing symetric Fe-Mg zonation from core to rim and also Ca enrichment at the outer rim. Mineral namesd written in plain are located in the matrix. Those in italics refer to minerals located within fractures and those in bold character refer to mineral inclusions.

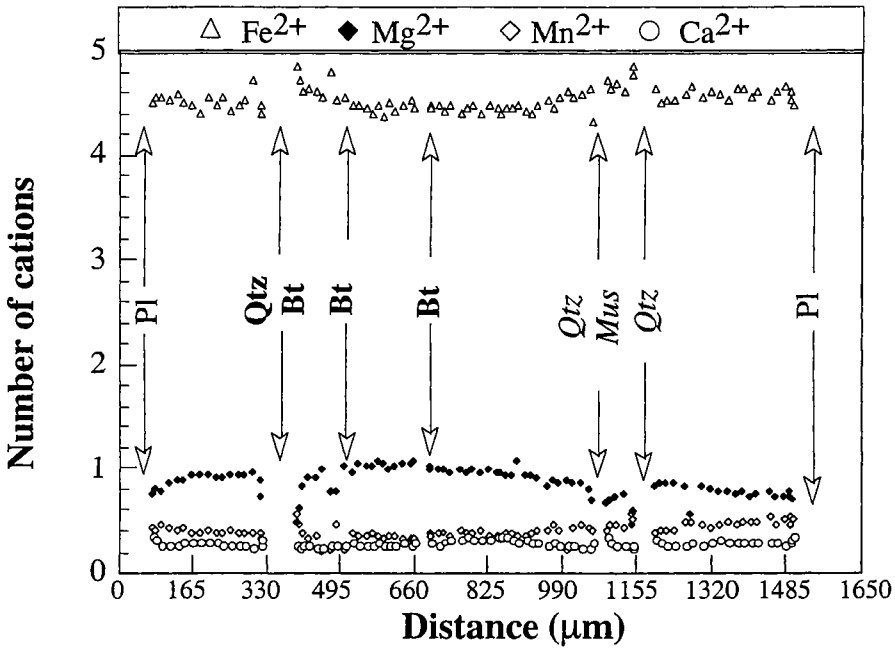


Figure I-38: Chemical compositions versus distance plot along garnet profile from sample 95/864, showing symetric Fe-Mg zonation from core to rim and also Ca enrichment at the outer rim. Mineral namesd written in plain are located in the matrix.

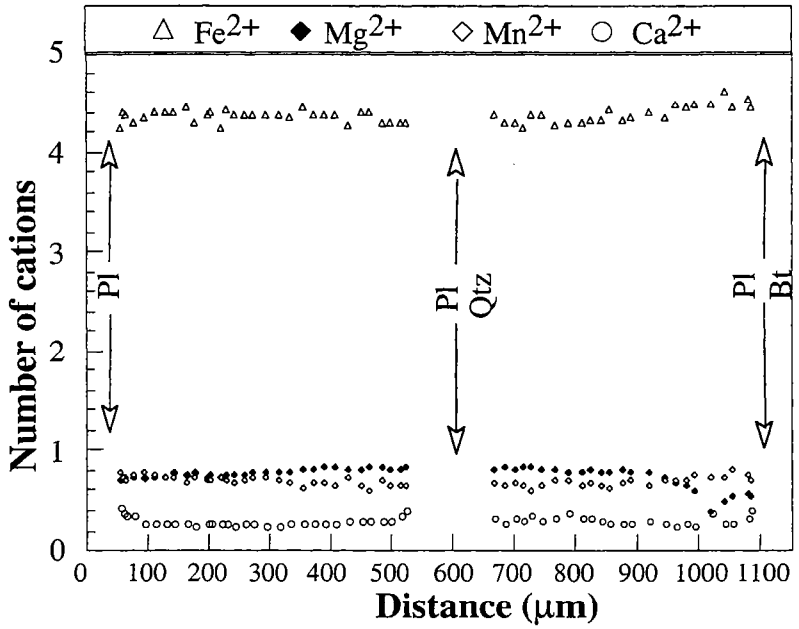

Figure I-39: Chemical compositions of garnet (sample 95/864) are plotted in a) Alm+Prp-Sps-Grs triangle and in b) Alm+Sps-Grs-Prp triangle. The chemical zonations are clearly shown. The major chemical variations are in Fe-Mg exchange and Ca-enrichment is only located at the outer rim of garnet when it is in contact with plagioclase.

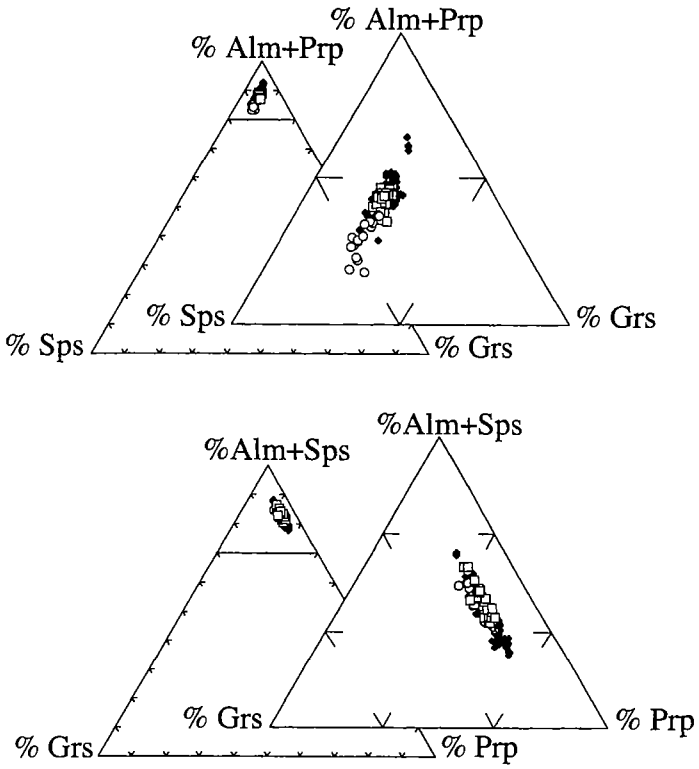


Figure I-40: Chemical compositions of garnet (sample 95/866) are plotted in a) Alm+Prp-Sps-Grs triangle and in b) Alm+Sps-Grs-Prp triangle. The chemical zonations are clearly shown. The major chemical variations are in Fe-Mg exchange and Ca-enrichment is only located at the outer rim of garnet when it is in contact with plagioclase.

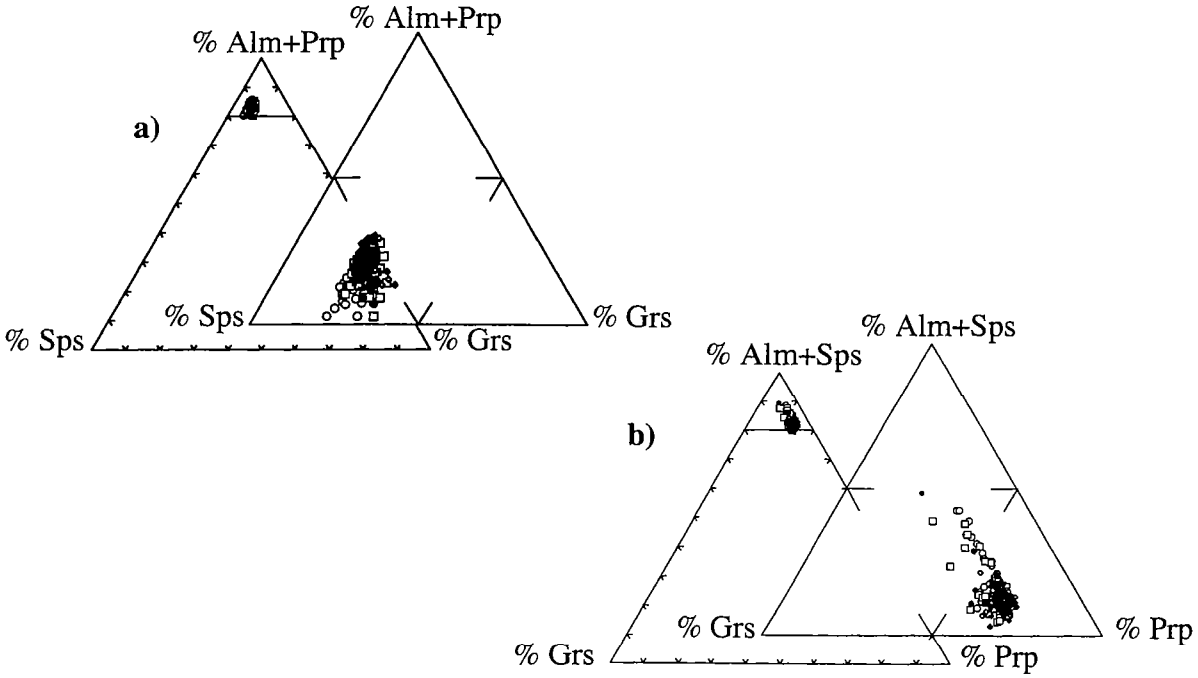

From the mineralogical associations and the microprobe analyses, it is difficult to discern the parageneses and pressure-temperature conditions of prograde metamorphism. Nevertheless, the chemical compositions of the minerals allow some conclusions on the metamorphic evolution of these rocks. The composite Qtz-Pl-Bt inclusions within garnet represent the typical precursor of garnet formation in metagreywackes. Garnet was probably formed during a melting reaction involving Bt + Pl + Qtz with incongruent melting of Bt (Vielzeuf and Montel, 1994; Patiño Douce and Beard, 1996). Opx is absent in the Fe-rich paleosomes; this is explained by their metagreywacke composition (Mg number = 0.4-0.6) and the fact that Opx is never stable in Fe-rich metagreywackes (Patiño Douce and Beard, 1996). Thus, Grt represents the main solid product of fluid-absent melting. Grt-Bt thermometry (TWEEQU, Berman, 1991) using the above presented chemical data gives temperatures of 700-750°C. This may reflect conditions of incipient retrogression. It is in accordance with thermobarometric results of Hisada et al. (1997) who describe upper amphibolite facies conditions at moderate pressure (P<5 kbars) in the Mahalapye Complex. The marginal Fe-Mg-Mn zonations in Grt are interpreted as retrograde diffusion zonations (Spear, 1992), which are associated with resorption of Grt to form Bt at temperatures below 700°C. The marginal Mn enrichment would be a direct effect of this resorption, as Mn is not easily incorporated into Bt. Such retrograde reactions may be associated with an evolution of the equilibrium between Grt and Pl as shown by the Ca zonation at the Grt rims. Local alterations at (sub-)greenschist facies conditions (chlorite, prehnite) document a late hydrothermal activity.

## 6. Geochemical results and discussion

The major and trace element data are presented in Table I-11 with Proterozoic granite (Condie, 1993) and Archean greywacke (Condie, 1993) added for comparison. All paleosome samples have a greywacke composition using the sedimentary classification of Pettijohn et al. (1972). They have very uniform primitive mantle-normalized spidergram patterns (Fig. I-41a) and are characterized by negative $TiO_2$, Sr and Nb anomalies, highly variable LILE contents and high Ni, Cr and Pb contents characteristic of Archean greywackes (Condie, 1993). Major element data agree fully with the modal mineral abundances (Table I-9). The leucosomes exhibit a restricted $SiO_2$ content between 72.04 and 73.66 wt% and portray a granitic composition in a Qtz-Or-Pl triangle using the normative composition (Streckeisen, 1976). All leucosomes have an $Al_2O_3$ contents above 13 wt% associated with A/CNK ratios above 1, implying a peraluminous character. Such peraluminous and granitic leucosomes are the typical partial melt produced by fluid-absent melting on Fe-rich metagreywackes, and the highly variable K/Na ratios and $FeO+MgO+TiO_2$ contents found match the features of melts produced by partial melting of Fe-rich metagreywacke at less than 7 kbars (Patiño Douce and Beard, 1996). The Na/Ca ratios of leucosomes (1.8 - 3.6) are markedly higher than those of paleosomes (0.6-2.2). This probably reflects the incongruent breakdown of Pl during Grt

Table I-11: Major and trace element contents of leucosomes and paleosomes. The compositions of Proterozoic granite and Archean greywacke (Condie, 1993) are listed for comparison.

| sample number | 95/860 | 95/861 | 95/8611 | 95/862 | 95/863 | 95/863b | 95/864 | 95/8641 | 95/865 | 95/866 | 95/868 | 95/8681 | Granite | Greywacke |
|---|---|---|---|---|---|---|---|---|---|---|---|---|---|---|
| type of rock | leucosome | leucosome | leucosome | leucosome | leucosome | Bt-rich part | metagreywacke | Grt-rich part | metagreywacke | metagreywacke | metagreywacke | Grt-rich part | Proterozoic | Archean |
| **major elements in wt% by XRF** | | | | | | | | | | | | | | |
| SiO2 | 72.72 | 72.04 | 73.66 | 72.29 | 72.14 | 65.65 | 66.02 | 69.06 | 60.63 | 64.65 | 55.94 | 52.65 | 73.30 | 65.00 |
| TiO2 | 0.18 | 0.2 | 0.05 | 0.01 | 0.11 | 0.4 | 0.5 | 0.4 | 0.79 | 0.78 | 1.14 | 0.37 | 0.28 | 0.61 |
| Al2O3 | 13.61 | 13.93 | 13.66 | 14.26 | 13.99 | 16.14 | 15.84 | 14.32 | 16.63 | 16.13 | 19.18 | 20.58 | 13.50 | 15.20 |
| Fe2O3 | 1.39 | 1.58 | 0.8 | 0.35 | 1.36 | 3.22 | 5.03 | 3.58 | 6.72 | 5.37 | 7.3 | 10.78 | 2.56 | 6.56 |
| MnO | 0.01 | 0.02 | 0.03 | 0.02 | 0.01 | 0.03 | 0.11 | 0.07 | 0.08 | 0.07 | 0.08 | 0.49 | - | - |
| MgO | 0.5 | 0.63 | 0.11 | 0 | 0.53 | 1.23 | 1.52 | 1.02 | 2.83 | 1.85 | 2.73 | 2.38 | 0.42 | 3.30 |
| CaO | 1.35 | 1.24 | 1.33 | 0.66 | 0.92 | 1.48 | 3.57 | 2.68 | 4.9 | 3.28 | 5.54 | 6.36 | 1.30 | 2.60 |
| Na2O | 2.36 | 2.67 | 2.84 | 2.29 | 2.44 | 3.11 | 3.66 | 3.29 | 2.99 | 3.74 | 3.47 | 3.45 | 3.20 | 3.10 |
| K2O | 6.07 | 5.86 | 5.47 | 8.23 | 6.99 | 6.36 | 1.69 | 2.74 | 1.98 | 2.69 | 2.56 | 1.2 | 4.80 | 2.10 |
| P2O5 | 0.11 | 0.06 | 0.06 | 0.05 | 0.06 | 0.08 | 0.14 | 0.1 | 0.25 | 0.25 | 0.44 | 0.48 | 0.08 | 0.14 |
| PF | 0.46 | 0.46 | 0.5 | 0.28 | 0.26 | 0.87 | 0.65 | 1.06 | 0.74 | 0.37 | 0.58 | 0.76 | - | - |
| total | 98.76 | 98.69 | 98.51 | 98.44 | 98.81 | 98.57 | 98.73 | 98.32 | 98.54 | 99.18 | 98.96 | 99.5 | 99.44 | 98.61 |
| A/NK | 1.302 | 1.298 | 1.290 | 1.125 | 1.208 | 1.345 | 2.018 | 1.709 | 2.355 | 1.779 | 2.262 | 2.951 | 1.29 | 2.06 |
| A/CNK | 1.054 | 1.072 | 1.050 | 1.028 | 1.056 | 1.099 | 1.105 | 1.081 | 1.041 | 1.073 | 1.034 | 1.110 | 1.05 | 1.26 |
| **trace elements in ppm by XRF** | | | | | | | | | | | | | | |
| Na/Ca | 1.81 | 2.23 | 2.21 | 3.59 | 2.74 | 2.17 | 1.06 | 1.27 | 0.63 | 1.18 | 0.65 | 0.56 | 2.54 | 1.23 |
| Ba/Rb | 2 | 3.05 | 3.08 | 3.47 | 5.7 | 4.32 | 2.05 | 4.54 | 2.99 | 4 | 1.82 | 3.66 | 4.80 | 5.57 |
| Na/Sr | 72.3 | 165 | 147 | 133 | 102 | 135 | 138 | 173 | 124 | 147 | 87.6 | 90.8 | 198.00 | 86.70 |
| Ca/Sr | 39.8 | 73.8 | 79.8 | 37.1 | 39.6 | 62.2 | 130.1 | 135.8 | 195 | 124.6 | 134.6 | 161.1 | 77.40 | 70.00 |
| Rb/Sr | 0.645 | 1.32 | 1.13 | 1.57 | 1.09 | 1.23 | 0.505 | 0.766 | 0.631 | 0.766 | 0.497 | 0.25 | 1.30 | 0.26 |
| Nb | 8.8 | 9.7 | 4.8 | 3.2 | 5.7 | 12.4 | 12.8 | 17.6 | 11.7 | 13 | 12.7 | 8.6 | 20 | 11 |
| Zr | 160 | 117 | 84 | 41 | 88 | 196 | 153 | 134 | 141 | 247 | 180 | 97 | 240 | 160 |
| Zr/Nb | 18.18 | 12.06 | 17.50 | 12.81 | 15.44 | 15.81 | 11.95 | 7.61 | 12.05 | 19.00 | 14.17 | 11.28 | 12.00 | 14.55 |
| Y | 13 | 17 | 32 | 18 | 10 | 33 | 20 | 30 | 17 | 21 | 17 | 99 | 45 | 25 |
| Sr | 242 | 120 | 119 | 127 | 166 | 170 | 196 | 141 | 179 | 188 | 294 | 282 | 120 | 265 |
| Rb | 156 | 158 | 135 | 200 | 181 | 210 | 99 | 108 | 113 | 144 | 146 | 73 | 156 | 70 |
| V | 13 | 12 | 6 | 2 | 9 | 26 | 34 | 30 | 78 | 67 | 108 | 62 | 20 | 115 |
| Ni | 8 | <1 | <1 | <1 | <1 | 3 | 2 | <1 | 34 | 14 | 18 | 8 | 15 | 75 |
| Cr | 20 | 5 | 10 | 2 | 10 | 3 | 24 | 14 | 54 | 41 | 55 | 42 | 18 | 175 |
| Cr/Th | 0.77 | 0.29 | 0.59 | 1.00 | 0.77 | 0.03 | 4.00 | 2.00 | 54.00 | 2.56 | 0.00 | 21.00 | 1.00 | 21.88 |
| Ba | 974 | 554 | 537 | 695 | 1031 | 909 | 402 | 490 | 338 | 576 | 535 | 345 | 750 | 390 |
| Ga | 17 | 19 | 17 | 15 | 16 | 23 | 21 | 21 | 22 | 22 | 28 | 24 | - | - |
| Cu | 7 | 7 | 12 | 8 | 8 | 4 | 14 | 14 | 32 | 6 | 48 | 98 | - | - |
| Zn | 20 | 19 | 4 | 1 | 14 | 47 | 52 | 39 | 83 | 68 | 95 | 68 | - | - |
| Th | 26 | 17 | 17 | 2 | 13 | 89 | 6 | 7 | 1 | 16 | 0 | 2 | 18 | 8 |
| Pb | 48 | 53 | 55 | 69 | 56 | 70 | 24 | 36 | 13 | 26 | 15 | 13 | 25 | 20 |
| U | 5.4 | 26.1 | 17.5 | 6.2 | 5.9 | 11.1 | 2.4 | 11 | 4.3 | 2.3 | 1.7 | 1.1 | 4.5 | 1.7 |
| **trace elements in ppm by INAA** | | | | | | | | | | | | | | |
| Cs (0.2) | 1.2 | 0.5 | 1.2 | 1.1 | 1.7 | 3.5 | 1.9 | 1.7 | 2.9 | 3 | 5.8 | 2.4 | - | - |
| Hf (0.2) | 4.3 | 2.4 | 3.4 | 1.4 | 2.9 | 6.3 | 3.9 | 3.1 | 3.3 | 5.5 | 3.7 | 2.3 | 7 | 4 |
| Mo (2) | 4 | 8 | <2 | 5 | 6 | 7 | <2 | 6 | 3 | <2 | 22 | <2 | - | - |
| Sb (0.1) | <0.1 | <0.1 | 0.1 | 0.1 | 0.3 | <0.1 | <0.1 | 0.1 | <0.1 | <0.1 | 0.2 | <0.1 | - | - |
| Sc (0.1) | 2.4 | 2.5 | 3.5 | 1.4 | 2 | 6.3 | 11.4 | 8.9 | 14.5 | 11.3 | 11.7 | 52.2 | 5.0 | 15.0 |
| Ta (0.3) | 2.2 | 3.8 | 3.5 | 3 | 2.7 | 4.2 | 2.5 | 6.9 | 2.3 | 2.1 | 1.1 | 2.7 | 1.5 | 0.7 |
| La (0.1) | 47.7 | 36.9 | 30.8 | 13.9 | 34.6 | 130 | 32.1 | 25.2 | 29 | 64.5 | 44.7 | 32.5 | 48.0 | 26.0 |
| Ce (1) | 84 | 69 | 58 | 28 | 64 | 243 | 57 | 40 | 57 | 125 | 89 | 67 | 115 | 52 |
| Nd (1) | 30 | 25 | 22 | 11 | 24 | 91 | 24 | 19 | 27 | 51 | 43 | 38 | 54 | 22 |
| Sm (0.01) | 4.91 | 4.41 | 4 | 2.17 | 3.87 | 15.5 | 3.91 | 3.04 | 5.02 | 8.04 | 7.69 | 8.8 | 8.70 | 3.90 |
| Eu (0.05) | 1.14 | 0.77 | 0.68 | 0.9 | 1.12 | 1.34 | 1.34 | 0.96 | 1.29 | 1.36 | 1.99 | 2.08 | 1.00 | 1.10 |
| Gd (0.1) | 3.5 | 2.7 | 4.1 | 2.5 | 3.5 | 9.9 | 3.1 | 3.3 | 3.5 | 4.1 | 3.1 | 9 | 8.17 | 3.69 |
| Tb (0.1) | 0.6 | 0.5 | 0.9 | 0.5 | 0.5 | 1.6 | 0.6 | 0.7 | 0.6 | 0.8 | 0.5 | 2.3 | 1.28 | 0.58 |
| Yb (0.05) | 1.02 | 2.59 | 4.62 | 3.38 | 0.97 | 1.4 | 1.67 | 2.76 | 1.26 | 1.8 | 0.96 | 10.3 | 3.50 | 1.40 |
| Lu (0.01) | 0.13 | 0.42 | 0.68 | 0.47 | 0.12 | 0.16 | 0.22 | 0.38 | 0.19 | 0.27 | 0.15 | 1.56 | 0.58 | 0.25 |
| (La/Yb)N | 30.88 | 9.41 | 4.40 | 2.72 | 23.55 | 61.32 | 12.69 | 6.03 | 15.20 | 23.66 | 30.75 | 2.08 | 9.06 | 12.26 |
| Eu/Eu* | 0.85 | 0.69 | 0.52 | 1.20 | 0.94 | 0.34 | 1.19 | 0.94 | 0.95 | 0.73 | 1.26 | 0.72 | 0.37 | 0.90 |

Figure I-41: a) Primitive mantle-normalized spidergrams for paleosomes. Note negative $TiO_2$, Sr and Nb anomalies typical of Archean greywacke. b) Primitive mantle-normalized spidergrams for leucosomes. They are characterized by negative $TiO_2$, $P_2O_5$, Sr and Nb anomalies similar to granite composition. Dotted area corresponds to the field of paleosomes.

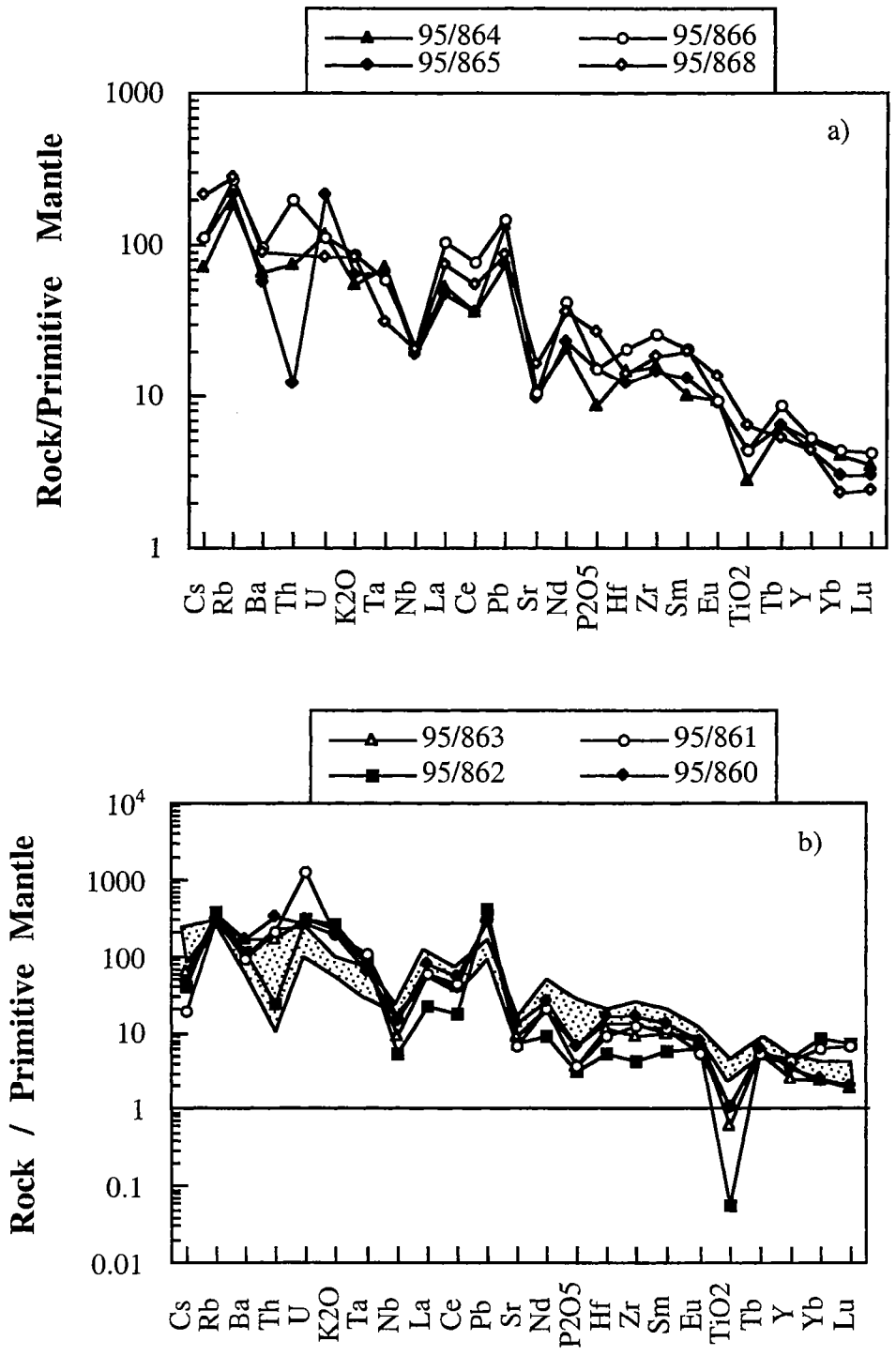

formation in melting, resulting in an enhanced albite component in the melt (Patiño-Douce and Beard, 1996). The values for paleosomes 95/864 and 95/866 are within the ranges of Pl compositions measured in these rocks (Fig. I-36, Table I-11).

Further information on equilibria during melting and melt extraction can be obtained from trace element data. The LIL elements reveal the behaviour of the feldspars and biotite. Leucosomes have on average 2x higher Rb/Sr ratios than the paleosomes, and a slightly less marked increase in Ba. These features are consistent with production of the leucosome through vapour absent biotite melting (Inger and Harris, 1993; Harris and Inger, 1992) and are also expected in preferential melting of Kfs over Pl. K/Rb ratios of the leucosomes range from 300 to 340, markedly higher than those of paleosomes which are between 130 and 250 (Note that the average "Proterozoic granite" and "Archean greywacke" both have K/Rb ratios of c. 250; Table I-11). This relation could either indicate equilibration between the melt and residual biotite (Rb is strongly compatible in biotite, Bea et al., 1994) or simply reflect that (as observed) Kf entered the melt preferentially to biotite, without much equilibration. However, leucosome K/Rb ratios are raised because of higher K and not lowered Rb (see Table I-11) and this points to the latter explanation. Further, there is no corresponding contrast in K/Ba or Na/Sr ratios between the leucosome and palaeosome. If extensive equilibration between melt and residue had occurred, a high leucosome K/Ba ratio would be expected through Ba scavenging by residual K Feldspar, and a high Na/Sr ratio through Sr incorporation in residual plagioclase (Bea et al., 1994). The LIL data thus indicate that the nascent melt did not equilibrate extensively with the residual feldspars and biotite in the paleosome (Nabaleck and Glascock, 1995). The scatter in Rb/Sr ratios of the leucosomes (0.6 - 1.6) most likely mirror the variable proportions of Kf and Pl entering the melt, as do the K/Na ratios.

Rb/Sr ratios and Ba concentrations can further be used to assess if the leucosomes represent melt, or if further melt has been extracted from them and they in fact represent residues. The observed values are not consistent with the equiibrium extraction of a further melt from a Kfs dominated leucosome, as this process would increase Ba and lower Rb/Sr in the "residual" leucosome (Ayres et al., 1997; Inger and Harris, 1993; Harris and Inger, 1992). It appears that the leucosome at Lose Quarry is not a residue, but is representative of the melt extracted from the paleosome. The rather uniform major and trace element composition of this leucosome leads to the conclusion that any melt which migrated away from this site would have had a similar composition.

It is expected that the distribution of Th, U, Hf and the REE between the leucosomes and the paleosomes will be largely determined by the degree to which monazite, apatite and zircon enter the melt during partial melting, either by entrainment or by dissolution.

Figure I-42: Chemical composition of paleosomes and leucosomes plotted in (a) Ce vs $P_2O_5$, (b) La vs Zr, (c) Zr vs $P_2O_5$, (d) La vs Th, (e) U vs Zr, (f) U vs Ce and (g) U vs Zr + Ce in order to assess the effect of accessory minerals on compositions.

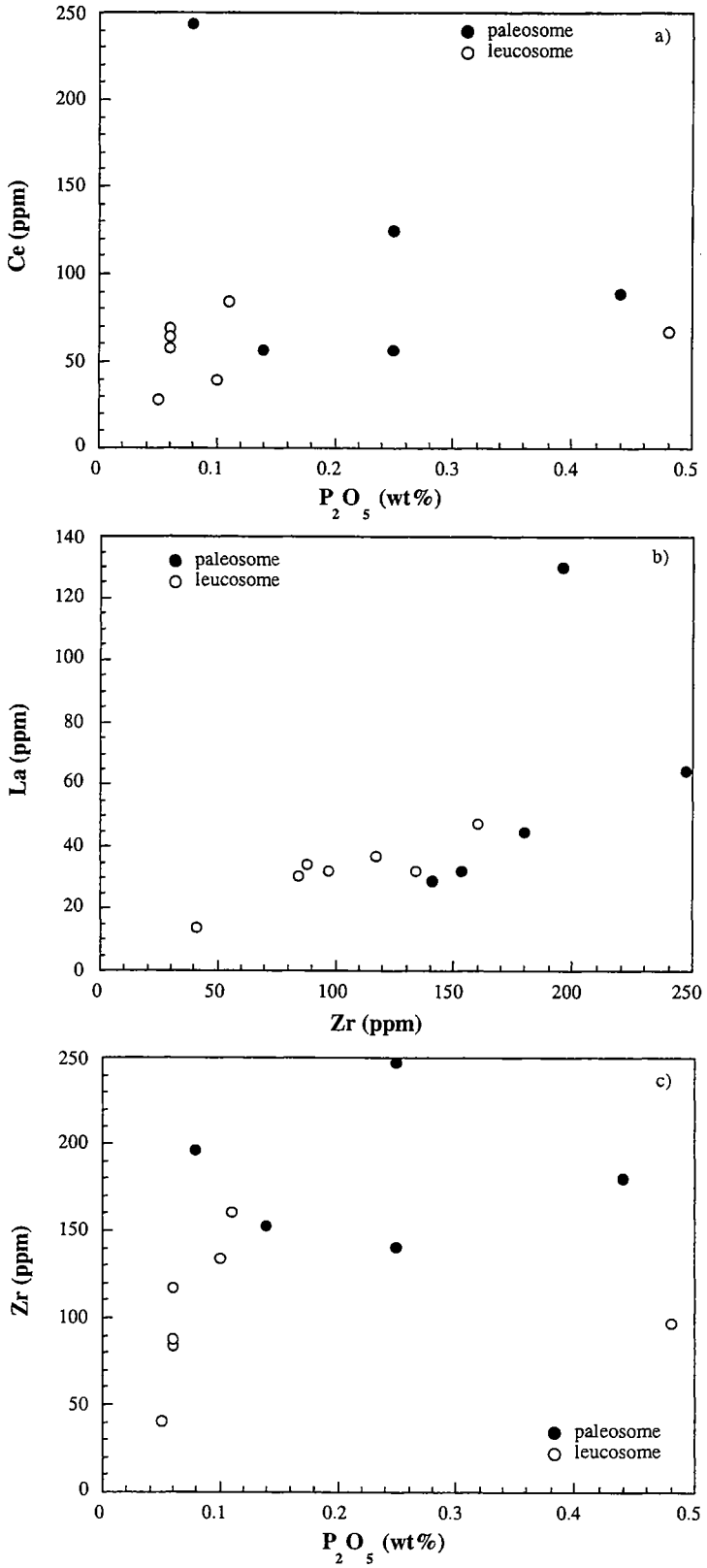

Figure I-42: Chemical composition of paleosomes and leucosomes plotted in (a) Ce vs $P_2O_5$, (b) La vs Zr, (c) Zr vs $P_2O_5$, (d) La vs Th, (e) U vs Zr, (f) U vs Ce and (g) U vs Zr + Ce in order to assess the effect of accessory minerals on compositions. Continued.

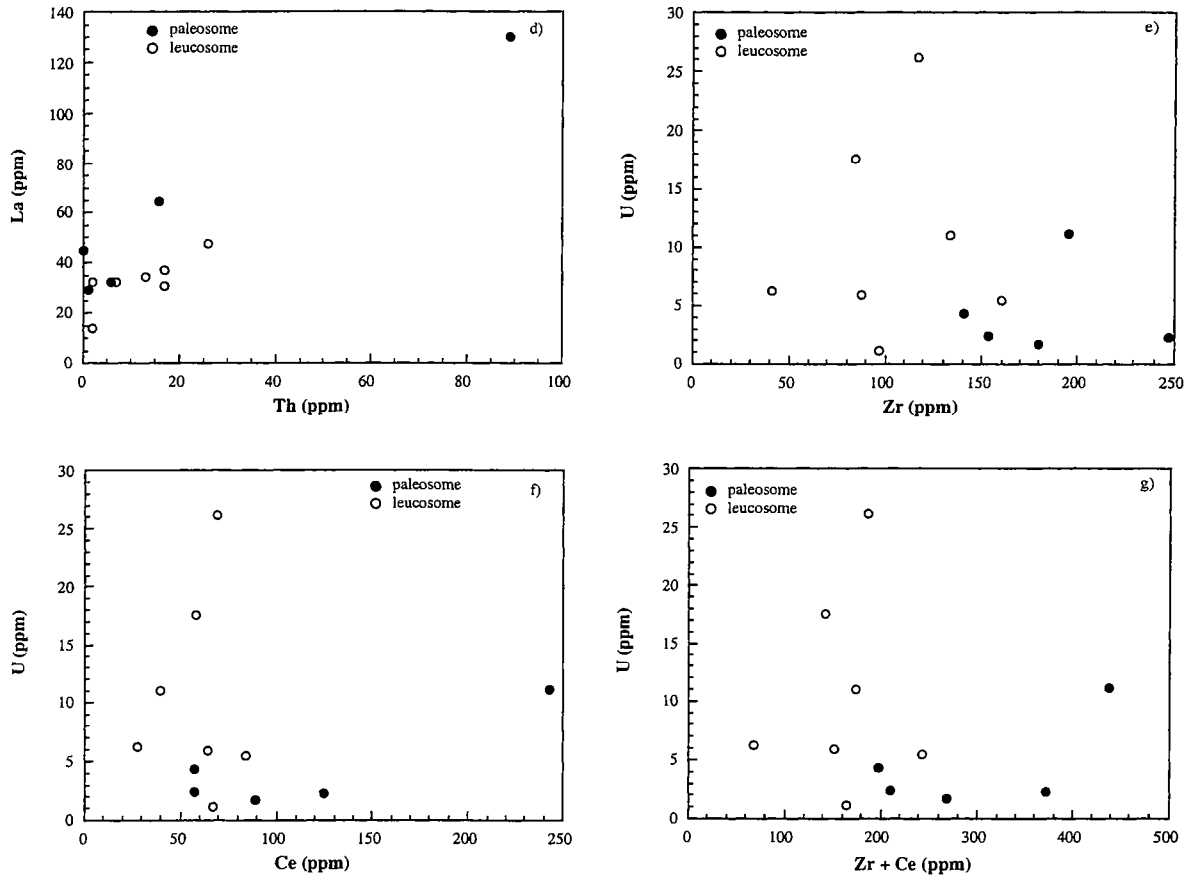

Chemical equilibrium of HFSE and REE will not necessarily be reached between the melt and incompletely dissolved accessory minerals remaining in the residue in fluid-absent partial melting, even under high-grade metamorphism, because the time scale of melt formation and transport may be short compared to the dissolution and trace element diffusion rates (Watt and Harley, 1993). A plot of Ce vs. $P_2O_5$ (Fig. I-42a) shows that the paleosomes have highly variable relative amounts of monazite and apatite. Both appear to have entered the melt to minor degrees. Zr correlates well with La (Fig. 10b) in the leucosomes, with an array pointing to the field of paleosomes, indicating that zircon and monazite have entered the melt approximately in the proportions of their occurrence in the source rock. In contrast, the array in the Zr vs $P_2O_5$ plot (Fig. I-42c) does not line up with the paleosomes field. The comparison between the two plots implies that monazite entered the leucosomes in preference to apatite. Th vs. La (Fig I-42d) shows parallel trends for leucosomes and paleosomes, suggesting both are dominated by monazite. The leucosomes have higher Th contents at similar La than the palaeosomes, which again suggests that proportionally more monazite than apatite entered the melt. The nonzero La "intercepts" at Th = 0 are probably mainly due to apatite.

Contrary to this behaviour, U is enriched in the leucosomes compared to the paleosomes (the one 'paleosome' with U> 10 ppm is a biotite rich band in leucosome 95/863), and shows no correlation to either Zr, Ce or the sum of both (Fig.I-42e, I-42f and I-42g). Further, U is too highly concentrated in all leucosomes, and two of the paleosomes, to be entirely contained in zircon and monazite. It probably resided in very minor interstitial phases, from where it was readily mobilized during melting, and does not appear to have been significantly scavenged by residual monazite, zircon or apatite in the paleosomes.

The rare earth patterns of all samples are summarized in Fig. I-43a to d. The paleosomes have uniform REE patterns similar to those of Archean TTG (Taylor and McLennan, 1985). The leucosomes have on average somewhat lower LREE concentrations. The garnet-free ones (95/860, 95/863) have patterns virtually indistinguishable from those of the paleosomes, whereas the garnet bearing ones (95/861 and 95/862) have marked HREE enrichment and in one case (95/862) strong LREE depletion relative to the paleosome population. Relative HREE enrichment is also shown by the garnet bearing leucosome pods of samples 95/864 and 95/868 (Fig. I-43c and I-43d). Thus garnet appears to affect the HREE concentrations of leucosomes strongly, and this means either that it scavenged HREE from very large areas during its growth, or that it was concentrated by mechanical processes during melt expression and migration. The above indications of lack of equilibrium make the second alternative much more likely. In the garnet-free cases, the REE pattern merely reflects the amount of monazite (the main LREE carrier of the rock) and zircon (its main HREE carrrier) present in the melt, and, as seen above, these minerals enter the melt in proportion to their abundance, which explains the unchanged REE pattern.

Figure I-43: a) Chondrite-normalized REE patterns for paleosomes. ($(La/Yb)_N$ = 12 to 30). b) for leucosomes. c) and d) Chondrite-normalized REE patterns for 95/864 and 95/868 and their associated Grt-bearing leucocratic patches 95/864L and 95/868L.

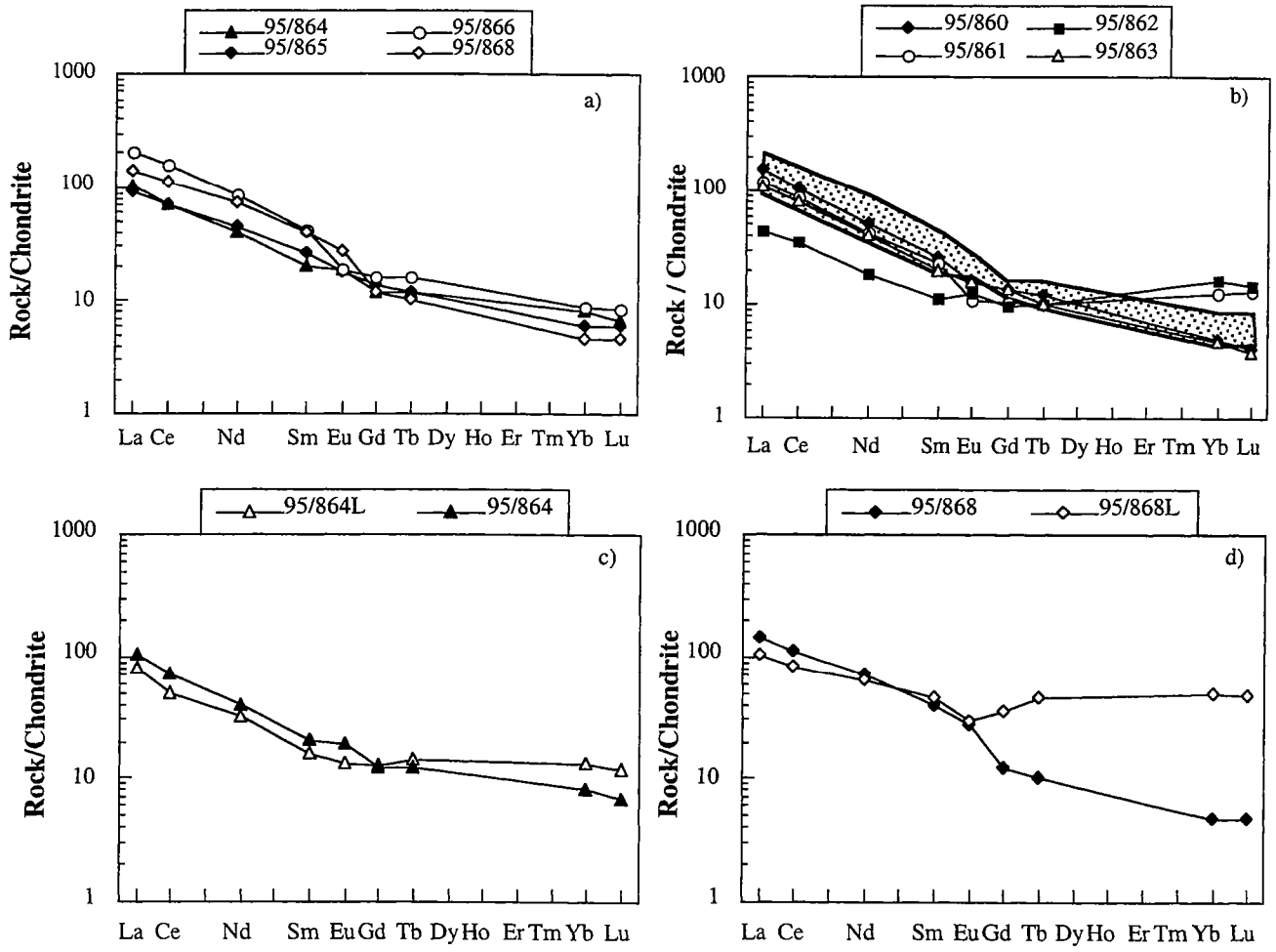

Table I-12: U-Pb isotope data of monazites from samples 95/862 and 95/863.

| sample | fraction size, color, shape | weight (mg) | 206/204Pb meas | 208/206Pb* | U (ppm) | Pb* (ppm) | Pbtot (ppm) | 207/206Pb* | ±2σ(%) | 207Pb/235U (Ma) | ±2σ(%) | 206Pb/238U (Ma) | ±2σ(%) | 207Pb/206Pb (Ma) | ±2σ(%) | r |
|---|---|---|---|---|---|---|---|---|---|---|---|---|---|---|---|---|
| 95/862a | <150µm, y, e | 0.29 | 476.4 | 1.39 | 3509.4 | 3148.1 | 3327.6 | 0.123287 | 1.06 | 7.024577 | 1.76 | 0.413241 | 1.32 | 2114.54 | 37.15 | 2229.72 | 29.40 | 2004.33 | 18.72, 18.96 | 0.798 |
| 95/862b | <150µm, o, a | 0.49 | 307.42 | 0.98 | 3365.7 | 2471.3 | 2737.7 | 0.122725 | 2.16 | 6.851455 | 2.49 | 0.404902 | 0.53 | 2092.4 | 52.14 | 2191.57 | 11.61 | 1996.21 | 37.93, 38.94 | 0.688 |
| 95/863a | >125µm, o, a | 0.18 | 1218.98 | 2.68 | 4095.4 | 5355.7 | 5355.7 | 0.123122 | 0.83 | 6.741323 | 1.40 | 0.397108 | 1.05 | 2078.06 | 29.17 | 2155.71 | 22.66 | 2001.95 | 14.58, 14.72 | 0.811 |
| 95/863b | <100µm, c, e | 0.45 | 542.01 | 2.59 | 3170.2 | 3275.2 | 3275.2 | 0.123096 | 1.98 | 5.46189 | 2.28 | 0.321809 | 0.48 | 1897.63 | 43.20 | 1798.56 | 8.60 | 2001.58 | 34.7, 35.54 | 0.696 |

y: yellow, o: yellow-orange, c: clear/pale yellow
e: euhedral, a: anhedral
r: correlation coefficient according to Ludwig (1988)
*: corrected for mass fractionation, blank and spike

Table I-13: Sm-Nd isotopic compositions of all leucosomes, paleosomes and mineral separates.

| Sample number | Rock type | Sm (ppm) | Nd (ppm) | 147Sm/144Nd | 143Nd/144Nd | ± 2 S(m) | eNd(0) | ±2σ(%) | eNd(2.0) 2.00 | T(DM)* Ga | T(DM)** Ga | f(Sm/Nd) |
|---|---|---|---|---|---|---|---|---|---|---|---|---|
| **95/860** | Leucosome | 5.31 | 30.50 | 0.1051 | 0.511067 | 6 | -30.65 | 1.32 | -7.93 | 2.91 | 2.750 | -0.466 |
| **95/861** | Leucosome | 4.45 | 23.34 | 0.1152 | 0.511195 | 8 | -28.15 | 0.53 | -8.03 | 3.01 | 2.840 | -0.414 |
| **95/861L** | Leucocome | 4.96 | 25.24 | 0.1188 | 0.511281 | 9 | -26.47 | 1.05 | -7.27 | 2.98 | 2.810 | -0.396 |
| | duplicate | 5.17 | 26.46 | 0.1180 | 0.511248 | 8 | -27.11 | 0.48 | -7.72 | 3.01 | 2.840 | -0.400 |
| **95/862** | Leucosome | 2.23 | 10.12 | 0.1334 | 0.511497 | 8 | -22.26 | 1.76 | -6.80 | 3.12 | 2.920 | -0.322 |
| **95/863** | Leucosome | 3.75 | 21.18 | 0.1071 | 0.511150 | 7 | -29.03 | 2.49 | -6.82 | 2.84 | 2.690 | -0.456 |
| **95/863B** | Bt-rich layer within 95/863 | 17.30 | 97.66 | 0.1071 | 0.511144 | 8 | -29.14 | 1.40 | -6.94 | 2.85 | 2.700 | -0.456 |
| **95/864** | Metagreywacke | 4.24 | 22.81 | 0.1123 | 0.511339 | 7 | -25.34 | 2.28 | -4.46 | 2.71 | 2.550 | -0.429 |
| **95/864L** | Leucosome | 3.25 | 16.83 | 0.1178 | 0.511358 | 7 | -24.97 | 0.48 | -5.50 | 2.83 | 2.660 | -0.401 |
| **95/864** | garnet >300µm | 4.81 | 9.42 | 0.3083 | 0.513857 | 16 | 23.78 | 0.32 | -5.69 | - | - | 0.568 |
| **95/864** | garnet 200-300µm | 3.28 | 3.04 | 0.6514 | 0.518338 | 42 | 111.19 | 0.93 | -6.39 | - | - | 2.312 |
| **95/864** | garnet 140-200µm | 3.49 | 5.26 | 0.4018 | 0.515113 | 23 | 48.28 | 0.93 | -5.18 | - | - | 1.042 |
| **95/864** | monazite | 10502.55 | 83359.89 | 0.0761 | 0.511900 | 16 | -14.40 | 0.93 | 15.88 | - | - | -0.613 |
| **95/865** | Metagreywacke | 4.87 | 23.08 | 0.1276 | 0.511577 | 7 | -20.70 | 2.28 | -3.74 | 2.77 | 2.580 | -0.351 |
| **95/865** | apatite 200-300µm | 489.35 | 1582.53 | 0.1869 | 0.512347 | 6 | -5.68 | 0.48 | -3.95 | - | - | -0.050 |
| **95/865** | euhedral apatite 100-200µm | 473.32 | 1468.34 | 0.1949 | 0.512441 | 7 | -3.84 | 0.48 | -4.16 | - | - | -0.009 |
| **95/865** | rounded apatite 100-200µm | 460.78 | 1535.77 | 0.1814 | 0.512428 | 7 | -4.09 | 0.48 | -0.93 | - | - | -0.078 |
| **95/866** | Metagreywacke | 8.77 | 54.41 | 0.0974 | 0.511171 | 6 | -28.62 | 1.76 | -3.90 | 2.58 | 2.440 | -0.505 |
| **95/868** | Metagreywacke | 8.52 | 45.42 | 0.1134 | 0.511382 | 8 | -24.50 | 1.40 | -3.90 | 2.67 | 2.510 | -0.423 |
| **95/868L** | Grt-rich part | 9.41 | 36.50 | 0.1558 | 0.511942 | 7 | -13.58 | 2.28 | -3.86 | 3.16 | 2.880 | -0.208 |
| **95/868** | garnet >160µm | 7.39 | 4.15 | 1.0762 | 0.524202 | 20 | 225.58 | 0.48 | -1.07 | - | - | 4.471 |

T(DM)*: calculated according to Goldstein et al. (1984).
T(DM)**: calculated according to Nägler and Kramers (1998).

Figure I-44: a) Concordia plot for monazites of samples 95/862 and 95/863B. b) Sm-Nd garnet-leucosome-paleosome isochron (sample 95/868). c) Sm-Nd garnet-leucosome-paleosome isochron (sample 95/864). d) Sm-Nd data for paleosome 95/865 and three apatite fractions. Age calculation according to Ludwig (1990).

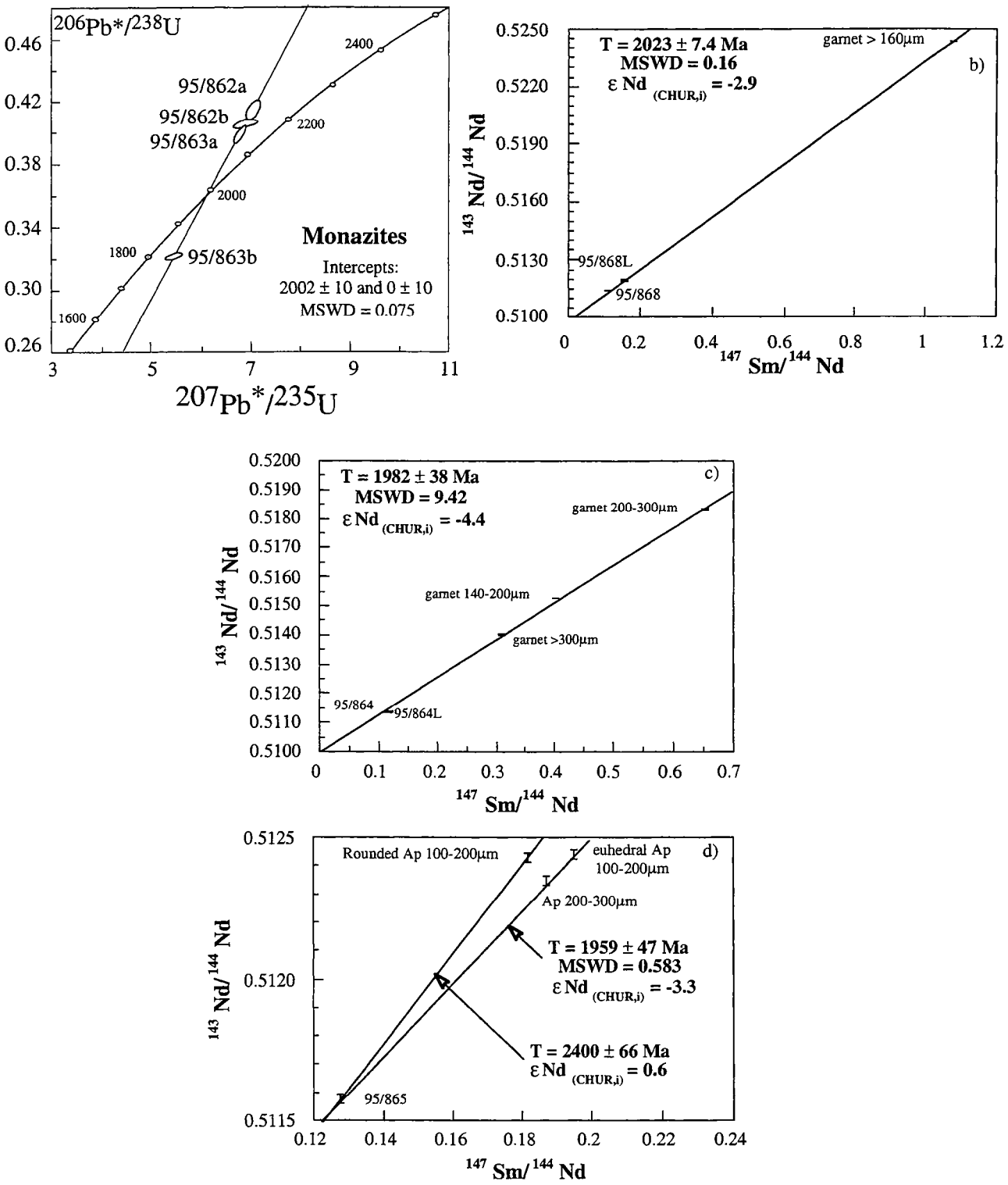

## 4.7. Age of the high grade metamorphism and migmatization.

As monazite grains in the leucosomes in part consist of cores and overgrowths, we have assumed that idiomorphic ones without cores crystallized from the mobilized melt and could thus be used for dating migmatization. Four core-free monazite fractions separated from two leucosomes, 95/862 and 95/863, were analyzed for U-Pb (see Table I-12). They have relatively low $^{208}Pb/^{206}Pb$ ratios for monazites, reflecting the high U/Th ratios of the leucosomes from which they crystallized (particularly 95/862, see Table I-11). Correction for common Pb was done using 2.0 Ga model Pb of Stacey and Kramers (1975). The four fractions are both positively and negatively discordant (Fig. I-44a) but yield a well defined concordia intercept age of 2002 ± 10 Ma (MSWD = 0.075), which we interpret as the age of crystallization of the monazite from the leucosome.

In a further effort to date metamorphism, three fractions of apatite from paleosome 95/865 were analyzed for Sm-Nd under the assumption that, due to the large radiogenic Nd component in old apatite, any possible initial Nd isotope heterogeneities would not be large enough to affect the apparent age greatly. The results are listed in Table 5 and shown in Fig. I-44d. Two fractions of sub- to prismatic apatite (100-200μm and 200-300 μm in size) yield together with the whole-rock paleosome an age of 1959 ± 47 Ma (MSWD = 0.58). The third fraction (100-200 rounded apatite) and the paleosome give an apparent age of 2400 ± 66 Ma. The first date is seen as that of either apatite recrystallisation, or resetting via diffusional exchange, hence of metamorphism, and is in broad agreement with the monazite ages. The second result is interpreted as a mixed age with an older, possibly originally detrital apatite component. The retention of the older age by part of the population may have been caused by armouring in other minerals; it illustrates that Nd isotope homogenization cannot be taken for granted even in apatites at high metamorphic grade.

Sm-Nd garnet-matrix dating was carried out on leucocratic pod samples 95/864 and 95/868. Initial disequilibrium should be even less significant here than in the case of apatite, and it should be possible to ascertain if the garnets were indeed formed in the same event that generated the leucosomes. Sm-Nd results are listed in Table I-13. In sample 95/868, the paleosome plus garnet-bearing leucocratic pod and one garnet fraction gave an age of 2023 ± 7 Ma (MSWD = 0.16; Fig. I-44b) and in sample 95/864, the garnet-bearing leucocratic pod *in toto*, three different garnet fractions and the locally associated paleosome yielded an age of 1982 ± 38 Ma (MSWD = 9.42; enhanced error; see Fig. I-44c). The fact that no isochron is defined in the case of 95/864 indicates that no full Nd isotope homogenization had been achieved in this sample prior to garnet growth. With this in mind, the ± 7 Ma error on the age for 95/868 should

Figure I-45: a) Sm-Nd whole rock diagram for all leucosomes and paleosomes at present time, b) Sm-Nd whole rock diagram for all leucosomes and paleosomes at 2.0 Ga.

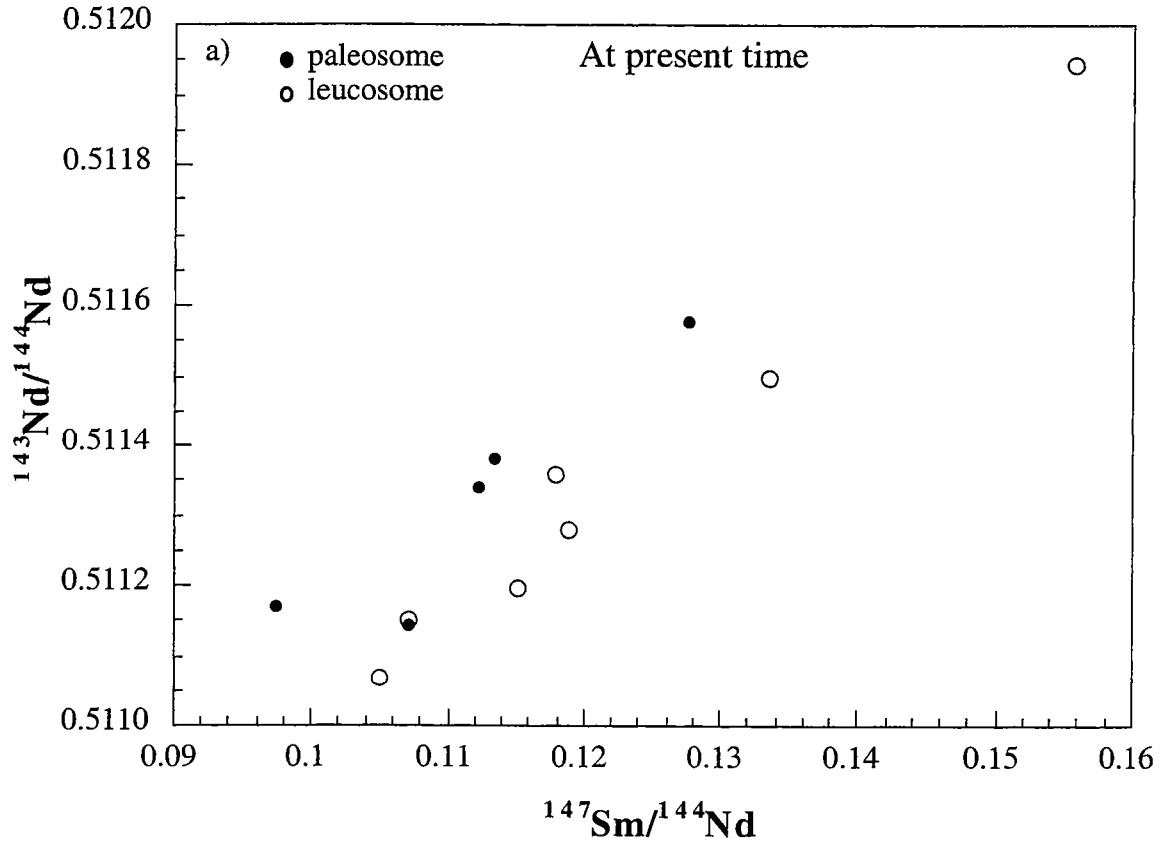


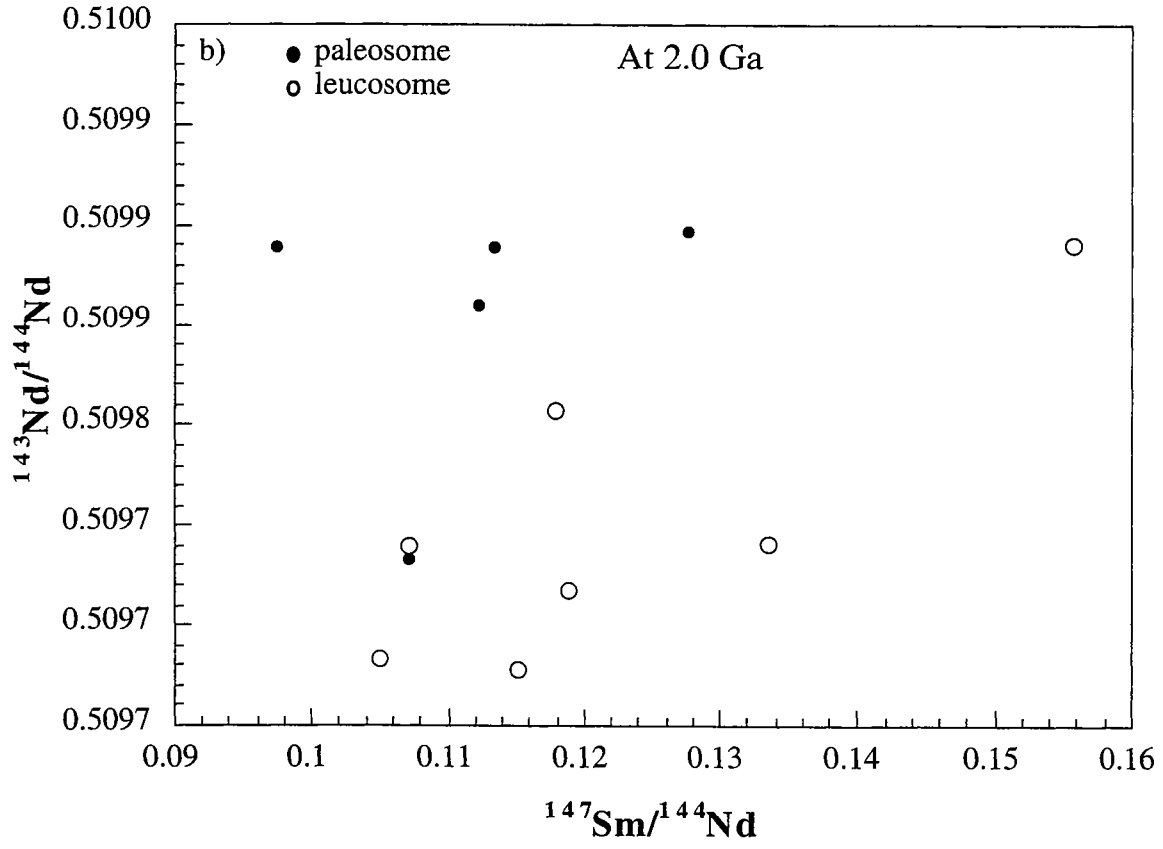

dates as approximating those of garnet crystallisation, and they show that the garnets indeed appear to have been formed in the migmatizing event. The initial $\varepsilon_{Nd}$ values for the samples (-4.4 for 95/864 and -2.9 for 95/868) document a considerable crustal history prior to 2 Ga for the Complex.

The evidence of high grade metamorphism (garnet growth in melting reactions) leading to migmatization (monazite crystallisation) very close to 2.0 Ga ago in the Mahalapye Complex is in good agreement with age data obtained regionally and further to the E in the CZ of the Limpopo Belt (Holzer et al., 1997, 1998; Kamber et al., 1995; Schaller et al., 1998) and in the Magondi Belt (Treloar and Kramers, 1989; Munyanyiwa et al., 1995). This metamorphic event in the MC can thus be attributed to the same 2.0 Ga orogenic episode manifested in these belts, and, together with the location of the MC close to the junction of these Belts, helps to strengthen the notion of a direct link between them. The age information obtained now allows us to assess the effects of the high grade metamorphism on the Sm-Nd systematics of these rocks.

## 4.8. Results and discussion on Sm-Nd systematics.

All Sm-Nd results on whole rocks as well as on separated minerals are presented in Table I-13. The WR and apatite data are plotted in a conventional Sm-Nd isochron diagram in Fig. I-45a. The Sm/Nd and $^{143}Nd/^{144}Nd$ ratios of all paleosomes are in narrow ranges from 0.0974 to 0.1276 and from 0.51117 to 0.51158, and they do not form an isochron. Their apparent $T_{DM}$ ages vary between 2.4 and 2.6 Ga. The clearly higher Sm/Nd ratio in the garnet bearing leucocratic pod of sample 95/868 relative to its host rock (with a similar $^{143}Nd/^{144}Nd$ ratios at 2.0 Ga, see Table I-13), results in an apparent $T_{DM}$ age 370 Ma older than that of the host rock. This exemplifies how partial melting can generate anomalous and wrong apparent $T_{DM}$ ages even without isotope disequilibrium. Further, in Fig. 13a all leucosomes, whether Gt bearing or Gt free, plot in a band below (or to the right of) that defined by the paleosomes, and apparent $T_{DM}$ ages for large leucosome bodies range from 2.69 to 2.92 Ga (Table I-13).

Fig. I-45b shows the results recalculated to 2.0 Ga b.p. This shows that significant differences in $^{143}Nd/^{144}Nd$ ratios existed at that time between different rock units and were not correlated with $^{147}Sm/^{144}Nd$ ratios. The paleosomes fall in a range of $^{143}Nd/^{144}Nd$ (2.0 Ga), of average of -3.3 $\varepsilon_{Nd}$ units, whereas leucosomes plot at lower values, averaging -7.7 $\varepsilon_{Nd}$ units, and show among themselves a much greater scatter ranging from equilibrium with the paleosome (95/868, see above) to 4.4 $\varepsilon_{Nd}$ units below the main population of paleosomes. Garnet bearing large leucosomes (95/861 and 95/862) have higher $^{147}Sm/^{144}Nd$ ratios than garnet free ones, as already discussed in connection with the general REE patterns, but their $^{143}Nd/^{144}Nd$ ratios at 2.0 Ga are similar to those of the other leucosomes. The Nd data of the

Figure I-46: TDM vs Sm/Nd ratio diagram shows a difference of at least 100 Ma between the Nd model ages of leucosomes compared to those of paleosomes.

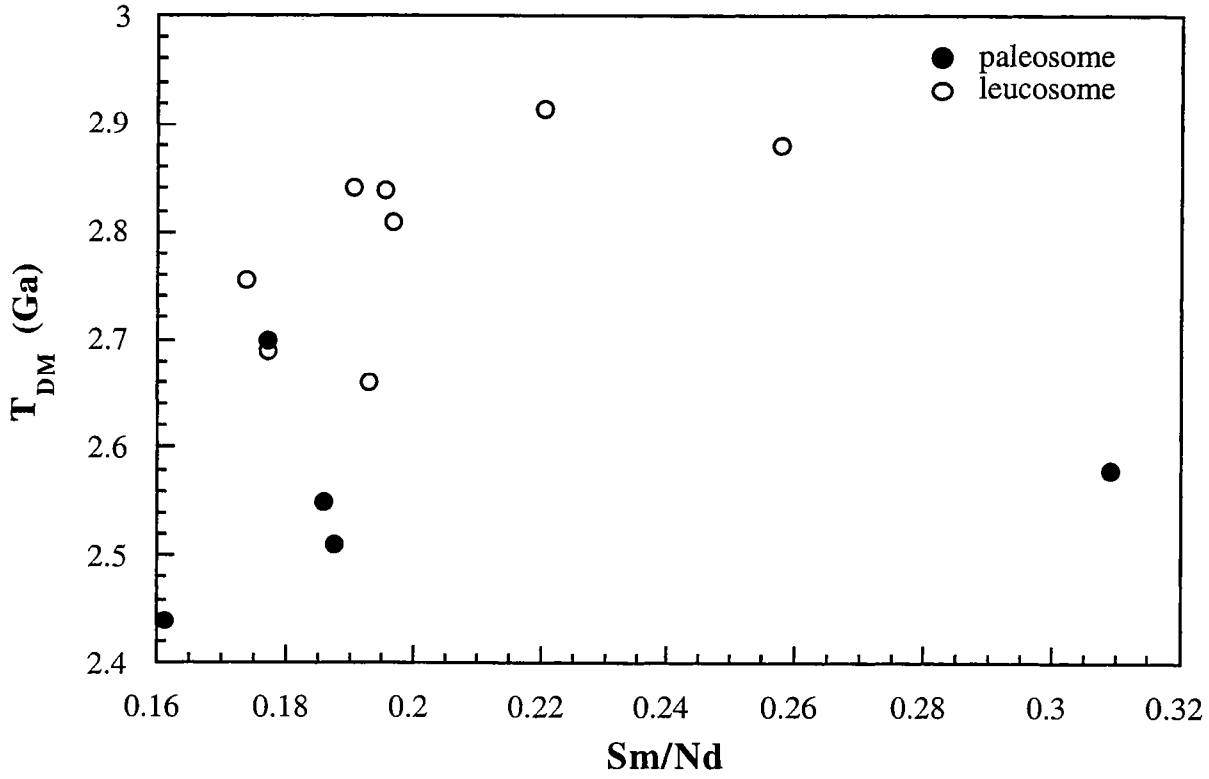

leucosomes and paleosomes thus show a lack of Nd isotope equilibration upon separation, and a systematic offset.

The significance of this offset has to be considered in combination with the trace element results. Above it has been argued on the basis of Th vs La and Ce vs. $P_2O_5$ plots (Fig. I-42d and I-42a), that proportionally more monazite than apatite entered the leucosomes. The apatites in the studied rocks appear to have, as is normal, high Sm/Nd ratios, and one case of unequilibrated radiogenic Nd in apatites was seen (see Table I-13). In contrast, the Sm/Nd ratios of monazites are lower than those of the whole rock samples, whose Sm-Nd budgets are mainly a composite of apatite and monazite. The $^{143}Nd/^{144}Nd$ ratios of monazites which existed before melting are thus expected to be lower than those of the whole rock at the time of melting. As there seems to be ample evidence that trace element equilibrium between the melt an the paleosome residue was not reached during partial melting and melt segregation, it follows that Nd isotopic homogenization between between these domains cannot have been complete either. Preferential incorporation of monazite over apatite in the melt (whether by entrainment or by dissolution) entails preferential incorporation of relatively unradiogenic Nd. The Nd isotopic observations are therefore in agreement with the geochemistry.

The Nd isotope offset of the leucosomes relative to the paleosomes, without a corresponding average offset in Sm/Nd ratios, results in the 250 Ma mean difference in $T_{DM}$ ages for the two sample groups (Table I-13, Fig. I-46). If upon migmatization the original rock were 'split' into paleosomes and leucosomes without any Sm-Nd exchange at all between the two parts, then paleosomes and leucosomes would be expected to be approximately colinear and an array giving broadly the original rock age would result in the Sm/Nd evolution ('isochron') diagram. If the larger, combined rock body of Lose Quarry resulted from a single mantle extraction event, we would also expect all $T_{DM}$ ages to be the same and similar to the age given by such an array, in spite of isotope offset and lack of equilibrium in migmatization. All this is contrary to observation, and there are two possible ways to interpret the offset in in Nd isotopes and thus $T_{DM}$ ages.

The first is, that some equilibration in Sm and Nd concentrations took place between the melt and residue before they were separated, but that this occurred without complete Nd isotope homogenization. Possible residual phases which could incorporate Nd preferentially over Sm and thus raise the Sm/Nd ratio of the melt would be feldspars, particularly plagioclase (Bea et al., 1994) and monazite. As chemical equilibrium must precede full isotope exchange, this is not inconceivable. However, it is unlikely because of the geochemical evidence against significant trace element equilibration between melt and residue discussed above, and the evidence that monazite was preferentially entrained. Neocrystallization of plagioclase and/or monazite in the migrating melt (as documented by the 2 Ga monazite U-Pb

age) would create heterogeneity in the Sm/Nd ratios of the leucosome. This is indeed seen, but a primary offset in average Sm/Nd between leucosomes and paleosomes would still be expected and is not observed.

The second possible explanation is that the original graywacke did not have a single source, and that most of the (detrital) monazite derived from an older crustal province than most of the other Nd bearing components of the rock (e.g. apatite and hornblende). If this is so, then the migmatization process could have in part unravelled the earlier mixing homogenization of sedimentation. We prefer this explanation over the former one, because of the problems mentioned above.

The consequences of the two hypotheses for deriving a crustal history from the Sm-Nd data are quite different. If the first is followed, the apparent $T_{DM}$ of the leucosomes is too old and that of the melanosomes is too young, and true $T_{DM}$ of the series should be between the ranges for the two rock types, probably closer to that of the paleosomes if the mass balance seen in the outcrop reflects the amount of melting. If the second is followed, then the $T_{DM}$ of the leucosomes should be a minimum age for the oldest material incorporated in the greywacke, and that of the paleosomes would be a maximum age for the youngest component. Considering that there are magmatic rock units ranging in age from c. 3.2 Ga (Sand river gneisses) to c. 2.6 Ga (e.g. Singelele and Bulai intrusives; Kröner et al., 1998; Barton et al., 1979) in the Central Zone of the Limpopo Belt, and that the Kaapvaal and Zimbabwe Cratons with similar age ranges are not far removed from the site, this is not an unlikely conclusion. It implies retentivity of the Sm-Nd system in monazites under high grade metamorphic conditions, a feature that has here been demonstrated for (possibly armoured) apatite. The adage that Sm-Nd systematics are able to 'look through' sedimentary and metamorphic episodes then takes on a new meaning: REE-fractionation can occur during migmatization, but LREE rich phases may in part retain their individual pre-sedimentary Nd isotope characteristics until they enter the melt - and then impart them to the leucosome. In this context the somewhat scattered distribution of paleosome Sm-Nd data in the 'isochron' diagram could be interpreted as also reflecting a primary heterogeneity, not improbable in clastic sediments.

## 4.9. Conclusions

The Mahalapye Complex is an entity belonging to the CZ of the Limpopo Belt and it underwent high grade metamorphism leading to migmatization during the 2.0 Ga event, as shown by U-Pb monazite and Sm-Nd mineral-WR ages.

If the timing of high grade metamorphism and migmatization is well constrained, age-correction can be used to assess the amount of isotope equilibrium during migmatization.

We found significant offsets in both Sm/Nd ratios and in $^{143}Nd/^{144}Nd$ between leucosomes and paleosomes. The former are due to mineral reactions, particularly garnet formation, and the latter appear to result from preferential incorporation of monazite, compared to apatite, in the melt. LREE -Th relations of the leucosome are in agreement with this. Lower $^{143}Nd/^{144}Nd$ ratios in leucosomes compared to paleosomes cause them to have apparent $T_{DM}$ ages on average 250 Ma older than those of these paleosomes. From LIL element concentration data it appears that leucosomic partial melts may be segregated from their residue without attaining trace element equilibrium with it, and therefore full isotope exchange should also not be expected.

Metasedimentary rocks can retain metre-scale primary Nd isotope heterogeneities during migmatization, and high REE mineral grains within them (apatite, monazite) may escape full Nd isotope exchange even where partial melts are being formed. As such grains can have been detrital in the original sediment, heterogeneities in Nd isotope characteristics of the original source area for those sediments may be retained, and may be expressed even after migmatization. In this way, differences in $T_{DM}$ ages within a metasedimentary migmatite terrain may to a large extent be due to source rocks of different ages, with additional scatter possibly being caused by Sm/Nd fractionation during crystallization of the leucosome. Rather than defining the protolith crustal age as a weighted average of the $T_{DM}$ ages derived from a migmatite outcrop, the true spread in mantle derivation ages for the sediment source region probably exceeds the range of $T_{DM}$ ages found in the outcrop.

## Acknowledgments

This work was supported by the SNF, grant 20-47157.96. We thank ACTLABS for the INAA analysis. VC thanks the technical staff from Bern and Rennes for their assistance in various phases of analytical works as well as many people from both universities for helpful discussions.

# 5. Metamorphic segregation at subsolidus conditions as migmatization process: Implications on Nd-Pb isotope exchange.

Valérie Chavagnac, Thomas F. Nägler and Jan D. Kramers

Universität Bern, Min. Pet. Inst., Gruppe Isotopengeologie, Erlachstr. 9a, 3012 BERN, SWITZERLAND.(FAX: 00-41-31-631-49-88) Corresponding author: chava@mpi.unibe.ch

**submitted to Lithos : 08/05/98**

## Abstract

We have carried out major and trace element analyses as well as Nd and Pb isotope measurements on a stromatic migmatite in the Phikwe Complex (Botswana) in order to assess the effect of high grade metamorphic event leading to migmatization on apparent Nd model ages.

The Phikwe Complex, considered as an entity of the Central Zone of the Limpopo Belt, underwent a high grade metamorphic event at 2.0 Ga leading to migmatite formation. Migmatites in this area present a very good layering of migmatitic components. Petrographic observations indicate the segregation of mafic layers either dominated by Hbl or by Bt, from leucocratic layers on a centimeter to millimeter scale. Accessory minerals such as Mnz, Ap and Zrn were not identified in Hbl and Qtz-fs layers. The combination of petrographic criteria and the trace element concentrations on all layers indicate that the migmatite may have been formed either by partial melting according to Bt and/or Hbl dehydration reactions, or by metamorphic segregation at subsolidus conditions. A clear descrimination between these two processes is obtained from REE modeling applying batch, fractional and disequilibrium melting equations. The modeled REE results of the Qtz-fs layers match those observed via metamorphic segregation at subsolidus conditions. Thus, the distribution of major and trace elements as well as the scatter Nd isotope data are interpreted as the direct consequence of the proportional amount of each mineral in the different migmatitic components. The positive $\varepsilon_{Nd}$ value of Hbl-rich layer suggests Hbl crystallization from a mantle-derived source and Sm/Nd fractionation at protolith formation age. Therefore, the apparent Nd model ages ranging from 2.3 to 3.1 Ga, do not reflect the crustal evolution in Southern Africa in Archean to Proterozoic time.

Based on the geochemical features and the Pb-Pb WR isochron at 2.0 Ga, mass conservation can be assumed to be maintained during migmatization. Therefore, chemical and Nd isotopic compositions of the protolith prior to migmatization are calculated applying mixing equations. The results indicate a quartz and potassium poor diorite as protolith. Moreover, calculated protolith composition results in a Sm-Nd isochron indicating an age of 2.7 Ga, and very similar Nd model ages of 2.73-2.75 Ga. Those ages are good indicators for the magmatic activity in the Phikwe Complex during the Archean.

**key words:** migmatization, Limpopo Belt, Proterozoic, mass balance, isotope

## 5.1. Introduction

The interpretation of Sm-Nd isotope data to constrain mantle source characteristics and crustal history, is based on the assumption that rocks studied remained closed with respect to these elements during intracrustal processes such as metamorphism, fractional crystallization or even partial melting. However, this requirement is not always valid, as shown by some recent studies on high-grade polymetamorphic terranes, which have provided examples of obvious disturbance of the Sm-Nd system (Arndt et al., 1989; Rosing, 1990; Tourpin et al., 1991; Bernard-Griffiths et al., 1991; Gruau et al., 1996; Whitehouse et al., 1996; Moorbath et al., 1997; Chavagnac et al., submitted). Migmatites provide an opportunity to look at the chemical fractionation which occurs during partial melting in the crust. In addition to resetting of Nd systematics in migmatites, some fractionation of the Sm/Nd ratio can take place during partial melting. As a consequence, the apparent Nd model ages of partial melts are too old and those of residual phases are too young (Chavagnac et al., submitted).

Mass balance and trace element modeling are powerful tools to evaluate quantitatively the extent of fractionation. Studies on the distribution of major and trace elements between partial melt and residue have shown that chemical equilibrium is not always reached, and have demonstrated that accessory minerals (zircon, monazite, allanite, apatite, titanite and xenotime) can dominate the distribution of trace element such as Zr, Hf, U, Th, Y and REE in migmatites and also granitoids (Miller and Mittlefehldt, 1982; Gromet and Silver, 1983; Sawyer, 1991). These can retard or inhibit equilibrium between nascent melts and their residue. In cases where accessory and major minerals are not completely chemically re-equilibrated during metamorphism, they may not give useful age information on the migmatization event. For all these reasons, an understanding of the mechanisms which govern the distribution of REE during migmatization are crucial for the interpretation of Nd whole rock studies in high and medium grade terrains.

The objective of the present study is to provide constraints on mechanisms controlling Sm and Nd redistribution during migmatization and to assess Pb and Nd isotope exchange in that process. From this perspective, a detailed study was carried out on a migmatitic sample from the Phikwe Complex in the Central Zone of the Limpopo Belt (Botswana). Petrographic criteria and geochemical results are combined to determine the process by which migmatites of this Complex were formed. A detailed REE study and mass balance calculation are reported. Geochemical data are used to evaluate the behaviour of major and accessory minerals relative to the composition of the migmatitic components and therefore, their influence on Pb and Nd isotope exchange. The question of open or closed system behaviour during migmatization is discussed. In the case of closed system, geochemical and Nd isotopic data can be used to reconstruct the history of the protolith.

Figure I-47: a) Geographical location of the Limpopo Belt in Africa. b) Geological map of the western part of the Limpopo Belt, in Botswana; modified after Geological Survey of Botswana, South Africa and Zimbabwe (1981). MoSZ: Mogagaphate Shear Zone, MSZ: Molabe Shear Zone, LSZ: Lepokole Shear Zone. Sample locality is also indicated.

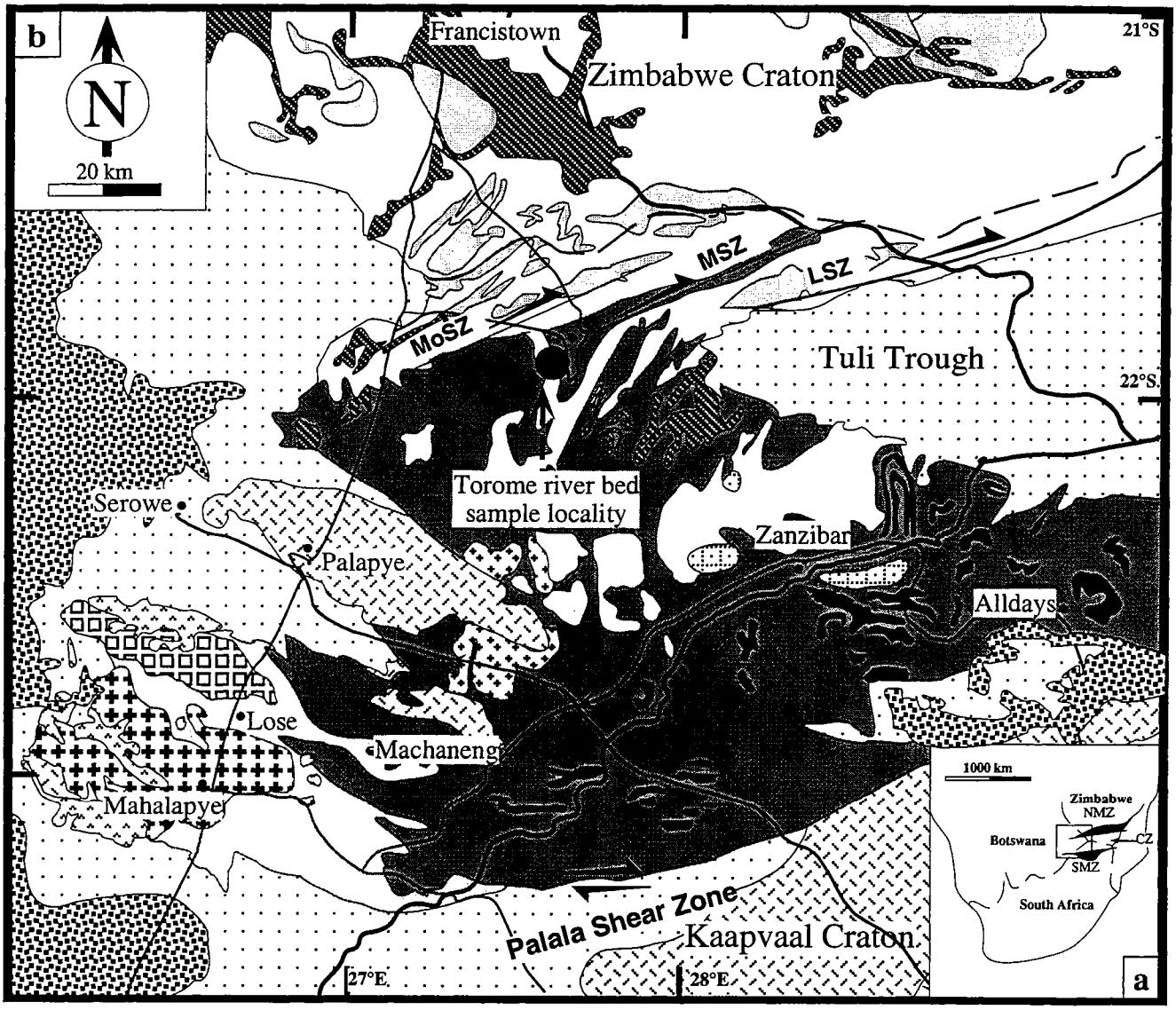

## 5.2. Geological setting

The Limpopo Belt which straddles the borders of South Africa, Zimbabwe and Botswana (Fig. I-47a), represents an example of a high-grade metamorphic belt wedged between two low-grade Archean granite-greenstone provinces, the Kaapvaal and Zimbabwe Cratons. It is separated from these cratons by late Archean inward dipping thrust zones (e.g. Van Reenen et al., 1992). Recent structural, petrological, geochemical and geochronological data have confirmed an important tectonic reworking associated with a high-grade metamorphic event in the Central Zone and Northern Marginal Zone of the Belt at 2.0 Ga (e.g. Barton et al., 1994; Kamber et al., 1995, 1996; Jaeckel et al., 1997; Holzer et al., 1997; Chavagnac et al., submitted). Crustal scale Proterozoic dextral strike slip shear zones, e.g. the Triangle Shear Zone to the north and the Palala Shear Zone to the south, constitute the sutures between the Central Zone and Northern and Southern Marginal Zones (Holzer et al., 1997). Henceforth, the Archean continent-continent collision of the two Cratons is uncertain and Holzer et al. (1997) favour a distinct tectono-metamorphic history in each zone during the Archean period followed by a final juxtaposition at 2.0 Ga.

The Phikwe Complex in eastern Botswana, forms part of the Central Zone of the Limpopo Belt (Fig. I-47b; Mason, 1973; Barton, 1983). The Complex is mainly composed of quartzo-feldspathic gneisses associated with concordant amphibolite layers, and granitic gneisses with ultrabasic intrusions. The quartzo-feldspathic gneisses are believed to be of sedimentary origin whereas the amphibolites are accepted as being generally metavolcanics (Carney et al., 1994). This lithological assemblage together with the metasediments encompasse a resemblance to greenstone-greywacke cratonic associations. The granitoid gneisses represent a wide range of compositions, from tonalitic to granitic, and are frequently migmatized.

The tectono-metamorphic evolution of the Phikwe Complex may be roughly summarized into two main events. The first regional event occurred under granulite facies conditions and the occurrence of charnockitic rafts within granitic gneiss bodies indicate that granulite facies metamorphism and granit formation were contemporaneous (Paya, 1996). The Swejane granitic gneisses which are quite similar to the Bulai granitic gneisses, have been dated by U-Pb in zircon at 2 517 ± 33 Ma, which has been interpreted as their intrusion age (Holzer et al., 1998). The second event is related to a single evolving continuous tectono-metamorphic episode during which partial melting under amphibolite facies took place. Field evidence indicates synkinematic migmatization (Holzer et al., 1998). This metamorphic event was dated by U-Pb on apatite and by Pb stepwise leaching on titanite from the Swejane granitic gneiss at 2001 ± 6 Ma and 1997 ± 7 Ma respectively (Holzer et al., 1998) and also by Rb-Sr biotite ages at 2.0 Ga (Van Breemen and Dodson, 1972). Migmatization is widespread and it is clear from

Figure I-48: Drawn in broad outline of a) all samples and b) each layer within each layer within each part of the migmatitic sample (95/859). In brackets are reported the volume proportion of each layer (in %) assuming the rocks as a parallelepiped.

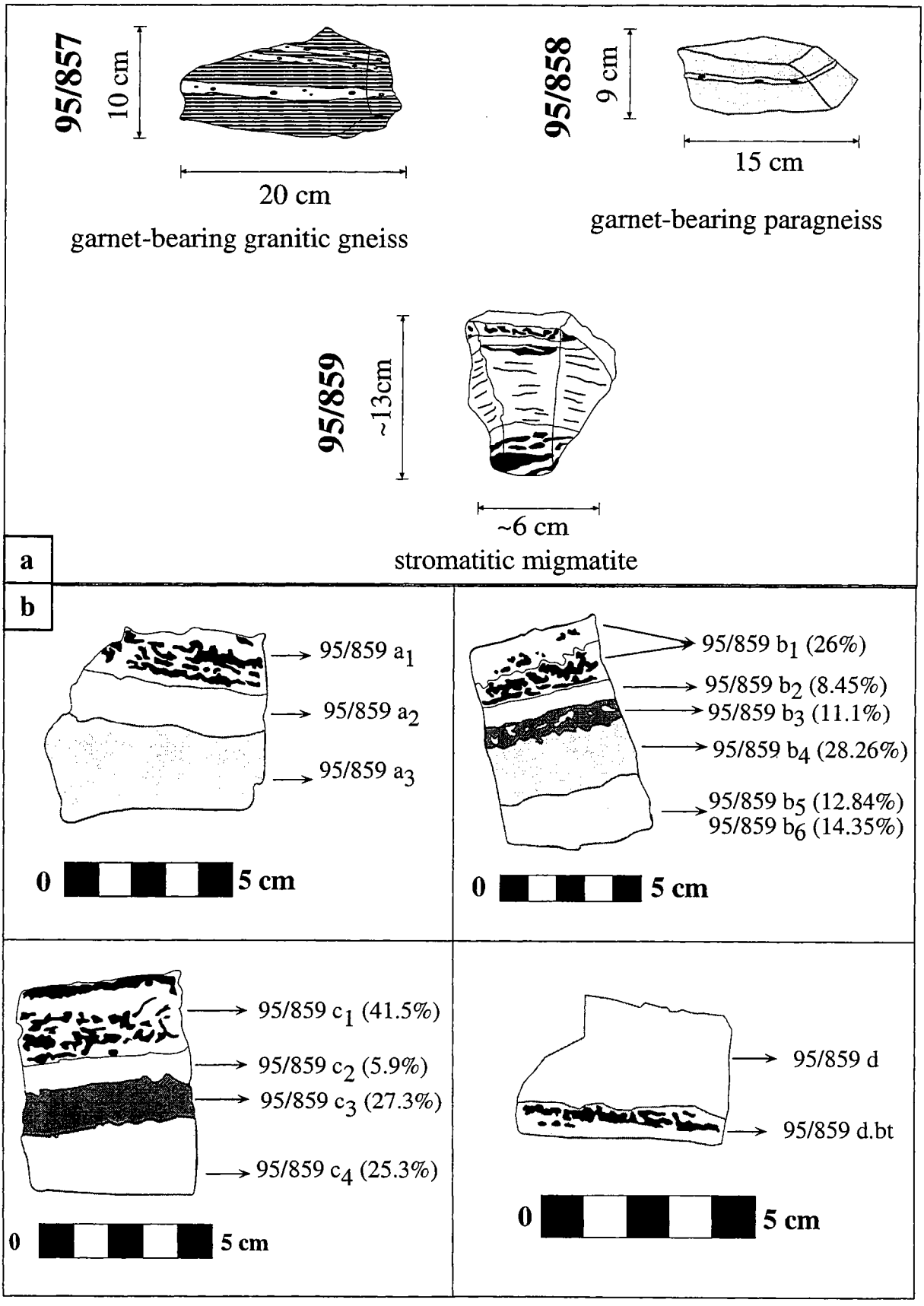

the field observations and the geochronological data, that this took place at 2.0 Ga under amphibolite facies metamorphism (T ~750-800°C, P = 4.5-6 kbar; Tsunogae et al., 1989).

## 5.3. Sample locality and description

The sample locality is situated in the Torome river bed (Fig. I-47b), which presents on an outcrop length of several hundred meters an interlayering of amphibolite, garnet-bearing leucosome, granitic gneiss, garnet-bearing paragneiss and migmatite. The amphibolite as well as garnet-bearing leucosome are sharply defined layers concordant with the granitoid gneisses whereas the garnet-bearing paragneiss occurs as lenses within it and is surrounded by mobilized garnet-bearing leucosome. Migmatites exhibit gradational contact with the other lithologies. Some pegmatitic veins crosscut the other lithologies and therefore are formed after the high-grade metamorphic event.

For this study, we collected samples of tonalitic migmatite, granitic gneiss containing small veins of garnet-bearing leucosome, and garnet-bearing paragneiss (Fig. I-48a).

*The country rock of the tonalitic migmatite*

The garnet-bearing paragneiss (95/858) has a heterogranular grano-nematoblastic texture and consists mainly of quartz (Qtz), plagioclase (Pl), alkali feldspar (K-fs), biotite (Bt), garnet (Grt), and magnetite (Mag) and small amounts of apatite (Ap), monazite (Mnz) and zircon (Zrn). The preferred alignment of Bt, Pl and Mag defines the foliation. Grt (up to 6mm in size) is subhedral but slightly cataclastic and was probably formed at the end of the deformation. Accessory minerals are present at grain boundaries and Zrn may contain an older core. The chemical composition of this paragneiss indicates a greywacke as protolith. Following the descrimination diagram of Bhatia and Cook ( 1986), it is similar to greywackes deposited in basins adjacent to volcanic arc developed in thin continental margins.

The granitic gneiss (95/857) is composed of foliated intermediate metamorphic rock and of Grt-bearing leucocratic veins. The foliated part has a heterogranular grano-nematoblastic texture and consists of Qtz, Pl, K-fs, Bt with minor amounts of Mnz, Ap and Zrn. The accessory minerals are only located within leucocratic minerals. The thin Grt-bearing leucosome in this sample consists essentially of Qtz, saussuritized Pl, K-fs, Grt and some alterated Bt. All minerals have irregular joint boundaries and the grain contact are curved. Grt occurs as elongated and fractured grains and probably crystallized during deformation. For our study this sample was cut in three pieces: (1) the thin Grt-bearing leucocratic veins (95/857L); (2) the foliated Grt-free granitic gneiss (95/857R); and finally (3) the part containing both previous lithologies (95/857WR).

The tonalitic migmatite (95/859) shows a very good layering of migmatitic components on a centimeter scale. The first layer is dominated by mafic minerals such as Bt, hornblende (Hbl) and Mag associated with Qtz, Pl, ± K-fs and Rutile. No accessory minerals such as Ap or Mnz were identified. The grain contact between mafic and leucocratic minerals are curved. This part is in contact with a very leucocratic layer which is composed of Qtz and Pl with minor amount of Bt and K-fs. Mnz only occurs as tiny grains at joint boundaries between leucocratic minerals. Along the edge of the leucocratic layer, we observe a strong accumulation of Bt defining the third layer. This layer is composed of Bt, Qtz, Pl ± K-fs forming a heterogranular nematoblastic texture. Accessory minerals are mainly Ap, with small amounts of Mnz and Zrn. They are not located within mafic minerals. The last different layer looks like an intermediate metamorphic layer and it consists of Qtz, Pl, Bt, ± K-fs with larger amounts of Ap, Mnz, Zrn than the other layers. The main petrographic observations are: (1) Hbl is only observed in one part which is mainly dominated by mafic minerals; (2) the size of the brownish Bt decreases from the contact with the quartzo-feldspathic layer toward the intermediate metamorphic part; (3) mafic and leucocratic minerals are segregated and form an internal layering of leucocratic and melanocratic veins on a millimeter scale within the fourth layer; (4) the An component in Pl varies between $An_5$ and $An_{20}$, and is in the same order in all layers; (5) accessory minerals do not occur randomly and disorderly between the different layers. Only minute Mnz occurs at joint boundaries within the quartzo-feldspathic layer whereas Ap is concentrated in the Bt-rich part and finally Ap, Mnz, Zrn occur in the intermediate metamorphic layer. 95/859 was split into 4 slices of several centimeter in size (Fig. 2b). Slices are termed a, b, c, and d. From the migmatitic assembly in each slice, we dissected one Hbl-rich layer (slice a, b and c), one Bt-rich layer (slice a, b, c and d), one quartzo-feldspathic layer (slice b and c), and finally one intermediate metamorphic layer (slice a, c) and three from slice b. We also analyzed two whole rock samples.

## 5.4. Analytical techniques

*Major and trace elements*

Major and trace elements were determined by X-ray fluorescence spectrometry (XRF) using a Philips spectrometer at the University of Rennes 1. Analytical uncertainties are ±1% to ±3% for major elements, ±5% for trace elements with concentrations above 20 ppm and ±10% for those below 20 ppm. Nb was determined with long counting times so that the precision was maintained at ±10% even for concentration less than 5 ppm. Some trace elements and REE were determined by INAA at ACTLABS, Canada. The detection limits are shown in brackets in table I-14.

*Chemical separation and isotope analyses*

About 100 mg of powdered samples (or 30 mg in the case of one Grt fraction) were spiked with a $^{150}Nd$-$^{149}Sm$ tracer before dissolution. Sample dissolution was carried out in two steps. First, the samples were attacked with a 1:3 mixture of ($HNO_3$ + HF) in a sealed savillex beaker at room temperature for one day. In order to suppress formation of any fluorite crusts and facilitate the dissolution, the savillex beaker was repeatedly placed in an ultrasonic bath for 20 minutes. After one day, the solution was evaporated to dryness. The same acid mix was added a second time and closed beaker was heated at 150 °C for 7 days and placed in an ultrasonic bath for 20 minutes twice a day. After evaporating to dryness, any remaining fluorites were dissolved in 6 N HCl on a hot plate during several hours. For U-Pb chemistry (95/859b), about 200 mg of sample were dissolved with a 1:3 mixture of ($HNO_3$ + HF) in a sealed savillex beaker at 120 °C for 7 days. The savillex beaker was repeatedly placed in an ultrasonic bath for 20 minutes each day. After evaporating to dryness, the sample was dissolved in a HBr : HCl mixture on a hot plate.

Separation of Sm and Nd was done using a routine two column ion-exchange technique, including first, a group separation of REE through a cation exchange column, followed by a separation of Nd from Sm through a second column packed with Kel-F Teflon coated with HDEHP. Chemical separations on whole rock samples were done at the University of Rennes 1. U and Pb were separated using standard anion exchange, at the University of Bern.

For the whole rock, Nd isotope analyses were done at the University of Rennes 1 using double Re filament ($Nd^+$ emission) in a seven collector Finnigan MAT 262 mass spectrometer. $^{143}Nd/^{144}Nd$ were normalized against $^{146}Nd/^{144}Nd = 0.7219$. During the period of data acquisition, the La Jolla standard gave $^{143}Nd/^{144}Nd = 0.511861 \pm 0.000006$ (2 standard deviation, n = 8; AMES standard value in 1997: $^{143}Nd/^{144}Nd = 0.511961 \pm 0.000007$; 2 standard deviation, n = 49). Nd isotopic compositions of part b were analyzed at the University of Bern using single Re filament ($NdO^+$ emission) in a modified VG Sector mass spectrometer in a single collector mode. The oxygen isotopic composition was determined by analysing pure $^{150}Nd$ spike as described by Wasserburg et al. (1981) and Chavagnac (in prep) and the average compositions gave $^{18}O/^{16}O = 2.024 \pm 0.23\ 10^{-3}$ close to Nier's (1950) value $^{18}O/^{16}O = 2.045\ 10^{-3}$, and $^{17}O/^{16}O = 3.83\ 10^{-4} \pm 0.03\ 10^{-4}$. Mass interference and oxygen corrections as well as fractionation and spike corrections are done on-line during the measurement. Le Jolla standard gave $0.511866 \pm 0.000029$ (2 standard deviation; n = 5). The Pb isotopic compositions were measured on a Re single filament on a VG Sector in static multi-collector mode; fractionation correction was done empirically using measurements of the NIST SRM 981 Pb standard, and amount to $0.08 \pm 0.02\%$ per mass unit. All Sm and U isotopic compositions were analyzed on triple Ta-Re-Ta filaments on an AVCO, single collector mass spectrometer at the University of

Figure I-49: Major and trace element distributions within the migmatitic sample: a) Fe2O3 versus MgO, b) TiO2 versus MgO, c) Ba versus Rb, d) Th versus MgO. Legend: black triangle: Hbl-rich layer, open circle: Qtz-fs layer, black circle: Bt-rich layer, and open star: intermediate metamorphic layer, cross: whole rock.

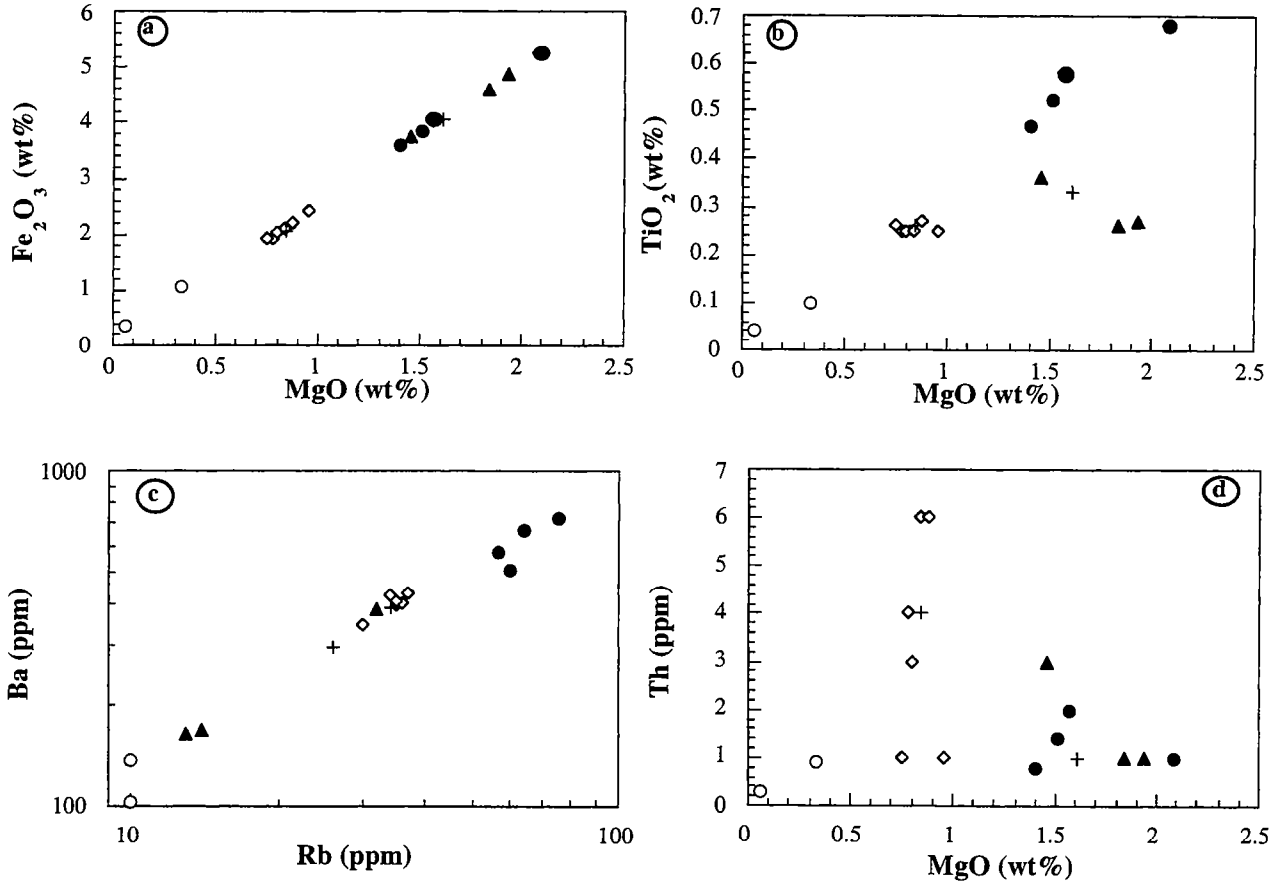

Table I-14: Major and trace element concentrations of sample 95/859.

| sample number | 95/859a.1 | 95/859a.2 | 95/859a.3 | 95/859b.1 | 95/859b.2 | 95/859b.3 | 95/859b.4 | 95/859b.5 | 95/859b.6 |
|---|---|---|---|---|---|---|---|---|---|
| type | Hbl-rich layer | Int. met. layer | Bt-rich layer | Hbl-rich layer | Qtz-Fs layer | Bt-rich layer | Int. met. layer | Int. met. layer | Int. met. layer |
| **major elements in weight %** | | | | | | | | | |
| SiO2 | 60.15 | 60.37 | 58.34 | 57.41 | 74.5 | 57.85 | 60.6 | 61.77 | 61.48 |
| TiO2 | 0.36 | 0.27 | 0.58 | 0.26 | 0.1 | 0.52 | 0.25 | 0.26 | 0.25 |
| Al2O3 | 20.17 | 21.46 | 21.29 | 21.09 | 13.97 | 21.71 | 21.48 | 20.58 | 21.46 |
| Fe2O3 | 3.73 | 2.21 | 4.03 | 4.59 | 1.05 | 3.83 | 2.03 | 1.93 | 2.11 |
| MnO | 0.06 | 0.03 | 0.05 | 0.11 | 0.01 | 0.05 | 0.02 | 0.02 | 0.02 |
| MgO | 1.46 | 0.88 | 1.57 | 1.84 | 0.33 | 1.51 | 0.8 | 0.76 | 0.84 |
| CaO | 7.48 | 7.44 | 7.01 | 8.79 | 5.06 | 7.19 | 7.45 | 7.15 | 7.5 |
| Na2O | 3.54 | 3.98 | 3.77 | 3.67 | 2.56 | 3.87 | 4.06 | 3.89 | 3.99 |
| K2O | 0.87 | 0.9 | 1.43 | 0.57 | 0.32 | 1.36 | 0.85 | 0.84 | 0.85 |
| P2O5 | 0.04 | 0.1 | 0.02 | 0.03 | 0.02 | 0.02 | 0.1 | 0.07 | 0.08 |
| PF | 0.57 | 0.52 | 0.6 | 0.51 | 0.66 | 0.81 | 0.63 | 0.66 | 0.42 |
| Total | 98.43 | 98.16 | 98.69 | 98.87 | 98.58 | 98.72 | 98.27 | 97.93 | 99 |
| **trace elements in ppm** | | | | | | | | | |
| Nb | 2.8 | 1 | 3.1 | 3.7 | - | - | 0.7 | 1.3 | 1.1 |
| Zr | 59 | 163 | 33 | 14 | - | - | 179 | 161 | 144 |
| Y | 6 | 2 | 0 | 12 | - | - | 1 | 1 | 0 |
| Sr | 285 | 323 | 299 | 286 | 169 | 169 | 324 | 307 | 320 |
| Rb | 32 | 37 | 64 | 14 | 10 | 60 | 36 | 35 | 34 |
| Co | 11 | 7 | 16 | 16 | - | - | 7 | 8 | 6 |
| V | 84 | 44 | 100 | 132 | - | - | 38 | 46 | 42 |
| Ni | 22 | 10 | 25 | 27 | - | - | 9 | 10 | 11 |
| Cr | 26 | 22 | 22 | 24 | 12 | 20 | 11 | 11 | 25 |
| Ba | 387 | 429 | 667 | 167 | 137 | 505 | 404 | 406 | 424 |
| Ga | 22 | 23 | 23 | 23 | - | - | 23 | 22 | 23 |
| Cu | 3 | 12 | 8 | 24 | - | - | 16 | 6 | 8 |
| Zn | 42 | 28 | 50 | 48 | 32 | 74 | 27 | 27 | 26 |
| Th# {0.1} | 3.5 | 6.3 | 2 | 1.1 | 0.9 | 1.4 | 4.3 | 1.4 | 6.4 |
| Pb | 8 | 10 | 11 | 10 | - | - | 10 | 10 | 10 |
| U# {0.1} | 1 | 1.6 | 0.3 | 2.8 | 1.9 | 3.7 | 1.4 | 1.4 | 1.4 |
| Sc# {0.1} | 8.7 | 3 | 4.6 | 12.2 | 1.4 | 6.2 | 2.6 | 1.4 | 2.6 |
| **Rare Earth Elements in ppm** | | | | | | | | | |
| La# {0.1} | 6.4 | 15.8 | 5 | 3.2 | 2.1 | 3.5 | 11.1 | 6.1 | 17.5 |
| Ce# {1} | 14 | 30 | 10 | 9 | 3 | 6 | 20 | 12 | 35 |
| Nd# {1} | 8 | 12 | 4 | 4 | 1 | 2 | 7 | 5 | 15 |
| Sm# {0.01} | 1.65 | 1.88 | 0.62 | 1.43 | 0.29 | 0.38 | 1.45 | 0.93 | 1.97 |
| Eu# {0.05} | 0.64 | 0.36 | 0.46 | 0.71 | 0.3 | 0.43 | 0.59 | 0.56 | 0.71 |
| Gd# {0.1} | 1.4 | 2 | 0.5 | 1.5 | 0.3 | 0.4 | 1.1 | 0.7 | 1.2 |
| Tb# {0.1} | 0.3 | 0.2 | 0.1 | 0.3 | <0.1 | 0.1 | 0.1 | 0.1 | 0.1 |
| Yb# {0.05} | 0.66 | 0.23 | 0.05 | 1.29 | 0.11 | 0.05 | 0.15 | 0.12 | 0.1 |
| Lu# {0.01} | 0.09 | 0.03 | 0.01 | 0.19 | 0.02 | 0.01 | 0.03 | 0.02 | 0.02 |
| (Eu/Eu*) | 1.30 | 0.58 | 2.56 | 1.50 | 3.15 | 3.42 | 1.45 | 2.15 | 1.43 |
| (La/Yb)N | 6.40 | 45.36 | 66.03 | 1.64 | 12.61 | 46.22 | 48.86 | 33.57 | 115.56 |
| **Norme in weight %** | | | | | | | | | |
| Qtz | 18.2 | 16.8 | 13.63 | 13.26 | 47.11 | 12.53 | 16.86 | 19.67 | 17.92 |
| Or | 5.14 | 5.32 | 8.45 | 3.37 | 1.89 | 8.04 | 5.02 | 4.96 | 5.02 |
| Ab | 29.95 | 33.68 | 31.9 | 31.05 | 21.66 | 32.75 | 34.35 | 32.92 | 33.76 |
| An | 36.58 | 36.26 | 34.65 | 39.39 | 24.97 | 35.54 | 36.31 | 35.01 | 36.69 |
| Mg-Hy | 3.54 | 2.19 | 3.91 | 3.13 | 0.82 | 3.76 | 1.99 | 1.89 | 2.09 |
| Mg-Di | 0.1 | - | - | 1.45 | - | - | - | - | - |
| Ca-Di | 0.11 | - | - | 1.68 | - | - | - | - | - |
| Ap | 0.09 | 0.23 | 0.05 | 0.07 | 0.05 | 0.05 | 0.23 | 0.16 | 0.19 |
| Ru | 0.29 | 0.24 | 0.52 | 0.14 | 0.09 | 0.46 | 0.23 | 0.24 | 0.23 |
| Cor | - | 0.65 | 0.84 | - | 0.26 | 0.85 | 0.57 | 0.44 | 0.53 |
| Hem | 3.73 | 2.21 | 4.03 | 4.59 | 1.05 | 3.83 | 2.03 | 1.93 | 2.11 |
| Mag | - | - | - | - | - | - | - | - | - |
| Ilm | 0.13 | 0.06 | 0.11 | 0.24 | 0.02 | 0.11 | 0.04 | 0.04 | 0.04 |

Table I-14: Major and trace element concentrations of sample 95/859. continued.

| sample number<br>type | 95/859c.1<br>Hbl-rich layer | 95/859c.2<br>Qtz-Fs layer | 95/859c.3<br>Bt-rich layer | 95/859c.4<br>Int. met. layer | 95/859d.WR<br>whole rock | 95/859d.bt<br>Bt-rich layer | 95/859d<br>Int. met. layer | 95/859WR<br>whole rock |
|---|---|---|---|---|---|---|---|---|
| **major elements in weight %** | | | | | | | | |
| SiO2 | 58.48 | 73.08 | 57.74 | 61.55 | 61.36 | 55.65 | 57.86 | 60.12 |
| TiO2 | 0.27 | 0.04 | 0.47 | 0.25 | 0.26 | 0.68 | 0.25 | 0.33 |
| Al2O3 | 20.15 | 15.66 | 22.07 | 21.22 | 21.33 | 21.88 | 23.06 | 20.18 |
| Fe2O3 | 4.86 | 0.37 | 3.58 | 1.91 | 2.07 | 5.26 | 2.41 | 4.05 |
| MnO | 0.12 | 0.01 | 0.04 | 0.02 | 0.03 | 0.07 | 0.04 | 0.08 |
| MgO | 1.94 | 0.06 | 1.4 | 0.78 | 0.84 | 2.09 | 0.96 | 1.61 |
| CaO | 8.56 | 5.68 | 7.37 | 7.39 | 7.45 | 7.2 | 8.3 | 7.89 |
| Na2O | 3.43 | 3.01 | 4.01 | 4 | 4.01 | 3.69 | 4.2 | 3.47 |
| K2O | 0.56 | 0.25 | 1.31 | 0.84 | 0.87 | 1.71 | 0.84 | 0.75 |
| P2O5 | 0.02 | 0.02 | 0.02 | 0.08 | 0.09 | 0.04 | 0.07 | 0.03 |
| PF | 0.43 | 0.22 | 0.45 | 0.47 | 0.54 | 0.64 | 0.62 | 0.55 |
| Total | 98.82 | 98.4 | 98.46 | 98.51 | 98.85 | 98.91 | 98.61 | 99.06 |
| **trace elements in ppm** | | | | | | | | |
| Nb | 3.5 | - | - | 0.9 | 0.7 | 3.5 | 1.5 | 3.3 |
| Zr | 15 | - | - | 165 | 163 | 61 | 11 | 27 |
| Y | 13 | - | - | 0 | 1 | 2 | 2 | 9 |
| Sr | 276 | 169 | 254 | 319 | 318 | 299 | 332 | 278 |
| Rb | 13 | 10 | 57 | 35 | 34 | 75 | 30 | 26 |
| Co | 15 | - | - | 7 | 7 | 19 | 10 | 14 |
| V | 128 | - | - | 39 | 39 | 131 | 65 | 110 |
| Ni | 29 | - | - | 8 | 8 | 32 | 16 | 23 |
| Cr | 31 | <1 | 20 | 14 | 21 | 29 | 6 | 32 |
| Ba | 164 | 103 | 574 | 396 | 391 | 718 | 346 | 297 |
| Ga | 22 | - | - | 23 | 22 | 25 | 23 | 22 |
| Cu | 22 | - | - | 8 | 9 | 6 | 15 | 29 |
| Zn | 47 | 28 | 50 | 26 | 27 | 63 | 32 | 43 |
| Th# {0.1} | 0.7 | 0.3 | 0.8 | 3 | 4.7 | 0.6 | 1 | 1 |
| Pb | 10 | - | - | 9 | 11 | 8 | 12 | 10 |
| U# {0.1} | 1.4 | 1.8 | 2.6 | 2 | 1.8 | 0.4 | 3.5 | 3.2 |
| Sc# {0.1} | 13.8 | 0.4 | 5.1 | 2.7 | 2.9 | 6.8 | 4 | 9.8 |
| **Rare Earth Elements in ppm** | | | | | | | | |
| La# {0.1} | 3.7 | 2.2 | 4.3 | 9.6 | 12.9 | 3.3 | 3.2 | 4 |
| Ce# {1} | 9 | 5 | 7 | 15 | 28 | 6 | 7 | 9 |
| Nd# {1} | 4 | 1 | 3 | 6 | 10 | 2 | 3 | 4 |
| Sm# {0.01} | 1.77 | 0.21 | 0.44 | 1.15 | 1.59 | 0.57 | 0.85 | 1.3 |
| Eu# {0.05} | 0.81 | 0.31 | 0.45 | 0.59 | 0.61 | 0.44 | 0.57 | 0.38 |
| Gd# {0.1} | 1.7 | 0.2 | 0.4 | 1.7 | 1.2 | 0.5 | 0.7 | 1.4 |
| Tb# {0.1} | 0.4 | 0.1 | 0.1 | 0.2 | 0.1 | 0.1 | 0.1 | 0.3 |
| Yb# {0.05} | 1.68 | 0.05 | 0.05 | 0.07 | 0.2 | 0.2 | 0.39 | 1.05 |
| Lu# {0.01} | 0.24 | 0.01 | 0.01 | 0.02 | 0.03 | 0.03 | 0.05 | 0.15 |
| (Eu/Eu*) | 1.45 | 4.68 | 3.32 | 1.31 | 1.37 | 2.55 | 2.29 | 0.87 |
| (La/Yb)N | 1.45 | 29.05 | 56.79 | 90.56 | 42.59 | 10.90 | 5.42 | 2.52 |
| **Norme in weight %** | | | | | | | | |
| Qtz | 16.16 | 42.41 | 11.58 | 18.3 | 17.74 | 9.21 | 11.2 | 18.21 |
| Or | 3.31 | 1.48 | 7.74 | 4.96 | 5.14 | 10.1 | 4.96 | 4.43 |
| Ab | 29.02 | 25.47 | 33.93 | 33.85 | 33.93 | 31.22 | 35.54 | 29.36 |
| An | 37.93 | 28.05 | 36.43 | 36.14 | 36.37 | 35.46 | 40.72 | 37.27 |
| Mg-Hy | 3.24 | 0.15 | 3.49 | 1.94 | 2.09 | 5.21 | 2.39 | 3.41 |
| Mg-Di | 1.59 | - | - | - | - | - | - | 0.6 |
| Ca-Di | 1.84 | - | - | - | - | - | - | 0.7 |
| Ap | 0.05 | 0.05 | 0.05 | 0.19 | 0.21 | 0.09 | 0.16 | 0.07 |
| Ru | 0.13 | 0.03 | 0.42 | 0.23 | 0.23 | 0.6 | 0.2 | 0.24 |
| Cor | - | 0.16 | 0.7 | 0.49 | 0.46 | 0.96 | 0.32 | - |
| Hem | 4.86 | 0.37 | 3.58 | 1.91 | 2.07 | 5.26 | 2.41 | 4.05 |
| Mag | - | - | - | - | - | - | - | - |
| Ilm | 0.26 | 0.02 | 0.09 | 0.04 | 0.06 | 0.15 | 0.09 | 0.17 |

Bern. The uncertainties on Sm/Nd ratios are less than ± 0.3%. Chemical procedural blank are 50 pg for Sm, 100 pg for Nd, and 50 pg for Pb.

Sm-Nd model ages were calculated relative to Depleted Mantle evolution. The Nd evolution of the Depleted Mantle is approximated by a third order polynomial fit:

$$\varepsilon_{Nd}(T) = 0.164\ T^3 - 0.566\ T^2 - 2.79\ T + 10.4$$ (Nägler and Kramers, 1998)

## 5.5. Results

### 5.5.1. Major and trace element results

The major and trace elements of all layers of 95/859 are reported in Table I-14.

Migmatitic layers range in $SiO_2$ contents from 55 wt% (Bt-rich layers) to 74 wt% (Qtz-fs layers). According to the rock classifications of Streckeisen (1976) and O'Connor (1965), all layers have a tonalitic composition. The migmatitic layers define a perfect linear correlation (R = 1) in a $Fe_2O_3$ versus MgO diagram (Fig. I-49a) whereas they highlight different compositions in $TiO_2$ versus MgO diagram (also in $K_2O$ versus MgO diagram not shown; Fig. I-49b). The Bt-rich layer is enriched in $TiO_2$, $K_2O$, $Fe_2O_3$ and MgO whereas the Hbl-rich layer is enriched in $Fe_2O_3$ and MgO but depleted in $TiO_2$ and $K_2O$. In addition, the Qtz-fs layer is depleted in all these elements compared to the other layers and the intermediate metamorphic layer has a very homogeneous and intermediate chemical composition between the three other chemical compositions. In Ba versus Rb diagram (Fig. I-49c), they define 4 different compositional fields according to the proportion of their best host mineral for the element of interest in the different layers. Th, U and REE data are added to evaluate the role of accessory minerals on the chemical compositions of the layer. Migmatitic layers have variable Th contents (Fig. I-49d). The chondrite-normalized REE patterns of Hbl-rich, Bt-rich, Qtz-fs and intermediate metamorphic layers are reported separately in Fig. I-50a, I-50b, I-50c, and I-50d. Hbl-rich layers are characterized by flat REE patterns ($(La/Yb)_N$ = 1.4 to 6.4) and weak positive Eu anomalies ((Eu/Eu*) = 1.4) whereas Bt-rich layers show LREE enriched patterns ($(La/Yb)_N$ = 11 to 66) and distinct positive Eu anomalies ((Eu/Eu*) = 2.6 to 3.5). Qtz-fs layers are characterized by low REE contents compared to the three other layers, LREE depletion, and large positive Eu anomalies ((Eu/Eu*) = 3.15 to 4.68). In contrast, the intermediate metamorphic layers are characterized by high REE contents, LREE enriched patterns $(La/Yb)_N$ = 34-115) and weak positive Eu anomalies (((Eu/Eu*) = 1.5).

Figure I-50: Chondrite-normalized REE patterns of Hbl-roch lqyer in a), Qtz-fs layer in b) Bt-rich layer in c) and intermediate metamorphic layer in d). Normalization values are those of Masuda et al. (1973).

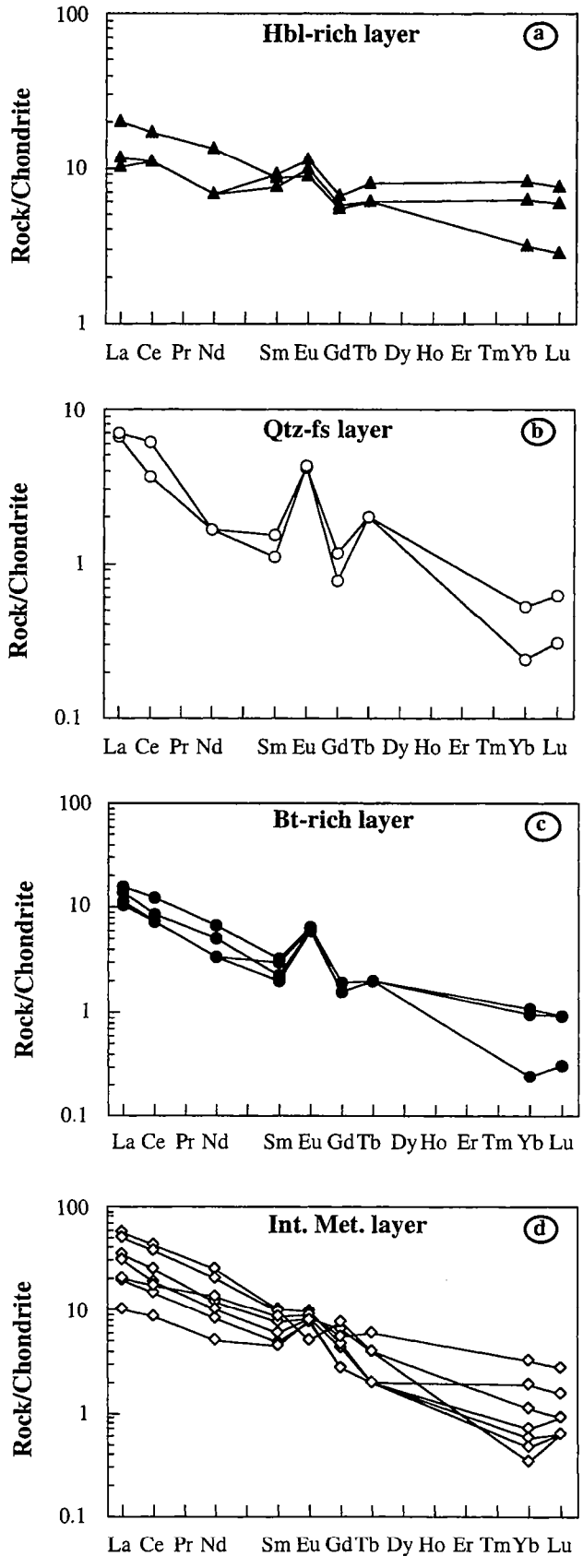

Table I-15: Sm-Nd isotopic compositions of all layers and samples from 95/859, 95/858 and 95/857 as well as mineral separates.

| Sample number | Rock type | Sm (ppm) by ID | Nd (ppm) by ID | 147Sm/144Nd | 143Nd/144Nd | ± 2 σ | ε(0) | ε (2.0) 2.00 | T(DM)* Ga | T(DM)** Ga | f(Sm/Nd) |
|---|---|---|---|---|---|---|---|---|---|---|---|
| **Tonalitic migmatite** | | | | | | | | | | | |
| **95/859a.1** | Hbl-rich part | 1.57 | 5.82 | 0.1628 | 0.512044 | 7 | -11.59 | -2.90 | 3.29 | 2.97 | -0.172 |
| **95/859a.2** | Int. Met. part | 1.72 | 9.9 | 0.1048 | 0.511124 | 7 | -29.53 | -5.96 | 2.82 | 2.67 | -0.467 |
| **95/859a.3** | Bt-rich part | 0.55 | 2.97 | 0.1110 | 0.511330 | 12 | -25.52 | -3.52 | 2.69 | 2.53 | -0.436 |
| **95/859b.1** | Hbl-rich part | 1.36 | 4.05 | 0.2027 | 0.512732 | 7 | 1.83 | 0.29 | 5.70 | nd | 0.031 |
| **95/859b.2** | Qtz-Fs part | 0.23 | 0.98 | 0.1438 | 0.511902 | 21 | -14.36 | -0.77 | 2.71 | 2.48 | -0.269 |
| **95/859b.3** | Bt-rich part | 0.36 | 1.98 | 0.1086 | 0.511433 | 22 | -23.51 | -0.88 | 2.48 | 2.33 | -0.448 |
| **95/859b.4** | Int. Met. part | 1.24 | 6.83 | 0.1101 | 0.511046 | 19 | -31.06 | -8.86 | 3.07 | 2.92 | -0.440 |
| **95/859b.5** | Int. Met. part | 0.79 | 4.09 | 0.1165 | 0.511380 | 17 | -24.54 | -3.96 | 2.76 | 2.59 | -0.408 |
| **95/859b.6** | Int. Met. part | 1.66 | 9.90 | 0.1014 | 0.511216 | 13 | -27.74 | -3.28 | 2.61 | 2.47 | -0.484 |
| **95/859c.1** | Hbl-rich part | 1.50 | 4.40 | 0.2066 | 0.512754 | 13 | 2.26 | -0.28 | 8.30 | nd | 0.050 |
| **95/859c.2** | Qtz-Fs part | 0.17 | 0.97 | 0.1048 | 0.511278 | 36 | -26.53 | -2.94 | 2.61 | 2.46 | -0.467 |
| **95/859c.3** | Bt-rich part | 0.39 | 2.20 | 0.1077 | 0.511366 | 14 | -24.81 | -1.97 | 2.55 | 2.40 | -0.452 |
| **95/859c.4** | Int. Met. part | 1.13 | 6.21 | 0.1096 | 0.511228 | 7 | -27.50 | -5.16 | 2.80 | 2.64 | -0.443 |
| **95/859d** | Int. Met. part | 0.75 | 2.63 | 0.1715 | 0.512182 | 16 | -8.90 | -2.44 | 3.47 | 3.10 | -0.128 |
| **95/859d.R** | Bt-rich part | 0.54 | 2.38 | 0.1382 | 0.511789 | 35 | -16.56 | -1.54 | 2.73 | 2.52 | -0.297 |
| **95/859WR** | Whole rock | 1.23 | 4.16 | 0.1793 | 0.512377 | 16 | -5.09 | -0.63 | 3.40 | 2.93 | -0.088 |
| **95/859d.WR** | Whole rock | 1.40 | 7.65 | 0.1109 | 0.51123 | 13 | -27.47 | -5.46 | 2.83 | 2.67 | -0.436 |
| **Garnet-bearing paragneiss** | | | | | | | | | | | |
| **95/858** | garnet 300-200µm | 7.65 | 11.33 | 0.4082 | 0.515129 | 19 | 48.59 | -5.76 | - | - | 1.075 |
| **95/858** | garnet 300-200 µm | 7.98 | 13.82 | 0.3492 | 0.514384 | 19 | 34.06 | -5.13 | - | - | 0.775 |
| **95/858** | garnet 200-100µm | 7.14 | 10.49 | 0.4115 | 0.515179 | 21 | 49.57 | -5.63 | - | - | 1.092 |
| **95/858** | Whole rock | 12.70 | 54.05 | 0.1420 | 0.511657 | 7 | -19.14 | -5.11 | 3.15 | 2.93 | -0.278 |
| **Granitic gneiss** | | | | | | | | | | | |
| **95/857WR** | Whole rock | 6.23 | 22.83 | 0.1648 | 0.512071 | 6 | -11.06 | -2.88 | 3.34 | 3.01 | -0.162 |
| **95/857** | garnet 300-200µm | 5.15 | 6.56 | 0.4742 | 0.51615 | 19 | 68.51 | -2.78 | - | - | 1.411 |
| **95/857L** | garnet-leucosome | 7.13 | 24.45 | 0.1762 | 0.512252 | 7 | -7.53 | -2.28 | 3.62 | 3.23 | -0.104 |
| **95/857R** | foliated part | 5.62 | 21.07 | 0.1612 | 0.512017 | 7 | -12.11 | -3.01 | 3.26 | 2.96 | -0.180 |

**T(DM)*: calculated according to Goldstein et al. (1984)**
**T(DM)**: calculated according to Nägler and Kramers (1998)**

Table I-16: U-Pb isotopic data of all layers from 95/859 slice b.

| sample | type | 206Pb/204Pb | 207Pb/204Pb | 208Pb/204Pb | U (ppb) | 1s(%) | Pb (ppb) | 1s (%) | μ 238 | μ 235 |
|---|---|---|---|---|---|---|---|---|---|---|
| **95/859b.1** | Hbl-rich part | 29.027 | 17.418 | 35.403 | 2422.3 | 0.44 | 7613 | 0.282 | 22.722 | 0.165 |
| **95/859b.2** | Qtz-Fs part | 24.303 | 16.785 | 34.891 | 1831.6 | 0.71 | 6061 | 0.088 | 20.054 | 0.145 |
| **95/859b.3** | Bt-rich part | 29.208 | 17.429 | 35.136 | - | - | 9404 | 0.072 | - | - |
| **95/859b.4** | Int. Met. part | 19.296 | 16.213 | 37.313 | 1104.1 | 0.33 | 6824 | 0.106 | 9.615 | 0.070 |
| **95/859b.5** | Int. Met. part | 19.069 | 16.185 | 35.782 | 1099.0 | 0.19 | 7885 | 0.138 | 8.659 | 0.063 |
| **95/859b.6** | Int. Met. part | 19.54 | 16.240 | 38.924 | 1042.7 | 0.42 | 6901 | 0.146 | 9.866 | 0.072 |

### 5.5.2. Nd and Pb isotopic compositions

Sm-Nd results are presented in Table I-15 and the U-Pb results on 95/859b are reported in Table I-16.

For the granitic gneiss, sections 95/857L, 95/857R, 95/857WR and one Grt fraction give a Sm-Nd isochron age of 2000 ± 66 Ma (MSWD = 5.7; Fig. I-51a). For the granetiferous paragneiss sample 95/858, the whole rock plus three different fractions of Grt yield an age of 1986 ± 12 Ma (MSWD = 1.8; Fig. I-51b). The initial $\varepsilon_{Nd}$ values for the samples (-2.7 for 95/857 and -5.2 for 95/858) document a considerable pre 2.0 Ga crustal history for the Complex. All migmatitic components from 95/859b were analyzed for U-Pb. The best regression line gives an age of 1998 ± 68 Ma (MSWD = 0.65; Fig. I-52a). The data plot well above the Stacey and Kramers (1975) curve, again indicating a long pre 2.0 Ga crustal history. Sm-Nd data of all layers from tonalitic migmatitic sample 95/859 are plotted in a Sm-Nd isochron diagram in Fig. I-52b. The slope of the regression line corresponds to an age of 2350 ± 220 Ma (MSWD = 56; 17 points). The scatter is essentially due to the highly variable Nd isotopic compositions (at similar Sm/Nd ratios) within the intermediate metamorphic layer. Their apparent Nd model ages vary between 2.4 and 3.1 Ga. Fig. I-52c shows the Nd isotopic compositions recalculated to 2.0 Ga in function of (1/Nd). The association of the Bt-rich layers and the intermediate metamorphic layers defines a trend in which the decreasing Nd contents is related to an increasing Nd isotopic composition, approaching those of Qtz-fs layers. Hbl-rich layers, Bt-rich layers and Qtz-fs layers broadly define a horizontal line. The behaviour of Sm-Nd system during metamorphism can be judged from the $f_{Sm/Nd}$ versus $\varepsilon_{Nd}(2.0)$ diagram (Fig. I-52d) which indicates the relative enrichment of Sm/Nd in a given layer relative to CHUR. In this diagram, only Hbl-rich layers have highly variable $f_{Sm/Nd}$ for the same $\varepsilon_{Nd}(2.0)$ whereas the other layers show variable $\varepsilon_{Nd}(2.0)$ values for the same $f_{Sm/Nd}$ value.

## 5.6. Discussion

### 5.6.1. Migmatization process

Since the earliest study of Mehnert (1968) on migmatites, several processes have been proposed to explain migmatite formation: (1) injection of foreign magma along the foliation planes (Sederholm, 1907, 1913, 1934; Weber and Barbey, 1986; Barbey et al., 1990); (2) metasomatism at subsolidus or hypersolvus conditions (Misch, 1968; Olsen, 1984, 1985; Babcock and Misch, 1989); (3) metamorphic differentiation at subsolidus temperature by chemical and/or mechanical processes (Robin, 1979; Ashworth and McLellan, 1985; Lindh and Wahlgren, 1985; Bloom, 1988; Whitney and Irving, 1994); and (4) partial melting (anatexis)

Figure I-51: a) Sm-Nd garnet-95/857R-95/857L-95/857WR isochron indicating an age of 2000 ± 66 Ma, b) Sm-Nd 3 garnet fractions-95/858WR isochron yielding an age of 1986 ± 12 Ma.

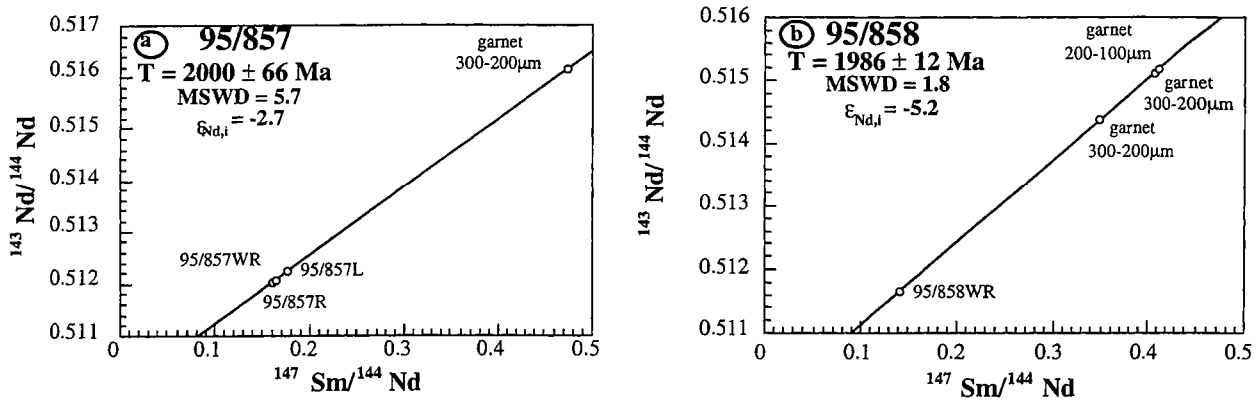


Figure I-52: a) Pb-Pb isochron diagram from 95/859b which indicates an age of 1998 ± 68 Ma, b) Sm-Nd whole rock diagram for all layers of sample 95/859 at the present time. The same legend as in Figure I-50, c) Nd isotopic compositions for all layers at 2.0 Ga in function of (1/Nd). The same legend as in Figure I-50, d) fSm/Nd in function of Nd epsilon values at 2.0 Ga for all layers within 95/859b and 95/859c.

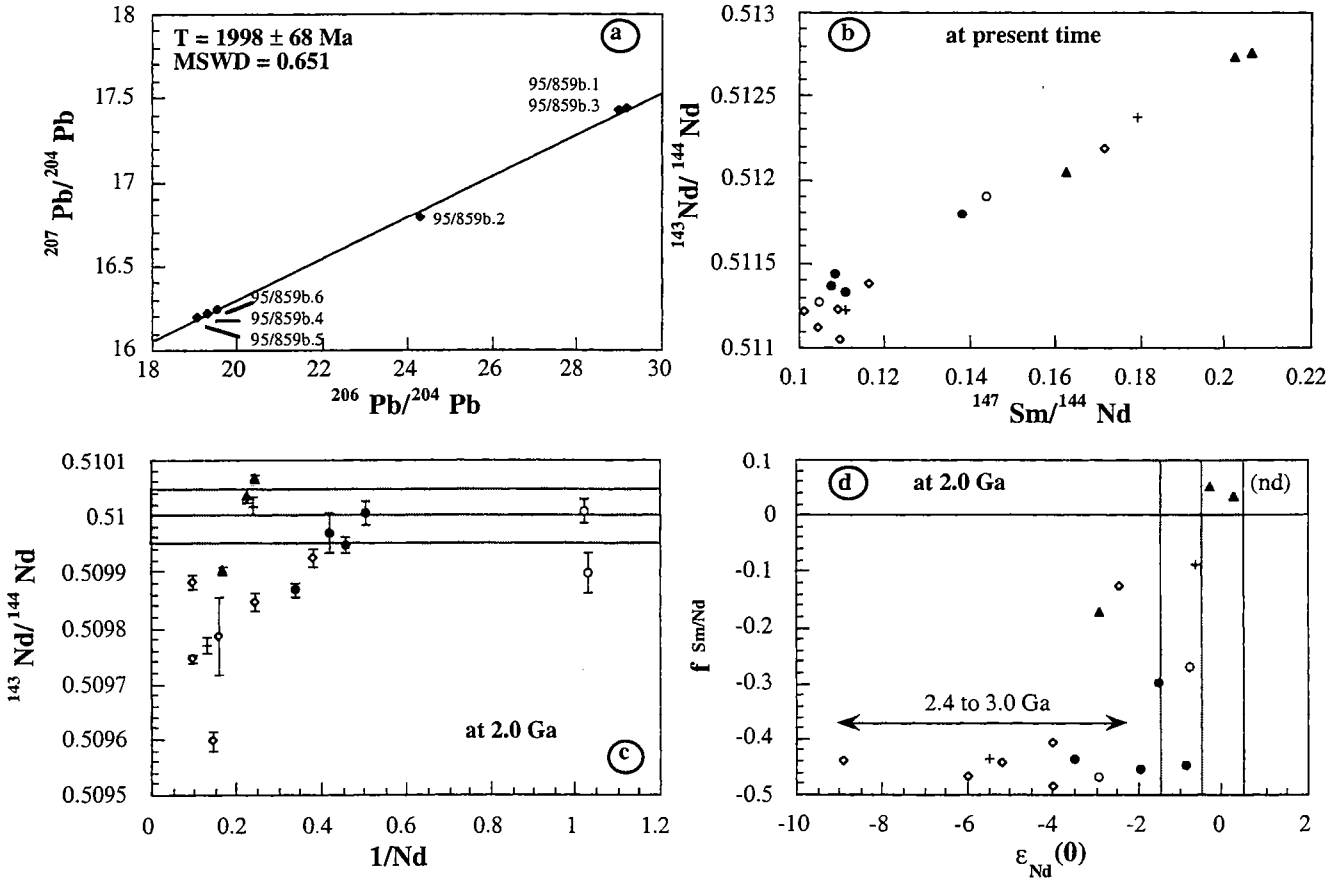

with or without segregation of initial melts (Holmquist, 1929; Winkler, 1961; Mehnert, 1968; Johannes and Gupta, 1982; Johannes et al., 1995; Whitney and Irving, 1994).

Following the first hypothesis, the quartzo-felspathic magma would have intruded along foliation planes and would have no relationship with the intruded gneiss (structurally, geochemically and isotopically). The consistent amounts of trace elements according to the proportion of mafic and leucocratic minerals (Fig. I-49) in the different layers are a strong argument against a foreign magma injection. Furthermore, the distinct occurrence of Bt-rich layer along the edge of the Qtz-fs layer can not be formed by such process. Therefore, magma injection can be ruled out as migmatization process.

Metasomatism at subsolidus or hypersolvus conditions can be evaluated using LIL element contents (Rb, Sr and Ba). This process implies the mobility of certain element due to the effect of an aqueous metamorphic hydrothermal fluid (Babcock and Misch, 1989), implying annihilation of chemical characteristics. In the studied sample, the contents of LIL elements are directly related in each layer to the proportions of their most probable host minerals. Therefore, each layer kept its own chemical feature. Thus, metasomatism at subsolidus or hypersolvus conditions can not explain the results.

Metamorphic differentiation at subsolidus conditions and partial melting (anatexis) with or without segregation of initial melts are widely recognized as the main processes of migmatite formation. In sample 95/859 microscopic observations indicate segregation of mafic from leucocratic minerals on a centimeter scale as well as on a millimeter scale within the intermediate metamorphic layer, favouring metamorphic segregation at subsolidus conditions. Nevertheless, no clear petrographic criteria are found against Hbl or Bt dehydration reactions to reject anatexis. In addition, the similar An contents in Pl from all layers suggest either anatexis (Whitney and Irving, 1994; Mehnert, 1968) or the re-equilibration of Pl during subsolidus recrystallization (Ashworth and McLennan, 1985). In the Qtz-Ab-Or triangular diagram (+ $H_2O$, + $CO_2$; Fig. I-53 modified after Inger and Harris (1993)), the normative composition of all layers is shown compared to the minimum eutectic normative melt composition for different $H_2O$ activities at 1, 2, 5 and 10 kbars. The Hbl-bearing layers, the Bt-rich layers and the intermediate metamorphic layers define three distinct but closely spaced groups whereas the Qtz-fs layers plot well above them with only a small Or component. Two explanations are possible: (1) the Qtz-fs layers represent the melt residue resulting from the previous extraction of a large volume of eutectic melt. This implies a very high degree of partial melting; and (2) Qtz-fs layers do not represent an anatectic melt but their normative composition only correspond to the proportion of their constituent minerals. The amount of melt produced by fluid-absent melting reactions in a hypothetical Qtz-fs source may be deduced from the T°-$H_2O$ wt% -melt% diagram (Fig. I-54; Johannes and Holtz, 1990). To use this diagram, we estimated the

Figure I-53: Qtz-Ab-Or triangular diagram for all layers of sample 95/859. Eutectic melt compositions are also reported for various pressure 1, 2, 5 and 10 kbar and water activity (open ssquare: $a_{H2O} = 1$, cross: $a_{H2O} = 0.5$). Modified after Inger and Harris (1993)

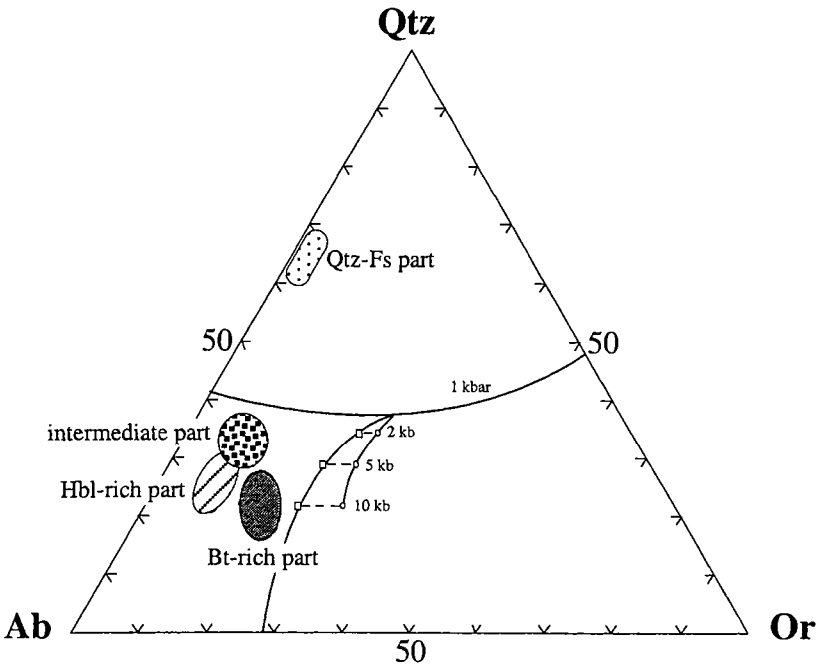


Figure I-54: The amount of melt (in wt %) formed by fluid-absent melting reactions in a possible quartzo-feldspathic protolith as a function of T° and water content of the source rock (curves) at 5 kbar according to Johannes and Holtz (1990).

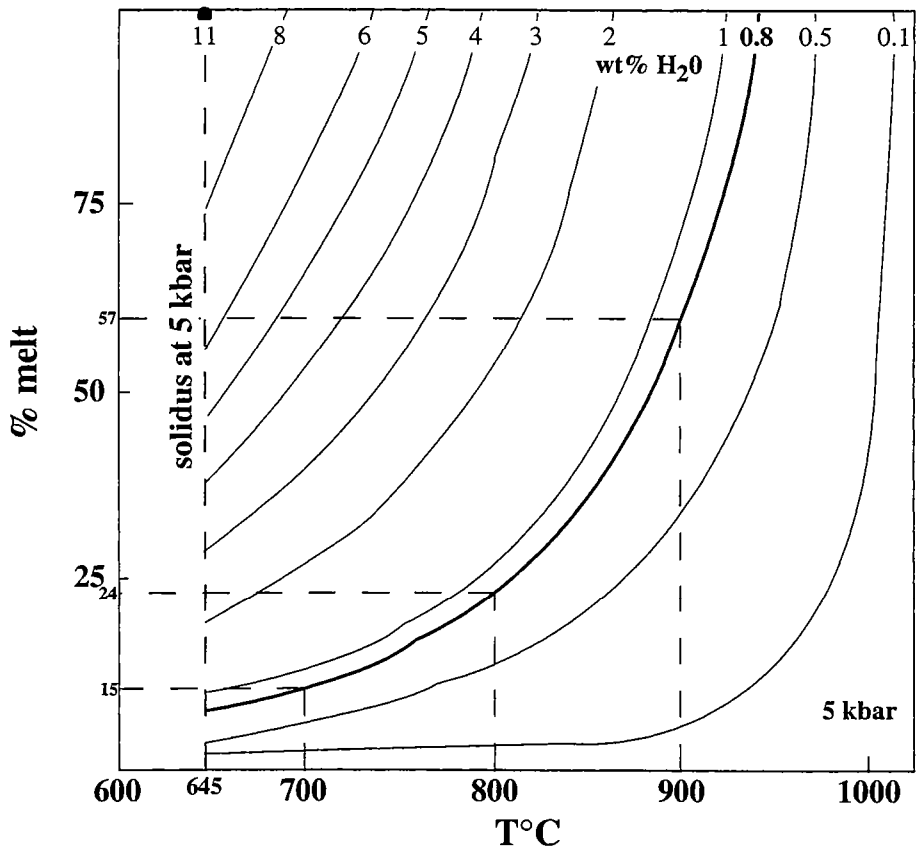

mineralogical composition of the source from the data compilation on Hbl-Bt gneisses in the Phikwe Complex by Hutton et al. (1974). For such a source, a pressure equal to 5 kbars and a tonalitic melting line above 700°C (Johannes, 1985) should be applied. If the source rock were composed entirely of 20% Hbl and 10% Bt, the maximum amount of $H_2O$ which could be released by dehydration reaction would be 0.8wt%. This quantity of water is able to generate 15 wt%, 24 wt% and 57 wt% of partial melt at 700°C, 800°C and 900°C respectively. The distribution of major and trace elements of the Qtz-fs layers combined with the extreme LREE depleted pattern and a strong positive Eu anomaly (Fig. I-49 and I-50b) would clearly indicate a high degree of partial melting (about 50 %) suggesting therefore very high temperature melting (above 900°C). At such a temperature, Hbl could still be present but Bt would have reacted completely with Pl to form a Grt-bearing partial melt. Thus, these considerations make it very unlikely that partial melting via Bt and/or Hbl dehydration reactions caused the migmatitic aspect of sample 95/859. Further, trace element abundances and modeling can provide a clear distinction between partial melting and metamorphic segregation at subsolidus conditions. REE concentrations in melt give information on the melting conditions, the mineralogical and chemical composition of the source during melting and the modification in melt composition by metasomatism, differentiation and fluid (Hanson, 1980). REE modeling was done on slices b and c using (1) batch, (2) fractional and (3) disequilibrium melting equations. These models assume no chemical re-equilibration by diffusion during cooling (Fourcade et al., 1992).

Equilibrium melting implies that thermodynamic equilibrium is attained between the melt and the solid and thus that equilibrium partition coefficients between melt and solid can be used (Allègre and Minster, 1978). The trace element concentrations in the leucosome (Qtz-fs layer of our study) are given by the following equation:

$$C_l^i = \frac{C_o^i}{\left(D_o^i + F*\left(1 - D_o^i\right)\right)} \qquad (1)$$

$C_l^i$ is the concentration of trace element $i$ in the leucosome, $C_0^i$ is the concentration of trace element $i$ in the source rock, $D_0^i$ is the total partition coefficient of element $i$ in the source rock and F is the degree of partial melting.

Fractional melting relates to the immediate migration of melt from the source, so that equilibrium is limited to the site of melting at infinitesimal melt batches (Allègre and Minster, 1978). The leucosome trace element concentrations are given by the following equation:

$$C_l^i = C_o^i * \left(\frac{1}{D_o}\right) * (1 - F)^{\left(\left(\frac{1}{D_o}\right) - 1\right)} \qquad (2)$$

Figure I-55: Chondrite-normalized REE patterns of the predicted leucosomes by a) batch melting, b) fractional melting and c) disequilibrium melting for part 95/859b and 95/859c.

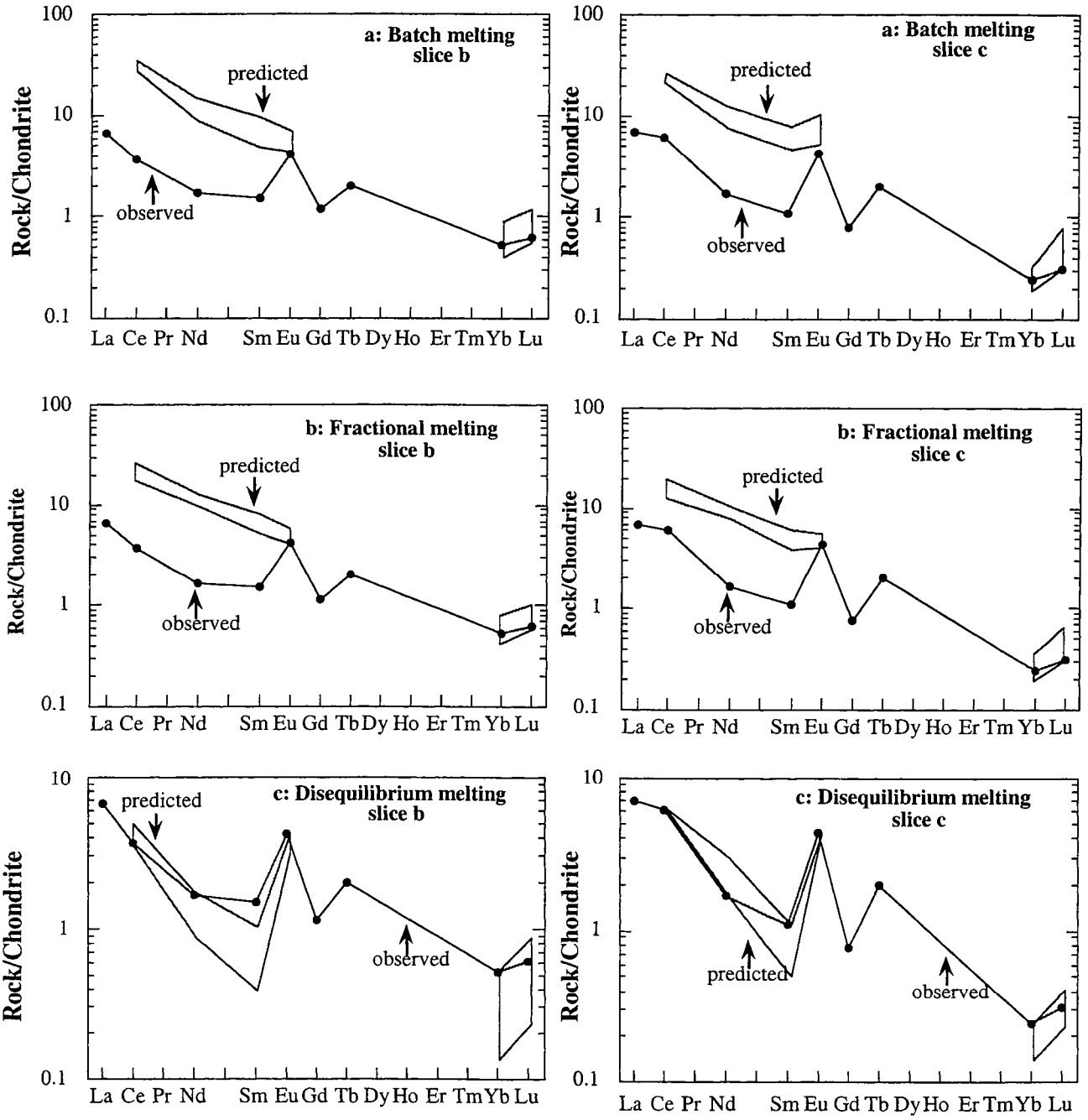

In disequilibrium melting, no trace element equilibration takes place between the residue and melt at all, and chemical compositions of leucosome depend only on the concentration of trace element in different minerals which enter the melt. Therefore, the same treatment applies to subsolidus metamorphic differentiation (Whitney and Irving, 1994). The leucosome trace element concentrations are given by the following equation (Prinzhofer and Allègre, 1985; Barbey et al., 1989; Sawyer, 1991):

$$C_l^i = C_o^i * \frac{\left( x_1 + \left( \frac{\sum_{j=2}^{n} x_j * D_j}{D_1} \right) \right)}{\left( X_1 + \left( \frac{\sum_{j=2}^{n} X_j * D_j}{D_1} \right) \right)} \qquad (3)$$

In Eq. (3), the variables are the same as in Eq. (1) plus $X_j$ which corresponds to the weight proportion of mineral $j$ in the source rock and $x_j$ to the weight proportion of mineral $j$ entering the leucosome.

Minerals used in all three models are Hbl, Bt, Qtz, Pl, Or, Ap, Mnz and Zrn. Petrographic features and arguments discussed earlier would indicate a high degree of partial melting, so that 50% was assumed for batch and fractional melting calculations. Furthermore, due to the very low concentrations in HREE, the modeling will focus on the LREE (Ce, Sm, Nd, and Eu) and Yb and Lu are calculated for completion. It was further assumed that : (1) no chemical re-equilibration by fluid/rock interractions modified the chemical features of the Qtz-fs layer (Babcock and Misch, 1989); (2) Qtz-fs layer did not undergo fractional crystallization (Cuney and Barbey, 1982; Sawyer, 1987); and (3) the intermediate metamorphic layers are interpreted as corresponding to the unmigmatized protolith and thus their REE contents are used as proxies for those of the source rock. Fig. I-55a and I-55b illustrate the REE results of the modelled Qtz-fs layer by batch as well as fractional melting on slices b and c. Both REE patterns show LREE enrichment and HREE depletion. However, they are substantially different from the observed one as they are 5 to 6 times more enriched in the LREE. In Fig. I-55c, the REE results of the Qtz-fs layer by disequilibrium melting are shown. The calculated values for slices b and c fit the observed REE pattern of the Qtz-fs layer using a range of source rock compositions.

In summary, the REE modeling results indicate that the disequilibrium model, e.g. metamorphic segregation at subsolidus conditions, match the observed REE contents of the Qtz-fs layer on slices b and c for the same range of source rock compositions.

### 5.6.2. Major and trace element distribution and Nd and Pb isotope exchange

Before assessing the extend of Nd and Pb isotope exchange during migmatization, it is crucial to discuss the distribution of major and trace elements between migmatitic components. Firstly, each layer clearly has a distinctive chemical composition (Fig. I-49). Bt-rich and Hbl-rich layers are enriched in Mg and Fe whereas Qtz-fs layers are depleted. Intermediate metamorphic layers have a homogeneous chemical composition between these two extremes. We interpret these results as the direct consequence of the proportional amounts of each mineral in the respective migmatitic component. The intermediate metamorphic layer has an intermediate LIL element concentrations (Ba, Rb, and Sr) between Bt-rich and Qtz-fs layers (Fig I-49). In addition, it has the highest Th and Ce contents indicating that the REE-Th bearing minerals are mainly concentrated in that layer (Fig. I-49). There is also no correlation between REE or Th contents with $SiO_2$ or MgO contents indicating that accessory minerals are not generally entrapped in mafic or leucocratic main minerals. Moreover, flat chondrite-normalized REE patterns of the Hbl-rich layers are dominated by Hbl whereas those of the intermediate metamorphic layers are characterized by LREE enrichment indicating the accumulation of accessory minerals (Fig. I-50). Thus, the distribution of major and trace elements reflect only a mixing of variable mineral proportions in the respective layers.

Significant scatter in the Sm-Nd regression line of sample 95/859 may be related to either an incomplete eradication of pre 2.0 Ga isotopic features within layer or a Sm/Nd fractionation during metamorphism or both (Fig. I-52b). The behaviour of the Sm-Nd system during migmatization can be unravelled by the use of the (1/Nd) versus $^{143}Nd/^{144}Nd(2.0)$ diagram (Fig. I-52c). This indicates a memory of Nd isotopic composition differences older than 2.0 Ga. A linear trend indicates a mixing line. The positive correlation of most samples with an almost linear array, indicates that the variation in $^{143}Nd/^{144}Nd(2.0)$ results from mixing. Thus, the age and the initial epsilon value are geologically meaningless. The array encompasses the Bt-rich layers and the intermediate metamorphic layers. It shows that layers with more Nd-rich mineral(s) (such as Mnz or Ap) have less radiogenic Nd isotopic compositions. The increase of $^{143}Nd/^{144}Nd(2.0)$ ratios is also correlated with decreasing Th contents, suggesting that Mnz is an important control factor. The $^{143}Nd/^{144}Nd(2.0)$ of Hbl-rich layers, the Bt-rich layers and the Qtz-fs layers broadly define (within $\pm$ 1 $\varepsilon_{Nd}$) a straight horizontal line, indicating that they have nearly the same Nd isotopic composition at that age. Note that one sample of Hbl-rich layer has a lower $^{143}Nd/^{144}Nd(2.0)$ and (1/Nd) ratios which may be explained by the occurrence of accessory minerals as it is characterized by lower $^{143}Nd/^{144}Nd$ ratio, higher Th and LREE contents compared to the two others.

We conclude, first, that nearly full Nd isotope exchange was attained between layers whose chemical compositions are dominated by main mineral phases, and second, that

accessory minerals which concentrate the REE budget of the intermediate metamorphic layer reflect Nd isotopic inheritance, due to the limiter diffusivity of their immediate surroundings (Kramers et al., 1998).

Similarly, Sévigny (1993) argued that Sm/Nd fractionation may be due to monazite fractional crystallization yielding an increase in Nd model ages. The use of the $f_{Sm/Nd}$ versus $\varepsilon_{Nd}(2.0)$ diagram provides a good indicator for Sm/Nd fractionation (Fig. I-52d). Nd model ages are also provided in brackets. The lower absolute $f_{Sm/Nd}$ values for Hbl-rich layers and the Qtz-fs layers may represent either the effect of Mnz fractionation or the effect of magmatic Hbl. In both case, $^{147}Sm/^{144}Nd$ of "Mnz-free layers" are higher than the others. However, the positive $\varepsilon_{Nd}(2.0)$ values of Hbl-rich layers cannot be accounted for by Mnz fractionation, this would change only the Sm/Nd ratio. The flat chondrite-normalized REE patterns and low Th content reflect the dominance of Hbl rather than accessory Mnz on the geochemistry of these layers. Their positive $\varepsilon_{Nd}(2.0)$ value (independant of age) indicates crystallization of the amphiboles from the melt when it was recently mantle derived. Consequently, the fractionation of the Sm/Nd ratios is not the result of the 2.0 Ga event or Mnz fractionation, but merely a primary feature of the protolith.

The Nd isotopic compositions indicate that Nd isotope exchange was not complete between the layers at 2.0 Ga but may have been attained between layers dominated by major minerals. Dahl (1996, 1997) has calculated the diffusivity of radiogenic isotopes from ionic porosity and his results predict Ap to be relatively unretentive for Nd, and Mnz retentive to Nd and Pb. Our above conclusions suggest that accessory minerals have influenced Nd isotope compositions of the intermediate metamorphic layers. The situation for Pb is different from Nd. All layers from 95/859b have been analyzed for U-Pb and they define a Pb-Pb isochron of 1998 ± 68 Ma (MSWD = 0.651; Fig. I-52a). This isochron suggests that: (1) all layers are cogenetic and magma injection is not realistic; (2) migmatization took place at 2.0 Ga; and (3) the U-Pb system was resetted during the high grade event. The comparison between Pb and Nd isotopic compositions on slice b give information on the completion of the U-Pb system resetting during migmatization compared with Nd isotopic inheritance. Three conclusions can be drawn: (1) the intermediate metamorphic layers have the highest Nd contents and $^{208}Pb/^{204}Pb$ ratio associated with the lowest $^{143}Nd/^{144}Nd$ and $^{206}Pb/^{204}Pb$ ratios emphazing the effect of Th-Nd rich minerals such as Mnz; (2) Hbl and Bt-rich parts have the same Pb isotopic compositions for scattered Nd isotopic composition; and (3) Pb isotope exchange was probably fairly complete at 2.0 Ga suggesting that Mnz and Ap are therefore not retentive to Pb. Diffusivities of U-Th-Pb between Ap or Mnz and their neighbours are not a limiting factor to full isotope exchange whereas Nd diffusivity is limiting factor in the sense that Nd is strongly enriched in those minerals compared to U or Th (for example Mnz: 8000ppm of Th compared to 10 wt% $NdO_2$). As a consequence, the relative proportions of accessory minerals in the source rock used in the mass balance

calculations, have a greater impact (at least 100 times) on modelled REE concentrations than on modeled trace element contents (for example Th).

### 5.6.3. Protolith prior to migmatization

Based on the discussed petrographical and geochemical features as well as U-Pb systematics, we can assume mass conservation during migmatization. Therefore, we propose to reconstruct the Sm-Nd characteristics of complete protoliths and attempt to determine their $T_{DM}$. The chemical and Nd isotopic compositions of the protolith prior to the high grade event can be determined by the equations given by Albarède (1995):

The concentration of element i in phase j is defined as:

$$C_0^i = \sum_{j=1}^{n} C_j^i * f_j \qquad (4)$$

with the closure equation:

$$\sum_{j=1}^{n} f_j = 1 \qquad (5)$$

In addition, the Sm-Nd isotopic composition in the protolith may be estimated by:

$$\left(\frac{C^{i2}}{C^{i1}}\right) = \sum_{j=1}^{n}\left(\frac{C^{i2}}{C^{i1}}\right)_j * \frac{C_j^{i2}}{C_{mix}^{i1}} * f_j = \sum_{j=1}^{n}\left(\frac{C^{i2}}{C^{i1}}\right)_j * \varphi_j^{i1} \qquad (6)$$

where $\sum_{j=1}^{n} \varphi_j^{i1} = \frac{\sum_{j=1}^{n} C_j^{i1} * f_j}{\sum_{k=1}^{n} C_k^{i1} * f_k} = 1$; we will assumed to be $C_{mix}^{^{144}Nd} = \sum_{j=1}^{n} C_j^{Nd} * f_j$ and $C_{layer}^{^{144}Nd} = C_{layer}^{Nd}$

For the modeling, we will consider only (1) 95/859b and 95/859c which show all migmatitic components; (2) in order to omit to the effect of unequal distribution of accessory minerals, all layers are considered; (3) chemical composition ( $C_j^i$ refers to concentration of species i in phase j) will be determined using the equation of mixing at n components (here n = 6 for slice b and n = 4 for slice c); (4) the mass proportion of the layers is estimated from the respective vol% in the "parallelepiped" rock at present time. Their respective proportion (referred to $f_j$) are indicated in the Fig. I-48b. If mass conservation remains a valid assumption, the results of 95/859b and 95/859c should be in the same order for chemical composition and Nd model ages.

Table I-17: Chemical composition and mineralogical constraints used for the determination of the migmatization process. The results of the chemical and Sm-Nd isotope compositions of the protolith prior to migmatization are reported.

| Possible source rock Minerals | A | B | C | D | E | F | G | H | I | J |
|---|---|---|---|---|---|---|---|---|---|---|
| **Hbl** | 0.2 | 0.15 | 0.1 | 0.2 | 0.15 | 0.1 | 0.2 | 0.2 | 0.3 | 0.5 |
| **Bt** | 0.1 | 0.15 | 0.2 | 0.1 | 0.15 | 0.2 | 0.1 | 0.1 | 0.1 | 0.05 |
| **Qtz** | 0.3 | 0.3 | 0.3 | 0.2 | 0.2 | 0.2 | 0.2 | 0.2 | 0.2 | 0.15 |
| **Or** | 0.05 | 0.05 | 0.05 | 0.05 | 0.05 | 0.05 | 0.05 | 0.05 | 0.05 | 0.05 |
| **Pl** | 0.3495 | 0.3495 | 0.3495 | 0.4495 | 0.4495 | 0.4495 | 0.4495 | 0.445 | 0.345 | 0.25 |
| **Ap** | 0.0002 | 0.0002 | 0.0002 | 0.0002 | 0.0002 | 0.0002 | 0.0003 | 0.005 | 0.005 | 0.0002 |
| **Zrn** | 0.0001 | 0.0001 | 0.0001 | 0.0001 | 0.0001 | 0.0001 | 0 | 0 | 0 | 0.0001 |
| **Mnz** | 0.0002 | 0.0002 | 0.0002 | 0.0002 | 0.0002 | 0.0002 | 0.0002 | 0 | 0 | 0.0002 |

| | Source | Kd (Ce) | Kd (Nd) | Kd(Sm) | Kd(Eu) | Kd(Yb) | Kd(Lu) |
|---|---|---|---|---|---|---|---|
| Arth and Barker (1976) | **Hbl** | 0.9 | 2.8 | 3.99 | 3.44 | 4.9 | 4.5 |
| Arth and Hanson (1975) | **Bt** | 0.32 | 0.29 | 0.26 | 0.24 | 0.44 | 0.33 |
| Green and Pearson (1985) | **Qtz** | 0.014 | 0.016 | 0.014 | 0.056 | 0.017 | 0.014 |
| Arth and Barker (1976) | **Or** | 0.037 | 0.035 | 0.025 | 4.45 | 0.03 | 0.033 |
| Arth and Barker (1976) | **Pl** | 0.27 | 0.21 | 0.13 | 2.15 | 0.049 | 0.046 |
| Onuma et al. (1968) | **Ap** | 34.7 | 57.1 | 62.8 | 30.4 | 23.9 | 20.2 |
| Higuchi and Nagasawa (1969) | **Zrn** | 2.64 | 2.2 | 3.14 | 3.14 | 270 | 323 |
| Brooks et al. (1981) | **Mnz** | 635 | 463 | 205 | 81 | 8.9 | 7.7 |

**Results**

| Major elements in wt% | 95/859 part b | 95/859 part c |
|---|---|---|
| **SiO2** | 61.76 | 59.92 |
| **TiO2** | 0.27 | 0.31 |
| **Al2O3** | 20.87 | 20.68 |
| **Fe2O3** | 2.83 | 3.5 |
| **MnO** | 0.05 | 0.07 |
| **MgO** | 1.12 | 1.39 |
| **CaO** | 7.61 | 7.77 |
| **Na2O** | 3.82 | 3.71 |
| **K2O** | 0.78 | 0.82 |
| **P2O5** | 0.06 | 0.04 |
| **PF** | 0.6 | 0.43 |
| **Total** | 99.77 | 98.64 |
| REE in ppm | | |
| **La** | 7.83 | 5.27 |
| **Ce** | 15.47 | 9.74 |
| **Nd** | 6.12 | 4.06 |
| **Sm** | 1.25 | 1.16 |
| **Eu** | 0.6 | 0.63 |
| **Gd** | 1.03 | 1.26 |
| **Tb** | 0.15 | 0.25 |
| **Yb** | 0.42 | 0.73 |
| **Lu** | 0.07 | 0.13 |
| Sm-Nd isotopic compositions | | |
| **147Sm/144Nd** | 0.1275 | 0.1529 |
| **143Nd/144Nd** | 0.511487 | 0.511936 |
| **TDM (Ga)** | 2.73 | 2.75 |

Figure I-56: a) Chondrite-normalized REE patterns of the protolith prior to migmatization according to the mixing calculations done on slices b and c. b) Sm-Nd isochron diagram for the two 95/859 whole rocks and the protolith calculated from mixing calculations.

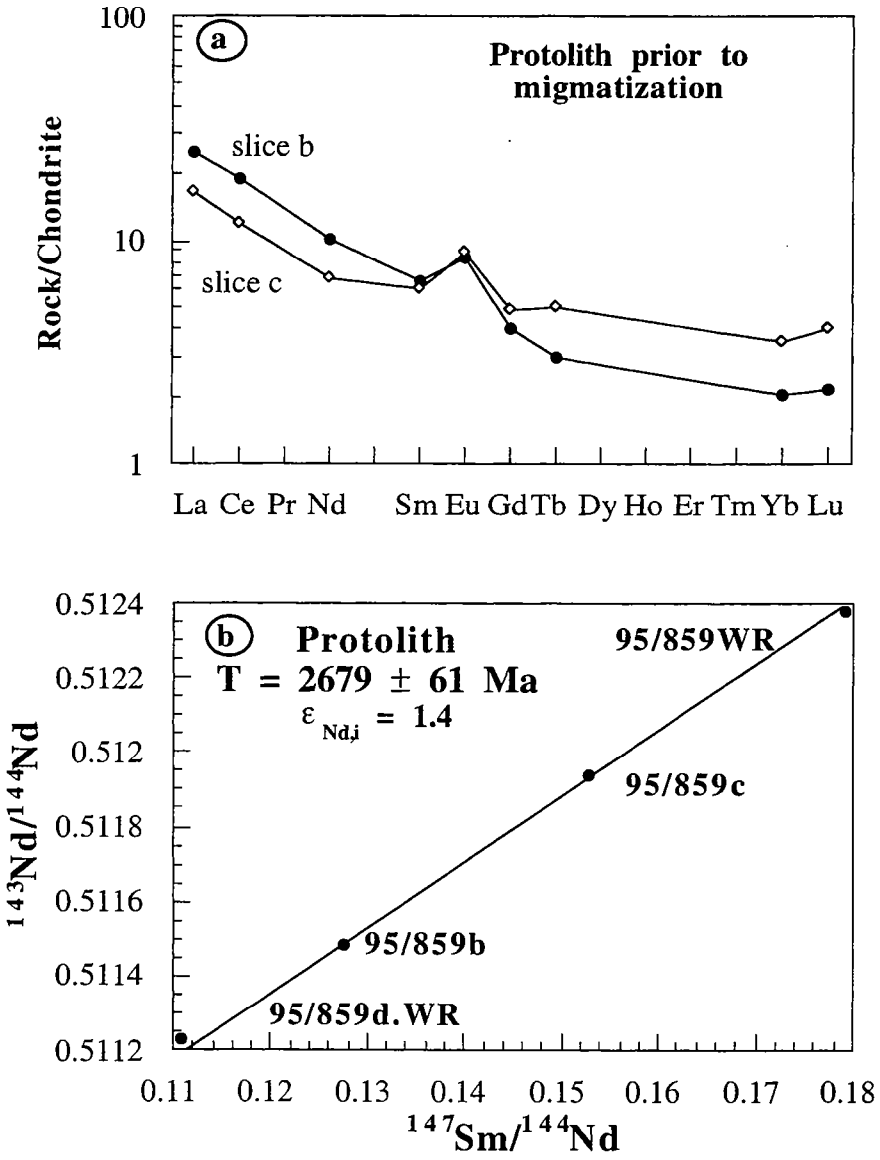

The data used in these calculations as well as the results are reported in Table I-17. Note that the intermediate metamorphic layer is dominant in slice b whereas it is the Hbl-rich layer in slice c. The chemical composition obtained is similar in calculations of slices b and c, and both indicate a quartz and potassium poor dioritic composition. They are also similar to the chemical composition of Hbl and Bt bearing gneisses found in the Phikwe Complex (Hutton et al., 1974). The chondrite-normalized REE patterns are characterized by low REE contents, HREE depletion ($(La/Yb)_N$ = 12.31-4.77) and a positive Eu anomaly ((Eu/Eu*) = 1.6) (Fig. I-56a). These features correspond to those of Archean (2.7 Ga) tonalite found in Ontario by Arth and Hanson (1975). Hanson (1978) indicated that such rocks may be formed by partial melting of an Archean basalt at mantle depth leaving a residue of Grt and/or Cpx. These features are in line with the results we obtained: (1) the protolith is potassium-poor which ruled out a sedimentary parent source, (2) Hbl is probably of magmatic origin and therefore fits a basaltic magma, (3) the 95/858 geochemical features indicate a magmatic activity during its deposition, and (4) the Phikwe Complex resembles greenstone belts.

We calculated Nd isotopic compositions of the protoliths as well as their Nd model ages. Sm-Nd data are plotted in a conventional Sm-Nd isochron diagram in Fig. I-56b and the "regression" line gives an age of 2 679 ± 61 Ma ($\varepsilon_{Nd,i}$ = 1.4). The calculated Nd model ages of 95/859b and 95/859c are 2.73 Ga and 2.75 Ga respectively. The WR isochron age is in agreement with the magmatic activity of this region at that time (Chavagnac et al., 1998). Therefore, the result supports the assumptions made in the modeling (closed system during migmatization).

## 5.7. Conclusions

The Phikwe Complex underwent high grade metamorphism leading to migmatization at 2.0 Ga, as suggested by Sm-Nd minerals-WR and Pb-Pb WR isochrons.

Petrographic criteria combined with the geochemical features indicate that the migmatization process may have been either metamorphic segragation at subsolidus conditions or partial melting (anatexis). REE modeling realized on two slices presenting all migmatitic components indicate that the observed REE patterns of leucosome - Qtz-fs layer in our study - can only be match by metamorphic segregation at subsolidus conditions. The distribution of major and trace elements reflects a mixing of variable mineral weight proportions in the layers. Due to the high REE concentrations compared to U-Pb-Th contents in accessory minerals, the relative proportion of these minerals used in mass balance calculations may have a strong impact on the REE modeled results. The apparent Nd model ages range between 2.3 and 3.1 Ga. These Nd model ages can not be used to constrain the crustal evolution in Southern Africa in Archean to Proterozoic time.

In the second order, the distribution of trace elements, the results of REE modeling and also the Pb-Pb WR isochron at 2.0 Ga are strong arguments for closed system and mass conservation during migmatization. Thus, mixing equations can be used so as to determine the chemical and Sm-Nd isotopic features of the protolith prior to migmatization. The results indicate a quartz and potassium-poor diorite as protolith which may have been formed via partial melting of an Archean basalt at mantle depth leaving a residue of Grt and/or Cpx. A Sm-Nd isochron using calculated protolith composition indicate an age of 2.7 Ga closed to the Nd model ages obtained by these calculations at 2.73-2.75 Ga indicating the validity of the model assumptions. Calculated Nd model ages can be used to constrain Archean crustal growth in this region of South Africa.

## Acknowledgements

This work is supported by the NSF (Switzerland), grant 20-47157.96. We thank ACTLABS for the INAA analyses. VC thanks the technical staff from Bern and Rennes for their assistance in various phases of analytical works as well as many people from both universities for helpfull discussions. Special thanks to Professor Bor-ming Jahn for organizing Nd isotope measurements at the University of Rennes 1. Fruitful discussions and support from Lorenz Holzer were quite appreciated.

# 6. Trace elements and Nd, Pb isotopes in migmatization at 2.0 Ga of a metapelitic rock in the Central Zone of the Limpopo Belt (South Africa)

Valérie Chavagnac, Jan D. Kramers, and Thomas F. Nägler

1: Universität Bern, Min. Pet. Inst., Gruppe Isotopengeologie, Erlachstrasse 9a, 3012 Bern, Switzerland. e-mail address of the corresponding author: chava@mpi.unibe.ch

**In prep for Contributions to Mineralogy and Petrology**

## 6.1. Introduction

The study of the Sm-Nd systematics has made an important impact in the field of crustal evolution by providing a way to determine "crust-formation" ages (McCulloch and Wasserburg, 1978). Nonetheless, some recent studies have provided examples of obvious disturbance of the Sm-Nd system either by resetting in a whole rock suites or by Sm/Nd fractionation during partial melting (Bock et al., 1994; Nabelek and Glascock, 1995; Gruau et al., 1996; Whitehouse et al., 1996; Moorbath et al., 1997; Ayres and Harris, 1997; Chavagnac et al., submitted). As that work could put wide ranging conclusions from Sm-Nd crustal studies into question, the mechanisms leading to resetting and fractionation should be studied in details.

Migmatites provide an opportunity to look at the extent of chemical equilibrium and isotope exchange during partial melting in the crust. Previous studies on migmatites suggest that chemical equilibrium between partial melts and refractory residues is not always reached. The main explanation invoked in chemical disequilibrium is the behaviour of accessory minerals during partial melting. As accessory minerals such as monazite, apatite, xenotime, or zircon, control the REE, Th and U contents of the bulk rock, their partial dissolution or their armouring within residual phases may strongly affect the REE chemical equilibration between nascent melt and restitic material (Sawyer, 1991; Watt and Harley, 1993; Nabelek and Glascock, 1995; Watt et al., 1996; Chavagnac et al., submitted). The extend of REE fractionation between partial melt and residus is of critical importance for crustal studies as Sm/Nd and $^{143}Nd/^{144}Nd$ ratios are needed to calculate Nd model ages. Partial chemical equilibrium during crustal anatexis may result in geologically meaningless Nd model ages as indicator of the time at which their protolith was initially extracted from the depleted mantle. Some isotopic studies suggested that accessory minerals may not reach full isotope exchange with the melt (Burton and O'Nions, 1990; Nabelek and Glascock, 1995), the extent of isotope exchange during anatexis however has not been clearly assessed yet.

The present study foccusses on the REE distributions and Nd and Pb isotopic compositions in partial melts and restitic components of a metapelite migmatite of the Mahalapye-Tshipise straightening zone in the Central Zone of the Limpopo Belt (South Africa). The trace element chemistry and Sm-Nd and U-Pb systematics of leucosomes in comparison to paleosomes will be examined in order to evaluate the trace element fractionation and the degree of equilibrium between nascent melt and residual phases. This will provide a framework for the assessment of Nd and Pb isotope exchange during migmatization. Finally, the Sm-Nd systematics of migmatized metapelite combined with previous isotopic studies perfomed on migmatized orthogneiss and metagreywacke are evaluated in terms of crustal history of the Limpopo Central Zone.

## 6.2. Geological setting and sample description

### 6.2.1. The Mahalapye-Tshipise Straightening Zone

The Limpopo Belt is a high-grade metamorphic terrane wedged between two low-grade granite-greenstone provinces, the Kaapvaal craton to the South and the Zimbabwe craton to the north (Fig. I-57). It covers parts of South Africa, Botswana and Zimbabwe. Late Archean inward dipping thrust zones mark the tectonic boundaries between the Limpopo Belt and its adjacent cratons. From North to South, the Limpopo Belt is subdivided into the Northern Marginal Zone (NMZ), the Central Zone (CZ) and the Southern Marginal Zone (SMZ). The subzones are separated from each other by two tectonic lineaments, the Triangle Shear Zone to the north and the Palala Shear Zone to the south.

The three subzones were thought to have been amalgamated in a simple continental collision at ~2.6 Ga (Roering et al., 1992; de Wit et al., 1992; Treloar et al., 1992). However, this idea may no longer hold because the Limpopo belt is now recognized to have undergone a poly-metamorphic evolution. The last event is characterized by a last transpressional event in the early Proterozoic affecting the CZ (Barton et al., 1994; Kamber et al., 1995; Holzer et al., 1998; Holzer et al., in press). This invoked major tectonism and a high-grade metamorphism. The structural, petrological and geochronological studies indicated that large amounts of granitic melt were produced at 2.0 Ga by fluid-absent melting reactions on various lithologies (Tsunogae et al., submitted; Holzer et al., in press; Chavagnac et al., submitted).On a regional scale, this Proterozoic tectono-metamorphic event also involves two Proterozoic thrust-fold belts, the Kheis and Magondi belts (Holzer et al., in press; Holzer et al., submitted).

From the Mahalapye Complex to the Tshipise area, the southern margin of the Limpopo CZ is characterized by a 5 to 10 km wide zone, strongly flattened and steeply dipping planar structures, termed the Mahalapye-Tshipise straightening zone (Fig. I-58; Holzer et al., in press). It is composed of highly deformed orthogneisses, calc-silicates, metapelites, metagreywackes and leucosomes with some occurrences of quartzites and ultramafic gneisses. From field observations, it appears that deformation within leucosomes is highly variable. The foliations of highly deformed paragneisses is related to upper-amphibolite facies mineral paragenesis which were formed close after the granulite facies peak metamorphism. Dating has yielded 2023 ± 7 Ma for garnet growth in granitic melt at the Mahalapye Complex (Sm-Nd Grts-WR-L, Chavagnac et al., submitted), 2020 ± 7 Ma to 2017 ± 6 Ma for the intense deformation fabrics in paragneisses (PbSL Titanite; Schaller et al., in press, Holzer et al., in press), 2002 ± 10 Ma for monazite crystallization in the youngest partial melt formation at the Mahalapye Complex (U-Pb Mnz, Chavagnac et al., submitted) and 1971 ± 26 Ma for syn-kinematic amphibolite facies biotite (Rb-Sr Bt-WR, Schaller et al., in press). It becomes

Figure I-57: Geological map of the Limpopo Belt. Map modified after Geological Survey of Botswana, South Africa and Zimbabwe (1981). NMZs.s.: Northern Marginal Zone sensu stricto, TZ: Transition Zone, TSZ: Triangle Shear Zone, CZ: Central Zone; PSZ: Palala Shear Zone, SMZ: Southern Marginal Zone, 1: Messina Layered Intrusion, 2: Bulai Granite Intrusion, 3: Great Dyke, 4: Bushveld Complex, 5: Matok Granite Intrusion. Location of the Figure I-58 is shown.

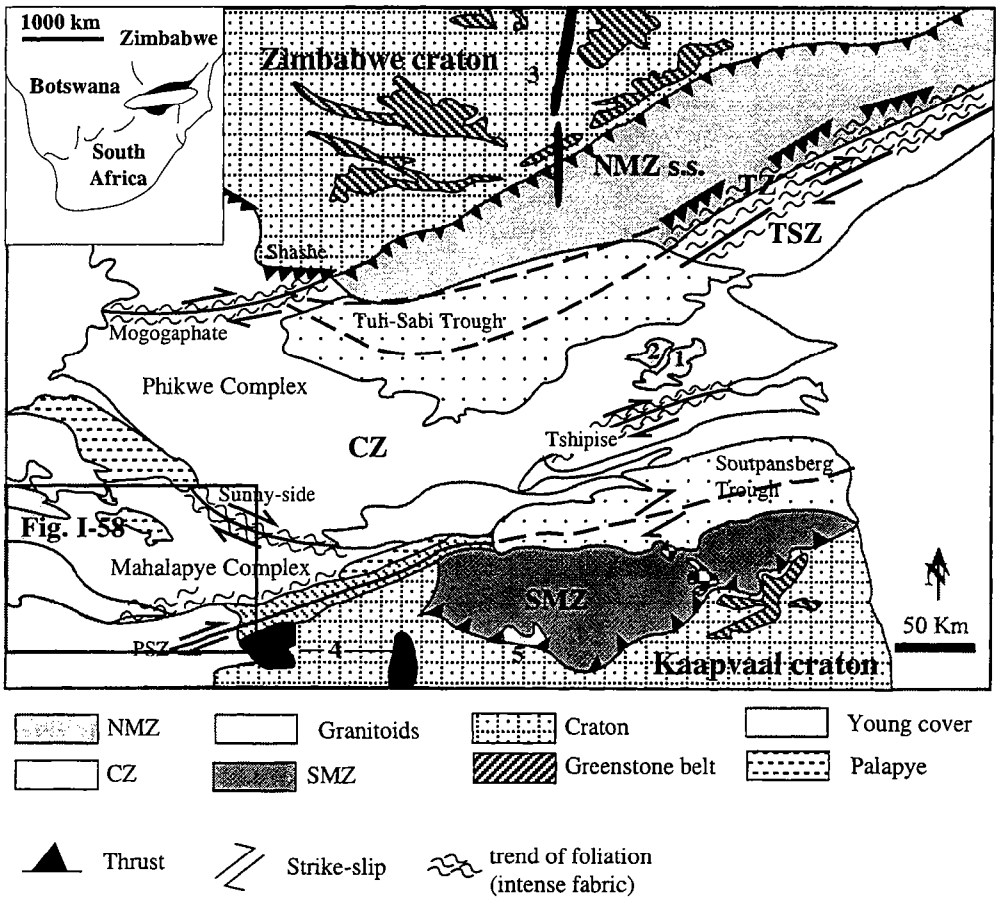


Figure I-58: Geological map of the Mahalapye Complex showing major structural features (after Holzer et al, in press). Sample location is indicated and previous geochronological data are also reported.

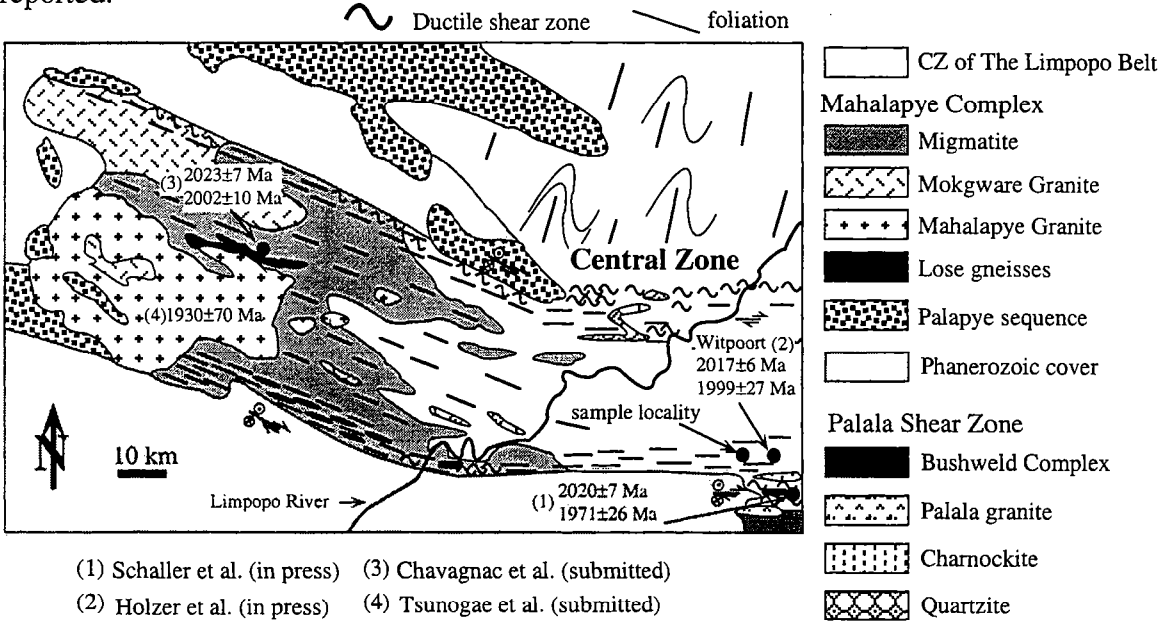


(1) Schaller et al. (in press) (3) Chavagnac et al. (submitted)
(2) Holzer et al. (in press) (4) Tsunogae et al. (submitted)

obvious that migmatization in the Mahalapye-Tshipise straightening zone is associated with a high-grade tectono-metamorphic event dated at 2.0 Ga.

### 6.2.2. Outcrop and sample descriptions

All migmatite samples belong to the same outcrop of migmatite within the Mahalapye-Tshipise straightening zone (Fig. 2; 21°25'N, 17°10'E; farm St Catharina, map 1:50000 2328AC Abbotspoort). They are strongly foliated and migmatized paragneisses of a metapelitic character.

Pods, veins and layers of garnet-bearing granitic melt occur as concordant material in a plastically deformed metamorphosed gneiss forming stromatic to nebulitic migmatite. Spatial relationships between partial melt and metapelitic gneisses are drawn in broad outline in Fig I-59. The meso-melanocratic gneisses are strongly foliated metapelite. They are mainly composed of plagioclase (Pl), alkali feldspar (K-fs), ± garnet (Grt), biotite (Bt), sillimanite (Sil), and quartz (Qtz) forming a grano-lepidoblastic texture. The preferential alignment of Pl, Bt and Sil define the foliation. Accessory minerals are mainly tiny euhedral apatite (Ap) and rounded monazite (Mnz) (~30-50 μm in size) situated at grain boundaries. Zircon (Zrn) may be observed as prismatic mineral as inclusions within Bt. Adjacent to leucosomes, the meso-melanocratic gneisses present a strong accumulation of Bt and Sil which may represent the "restitic" material after Bt dehydration reaction. From macroscopic observations, paleosome and melanosome are difficult to distinguish and therefore the term "paleosome" in this study refers to meso-to melanocratic gneisses which may include some thin layers of "restitic" material. In addition, very thin Bt-Sil-rich layer may be entrained in the leucosome in the same way as very thin granitic layer is observed in the gneisses.

Leucosomes are texturally associated with migmatitic metapelite with which they formed concordant layers or veins. They are interpreted as in-situ produced leucosomes. Partial melts have granitic composition with about 10 vol% of Grt. They are characterized by heterogranular and granoblastic textures. Lobate grain boundaries between feldspar and Qtz and myrmekite formation at Pl and K-fs boundaries indicate high temperature subsolidus recrystallization. Grt is located either in the matrix as cataclastic and irregularly shaped grains or as lobate grains associated with fibrolite Sil, tabular Sil, K-fs and Bt along the leucosome-melanosome interface as shown in Fig. I-60. This feature argues strongly against foreign magma injection. The association of Bt, Sil, Pl and Qtz may be observed as kidney shaped inclusion within Grt. The growth of Grt is interpreted to be related to partial melt, either growing during Bt dehydration reaction or precipitating from the melt itself. Furthermore, the occurrence of fibrolite Sil associated with K-fs may suggests also that muscovite dehydration reaction may have occurred at the early stage of melting reaction. Accessory minerals are tiny

Figure I-59: Spatial relationship between leucosomes and paleosomes are drawn in broad outline. Nebulitic migmatite is represented in a) and stromatic migmatite in b).

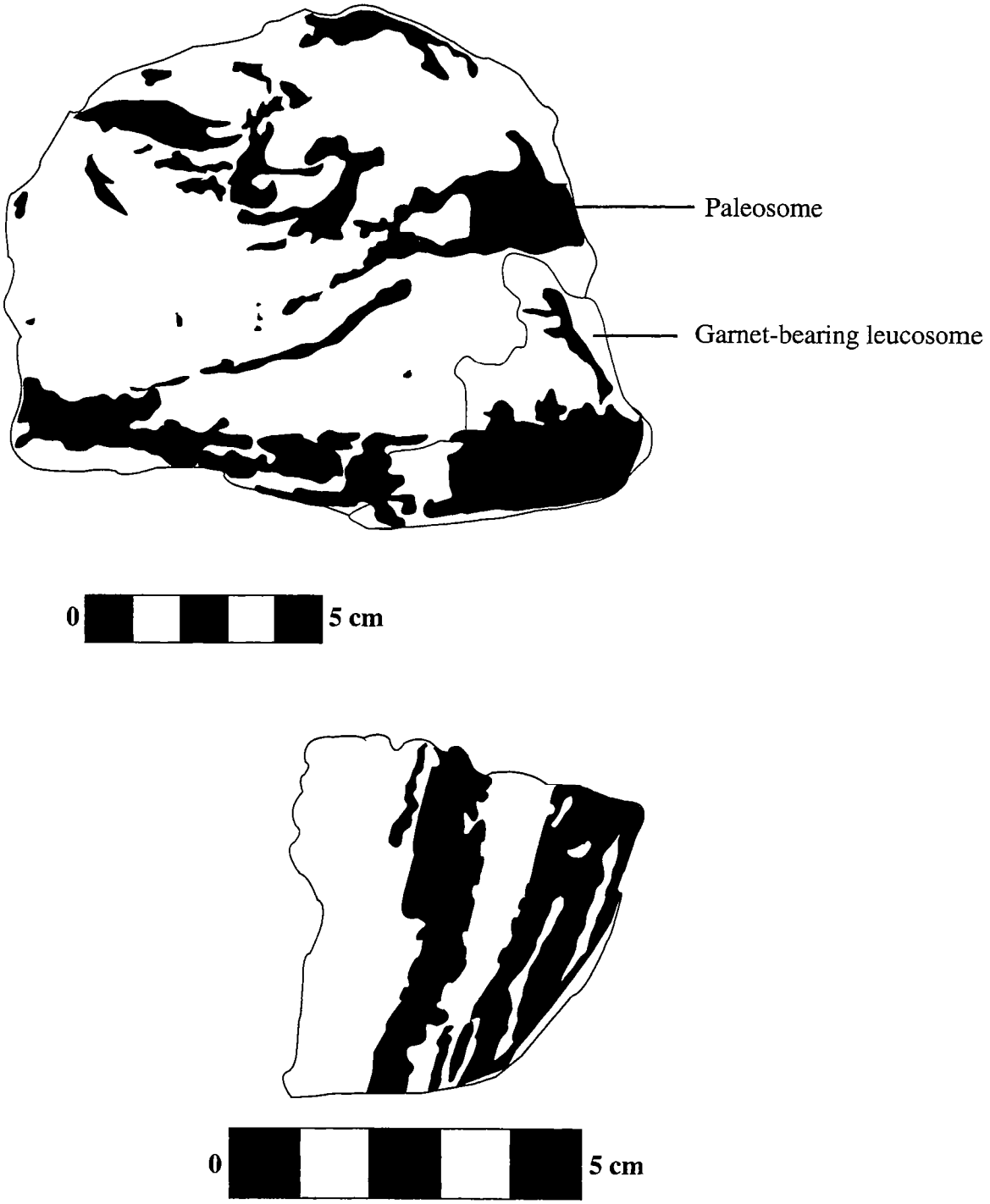

Figure I-60: Fabric and mineral association of the metapelitic migmatite. Lobate grain is associated with Bt, Sil, Pl and K-fs. The foliation is marked by the preferential alignment of Bt and Sil whereas leucosome presents a heterogranular granoblastic texture.

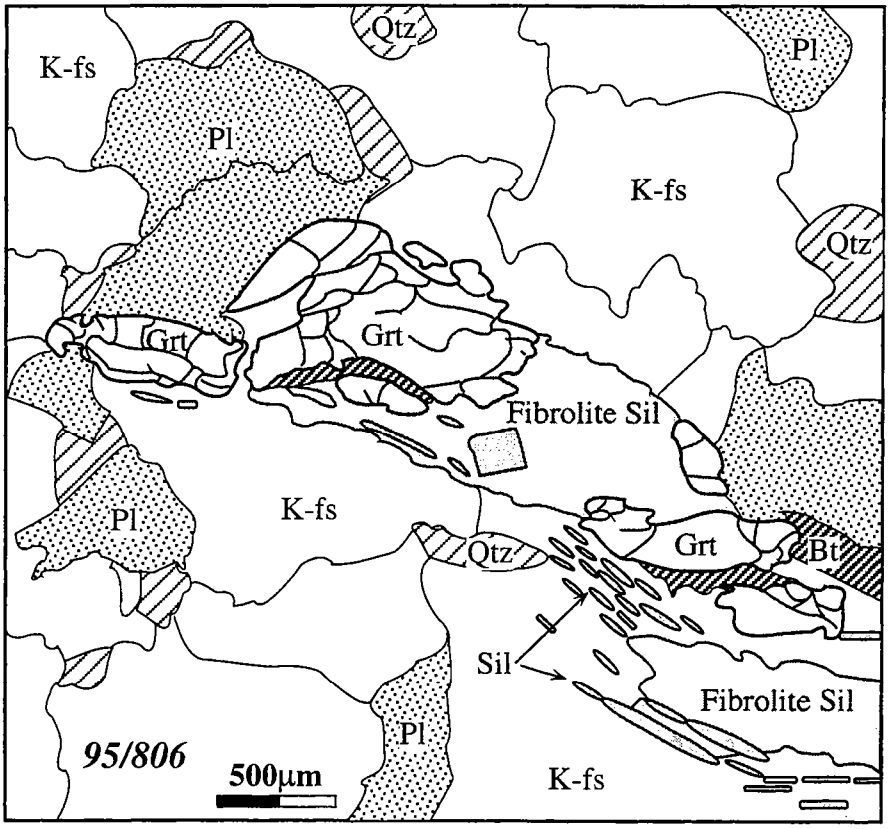


Figure I-61: Isocon diagram accroding to the graphical representation of Grant (1985). We used as parental protolith Proterozoic cratonic shale and as a result of migmatization a leucosome which is characterized by eutectic melt composition. The best fit isocon is represented by the mass conservation isocon defined by the alignment of P, Al, Eu, Rb, La, Nd, and Sm.

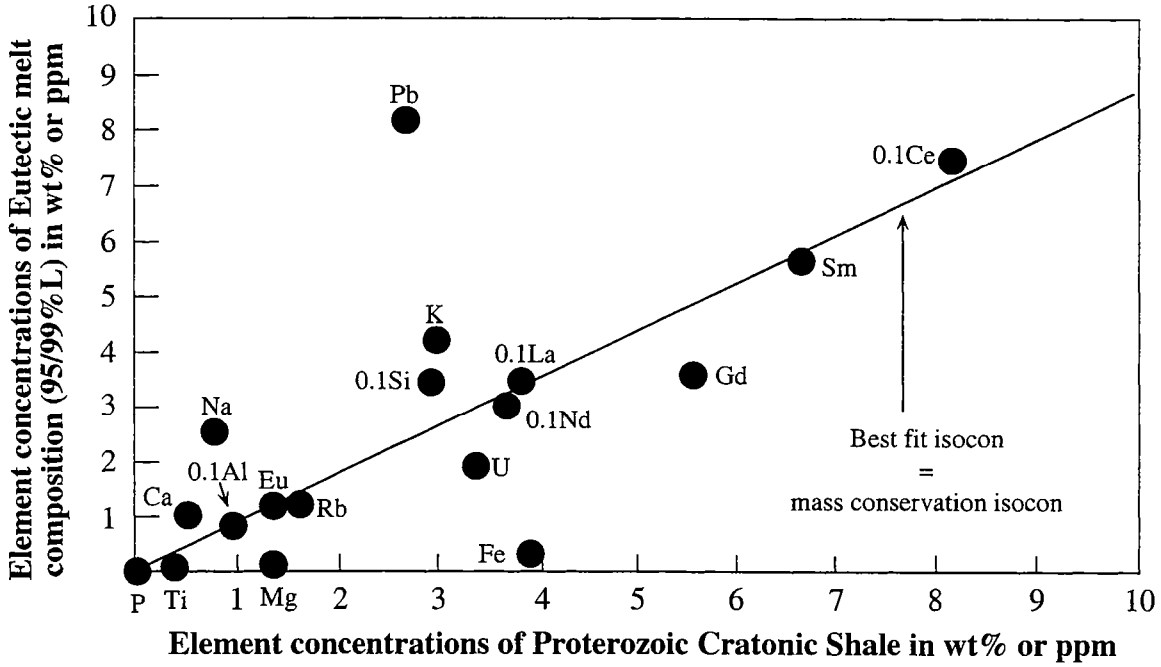

Mnz and Ap which are located either at grain boundaries or as inclusions within Pl and Qtz. Zrn is only observed as prismatic inclusion in Bt. Accessory minerals do not show an overgrowth.

A test for cogenetic relation between the migmatitic components from the chemical composition (see §6.5) was done using the Gresens' method (Gresens, 1967) which allows to assess changes in volume and concentrations of chemical species during migmatization. Results using the graphical representation of Grant (1986) are reported in Fig. I-61. The best fit isocon corresponds to the mass conservation isocon and it is defined by P, Al, Eu, Rb, La, Nd, and Sm. The migmatization process entailed enrichment of Na, Ca, Si and K in the leucosome and the enrichment of Fe, Mg and Ti in the paleosome. The distribution of major and trace element are in accord with the participation of particularly Bt and Pl melting. In addition, Nd and Sm plot on the best fit isocon which may suggest already that full Nd isotope exchange during migmatization may have been reached.

In all samples, retrogression is expressed by the damouritization of Pl, the replacement of Bt by chlorite, and the growth of Bt at the expense of Grt. Muscovite as secondary phase may be observed in Grt fractures during late hydrothermal overprint.

5 samples of migmatitic metapelite (1 to 5 kg each) were taken from the same outcrop, and they are termed 95/806, 95/806b, 95/806c, 95/806d, and 95/806e. As garnet-bearing leucosomes are texturally intimately associated to paleosomes, pure migmatitic end-members are difficult to separate from others. Therefore, leucosomes and paleosomes are annotated in the text by the estimated amount of pure end-member. For example, a leucosome which contains 5% of paleosome is annotated by 95%L.

## 6.3. Analytical techniques

### 6.3.1. Microprobe analyses

Mineral compositions were analyzed with a Cameca SX50 electron microprobe at the University of Bern, operating at 15 kV high voltage and 20 nA beam current.

### 6.3.2. Major and trace-element analyses

Major and trace elements were determined by X-ray fluorescence spectrometry (XRF) using a Philips spectrometer at the University of Rennes 1. Relative analytical uncertainties range from ±1% to ±3% for major elements, around ±5% for trace elements with concentrations around 20 ppm and around ±10% for those < 20 ppm. Nb was determined with long counting time so that the precision was maintained at ~±10% even for concentration less

than 5 ppm. Some trace elements and REE were determined by INAA at ACTLABS, Canada. The detection limits are shown in brackets in Table I-19.

### 6.3.3. Chemical separation and isotope analyses

About 100 mg each of powdered samples and 50 mg of sillimanite, biotite, and different size fractions of garnet were spiked with $^{150}Nd$-$^{149}Sm$ tracer before dissolution. Chemical procedure is detailed in Chavagnac et al. (submitted). For U-Pb analyses, about 200mg of powdered samples were dissolved using an acid digestion (40% HF 2xdist : $HNO_3$) in a Savillex beaker at 150°C for several days. After total dissolution, a mixed tracer ($^{205}Pb$-$^{235}U$) was added. U and Pb were separated using standard anion exchange. Mineral and chemical separations have been done at the University of Bern.

For some whole rock samples, Nd isotope analyses were done at the University of Rennes 1 using double Re filament ($Nd^+$ emission) in a seven-collector Finnigan MAT 262 mass spectrometer in semi-dynamic mode due to technical problem on mass spectrometer at the University of Bern at that time. $^{143}Nd/^{144}Nd$ ratios were normalized against $^{146}Nd/^{144}Nd$ = 0.7219. During the period of data acquisition, the AMES standard gave $^{143}Nd/^{144}Nd$ = 0.511961 ± 0.000007 (2 σ) and the La Jolla standard gave 0.511858 ± 0.000007 (2 σ). The others Nd isotope analyses were done at the University of Bern using single Re filament ($NdO^+$ emission). La Jolla standard gave 0.511858 ± 0.000030 (2 σ). Details on Nd measurement as oxyde as well as Sm, U and Pb are presented in Chavagnac et al. (submitted). The uncertainty on Sm/Nd ratios is less than ±0.3%. Chemical procedural blanks are Sm ~50pg and Nd ~150 pg and Pb ~50pg.

Sm-Nd model ages were calculated relative to depleted mantle evolution. The Nd evolution of the Depleted Mantle is approximated by a third order polynomial fit:

$$\varepsilon_{Nd}(T)_{sample} = 0.164T^3 - 0.566T^2 - 2.79T + 10.4 \text{ (Nägler and Kramers, 1998)}$$

## 6.4. Metamorphic conditions

Representative chemical composition of the major minerals forming the metapelitic migmatite are reported in Table I-18. The stochiometric formulas are calculated on the basis of 8 (Pl), 16 (Grt) and 22 oxygen atoms and 4(OH, Cl, F) ions for Bt.

Muscovite (Ms) occurs only as a secondary mineral phase at grain boundaries and peak metamorphic conditions were clearly above its stability field. However, the presence of fibrolite Sil along the edge of tabular Sil crystal suggests that Ms breakdown may have occurred

Table I-18: Representative chemical analyses and cation proportions of Bt, Pl, K-fs and Grt of sample 95/806. Mineral abbreviation according to Kretz (1983).

| | Biotite | | | |
|---|---|---|---|---|
| SiO2 | 36.63 | 36.75 | 36.87 | 37.03 |
| TiO2 | 3.84 | 3.87 | 3.87 | 3.53 |
| Al2O3 | 18.5 | 18.11 | 18.28 | 18.39 |
| Fe2O3 | 1.55 | 1.4 | 0.99 | 0.42 |
| FeO | 12.76 | 13.16 | 13.04 | 13.04 |
| MnO | 0.04 | 0.1 | 0.01 | 0.01 |
| MgO | 12.94 | 13.04 | 13.11 | 13.49 |
| CaO | 0.07 | 0.01 | 0 | 0 |
| Na2O | 0.09 | 0.09 | 0.07 | 0.12 |
| K2O | 9.77 | 10.21 | 10.12 | 9.95 |
| H2O | 4.08 | 4.09 | 4.08 | 4.08 |
| Total | 100.27 | 100.83 | 100.44 | 100.06 |
| | | | | |
| Si | 2.6882 | 2.6939 | 2.7044 | 2.7185 |
| Al(IV) | 1.3118 | 1.3061 | 1.2956 | 1.2815 |
| Ti | 0.2121 | 0.2136 | 0.2137 | 0.1947 |
| Al(VI) | 0.2885 | 0.2585 | 0.2844 | 0.3093 |
| Fe(3+) | 0.0856 | 0.0772 | 0.0545 | 0.0234 |
| Fe(2+) | 0.7831 | 0.8066 | 0.8001 | 0.8008 |
| Mn | 0.0024 | 0.006 | 0.0006 | 0.0007 |
| Mg | 1.4161 | 1.4246 | 1.433 | 1.4763 |
| Ca | 0.0055 | 0.001 | 0 | 0 |
| Na | 0.0121 | 0.0134 | 0.0098 | 0.0171 |
| K | 0.9147 | 0.9551 | 0.9469 | 0.9318 |

| | Pl | | | |
|---|---|---|---|---|
| SiO2 | 62.09 | 61.04 | 61.41 | 62.11 |
| Al2O3 | 24.92 | 25.95 | 24.97 | 25 |
| Fe2O3 | 0 | 0 | 0 | 0 |
| FeO | 0.05 | 0.07 | 0.06 | 0.03 |
| MnO | 0 | 0 | 0 | 0 |
| MgO | 0 | 0 | 0 | 0 |
| CaO | 6.04 | 4.97 | 6.43 | 6.18 |
| Na2O | 8.16 | 7.32 | 7.9 | 8.06 |
| K2O | 0.25 | 1.6 | 0.28 | 0.24 |
| Total | 101.51 | 100.95 | 101.05 | 101.62 |
| | | | | |
| Si | 2.7207 | 2.6951 | 2.7066 | 2.7205 |
| Al | 1.2868 | 1.3507 | 1.297 | 1.2908 |
| Ca | 0.2838 | 0.2351 | 0.3036 | 0.2899 |
| Na | 0.6931 | 0.6265 | 0.675 | 0.6842 |
| K | 0.0139 | 0.09 | 0.0156 | 0.0133 |
| | | | | |
| Or | 0.014 | 0.095 | 0.016 | 0.013 |
| Ab | 0.7 | 0.658 | 0.679 | 0.693 |
| An | 0.286 | 0.247 | 0.305 | 0.294 |

Table I-18: Representative chemical analyses and cation proportions of Bt, Pl, K-fs and Grt of sample 95/806. Mineral abbreviation according to Kretz (1983). Continued.

| | K-fs | | | |
|---|---|---|---|---|
| SiO2 | 65.66 | 65.76 | 65.66 | 65.76 |
| Al2O3 | 18.72 | 18.74 | 18.72 | 18.74 |
| Fe2O3 | 0 | 0.08 | 0 | 0.08 |
| FeO | 0 | 0 | 0 | 0 |
| MnO | 0 | 0 | 0 | 0 |
| MgO | 0 | 0 | 0 | 0 |
| CaO | 0.08 | 0.08 | 0.08 | 0.08 |
| Na2O | 1.35 | 1.45 | 1.35 | 1.45 |
| K2O | 15.27 | 14.99 | 15.27 | 14.99 |
| Total | 101.08 | 101.1 | 101.08 | 101.1 |
| Si | 2.9871 | 2.9909 | 2.9871 | 2.9909 |
| Al | 1.0039 | 1.0044 | 1.0039 | 1.0044 |
| Ca | 0.0038 | 0.0039 | 0.0038 | 0.0039 |
| Na | 0.1191 | 0.1281 | 0.1191 | 0.1281 |
| K | 0.8861 | 0.8699 | 0.8861 | 0.8699 |
| Or | 0.878 | 0.868 | 0.878 | 0.868 |
| Ab | 0.118 | 0.128 | 0.118 | 0.128 |
| An | 0.004 | 0.004 | 0.004 | 0.004 |

| | Grt | | | |
|---|---|---|---|---|
| SiO2 | 38.64 | 38.75 | 38.41 | 38.8 |
| TiO2 | 0 | 0.02 | 0 | 0.01 |
| Al2O3 | 21.68 | 21.62 | 21.7 | 21.7 |
| FeO | 31.41 | 31.4 | 30.73 | 31.22 |
| MnO | 1.03 | 1.04 | 1.09 | 1.03 |
| MgO | 7.01 | 7.01 | 7.23 | 7.21 |
| CaO | 0.87 | 0.84 | 0.84 | 0.85 |
| Na2O | 0.02 | 0.03 | 0.03 | 0.01 |
| Total | 100.66 | 100.71 | 100.62 | 100.83 |
| Si | 3.0088 | 3.0166 | 2.9895 | 3.0125 |
| Ti | 0 | 0.0009 | 0 | 0.0007 |
| Al | 1.9893 | 1.9832 | 1.9907 | 1.9853 |
| FeII | 2.0454 | 2.044 | 2.0002 | 2.0266 |
| Mn | 0.068 | 0.0684 | 0.0716 | 0.0674 |
| Mg | 0.8134 | 0.8132 | 0.8386 | 0.8348 |
| Ca | 0.0727 | 0.0699 | 0.0702 | 0.0711 |
| Na | 0.0024 | 0.0039 | 0.0045 | 0.0016 |
| Alm | 0.682 | 0.682 | 0.671 | 0.676 |
| And | 0 | 0 | 0.017 | 0 |
| Grs | 0.024 | 0.023 | 0.006 | 0.024 |
| Prp | 0.271 | 0.271 | 0.281 | 0.278 |
| Sps | 0.023 | 0.023 | 0.024 | 0.022 |

| | Grt | | | |
|---|---|---|---|---|
| SiO2 | 39.1 | 39.19 | 39.19 | 39.27 |
| TiO2 | 0.01 | 0.01 | 0.03 | 0.03 |
| Al2O3 | 21.65 | 21.61 | 21.79 | 21.65 |
| FeO | 27.78 | 27.61 | 27.73 | 27.54 |
| MnO | 0.69 | 0.67 | 0.75 | 0.74 |
| MgO | 9.56 | 9.61 | 9.55 | 9.64 |
| CaO | 0.87 | 0.96 | 0.91 | 0.93 |
| Na2O | 0.01 | 0 | 0.01 | 0.01 |
| Total | 99.67 | 99.66 | 99.96 | 99.81 |
| Si | 3.0182 | 3.0237 | 3.0166 | 3.0251 |
| Ti | 0.0003 | 0.0006 | 0.0018 | 0.002 |
| Al | 1.97 | 1.9657 | 1.9766 | 1.9655 |
| FeII | 1.7933 | 1.7816 | 1.7846 | 1.7744 |
| Mn | 0.0453 | 0.0435 | 0.0487 | 0.0485 |
| Mg | 1.0996 | 1.1057 | 1.095 | 1.1067 |
| Ca | 0.0723 | 0.0792 | 0.0752 | 0.0768 |
| Na | 0.001 | 0 | 0.0014 | 0.001 |
| Alm | 0.596 | 0.592 | 0.594 | 0.59 |
| And | 0 | 0 | 0 | 0 |
| Grs | 0.024 | 0.026 | 0.025 | 0.026 |
| Prp | 0.365 | 0.367 | 0.365 | 0.368 |
| Sps | 0.015 | 0.014 | 0.016 | 0.016 |

Figure I-62: Ti versus $Al_{VI}$ diagram for the biotite chemical composition after Schreurs (1985). The Ti contents indicate a temperature of 650°-700°C for the biotite crystallization at the expense of garnet.

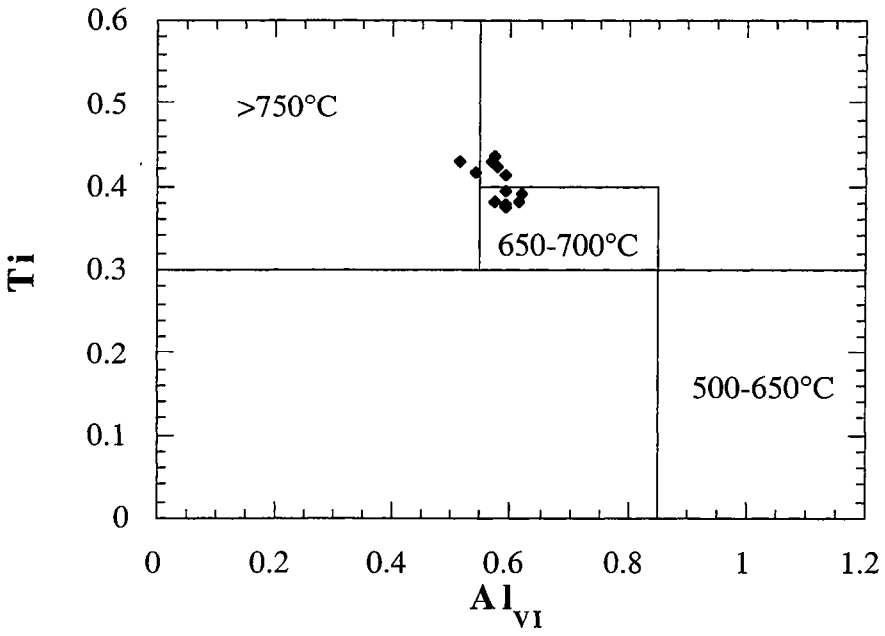


Figure I-63: The chemical compositions of Pl and K-fs are plotted in an Or-Ab-An triangle. Pl has an oligoclase composition and K-fs are composed of 80 to 95% Or contents.

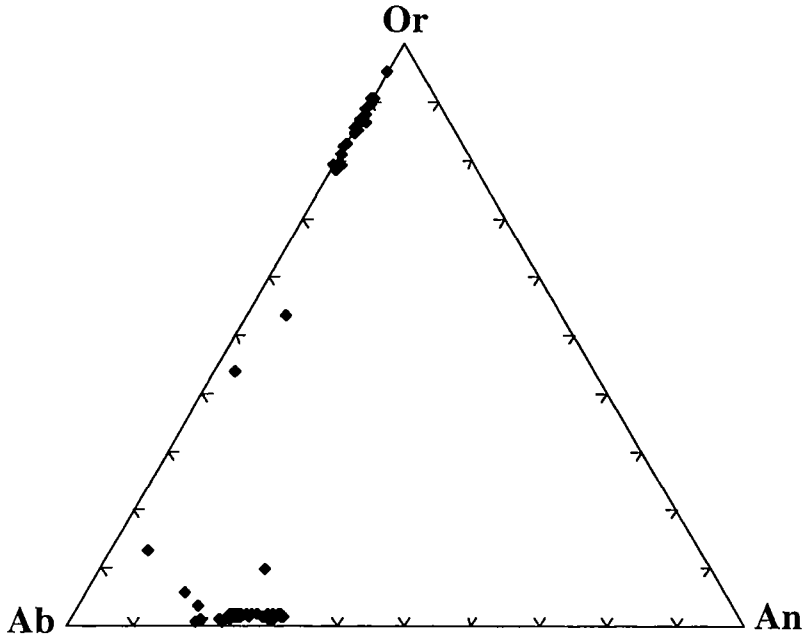

at the early stage of partial melting according to the following reaction (Le Breton and Thompson, 1988, Gardien et al., 1995) :

$$Ms + Pl + Qtz <=> Sil + K\text{-}fs + melt$$

After Ms was used up, further heating induced melt formation via the Bt fluid-absent melting. This is shown by inclusions of Bt-Sil-Pl-Qtz in Grt which is the typical mineral paragenesis association with garnet formation in a metapelite in the following reaction (Vielzeuf and Montel, 1994; Patiño Douce and Beard, 1996; Stevens et al., 1997):

$$Bt + Sil + Pl + Qtz <=> Grt + K\text{-}fs + melt$$

As matrix Bt grains were mostly altered, analyzed Bt grains are texturally associated with resorbed Grt. The Ti versus $Al_{VI}$ diagram (Schreurs, 1985) can be used to estimate the metamorphic grade as Bt is always associated with Fe-Ti oxydes (Fig.I-62). For Bt which grew at the expense of Grt during the retrograde path, a formation temperature of 650° to 700°C is indicated by the Ti and $Al_{VI}$ contents. Temperatures above 750°C is however suggested by the highest Ti contents in Bt intimately associated with Grt. Experimental studies on Ms and Bt dehydration reactions support continuous evolution of Grt and melt modes from Ms to Bt dehydration reactions (Vielzeuf and Holloway, 1988; Patiño Douce and Johnston, 1991; Gardien et al., 1995). Spear and Kohn (1996) suggest that the modal proportion of minerals may change significantly during the transition, and chemical zonation in Grt may be observed. Pl compositions are plotted in an Or-Ab-An triangular diagram (Fig. I-63). It can be seen that (1) Pl has an oligoclase composition, (2) K-fs are composed of 80 to 95% Or, (3) some Pl have a high Or content (up to 40%) suggesting antiperthite formation. In addition, chemical compositon variations in Grt are documented by microprobe scan profiles (Fig. I-64a, I-64b). Several features are suggested: (1) one generation of Grt is characterized by $X_{Mg}$ ~0.38 whereas the second generation presents $X_{Mg}$ ~0.25, the chemical variation is not related to the grain size of the Grt analyzed; (2) chemical zonations are restricted to a thin rim (~50μm) at the contact with Bt either in the matrix or occurring as inclusions; (3) Sps and Grs contents form a linear trend from core to rim and no variation is observed at the contact with Bt or Pl; (4) Both Grt have an almandin-rich composition. Therefore, two distinct chemical compositions of Grt may represent the change in element partition coefficients between products and melt. The determination of the P-T conditions related to each melting reaction cannot be established as original Ms is no longer present. Grt grains cannot be ascribed to a specific melting reaction, and the water activity may have changed as temperature increased.

The lack of Opx as a main phase product during the dehydration reaction may be explained by the high bulk $X_{Fe}$ in metapelite which do not allow its crystallization. Therefore, Grt is the main Fe-Mg solid product of the fluid-absent melting.

Figure I-64: Chemical compositions versus distance along garnet profile. Two generations of garnet are suggested. Both garnets presents a Fe-Mg zonation at the outer rim.

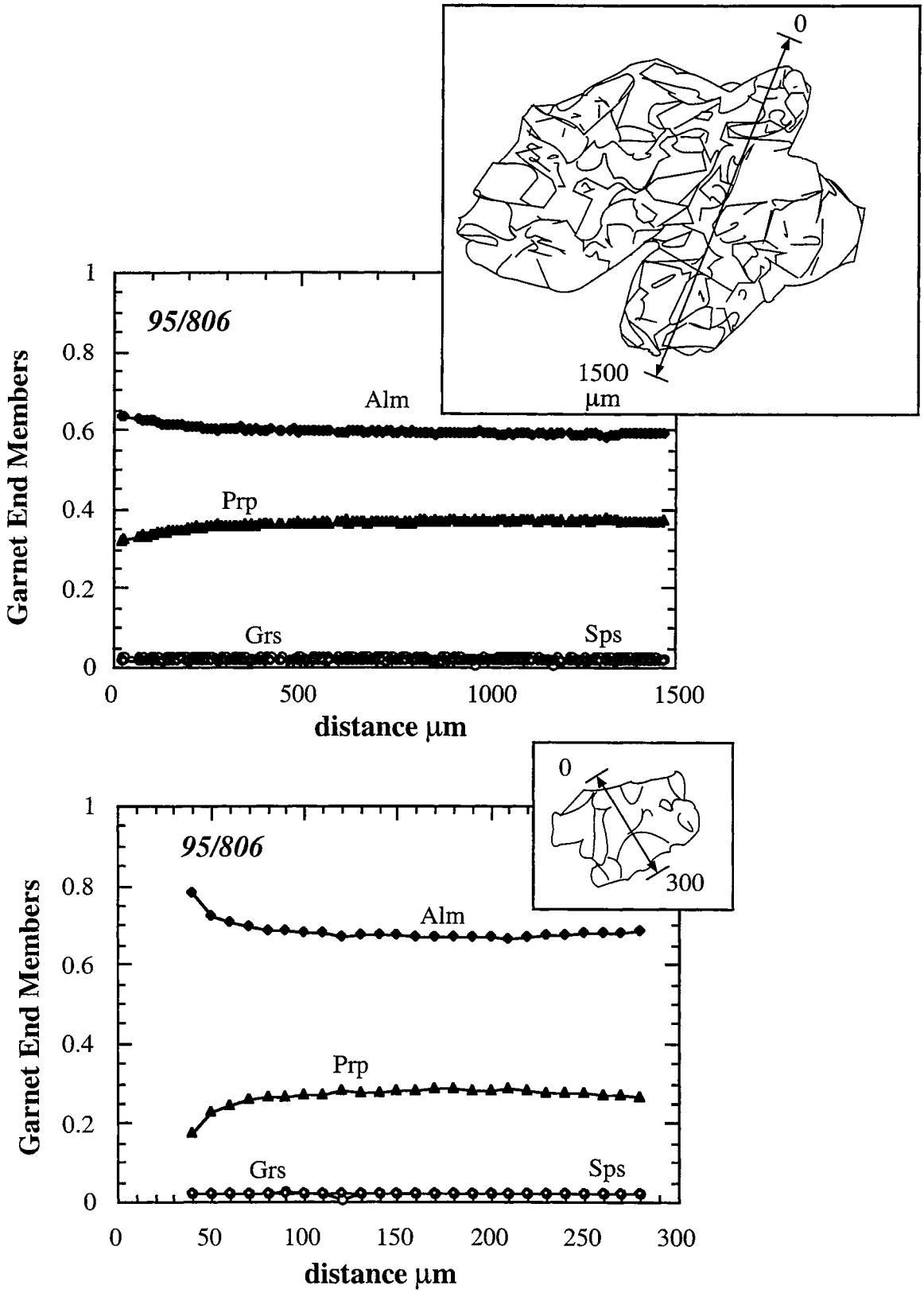

The marginal Fe-Mg zonations in garnets are interpreted as retrograde diffusion zonations (Spear, 1992), which are associated with the resorption of Grt to form Bt at temperature below 700°C. The rehydration may be the product of fluid oversaturation reached during nearby crystallization of granitic melts. Local alteration at greenschist facies conditions document a late hydrothermal activity.

## 6.5. Geochemical results and discussion

The major and trace element data are presented in Table I-19 with Proterozoic cratonic shale (Condie, 1993) and Proterozoic granite added for comparison. All whole rock samples have a shale composition according to the sedimentary classification of Herron (1988). Their spidergram patterns normalized to primitive mantle are similar to Proterozoic cratonic shale (Fig. I-65a). They are characterized by negative Nb, Sr, $P_2O_5$ and $TiO_2$ anomalies and variable LILE contents. On the whole, the patterns of the paleosomes are also characterized the same negative anomalies as the Proterozoic cratonic shale and by severe depletion in all LILE (Fig. I-65b). The leucosomes portray a granitic composition in a Qtz-Pl-Or triangle (Streckeisen, 1976). Their primitive-mantle-normalized spidergram patterns ressemble those of a Proterozoic granite, exhibiting negative Nb, Sr, $P_2O_5$ and $TiO_2$ anomalies and LILE enrichment relative to paleosomes (Fig. I-65c). Leucosomes which present a chemical composition close to the minimum eutectic melt composition show the highest negative anomalies and Th, Zr and HREE depletion. The $Al_2O_3$ contents of leucosomes above 13 wt% associated with their A/CNK ratios above 1 (1 exception) imply a peraluminous character. Such compositions are typical for the partial melt produced by fluid-absent melting of metapelite (Le Breton and Thompson, 1988; Patiño Douce and Johnston, 1991; Stevens et al., 1997).

All migmatitic components define a positive linear correlation in the $Fe_2O_3$ and $TiO_2$ versus MgO diagrams (Fig. I-66a, I-66b). Eutectic melts are depleted in $TiO_2$, MgO and $Fe_2O_3$ and the $TiO_2$, MgO and $Fe_2O_3$ contents of leucosomes vary with the amount of paleosome incorporqted in them. In addition, the Na/Ca and K/Na ratios of leucosomes (1.4-3.8 and 0.8-2.7 respectively at one exception) are markedly higher than those of the paleosomes (0.5-0.8 and 1-1.5 respectively). Pl, Bt and perhaps Ms are the main contributors of Na, Ca and K to the partial melt and these offsets correspond qualitatively to the proportions in which these entered the melt.

The extent of chemical equilibrium between partial melts and refractory residues may be investigated from trace element data. All leucosomes present significantly higher LILE concentrations compared to paleosomes arguing for melt formation via Bt (and Ms) fluid-absent dehydration reaction (Harris and Inger, 1992; Inger and Harris, 1993). K/Rb ratios of leucosomes range from 240 to 427 (K/Rb = 256 for Proterozoic granite) are higher than those

Table I-19:Major and trace element contents of all migmatitic components and 4 whole rocks. The compositions of Proterozoic granite and Proterozoic cratonic shale (Condie, 1993) are listed for comparison.

| sample number<br>rock | 95/806.wr<br>whole rock | 95/806.r<br>paleosome | 95/806.99l<br>leucosome | 95/806.95l<br>leucosome | 95/806.80l<br>leucosome | 95/806b.wr<br>whole rock | 95/806b.95l<br>leucosome | 95/806b.85l<br>leucosome | 95/806c.98r<br>paleosome |
|---|---|---|---|---|---|---|---|---|---|
| **Major elements by XRF in wt%** | | | | | | | | | |
| SiO2 | 71.75 | 62.56 | 72.44 | 71.89 | 73.66 | 64.4 | 66.63 | 63.23 | 68.34 |
| TiO2 | 0.36 | 0.93 | 0.04 | 0.08 | 0.25 | 0.81 | 0.34 | 0.57 | 0.69 |
| Al2O3 | 12.76 | 14.02 | 14.81 | 15.64 | 13.68 | 14.14 | 15.84 | 16.31 | 12.96 |
| Fe2O3 | 4.07 | 9.69 | 0.41 | 0.8 | 2.84 | 8.34 | 4.06 | 7.25 | 7.08 |
| MnO | 0.07 | 0.14 | 0 | 0.01 | 0.04 | 0.12 | 0.07 | 0.16 | 0.09 |
| MgO | 1.82 | 4.83 | 0.11 | 0.57 | 1.65 | 4.13 | 1.89 | 3.26 | 3.51 |
| CaO | 1.32 | 1.76 | 1.46 | 0.81 | 1.55 | 1.76 | 1.97 | 1.87 | 1.93 |
| Na2O | 2.31 | 1.83 | 3.4 | 2.95 | 2.44 | 2.18 | 3.93 | 3.1 | 2.36 |
| K2O | 2.94 | 1.35 | 5.04 | 7.16 | 2.96 | 1.83 | 2.64 | 2.52 | 1.05 |
| P2O5 | 0.04 | 0.03 | 0.06 | 0.07 | 0.04 | 0.05 | 0.06 | 0.06 | 0.04 |
| PF | 0.93 | 1.62 | 0.22 | 0.42 | 1 | 1.43 | 1.05 | 0.81 | 1.37 |
| Total | 98.37 | 98.76 | 97.99 | 100.4 | 100.11 | 99.19 | 98.48 | 99.14 | 99.42 |
| **Trace elements by XRF in ppm** | | | | | | | | | |
| Rb/Sr | 0.798 | 1.087 | 0.616 | 0.842 | 0.689 | 0.953 | 0.597 | 0.674 | 0.674 |
| K/Na | 1.424 | 0.825 | 1.659 | 2.716 | 1.357 | 0.939 | 0.752 | 0.910 | 0.498 |
| K/Ba | 30.93 | 39.18 | 25.84 | 27.49 | 27.30 | 37.23 | 31.49 | 31.22 | 44.47 |
| Na/Sr | 164.79 | 196.76 | 158.65 | 127.99 | 152.12 | 188.06 | 217.59 | 178.29 | 203.59 |
| Na/Ca | 1.82 | 1.08 | 2.42 | 3.78 | 1.63 | 1.29 | 2.07 | 1.72 | 1.27 |
| Ca/Sr | 90.71 | 182.30 | 65.63 | 33.85 | 93.09 | 146.26 | 105.07 | 103.60 | 160.39 |
| K/Rb | 294.04 | 149.42 | 426.91 | 412.74 | 299.65 | 185.25 | 273.93 | 240.44 | 150.28 |
| Nb | 16.4 | 28.5 | 1.1 | 3.3 | 10.1 | 31.3 | 13.8 | 20.3 | 12 |
| Zr | 80 | 157 | 6 | 28 | 56 | 141 | 85 | 120 | 141 |
| Y | 49 | 69 | 4 | 8 | 27 | 71 | 50 | 85 | 41 |
| Sr | 104 | 69 | 159 | 171 | 119 | 86 | 134 | 129 | 86 |
| Rb | 83 | 75 | 98 | 144 | 82 | 82 | 80 | 87 | 58 |
| Co | 15 | 39 | <1 | 3 | 19 | 35 | 15 | 32 | 33 |
| V | 74 | 214 | 10 | 18 | 49 | 176 | 72 | 125 | 152 |
| Ni | 72 | 144 | 6 | 12 | 78 | 126 | 57 | 94 | 128 |
| Cr | 207 | 466 | 21 | 35 | 115 | 423 | 184 | 311 | 345 |
| Ba | 789 | 286 | 1619 | 2162 | 900 | 408 | 696 | 670 | 196 |
| Ga | 18 | 24 | 14 | 14 | 17 | 22 | 20 | 21 | 17 |
| Cu | 22 | 7 | 2 | 3 | 9 | 12 | 6 | 3 | 57 |
| Zn | 58 | 128 | 14 | 19 | 78 | 107 | 48 | 95 | 96 |
| Th | <1 | 7 | 2 | <1 | 5 | 13 | 3 | 13 | 7 |
| Pb | 47 | 25 | 81 | 102 | 49 | 33 | 48 | 47 | 27 |
| U | <0,7 | 1.1 | 1.9 | 2.5 | 2.2 | 1.7 | 1.3 | 2.5 | <1,0 |
| **Rare Earth Elements by INAA in ppm** | | | | | | | | | |
| La {0.1} | 21.7 | 34.4 | 34.2 | 23.2 | 34.3 | 45.1 | 33.3 | 47.9 | 32 |
| Ce {1} | 54 | 75 | 73 | 44 | 71 | 108 | 80 | 110 | 73 |
| Nd {1} | 15 | 30 | 29 | 15 | 32 | 38 | 22 | 44 | 24 |
| Sm {0.01} | 4.01 | 6.34 | 5.49 | 3.63 | 5.68 | 8.87 | 5.34 | 8.89 | 5.55 |
| Eu {0.05} | 1.04 | 0.74 | 1.22 | 1.39 | 0.73 | 0.84 | 1.21 | 1.18 | 0.65 |
| Gd {0.1} | 4.7 | 7.4 | 3.5 | 3 | 4.6 | 8.3 | 4.9 | 8 | 5.5 |
| Tb {0.1} | 1.1 | 1.6 | 0.4 | 0.4 | 0.9 | 1.9 | 1 | 1.7 | 1.1 |
| Yb {0.05} | 5.63 | 7.6 | 0.95 | 0.9 | 3.23 | 7.55 | 6.54 | 10.4 | 4.38 |
| Lu {0.01} | 0.78 | 0.95 | 0.15 | 0.13 | 0.44 | 1.01 | 0.9 | 1.28 | 0.6 |
| ΣHREE | 7.51 | 10.15 | 1.5 | 1.43 | 4.57 | 10.46 | 8.44 | 13.38 | 6.08 |
| Eu/Eu* | 0.742 | 0.335 | 0.862 | 1.305 | 0.442 | 0.303 | 0.733 | 0.433 | 0.364 |
| (La/Yb)N | 2.55 | 2.99 | 23.77 | 17.02 | 7.01 | 3.94 | 3.36 | 3.04 | 4.82 |
| **Norme CIPW in weight %** | | | | | | | | | |
| Qtz | 41.63 | 35.86 | 30.25 | 24.94 | 42.47 | 34.93 | 26.8 | 26.86 | 41.34 |
| Or | 17.37 | 7.98 | 29.78 | 42.31 | 17.49 | 10.81 | 15.6 | 14.89 | 6.2 |
| Ab | 19.55 | 15.48 | 28.77 | 24.96 | 20.65 | 18.45 | 33.25 | 26.23 | 19.97 |
| An | 6.29 | 8.54 | 6.85 | 3.56 | 7.43 | 8.4 | 9.38 | 8.89 | 9.31 |
| Mg-Hy | 4.53 | 12.03 | 0.27 | 1.42 | 4.11 | 10.29 | 4.71 | 8.12 | 8.74 |
| Ap | 0.09 | 0.07 | 0.14 | 0.16 | 0.09 | 0.12 | 0.14 | 0.14 | 0.09 |
| Ru | 0.28 | 0.77 | 0.04 | 0.07 | 0.2 | 0.67 | 0.26 | 0.39 | 0.59 |
| Cor | 3.47 | 6.42 | 1.25 | 1.73 | 3.74 | 5.49 | 3.08 | 5.23 | 4.53 |
| Hem | 4.07 | 9.69 | 0.41 | 0.8 | 2.84 | 8.34 | 4.06 | 7.25 | 7.08 |
| Ilm | 0.15 | 0.3 | - | 0.02 | 0.09 | 0.26 | 0.15 | 0.34 | 0.19 |

Table I-19:Major and trace element contents of all migmatitic components and 4 whole rocks. The compositions of Proterozoic granite and Proterozoic cratonic shale (Condie, 1993) are listed for comparison.

| sample number<br>rock | 95/806c.90r<br>paleosome | 95/806c.95l<br>leucosome | 95/806d.wr<br>whole rock | 95/806d.r<br>paleosome | 95/806d.92l<br>leucosome | 95/806d.70l<br>leucosome | 95/806e.wr<br>whole rock | 95/806e.l<br>leucosome | Cratonic shale<br>Proterozoic | Granite<br>Proterozoic |
|---|---|---|---|---|---|---|---|---|---|---|
| **Major elements by XRF in wt%** | | | | | | | | | | |
| SiO2 | 66.2 | 70.08 | 67.53 | 67.3 | 72.04 | 71.32 | 66.1 | 73.08 | 63.1 | 73.3 |
| TiO2 | 0.66 | 0.45 | 0.19 | 0.8 | 0.07 | 0.48 | 0.71 | 0.09 | 0.64 | 0.28 |
| Al2O3 | 14.21 | 13.73 | 17.01 | 12.26 | 14.44 | 11.9 | 14.3 | 14.9 | 17.5 | 13.5 |
| Fe2O3 | 6.66 | 4.2 | 2.65 | 8.3 | 0.77 | 5.82 | 7.46 | 1.25 | 6.28 | 2.45 |
| MnO | 0.09 | 0.06 | 0.04 | 0.12 | 0.01 | 0.1 | 0.11 | 0.02 | | |
| MgO | 3.38 | 2.2 | 1.25 | 4.23 | 0.33 | 2.56 | 3.83 | 0.53 | 2.2 | 0.42 |
| CaO | 1.94 | 1.56 | 1.36 | 1.56 | 0.87 | 1.54 | 1.88 | 2.31 | 0.71 | 1.3 |
| Na2O | 2.78 | 3.21 | 2.79 | 1.83 | 2.78 | 2.12 | 2.78 | 4.29 | 1.06 | 3.2 |
| K2O | 1.49 | 2.18 | 4.8 | 1.13 | 6.5 | 1.8 | 1.39 | 1.63 | 3.62 | 4.8 |
| P2O5 | 0.05 | 0.05 | 0.05 | 0.03 | 0.06 | 0.03 | 0.05 | 0.06 | 0.12 | 0.08 |
| PF | 1.44 | 1.11 | 0.85 | 1.42 | 0.38 | 0.95 | 1.49 | 0.28 | | |
| Total | 98.9 | 98.83 | 98.52 | 98.98 | 98.25 | 98.62 | 100.1 | 98.44 | 95.23 | 99.33 |
| **Trace elements by XRF in ppm** | | | | | | | | | | |
| Rb/Sr | 0.720 | 0.580 | 0.773 | 0.934 | 0.828 | 0.628 | 0.745 | 0.285 | 1.528 | 1.300 |
| K/Na | 0.600 | 0.760 | 1.925 | 0.691 | 2.616 | 0.950 | 0.559 | 0.425 | 3.821 | 1.678 |
| K/Ba | 42.80 | 28.14 | 28.18 | 40.09 | 29.06 | 29.88 | 47.68 | 27.67 | 46.81 | 53.13 |
| Na/Sr | 192.76 | 200.13 | 126.99 | 222.57 | 136.59 | 201.64 | 219.41 | 201.44 | 72.82 | 197.84 |
| Na/Ca | 1.49 | 2.14 | 2.13 | 1.22 | 3.32 | 1.43 | 1.54 | 1.93 | 1.55 | 2.56 |
| Ca/Sr | 129.58 | 93.69 | 59.63 | 182.78 | 41.18 | 141.11 | 142.94 | 104.49 | 46.98 | 77.43 |
| K/Rb | 160.63 | 262.26 | 316.23 | 164.56 | 431.65 | 304.93 | 164.83 | 300.68 | 182.12 | 255.42 |
| Nb | 12.6 | 15.3 | 9.6 | 19 | 2.5 | 20.3 | 23.3 | 3.1 | 16.8 | 20 |
| Zr | 130 | 91 | 65 | 160 | 20 | 100 | 145 | 26 | 196 | 240 |
| Y | 37 | 38 | 32 | 51 | 6 | 70 | 64 | 14 | 35 | 45 |
| Sr | 107 | 119 | 163 | 61 | 151 | 78 | 94 | 158 | 108 | 120 |
| Rb | 77 | 69 | 126 | 57 | 125 | 49 | 70 | 45 | 165 | 156 |
| Co | 31 | 20 | 13 | 35 | 2 | 22 | 30 | 8 | 18 | 5.5 |
| V | 154 | 99 | 43 | 172 | 16 | 88 | 157 | 20 | 100 | 20 |
| Ni | 131 | 72 | 67 | 130 | 15 | 94 | 116 | 31 | 52 | 15 |
| Cr | 334 | 214 | 122 | 397 | 33 | 202 | 376 | 51 | 115 | 18 |
| Ba | 289 | 643 | 1414 | 234 | 1857 | 500 | 242 | 489 | 642 | 750 |
| Ga | 19 | 18 | 22 | 19 | 13 | 17 | 21 | 17 | - | - |
| Cu | 44 | 7 | 18 | 11 | 4 | 31 | 17 | 1 | - | - |
| Zn | 98 | 63 | 83 | 108 | 16 | 56 | 89 | 31 | - | - |
| Th | 7 | 8 | <1 | 9 | <1 | 6 | 10 | 4 | 14.3 | 18 |
| Pb | 26 | 47 | 66 | 22 | 90 | 37 | 31 | 46 | 27 | 25 |
| U | 1.9 | 1.4 | 1.9 | <0,6 | 1.9 | 2.4 | 2.2 | 1.7 | 3.4 | 4.5 |
| **Rare Earth Elements by INAA in ppm** | | | | | | | | | | |
| La {0.1} | 38.7 | 36.8 | 26.5 | 39 | 20.2 | 26.7 | 43.8 | 33.5 | 38 | 48 |
| Ce {1} | 84 | 86 | 55 | 89 | 41 | 61 | 98 | 67 | 81.7 | 115 |
| Nd {1} | 35 | 29 | 18 | 37 | 14 | 20 | 38 | 25 | 37.5 | 54 |
| Sm {0.01} | 6.72 | 6.36 | 4.21 | 7.01 | 2.81 | 5.49 | 8.06 | 4.99 | 6.68 | 8.7 |
| Eu {0.05} | 0.95 | 1.06 | 1.21 | 0.65 | 1.3 | 0.65 | 0.89 | 1.11 | 1.32 | 1 |
| Gd | 6.9 | 5.7 | 3.4 | 6.8 | 1.8 | 6.3 | 7.5 | 3.9 | 5.6 | 8.17 |
| Tb {0.1} | 1 | 0.9 | 0.8 | 1.3 | 0.2 | 1.4 | 1.5 | 0.5 | 0.9 | 1.28 |
| Yb {0.05} | 4.53 | 5.2 | 5.59 | 5.18 | 1.11 | 9.83 | 7.07 | 2.02 | 2.86 | 3.5 |
| Lu {0.01} | 0.6 | 0.75 | 0.75 | 0.7 | 0.17 | 1.35 | 0.9 | 0.29 | 0.48 | 0.58 |
| ΣHREE | 6.13 | 6.85 | 7.14 | 7.18 | 1.48 | 12.58 | 9.47 | 2.81 | 4.24 | 5.36 |
| Eu/Eu* | 0.432 | 0.545 | 0.99 | 0.291 | 1.79 | 0.342 | 0.355 | 0.779 | 0.668 | 0.367 |
| (La/Yb)N | 5.64 | 4.67 | 3.13 | 4.97 | 12.02 | 1.79 | 4.09 | 10.95 | 8.77 | 9.06 |
| **Norme CIPW in weight %** | | | | | | | | | | |
| Qtz | 35.27 | 36.59 | 28.3 | 42.77 | 28.81 | 45.07 | 35.01 | 36.32 | | |
| Or | 8.8 | 12.88 | 28.36 | 6.68 | 38.41 | 10.64 | 8.21 | 9.63 | | |
| Ab | 23.52 | 27.16 | 23.61 | 15.48 | 23.53 | 17.94 | 23.52 | 36.3 | | |
| An | 9.3 | 7.41 | 6.42 | 7.54 | 3.92 | 7.44 | 9 | 11.07 | | |
| Mg-Hy | 8.42 | 5.48 | 3.11 | 10.53 | 0.82 | 6.38 | 9.54 | 1.32 | | |
| Ap | 0.12 | 0.12 | 0.12 | 0.07 | 0.14 | 0.07 | 0.12 | 0.14 | | |
| Ru | 0.56 | 0.38 | 0.14 | 0.66 | 0.06 | 0.37 | 0.59 | 0.07 | | |
| Cor | 4.62 | 3.37 | 4.87 | 5.26 | 1.39 | 3.74 | 4.92 | 2.02 | | |
| Hem | 6.66 | 4.2 | 2.65 | 8.3 | 0.77 | 5.82 | 7.46 | 1.25 | | |
| Ilm | 0.19 | 0.13 | 0.09 | 0.26 | 0.02 | 0.21 | 0.24 | 0.04 | | |

Figure I-65: Primitive mantle-normalized spidergram patterns of whole rocks in a), paleosomes in b) and leucosomes in c). They are characterized by negative Nb, Sr, P2O5 and TiO2 anomalies. Whole rocks present chemical features similar to Proterozoic cratonic shale and leucosomes to Proterozoic granite. Note a strong enrichment of LILE in leucosomes compared to paleosomes and the highly variable HREE contents in leucosomes.

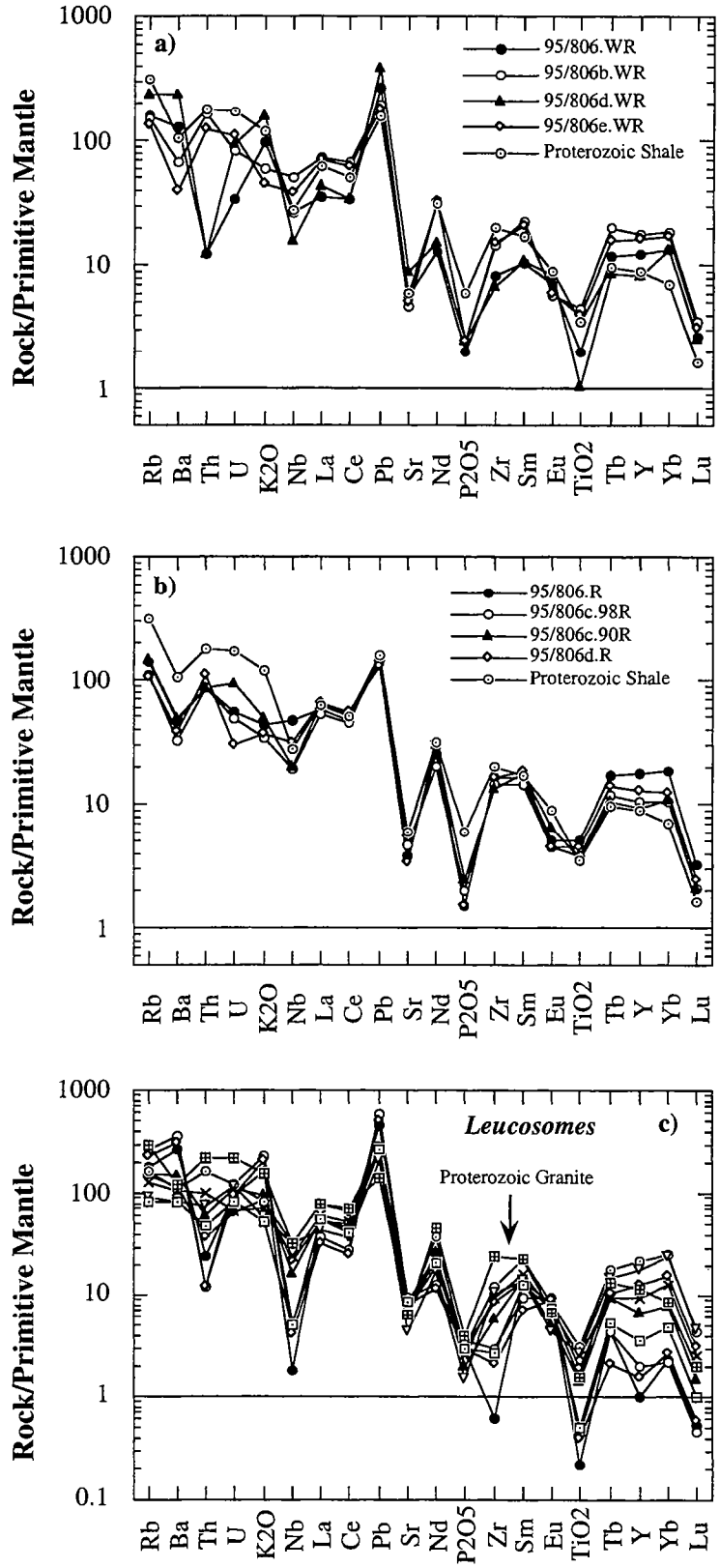

Figure I-66: Major and trace element distribution within migmatitic components: a) Fe2O3 versus MgO, b) TiO2 versus MgO, and c) Rb/Sr ratio versus Ba. Legend: open circle: leucosome, black circle: whole rock, and black triangle: paleosome.

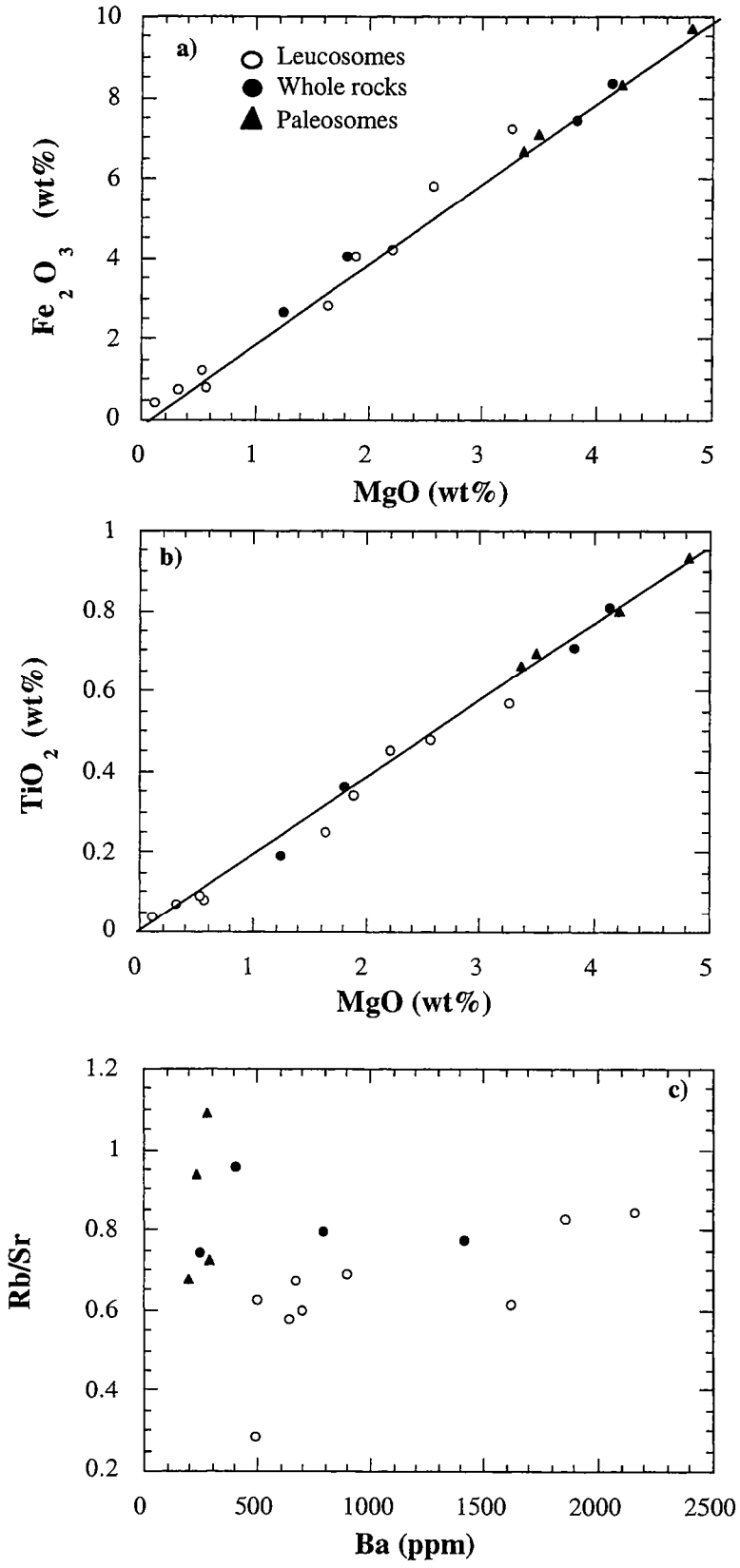

of paleosomes which are between 149 and 165 whereas the leucosomes are characterized by lower K/Ba, Na/Sr and Ca/Sr ratios (26-32, 128-218, and 33-141 respectively) compared to those of paleosomes (39-45, 193-223 and 130-183 respectively). These chemical features could either reflect a poor chemical equilibrium between Bt, K-fs and Pl with the melt, or reflect a melt residue. Na/Sr, Ca/Sr and K/Ba correlate positively with Sr and Ba contents respectively emphazing that Ba and Sr were not scavenged by residual Pl and K-fs. Furthermore, the leucosomes K/Rb ratios raised up because of higher K contents and not lowered Rb. On the whole, the K/Rb ratios of leucosomes increase with increasing Rb contents pointing the control that Bt has on the chemical composition of leucosomes. It appears that the chemical compositions of the partial melts are related to the incongruent melting of feldspars and Bt.

The question whether leucosomes represent pure melts or contain much restitic material (i.e. of how much melt left the system) cannot be answered from the distribution of major elements nor from the isocon diagram. While Bt, K-fs and Pl (perhaps Ms) controlled the major elements of the leucosomes, the concentrations of the most incompatible element namely Rb, Sr and Ba may provide further information on this aspect. In Fig. 10c the Rb/Sr ratios of all migmatitic components and whole rocks are shown as a function of their Ba contents. In chemical equilibrium, it is expected that leucosomes present higher Rb/Sr ratios and lower Ba contents compared to paleosomes. In the present case, palesomes are characterized by higher Rb/Sr ratios and lower Ba contents (0.65-1.15 and 200-300 ppm respectively) compared to leucosomes (Rb/Sr = 0.3-0.8 and Ba = 500-2200 ppm). The low Rb/Sr ratios do not correspond to real eutectic melt. Consequently, it appears that some partial melt have escaped. In addition, it does not mean that the melt fraction that escaped, did reach chemical equilibrium with the paleosomes.

The distribution of Zr, Th, Y and REE between paleosomes and leucosomes is expected to picture the degree to which accessory minerals and Grt enter the melt during partial melting. Even in a high-grade metamorphic event, chemical equilibrium of HFSE and REE is not necessarely achieved as melt formation and transport is after markedly faster than the dissolution and trace element diffusion rates (Watt and Harley, 1993). The paleosomes are characterized by a "bird" REE patterns with LREE and HREE enrichments ($(La/Yb)_N$ = 3-5) associated with a strong negative Eu anomalies ((Eu/Eu*) = 0.3-0.4; Fig. I-67b). Two distinct REE patterns of leucosomes can be distinguished: (1) the first group presents LREE enrichment ($(La/Yb)_N$ = 11-24) and slightly negative to positive Eu anomalies ((Eu/Eu*) = 0.78-1.79; Fig. I-67c), and (2) the others show LREE and HREE enrichments ($(La/Yb)_N$ = 1.8-7) and a strong negative Eu anomalies ((Eu/Eu*) = 0.3-0.7; Fig. I-67d). Finally, the whole rocks REE patterns (Fig. I-67a) reveal a mixing between various proportions of leucosomes and paleosomes of which they are composed of. The large variations in the HREE contents of leucosomes may be explained either by the entrainment of Grt or by the partial dissolution and/or the entrainment of

Figure I-67: Chondrite-normalized REE patterns of whole rocks in a), paleosomes in b) and leucosomes in c) and d). Normalization values are those of Masuda et al. (1973).

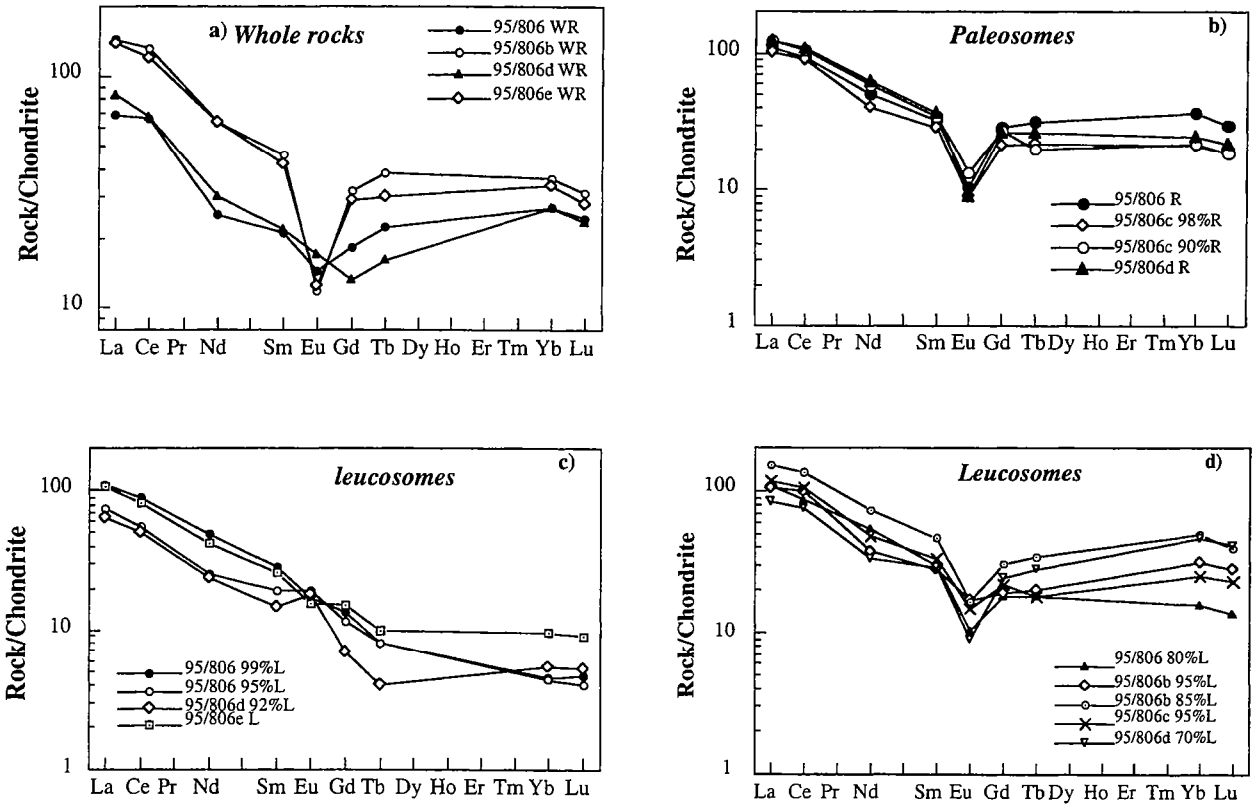

Zrn. The Zr versus MgO diagram shows a linear positive correlation in which the LREE-enriched leucosomes contain the lowest Zr and MgO contents whereas the paleosomes are significantly enriched in Zr and MgO. This indicates that Zrn behaviour during partial melting is related to a Mg-rich mineral phase, namely Bt, in which Zrn occurs as inclusions. In addition, the influence of Grt over Zrn on the distribution of HREE is confirmed by the positive correlation of the ∑HREE with Y for both leucosomes and paleosomes (Fig. I-68c). Nonetheless, the Zrn ∑HREE budget may have contributed to those of paleosomes as it increases the HREE and Zr concentrations of paleosomes (Fig. I-68b). The comparison between the three plots indicate that Grt is a more important contributor of leucosome HREE than Zrn, and the occurrence of Zrn into the melt is related to the incorporation of Bt-rich paleosome into the leucosomes. Furthermore, the occurrence of tiny Mnz grains within leucosomes suggests its crystallization from the melt. Mnz which entered the melt can influence the Th and LREE distributions between melts and refractory residues. The variations of the Eu anomalies from markedly negative to posive values can reflect the entrainment either of Mnz or feldspars. Note Eu/Eu* is stronlgy negative where Th is low. The comparison of La, Eu/Eu* values as function Th and/or Sr (or Ba) provide three main conlusions: (1) La concentrations of leucosomes and paleosomes increase for variable Th values (Fig. I-68d), (2) Eu/Eu* values of leucosomes decrease with increasing Th contents (Fig. I-68e), and (3) Eu/Eu* values of paleosomes and leucosomes correlate with Sr contents (Fig. I-68f). In addition, La correlates positively with CaO (not shown) picturing the feldspars domination on the distribution of LREE. Large amount of feldspars entering the melt implies positive Eu anomaly associated with high Sr and/or Ba contents as chemical characteristics. Nonetheless, Mnz may have increased the LREE budget of leucosomes either by its entrainment of its dissolution but it did mask the control of felspars.

From the major and trace element data, we demonstrated that some partial melt may have escape leaving a further melf dominated by feldspars. Nonetheless, the REE contents of all migmatitic components are dominated by main minerals such as feldspars for LREE and Grt for HREE. The effect of accessory minerals on the chemical features of partial melt is also suggested as a minor contributions without hiding feldspars and Grt.

## 6.6. Nd and Pb isotope results and discussion

The Sm-Nd isotope results on all migmatitic components and minerals separates are reported in Table I-20 and the U-Pb isotope results on whole rocks, leucosomes and paleosomes are listed in Table I-21.

Previous discussions (§6.4 and 6.5) on the in-situ partial melting and on the trace element distributions argued for the Sm and Nd affiliation to isochemical elements during fluid-

Figure I-68: Distribution of LIL, HFS and RE Elements between migmatitic components in order to assess the behaviour of main and accessory minerals on the chemical compositions of leucosomes. a) Zr versus MgO, b) ΣHREE versus Zr, c) ΣHREE versus Y, d) La versus Th, e) Eu/Eu* versus Th, and f) Eu/Eu* versus Sr.

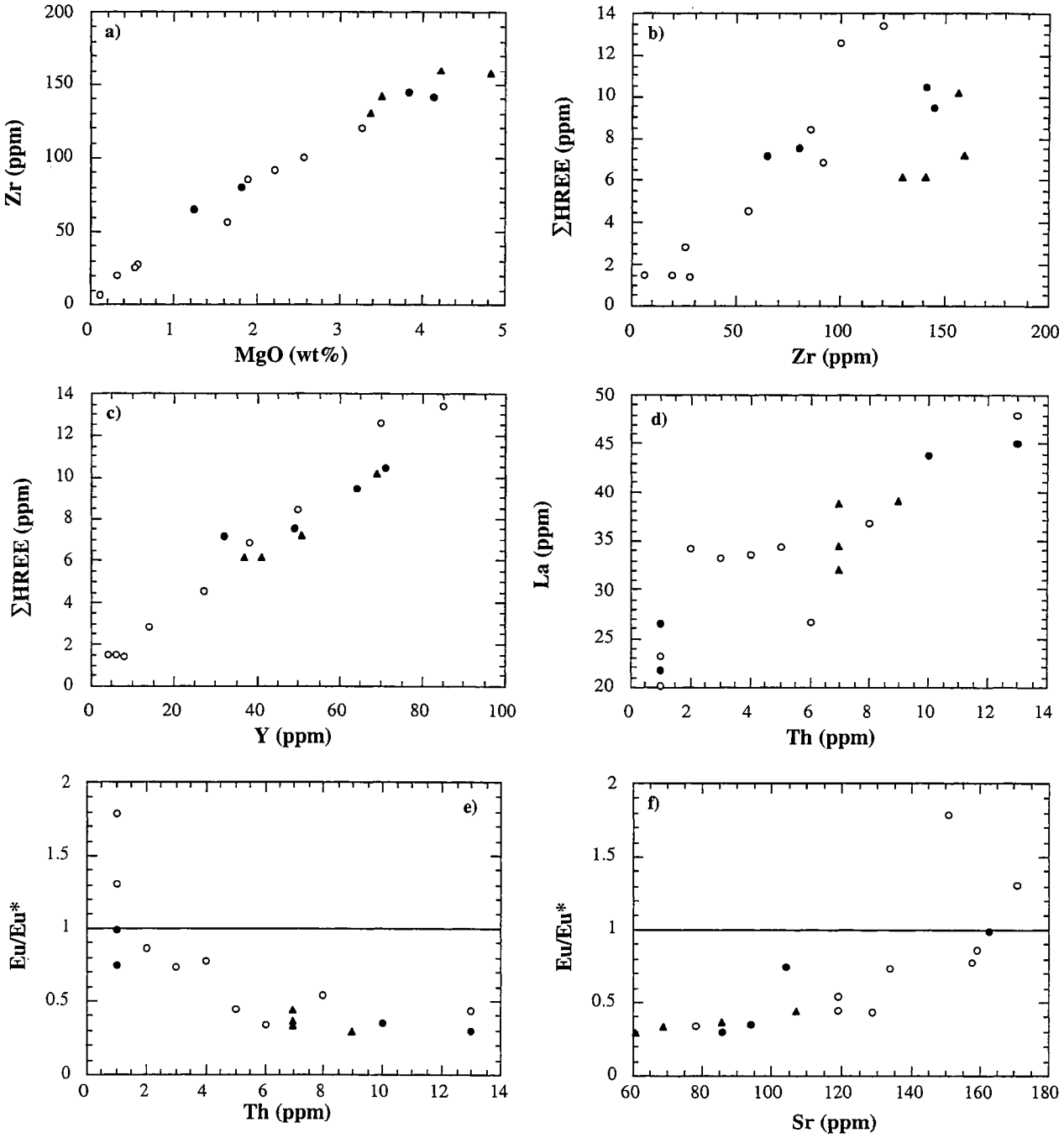

Table I-20: Sm-Nd isotopic compositions of all leucosomes, paleosomes, whole rocks and mineral separates from sample 95/806.

| Sample number | Rock type | Sm (ppm) by ID | Nd (ppm) by ID | 147Sm/144Nd | 143Nd/144Nd | ±2 σ | ε(0) | ε 2.00 | T(DM) Ga | f(Sm/Nd) |
|---|---|---|---|---|---|---|---|---|---|---|
| **Migmatitic metapelite** | | | | | | | | | | |
| **95/806 WR** | Whole rock | 3.03 | 13.12 | 0.1393 | 0.511521 | 0.000014 | -21.79 | -7.08 | 3.1 | -0.292 |
| **95/806 99%L** | Leucosome | 4.75 | 24.12 | 0.1189 | 0.511231 | 0.000018 | -27.45 | -7.50 | 2.89 | -0.396 |
| **95/806 95%L** | | 2.94 | 14.18 | 0.1253 | 0.511335 | 0.000026 | -25.42 | -7.12 | 2.93 | -0.363 |
| **95/806 R** | Paleosome | 5.14 | 21.92 | 0.1417 | 0.511490 | 0.000027 | -22.39 | -8.30 | 3.29 | -0.280 |
| **95/806 80%L** | | 5.27 | 25.58 | 0.1245 | 0.511500 | 0.000015 | -22.20 | -3.67 | 2.62 | -0.367 |
| **95/806b WR** | Whole rock | 10.56 | 47.63 | 0.1325 | 0.511401 | 0.000005 | -24.13 | -7.68 | 3.07 | -0.326 |
| **95/806b 95%L** | | 4.53 | 20.71 | 0.1324 | 0.511377 | 0.000025 | -24.60 | -8.13 | 3.11 | -0.327 |
| **95/806b 85%L** | | 8.35 | 37.37 | 0.1350 | 0.511421 | 0.000006 | -23.74 | -7.93 | 3.13 | -0.314 |
| **95/806c 95%L** | | 5.23 | 25.04 | 0.1262 | 0.511294 | 0.000007 | -26.22 | -8.15 | 3.03 | -0.358 |
| **95/806c 98%R** | | 5.65 | 27.30 | 0.1251 | 0.511224 | 0.000005 | -27.58 | -9.24 | 3.12 | -0.364 |
| **95/806c 90%R** | | 5.45 | 26.38 | 0.1249 | 0.511238 | 0.000006 | -27.31 | -8.91 | 3.08 | -0.365 |
| **95/806d WR** | Whole rock | 3.17 | 14.57 | 0.1314 | 0.51142 | 0.000006 | -23.76 | -7.02 | 2.99 | -0.332 |
| **95/806d R** | | 6.13 | 28.93 | 0.1280 | 0.511274 | 0.000007 | -26.61 | -9.01 | 3.13 | -0.349 |
| **95/806d 92%L** | | 2.08 | 10.83 | 0.1163 | 0.511159 | 0.000007 | -28.85 | -8.24 | 2.93 | -0.409 |
| **95/806d 70%L** | | 5.32 | 21.94 | 0.1465 | 0.51178 | 0.000017 | -16.74 | -3.86 | 2.84 | -0.255 |
| **95/806e WR** | Whole rock | 6.79 | 30.61 | 0.1341 | 0.511367 | 0.000024 | -24.79 | -8.76 | 3.20 | -0.318 |
| **95/806e L** | Leucosome | 4.87 | 24.60 | 0.1197 | 0.511207 | 0.000007 | -27.91 | -8.18 | 2.96 | -0.391 |
| **95/806** | Garnet 300-250µm | 4.35 | 3.86 | 0.6819 | 0.518544 | 0.000023 | 115.21 | -9.44 | - | 2.466 |
| **95/806** | Garnet 250-160µm | 3.83 | 1.89 | 1.2261 | 0.525779 | 0.000018 | 256.34 | -8.08 | - | 5.233 |
| **95/806** | Garnet <160µm | 3.54 | 1.47 | 1.4576 | 0.528752 | 0.000031 | 314.33 | -9.55 | - | 6.410 |
| **95/806** | Bt | 5.73 | 23.11 | 0.1498 | 0.511562 | 0.000016 | -20.99 | -8.99 | - | -0.238 |
| **95/806** | Sil | 4.54 | 19.14 | 0.1433 | 0.511579 | 0.000019 | -20.66 | -6.97 | - | -0.272 |
| **Messina, Tshipise** | | | | | | | | | | |
| **95/813** | Leucosome | 3.46 | 25.11 | 0.0833 | 0.510584 | 0.000019 | -40.07 | -11.00 | 2.86 | -0.577 |
| **95/814** | Leucosome | 3.68 | 22.53 | 0.0986 | 0.510785 | 0.000021 | -36.15 | -11.01 | 2.97 | -0.499 |
| **95/832** | Leucosome | 1.99 | 7.32 | 0.1643 | 0.511916 | 0.000007 | -14.08 | -5.79 | 3.54 | -0.165 |
| **Botswana, Phikwe Complex** | | | | | | | | | | |
| **95/874** | Metapelite | 10.44 | 51.33 | 0.1229 | 0.511246 | 0.000006 | -27.15 | -8.24 | 3.00 | -0.375 |
| **95/873** | Metapelite | 4.44 | 20.97 | 0.1279 | 0.511458 | 0.000008 | -23.02 | -5.38 | 2.79 | -0.350 |
| **Alldays** | | | | | | | | | | |
| **95/896** | Semi-pelite | 3.17 | 14.57 | 0.1314 | 0.51142 | 6.000000 | -23.76 | -7.02 | 2.99 | -0.332 |
| **95/909** | Leucosome | 4.57 | 27.4 | 0.1009 | 0.510926 | 0.000020 | -33.40 | -8.84 | 2.84 | -0.487 |
| **95/905** | Metapelite | 5.76 | 29.82 | 0.1167 | 0.51091 | 0.000019 | -33.71 | -13.23 | 3.35 | -0.407 |
| **95/906** | Leucosome | 1.45 | 6.08 | 0.1447 | 0.511543 | 0.000005 | -21.36 | -8.05 | 3.32 | -0.264 |
| **PSZ** | | | | | | | | | | |
| **95/833** | Metapelite with leucosome | 1.55 | 8.49 | 0.1100 | 0.510893 | 0.000007 | -34.04 | -11.83 | 3.15 | -0.441 |
| **95/834** | Metapelite | 6.90 | 31.01 | 0.1267 | 0.511471 | 0.000008 | -22.76 | -4.81 | 2.73 | -0.356 |

Table I-21: U-Pb isotope data of all migmatitic components and whole rocks from sample 95/806.

| sample | 206Pb/204Pb | ±2σ | 207Pb/204Pb | ±2σ | 208Pb/204Pb | ±2σ | r1 | r2 | μ | t (Ga) | 206Pb/204Pb corrected | 207Pb/204Pb corrected |
|---|---|---|---|---|---|---|---|---|---|---|---|---|
| 95/806 WR | 16.830 | 0.043 | 15.418 | 0.041 | 34.625 | 0.094 | 0.987 | 0.980 | 2.318 | 2 | 15.987 | 15.314 |
| 95/806 99%L | 15.850 | 0.011 | 15.277 | 0.014 | 34.601 | 0.038 | 0.967 | 0.940 | 0.757 | 2 | 15.575 | 15.243 |
| 95/806 95%L | 17.144 | 0.009 | 15.453 | 0.012 | 34.352 | 0.034 | 0.973 | 0.969 | | 2 | | |
| 95/806 R | 17.096 | 0.026 | 15.455 | 0.025 | 36.110 | 0.063 | 0.978 | 0.963 | 6.328 | 2 | 14.794 | 15.172 |
| 95/806 80%L | 19.634 | 0.125 | 15.846 | 0.149 | 35.025 | 0.230 | 0.679 | 0.974 | 3.215 | 2 | 18.464 | 15.702 |
| 95/806b WR | 17.241 | 0.011 | 15.479 | 0.013 | 36.031 | 0.038 | 0.972 | 0.942 | 4.138 | 2 | 15.736 | 15.294 |
| 95/806b 95%L | 16.155 | 0.015 | 15.329 | 0.017 | 34.638 | 0.044 | 0.965 | 0.936 | 1.613 | 2 | 15.568 | 15.257 |
| 95/806b 85%L | 16.967 | 0.035 | 15.437 | 0.034 | 35.512 | 0.080 | 0.976 | 0.969 | 1.457 | 2 | 16.437 | 15.372 |
| 95/806c 95%L | 16.303 | 0.050 | 15.359 | 0.049 | 34.960 | 0.113 | 0.988 | 0.981 | 1.959 | 2 | 15.590 | 15.271 |
| 95/806c 98%R | 16.660 | 0.016 | 15.414 | 0.017 | 35.800 | 0.046 | 0.967 | 0.935 | 3.45 | 2 | 15.405 | 15.260 |
| 95/806c 90%R | 16.506 | 0.015 | 15.389 | 0.016 | 35.295 | 0.043 | 0.974 | 0.935 | 3.815 | 2 | 15.118 | 15.218 |
| 95/806d WR | 16.406 | 0.038 | 15.351 | 0.037 | 34.709 | 0.087 | 0.982 | 0.969 | 2.389 | 2 | 15.537 | 15.244 |
| 95/806d R | 16.907 | 0.015 | 15.432 | 0.017 | 35.909 | 0.046 | 0.955 | 0.890 | 4.481 | 2 | 15.277 | 15.232 |
| 95/806d 92%L | 15.612 | 0.012 | 15.260 | 0.015 | 34.271 | 0.040 | 0.955 | 0.911 | 0.585 | 2 | 15.399 | 15.234 |
| 95/806d 70%L | 18.182 | 0.018 | 15.628 | 0.018 | 35.006 | 0.046 | 0.973 | 0.942 | 4.983 | 2 | 16.369 | 15.405 |
| 95/806e WR | 17.584 | 0.012 | 15.536 | 0.013 | 35.819 | 0.038 | 0.973 | 0.946 | 4.592 | 2 | 15.914 | 15.331 |
| 95/806e L | 15.913 | 0.009 | 15.292 | 0.012 | 34.955 | 0.036 | 0.978 | 0.956 | 1.361 | 2 | 15.418 | 15.231 |

Figure I-69: a) Sm-Nd Grts-WRs-Bt-Sil isochron indicating and age of 1990 ± 19 Ma. Legend: the same as in Figure I-66 plus circle with a point at the middle for minerals, b) Nd isotopic compositions of all migmatitic components and minerals at 2.0 Ga in function of 147Sm/144Nd, c) zoom in the Figure I-69b around whole rocks, d) Pb-Pb isochron diagram from all migmatitic components reflecting an incomplete Pb-Pb resetting. The Stacey-Kramers curve is also reported, e) Comparison between Pb and Nd isotopic compositions on paleosomes and leucosomes.

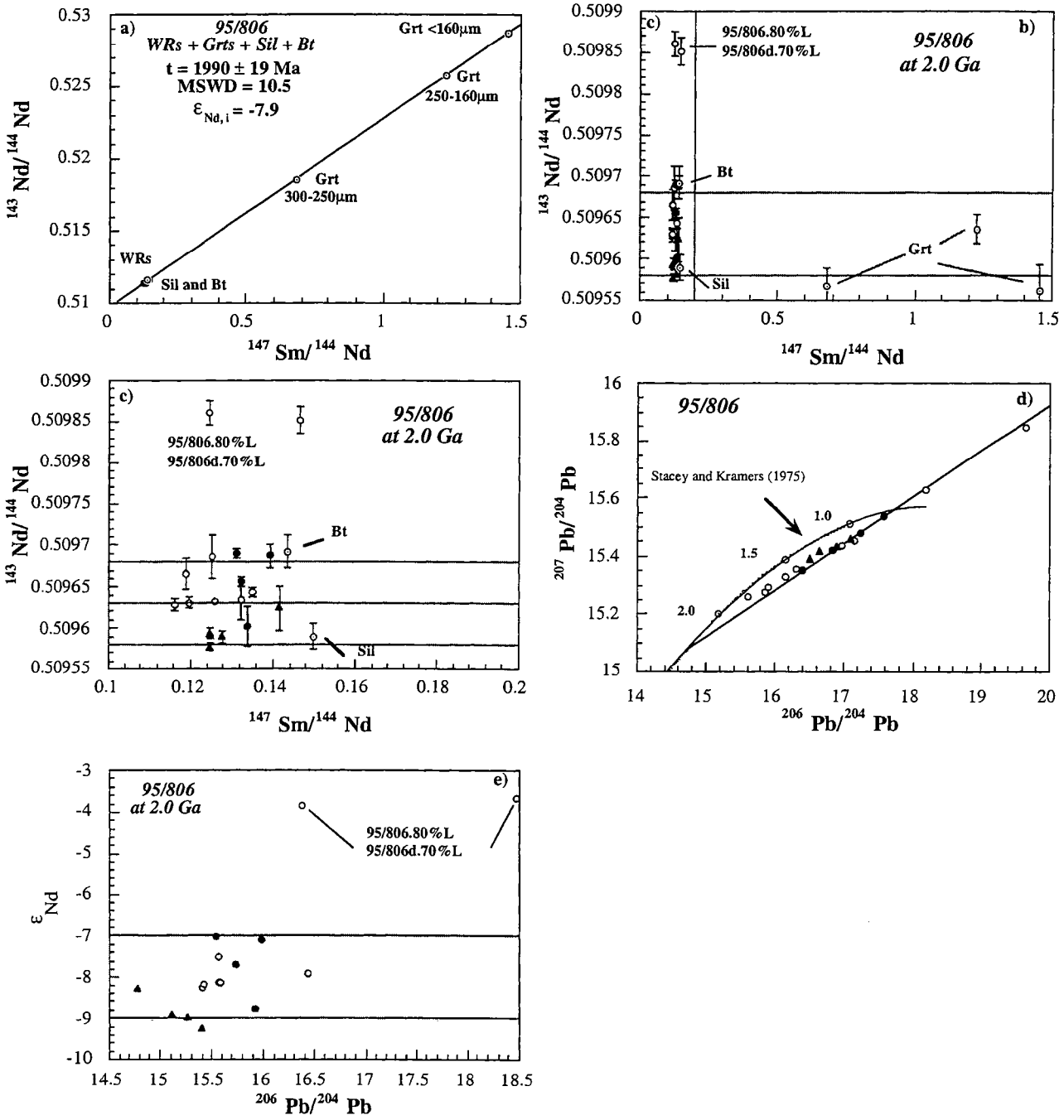

absent melting reaction and for the domination of main minerals over accessory minerals on the trace element distribution. We have carried out Sm-Nd analyses on the metapelitic migmatite. The 4 whole rocks, plus Bt, Sil and three fractions of different Grt sizes yielded an age of 1990 ± 19 Ma (9 points; MSWD = 10.5; Fig. I-69a). This age is in agreement with the previous geochronological data ranging from 2.02 to 2.0 Ga in the Mahalapye-Tshipise straightening zone (Holzer et al., in press; Schaller et al., in press; Chavagnac et al., submitted). Thus, we interpret it as dating Grt crystallization via Bt dehydration reaction. However, the initial epsilon Nd value of -7.9 documents a considerable pre 2.0 Ga crustal history in this area. In addition, the high MSWD value suggests that no full isotope homogeneization prior to Grt growth had been achieved.

The behaviour of the Sm-Nd system during migmatization can be unravelled by the use of the $^{147}Sm/^{144}Nd$ versus $^{143}Nd/^{144}Nd(2.0)$ diagram (Fig. I-69b, I-69c). The $^{143}Nd/^{144}Nd(2.0)$ of all minerals and migmatitic components with two exceptions, cluster within ± 1 $\varepsilon_{Nd}$. The two exceptions are leucosomes with much higher $^{143}Nd/^{144}Nd(2.0)$ which have $^{147}Sm/^{144}Nd$ ratios in the same range as the other migmatitic components (Fig. I-69b and I-69c). Further information on the extend of isotope exchange between the migmatitic components is given by the U-Pb isotopic compositions (Fig. I-69d). The Pb isotopic compositions picture that: (1) Pb-Pb systematics are not fully reset and reflect an errorchron of c. 2300 Ma, (2) they plot well below the Stacey-Kramers curve suggesting a significant pre 2.0 history, and (3) two leucosomes have markedly higher Pb isotopic compositions than the others. These are the same samples that also showed high $\varepsilon_{Nd}(2.0)$ values. The other migmatitic components are scattering between ± 1$\varepsilon_{Nd}$ and ± 1 $^{206}Pb/^{204}Pb$ unit (Fig. I-69e). The distinct Nd and Pb isotopic compositions of leucosomes 95/806.80%L and 95/806d.70%L could reflect the incomplete Nd and Pb isotope exchanges of either Grt or accessory minerals. The high $^{143}Nd/^{144}Nd(2.0)$ and $^{206}Pb/^{204}Pb(2.0)$ ratios of these two leucosomes are related neither to high Th concentrations (5-6 ppm) nor to high $^{208}Pb/^{204}Pb$ ratios. Consequently, Mnz as the agent of isotope perturbation can be rulled out. Grt and Zrn both have high Sm/Nd ratios and high HREE contents compared to other rock-forming minerals and they are also both characterized by U/Pb ratios. Thus, involvement of pre-existing Grt or Zrn could induce the perturbation of Nd and Pb isotope exchanges. The Y, Zr and HREE concentrations in these two partial melts do not favoured Grt over Zrn or Zrn over Grt. Furthermore, Zrn occurs only as inclusions in Bt which is one of the mineral precursor for Grt formation. Therefore, we cannot exclude the incorporation of small Zrn grains within Grt during its crystallization. The combination of Grt and Zrn can also be invoked for the distinct Nd and Pb isotopic compositions of 95/806.80%L and 95/806d.70%L. Furthermore, microprobe analysis highlighted two Grt generations suggesting that the older Grt might not have reached Nd and Pb isotopic equilibrium with the paleosomes during migmatization. Its entrainment or its occurrence in certain leucosomes and/or paleosomes could correspond to the higher $\varepsilon_{Nd}(2.0)$.

Figure I-70: Nd model ages map of the Limpopo Central Zone.

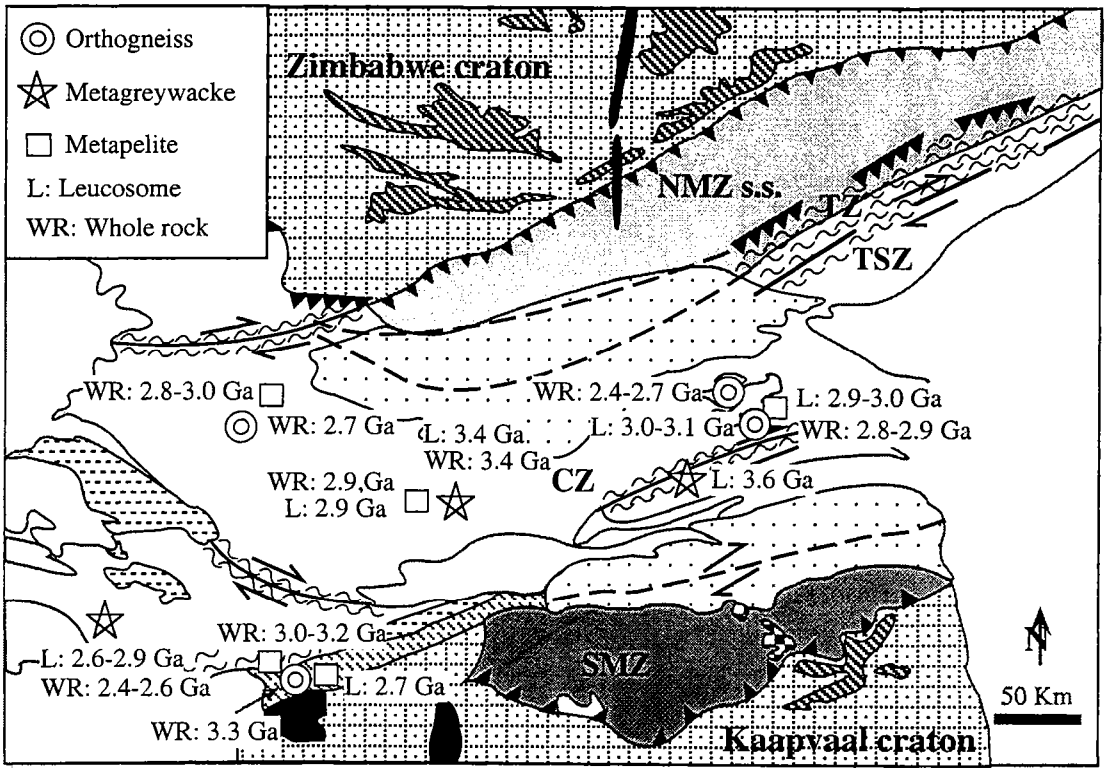

Nd model ages obtained on each migmatitic components range from 2.9 to 3.3 Ga. Older Nd model ages are not necessarely associated with higher proportion of paleosomes into leucosomes. Therefore, the Nd isotopic compositions of the whole rocks represent a good approximation of those of the original protolith. $T_{DM}$ suggests a 3.0-3.2 Ga old protolith and these ages may be used as markers of the crustal evolution of the Limpopo Central Zone. In addition, $T_{DM}$ ages obtained on the two distinct leucosomes are younger 2.6-2.8 Ga. If entrained Grt or Zrn is significant, they reflect a multistage history and thus and cannot be considered as good indicators for the crustal growth in southern Africa.

## 6.7. Nd model ages as crustal growth indicators

Detailed isotopic studies have been performed on migmatites which were formed either by partial melting or metamorphic segregation at subsolidus conditions on metapelite and metagreywacke, and orthogneiss respectively (this present study; Chavagnac et al., submitted; Chavagnac et al., submitted). Partial melting following Bt breakdown reaction in high temperature and low pressure rocks did lead to different behaviour of Sm-Nd systematics for metagreywacke and metapelite. In the first case, chemical equilibrium and full Nd isotope exchange were not reached due to the effect of accessory minerals on the compositions of the partial melt (Chavagnac et al., submitted). As a consequence, the Nd model ages on partial melt are up to 400 Ma older than those on paleosomes and the Nd model ages of these rocks cannot be used to constrain the evolution of the Central Zone continental crust (Chavagnac et al., submitted). In contrast, this present study suggest that partial melts formed by the same metamorphic reaction on metapelite exhibit chemical equilibrium with paleosomes and nearly full Nd isotope exchange was reached, but Pb-Pb systematics was not fully reset. The question is also how much Nd isotope variability was achieved in the metapelite before migmatization. Consequently, the Sm-Nd isotope signatures of whole rocks may be used as indicators of crustal growth in the Limpopo Central Zone. Finally, in migmatites formed by metamorphic segregation at subsolidus consitions, chemical equilibrium and Nd isotope exchange were not reached during migmatization. Nonetheless, geochemical characteristics and REE modelling provided arguments for closed system behaviour of the whole rock during migmatization. Therefore, the Sm-Nd isotopic features of the protolith could be determined via mass balance calculations and they can be used as marker of the crustal evolution.

The Pb-Pb isotopic compositions of various lithologies which composed the Limpopo Belt confirmed the occurrence of three entities as suggested previously from structural works (Kreissig and Holzer, 1997). Both Marginal Zones present similar Pb-Pb isotopic features of their adjacent cratons (Berger et al., 1995; Kreissig and Holzer, 1997), whereas the Central Zone is isotopically distinct from its northern and southern edges. The field observations and structural studies associated with geochonological works reveal three high-

grade metamorphic events associated with deformation, migmatization and magmatism in the Central Zone: (1) 3.2-2.9 Ga, (2) ~2.6 Ga, and (3) 2.0 Ga (Holzer et al., 1998; Holzer, 1998). The behaviour of the Sm-Nd system during migmatization is shown to be variable and the detailed isotopic studies performed on migmatites provide a framework for the evaluation of Sm-Nd systematics on the high-grade metamorphic rocks of the Limpopo Central Zone. In Fig. I-70 and Table I-20 are reported Nd model ages obtained on migmatites of various protoliths as well as other lithologies done by Harris et al. (1987), Chavagnac et al. (submitted), and Chavagnac et al. (submitted). The Archean high-grade metamorphic event is represented essentially by magmatic activity which produced large amount of TTG suite in the whole Central Zone such as the Sand River Gneiss in the Messina area ($T_{DM}$ = 3.1 to 3.0 Ga). Granitic melt in the Sand River Gneiss are also characterized by $T_{DM}$ of 2.9-3.0 Ga. The erosion of the basement produced cratonic shale which may be traced in the eastern part of the Central Zone such as the Beitbridge Gneisses ($T_{DM}$ ~2.9 Ga) as well as in the western part within the Phikwe Complex ($T_{DM}$ = 2.8-3.0 Ga). The Late Archean event (~2.6 Ga) took place under low pressure granulite metamorphic condition associated with deformation in the whole Central Zone and with mantle-derived magmatism. Structural, petrographic and geochronological studies suggested several pulses of thermal disturbance associated with magmatism and tectono-metamorphism characterized by an anti-clockwise P-T path (Holzer et al., 1998; Holzer, 1998). The magmatic activity led to charnockitic-granitic intrusions such as the Bulai in the Messina area (Barton et al., 1994), or to formation of quartz and potassium poor diorite in the Phikwe Complex (Chavagnac et al., submitted). Igneous intrusions occurred at the same time in the Southern Marginal Zone by the Matok Granite intrusion and its associated charnockites (Barton and van Reenen, 1992) and in the Northern Marginal Zone expressed by charno-enderbite and porphyric granite intrusions (Berger et al., 1995; Mkweli et al., 1995). The last high-grade tectono-metamorphic event in the Central Zone was dated at about 2.0 Ga (Barton et al., 1994; Kamber et al., 1995; Holzer et al., 1998; Chavagnac et al., submitted). It is characterized by a clockwise P-T path during which voluminous migmatitic complexes have been produced. The Sm-Nd systematics on migmatitic metagreywacke were demonstrated to be not fully equilibrated during anatexis leading to meaningless Nd model ages such as obtained in Tshipise, Alldays and Mahalapye migmatites (Fig. I-70). A totally different statement have been obtained on metapelite arguing for nearly full Nd isotope homogeneization and consequently the Nd model ages constitute reliable contraints on the crustal evolution of the Central Zone (Fig. I-70). It arises that granitic melts are essentially formed via fluid-absent melting reaction corresponding to crustal anatexis on older lithologies ($T_{DM}$ = 2.8-3.2 Ga). Nonetheless, igneous intrusions such as the Bushweld Complex or the Palala Granite intruded older basement in the soutwestern part of the Central Zone at about 2.0 Ga (Schaller et al., 1997; Schönberg et al., 1998). The 2.0 Ga metamorphic event may be related to a crustal thickening event due to the transpressional orogeny between the Central Zone and the amalgamated NMZ-Zimbabwe craton and SMZ-Kaapvaal craton. Holzer et al. (in press)

concluded that the PSZ and the TSZ represented two major transcurrent lineaments between the Central Zone and the respective adjacent cratons along which the exhumation strain was localized after the 2.0 Ga tectono-metamorphic event.

## 6.8. Conclusions

A detailed trace element and Nd and Pb isotopic study has been performed on a migmatitic metapelite to decipher whether chemical equilibrium and full Nd and Pb isotope exchanges were achieved during migmatization. Three main conclusions are shown:

(1) Garnet-bearing granitic melts were formed by fluid-absent melting reaction by Bt breakdown reaction. The leucosomes are significantly enriched in LIL elements compared to paleosomes but their low Rb/Sr ratios suggested melt escape from the site of partial melting. However, the distribution of Rb, Sr, Ba, K, Na and Ca elements between leucosomes and paleosomes are related to the influence of the incongruent Bt, Pl and K-fs melting on the leucosome chemical compositions. The large variations in the REE and HFSE concentrations of partial melts reflect the control of Grt on the HREE and of feldspars on the LREE. The accessory minerals such as Mnz or Ap might have contributed to the LREE budget of leucosomes without perturbing the effect of main minerals.

(2) Nd and Pb isotopic compositions on all migmatitic components indicate that nearly full Nd isotope exchange was reached at 2.0 Ga the age of high-grade metamorphic event whereas Pb-Pb systematics were not fully reset. However, two leucosomes present higher Nd and Pb isotopic compositions at 2.0 Ga that we interpreted as the consequence of incomplete homogeneization of Zrn or an older Grt. As nearly full Nd homogenization occurred at 2.0 Ga, the Nd model ages obtained on whole rocks are a good approximation of the magma source, 3.2-3.0 Ga.

(3) Early to late Archean magmatic activity in the Central Zone of the Limpopo Belt led to the formation of granitic to charno-enderbite intrusion from a mantle-derived source. Some crustal reworking took place as well but as a minor process for melt formation. In contrast, large migmatitic complexes in the whole Central Zone were formed during the 2.0 Ga transpressional orogeny between the Central Zone and the adjacent cratons. Garnet-bearing granitic melt represent the product of fluid-absent melting reaction on fertile lithologies suggesting an important tectonic reworking at about 2.0 Ga.

**Acknowledgments**

This work was supported by the Swiss National Foundation (Grant 20-47157.96 to JDK). We thank ACTLABS for the INAA analysis. We acknowledge support for the electron microprobe of the University of Bern by Swiss National Foundation (Grant 21-26579.89).

# 7. Conclusions

The behaviour of the Sm-Nd system during migmatization has been investigated in three examples of migmatites which belong to the high-grade Limpopo Central Zone in order to evaluate the significance of the Nd model ages in terms of crustal growth.

Partial melting following fluid-absent melting reactions during the high-grade metamorphic event at 2.0 Ga in this zone led to different behaviour of the Sm-Nd systematics on metagreywacke (the Mahalapye Complex) and on metapelite (The Mahalapye-Tshipise Straightening Zone).

In the first case, garnet-bearing granitic and peraluminous leucosomes were formed by biotite dehydration reactions. The leucosomes are characterized by higher K/Ba, K/Rb and Na/Sr ratios compared to paleosome without lowered Rb, Ba or Sr contents. These geochemical features exhibit the incongruent melting of feldspars and biotite during migmatization. The LILE data indicate also that the nascent melt did not equilibrate extensively with the residual biotite and feldspars in the paleosome. In addition, the high LREE and Th contents picture the dominant effect of monazite on the geochemical characteristics of the partial melt. It appears that monazite entered the melt in preference to apatite either by dissolution or entrainment and its unradiogenic Nd isotopic signature dominates those of leucosomes. Significant differences in $^{143}Nd/^{144}Nd$ ratios existed at 2.0 Ga between paleosomes and leucosomes, corresponding to $^{147}Sm/^{144}Nd$ ratios clustering in the same range. Therefore, the Nd data of the leucosomes and paleosomes show lack of Nd isotope equilibration upon separation, and a systematic offset, as a consequence of the unradiogenic monazite Nd. The Nd model ages obtained on leucosomes (2.7-2.9 Ga) are up to 400 Ma older than those on paleosomes (2.4-2.5 Ga). Rather than defining the protolith crustal age as a weighted average of the $T_{DM}$ ages derived from a migmatite outcrop, the true spread in mantle derivation ages for the sediment source region probably exceed the range of $T_{DM}$ found in the outcrop. These Nd model ages cannot be considered as good indicators for the crustal evolution in southern Africa.

In the case of anatexis on metapelite, the mineralogic association of biotite, sillimanite, plagioclase and quartz as small inclusions within garnet represent the precursor of garnet formation. In addition, the occurrence of fibrolite sillimanite in association with alkali feldspar suggested that muscovite breakdown may have occurred at the early stage of partial melting. The two distinct chemical compositions of garnet may represent changing conditions during the transition between muscovite and biotite fluid-absent melting reactions. The effect of incongruent melting of feldspars during migmatization is also highlighted by the chemical

compositions of partial melts. Leucosomes present the same LILE features as those produced by biotite dehydration reaction in metagreywacke. Furthermore, the REE distribution between paleosome and leucosome shows that the HREE are dominated by the behaviour of garnet and zircon whereas the LREE are controlled by the feldpars. It appears that the LREE-bearing minerals such as monazite or apatite may have contributed to the LREE budget of the leucosomes without masking the domination of feldspars. The $^{143}Nd/^{144}Nd$ ratios at 2.0 Ga of all migmatitic components with two exceptions cluster within ± 1 $\varepsilon_{Nd}$ indicating that they have nearly the same isotopic composition at that age. The two exceptions are two garnet-bearing leucosomes with much higher $^{143}Nd/^{144}Nd(2.0)$ corresponding to $^{147}Sm/^{144}Nd$ ratios in the same range as the other migmatitic components. The Pb-Pb systematics show incomplete Pb isotope exchange at 2.0 Ga. The two leucosomes that showed high $\varepsilon_{Nd}(2.0)$ values, also present higher $^{207}Pb/^{204}Pb$ and $^{206}Pb/^{204}Pb$ isotopic compositions. These Nd and Pb isotopic features of the two leucosomes may be explained by the involvment of pre-existing garnet or zircon as both have high Sm/Nd ratios and HREE contents compared to other rock-forming minerals as well as high U/Pb ratios. Considering that nearly full Nd isotope exchange was reached during migmatization, Nd model ages on the whole rocks represent a good approximation of those of the original protolith (3.0-3.2 Ga).

The last example is a migmatitic orthogneiss in the Phikwe Complex. Petrographic criteria combined with REE modeling performed on two slices presenting all migmatitic components indicate that the REE patterns of leucosome can only be match by metamorphic segragation process at subsolidus conditions. The distribution of major and trace elements correspond to the mixing between variable mineral weight proportions in the layers. The mixing between minerals is also highlighted in the Nd isotope features of each migmatitic components. The $\varepsilon_{Nd}(2.0)$ values are highly variable emphazing the lack of Nd isotope exchange at 2.0 between each layers. Nonetheless, the geochemical features, REE modeling and Pb-Pb WR isochron at 2.0 Ga suggest that the system remained closed at the whole rock scale during migmatization, i.e. mass conservation may be assumed to be maintained. Consequently, the geochemical and Nd isotopic features of the protolith prior to migmatization is obtained via mass balance calculations. A quartz and potassium poor diorite as protolith is suggested. A Sm-Nd isochron using calculated protolith compositions indicates an age of 2.7 Ga, close to the 2.73-2.75 Ga Nd model ages obtained by these calculations. Then while $T_{DM}$ of individual migmatitic components cannot be used to constrain crustal evolution, the calculated protolith Nd model ages can be used as marker of crustal growth in the Phikwe Complex.

From these additional published data, it can be summarized that the crustal evolution of the Limpopo Central Zone took place in three main periods in line with the structural, geochronological and petrographic studies. The period between 3.2 and 2.9 Ga is

mainly characterized by a magmatic activity which led to the formation of early tonalitic crust examplified by the Sand River Gneiss. The Late Archean ~2.6 Ga event was a low-pressure and high temperature metamorphic event associated with a main deformation phase affecting the entire Central Zone of the Limpopo Belt and with a magmatitic activity (e.g. the Bulai Intrusion). The Early Proterozoic event took place under high-grade metamorphic conditions during which partial melting on "fertile" lithologies formed migmatites and locally produced large amounts of garnet-bearing granitic melt. The 2.0 Ga metamorphic event may be related to crustal thickening due to the transpressional orogeny between the Central Zone and the amalgamation of the Southern and Northern Marginal Zone with their adjacent cratons.

# *Part II: The Ultra-High Pressure Metamorphic Terrane*

# 1. Introduction

Metamorphism is the process by which a rock changes its mineral contents towards a new state of chemical equilibrium in the course of changing environmental condition which it is being subjected to within the Earth (Schreyer, 1995). Eskola (1921) defined specific mineral facies, now called metamorphic facies to be characteristics for various combinations of pressure and temperature which both increase with depth. Depending on whether the tectonic movement of a rock is downward or upward, its metamorphism is prograde or retrograde.

Among metamorphic rocks recognized in orogenic belts, geologists focus principally on eclogites as they represent the deepest ones. Eclogites are mainly related to a basaltic composition and so forth they may provide information on the depth at which the oceanic crust was eclogitized. However, the discovery of metamorphic coesite in metapelites either in the Western Alps (Chopin, 1984) or in the Caledonides (Smith, 1984) highlights that not only basaltic rocks but also metasedimentary rocks may be buried at mantle depth, i.e. at depth greater than the normal continental crust. Therefore, the ultradeep metamorphism carries important geodynamic implications on subduction zones (Schreyer, 1995).

According to Miyashino (1961), eclogites are referred to high pressure metamorphism, characterized by geothermal gradient about 10°C/km. Due to the discovery of coesite which implies a geothermal gradient lower than 10°C/km, the term "UltraHigh Pressure Metamorphism" (UHPM) has been defined in terms of high pressure metamorphism in which coesite could be formed, i.e. metamorphism conditions in the stability field of coesite ($P > 27$ kbar). As a consequence, the metamorphic classification of eclogites is largely based now on the studies of Carswell (1990) who tried to separate eclogite facies rock into high-temperatue, medium-temperature and low-temperature, and also of Chopin et al. (1991) who tried to divide eclogite facies rock into "hot eclogite" (in the coesite stability field) and "cold eclogite" ($P < 27$ kbar). Figure II-1 represents the updated P-T petrogenetic grid of ultrahigh pressure metamorphism.

On the basis of this P-T grid of the UHPM rocks, Liou et al. (1995) report the recognized UHPM terranes as well as those suppected (Fig. II-2) in a world map. The investigated UHPM terrane for this Ph.D. is the Dabie, Su-Lu terrane located in Eastern Central China.

In the Dabie, Su-Lu UHPM terrane, coesite and its quartz pseudomorph were largely identified as phases produced during the UHPM event. They occur in protoliths of

Figure II-1: P-T petrogenetic grid of Ultrahigh Pressure Metamorphism after Liou et al. (1995).

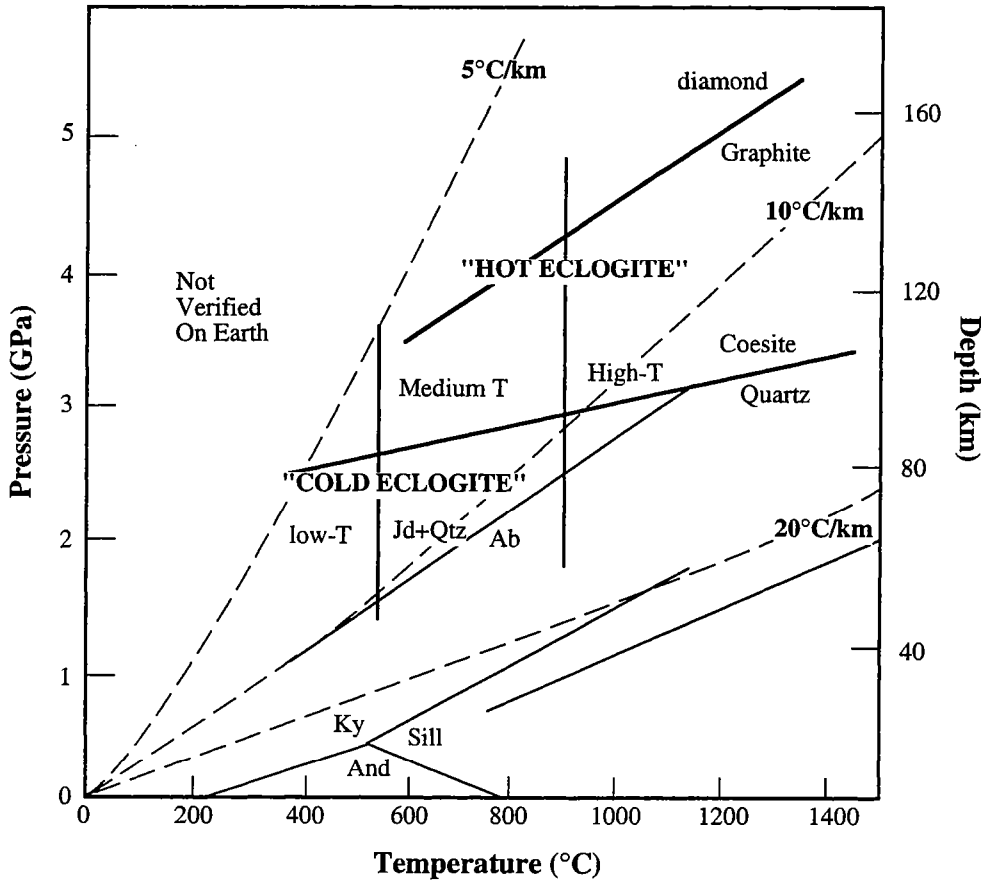


Figure II-2: Distribution of recognized UHP terranes in the world. Those with occurrences of index minerals such as coesite ± diamond are indicated as definite UHP terranes whereas those suggested by thermochemical are listed as suspected terranes (Liou et al., 1995).

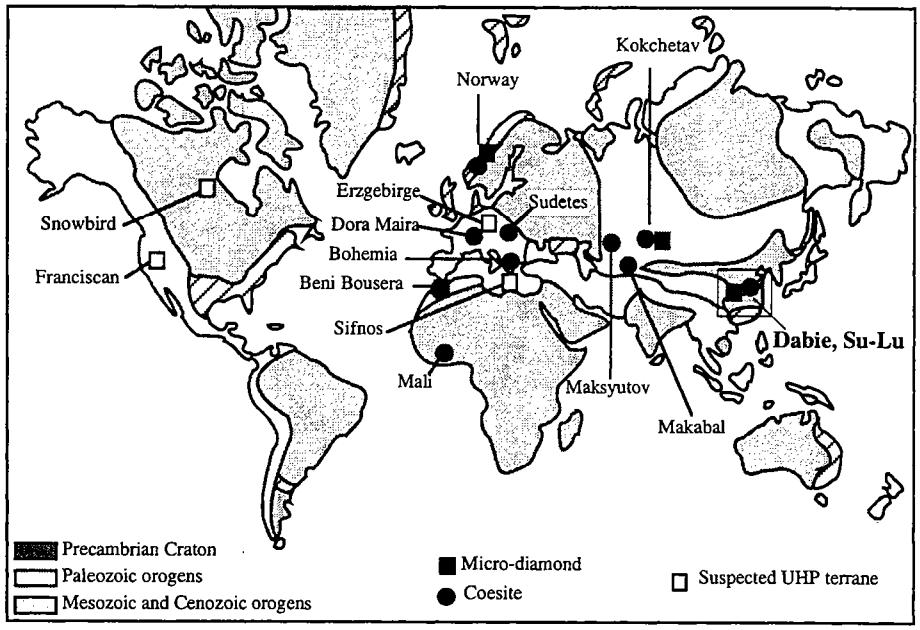

basaltic composition, for example the Bixiling Complex (Zhang and Liou, 1995), but also in protoliths of undoubted crustal origin, for example the UHPM slab of Shuanghe (Cong et al., 1995). These coesites are located as inclusions in garnet, omphacite but also in epidote and kyanite (Zhang, 1992; Zhang et al., 1993). Finally, Xu et al. (1992) discovered micro-diamond in eclogites from the Dabie Mountains.

As a consequence of coesite and micro-diamond in crustal rocks, subduction at mantle depth may be also applied to continental material, with important implications for the plate tectonic processes at convergent margins. These implications are of several order: 1) the spatial relationships between eclogites and their country rocks during the UHPM event, "In situ" or "Foreign"?, 2) the P-T conditions during exhumation allowing the preservation fo UHPM minerals (i.e. coesite and micro-diamond), 3) the problem of mechanism and rate by which deep-seated rocks returned to the surface, 4) the role, nature and source of fluids during the formation of the UHPM rocks. These few points represent only a restricted list of geological problems that geologists have to resolve in such terranes.

The aims of this Ph.D is certainly not to provide information on each problems but merely to yield arguments on the coalescence or no-coalescence of eclogites and their country rocks during the UHPM event. To do so, I focus on two famous outcrops in the Dabie Mountains: The Bixiling Complex and the UHPM slab of Shuanghe. The aims are fourfolds: 1) the geochemical characterization of the country rocks which surround eclogites, 2) the dating of eclogite and the country rocks, 3) the estimation of cooling and exhumation rates in both localities, and finally 4) the examination of Sm-Nd and also Rb-Sr dating on metamorphic rocks which underwent UHPM event.

# 2. Geological setting

## 2.1. Introduction

The Qinling-Dabie-SuLu orogenic belt is located in Eastern Central China, and it is recognized as one of the biggest UHPM terrane in the World (Fig. II-2). It is considered as the suture zone between the Yangtze Craton to the South and the Sino-Korean Craton to the North after the continent-continent collision. The 2 000 km long orogenic belt is composed of a principal E-W trending zone and of a N-S trending zone - Su-Lu region - which has been displaced approximately 500 km northward by the NE trending left-lateral Tan-Lu Fault (Okay and Sengör, 1992; Yin and Nie, 1993) (Fig. II-3). Ernst et al. (1995) documented the Eastern extension of the UHP-HP Su-Lu region across the Yellow Sea in Central Korea.

Figure II-3: The Qinling-Dabie-SuLu orogenic belt located in Eastern Central China..

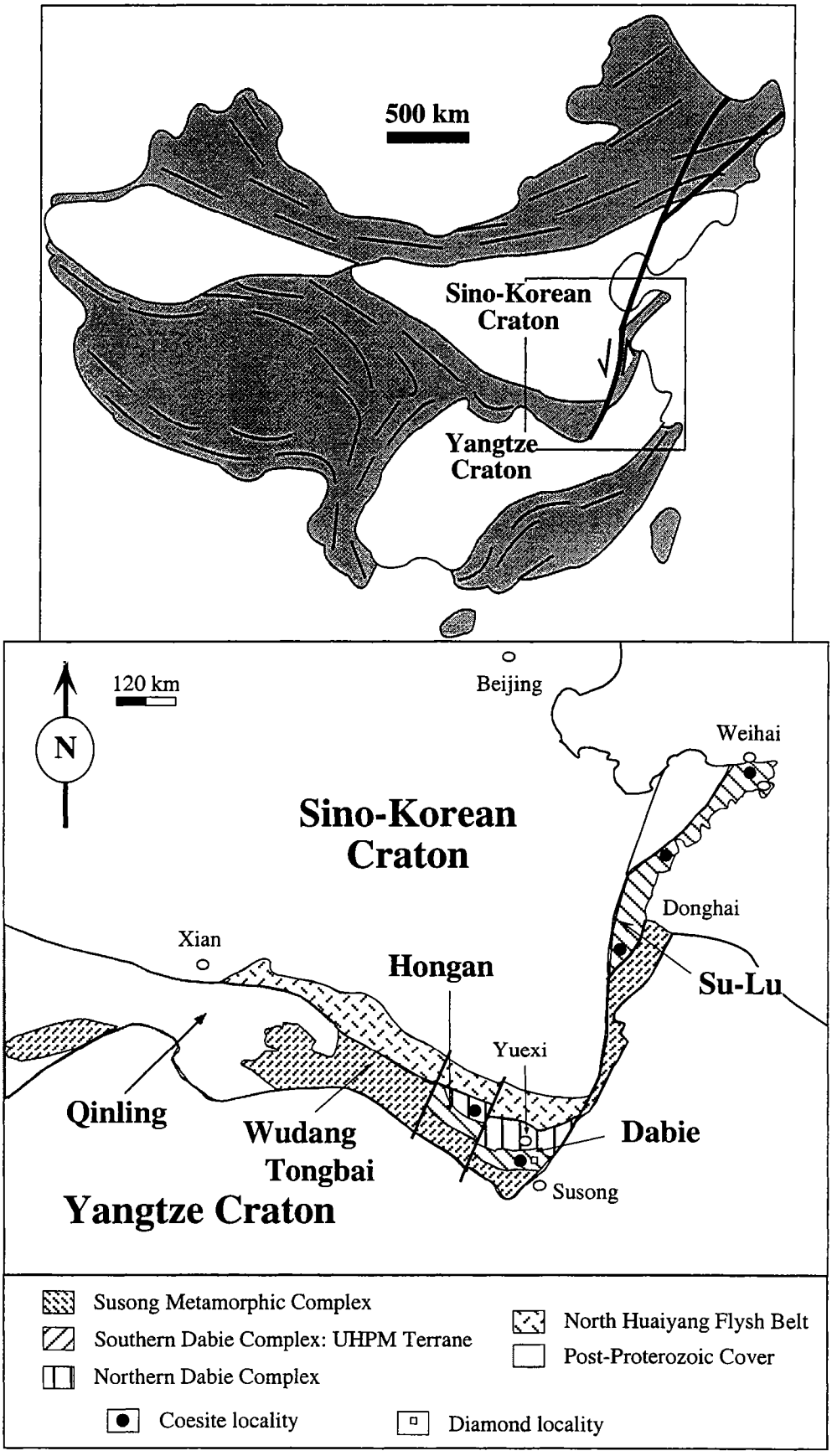

Coesite and coesite pseudomorphs are widespread as minor fine-grained inclusions in garnet, omphacite, kyanite and epidote from eclogites (Wang et al., 1989; Okay 1993a; Yang et Smith, 1989; Wang et al., 1992; Zhang et al., 1993), marbles (Wang and Liou, 1991, 1993; Xu et al., 1992) and gneiss (Wang and Liou, 1991; Enami and Zhang, 1990; Hirajima et al., 1990; Zhang et al., 1995). Xu et al. (1992) described the occurence of microdiamond within garnet of eclogite, in the Dabie Mountains. These UHPM relics are coarser than those described in the Kokchetav Massif, with a grain size ranging from 150 to 700 μm.

The subparallel nearly E-W striking set of faults divides the Qinling-Dabie belt into several subunits which are from north to south: (1) the Sino-Korean Craton; (2) the paleozoic accretionary complex (Zhang, 1985; Liu et Hao, 1989; You et al., 1993); (3) the Qinling-Dabie metamorphic complex sensu-stricto; and (4) the Yangtze Craton. The second set of faults are NE-SW, subvertical, subparallel to the Tan-Lu fault. It divides the E-W trending orogenic belt into sevreal subunits which are from W to E: 1) the Qinling region; 2) the Wudang-Tongbai region; 3) the Hongan region; 4) the Dabie Mountains, and finally 5) the Su-Lu province as shown in broad outline in Figure II-3.

Abundant eclogites occur as small lenses or blocks less than 20 m in size within serpentinized ultramafics, or as thin layers in gneisses or marbles in the Dabie and Su-Lu regions. From the field relationships, three distinct types of eclogite can be distinguished: (1) in ultramafics, eclogites are exposed as thin lenticular lenses or small pods within garnet-bearing peridotite which, in turn, are enclosed in amphibole and biotite gneisses; (2) the eclogites are interlayered with hornblende and biotite gneiss and marbles; sometimes they occur as boudinaged blocks of various size; and (3) the last occurrence of eclogite is as layers within gneiss.

The investigated area is within the Dabie Mountains and therefore, I will described briefly the Sino-Korean and Yangtze Cratons and the SuLu region.

## 2.2. The Sino-Korean Craton

The Sino-Korean Craton bound the Qinling-Dabie-SuLu orogenic belt to the north. It consists of an early Archean to Proterozoic crystalline basement (3.8 Ga by Liu et al., 1992, some areas 2.5-2.8 Ga Kröner et al., 1988) overlain by a thick sedimentary cover (4-8 km thick) dated from Proterozoic to early Cambrian (Hsü et al., 1987, R.G.S. Henan, 1989). The sediments are mainly composed of shallow marine sequence, carbonate rocks or coal-bearing strata. Closed to the orogenic belt, the rocks are metamorphosed and deformed into a north vergent fold thrust belt (R.G.S. Henan, 1989).

## 2.3. The Yangtze Craton

The Yangtze Craton forms the southern boundary of the Qinling-Dabie-SuLu orogen. It has a Proterozoic crystalline basement overlain by dominantly sedimentary Sinian to Mesozoic strata (12 km thick). The oldest unmetamorphosed sedimentary cover has been dated at 0.9 Ga by Liu et al. (1989). From late Proterozoic to Trias, the shallow marine sequence is nearly continuous.

## 2.4. The SuLu region

The Su-Lu region belongs to the Qinling Dabie orogenic belt but it has been offset about 500 km northward from Dabie Mountains by a sinistral strike slip Tan-Lu Fault (Xu et al., 1987; see fig. II-3). The Dabie Mountains and the Su-Lu region have similar geologic and lithologic units and metamorphic histories. The Su-Lu area is underlained mainly by gneisses and amphibolites of amphibole and granulite facies (Jiaonan-Jiaodong and Haizhou Groups) and schist of greenschist and glaucophane schist facies (Yuntai Group) (Enami et al., 1993). Biotite gneiss and granitic gneiss are most common and they were never equilibrated above medium pressure amphibolite facies metamorphism (Enami et al., 1993). Eclogites are abundant within biotite gneiss and granulite and they occur mostly as isolated lenses or blocks in country rocks gneisses, partly serpentinized garnet peridotite and marble (Enami et al., 1986; Enami et al., 1993; Ishiwatari et al., 1990b). The coesite-bearing rocks are gneiss with marble, ultramafic, eclogite. Hirajima et al. (1990) described the occurence of coesite at Donghai and at Rongchen, Zhucheng, Junan and Lanshantou, quartz pseudomorphs have been described by Yang and Smith (1989) and Enami and Zhang (1990).

## 2.5. The Dabie Mountains

The Dabie Mountains represents the Eastern part of the Qinling-Dabie orogenic belt. It is sandwiched between the Sino-Korean Craton and the Yangtze Craton. It has a triangular shape bounded to the north as well as the south by major E-W striking steeply north-dipping fault (Liou et al., 1995). From north to south, the Dabie metamorphic complex shows a decreasing metamorphic grade from migmatite to greenschist facies metamorphism. The Dabie Mountains sensu stricto can be divided into four metamorphic belts which are from north to south (see Fig. II-4a, b): (1) North Huaiyang Flysch belt, (2) the Northern Dabie Complex belt, (3) the Southern Dabie Complex belt and (4) the Susong Metamorphic Complex belt.

Figure I-4a: Geological map of the Dabie Mountains.

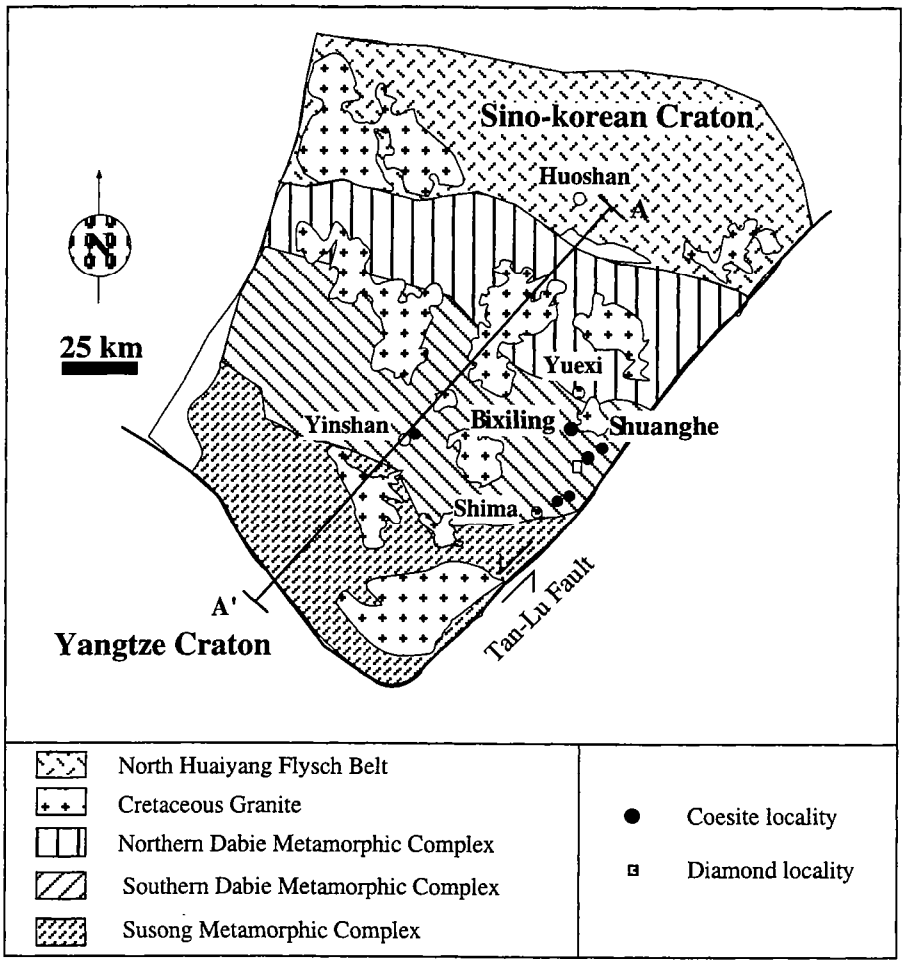


Figure I-4b: Metamorphic cross section through the Dabie Mountains (Modified after Zhang et al., 1996). NHF: North Huaiyang Flysch Belt, NDC: Northern Dabie Complex, SDC: Southern Dabie Complex, SMC: Susong Metamorphic Complex. Cold-e: Cold- clogite, Hot-e: Hot eclogite.

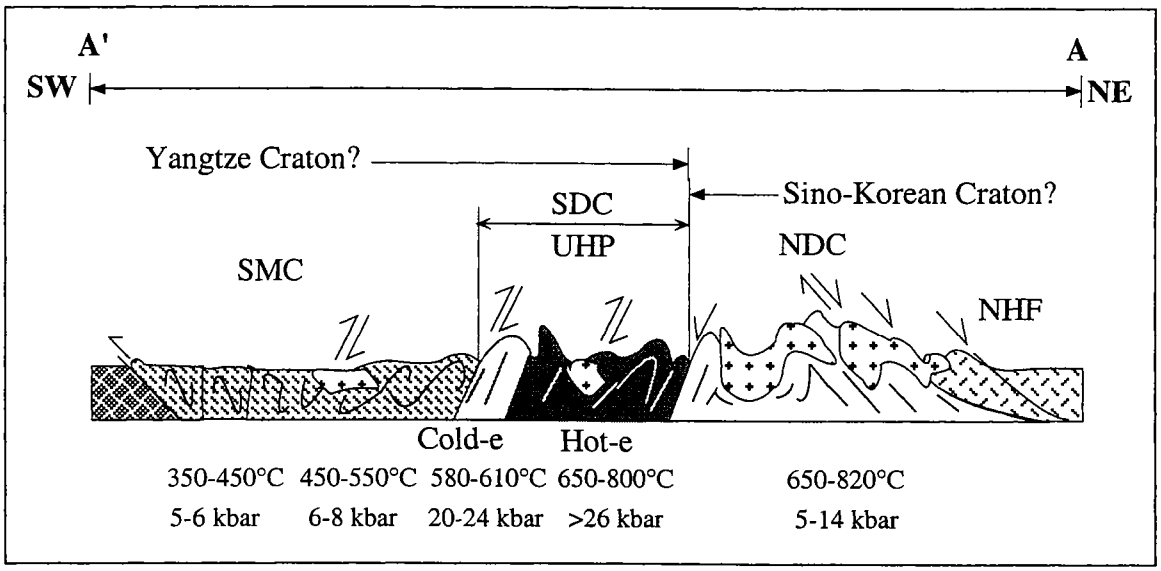

### 2.5.1. The North Huaiyang Flysch belt (NHF)

The NHF is the northernmost part of the Dabie Mountains (Fig. II-5). and it is seperated from the Northern Dabie Complex by a WNW-ESE trending, steeply dipping, major strike slip fault, called Xiaotian-Mozitan Fault (Mattauer et al., 1985). It can be traced as a 13 km wide zone from the North of Dabie Shan westward for over 400 km to Tonghai-Shan (Okay et al., 1993).

The NHF or "the Foziling Group" is subdivided into the Xiaoxihe formation, the Xianrenchong formation, the Xiangyunzhai formation, the Panjialing formation and Zhufo'an formation (Anhui Geological Survey, 1974, unpublished data). The NHF constitutes a very thick, monotonous, fine-grained to very fine-grained thin to medium bedded metapelites with intercalations of orthoquartzites and marbles. The metapelites present an interlayered bedding of medium to fine-grained, mafic minerals and quartz-plagioclase layers. Mafic minerals are mainly represented by biotite and muscovite ± chlorite. Marbles show a coarse-grained matrix mainly composed of calcite but we cannot call them "pure marble" because of the occurrence, in a centimeter scale, of mafic minerals such as biotite and/or chlorite. Small deformed boudins of amphibolites (about 1 m long and 0,5 m wide) are enclosed in marbles. The quartzites have a very fine-grained texture and they are mainly composed of quartz and muscovite ± chlorite. The age of this formation is not well constrained with a variation from Devonian (Mattauer et al., 1985; Xu et al., 1992; Kröner et al., 1993) to Triassic (Hsü et al., 1987) but the total range may represent the total age of the NHF.

These rocks have been metamorphosed in greenschist facies with the typical mineral assemblage of quartz + plagioclase + muscovite + biotite + ilmenite ± chlorite ± epidote. Only at Luzenguan, this formation shows the typical paragenese of amphibolite facies metamorphism.

All these lithologies have a well developed foliation with a general direction N120-130° 30°NE and an E-W stretching lineation defined by elongated quartz, calcite or chloritein quartzite, marble and metapelite respectively. In addition, they suffered ductile deformation after the foliation formation as expressed by isoclinal folds with fold axes parallel to the stretching lineation. Along the Foziling reservoir area, the foliated metapelites have been deformed by northward kink folds and eastward boudinage.

The NHF is cutted by mesozoic andesite, lamprophyre dykes and microdioritic intrusions and they are unconformably overlain by the jurassic volcano-clastic rocks and red sandstones.

Figure II-5: Location of the NHF in the Dabie Mountains. P-T metamorphic conditions are indicated.

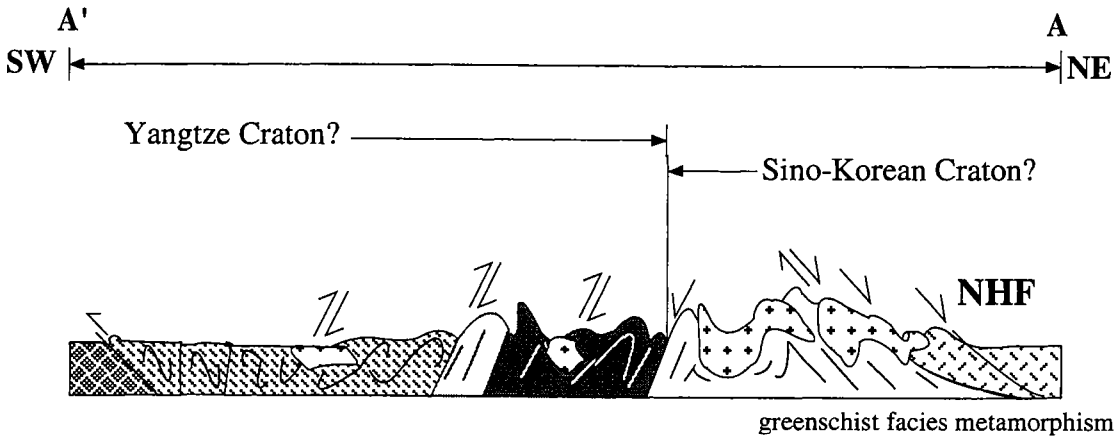

The signification of the very thick sedimentary NW-SE trending zone is still controversial and several interpretations have been proposed: 1) molassic foredeep (Mattauer et al., 1985); 2) accretionary wedge (Hsü et al., 1987) or flysch sequence (Xu et al., 1994); 3) forearc setting (Xu et al., 1992); 4) a thick clastic wedge deposited at the northern passive continental margin of the Yangtze plate (Okay et al., 1993).

### 2.5.2. The Northern Dabie Complex (NDC)

The Northern Dabie Complex (NDC) is separated from the adjacent units by ductile shear zone called Xiaotian-Mozitan Fault (XMF) to the north and Wuhe-Shuihou Fault (WSF) to the south (Fig. II-6; Liou et al., 1995; Hacker and Wang, 1995; Wang et al., 1995). The contact at the north is represented by "overhotted" gneisses which present a fine grained texture and a cataclastic deformation. Within a few meters, the metapelites corresponding to the NHF and the migmatites belonging to the NDC, have totally different foliation and stretching lineation. The NDC is composed of four different lithologies: (1) gneiss, augen-gneiss, migmatite and minor amphibolite, (2) metasedimentary horizons such as calc-silicates and marbles, (3) lenses of mafic-ultramafic rock and mafic-ultramafic intrusive bodies, and (4) granitic bodies.

The orthogneiss lithology constitutes about 60 vol% of the NDC. It is banded, strongly foliated, medium grained frequently porphyroblastic (e.g. alkali feldspar augen). The mineral assemblage of quartz + plagioclase + alkali feldspar + hornblende + biotite + opaques ± chlorite corresponds to a pale gray trondhjemite-granodiorite suite. In several localities, these orthogneisses show clearly a migmatitic structure with sharp alternance of thin layers of mafic minerals (biotite and hornblende) and thick coarse-grained layers of leucosome with typical assemblage quartz + plagioclase + alkali-feldspar ± biotite. But, banded gneisses of pale and dark bands with varying proportions of felsic and mafic minerals are also common. Migmatites are strongly foliated (N140° 18°E to N150° 30°E) defined by irregular thickness of mafic layers and alkali-felspar augen leucocratic layers, and a westward to southward dipping stretching lineation. In addition, they suffered fluidal folding and later a hot water fracturation (i.e. brechia). In some localities (for example at Manshuishe), amphibolite boudins of decimeter to meter in size, occur as enclaves within migmatites. These enclaves have a medium to coarse-grained mineral assemblage composed of hornblende + plagioclase ± clinopyroxene + ilmenite/titanite ± biotite ± alkali feldspar ± quartz. The foliation goes round these boudins suggesting the amphibolite formation before partial melting. Migmatites as well as amphibolite boudins present the same NW-SE stretching lineation either defined by elongated alkali-feldspar or by plagioclase. From the metamorphic point of view, the orthogneisses are characterized by amphibolite facies assemblage. However, Zhang et al. (1996) described only a few case of relics of granulite facies assemblages such as garnet and

Figure II-6: Location of the NDC in the Dabie Mountains. P-T metamorphic conditions are indicated.

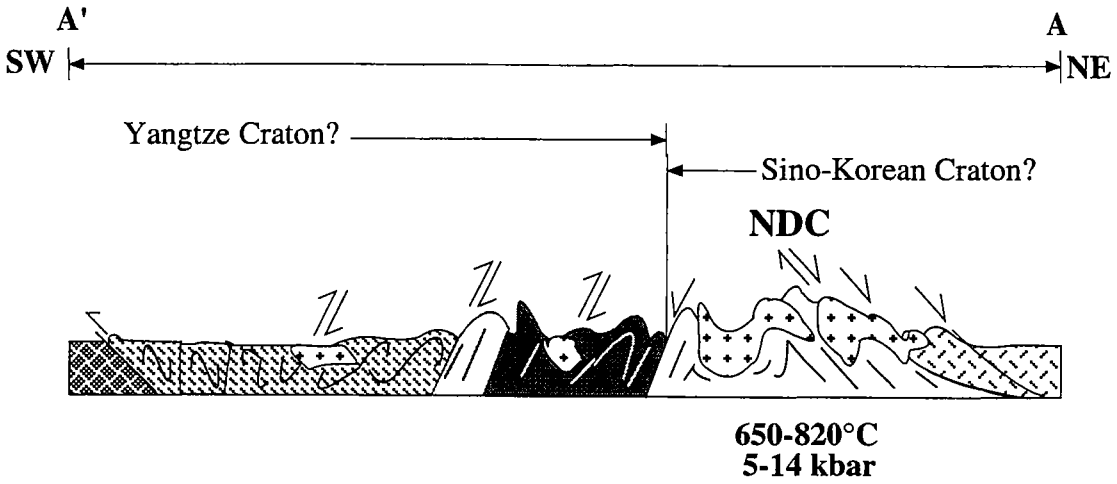

vermicular intergrowths of clinopyroxene + plagioclase from garnet. Thus, the occurence of granulitic relics may suggest an initial granulite facies metamorphism probably associated to migmatization, overprinted by amphibolite facies metamorphism during the retrograde P-T path. The gneissosity dips to the north and northeast with moderate angle (30-60°) closed the XMF whereas it dips to the south-southeast with the same angle at the contact with the Southern Dabie Complex (Fig. II-6). This variation in the foliation direction seems to form a dome of orthogneisses. Ductile shear zones subparallel to the layering are generally strike to NW-SE with a northward sense of shear within the migmatitic gneisses.

The metasedimentary horizons are composed of interlayered fine-grained gneisses, metamorphosed calc-silicates, marbles, metaquartzites and amphibolites. As the orthogneisses, this formation contain in some area granulitic relics. but the present mineralogic assemblage corresponds to amphibolite facies metamorphism.

The third lithology is represented by the mafic-ultramafic bodies which occur as complex within the migmatites. They may be separated into two groups: (1) undeformed and unmetamorphosed ultramafic rocks and (2) mafic rocks which are metamorphosed under granulite facies metamorphism. The first group of ultramafic bodies consists of lherzolite, dunite, harzburgite, hornblende-bearing peridotite, pyroxenite, garnet-bearing pyroxenite, gabbro and anorthositic gabbro. These rocks are totally undeformed and show only a magmatic texture composed of olivine, clinopyroxene and orthopyroxene with a variable amount of plagioclase. They probably crystallized either at mid-crustal level as suggested by the lack of garnet or at deeper depth for garnet-bearing bodies. The second kind occured also in the migmatites but they undergone deformation and metamorphism as expressed by their granulitic mineral paragenese. It seems that the petrogenesis of these ultramafic rocks can not be interpreted only in a single history according to their metamorphic grade and their geochemistry. Li et al. (1989), Liu et Hao (1989), Xu et al. (1992) and Okay (1993) suggest that these mafic-ultramafic bodies represent an ophiolitic melange in the eclogite facies with granulite-amphibolite overprint.

Finally, the granitic plutons represent the last lithology which occurs in the NDC (fig. II-6). This formation may contain xenoliths of gneiss, mafic and ultramafic rocks (Zhang et al., 1996). The main question which still remains unresolved, is their time formation, syn or post tectonic? For example, at the SW area from Laibang, it was clear that the granitic pluton called Beimajian is syn-tectonic owing to its S-C structure with a possible southward sense of shear (2-3 m wide mylonitic zone). The foliation in the coarse-grained granitic body is N38° 48°SE associated with a N126°-140° southeastward stretching lineation. However, these granitic plutons may be also totally undeformed.

Otherwise, monzogranitic, granitic and dioritic dykes go through the migmatite and they are probably related to these granitic plutons. Pegmatitic veins composed of quartz + plagioclase + alkali feldspars ± biotite cut the migmatite and the amphibolites like the other dykes. The cross-cutting of these different dykes seem to be associated with some post-collisional granitic bodies and not with the partial melting event.

### 2.5.3. The Sourthern Dabie Complex (SDC)

The Southern Dabie Complex (SDC) termed the eclogite zone by Okay et al. (1993), has an unclear limit with the NDC (Fig. II-7). In fact, the boundary between these two units doesn't seem to be well constrained geographically and its location changes strongly among the scientific community. Nevertheless, everybody agreed that the lithologies of the SDC are totally different than those of NDC. The gneiss from the SDC is distinct by its fine-grained size and the general absence of porphyroblastic texture. This zone is composed of more than 80 % of quartzofeldspathic gneisses intercalated with amphibolitized eclogites, marbles, ultramafics, rare metapelites and late cretaceous granitic intrusions. Some undeformed ultramafic-mafic rocks are enclosed in quartzofeldspathic gneisses like in the NDC. Pyroxenites at Shachun are composed of orthopyroxene + clinopyroxene + plagioclase assemblage. They present only a magmatic texture and no trace of UHPM minerals are observed in thin sections. Therefore, pyroxenites do not exhibit relics of the UHP metamorphic event. Thus, this may suggest that these ultramafic bodies are related to undeformed and unmetamorphosed bodies of the NDC. However, their petrogenesis, their age, and their geochemical signature are still unclear in regards to the tectono-metamorphic evolution of the Qinling-Dabie-SuLu orogenic belt.

Okay et al. (1993) subdivided the SDC into two subunits: the northern one termed "hot eclogites" zone with P-T conditions T = 800 ± 50°C and P = 38 ± 5 kbars and a southern one ("cold eclogites" zone) which is lithologically and structurally similar to the northern part (Fig. II-7). The separation between these two subunits are based on the lack of coesite, microdiamond and marble bands, and also on the occurrence of Na-amphibole-bearing eclogite (T = 635 ±40 °C and P = 23 ± 3 kbars). Okay et al (1993) described the boundary between these two units as a shear zone with a southward normal sense of displacement corresponding to a decrease in pressure of about 15 kbars. Three distinct types of eclogite were recognized in association with gneiss, marble, and ultramafic rock.

Country rock gneiss and quartzite: The most common gneissic rocks consist of white pale gray banded quartzofelspathic gneisses composed of quartz + plagioclase + alkali feldspar + muscovite + epidote ± garnet ± biotite ± hornblende ± titanite ± opaques. In some area, the gneissic rocks show a wide variation in thickness of felsic/mafic layers. They are

Figure II-7: Location of the SDC in the Dabie Mountains. P-T metamorphic conditions are indicated.

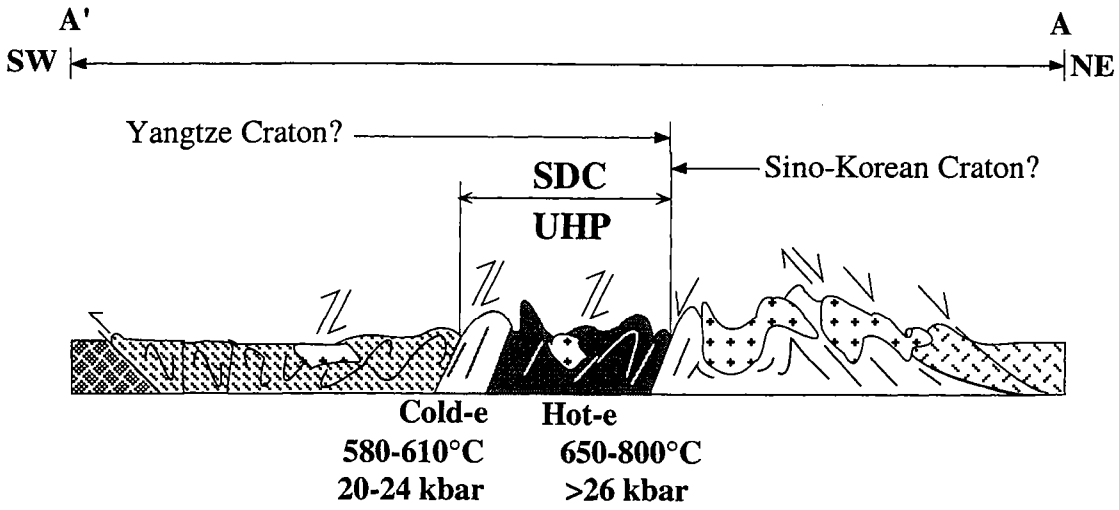

interlayered with metapelites, marbles, or amphibolized eclogites. This may suggest that the country rocks and the eclogites were together during the UHPM event. However, the lack of typical UHPM minerals such as coesite, pyrope, and Si-rich phengite in the gneiss provides a no-uniform interpretation on the coalescence or no-coalescene of eclogites and their country rocks during the UHPM event. According to Carswell et al. (1993), the quartzofeldspathic gneisses have never been equilibrated at pressure above the plagioclase stability field. But, Wang and Liou (1991) and Okay (1993) described the occurence of high-Si phengite and/or coesite pseudomorphs as inclusions in garnet from metapelitic and metapsammitic gneisses. At Shuanghe, several authors described coesite-bearing jadeite quartzites within gneisses interbedded with eclogite-bearing marbles and coesite-eclogite layers (Xu et al., 1992; Zhang et al., 1993; Okay, 1993; Cong et al., 1995). Different localities in the SDC present the occurrence of coesiteas in supracrustal rocks as well as ultramafic rocks, thus suggesting a regional UHP metamorphic event, although it is still a hot debate.

Eclogite in gneiss: The coesite-bearing eclogites occur mainly as disrupted blocks and discontinuous layers in gneiss and marbles or as lenses, blocks or layers in ultramafic rocks (Liou et al., 1995). These eclogites are composed of garnet, omphacite, kyanite, zoïsite, rutile, phengite plus coesite and quartz pseudomorphs after coesite as minor minute inclusions in garnet, kyanite, omphacite and zoïsite. Many eclogitic layers exhibit conformable contact with layering in host gneisses and marbles. The "hot eclogites" show two stages of recrystallization: (1) eclogitic stage composed of kyanite, omphacite, garnet, zoïsite, talc, magnesite and coesite and (2) amphibolite stage corresponding to the retrograded assemblage amphibole + plagioclase ± Ca-clinopyroxene after omphacite, amphibole ± epidote ± plagioclase ± biotite ± calcite after garnet and replacement of kyanite by corona assemblage of zoïsite + phlogopite + plagioclase ± muscovite and/or margarite. Only a few authors reported the microdiamond occurence as small inclusions in garnet (Xu et al., 1992; Okay, 1993). The main difference between the "hot eclogites" and "cold eclogites" are the lack of coesite and microdiamond, the absence of marbles as country rocks and the occurence of glaucophane in kyanite-bearing eclogite.

Eclogite in marble: Eclogites situated in marbles, occur as isolated blocks (for example the UHPM slab of Shuanghe) or as discontinuous layers. The typical mineralogical assemblage is composed of garnet, omphacite, zoïsite, phengite, calcite, dolomite and sometime microdiamond and coesite which have been described as inclusions in garnet (Okay, 1993).

Eclogite in ultramafic rock: Eclogites occur as layers or lenticular bodies in garnet-bearing ultramafics. The mineralogical association is garnet + omphacite + phengite + rutile and minor kyanite + zoïsite. Minute coesite pseudomorphs have been found as inclusions in

garnet. They are believed to be formed at 740 ± 50°C and P > 40 kbars (Wang et al., 1989; Okay, 1993).

#### 2.5.4. The Susong Metamorphic Complex (SMC)

The Susong Metamorphic Complex (SMC) occurs in the southern margin of the Dabie Mountains. It comprises metamorphosed quartz sandstone, schist, marble, quartz-rich amphibolite, biotite gneiss and metaphosphorite (Liou et al., 1995). These rocks have a regional schistosity and gneiss foliation that dip to the southwest and they were folded later on. Most of the lithologies were metamorphosed under grenschist to amphibolite facies (Fig. II-8).

The SMC can be subdivided into three subunits: (1) a northern belt which is composed of thick metamorphosed magnetite-bearing quartz sandstone with thin layers of mica schist and granitic gneiss; (2) a middle belt which comprises interlayered magnetite-bearing quartz sandstone, marble, talc quartzite and garnet-biotite gneiss, quartz hornblendite and characteristically metaphosphorite and kyanite-quartzite; and (3) a southern belt where we can find interlayers of chlorite-sericite schist, greenschist and fine-grained biotite gneiss.

### 2.6. Overview on the tectono-metamorphic evolution of the UHPM Qinling-Dabie terrane

Ultra-High Pressure Metamorphic terranes within which coesite and/or diamond are found, are represented by three main orogenic belts which are: the Western Caledonides in Norway, the Dora Maira Massif in the Alps and the Dabie Shan in Central China. Geological investigations in these metamorphic terranes highlighted the subduction of crustal material to depth greater than a thicker continental crust. It arises the profound problem of the exhumation of UHPM rocks which preserved the UHPM mineral index (coesite for example). Coesite occurs as inclusions within silicate minerals such as garnet or omphacite, emphazing the extreme metamorphic conditions of UHPM event. Whatever the UHPM terrane considered, coesite-bearing eclogites occuring as disrupted blocks, are enclosed within low-pressure gneisses. These field observations rise up the on-going controversy regarding the "exotic/tectonic emplacement" or "in-situ" origin of the coesite-bearing eclogites (Krogh, 1977; Cuhbert and Carswell, 1990; Griffin et al., 1985; Smith, 1988). "... it remains a challenging task to discriminate between gneisses which have witnessed UHP conditions, but were extensively overprinted by retrograde assemblages ... and those gneisses with only prograde lower-pressure assemblages which were tectonically interleaved alongside the UHP rocks at a late stage in the overall P-T history. ..." (Schreyer, 1995). Consequently, the tectonic model unraveling the exhumation of coesite-bearing eclogite should combined

Figure II-8: Location of the SMC in the Dabie Mountains. P-T metamorphic conditions are reported.

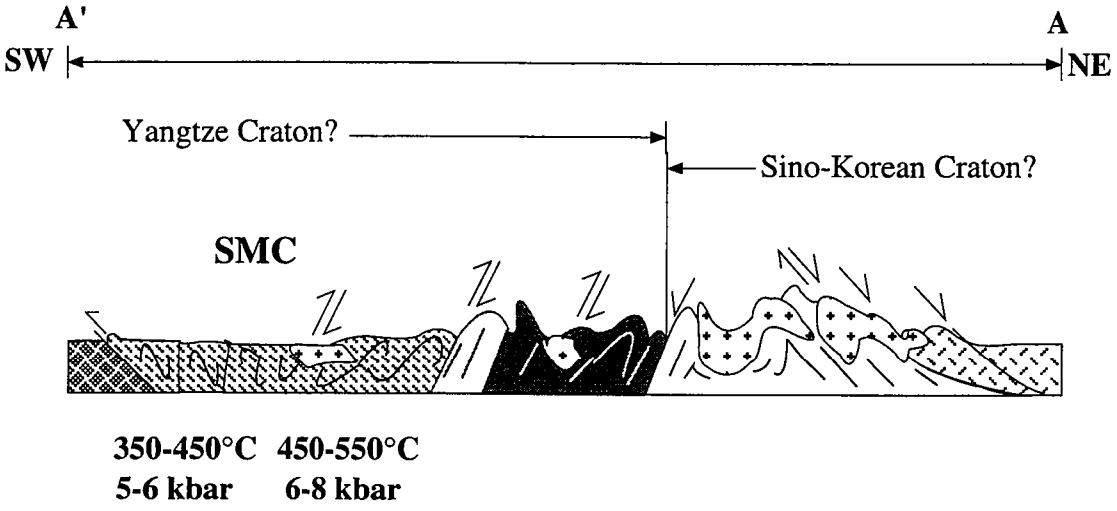


Figure II-9: Sketch drawing illustrating the inclusion of coesite pseudomorph retrogressed to quartz within garnet porphyroblast. Typical radial cracks are formed during the expansion of the inclusion during decompression.

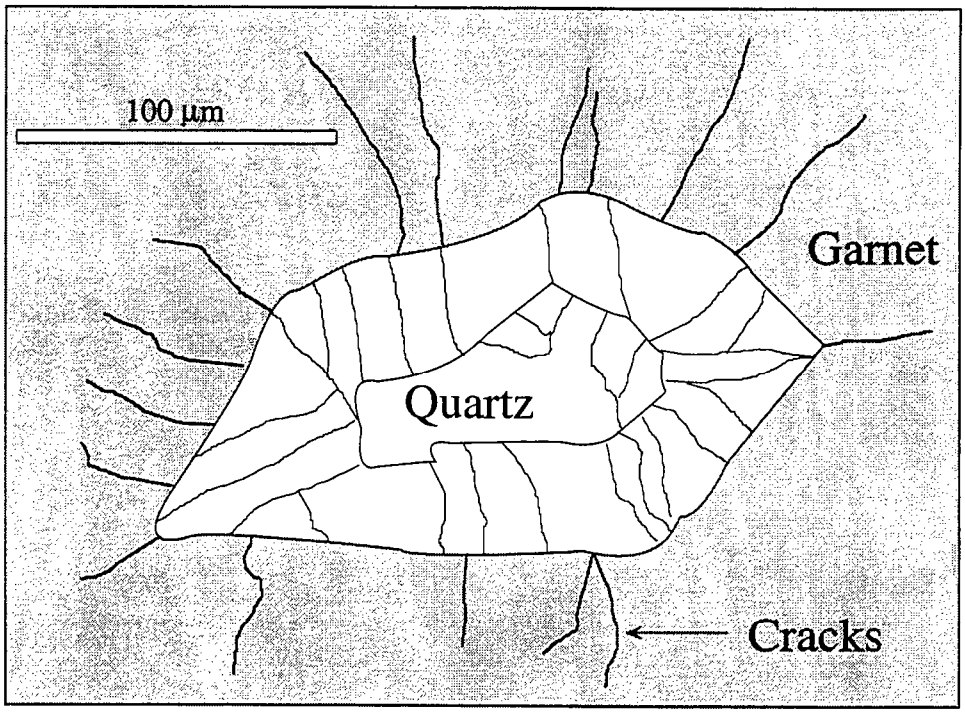

judicious mineralogical, geochemical, structural, geochronological and geophysical data to decipher the prograde from the retrograde metamorphic histories.

The first requirement for that model is given from the mineralogical point of view, by the occurrences of coesite and/or diamond. Diamond is found as large crystals from 150 to 700 μm in size in garnets from eclogite, garnet-pyroxenite and jadeite quartzite (Xu et al., 1992; Hu and Liu, 1992; Okay, 1993). Coesite is located essentially as inclusions within porphyroblast of garnet, omphacite or kyanite as shown in Fig. II-9.

These minerals are able to avoid the total transformation of coesite into quartz as they can maintain a high internal pressure during decompression (Gillet et al., 1984, van der Molen and van Roemund, 1986). In addition, the experimental work indicated the sluggish transformation of coesite into quartz pseudomorph in the absence of water (Bohlen and Boettcher, 1982). Therefore, fluid activity during decompression had to be low in order to preserve coesite.

Metamorphic evolution of coesite-bearing eclogite provides the second constraint for the tectonic model. P-T paths of three well known coesite-bearing eclogites are reported in Fig. II-10.

Their metamorphic evolution is related to a clockwise P-T where three important points are reported: (1) the prograde P-T path is not precisely determined due to the "altered" mineral phases situated as inclusions in the eclogite facies paragenesis and to the difficulty to analyze them; (2) the peak metamorphism under eclogite facies took place at low temperature, generally around 650°-700°C, and high pressure above 27kbars; (3) all retrograde metamorphic evolution of coesite-bearing eclogites are characterized by decompression nearly isothermal, followed by cooling as UHP and HP rocks reached the mid-crustal level. Such features should be seriously considered in the future tectonic model as the point 2 implyes an extreme metamorphic environment for the formation of coesite-bearing eclogite, also true for crustal material which preserved coesite, and as the point 3 strongly suggests either rapid exhumation of UHPM rocks or continued subduction at deeper level while exhumation was occuring. In addition, large greenschist to amphibolite facies overprint is expressed in most retrograde paths suggesting that geochronological data considered as cooling age must be interpreted with caution.

The geochemical and Sr-Nd isotopic data on eclogites from the whole Qinling-Dabie orogenic belt have been compiled by Jahn (1998). Most of the eclogites are of basaltic composition but some of them are from marble or siliceous carbonate origin, arguing for the deep subduction of continental material. Their geochemical characteristics are similar to those

Figure II-10: Pressure-Temperature (P-T) paths for coesite-bearing eclogites from Dora Maira massif (Chopin, 1984; Schertl et al., 1991; Sharp et al., 1993), Western Alps (Reinecke, 1991), Qinling-Dabie orogenic belt (Enami and Zhang, 1990; Wang and Liou, 1991, 1992). After Hacker and Peacock (1997).

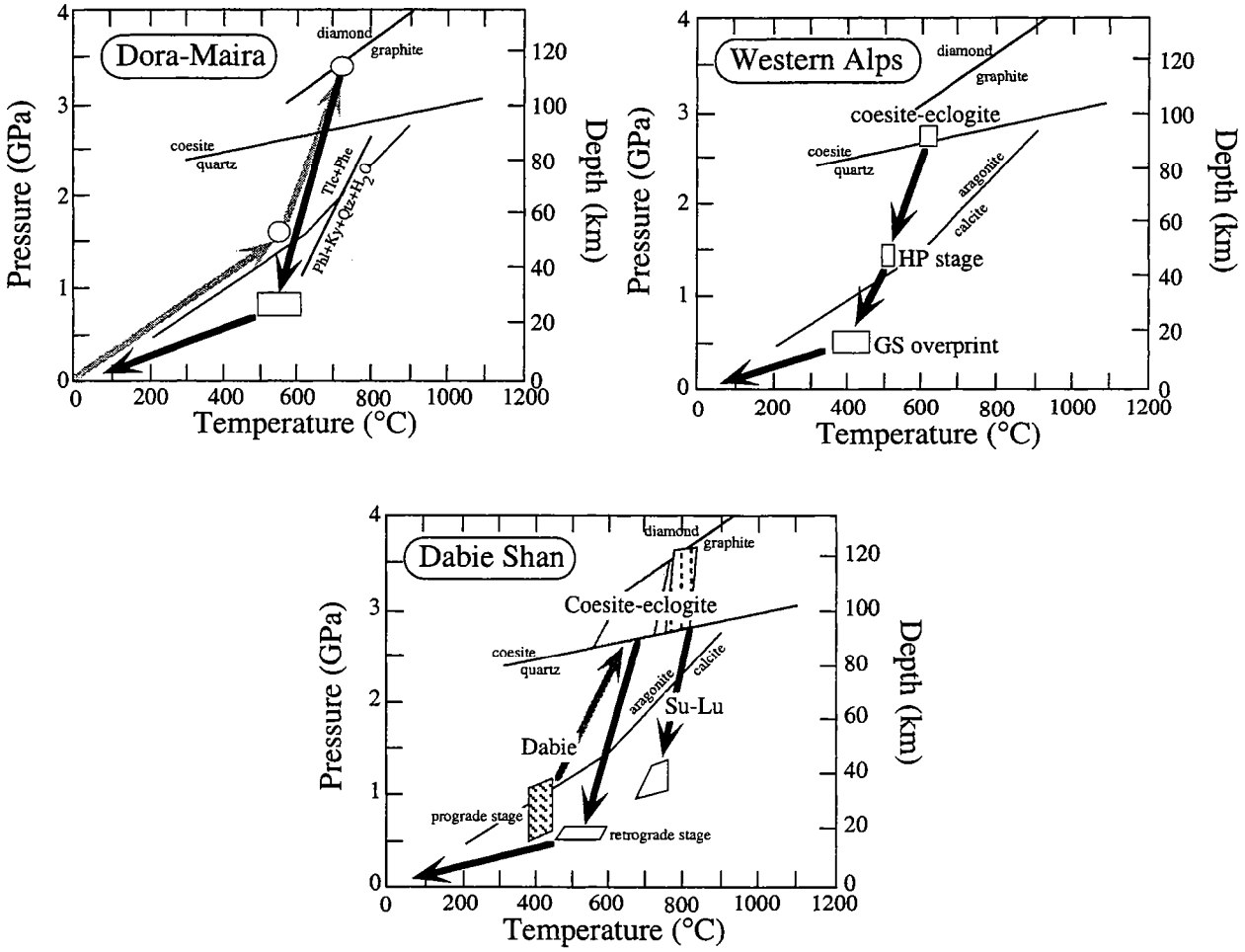

of mafic rocks of Precambrian gneiss terranes, probably Proterozoic in age. No eclogite of MORB composition has been yet found in the entire orogenic belt. In contrast to small disrupted eclogite boudins, large and layered eclogite massifs occur in the Dabie Mountains. Geochemical and Sr-Nd isotopic features indicate a mantle-derived magma as parental source, which was either contaminated by the lower crust in the case of the Bixiling Complex or by the upper continental crust for the Maowu intrusion. "... The UHP paragenesis of layered intrusions have a connotation of continental subduction, ..." (Jahn, 1998). Thus, the geochemical and isotopic features of the coesite-bearing eclogites confirm the subdution of continental material.

From the geochronological point of view, a large dataset is now available on the coesite-bearing eclogites, eclogites, paragneisses and orthogneisses. Peak metamorphism ages, cooling ages and also protolith ages were obtained using U-Pb, Sm-Nd, Ar-Ar, Rb-Sr and fission tracks methods on their best destined minerals (Fig. II-11).

U-Pb zircon ages associated with Sm-Nd garnet ages indicate that the peak metamorphism under eclogite facies metamorphism took place at ~220 Ma. Nevertheless, it has to be noticed that some Sm-Nd garnet ages are older than the U-Pb zircon ages suggesting that isotopic systems in general, might not reach necessarely equilibrium under such metamorphic conditions (Jagoutz, 1988, Vidal and Hunziker, 1985). In addition, Ar-Ar analysis on phengite may give older ages than U-Pb zircon ages, interpreted as due to excess of $^{40}Ar$ (Vidal and Hunziker, 1985; Tonarini et al., 1993; Li et al., 1994). The combination of multi-chronometric data on the same sample argue for a high initial exhumation rate and a high initial cooling rate of coesite-bearing eclogites about 10mm/yr and ~40°C/Ma. respectively.

The contraints mentioned above constitute the framework for the explanation of the exhumation of UHPM rocks which preserved the UHPM mineral index. Typical geotherm characterizing stable continental or oceanic settings indicate that a temperature above 1000°C should be reached for a pressure above 27 kbars (Pollack and Chapmann, 1977). However, the coesite-bearing eclogites recorded only 700°C for the peak temperature. Therefore, such findings are applied exclusively in a subduction setting where cooler conditions may be still maintained at great depth and thus, the (P-T) determinations calculated on the coesite-bearing eclogites are consistent with those obtained within a subduction zone (Peacock, 1990, 1993). Several metamorphic studies in the Dabie Shan reported the occurrence of coesite in both basaltic and crustal material implying therefore the subduction of the continental crust. 4 P-T paths subsequent to coesite-eclogite facies metamorphism may be proposed as reported in Fig. II-12.

Figure II-11: Radiometric ages related to the UHPM Qinling-Dabie etrrane. Modified after Hacker and Wang (1995).

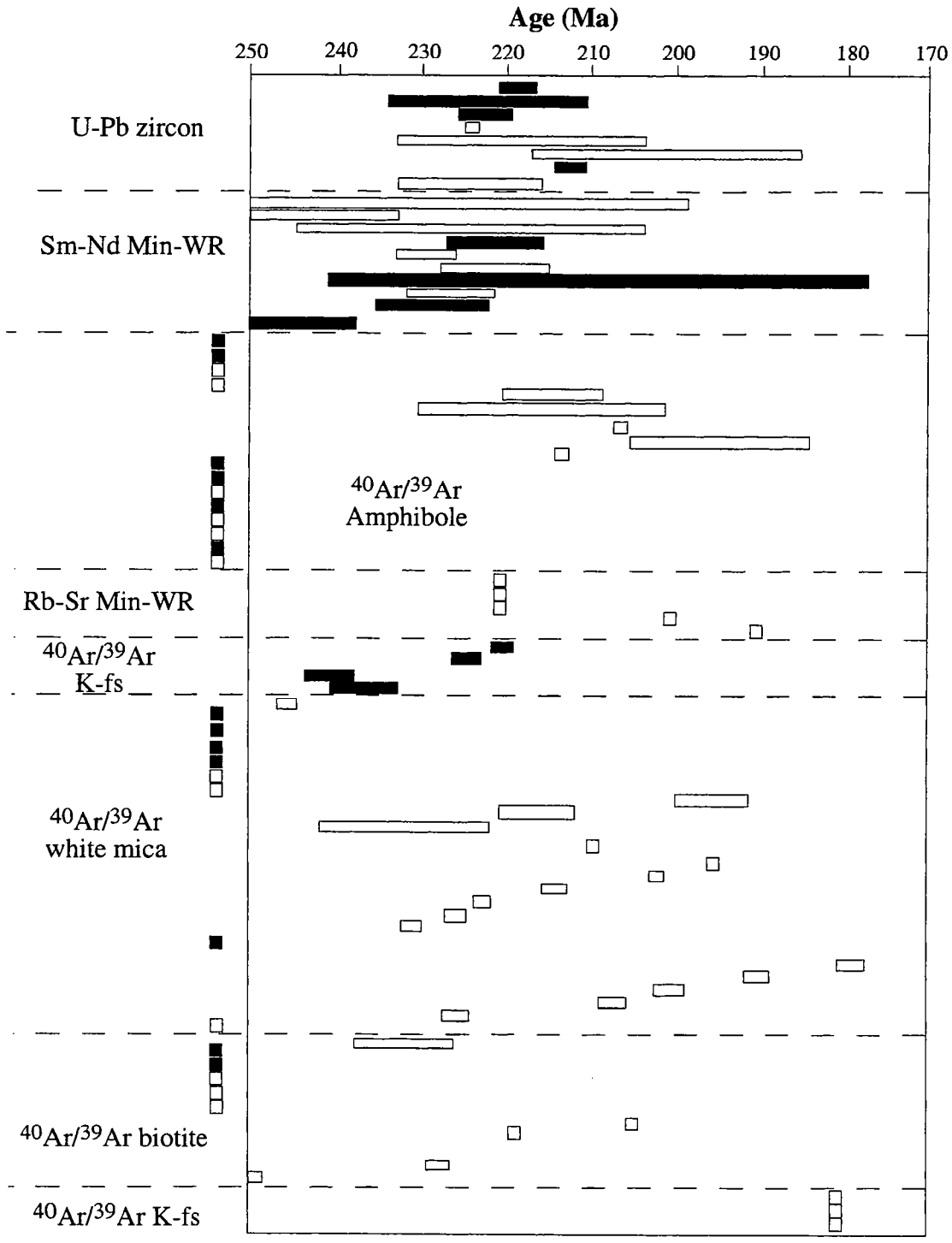

Figure II-12: Possible P-T paths after coesite-eclogite facies metamorphism. After Hacker and Peacock (1997).

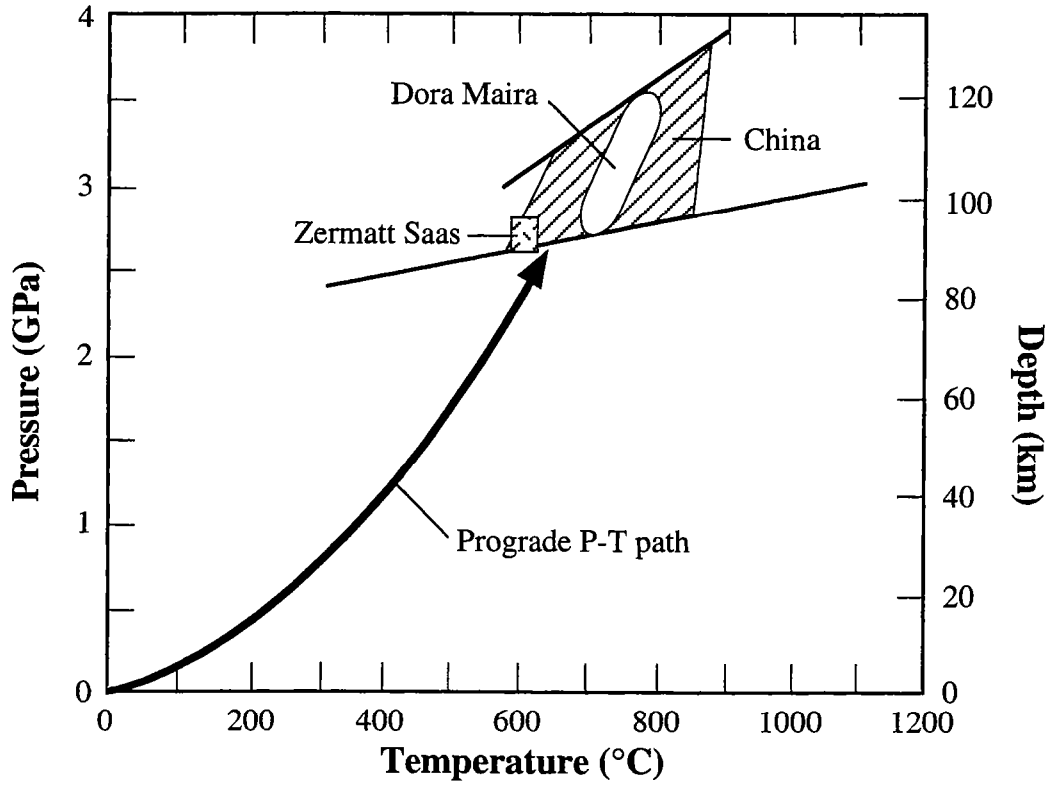


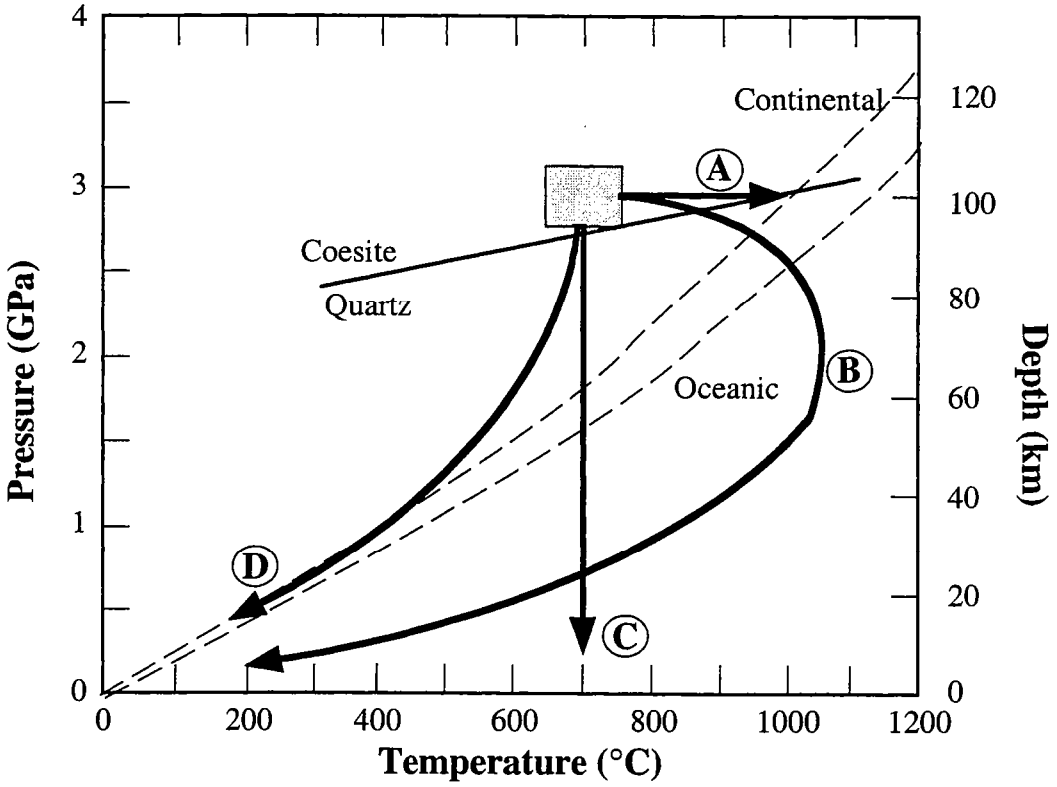

The path A corresponding to the subduction stop with no exhumation of buried rocks, expresses a heat up nearly isobarically after the peak eclogite facies metamorphism, related to thermal relaxation in a new warmer steady state. In that case, the isotherms are no longer deflected downward and new mineral paragenesis are expected to form. Therefore, this P-T trajectory cannot be applied to the UHPM rocks which preserved coesite. Still considering the suspension of subduction but with additional exhumation by erosion (path B according to the calculation of England and Thompson (1984)) of UHP rocks, coesite-eclogite suffer a heat up at the early stage of decompression due to the thermal re-equilibration. Consequently, HP rocks become hotter during decompression and a newly formed mineral assemblage is expected to appear near the peak temperature. In such metamorphic evolution it should be totally fortituous to preserve coesite from its total transformation into quartz speudomorph. Thus, the path B cannot be applied on coesite-bearing eclogite as the cooling path during exhumation. Furthermore, suspension of subduction may be associated with a very high erosion rate provoking the instantaneous exhumation of coesite-bearing eclogite. Thus, the UHP rocks undergo adiabatic nearly isothermal decompression and this cooling path may correspond to the P-T path calculated on the UHPM rocks. However, there is still lacking convincing observations of metamorphic reactions which should occur in such P-T conditions (Chopin, 1984). Finally, the last possible cooling path for coesite-bearing eclogite is represented by the path D. If the subduction is still activated during exhumation of UHP rocks, the isotherms are still depressed in the region of the subducted slab and the UHP rocks which are transported towards the surface, evolve in cool environment during decompression (Rubie, 1984; Davy and Gillet, 1986; Gillet et al., 1986; Ernst, 1988). Consequently the path D may account for the preservation of coesite from the total transformation into quartz pseudomorph and also for the P-T paths calculated on the UHPM rocks.

Exhumation corresponds to the displacement of rocks towards the surface (England and Molnar, 1990). Several mechanisms have been proposed to interpret the exhumation of UHPM rocks from the Dabie Shan which records the highest P-T condition. They require either the removal of the overburden, or the transport of UHP rocks through the overburden, but they cannot only be related to thrusting or strike slip faulting (Platt, 1993). Among an exhaustive list of exhumation mechanisms, only three are described below: (1) buoyancy forces acting directly on metamorphic rocks (Ernst, 1988) or corner flow of low viscosity material (Cowan and Silling, 1978; England and Holland, 1979; Cloos, 1982; Palvis and Bruhn, 1983); (2) extension (Platt, 1986, 1987; Dewey, 1988); and (3) slab breakoff (von Blankenburg and Davies, 1995).

*Buoyancy forces and corner flow*

Both exhumation models suggest the activation of buoyancy forces either in the subducted slab or in the accretionary prism respectively. These forces allow some portions of continental crust which have been buried to mantle depth, to ascend up to crustal level. The important factor is the lower density of crustal material compared to mantle material. "... Upward motion took place as tectonically imbricated slices, as laminar return flow in melanges zones, and perhaps partly lateral spreading/extension of the underplated accretionary prism. ..." (Ernst, 1988). For the corner flow model (Cowan and Silling, 1978; England and Holland, 1979; Cloos, 1982; Palvis and Bruhn, 1983), an accretionary prism is formed between the subducted slab and the overlying plate as a result of on-going convergence. This develops an upward flow of deeply buried rocks. Such tectonic mechanism may explain the occurrences of HP metamorphic rocks in melange zone (Platt, 1993).

*Extension*

The models invoke either the underplating-wedge extension (Platt, 1986, 1987) or the lithospheric extension (Dewey, 1988). Firstly, subduction-accretion complexes form a wedge-shaped continua at the junction between the subducted slab and the overlying plate. The accretion of material implyes the increasing length and thickness of the wedge during the on-going subduction. Internal shortening deformation maintaining a stable geometry is expressed as thrusting, backthrusting, and folding. The thickness of the wedge is due to the underplating of sediment or crustal slices. It is reduced via extension (listric normal faults). The association of underplating and extension allow the ascend of HP-LT rocks to upper levels in the rear of the wedge. Secondly, the lithospheric extension model is generally invoked in orogenic belt to explain the return of normal crustal thickness without very much erosional denudation. The lithospheric extension is active whereas the plate motions are convergent (Dewey, 1988). Consequently, the forces leading to extension are generated at the site of convergent due to the high surface elevation in the region of crustal thickening (Molnar and Taponnier, 1978). The forces are still localized within the wegde previously mentioned but their precursors are different to the underplating-wedge extension. The deformation within the wedge is dominated by strike slip faulting (Houseman and England, 1986).

*Slab Breakoff*

This model is related in some way with the buoyancy forces suggested by Ernst (1988), with the decoupling of the Thermal Boundary Layer in the subducted lithosphere (Andersen et al., 1991) and also with the "breakup" model proposed by van den Beukel (1992). In that model, oceanic lithosphere detaches from continental lithosphere during continental collision ("slab breakoff") (Davies and von Blankenburg, 1995; von Blankenburg and Davies, 1995).

The "easier" subduction of oceanic crust compared to continental material leads to an opposite buoyancy forces within the subducted slab. Consequently, as strain localizes, the detachment of the oceanic lithosphere from the continental lithosphere may occur. Such model can explain the bi-modal magmatism as due to the heating of the overriding lithosphere mantle by upwelling asthenosphere inducing melting, the thermal weakening of the subducted crustal lithosphere allowing buoyant race of the relaxed crustal slices from mantle depths, and finally the short time interval between uplift and onset of magmatism.

Some special features of these exhumation mechanisms may be applied to the UHPM rocks from the Qinling-Dabie orogenic belt but in general term, no "absolute exhumation mechanism" have been yet established. The occurence of serpentinite and/or carbonate-material with the UHPM rocks may promote the buoyancy forces model. The low thermal gradient which is maintained in the subducted slab is a requisite for the exhumation of UHPM rocks and it is maintained in the corner flow or undeplating-wedge extension models. The bi-modal magmatism is explained by the "slab breakoff" model. However, special improvements from the structural and petrographical data may be made in order to elucidate obscurs points such as the tectonic relationship between the UHPM rocks and their country rocks, the metamorphic conditions undergone by the host gneisses, the larga time interval between the peak eclogite metamorphism and the onset of magmatism.

## 2.7. The investigated UHPM Complexes

### 2.7.1. The Bixiling Complex

This mafic-ultramafic Bixiling Complex is the largest coesite-bearing mafic-ultramafic body around 1.5 $km^2$ in outcrop. This complex is really interesting by its occurence which is in quite contrast with the other eclogites, its unusual talc occurence and Ti-clinohumite and magnesite minerals in ultramafics rocks. The Bixiling complex mainly composed of eclogites, is enclosed within foliated quartzofeldspathic gneiss (Fig. II-13).

About 20 elongated lenses of garnet-bearing ultramafic rocks ranging from 50 to 300 m in length and from 5 to 50 m in width, occur within eclogites. According to the extent of serpentinization and the content of titano-clinohumite and garnet, these lenses display color ranging from black-greenish to reddish layering. Contact between eclogites and ultramafic rocks is either sharp or gradational. The layered eclogites dips about 45-65° to the NW and the thickness ranges from about 2 to 10 m. Each eclogitic layer of the Bixiling Complex is associated with a distinct mineralogical paragenesis as drawn in broad outline in Fig. II-14.

Figure II-13: Sketch geological map of the Bixiling Complex. Sample location are indicated.

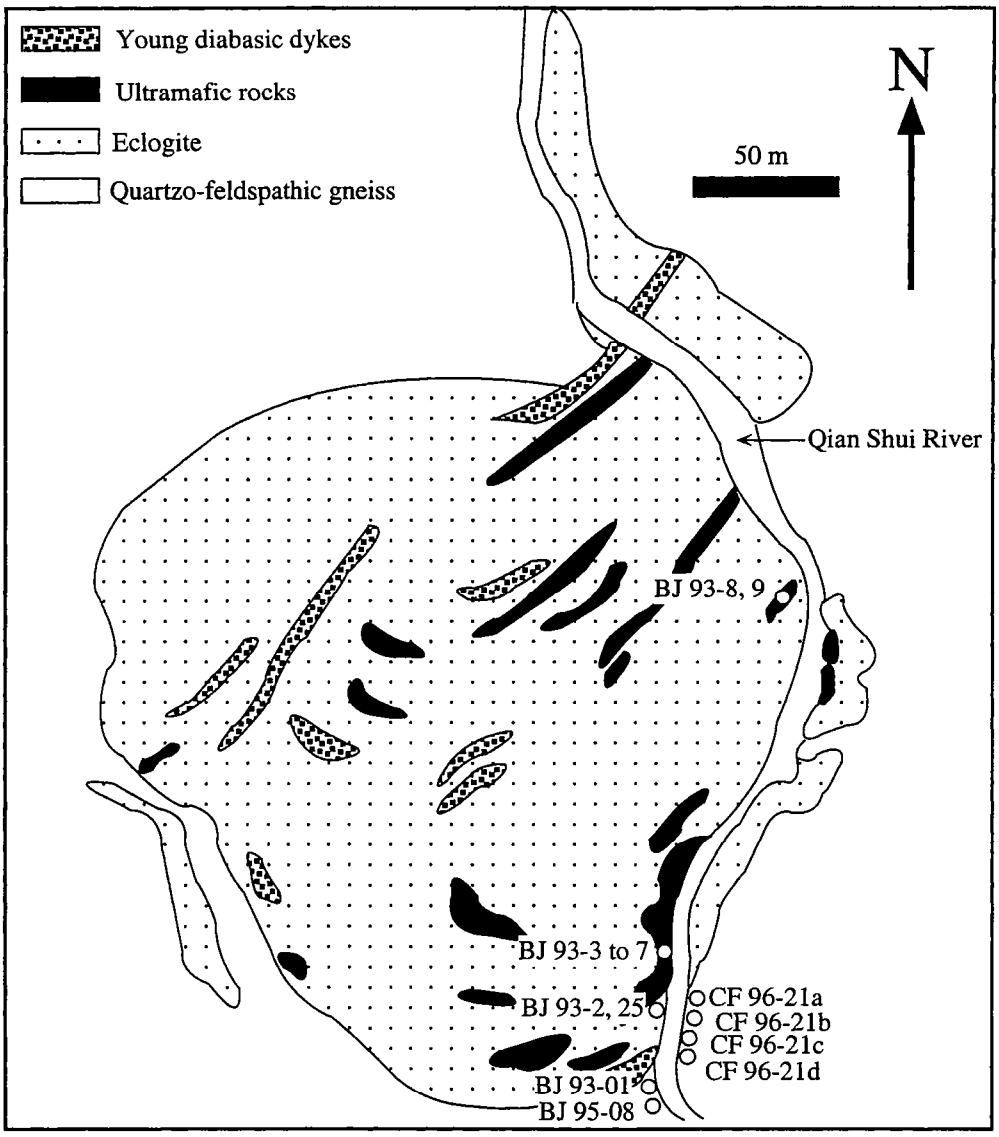

Figure II-14: Field observations at the southwestern part of the Bixiling Complex presenting a well layering of eclogites. Each eclogitic layer is associated with a distinct mineralogical association.

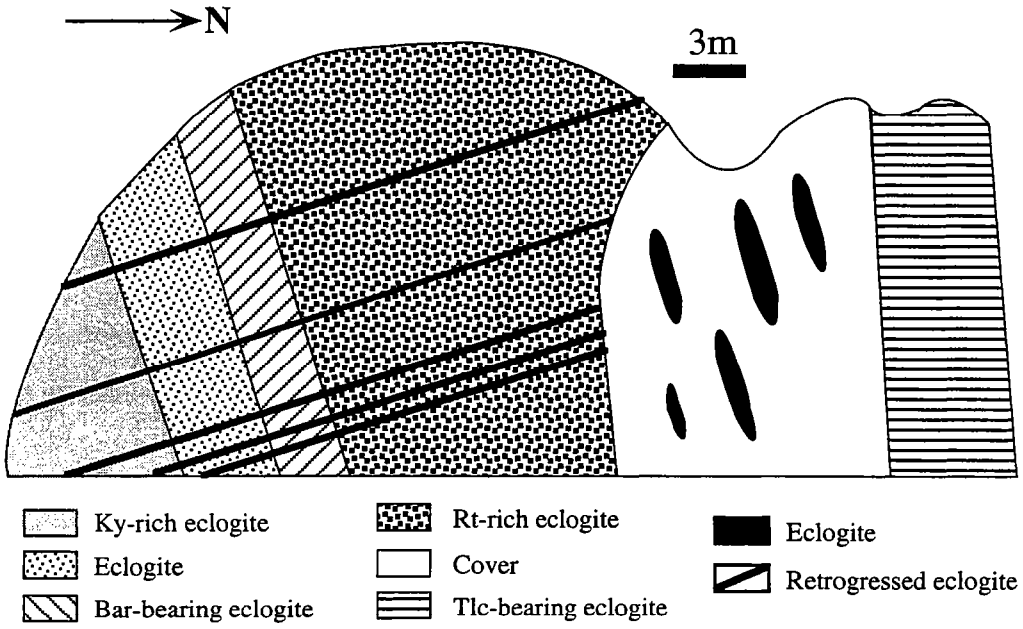


Figure II-15: P-T metamorphic conditions of the eclogites and the mafic-ultramafic rocks after Zhang et al. (1995).

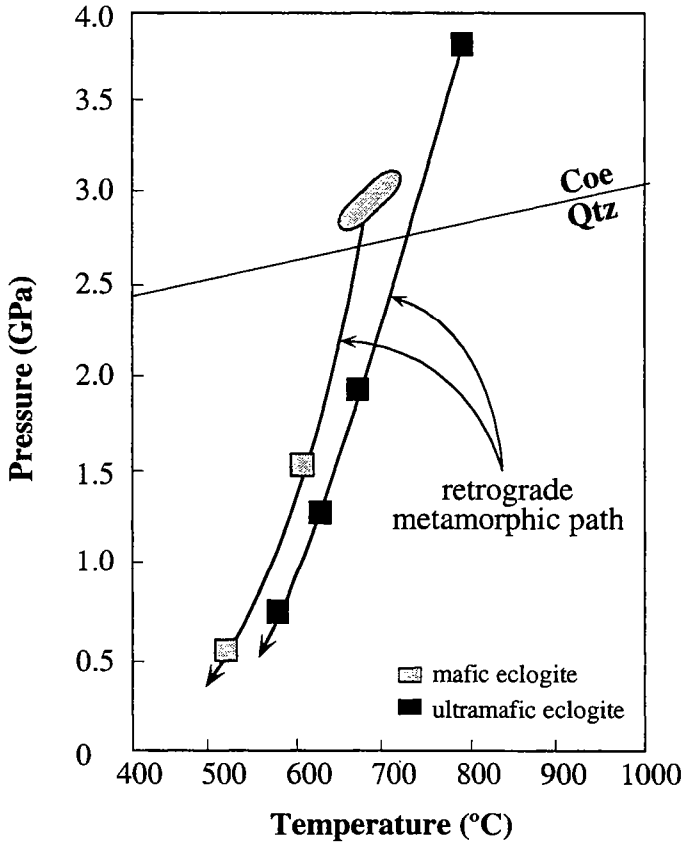

We can distinguish kyanite-rich eclogite, kyanite-bearing eclogite, rutile-bearing eclogite, phengite-bearing eclogite, barroisite-bearing eclogite and zoïsite and talc-bearing eclogites. The layers are crosscut by several subparallel thin (1 cm to 10 cm thick) dark, amphibolitized bands. Thin colorless layers of plagioclase plus quartz occur at the center of these bands as the last stage of recrystallization.

From the metamorphic point of view, most eclogites and ultramafic rocks preserve mineral paragenesis related to the peak metamorphism. However, two stages of recrystallization from the eclogites may be observed: (1) the peak metamorphic paragenesis expressed by garnet + omphacite + coesite + talc + zoïsite ± kyanite ± phengite ± rutile, is related to a temperature at 610-700°C and a pressure over 27 kbars; (2) the retrograded association is characterized by polycrystalline quartz aggregates after coesite, tremolite rim around talc, poorly developed symplectites of plagioclase plus Na-clinopyroxene and hornblende around omphacite, garnet destabilization into amphibole and rutile into ilmenite. In the extensive retrogressed rocks, omphacite is completely replaced by amphibole plus plagioclase, rutile is altered in ilmenite and titanite, and finally garnet is partially replaced by amphibole, epidote and plagioclase. The P-T conditions associated with these transformations are below 600°C and below 6-15 kbars (Fig. II-15).

The ultramafic rocks undergone two stages of recrystallization like the eclogites. The peak metamorphic assemblage of common peridotite is garnet ± enstatite + diopside ± olivine ± magnesite ± Ti-clinohumite. During the retrograded recrystallization, several transformations occur such as Ti-clinohumite in symplectite of secondary olivine plus ilmenite, or dolomite rimmed magnesite or diopside in tremolite. The last recrystallization of these ultramafic rocks which occur with more fluid, is characterized by the remplacement of olivine by serpentine and pyroxene by chlorite. Totally retrograded eclogites at Bixiling, expose either at the margin of the complex or along the fractures within the massif. Eclogites are retrograded in amphibolites due to the fluid circulation along fractures which are perpendicular to the eclogite layering. These amphibolites are composed of green amphibole (> 80 vol%), epidote and minor plagioclase, biotite and ilmenite, only minor relic eclogitic phases persist. Only along the Qian Shui river, the country rocks i.e. the quartzofeldspathic gneiss, may be observed. They are strongly foliated but they do not show the typical eclogitic mineral assemblage. They are composed of muscovite, biotite, epidote, plagioclase and quartz which correspond to the retrograded assemblage under the amphibolite facies metamorphism.

### 2.7.2. The UHPM slab of Shuanghe

Cong et al. (1995) described the UHPM rocks at Shuanghe as a thrust slab. It occurs as an elongated tectonically-bounded slab (NNW-SSE trend) within foliated orthogneiss (fig. II-16).

This slab is offset by a dextral strike slip fault, and is intruded by younger granitic body to the NW (Liou et al., 1995). A few fragments of actinolitized pyroxenite and sepentinitized peridotite occur along the eastern margin (in the eastern fault boundary) in a zone of about 20 m width (Cong et al., 1995). From the field observations, we can distinguish several lithologies which compose the UHPM slab: (1) grey-green massive eclogite, (2) dark green foliated and retrograded eclogite, (3) epidote-two mica schist, (4) garnet and biotite bearing gneiss, (5) marble with or without eclogite nodules or boudins, (6) dark grey jadeite quartzite, and finally (7) amphibolite. The UHPM slab show an apparent compositional layering more or less parallel to the foliation but it is clearly discordant to the granitic foliation of the country rock.

UHPM eclogites occur in different places : (1) as asymetric boudins of 10 cm in size within marbles including pure white marble, pale light green "impure marble" and calc-silicate rock; the foliation in marble dips to the southwest and the southward sense of shear is clearly expressed by the pressure shadow around small eclogitic boudins; (2) as thin disrupted layers or disrupted boudins in gneisses; and (3) as distinct layers of various composition and extent of retrogression intercalated with gneiss. Therefore, three kinds of eclogite may be distinguished: (1) "common" eclogite as composed of the typical garnet and omphacite association; (2) quartz-bearing eclogite; and 3) carbonate-bearing eclogite. The quartz-eclogite do not show a well preserved peak metamorphic association. The present mineral paragenesis, mainly composed of large garnet porphyroblasts in a fine grained amphibole, quartz, plagioclase matrix, corresponds to retrograded P-T condition under amphibolite facies metamorphism. During the decrease of pressure and temperature, omphacite is replaced by a corona of Ca-pyroxene and Na-plagioclase which is, sometimes, overgrown by late epidote at further lower metamorphic condition. Garnet and quartz are rimmed by a symplectite of green amphibole and yellow green Na-Ca aegyrine-augite pyroxene. A biotite and plagioclase intergrowth surrounds remainder phengite. Rutile is destabilized into titanite and ilmenite. Finally, coesite is rimmed by polycrystalline quartz aggregate as inclusions in garnet porphyroblasts. In addition, the carbonate-bearing eclogite which occurs as small boudins within marble, shows also a mineralogical paragenesis related to retrograde metamorphic grade.

Figure II-1-16: Geological map of the UHPM slab of shuanghe. Foliation is reported after Cong et al. (1995). Sample locations are indicated.

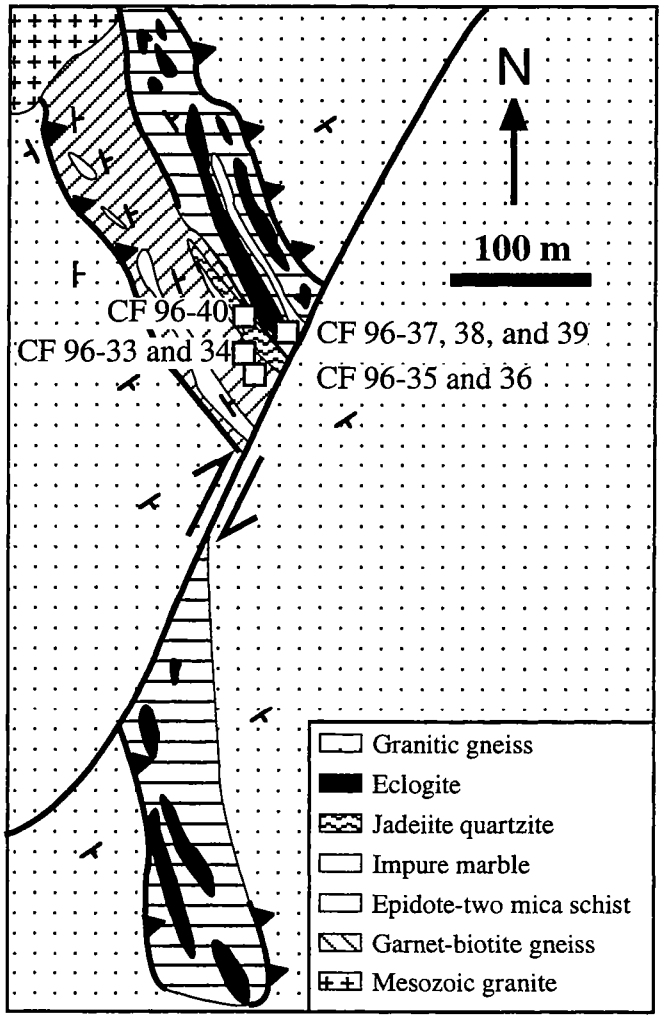

Figure II-17: P-T loop of the UHPM slab of Shuanghe after Cong et al. (1995).

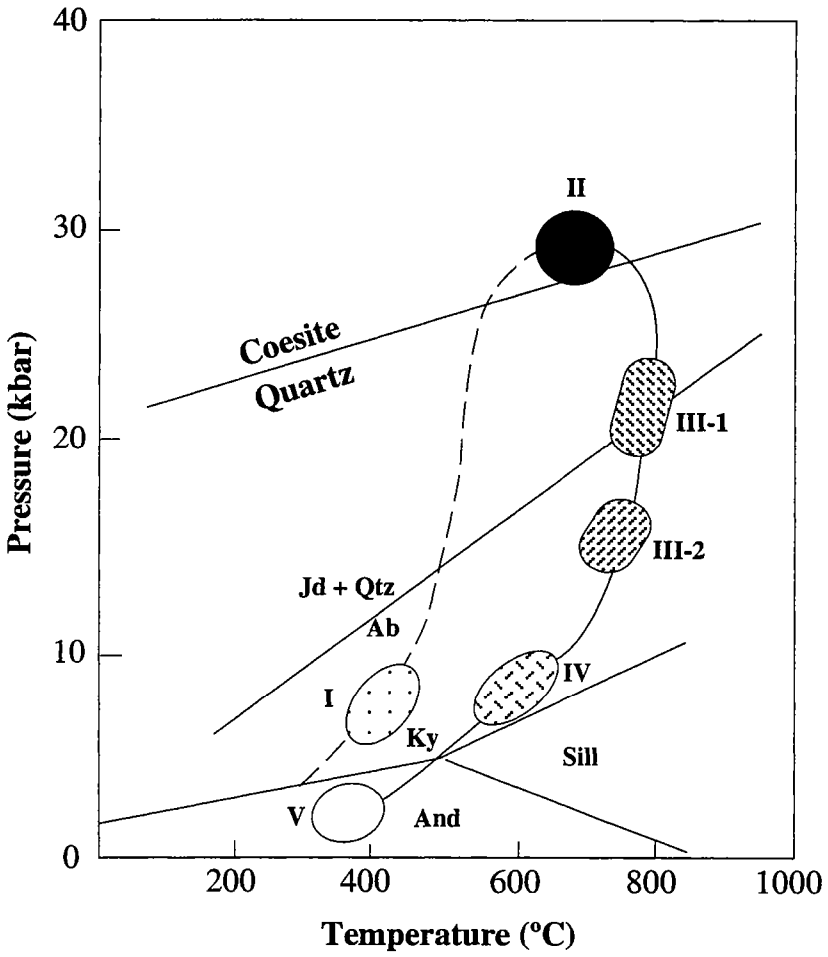

Jadeite quartzite is up to now, the single locality of such lithology in the entire Qinling-Dabie-SuLu orogenic belt, undergoing the UHPM event. It occurs as layer of several meters in size intercalated between epidote-two mica schist and marble. Jadeite quartzite is mainly composed of remainder garnet and jadeite prophyroblast in a matrix of very fine grained albite, quartz, Na-pyroxene, Na-Ca amphibole and Fe-rich oxydes (Cong et al., 1995). Blue amphibole which replaced garnet in the early stage of retrogression, is also surrounded by chlotite and magnetite aggregates. Jadeite is destabilized into symplectites of fine grained albite and acicular Na-amphibole. The occurrence of polycrystalline textute of quartz as inclusions in garnet and jadeite may suggest the earlier occurrence of coesite at the peak metamorphism. Rutile and ilmenite are also present.

Marble occurs as white massive and "impure marble". This lithology is composed of calcite, Fe-dolomite, phlogopite, epidote and titanite.

At the northwestern part of the UHPM slab occurs the epidote-two mica schist which surrounds boudins and layers of quartz eclogite. They present a mineral association of biotite, phengite, epidote (± zoïsite), quartz with minor amounts of garnet, kyanite, titanite, rutile, amphibole and plagioclase. Phengite is replaced by aggregates of biotite and plagioclase. The occurrence of symplectite intergrowth of amphibole and Na-plagioclase may suggest the previous occurrence of omphacite before the retrograde metamorphism (Cong et al., 1995). Therefore, this lithology is interpreted as the product of retrograde metamorphism under amphibolite facies, of quartz eclogite.

Garnet-biotite gneiss is located along the western edge of epidote-two mica lithology. It contains concordant layers of "impure marble" and jadeite quartzite. It is composed of biotite, quartz, plagioclase, garnet, phengite and epidote with minor amounts of titanite rutile and ilmenite. The occurrence of high-Si phengite as inclusion in garnet suggests a previous higher metamorphic grade approaching coesite-stability field.

Finally, the country rock of the UHPM slab is mainly represented by granitic gneiss which have clearly a distinct foliation. Its mineral association of Na-plagioclase, microcline, quartz, biotite, epidote, phengite and also titanite and garnet, encompasses amphibolite facies metamorphism.

From the metamorphic point of view, the occurrence of coesite and polycrystalline aggregates of quartz after coesite as well as the high-Si phengite as inclusions within garnet, indicate that not only metamafic eclogite but also meta-sedimentary rocks have undergone the UHPM event. The entire UHPM slab underwent the UHPM event whereas the granitic gneiss does not exhibit any relevant witness of that event. The concordant layering of

quartz eclogite, garnet-biotite gneiss and epidote-two mica schist may correspond to the metamorpho-chronological evolution of eclogite from the coesite stability field through amphibolite facies to greenschist facies. The metamorphic evolution of the UHPM slab follows a clockwise P-T loop where subduction and exhumation are related (Fig. II-19). This P-T trajectory is similar to those obtained on other UHPM terranes in the world (for example the Western Alps).

# 3. Coesite-bearing Eclogites from the Bixiling Complex, Dabie Mountains, China: Sm-Nd Ages, Geochemical Characteristics and Tectonic Implications

**Valérie Chavagnac[1] and Bor-ming Jahn**

Géosciences Rennes (UPR 4661-CNRS), Université de Rennes 1, Avenue du Général Leclerc, 35042 Rennes Cedex, France

1. Present address: Mineralogisch-petrographisches Institut, Gruppe Isotopengeologie, Universität Bern, Erlachstr. 9a,3012 Bern, Switzerland

**Chemical Geology 133 (1996) 29-51**

**Abstract**

The Bixiling mafic-ultramafic complex occurs as a tectonic block within biotite gneisses in eastern part of the Dabie ultrahigh-pressure metamorphic (UHPM) terrane. Geochemical and isotopic (Rb-Sr and Sm-Nd) analyses were performed on whole-rock and mineral constituents in order to constrain the age of metamorphism, to discuss the age and nature of protoliths, and to estimate the rates of initial cooling and uplift of the Complex as well as much of the Dabie UHPM terrane.

The Bixiling eclogites and ultramafic rocks have narrow ranges of near-chondritic $\varepsilon_{Nd}(0)$ values (-0.6 to -2.7) and $^{147}Sm/^{144}Nd$ ratios ($\approx$ 0.16 to 0.19), which is in strong contrast with the majority of eclogites from the Su-Lu and Dabie terranes which have low $\varepsilon_{Nd}(0)$ values (-6 to -20) and smaller $^{147}Sm/^{144}Nd$ ratios ($\approx$ 0.1 to 0.15). Trace element and Sr-Nd isotopic characteristics suggest that the original mantle-derived magma intruded in the lower crust and was contaminated by crustal rocks (granulites) during magma differentiation.

Sm-Nd isotopic analyses on garnet and omphacite from 6 eclogites and 1 garnet peridotite give tightly grouped isochron ages ranging from 210 to 218 Ma, with near-chondritic $\varepsilon_{Nd}(T)$ values (-0.1 to -1.8). When all garnet data are treated alone, they form a similar "isochron" age of 225 $\pm$ 7 Ma with $\varepsilon_{Nd}(T) = -2.5 \pm 1.1$. Similarly, Rb-Sr isotopic analyses on phengite and other minerals yield almost the same age results; and the phengite-only data also define a similar isochron age of about 210 Ma. These results lead to several important conclusions: (1) The concordant mineral Sm-Nd ages obtained for both mafic and ultramafic rocks from the same intrusion indicate attainment of isotopic equilibrium during the UHP metamorphism. (2) The Sm-Nd mineral ages are identical within error limits with the zircon U-Pb ages of $\approx$ 220 Ma from nearby eclogites. Thus, 210-220 Ma is considered the best estimate for the age of the UHP metamorphism and continental collision. (3) The fact that the garnet data points alone also give a similar (or slightly older) age and a slightly lower initial $\varepsilon Nd(T)$ value as the other garnet-omphacite pairs strongly suggests that the Bixiling complex intruded shortly before the UHP metamorphism. The same conclusion can be drawn from the phengite-only Rb-Sr isochron argument.

Using the known P-T conditions and probable blocking temperatures for Sm-Nd and Rb-Sr sytems in garnet and phengite, high rates of initial cooling ($\approx$ 40°/Ma) and early stage of uplift ($\approx$ 10 mm/yr) were calculated for the Bixiling Complex. This is in strong contrast with the Weihai eclogites from the Su-Lu terrane in which slow cooling and slow uplift ($\approx$ 1 mm/yr) rates were estimated. Evidently, differential exhumation of UHPM rocks prevails in the Dabie and Su-Lu terranes.

## 3.1. Introduction

The Qinling-Dabie orogenic belt is generally considered as the suture zone formed by collision between the Sino-Korean and Yangtze cratons (Fig. II-18). Coesite-bearing rocks are widely distributed in the Dabie and Su-Lu ultrahigh-pressure metamorphic (UHPM) terranes, which are trancated by the Tanlu Fault and probably offset by about 500 km to the north (Xu et al., 1987). Study of such UHPM rocks is important to our understanding of continental tectonics, particularly in the aspects of subduction of sialic crustal blocks and of preservation and exhumation of UHP rock assemblages (e.g., see reviews by Schreyer, 1995 and Harley and Carswell, 1995).

A key issue about the Qinling-Dabie orogenic belt is the timing of the UHP metamorphic event(s) as well as the collision between the Sino-Korean and Yangtze cratonic blocks. Based on Sm-Nd analyses of eclogitic minerals, Li et al. (1993) proposed that the UHP metamorphism and collisional events took place at about 200-240 Ma. This hypothesis has since been supported by U-Pb zircon analyses (Ames et al., 1993, 1995; Maruyama et al., 1995) and is basically in agreement with the conclusions deduced from paleomagnetic studies (Lin et al., 1985; Zhao and Coe, 1987; Yang et al., 1991, 1992).

On the other hand, different opinions have also surfaced. These include (1) a Devonian collision based on a regional geochemical study of fine-grained clastic sediments in the S. Qinling Belt (Gao et al., 1995), (2) an Archean ($\approx$ 2.7 Ga) or a Proterozoic ($\approx$ 0.8 Ga) UHP metamorphic event based on U-Pb zircon dating of the Bixiling eclogites (Cao et al., 1995; Liu et al., 1995), and (3) a prolonged UHP metamorphism from 480 Ma to $\approx$ 200 Ma based on Sm-Nd, U-Pb and Ar-Ar age results of the Dabie eclogites (You et al., 1995). Earlier, Mattauer et al. (1991) also proposed a minimum age of 600 Ma for the UHP metamorphism using phengites Ar-Ar dates. It is now known that the presence of excess Ar in phengitic mica is a common phenomenon (Li et al., 1994; Hacker and Wang, 1995). Nevertheless, it is clear that the metamorphic history and tectonic evolution of the Qinling-Dabie orogenic belt are extremely complex.

The purposes of our study are: (1) to establish the age of UHP metamorphism and the time of collision between the Sino-Korean and Yangtze cratons, using the Sm-Nd and Rb-Sr mineral isochron techniques. Unlike the other isolated eclogite blocks in the Dabie terrane, the different rock types of the layered complex are assumed comagmatic and have shared the same metamorphic evolution. Therefore, they should yield the same garnet-omphacite isochron ages if Sm-Nd isotopic equilibrium in all rocks has been reached; (2) to use Sr-Nd isotopic data to examine the nature of the mantle source and to evaluate possible crustal contamination during differentiation in the magma chamber; (3) to use the P-T information

Figure II-18: General geological map showing the Qinling-Tongbai-Dabie orogenic belt which separates the Sino-Korean craton in the north from the Yangtze craton to the south. The Su-Lu terrane is considered as the eastern extension of the Dabie terrane, offset to the north by the gigantic Tanlu Fault.

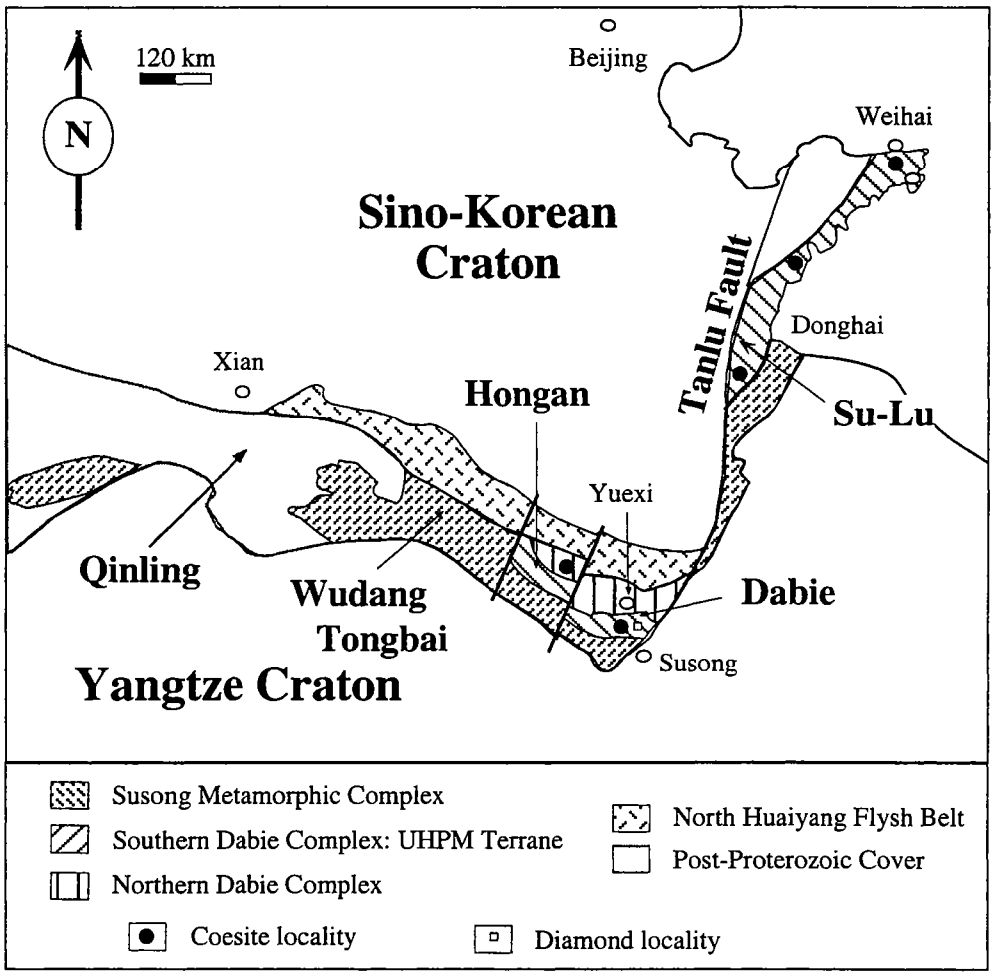

derived from previous petrological studies and the reasonably known isotopic blocking temperatures in different minerals to estimate the rates of cooling and uplift of the Bixiling complex following the continental collision. In the end, we also estimate the age of magma intrusion using garnet-only Sm-Nd and phengite-only Rb-Sr isotopic systematics, and conclude that the intrusion must have taken place shortly (≤ 300 Ma) before the UHP metamorphic event.

## 3.2. Geological Background of the Bixiling Complex

The geological setting of the Dabie orogenic belt has been described by many authors. The most up-to-date information can be found in Liou et al. (1995), Coleman and Wang (1995) and Hacker et al. (1995). The Bixiling Complex, the largest coesite-bearing mafic-ultramafic body (≈ 1.5 $km^2$) in the Dabie Mountains, occurs as a tectonic block enclosed within foliated quartzofeldspathic gneisses in eastern part of the Dabie ultrahigh-pressure (UHP) metamorphic terrane (Fig. II-19). Because of heavy vegetation, the best exposure of the complex is found along the Qianshui River and road-cuts on the eastern side of the hill, from where our samples were collected (Fig. II-19).

The complex consists predominantly of banded eclogites that contain many lenticular bodies of ultramafic rocks (garnet peridotite, garnet pyroxenite and wehrlite; Zhang et al., 1995). The contact between eclogite and ultramafic rocks is gradational. The occurrence of this complex is in contrast to most other eclogite bodies, which commonly form small disrupted blocks, lenses or nodules in enclosing gneisses. Field relationships and petrological studies suggest a cumulate origin of the mafic-ultramafic complex (Zhang et al., 1995). The diverse rock types are hence considered, at least to a first approximation, magmatically cogenetic. The ultramafic rocks show variable color, depending on the degree of serpentinization (dark green bands) and the presence of titanoclinohumite and garnet (reddish yellow bands). The complex and the surrounding granitic gneiss are cut by younger diabasic dykes.

The present mineral assemblages of the Bixiling eclogites include not only the common eclogitic phases (garnet, omphacite, kyanite, phengite, zoisite, and rutile) but also diagnostic parageneses of UHPM origin, including coesite and talc in eclogite, and magnesite and Ti-clinohumite in meta-ultramafic rocks (Zhang et al., 1995). Coesite relics and their quartz pseudomorphs occur as inclusions in garnet, omphacite, kyanite and zoisite of certain eclogite bands.

According to Zhang et al. (1995), the peak eclogite metamorphism took place at 610-700°C and P > 27 kb, whereas the retrograde amphibolite facies, which is characterized

Figure II-19: Sketch map of the Bixiling Complex (after Zhang et al., 1995) and sampling localities.

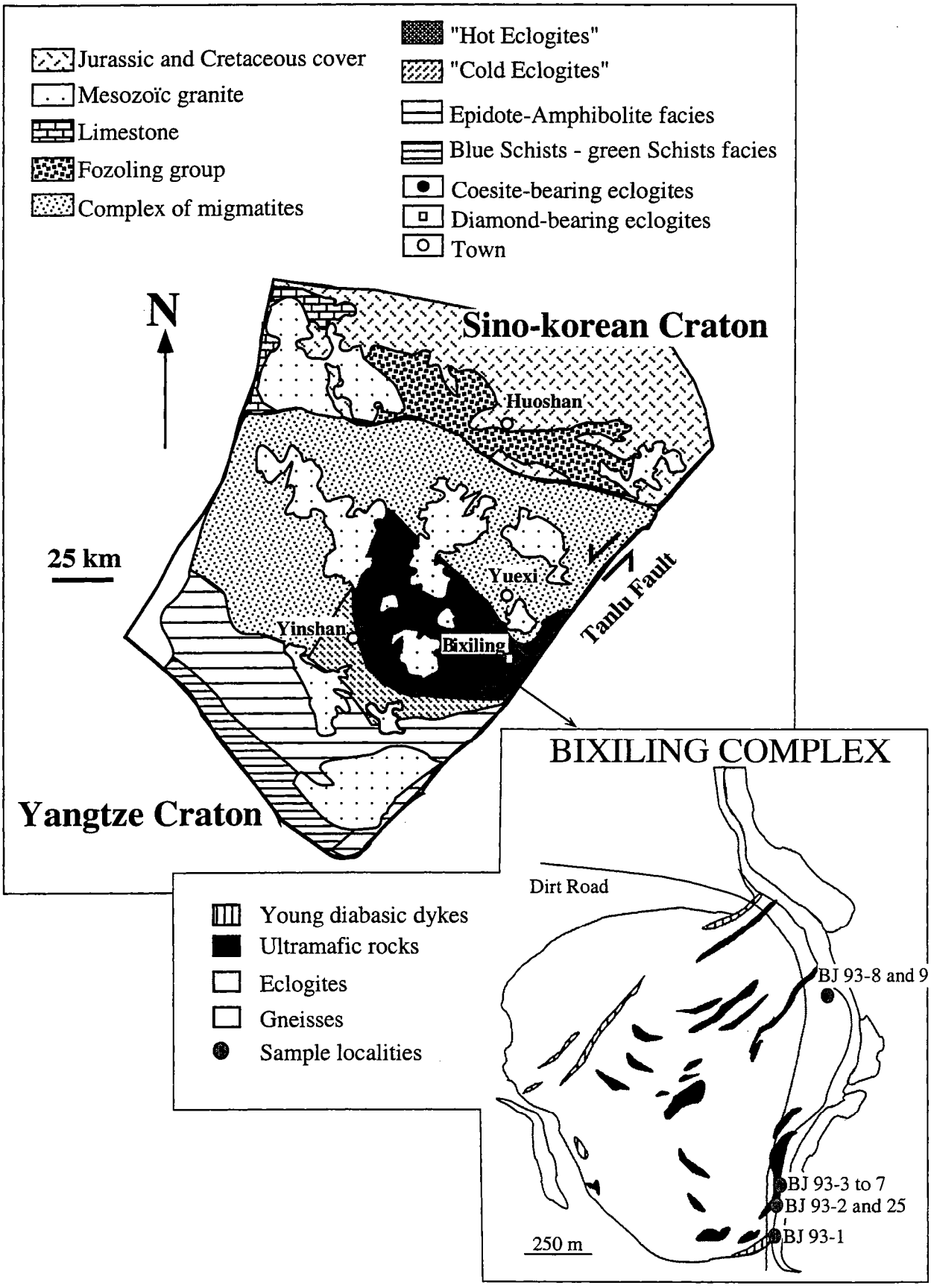

by symplectites of plagioclase and hornblende after omphacite, and replacement of tremolite after talc, formed at T < 600°C, and P < 6-15 kb. The meta-ultramafic assemblages (olivine + enstatite + diopside + garnet; Ti-clinohumite + diopside + enstatite + garnet + magnesite ± olivine) indicate their formation at 700-800°C and 47-67 kb. Thus, the ultramafic rocks appear to have recorded higher P and possibly higher T conditions than the associated mafic rocks. The discrepancy of P-T estimates may suggest (1) some uncertainties in the different geothermobarometers used, (2) neglect of ferric Fe in P-T calculations for the meta-ultramafic rocks, and (3) possible compositional change of constituent phases in mafic (eclogite) and ultramafic rocks in response to decompression and retrograde metamorphism (Zhang et al., 1995).

The primary intrusive and metamorphic ages of the Bixiling Complex have not been determined before, although a range of 200-240 Ma has been considered as the best estimate for the age of continental collision and UHP metamorphism in the Dabie terrane, based on both Sm-Nd garnet-omphacite (Li et al., 1993, 1994) and U-Pb zircon age studies (Ames et al., 1993, 1995). In addition, drastically different U-Pb zircon ages ranging from 420 Ma to ≈ 2.7 Ga (including upper and lower intercept ages) have been reported for the Bixiling eclogites (Liu et al., 1995; Cao et al., 1995). These authors considered that the UHP metamorphism took place in late Archean (≈ 2.7 Ga, Cao et al., 1995) or late Proterozoic (≈ 0.8 Ga, Liu et al., 1995). We will demonstrate that any Precambrian ages are not likely for the Bixiling Complex from geochronological and isotopic constraints.

## 3.3. Sample description

Representative rock types of the Bixiling Complex were sampled for the present study. They include six eclogites, two garnet peridotites of the eclogite facies, one amphibolite, and one granitic gneiss representing the country rock. Eclogite samples are essentially composed of garnet and omphacite, with variable amounts of phengite, kyanite, rutile, zoisite and opaques. The UHP metamorphism is clearly expressed by the presence of coesite as inclusions in garnet and omphacite (Fig. II-20). Other petrographic features of the eclogites include: (1) presence of symplectites of amphibole and plagioclase along the margin of omphacite, (2) presence of fine-grained amphiboles around garnet, and (3) transformation of phengite to fine-grained biotite. Overall, most of these rocks have preserved the eclogite facies parageneses.

The two meta-ultramafic rocks are garnet peridotite in composition. They contain variable amounts of garnet, clinopyroxene, orthopyroxene and titano-clinohumite (BJ93-9). Olivine is found in sample BJ93-8 and shows effects of serpentinization. The associated amphibolite (BJ93-2) occurs as small blocks enclosed in granitic gneiss. Zhang et al. (1995)

Figure II-20: Photomicrograph of a coesite-bearing eclogite (BJ 95-5). Coesite occurs as inclusion in omphacite. The characteristic radial fractures around coesite or quartz pseudomorph is shown. Total horizontal width ~1000μm. Upper view with open nicols; lower view crossed nicols.

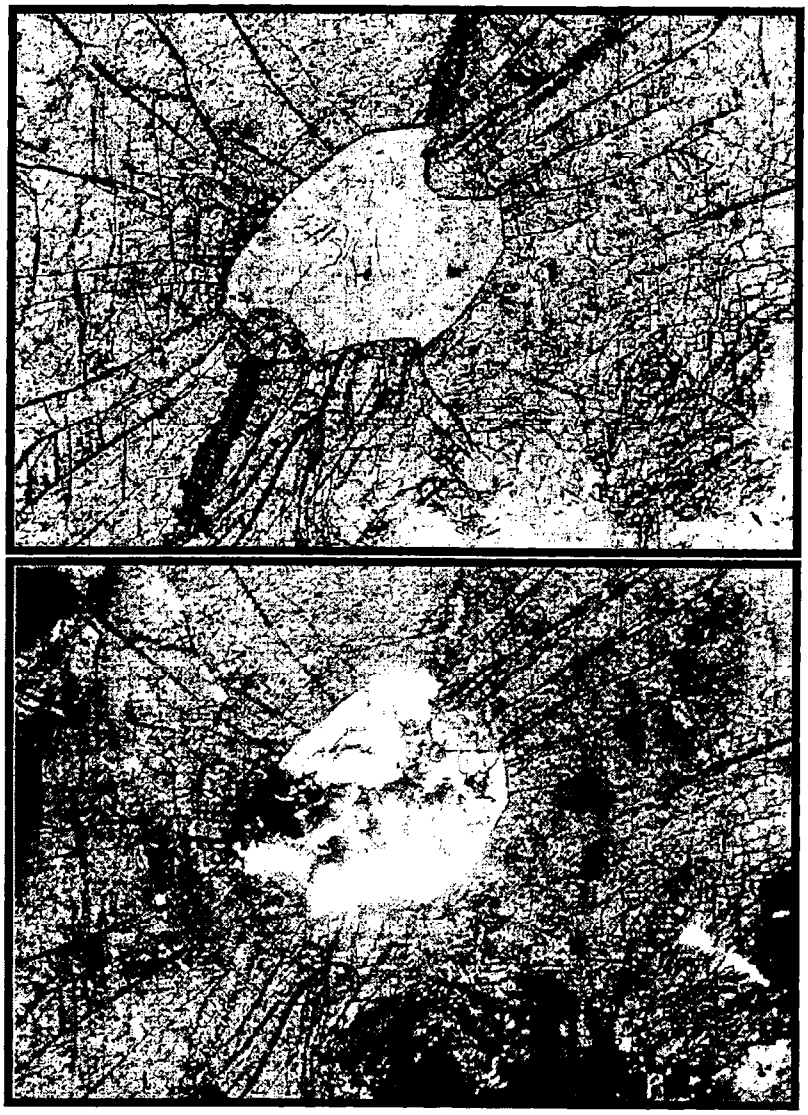

proposed that the amphibolite was produced by retrograde metamorphism from eclogite through extensive amphibolitization. The present mineral assemblage is composed of amphibole, plagioclase, epidote, garnet, quartz, biotite and accessory apatite and opaques. In addition to this occurrence, amphibolite bands may develop along fractures of eclogite layers (see Fig. II-19 of Zhang et al., 1995). From textural and field relations it is clear that this amphibolite is either completely or extensively retrograded eclogite.

The only sample of country gneiss (BJ 93-1) is of trondhjemitic composition. It consists of quartz, plagioclase, alkali feldspar, biotite, zoisite, sphene, muscovite and accessory apatite and zircon.

## 3.4. Analytical Procedures

### 3.4.1. Major and trace element analyses

Major elements and most trace elements were determined by XRF using a Philips spectrometer at the Université de Rennes 1. Analytical uncertainties range from 1 to 3% for major elements; ≈ 5% for trace elements with concentrations ≥ 20 ppm, and ≈ 10% for those < 20 ppm. Nb was determined with long counting time so the precision was maintained at ≈ 10% even for concentrations less than 5 ppm. REE abundances were determined by the isotope dilution method using the routine procedures employed at Rennes. Overall analytical uncertainties are ≈ 3% for all rare earth elements.

### 3.4.2. Isotopic analyses

In order to facilitate sample dissolution, garnet (0.8 to 1.8 g) grains were first ground in a boron carbide mortar with a small amount of silica gel (60 silonized; Merck), and then washed ultrasonically in quartex water. This grinding procedure was not applied to omphacite samples (0.2 to 0.7 g). Sample dissolution was carried out in two steps: (1) acid digestion ($HNO_3$ + HF) in sealed Savillex beaker on a hot plate (80°C) for 7 to 14 days (14 days for garnets and 7 days for other minerals), and followed by (2) 7-day teflon bomb dissolution for the residue (especially for garnets). Total dissolution is guaranteed in all cases. Separation of Sm and Nd was done using the routine two-column ion exchange techniques which include (1) a group separation of light rare earth elements through a cation exchange column (1 x 18 cm, packed with Bio-Rad AG50W-X8, 200-400 mesh resin), and (2) a purification of Sm and Nd through a second exchange column (0.6 x 7 cm, packed with Kel-F teflon powder with HDEHP as exchange medium), conditioned and eluded with dilute HCl. For the phengite Rb-Sr analyses, samples of 50-60 mg were used and the dissolution followed that for garnet and omphacite except teflon bomb. Complete dissolution took two to three days.

Mass analyses were performed using a 7-collector Finnigan MAT-262 mass spectrometer in static mode for Sr and in semi-dynamic mode for Nd. $^{87}Sr/^{86}Sr$ ratios were normalized against the value of $^{86}Sr/^{88}Sr = 0.1194$. The long-term analyses on NBS-987 Sr standard yielded $^{87}Sr/^{86}Sr = 0.710233 \pm 16$ (for 26 analyses). $^{143}Nd/^{144}Nd$ ratios were normalized against the value of $^{146}Nd/^{144}Nd = 0.7219$ and were further adjusted to the La Jolla Nd standard = 0.511860. During the period of data aquisition, the La Jolla Nd standard gave $^{143}Nd/^{144}Nd = 0.511854 \pm 11$ (2 $\sigma_D$, for 14 analyses).

The uncertainty in concentration measurement by isotope dilution is 1 to 2% for Rb, 0.5 to 1% for Sr, and 0.2 to 0.5% for Sm and Nd depending on concentration levels. However, the uncertainties for ratio measurements using mixed spikes are better than those calculated from individual errors for concentrations. We estimated the uncertainty on Rb/Sr ratios 1-2% and Sm/Nd ratios 0.2-0.5%. Procedural blaks are Rb = 90 pg, Sr = 300 pg, Sm = 50 pg, Nd = 180 pg.

The decay constants ($\lambda$) used in age calculations are 0.0142 $Ga^{-1}$ for $^{87}Rb$ and 0.00654 $Ga^{-1}$ for $^{147}Sm$. Sm-Nd model ages were calculated based on depleted mantle ($T_{DM}$) assuming a linear evolution from $\varepsilon_{Nd}(T) = 0$ at 4.56 Ga to +10 at the present time. The equation used can be found in the footnote of Table II-2. Isochron ages were calculated using the regression program of ISOPLOT (Ludwig, 1990). Input errors used in age computations are $^{147}Sm/^{144}Nd = 0.2\%$, $^{143}Nd/^{144}Nd = 0.005\%$; $^{87}Rb/^{86}Sr = 2\%$, $^{87}Sr/^{86}Sr = 0.005\%$. The quoted errors throughout this paper represent $\pm 2\ \sigma_D$.

## 3.5. Results

### 3.5.1. Geochemical characteristics

The major and trace element concentration data are given in Table II-1. The eclogitic rocks of the Bixiling Complex show a large variation in chemical composition. In a TAS (total alkali vs silica) diagram (Fig. II-21) of Le Maître et al. (1989), all of them fall in the category of sub-alkaline basalt, although at least one sample (BJ93-25) is clearly of cumulate origin as evidenced from its low $SiO_2$ and high $Fe_2O_3$, $TiO_2$ and V contents (Table II-1).

Two garnet peridotites (BJ93-8 and -9) have rather peculiar chemical compositions. They are not only distinguished from each other in $Al_2O_3$, MgO, CaO, $Na_2O$, and Cr contents, but also from the "typical" upper mantle garnet peridotites, as represented by those from kimberlite pipes of southern Africa (Erlank et al., 1987). The Bixiling peridotites are lower in MgO (25-30%), but are much higher in "fertile elements" such as Al, Ca, Fe, Ti

Table II-1: Chemical compositions of eclogites and associated rocks from the Bixiling Complex.

| Sample No. | BJ 93-1 | BJ 93-2 | BJ 93-3 | BJ 93-4 | BJ 93-5 | BJ 93-6 | BJ 93-7 | BJ 93-8 | BJ 93-9 | BJ 93-25 | Chondrite |
|---|---|---|---|---|---|---|---|---|---|---|---|
| Analysis No. | 12377 | 12378 | 12379 | 12380 | 12381 | 12382 | 12383 | 12384 | 12385 | 12398 | Values |
| Rock type | trondhjem. | amphib. | eclogite | eclogite | eclogite | eclogite | eclogite | ga perid. | ga perid. | eclogite | used for normalization |
| SiO2 | 73.40 | 52.17 | 48.53 | 50.58 | 48.91 | 49.77 | 50.77 | 43.16 | 45.57 | 45.70 | |
| Al2O3 | 12.98 | 13.83 | 18.59 | 16.10 | 17.57 | 16.65 | 15.90 | 9.75 | 2.43 | 13.47 | |
| Fe2O3 | 2.08 | 11.84 | 7.58 | 9.09 | 8.78 | 8.14 | 8.87 | 15.29 | 16.81 | 18.56 | |
| MnO | 0.06 | 0.30 | 0.14 | 0.17 | 0.15 | 0.16 | 0.17 | 0.23 | 0.20 | 0.22 | |
| MgO | 0.64 | 3.66 | 7.19 | 8.39 | 7.70 | 8.96 | 8.40 | 24.63 | 30.44 | 7.01 | |
| CaO | 2.09 | 7.68 | 13.69 | 11.26 | 13.06 | 12.07 | 11.22 | 4.98 | 1.99 | 10.98 | |
| Na2O | 5.04 | 3.37 | 1.91 | 2.40 | 2.06 | 2.25 | 2.41 | 0.47 | 0.14 | 2.40 | |
| K2O | 1.30 | 1.67 | 0.00 | 0.25 | 0.26 | 0.20 | 0.27 | 0.00 | 0.00 | 0.05 | |
| TiO2 | 0.32 | 2.30 | 0.65 | 0.73 | 0.68 | 0.42 | 0.71 | 0.34 | 0.53 | 2.34 | |
| P2O5 | 0.03 | 0.71 | 0.09 | 0.10 | 0.03 | 0.02 | 0.11 | 0.02 | 0.01 | 0.01 | |
| LOI | 0.82 | 1.03 | 0.51 | 0.35 | 0.39 | 0.44 | 0.38 | 0.29 | 0.94 | -0.49 | |
| TOTAL | 98.76 | 98.56 | 98.88 | 99.42 | 99.59 | 99.08 | 99.21 | 99.16 | 99.06 | 100.25 | |
| Trace elements (in ppm), by XRF | | | | | | | | | | | |
| Nb | 5.8 | 5.7 | 1.1 | 1.2 | 0.8 | 0.7 | 1.2 | 1.3 | 0.9 | 3.5 | |
| Zr | 182 | 127 | 47 | 33 | 24 | 20 | 35 | 19 | 14 | 36 | |
| Y | 30 | 50 | 14 | 12 | 12 | 10 | 12 | 4 | 5 | 26 | |
| Sr | 193 | 177 | 458 | 235 | 209 | 174 | 231 | 185 | 91 | 60 | |
| Rb | 28 | 39 | 2 | 7 | 6 | 6 | 8 | 0 | 1 | <1 | |
| Co | 3 | 23 | 25 | 40 | 33 | 35 | 38 | 127 | 154 | 51 | |
| V | 35 | 229 | 158 | 198 | 226 | 158 | 201 | 77 | 116 | 794 | |
| Ni | 5 | 6 | 89 | 45 | 90 | 66 | 46 | 760 | 890 | 22 | |
| Cr | 15 | 11 | 647 | 217 | 429 | 109 | 221 | 1416 | 2766 | 42 | |
| Ba | 474 | 487 | 31 | 668 | 72 | 105 | 820 | 15 | 25 | 68 | |
| Ga | 15 | 18 | 14 | 15 | 15 | 14 | 15 | 7 | 5 | 22 | |
| Cu | 3 | 19 | 81 | 46 | 48 | 41 | 50 | 46 | 70 | 27 | |
| Zn | 45 | 99 | 49 | 59 | 60 | 56 | 57 | 110 | 152 | 124 | |
| Th | 3 | 2 | <1 | <1 | 1 | <1 | <1 | 1 | 2 | <1 | |
| Pb | 10 | 7 | 6 | 2 | 2 | 3 | <1 | 2 | 4 | 5 | |
| Trace elements (in ppm), by Isotope Dilution Method | | | | | | | | | | | |
| La | 44.52 | | | 3.48 | | 1.72 | 4.46 | 1.19 | 0.43 | | 0.315 |
| Ce | 92.41 | | | 7.81 | | 4.37 | 9.71 | 3.64 | 1.45 | | 0.813 |
| Nd | 43.53 | | | 5.55 | | 3.31 | 6.66 | 2.80 | 1.35 | | 0.595 |
| Sm | 8.01 | | | 1.63 | | 1.01 | 1.82 | 0.761 | 0.435 | | 0.193 |
| Eu | 1.692 | | | 0.758 | | 0.507 | 0.820 | 0.346 | 0.174 | | 0.0722 |
| Gd | 6.59 | | | 2.09 | | 1.40 | 2.15 | 0.869 | 0.575 | | 0.259 |
| Dy | 5.31 | | | 2.20 | | 1.61 | 2.20 | 0.905 | 0.752 | | 0.325 |
| Er | 3.22 | | | 1.32 | | 1.00 | 1.29 | 0.579 | 0.620 | | 0.213 |
| Yb | 3.08 | | | 1.21 | | 0.94 | 1.19 | 0.577 | 0.779 | | 0.208 |
| Lu | 0.464 | | | 0.182 | | 0.140 | 0.178 | 0.093 | 0.128 | | 0.0323 |

Figure II-21: TAS (total alkali vs silica) classification diagram for eclogites from the Dabie and Su-Lu terranes. The Bixiling rocks are shown in solid dots. Additional data are from Jahn (unpublished). Symbols: pic-b = picritic basalt, teph basn: tephrite basanite; phon = phonolite; tr-bas = trachybasalt; bas = basalt; tr-and = trachyandesite; b-and = basaltic andesite; and = andesite; trach = trachyte; dac = dacite; rhy = rhyolite.

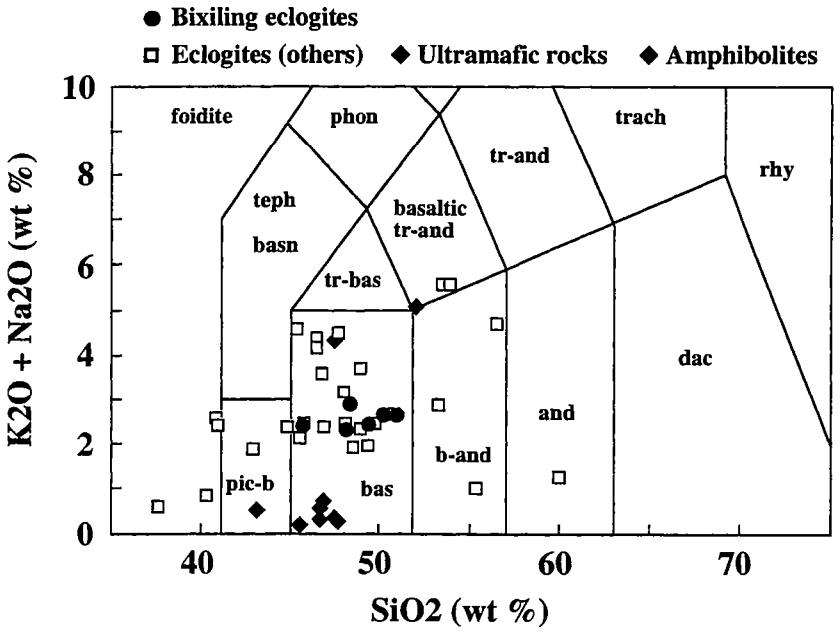


Figure II-22: REE distribution patterns of (a) eclogites, (b) ultramafic rocks, (c) trondhjemitic gneiss from the Bixiling Complex. REE patterns of N-MORB, CFB, and Archean trondhjemitic gneisses (or TTG) are also shown for comparison. Reference data from the literature.

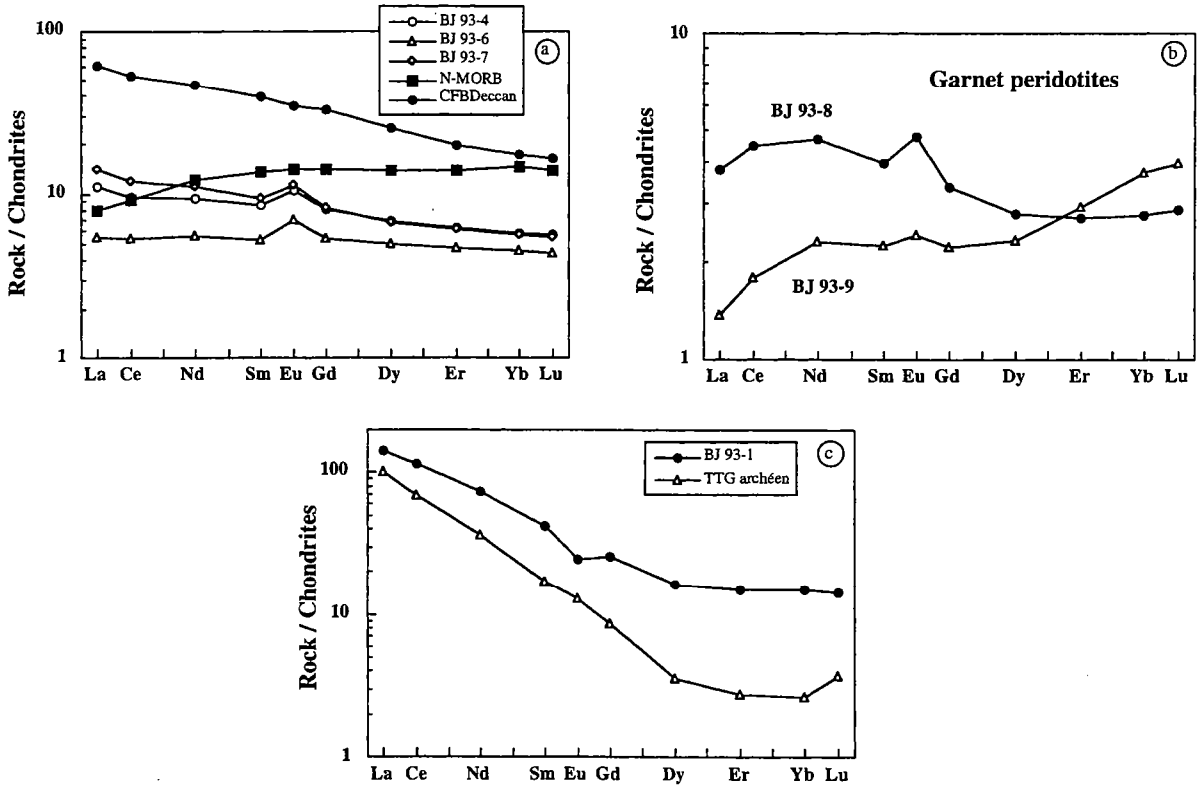

and Na. Trace elements Zr, Sr and V are relatively enriched, too. To some extent, their relatively low MgO make them similar to some peridotitic komatiites, but other features such as the low $CaO/Al_2O_3$ ratio (about 0.5 for BJ93-8) and low CaO and $Al_2O_3$ contents (about 2% in BJ93-9) make their direct comparison untenable. In any case, these rocks are not likely to represent residues after mantle melting (as garnet peridotite xenoliths in kimberlite pipes), nor to represent ultrabasic liquids like komatiites. They were probably formed as cumulates during the differentiation of the Bixiling Complex.

The REE data for three eclogites, two garnet peridotites and one trondhjemitic gneiss are given in Table II-1 and their distribution patterns are shown in Fig. II-22. PM (Primitive Mantle)-normalised spidergrams are presented in Fig. II-23. The three eclogites have rather similar patterns with variable degrees of LREE enrichment (Fig. II-22a). They are distinguished from the typical N-MORB pattern by the relatively low HREE and slightly enriched LREE. This suggests that they were not derived by differentiation from an N-MORB parental magma. The consistent positive Eu anomalies indicate an original plagioclase cumulate. For the three eclogites, significant negative Nb anomalies and discernible positive Sr and Ba anomalies are found in all cases (Fig. II-23). The negative Nb anomaly is particularly important because it is indicative of crustal contamination in the pre-metamorphic magmatic evolution. The positive Sr anomalies could be interpreted as due to the presence of plagioclase cumulate.

The REE patterns of two garnet peridotites (Fig. II-22b) are unusual and difficult to interpret. Like the three eclogites, they also possess positive Eu anomalies. Their relatively high abundances are significantly different from those of garnet peridotites from kimberlite pipes, or common alpine-type peridotites (MacDonough and Frey, 1989). The patterns suggest that these two peridotites represent a more advanced crystal cumulation or as a residual solid after separation of liquid. In addition, the spidergrams for two garnet peridotites show positive Sr and Th anomalies and enrichment in K and Ba. These features are not inconsistent with crustal contamination. Further petrogenetic modelling is not warranted given the limited data set. In conclusion, from the elemental abundance patterns it appears that the original magma chamber of the eclogite and peridotite protoliths has experienced crustal contamination during the differentiation process.

Amphibolite (BJ93-2) shows a composition sufficiently different from those of eclogites, and it cannot be easily explained by fractional crystallization of the same magma batch or by retrograde metamorphism from the associated eclogites. A comparison of immobile elemental abundances (Table II-1) clearly indicates that it is higher in $Fe_2O_3$, $TiO_2$, $P_2O_5$, Nb, Zr, and Y, but is significantly lower in $Al_2O_3$, MgO, CaO, Ni and Cr than the eclogites. This casts doubt on the hypothesis that this rock represents a retrograde

Figure II-23: PM- (Primitive Mantle) normalized spidergrams for the Bixiling rocks. Negavie Nb anomalies are clearly shown in eclogites. Trondhjemitic gneiss shows characteristic negative anomalies in Nb, P2O5 and TiO2. PM values used are from Sun and McDonough (1989).

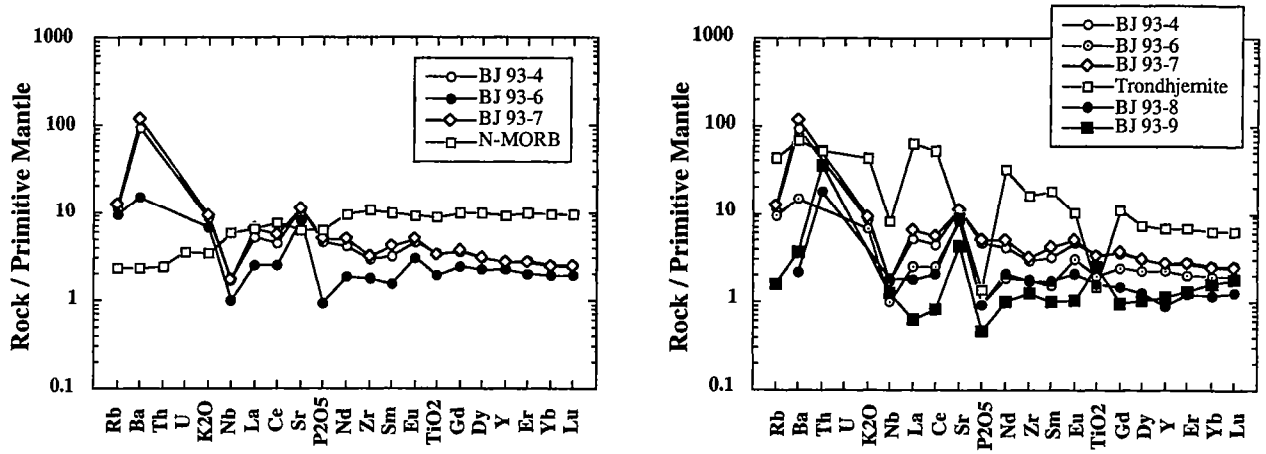


Figure II-24: Whole-rock $\varepsilon_{Nd}$ vs $^{147}Sm/^{144}Nd$ diagram for eclogites from the Bixiling Complex and other occurrences in the Dabie and Su-Lu terranes. Data are mainly from Jahn et al. (1994; 1995a; in preparation). Additional data are from Li et al. (1993), Okay et al. (1993) and Ames et al. (1995).

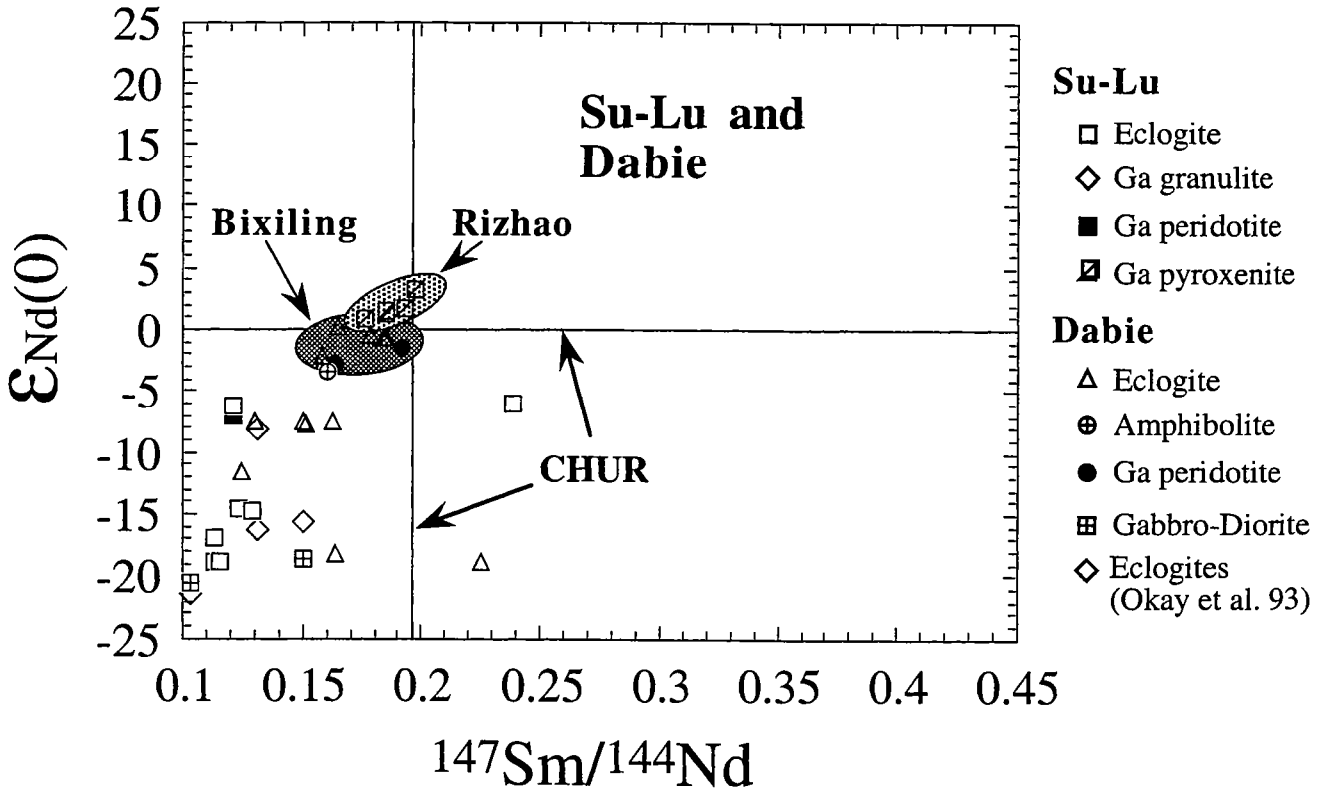

metamorphism from these eclogites (Zhang et al., 1995). It is possible that chemical composition might have been modified during metamorphic recrystallisation through the increase of water activity, but the obvious distinction between amphibolite and eclogites in terms of "immobile elements" such as $Al_2O_3$, $TiO_2$, Nb, Zr, Ni and Cr does not support this possibility. Therefore, the amphibolite appears to have a genetically different protolith. Note that the amphibolite analyzed here is not the same as the amphibolite layers developed along fractures of eclogite layers described by Zhang et al. (1995).

The only granitic gneiss sample (BJ 93-1) is of trondhjemitic composition with $Na_2O/K_2O \approx 3.8$. It shows a typical post-Archean granitic REE pattern with enriched LREE, nearly flat HREE and distinct negative Eu anomaly (Fig. II-22c). The trondhjemite shows negative anomalies in Nb, P and Ti, a feature commonly observed for granitic or upper continental crustal rocks.

### 3.5.2. Whole-rock isotopic data

Rb-Sr and Sm-Nd whole-rock and mineral isotopic data are given in Table II-2. When compared with all the eclogites from the Dabie and Su-Lu terranes, the Bixiling Complex has distinctive Sr and Nd isotopic compositions (Figs. II-26 and II-25).

The eclogites and ultramafic rocks (garnet peridotites) have narrow ranges of $^{147}Sm/^{144}Nd$ ratios (0.16 to 0.19) and $\varepsilon_{Nd}(0)$ values (-0.6 to -2.7; Fig. II-23). This is in strong contrast with the majority of eclogites from the Su-Lu and Dabie terranes which have generally lower but more variable $^{147}Sm/^{144}Nd$ ratios and much lower $\varepsilon_{Nd}(0)$ values (-6 to -20), the lowest among the world's known eclogite occurrences (Jahn et al., 1994, 1995a). In an $\varepsilon_{Nd}(0)$ vs $^{87}Sr/^{86}Sr$ diagram (not age-corrected, Fig. II-25), the Bixiling rocks fall just beneath the "mantle array" in the third quadrangle. When the Nd-Sr isotopic compositions are age-corrected, the data points would be placed closer to the contemporary paleo-mantle array. Although not clearly shown in Fig. II-25, the age-corrected $\varepsilon_{Nd}(T)$ values are chondritic within analytical errors (Table II-2). Thus, the range of isotopic compositions and trace element characteristics as outlined earlier suggest that the original magma was derived from the upper mantle and probably contaminated by small amounts of crustal rocks during the differentiation process. For comparison, the Nd-Sr isotopic data of garnet pyroxenites from the Rizhao area (Su-Lu terrane) fall in the "mantle array". Such a feature is consistent with that the Rizhao ultramafic bodies represent "mantle xenoliths of tectonic origin" (as opposed to mantle xenoliths of volcanic origin brought to the surface by volcanism, these are pieces of mantle peridotites and pyroxenites emplaced in crustal environments through tectonic processes). Their Sr and Nd isotopic compositions could be representative of the lithospheric mantle in the Su-Lu and Dabie regions. The Bixiling magma, on the other hand, was

Figure II-25: $\varepsilon_{Nd}$ vs 87Sr/86Sr diagram for eclogites and ultramafic rocks from the Bixiling Complex and other occurrences in the Dabie Su-Lu terranes. Data are mainly from Jahn et al. (1994; 1995a; in prep.), Ames et al. (1995) and Li et al. (1993). The Bixiling data fall slightly below the present "mantle array", which may be indicative of contamination by the lower crust or depleted granulite rocks during magma differentiation processes. Dashed lines represent the primitive mantle Nd-Sr isotopic compositions at T = 220 Ma. The Bixiling data at 220 Ma fall within the "paleo-mantle array".

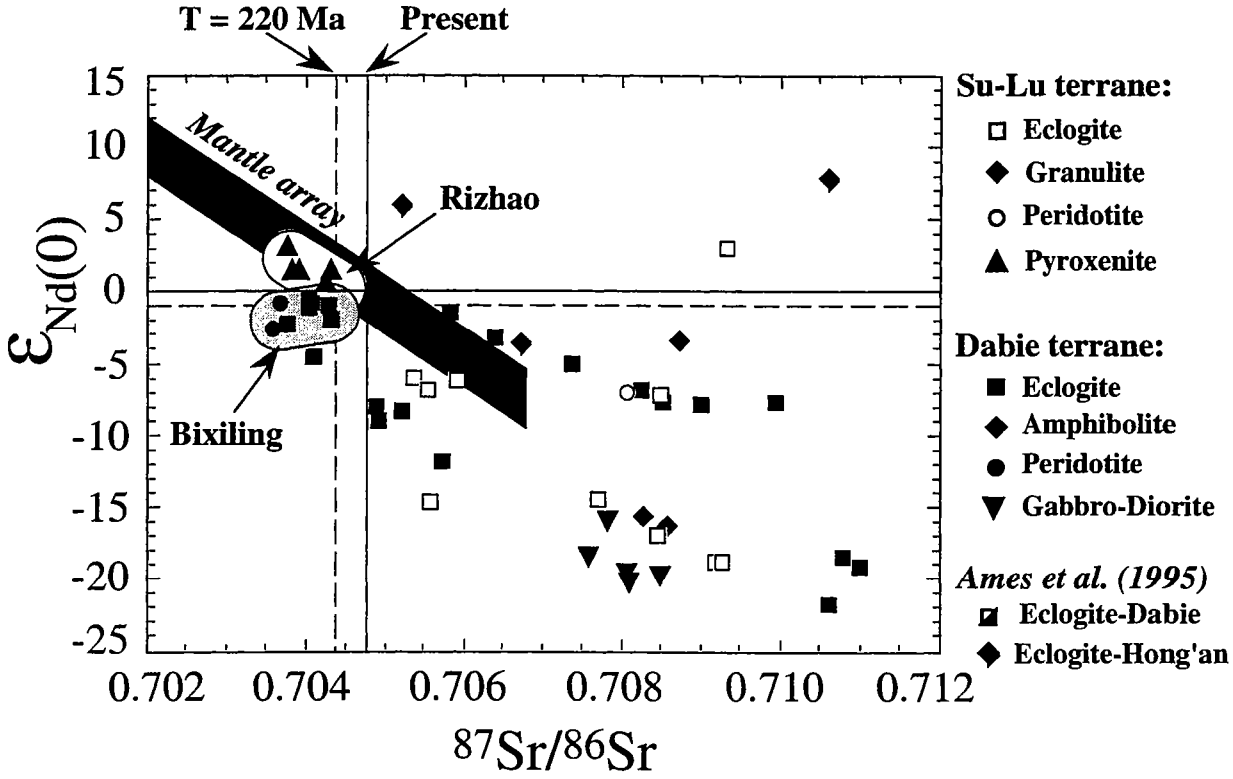


Figure II-26: Whole-rock Sm-Nd isotopic data showing no isochron relationship. However, the display of data points suggest a relatively young age, but not a Proterozoic or Archean age.

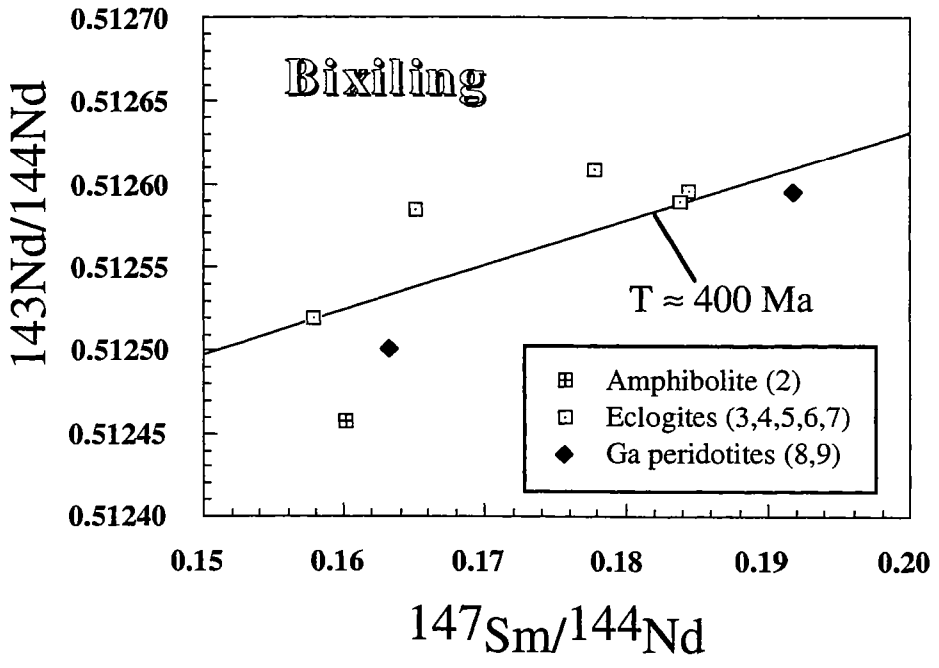

Table II-2: Whole rock and mineral Rb-Sr and Sm-Nd isotopic data for the Bixiling eclogites and associated rocks.

| Sample No. | Analysis No. | Rock type/Mineral | [Rb] (ppm) | [Sr] (ppm) | 87Rb/ 86Sr | 87Sr/ 86Sr | ± 2 sm | I(Sr) (220 Ma) | [Sm] (ppm) | [Nd] (ppm) | 147Sm/ 144Nd | 143Nd/ 144Nd | ± 2 sm | eNd(0) | eNd(T) (220 Ma) | f(Sm/Nd) | T(DM) (Ga) |
|---|---|---|---|---|---|---|---|---|---|---|---|---|---|---|---|---|---|
| BJ93-01 | 12377 | trondhjemite WR | 28.65 | 198.35 | 0.418 | 0.710847 | 8 | 0.709539 | 8.00 | 43.53 | 0.1111 | 0.512407 | 5 | -4.5 | -2.1 | -0.43 | 1.10 |
| | duplicate (non-spiked) | | | | | | | | | | | 0.512410 | 4 | -4.4 | | | |
| | | clinozoisite | 3.77 | 52.27 | 0.209 | 0.709760 | 8 | | | | | | | | | | |
| BJ93-02 | 12378 | amphibolite WR | 38.08 | 172.60 | 0.638 | 0.708761 | 8 | 0.706765 | 6.84 | 25.82 | 0.1601 | 0.512457 | 8 | -3.5 | -2.5 | -0.19 | 1.96 |
| | duplicate (non-spiked) | | | | | | | | | | | 0.512434 | 3 | -4.0 | -4.0 | | |
| | | biotite | 308.34 | 4.78 | 195.79 | 1.204429 | 8 | | | | | | | | | | |
| BJ93-03 | 12379 | eclogite WR | 0.14 | 456.33 | 0.001 | 0.703755 | 5 | 0.703752 | 1.96 | 7.51 | 0.1578 | 0.512520 | 4 | -2.3 | -1.2 | -0.20 | 1.71 |
| | | garnet | 0.02 | 7.25 | 0.007 | 0.703842 | 8 | | 0.21 | 0.17 | 0.7281 | 0.513307 | 8 | 13.1 | -1.9 | 2.70 | |
| | | omphacite | | 1013.2 | | 0.703789 | 8 | | 4.34 | 16.59 | 0.1582 | 0.512530 | 5 | -2.1 | -1.0 | -0.20 | |
| BJ93-04 | 12380 | eclogite WR | 5.81 | 232.31 | 0.072 | 0.704026 | 8 | 0.703799 | 1.63 | 5.55 | 0.1778 | 0.512608 | 6 | -0.6 | -0.1 | -0.10 | 2.29 |
| | | garnet | | | | | | | 0.99 | 0.37 | 1.6304 | 0.514634 | 13 | 38.9 | -1.3 | 7.29 | |
| | | omphacite | | 199.8 | | 0.701753 | 8 | | 0.78 | 2.81 | 0.1676 | 0.512572 | 8 | -1.3 | -0.5 | -0.15 | |
| | | phengite | 131.52 | 192.88 | 1.973 | 0.709764 | 8 | | | | | | | | | | |
| BJ93-05 | 12381 | eclogite WR | 6.35 | 206.97 | 0.089 | 0.704063 | 9 | 0.703785 | 1.45 | 4.75 | 0.1845 | 0.512596 | 4 | -0.8 | -0.5 | -0.06 | 2.88 |
| | | garnet | 0.1 | 1.85 | 0.149 | 0.704449 | 8 | | 0.30 | 0.12 | 1.4620 | 0.514369 | 9 | 33.8 | -1.8 | 6.43 | |
| | | omphacite | 3.87 | 243.05 | 0.046 | 0.703861 | 8 | | 1.63 | 5.36 | 0.1841 | 0.512609 | 7 | -0.6 | -0.2 | -0.06 | |
| | | phengite | 119.92 | 67.46 | 5.15 | 0.719472 | 10 | | | | | | | | | | |
| BJ93-06 | 12382 | eclogite WR | 4.40 | 168.40 | 0.076 | 0.704278 | 6 | 0.704041 | 1.03 | 3.37 | 0.1839 | 0.512590 | 4 | -0.9 | -0.6 | -0.07 | 2.84 |
| | | garnet | | | | | | | 0.45 | 0.14 | 1.8772 | 0.514980 | 6 | 45.7 | -1.5 | 8.54 | |
| | | phengite | 141.22 | 138.91 | 2.943 | 0.712345 | 8 | | | | | | | | | | |
| BJ93-07 | 12383 | eclogite WR | 6.56 | 229.74 | 0.083 | 0.704033 | 8 | 0.703774 | 1.84 | 6.74 | 0.1651 | 0.512584 | 4 | -1.1 | -0.2 | -0.16 | 1.77 |
| | | garnet | | | | | | | 0.90 | 0.46 | 1.1986 | 0.514016 | 14 | 26.9 | -1.2 | 5.09 | |
| | | omphacite | 0.45 | 747.64 | 0.002 | 0.703708 | 7 | | 0.88 | 2.82 | 0.1882 | 0.512585 | 8 | -1.0 | -0.8 | -0.04 | |
| | | phengite | 138.71 | 189.8 | 2.115 | 0.710436 | 9 | | | | | | | | | | |
| BJ93-08 | 12384 | ga peridotite WR | 0.09 | 177.64 | 0.002 | 0.703618 | 9 | 0.703612 | 0.77 | 2.85 | 0.1633 | 0.512500 | 5 | -2.7 | -1.8 | -0.17 | 1.96 |
| | duplicate (non-spiked) | | | | | | | | | | | 0.512503 | 4 | -2.6 | | | |
| | | garnet | | | | | | | 0.48 | 0.33 | 0.8665 | 0.513465 | 6 | 16.1 | -2.7 | 3.41 | |
| | | omphacite | 0.39 | 890.7 | 0.001 | 0.703645 | 9 | | 2.82 | 12.95 | 0.1319 | 0.512456 | 6 | -3.6 | -1.7 | -0.33 | |
| BJ93-09 | 12385 | ga peridotite WR | 0.22 | 86.91 | 0.007 | 0.703681 | 9 | 0.703658 | 0.43 | 1.36 | 0.1919 | 0.512594 | 17 | -0.9 | -0.7 | -0.02 | 3.85 |
| | duplicate (non-spiked) | | | | | | | | | | | 0.512574 | 5 | -1.2 | | | |
| BJ93-25 | 12398 | eclogite WR | | | | | | | | | | | | | | | |
| | | garnet | | | | | | | 1.60 | 0.55 | 1.7482 | 0.514784 | 16 | 41.9 | -1.7 | 7.89 | |
| | | omphacite | 16.74 | 95.08 | 0.509 | 0.704368 | 8 | | 1.51 | 3.48 | 0.2629 | 0.512664 | 7 | 0.5 | -1.4 | 0.34 | |

Note:
(1) eNd(0) = [(143Nd/144Nd)s / (143Nd/144Nd)CHUR - 1] x 10000, where s = sample, (143Nd/144Nd)CHUR = 0.512538.
(2) eNd(T), same definition, calculated as eNd(T) = eNd(0) - Q.f(Sm/Nd),T, where Q = 25.1 Ga-1, T = age, and f(Sm/Nd), see (3).
(3) f(Sm/Nd) = (147Sm/144Nd)s / (147Sm/144Nd)CHUR - 1, where (147Sm/144Nd)CHUR = 0.1967.
(4) TDM = 1/l . ln { 1 + [(143Nd/144Nd)s - 0.51315] / [(147Sm/144Nd)s - 0.2137]}

contaminated, probably by LIL-depleted lower crustal granulites of Proterozoic or late Archean age. This process might not modify significantly the Sr isotopic compositions, but could lower $\varepsilon_{Nd}$ values and introduce negative Nb anomalies as observed. Furthermore, the ancient zircon components as revealed in recent works (Cao et al., 1995; Liu et al., 1995) might find their potential sources.

Amphibolite sample BJ93-2 has a Nd isotopic composition similar to that of eclogites and peridotites, but its $^{87}Sr/^{86}Sr$ ratio is distinctly higher ($\approx$ 0.7088). This high ratio could have been acquired from enclosing granitic gneiss during retrograde metamorphism.

Trondhjemitic gneiss BJ93-1 has an $\varepsilon_{Nd}(0)$ value of -4.5, an $f_{Sm/Nd}$ of -0.43, and a model age ($T_{DM}$) of 1.1 Ga (Table II-2). This model age argues against any Archean ages for the gneisses in the Dabie terrane, a hypothesis held by many local geologists in the past and most recently, by Cao et al. (1995). Ames et al. (1995) obtained zircon U-Pb ages for some granitic gneisses. Their analytical data points are very close to the lower intercepts in concordia diagrams and give precise lower intercept ages of about 220 Ma. Their upper intercept ages, however, are loosely constrained at about 800 Ma. These ages of about 800 Ma are compatible with the young Sm-Nd model age, which together suggest that the trondhjemitic rock was formed in late Proterozoic.

For the eclogitic and peridotitic rocks, their relatively high $^{147}Sm/^{144}Nd$ ratios ($\approx$ 0.16 - 0.19) and likely crustal contamination render the calculated model ages (1.7 - 2.9 Ga, Table II-2) not very meaningful. The whole-rock Sm-Nd and Rb-Sr data do not allow construction of any significant isochrons (Fig. II-26).

### 2.5.3. Mineral isotopic data and mineral isochrons

Garnet, omphacite, and phengite were separated from 6 eclogites and 1 garnet peridotite for Sm-Nd and Rb-Sr isotopic analyses. The results are given in Table II-2. Sm-Nd and Rb-Sr mineral isochrons are shown in Figs. II-27 and II-28.

For the Sm-Nd analyses, all garnet-omphacite or garnet-omphacite-WR isochrons give a small range of ages from 210 to 218 Ma (2 sigma errors from 3 to 9 Ma; Figs. II-27b to II-27g). All of them have near-chondritic $\varepsilon_{Nd}(T)$ values of -0.1 to -1.8, but with errors of about $\pm$ 0.5 $\varepsilon$ unit. In addition, when all garnet data points aretreated alone, they form an "isochron" of similar or slightly greater age of 225 $\pm$ 7 Ma with $\varepsilon_{Nd}(T) = -2.5 \pm 1.1$ (Fig. II-27h).

For the Rb-Sr analyses, four eclogites produce a small range of phengite-WR or phengite-omphacite ages from 198 $\pm$ 13 Ma to 223 $\pm$ 15 Ma (Figs. II-28b to II-28e). This

Figure II-27: Sm-Nd mineral isochrons for 6 eclogites (a to f) and 1 peridotite (g). Garnet data alone also define an isochron (h) of very similar age and initial $\varepsilon_{Nd}$ value.

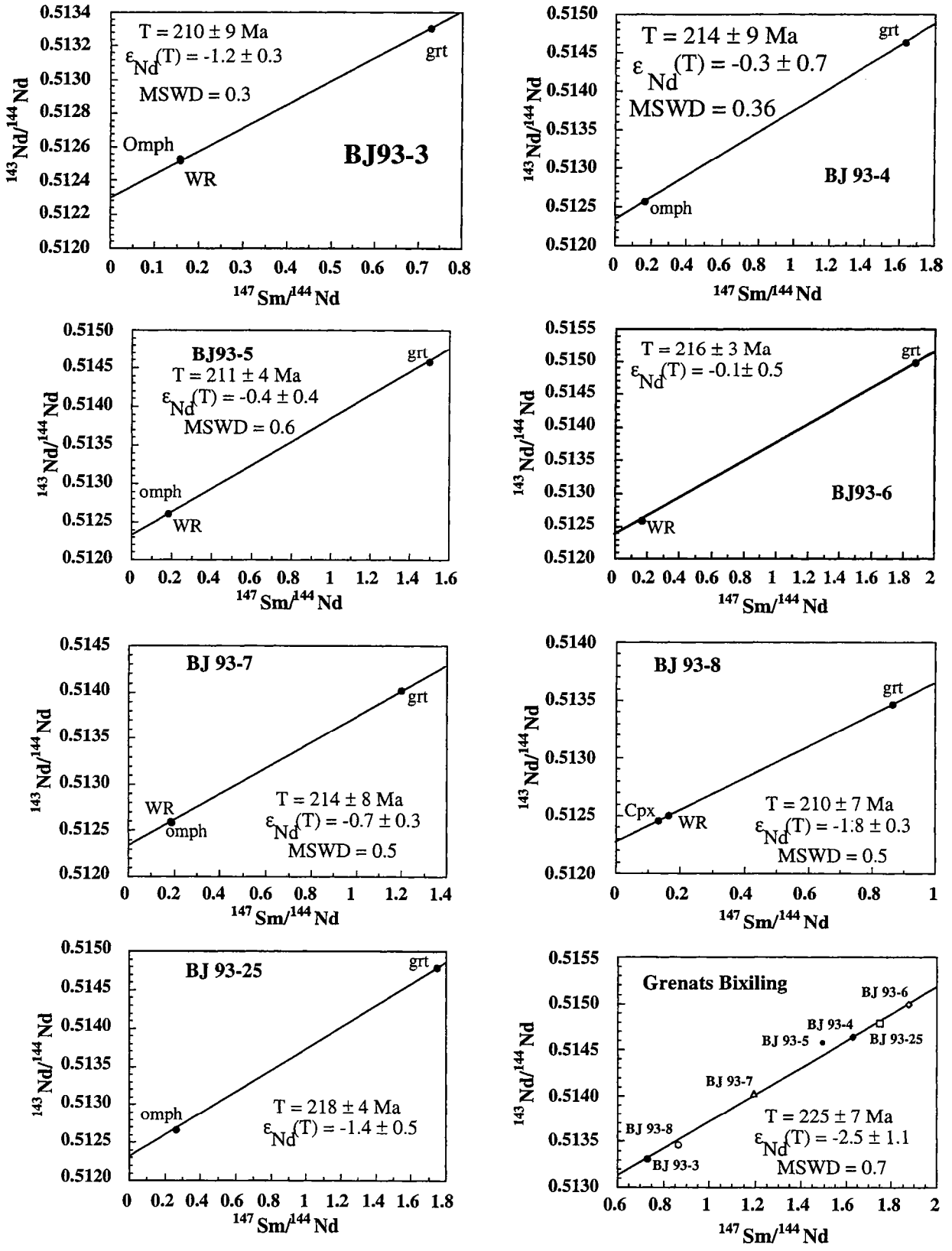

Figure II-28: Rb-Sr mineral isochrons for 1 amphibolite (a) and 4 eclogites (b to e). Phengite data alone also define an isochron (f) of very similar age and initial $^{87}Sr/^{86}Sr$.

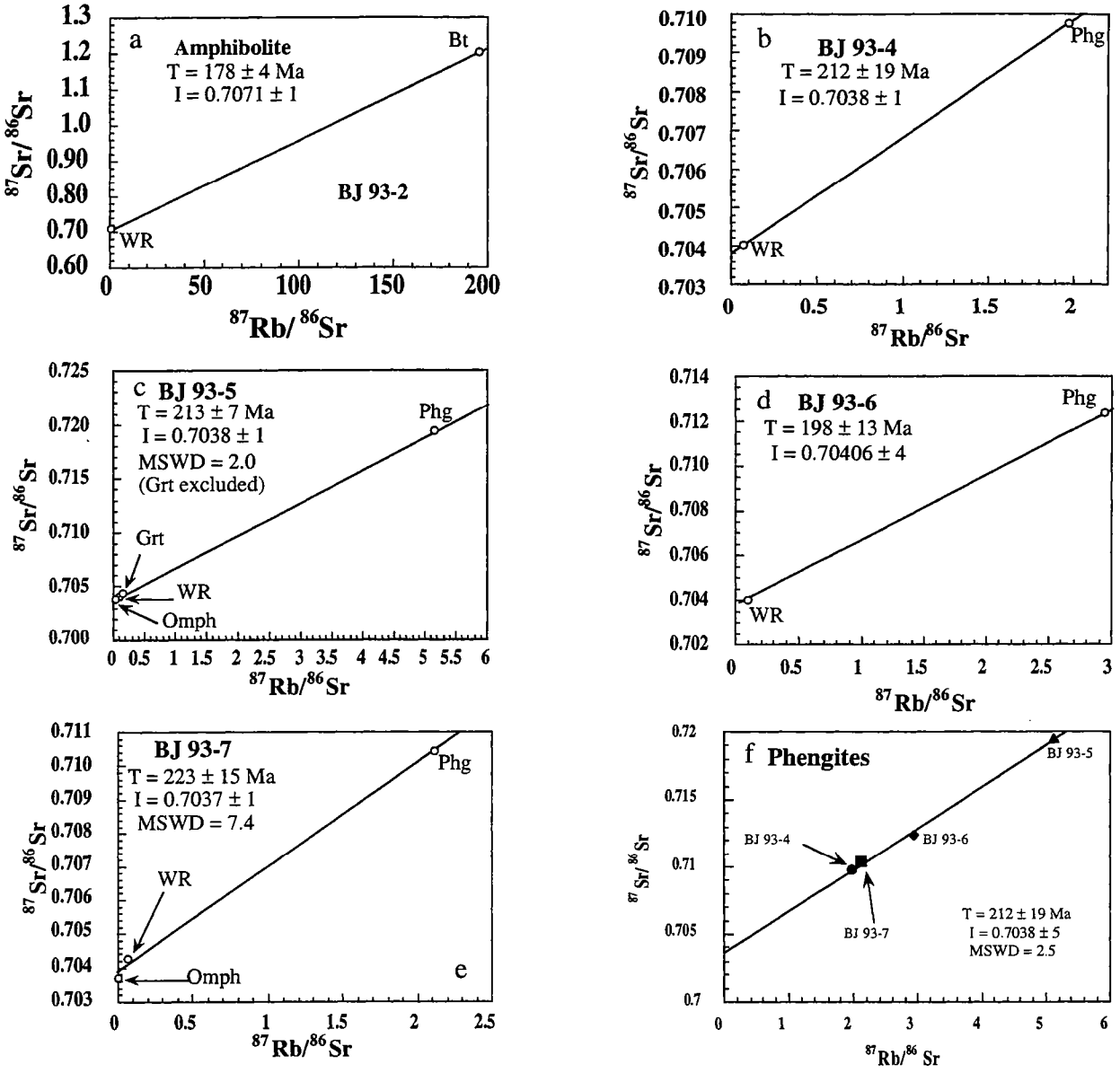

range is similar to that of the Sm-Nd mineral isochron ages. Again, if the four phengite data points are used alone, they yield a phengite isochron age of 213 ± 5 Ma. We shall address the special significance of the phengite Rb-Sr and garnet Sm-Nd ages in a later section.

Finally, a significantly younger Rb-Sr biotite-WR isochron age (179 ± 4 Ma) was obtained for amphibolite sample BJ93-2 (Fig. II-28a). All the above mineral isochron ages will be used to construct the cooling and uplift rates of the Bixiling complex in the following section.

## 3.6. Discussion

### 3.6.1. Age of the eclogite facies metamorphism and time of collision between the Sino-Korean and Yangtze cratons

The age of the UHP-HP (high-pressure) metamorphism and time of collision between the Sino-Korean and Yangtze cratons has long been debated and the issue is not yet completely resolved (Li et al., 1993, 1994; Gao et al., 1995; You et al., 1995). Isotopic age determinations on UHP rocks from the Dabie and Su-Lu terranes (Li et al., 1993, 1994; Ames et al., 1993, 1995; Maruyama et al., 1995) as well as the results of paleomagnetic studies (Lin et al., 1985; Zhao and Coe, 1987; Yang et al., 1991; Enkin et al., 1992) favor a Triassic time of collision. By contrast, sedimentological studies in the Qinling orogen to the west of Dabie Mountains indicate that the collision likely took place earlier in Ordovician about 400 Ma ago (Gao et al., 1995).

Published Sm-Nd isotopic ages generally range from 200 to 240 Ma (Li et al., 1993). Our new results of Sm-Nd garnet-omphacite(-WR) isochrons confirm this range and lead to several significant conclusions: (1) The concordant mineral Sm-Nd ages obtained for different rock types from the same layered complex indicate the attainment of isotopic equilibrium during the UHP metamorphism (T = 700 - 800°C, P ≥ 27 kb, from the combined P-T information of eclogite and ultramafic rocks). (2) The Sm-Nd mineral ages are identical with the zircon U-Pb ages of about 220 Ma for eclogites from the same region (Ames et al., 1993, 1995). This suggests that the blocking temperatures for garnet Sm-Nd and zircon U-Pb systems are either comparable or the cooling rate for the Bixiling Complex is very high. (3) The age of 210-220 Ma is considered as the most reliable estimate for the time of the UHP metamorphism and also the continental collision between the Sino-Korean and Yangtze cratons.

Different isotopic ages have also been reported. For example, Mattauer et al. (1991) gave several phengite $^{40}Ar/^{39}Ar$ plateau ages (668 ± 5, 491 ± 5, 500 ± 5 Ma) for the

eclogite from a small region near Yueshi, Dabie terrane. Ar/Ar ages older than about 220 Ma have been attributed to the presence of excess Ar in phengitic mica of HP-UHP origin (Li et al., 1994; Eide et al., 1994; Hacker and Wang, 1995). A similar case for the Dora Maira Massif in the western Alps has been clearly demonstrated (Tilton et al., 1989, 1991; Monié and Chopin, 1991; Arnaud and Kelley, 1994). More recently, a garnet-WR Sm-Nd isochron age of 481 ± 25 Ma was determined for a kyanite eclogite from central Dabie (Hubei Province), and two zircon U-Pb lower intercept ages of 471 ± 2 and 326 ± 25 Ma were reported for eclogite at Shima, eastern Dabie (You et al., 1995). Thus, it is possible that the orogenic history of the Dabie Mountains is highly complicated.

### 3.6.2. Fast cooling and fast uplift of the Bixiling Complex

In order to understand the significance of mineral isochron ages, the concept of blocking temperatures is important to keep in mind. As mentioned above, the comparable zircon U-Pb and garnet Sm-Nd ages suggest that the blocking temperature for the garnet Sm-Nd system may be as high as that of the zircon U-Pb system or the initial cooling rate after peak metamorphism must be very high. The zircon U-Pb system is commonly believed to be blocked as soon as the mineral is crystallized from an igneous or a metamorphic system. Watson and Harrison (1983) determined that the blocking temperature of zircon U-Pb system is ≥ 800°C.

A blocking temperature of ≈ 600°C for garnet Sm-Nd system has been suggested by Humphries and Cliff (1982) and Mezger et al. (1992). Other studies have proposed that garnet is more likely to have higher blocking temperatures (≥ 750°C; Jagoutz, 1988; Thöni and Jagoutz, 1992; Hensen and Zhou, 1995; Zhou and Hensen, 1995). As underlined by Burton et al. (1995), the blocking temperature is dependent on a number of factors including grain size, chemical composition, the nature of coexisting phases and the thermal histroy of the rock concerned. Therefore, garnet is not likely to possess a unique blocking temperature for U-Pb or Sm-Nd system. Here we add that the presence or absence of water in metamorphic condition may affect the elemental and isotopic diffusion rate, hence the calculation of blocking temperatures.

In an anhydrous system, Jagoutz (1988) suggested a high blocking temperature of about 850°C for cessation of Sm-Nd exchange between garnet and clinopyroxene. For the Bixiling eclogites, retrograde metamorphism is rather insignificant, but the presence of hydrous phases (e.g., Ti-clinohumite) in these rocks suggests that the system was not completely anhydrous (Zhang et al., 1995; Liou and Zhang, 1995). Consequently, the blocking temperature for the Bixiling Complex would likely be lower than 850°C. Moreover, Zhang et al. (1995) have identified garnet zoning in these eclogites (higher Mg towards grain

Figure II-29: Cooling and uplift paths for the Bixiling Complex as constructed from the ages and known blocking temperature data. Note the very high initial cooling rate (~40°C/Ma) and the rapid early uplift (~10mm/yr).

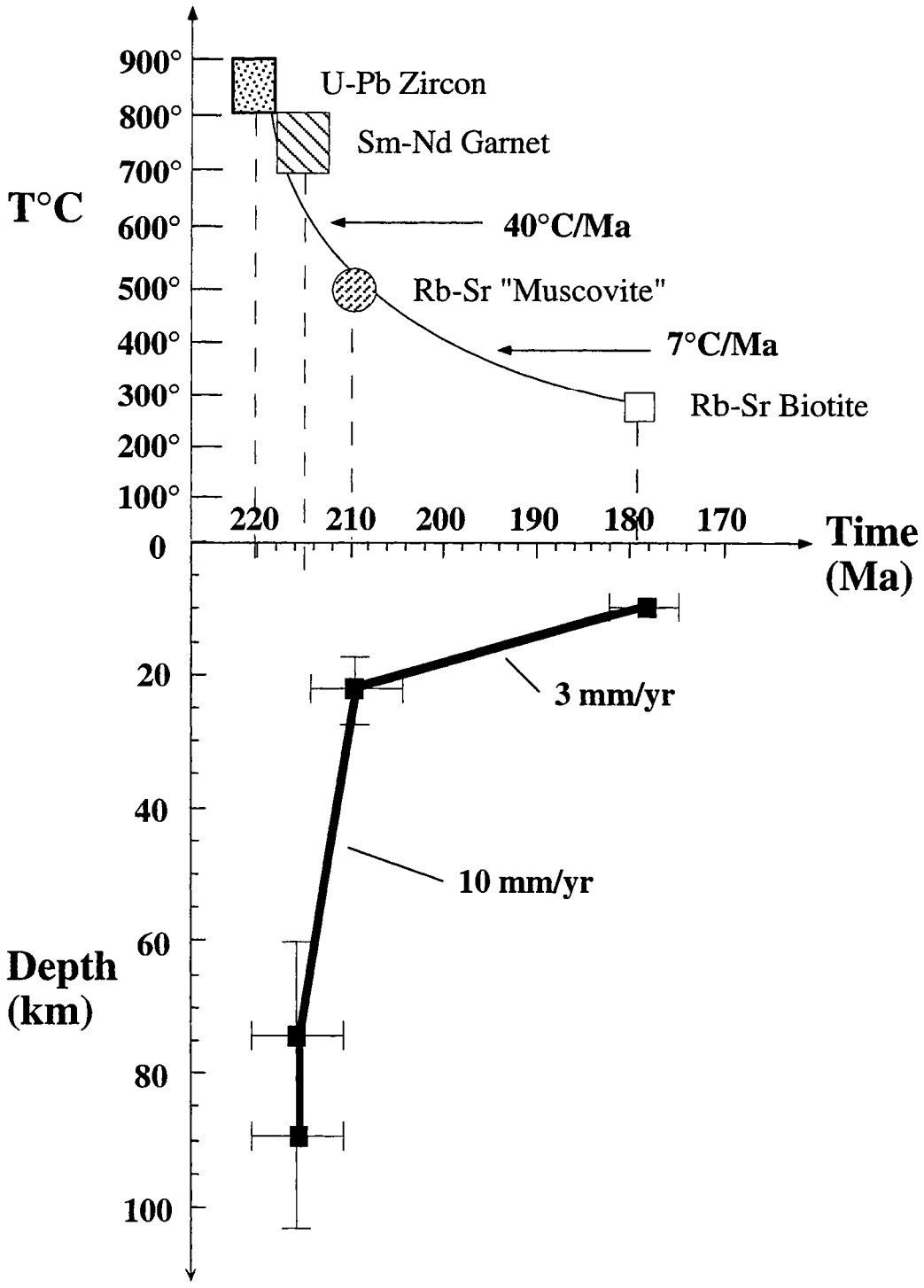

boundary) and determined the temperature of the peak metamorphism at 610-700°C based on a grt-cpx geothermometer. This temperature represents the cessation of Fe-Mg exchange in the minerals. For the Bixiling Complex and its vicinity, the close range of ages obtained by zircon U-Pb (219 ± 2, 218 ± 3, 214 ± 10, Ames et al., 1995), garnet Sm-Nd (averaged 213 Ma, see Fig. II-27) and phengite Rb-Sr (averaged 210 ± 10 Ma) methods strongly indicate a high initial cooling rate (≈ 40°C/Ma). This is deduced from zircon U-Pb (≥ 800°C) and muscovite Rb-Sr (≈ 500°C, Cliff, 1993; also assumed for phengite here) blocking temperatures. In this case, the garnet Sm-Nd blocking temperature cannot be uniquely determined.

The estimated high rate of cooling (about 300°C in 8 Ma or ≈ 40°C/Ma) is hinged on the assumption that the zircon U-Pb ages obtained by Ames et al (1995) are also valid for the Bixiling Complex. The zircon data of Liu et al. (1995) give an imprecise lower intercept age of 247 ± 68 Ma, which may be compared with the more precise ages of Ames et al. (1995).

The very high initial cooling rate recorded in the Bixiling Complex is exceptional. We note that the cooling rate for both the Dora Maira Massif in the western Alps and the Kotchetav Massif in Karzarkstan is about 20°C/Ma (Schertl et al., 1991; Jagoutz et al., 1990). The Bixiling thermal history is also in strong contrast to that of the eclogites from the Weihai area in the eastern end of the Su-Lu terrane (Jahn et al., 1995b). In the Weihai eclogites, garnet-WR tie-lines yield ages of 156 ± 3 Ma and 159 ± 3 Ma for two retrograded eclogites (now as garnet granulites). The young ages were interpreted to reflect a prolonged granulite facies recrystallisation at temperatures greater than the garnet Sm-Nd blocking temperature. Regardless of the controversial warming or cooling paths during the retrograde metamorphism from the eclogite to granulite facies (see discussion by Jahn et al;, 1995b), the temperatures at ca. 8-10 kb were estimated at 850° to 750°C, which are higher than the known garnet Sm-Nd blocking temperature of ≈ 600°C proposed by Mezger et al. (1992) or 700-750°C proposed by Hensen and Zhou (1995). This temperature could have lasted for a lengthy period and continuously reset the garnet Sm-Nd isotopic system until the blocking temperature was reached about 160 Ma ago.

Using the known P-T conditions of metamorphism and the various mineral ages obtained, an uplift trajectory (depth vs time) is also constructed (Fig. II-29). We note that the major exhumation event took place between 220 to 210 Ma, during which a very high initial uplift rate of ≈ 10 mm/year is deduced. By contrast, a much slower initial uplift rate of 1 mm/yr was estimated for the Weihai eclogites.

The implication derived from the very different rates of cooling and uplift recorded in the Bixiling Complex and the Weihai eclogites is that exhumation of UHP metamorphic rocks in the Dabie and Su-Lu terranes was not of the same pattern everywhere. Petrological and geochronological studies on other regions of the Dabie and Su-Lu terranes suggest a differential tectonic unroofing along strike of the collision zone (Liou et al., 1995; Ernst and Liou, 1995). Differential uplift and cooling within the Dabie terrane has been well documented by Chen et al. (1995).

### 3.6.3. Age of the protolith

In normal circumstances, the intrusive age of a layered complex may be determined by the WR isochron method provided the WR samples have maintained closed systems and possess sufficiently large spreads in Sm/Nd and $^{143}Nd/^{144}Nd$ ratios. Unfortunately, this is not the case for the Bixiling Complex. We have argued that the significant negative Nb anomalies (Fig. II-23) and the Nd isotopic signature (Figs. II-26 and II-25) can be best explained by crustal contamination during the magma differentiation. So the WR chemical and isotopic systems have not remained closed prior to the metamorphism (Fig. II-26). Moreover, the small range in Sm/Nd ratios is not really favorable for isochron construction, but this is not the principal obstacle because the range is *in theory* enough to make a crude estimate of age. Fig. II-26 shows that the scatter is much greater than expected and is most probably due to crustal contamination. Consequently, a direct age estimate using WR Sm-Nd systems is not possible.

Here we present an indirect method of estimating the intrusive age based on the garnet Sm-Nd and phengite Rb-Sr mineral isotopic systematics. The argument is based on the fact that the six garnet Sm-Nd data points alone (Fig. II-27h) give an "isochron" age and initial $\varepsilon_{Nd}(T)$ value similar to or slightly older than the seven garnet-omphacite pairs (Fig. II-27a to II-27g). A graphical representation is shown in Fig. II-30 and the relevant equations are given in Appendix 1 to explain why when a garnet-only isochron age approaches the ages of garnet-WR or garnet-omphacite ages, the intrusive and metamorphic events cannot be separated by a long time interval. In Fig. II-30, the cogenetic WR samples R1 and R2 are assumed to have the same initial Nd isotopic ratio. This assumption is not strictly valid because of the observed isotopic inhomogeneity shown in Fig. II-26. However, if the range of $^{143}Nd/^{144}Nd$ and $^{147}Sm/^{144}Nd$ ratios of WR samples (0.5125-0.5126; 0.16-0.19) are to be compared with those of garnet data (0.5133-0.5150; 0.7-1.9), then the isotopic inhomogeneity of WR samples becomes trivial and the argument presented in Fig. II-30 remains valid.

Fig. II-30 shows that if metamorphism took place some significant length of period after the initial magmatic intrusion, then we may obtain a series of mineral isochrons

Figure II-30: Sm-Nd isochron diagram explaining why the Bixiling Complex was intruded shortly before the UHP metamorphism (see text and Appendix 1 for explanation).

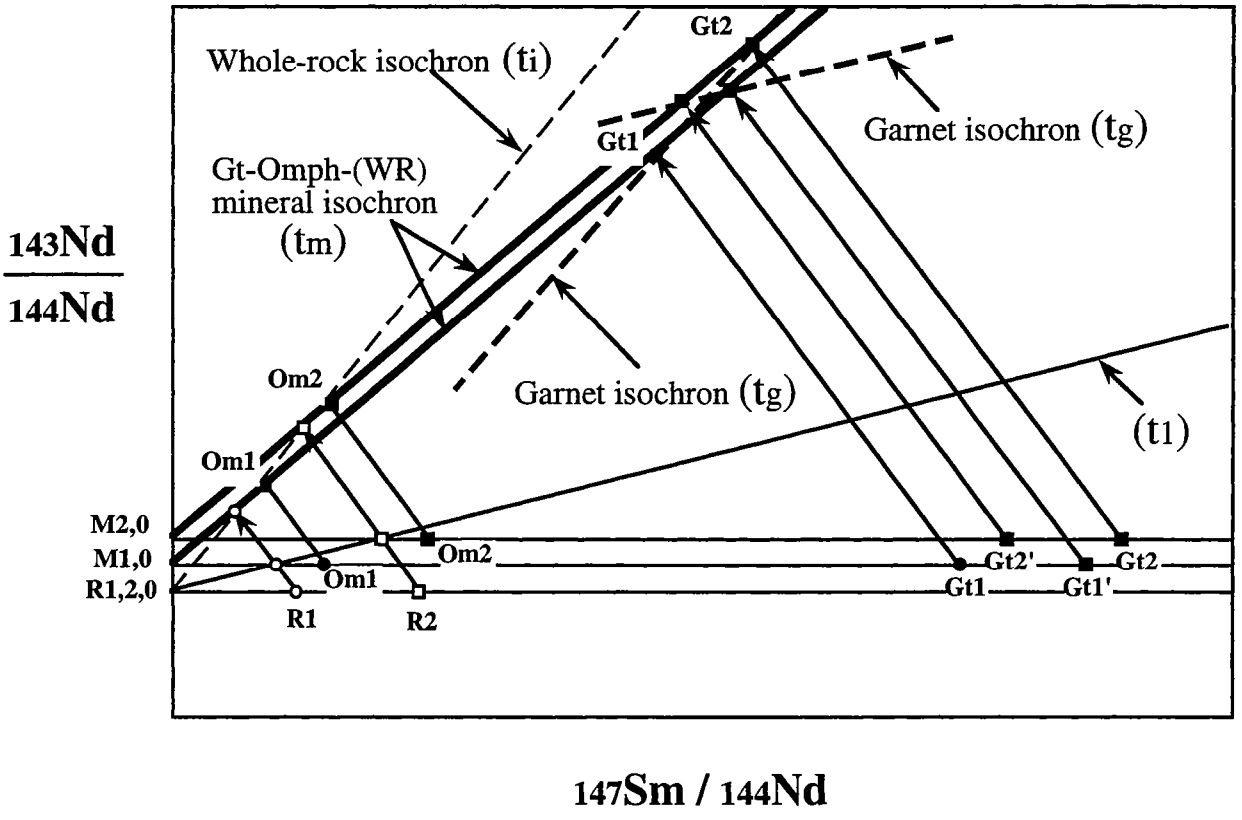

of identical metamorphic ages ($t_m$) from Gt-WR or Gt-Omph-WR data points. This is precisely what we have obtained in Fig. II-27. However, depending on the Sm/Nd ratios in metamorphic garnets ($Gt_1$ and $Gt_2$), garnet data points may have different slopes (positive or negative) or simply scattered. Only in a very strict condition that garnet-only isochron may give the same age as the other mineral isochrons. This would occur only when the metamorphism took place shortly after the initial magmatic intrusion. The equations in Appendix 1 fully explain the restricted condition.

Here we make a semi-quantitative calculation for the time interval between intrusive and metamorphic events (denoted as $\Delta t$). Using the range of $^{147}Sm/^{144}Nd$ (denoted as $\Delta Sm/Nd$) observed for the Bixiling WR samples, 0.03, we may calculate the differences in Nd isotopic growth (denoted as $\Delta^{143}Nd$) between eclogitic samples for any defined $\Delta t$ values. The results show that in $\Delta t$ = 1 Ga, 500 Ma and 300 Ma, the $\Delta^{143}Nd$ values would be increased by 0.000197, 0.000098, and 0.000059, respectively. The garnet-only isochron (Fig. II-27h) has an age of 225 ± 7 Ma and initial ratio of 0.512224 ± 0.000059 (2σ). If we allow the 2σ (about 1 ε-unit) to represent the time interval $\Delta t$, we then conclude that the intrusion and metamorphism could not be separated by more than 300 Ma. Note that this 2σ could be due only to the initial Nd isotopic variation produced by crustal contamination (Table 2 and Fig. II-26). If any Archean intrusive age is assumed as preferred by Cao et al. (1995), the rock samples would have $\Delta^{143}Nd$ as high as 0.000495 (for $\Delta t$ = 2.5 Ga). In this case the garnet data points would most likely show a considerable scatter.

The same excercise could be done for the phengite Rb-Sr systems, and similar conclusions are reached. Consequently, we conclude that the Bixiling complex has an intrusive age not much older than the metamorphic age of about 220 Ma. The two events could be contemporaneous or separated by a maximum time interval of 300 Ma. If the Complex was intruded in Proterozoic or Archean, it would be extremely fortuitous to have the garnet-only or phengite-only age similar to the other mineral isochron ages. In fact, the "young" protolith age is also consistent with the near-chondritic εNd values and relatively low $^{87}Sr/^{86}Sr$ ratios (Table II-2; Fig. II-25). At any rate, the Bixiling complex is a very special case in the entire Dabie and Su-Lu terranes.

### 3.6.4. Interpretation of ancient zircon ages

Recent publications of very old zircon U-Pb ages for the Bixiling eclogites by Cao et al. (1995) and Liu et al. (1995) have aroused much debate inside the Chinese science community about the time of the UHP metamorphism and continental collision, as well as the age of the Dabie and Su-Lu terranes. Cao et al. (1995) separated zircons from a single Bixiling eclogite sample and obtained a 4-point discordia with an upper intercept age of 2775

± 23 Ma, and a lower intercept age of 452 ± 78 Ma. They also obtained two phengite Ar-Ar plateau ages of 665 ± 13 and 662 ± 13 Ma. They considered that the Bixiling Complex intruded in the late Archean as revealed by the upper intercept age and took the "average" of four $^{207}Pb/^{206}Pb$ ages (2660 Ma) as the time of UHP metamorphism. Furthermore, they suggested that the entire Dabie Group was formed in the Archean. This is in contradiction with our young Sm-Nd $T_{DM}$ age of 1.1 Ga for the trondhjemitic gneiss (BJ93-1, Table II-1) and the late Proterozoic U-Pb upper intercept ages (800-900 Ma) for the gneisses and eclogites in this region (Ames et al., 1995). The phengite Ar-Ar ages of about 660 Ma are evidently due to the presence of excess Ar, which has been well documented by Li et al. (1994) and Hacker and Wang (1995), but considered geologically significant by Cao et al. (1995). We emphasize that the use of the average $^{207}Pb/^{206}Pb$ age as the time of UHP metamorphism is considered geochronologically groundless.

Nevertheless, the above Archean zircon ages have inspired a subsequent re-examination work of Liu et al. (1995). Their new zircon analyses failed to reproduce any late Archean ages as obtained by Cao et al. (1995). Instead, for the dark brown prismatic zircon suite they got an upper and lower intercepts of 2210 ± 39 and 907 ± 100 Ma; whereas for the yellowish brown suite, 818 ± 163 and 247 ± 68 Ma, respectively. These ages are difficult to interpret. However, using a variety of age information, Liu et al. (1995) suggested that the Bixiling protoliths were formed 2.2 Ga ago or earlier, and argued that the UHP metamorphism of the Bixiling complex most likely took place between 800-900 Ma. They interpreted the age of 400-500 Ma as a "second collision" between the Sino-Korean and Yangtze blocks, or as the time of retrograde metamorphism. The available Sm-Nd garnet ages of 210-250 Ma were considered as the time of recrystallization accompanying the exhumation and later amphibolitization.

We admit that the presence of old zircon components in the Bixiling complex is possible. As mentioned earlier, the presence of negative Nb anomalies in the eclogites (Fig. II-23) provides evidence for crustal contamination during the magma differentiation. Negative Ta and Nb anomalies have also been identified by Liu et al. (1995), but they ascribe them to a petrogenetic environment of island arc or continental margin. We consider that the ancient zircons could be interpreted as being derived from a lower crustal contaminant. Their ages could only reflect the time of their crystallisation in the lower crustal rock, but not necessarily the intrusive time of the Bixiling Complex. We reiterate that the overall geochemical features, the Sr-Nd isotopic signature, and the Sm-Nd and Rb-Sr mineral isochron ages point to the conclusion that the Bixiling Complex is a "young" intrusive body which underwent UHP metamorphism at about 220 Ma.

## 3.7. Conclusions

1. The eclogites and ultramafic rocks of the Bixiling Complex have trace element and Sr-Nd isotopic compositions characteristic of a mantle origin with small but variable amounts of lower crustal contamination.

2. The garnet-omphacite (or garnet-omphacite-WR) Sm-Nd isotopic data of five eclogites and one garnet peridotite yield a narrow age range of 210-220 Ma, which is identical with the zircon U-Pb ages for the eclogites from the same region in the Dabie Mountains (Ames et al., 1993, 1995). The phengite Rb-Sr ages are slightly but arguably younger (≈ 210 Ma). The age of 210-220 Ma represents the best estimate for the UHP metamorphism and the collision between the Yangtze and Sino-Korean cratons. We hence endorse the earlier conclusions reached by Li et al. (1993).

3. The garnet-only Sm-Nd isochron yields an age similar to or slightly older than the garnet-omphacite (or garnet-omphacite-WR) isochrons. This provides a strong argument for the Bixiling Complex to have been intruded shortly before the UHP metamorphism ($\Delta t \leq$ 300 Ma). The same conclusion is also reached with the phengite-only Rb-Sr isochron age argument. This intrusion is definitely not of Archean or Proterozoic age as the majority of the eclogites from the Su-Lu and Dabie terranes. In this sense, the Bixiling Complex is unique among the eclogites of the Dabie and Su-Lu terranes.

4. Differential tectonic unroofing along the strike of the Dabie and Su-Lu collision belt has been recognized (Zhang and Liou, 1995) and clearly demonstrated by the two contrasting cases: the Weihai eclogites (Jahn et al., 1995b) and the Bixiling complex. The Bixiling complex has recorded a very high initial cooling rate of ≈ 40°C/Ma and a rapid initial uplift of ≈ 10 mm/yr.

## Appendix 1. Intrusive Age of the Bixiling Complex

Referring to Fig. II-30, the Bixiling magma was intruded at time $t_i$ (= hypothetical whole-rock isochron age). Assuming that two cogenetic whole-rock samples $R_1$ and $R_2$ underwent eclogite facies metamorphism at time $t_1$, producing two metamorphic minerals (omphacite and garnet) $Om_1$, $Om_2$ and $Gt_1$, $Gt_2$. The Sm/Nd ratios of garnets are substantially higher than those of $R_1$ and $R_2$. At present, $R_1$-$Om_1$-$Gt_1$ and $R_2$-$Om_2$-$Gt_2$ isochrons or $R_1$-$Gt_1$ and $R_2$-$Gt_2$ tie-lines form two mineral isochrons of identical age $t_m$ but with different metamorphic initial ratios ($M_{1,0}$ and $M_{2,0}$). The Nd isotopic composition of metamorphic garnet ($Gt_1$) can be written as:

$$(^{143}Nd/^{144}Nd)_{Gt1} = (^{143}Nd/^{144}Nd)_{M1,0} + (^{147}Sm/^{144}Nd)_{Gt1}(\exp(\lambda t_m) - 1)$$

$$= [(^{143}Nd/^{144}Nd)_{R1,0}+(^{147}Sm/^{144}Nd)_{R1}(\exp(\lambda t_1) - 1)]$$

$$+ (^{147}Sm/^{144}Nd)_{Gt1}(\exp(\lambda t_m) - 1) \quad \text{---------- (1)}$$

Similarly, we may write:

$$(^{143}Nd/^{144}Nd)_{Gt2} = [(^{143}Nd/^{144}Nd)_{R2,0} + (^{147}Sm/^{144}Nd)_{R2}(\exp(\lambda t_1) - 1)]$$

$$+ (^{147}Sm/^{144}Nd)_{Gt2}(\exp(\lambda t_m) - 1) \quad \text{---------- (2)}$$

The slope connecting data points $Gt_1$ and $Gt_2$ defines a garnet isochron age $t_g$

$$[(^{143}Nd/^{144}Nd)_{Gt2} - (^{143}Nd/^{144}Nd)_{Gt1}] / [(^{147}Sm/^{144}Nd)_{Gt2} - (^{147}Sm/^{144}Nd)_{Gt1}]$$

$$= \exp(\lambda t_g) - 1 \quad \text{---------- (3)}$$

This slope could be of any degree, either positive or negative, depending on the Sm/Nd ratios of individual garnets formed during the metamorphism.

Subtracting equation (1) from (2), and with $(^{143}Nd/^{144}Nd)_{R1,0} = (^{143}Nd/^{144}Nd)_{R2,0}$, we obtain :

$$(^{143}Nd/^{144}Nd)_{Gt2} - (^{143}Nd/^{144}Nd)_{Gt1}$$

$$= [(^{147}Sm/^{144}Nd)_{R2} - (^{147}Sm/^{144}Nd)_{R1}](\exp(\lambda t_1) - 1)$$

$$+ [(^{147}Sm/^{144}Nd)_{Gt2} - (^{147}Sm/^{144}Nd)_{Gt1}](\exp(\lambda t_m) - 1) \text{ ------- (4)}$$

For the Bixiling Complex, the garnet isochron age happens to be nearly identical to the garnet-omphacite or garnet-omphacite-WR isochron ages; that is, $t_g = t_m$ . The only condition that satisfies both equations (3) and (4) is when the term :

$$[(^{147}Sm/^{144}Nd)_{R2} - (^{147}Sm/^{144}Nd)_{R1}](\exp(\lambda t_1) - 1)$$

equals to zero. In other words, $t_1$ is $\approx 0$. It is therefore concluded that the intrusion took place almost contemporaneously with, or very shortly before the UHP metamorphism.

Equations for the phengite and WR Rb-Sr systematics can be similarly derived. The phengite-only Rb-Sr isochron age (Fig. 11f) reinforces the conclusion for a very young intrusive age as obtained from the garnet-only Sm-Nd isochron age.

**Acknowledgments:**

VC is most grateful to the laboratory staff in Rennes for the tutoring of analytical techinques and to many members of the isotope geochemistry and petrology group for discussion on a variety of problems. BMJ is indebted to Prof. BL Cong of the Chinese Academy of Sciences for his invitation to the field work and sampling in the Dabie Mountains. We thank Jean Cornichet, Joël Macé, Nicole Morin, Odile Henin, and Martine Le Coz-Bouhnik for their assistance in various phases of analytical works. This paper is benefitted by the constructive comments of J.G. Liou and critical reviews of Klaus Mezger and Simon Harley. Nick Arndt provided useful suggestion for improvement of the final version.

# 4.Multichronometric approach on the Ultra-High Pressure Metamorphic terrane of Dabie Shan, Central China. Implications on the cooling rates.

**Valérie Chavagnac[1,2], Bor-ming Jahn[2]**

1: Universität Bern, Min. Pet. Inst., Gruppe Isotopengeologie, Erlachstrasse 9a, CH-3012 Bern, Switzerland; chava@mpi.unibe.ch

2: Géosciences Rennes (UPR 4661-CNRS), Université de Rennes1, Avenue du Général Leclerc, F-35042 Rennes Cedex, France; jahn@univ-rennes1.fr

**In prep for Journal of Geology**

## 4.1. Introduction

The Dabie Mountains and the Su-Lu region in the Central China are known to contain the largest distribution of Ultra-High Pressure Metamorphic rocks (UHPM) in the world. They are parts of the 2 000 km long Qinling-Dabie orogenic belt which was formed during the continent-continent collision between the Sino-Korean and Yangtze cratons. The discovery of coesite and its quartz pseudomorph in eclogites and metasedimentary rocks implies an UHP metamorphism, hence a subduction of crustal fragment to mantle depths. Consequently, the consensus on plate tectonic processes at convergent margins should be revised. Preservation of UHPM minerals has inspired numerous studies in an attempt to understand the deep subduction of continental crust but still the exhumation of UHPM rocks which preserved UHPM mineral relics is not well understood. Coesite occurs mainly as small inclusions within silicate minerals such as garnet, omphacite, kyanite and jadeite emphazing the extreme metamorphic conditions of the UHPM event. From field observations, coesite-bearing metamorphic rocks are found as disrupted lenses, layers or blocks within low-pressure gneisses. It rises up the on-going controversy regarding the "exotic/tectonic emplacement" or "in-situ" origin of the coesite-bearing metamorphic rocks. Although the eclogite host gneisses display not obvious UHPM features, it does not necessarily mean that they did not undergo the UHPM event. They may have metastably overstepped the short-lives UHPM conditions, and/or be extensively overprinted by retrograde metamorphism. Critical parameters such as field observations, P-T conditions, cooling/exhumation rates, protolith nature must be taken into consideration in any tectonic models. The tectonic relationship between coesite-bearing metamorphic rocks and their host gneisses can be provided by geochronological data performed on associated eclogites and quartzo-feldspathic gneisses.

In this present paper, we report new geochemical and isotopic data on a variety of host gneisses that surround two well known coesite-bearing eclogite bodies within the Dabie terrane: the Bixiling Complex and the UHPM rocks of Shuanghe. Multi-chronometric approach was employed to tackle the problem of eclogite-gneiss tectonic relationship. U-Pb SIMS, Sm-Nd, Rb-Sr, and Ar-Ar methods were applied on appropriate minerals (zircon, garnet, biotite and muscovite) in order to provide age contraints on the metamorphic evolution of the host gneisses. These data will be used (1) to discuss the protolith age of the host gneisses, (2) to examine whether the host gneisses have undergone an event coeval to UHP, and (3) to discuss the validity of exhumation and cooling rates from the literature.

Figure II-31: Geological map showing the Qinling-Dabie orogenic belt wedged between the two low-grade metamorphic terranes of the Sino-Korean craton to the north and the Yangtze craton to the south. The Su-Lu terrane considered as the extension of the Dabie terrane is offsetted to the north by the TanLU Fault. a) Location of the Qinling-Dabie orogenic belt in China, b) Note the occurrence of coesite and diamond only in the Dabieshan.

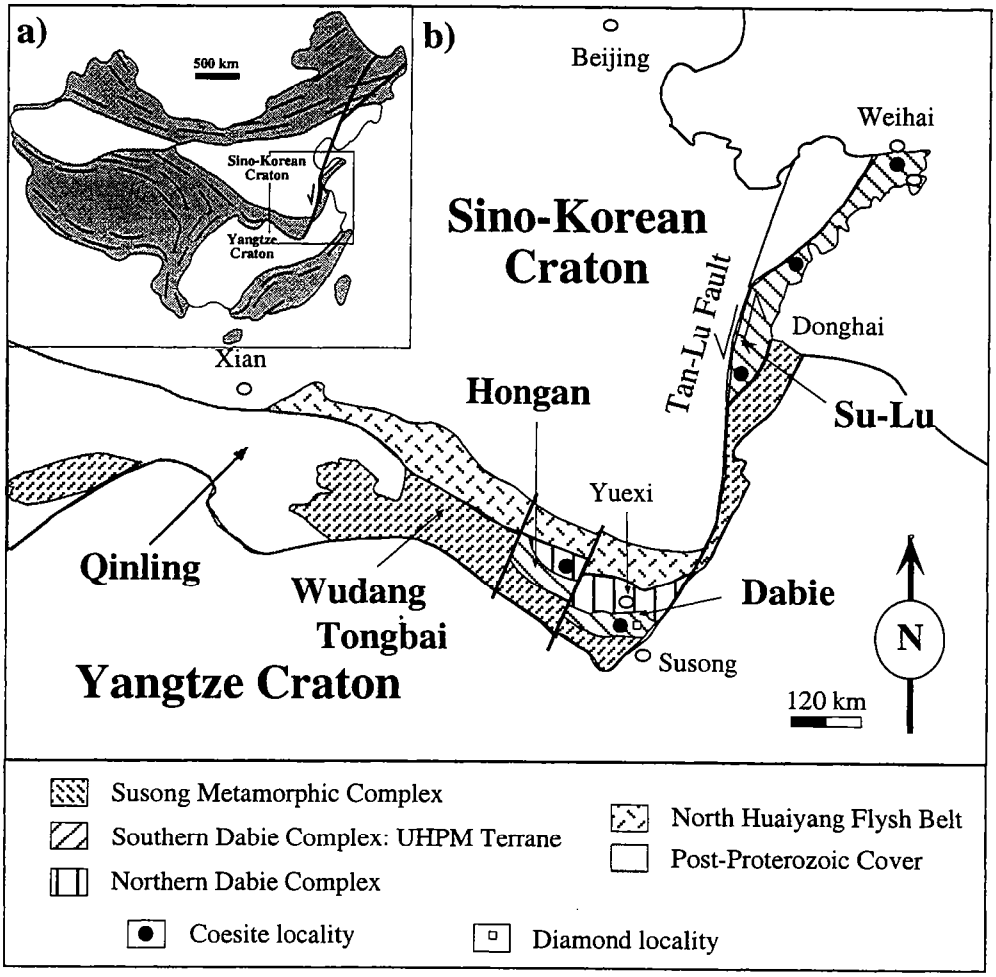

## 4.2. Geological setting and sample description of the Bixiling Complex and the UHPM tectonic slab of Shuanghe

The Qingling-Dabie orogenic belt is wedged between two low-grade metamorphic cratons, the Sino-Korean Craton to the north and the Yangtze Craton to the south (Fig. II-31a). It is considered as the product of the continental collision between these two cratons in the early Jurassic (Li et al. 1994, Ames et al. 1995, Chavagnac and Jahn, 1996). The orogenic belt is composed of a principal E-W trending zone of which the Dabie Shan represents the eastern part, and of a N-S trending zone (Su-Lu region) which have been displaced approximately 500 km northward by the NE trending left-lateral Tan-Lu Fault (Fig. II-31b; Okay and Sengör 1992, Yin and Nie 1993). Coesite and its quartz pseudomorph are widespread as minor fine-grained inclusions in garnet, omphacite, kyanite and epidote from eclogites (Wang et al. 1989, Okay 1993, Yang and Smith 1989, Wang et al. 1992, Zhang et al. 1993), marbles (Wang and Liou 1991, 1993, Xu et al. 1992), and very rarely gneisses (Wang and Liou 1991, Enami and Zhang 1990, Hirajima et al. 1990). Abundant eclogites occur as small lenses or blocks less than 20 m in size within serpentinized ultramafics, or as thin layers in gneisses or marbles. Compared to disrupted blocks, the Bixiling Complex represents the largest mafic-ultramafic eclogitic complex. The UHPM rocks of Shuanghe are of special interest as they are of metasedimentary origin and as coesite is located as small inclusions within jadeite of jadeite quartzite (Cong et al. 1995).

(A) The Bixiling Complex

The Bixiling Complex (1.5 $km^{2)}$ occurs as a layered intrusion enclosed within quartzo-feldspathic gneisses in the eastern part of the Dabie UHPM terrane (Fig. II-32a and II-32b). The eclogite rocks present the typical bi-mineralic paragenesis of garnet and omphacite but also the occurrence of coesite as inclusions within both of them. Petrological metamorphic studies on the mafic and ultramafic eclogites indicate that the metamorphic evolution followed a clockwise P-T loop from peak eclogitic conditions (T = 610-700°C; P > 27 kbars) to amphibolite facies metamorphism (T < 600°C; P < 6-15 kbars) (Zhang et al. 1995). From geochemical and Sr-Nd isotopic criteria, the complex is considered as a mantle-derived intrusive body which was slightly contaminated by the lower crust during its crystallization (Chavagnac and Jahn 1996). The quartzo-feldspathic gneisses are strongly foliated but they do not show any evidence of HP-HT metamorphic assemblages. They are composed of phengite, epidote, ± biotite, quartz, albite, titanite, zircon, apatite, ilmenite. This mineral association corresponds to the albite-epidote metamorphic facies related to the retrograde P-T path of the eclogite determined by Zhang et al. (1995). However, the chemical zonation of epidote and the destabilization of rutile into ilmenite are probably associated with higher P-T conditions, which may suggest that the gneisses have also undergone UHP metamorphism.

Figure II-32: a) General geological map of the DabieShan terrane. The tectonic contact between the differents units of the DabieShan are not well defined and are represented by a dashed line with question mark. The Bixiling Complex and the UHPM slab of Shuanghe belong to the Southern Dabie Metamorphic Complex which underwent the highest metamorphic conditions. b) Geological sketch of the Bixiling Complex. Sampling area of gneisses are reported with those of coesite-bearing eclogites given by Chavagnac and Jahn (1996). c) Sampling localities of gneisses within the UHPM slab of Shuanghe are indicated..

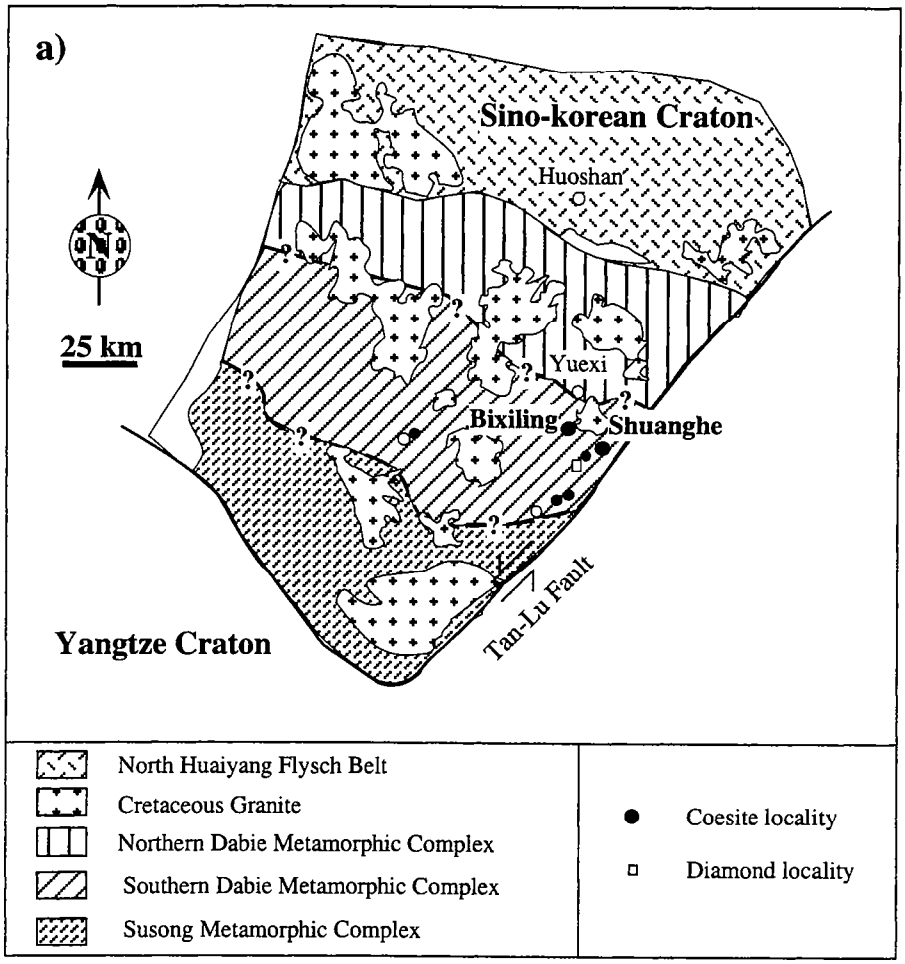


The Bixiling Complex

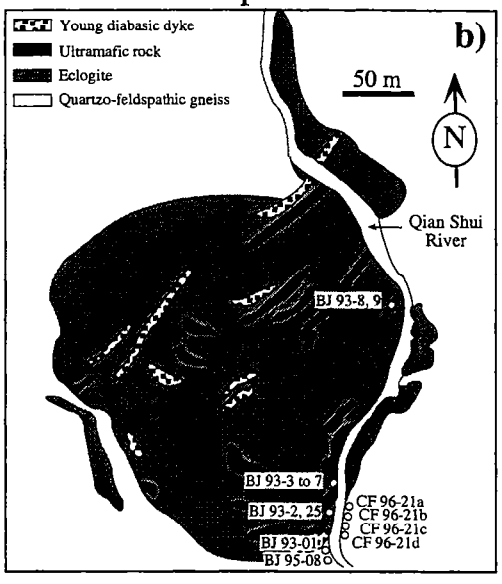


The UHPM slab of Shuanghe

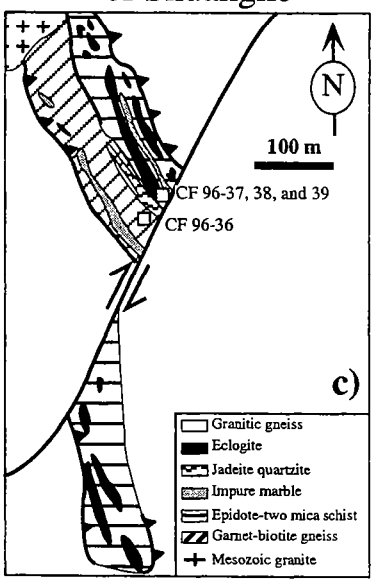

The UHP metamorphic age of the Bixiling Complex was based on seven Sm-Nd garnet-omphacite-WR isochrons at 210 ± 9 to 218 ± 4 Ma (Chavagnac and Jahn 1996) which are close to the 218.5 ± 1.8 Ma and 218.4 ± 2.5 Ma obtained on U-Pb zircon ages (Ames et al. 1993, 1995). The primary intrusive age was constrained from a Sm-Nd garnet only isochron. The garnets isochron provided an age as well as an initial epsilon Nd value similar to those on garnet-omphacite-WR isochrons, emphazing the reproducibility and the consistency in the age and also suggesting a mantle-derivation age for the Bixiling Complex shortly before the UHPM event, approximately 300 Ma (Chavagnac and Jahn 1996). The previous geochronological data have been interpreted in terms of thermochronology leading to the conclusion that the Bixiling Complex has recorded very high initial cooling rate ~40°C/Ma and a rapid initial exhumation rate of ~10mm/yr. However, no geochronological data have been done on the country rocks to examine whether they underwent a similar metamorphic chronology as the coesite-bearing eclogites. We sampled representative rock types of the host gneisses, which include 2 paragneisses (CF 96-21b and c) and 3 orthogneisses (CF 96-21a and d, BJ 95-08) collected along the Qianshui River as shown in Fig. II-32b.

(B) The UHPM rocks of Shuanghe

The second best known coesite-bearing eclogite locality is situated at Shuanghe, approximately 25 km south east of the Bixiling Complex, still in the Southern Dabie Metamorphic Complex (Fig. II-32a). It is exposed as an elongated tectonically-bounded thrust slab within foliated orthogneisses (Cong et al. 1995). The slab is offset by a dextral strike slip fault (Fig. II-32c; Liou et al. 1995). It is composed of an apparent layering of massive eclogite, retrograded eclogite, epidote-two mica schist, garnet and biotite bearing gneiss, marble with or without eclogite boudin, jadeite quartzite and amphibolite. The field association of these lithologies is more or less parallel to the foliation but it is clearly discordant to that of the host orthogneisses. The particular feature of this UHPM slab is the occurrence of coesite as inclusions in jadeite quartzite, arguing for the subduction of crustal material to mantle depth. In addition, the epidote-two mica schist presents the mineral association of biotite, ± phengite, epidote, quartz with minor amounts of garnet, kyanite, titanite, rutile, amphibole and plagioclase, and it is considered as the retrograde amphibolite association of a quartz eclogite (Cong et al. 1995). Furthermore, the close field association of quartz eclogite, garnet-biotite gneiss and epidote two mica schist may express the retrograde metamorphic path from the eclogite to the amphibolite facies metamorphism (Cong et al. 1995). Although the tectono-metamorphic evolution has been extensively studied (Cong et al. 1995, Liou et al. 1995, Liou et al. 1997), no geochronological data have been previously obtained on these gneisses to examine the peak eclogite facies age. Consequently, we sampled three epidote-two mica schists (CF 96-36, 37 and 38) and one garnet-biotite gneiss (CF 96-39) for a detailed geochronological study (Fig. II-32c).

## 4.3. Analytical procedures

### 4.3.1. Major and trace element analyses

Major elements were determined by X-ray fluorescence spectrometry (XRF) using a Philips spectrometer at the University of Rennes 1 (France). Analytical uncertainties range from ± 1% to ± 3%. Depending on concentrations levels of trace element whole rock sample were analyzed by ICP-MS (Elan 6000, Perkin Elmer) at the Laboratory of Geochemistry (C.A.S., Canton, China). The international standard of a granitic composition USGS-G2 was used to check the validity of the dataset. The samples were either dissolved with a mixture of HF and $HNO_3$ or with alkali fusion method.

### 4.3.2. Sr-Nd isotopic analyses

About 100 mg of powdered samples (or several mg in the case of mineral separates) were spiked with a $^{150}Nd$-$^{149}Sm$ and/or $^{87}Rb$-$^{84}Sr$ tracers before dissolution. Sample dissolution was carried out in two steps. First, the samples were attacked with a 3 : 1 mixture of (HF : $HNO_3$) in a sealed Savillex beaker at room temperature for one day. In order to suppress formation of any fluoride and facilitate the dissolution, the beaker was placed 3 times in an ultrasonic bath for 20 minutes. After one day, the solution was evaporated to dryness. The same acid mix was added a second time and closed beaker was heated at about 90°C (10 days for whole rock, 4 days for micas, 7 to 10 days for the other mineral separates) and placed in an ultrasonic bath for 10 minutes twice a day. After evaporating to dryness, any remaining fluorides were dissolved in 6 N HCl on a hot plate during several hours.

Separation of Rb, Sr, Sm and Nd was done using a routine two column ion-exchange technique. Firstly, a cation exchange column allowed the separation of Rb, Sr and a group of REE. The chemical separation of Sm and Nd from the other REE was done using a second column packed with Kel-F teflon® coated with HDEHP. Chemical separations were done at the University of Rennes 1 except for the garnet and kyanite fractions which were done at the University of Bern using the same chemical procedure.

For the whole rocks, Nd isotope analyses were done at the University of Rennes 1 using a double Re filament ($Nd^+$ emission) in a seven collector Finnigan MAT 262 mass spectrometer. $^{143}Nd/^{144}Nd$ were normalized against $^{146}Nd/^{144}Nd = 0.7219$. During the period of data acquisition, the AMES standard gave $^{143}Nd/^{144}Nd = 0.511962 \pm 0.000007$ (2 $\sigma$; n = 6). Nd isotopic compositions of garnet and kyanite were analyzed at the University of Bern using single Re filament ($NdO^+$ emission) in a VG Sector mass spectrometer in a single collector mode. The oxygen isotopic composition was determined by analysing pure $^{150}Nd$

spike as described by Wasserburg et al. (1981) and the average compositions gave $^{18}O/^{16}O$ = 2.074 $10^{-3}$ ± 1.16 $10^{-5}$ (1 σ) and $^{17}O/^{16}O$ = 3.86 $10^{-4}$ ± 1.32 $10^{-5}$ (1 σ). Mass interference and oxygen corrections as well as fractionation and spike corrections are done on-line during the measurement. La Jolla standard gave 0.511855 ± 0.000020 (2 σ; n = 3). The Sm isotopic compositions were analyzed either using a double Re filament in a seven collector Finnigan MAT 262 at the University of Rennes 1, or on a triple Ta-Re-Ta filaments on an AVCO, single collector at the University of Bern. Uncertainties on Sm/Nd ratios are less than ± 0.3%. Chemical procedural blank are below 150 pg for Sm and Nd.

Sm-Nd model ages were calculated relative to Depleted Mantle evolution. The Nd evolution of the Depleted Mantle is approximated by a third order polynomial fit:

$$\varepsilon_{Nd}(T) = 0.164\ T^3 - 0.566\ T^2 - 2.79\ T + 10.4$$ (Nägler and Kramers 1998)

For all whole rocks and mineral separates, Sr isotope analyses were done at the University of Rennes 1 using a single W filament with an additional acid (tantalum fluoride) in a seven collector Finnigan MAT 262 mass spectrometer. $^{87}Sr/^{86}Sr$ were normalized against the $^{88}Sr/^{86}Sr$ = 8.375209. During the period of data acquisition, the NBS 987 Sr standard gave 0.710264 ± 0.000015 (2 $\sigma_D$; n = 6). Rb isotopic compositions were analyzed by the same mass spectrometer on double Re filament. The uncertainty on Rb/Sr ratios was 2%. Chemical procedural blank is ~300pg for Sr and ~100pg for Rb.

The decay constants (λ) used in age calculations are 0.0142 $Ga^{-1}$ for $^{87}Rb$ and 0.00654 $Ga^{-1}$ for $^{147}Sm$. Isochron were calculated using the regression program of ISOPLOT (Ludwig, 1990).

#### 4.3.3. $^{39}Ar$-$^{40}Ar$ isotopic compositions

About 5 to 10 mg of each muscovite and biotite fractions were handpicked under the binocular microscope to achieve visual purity close to 100%. The samples were step-heated in a double vacuum resistance oven connected to a MAP® 215-50B mass spectrometer. Data are corrected for mass spectrometer background and discrimination (0.13%/amu favouring heavy masses).

Table II-3: Major and trace element concentrations of gneisses from the Bixiling locality and the UHPM slab of Shuanghe. Additional data: BJ 93-: Chavagnac and Jahn (1996) and BJ 93-32: Liou et al. (1997).

| sample | CF 96-21a | CF 96-21b | CF 96-21c | CF 96-21d | BJ 95-08 | BJ 93-01 | CF 96-36 | CF 96-37 | CF 96-38 | CF 96-39 | BJ 93-32 |
|---|---|---|---|---|---|---|---|---|---|---|---|
| locality | Bixiling | Bixiling | Bixiling | Bixiling | Bixiling | Bixiling | Shuanghe | Shuanghe | Shuanghe | Shuanghe | Shuanghe |
| rock | orthogneiss | paragneiss | paragneiss | orthogneiss | orthogneiss | orthogneiss | Ep-Bt-Ms schist | Ep-Bt-Ms schis | Ep-Bt-Ms schist | Grt-Bt gneiss | Bt gneiss |
| **Major elements by XRF in wt%** | | | | | | | | | | | |
| SiO2 | 72.44 | 74.41 | 73.39 | 72.90 | 70.97 | 73.40 | 70.74 | 59.30 | 67.79 | 66.20 | 59.65 |
| TiO2 | 0.39 | 0.37 | 0.41 | 0.39 | 0.38 | 0.32 | 0.29 | 0.63 | 0.30 | 0.31 | 0.65 |
| Al2O3 | 13.41 | 12.96 | 12.78 | 13.32 | 14.29 | 12.98 | 14.52 | 14.79 | 14.77 | 16.31 | 16.03 |
| Fe2O3 | 2.68 | 2.72 | 2.81 | 2.63 | 2.87 | 2.08 | 3.05 | 7.70 | 4.10 | 3.70 | 7.35 |
| MnO | 0.06 | 0.03 | 0.03 | 0.06 | 0.07 | 0.06 | 0.05 | 0.12 | 0.06 | 0.05 | 0.11 |
| MgO | 0.59 | 1.20 | 1.09 | 0.50 | 0.55 | 0.64 | 0.72 | 2.82 | 2.35 | 1.93 | 2.86 |
| CaO | 1.76 | 1.24 | 1.44 | 2.05 | 2.53 | 2.09 | 2.17 | 5.90 | 2.88 | 4.52 | 5.20 |
| Na2O | 4.17 | 0.50 | 0.30 | 4.55 | 4.68 | 5.04 | 4.88 | 2.77 | 4.08 | 4.22 | 3.27 |
| K2O | 2.36 | 4.30 | 4.44 | 2.15 | 1.94 | 1.30 | 1.95 | 2.76 | 2.12 | 1.03 | 2.77 |
| P2O5 | 0.09 | 0.09 | 0.09 | 0.09 | 0.09 | 0.03 | 0.10 | 0.11 | 0.13 | 0.10 | 0.14 |
| PF | 0.94 | 1.93 | 1.95 | 0.60 | 1.06 | 0.82 | 0.44 | 1.96 | 0.61 | 0.60 | 1.06 |
| Total | 98.89 | 99.75 | 98.73 | 99.24 | 99.43 | 98.76 | 98.91 | 98.86 | 99.19 | 98.97 | 99.09 |
| DF | 2.12 | -3.50 | -3.31 | 2.73 | 3.35 | 2.94 | 3.27 | 1.54 | 1.27 | 2.67 | 1.89 |
| **Trace elements by ICPMS in ppm** | | | | | | | | | | | |
| Nb | 5.1 | 3 | 3.5 | 4.8 | 6 | 5.8 | 7.8 | 5.9 | 3.2 | 2.8 | 8.9 |
| Zr | 184 | 131 | 117 | 185 | 215 | 182 | 130 | 10 | 9 | 3 | 141 |
| Zr/Nb | 36.1 | 43.7 | 33.4 | 38.5 | 35.8 | 31.4 | 16.7 | 1.7 | 2.8 | 1.1 | 15.8 |
| Y | 35.8 | 25.7 | 33.6 | 30.1 | 38 | 30 | 21.4 | 22.9 | 13.2 | 7.8 | 23 |
| Sr | 277 | 347 | 434 | 224 | 244 | 193 | 950 | 257 | 93 | 384 | 247 |
| Rb | 59 | 92 | 98 | 46 | 46 | 28 | 45.0 | 79.9 | 55.5 | 32.9 | 88.85 |
| Co | 4 | 6 | 6 | 4 | 2 | 3 | 4 | 21 | 12 | 11 | 21 |
| V | 28 | 41 | 44 | 22 | 32 | 35 | 23 | 191 | 110 | 62 | 122 |
| Ni | - | - | - | - | 2 | 5 | - | 49 | 32 | 30 | 17 |
| Cr | - | - | - | - | 4 | 15 | - | 138 | 50 | 43 | 47 |
| Cr/Th | - | - | - | - | 0.7 | 5.0 | - | 475.9 | 82.0 | 119.4 | 23.5 |
| Ba | 1656 | 1584 | 1630 | 941 | 1325 | 474 | 866 | 952 | 799 | 242 | 686 |
| Ga | 16 | 14 | 15 | 14 | 15 | 15 | 15 | 21 | 17 | 14 | 20 |
| Cu | - | - | - | - | 1 | 3 | - | 22 | 5 | 28 | |
| Zn | 46.0 | 43.0 | 45.0 | 34.0 | 31.0 | 45.0 | 46 | 86 | 33 | 70 | 10 |
| Th | 11.8 | 3.4 | 4.1 | 3.8 | 6.0 | 3.0 | 6.7 | 3.2 | 3.5 | 1.2 | 106.0 |
| U | 1.37 | 1.55 | 1.8 | 1.18 | 2 | - | 1.1 | 0.3 | 0.6 | 0.4 | 2.0 |
| Pb | - | - | - | - | <1 | 10 | - | 4.52 | 1.12 | 6.39 | - |
| Hf | 5.47 | 4.07 | 3.69 | 5.9 | - | - | 4.14 | 0.31 | 0.20 | 0.08 | - |
| Ta | 0.23 | 0.15 | 0.20 | 0.24 | - | - | 0.44 | 0.30 | 0.29 | 0.25 | - |
| Cs | 2.80 | 2.50 | 2.60 | 2.10 | - | - | 0.90 | 1.13 | 1.79 | 0.96 | - |
| La | 29.6 | 25.6 | 27.4 | 17.8 | - | 44.52 | 40.50 | 21.73 | 16.95 | 13.29 | 15.78 |
| Ce | 52.3 | 51 | 52 | 40.4 | - | 92.41 | 76.10 | 39.55 | 34.49 | 29.03 | 30.64 |
| Pr | 6.52 | 6.68 | 6.88 | 5.25 | - | - | 8.95 | 4.19 | 4.00 | 3.57 | - |
| Nd | 26.3 | 27.4 | 29.2 | 22.5 | - | 43.53 | 33.40 | 14.56 | 15.11 | 14.24 | 14.82 |
| Sm | 5.13 | 5.92 | 6.19 | 4.59 | - | 8.01 | 5.16 | 2.86 | 2.67 | 2.60 | 3.28 |
| Eu | 1.13 | 1.65 | 1.97 | 1.06 | - | 1.692 | 1.08 | 0.72 | 0.68 | 0.75 | 0.78 |
| Gd | 4.92 | 5.44 | 6.56 | 4.18 | - | 6.59 | 3.77 | 4.03 | 2.31 | 1.73 | 3.57 |
| Tb | 0.9 | 0.85 | 1.13 | 0.8 | - | - | 0.59 | 0.73 | 0.39 | 0.24 | - |
| Dy | 5.98 | 5.07 | 6.71 | 5.38 | - | 5.31 | 3.83 | 4.27 | 2.24 | 1.30 | 3.45 |
| Ho | 1.31 | 0.95 | 1.27 | 1.16 | - | - | 0.79 | 0.82 | 0.46 | 0.25 | - |
| Er | 3.92 | 2.46 | 3.42 | 3.45 | - | 3.22 | 2.13 | 2.17 | 1.33 | 0.71 | 1.91 |
| Tm | - | - | - | - | - | - | - | - | - | - | - |
| Yb | 4.4 | 2.28 | 3.46 | 3.92 | - | 3.08 | 2.41 | 1.94 | 1.42 | 0.70 | 1.68 |
| Lu | 0.67 | 0.32 | 0.51 | 0.62 | - | 0.464 | 0.37 | 0.27 | 0.22 | 0.10 | 0.24 |

The concentration of trace elements on sample BJ 93-08, BJ 93-01 and BJ 93-32 are determined by XRF at the University of Rennes 1.
The concentration of REE on sample BJ 93-01 and BJ 93-32 are determined by isotopic dilution performed at the University of Rennes 1.

#### 4.3.4. Microprobe analyses

Mineral compositions on all muscovite fractions were analyzed by an electron microprobe (CAMECA SX50) at the University of Bern, operating at 15 kV accelerating voltage and 20nA beam current.

#### 4.3.5. U-Pb SIMS measurements

The zircon U-Pb isotope analyses were performed using a secondary ion microprobe spectrometer (SIMS: CAMECA IMS 1270) in Laboratory for Isotope Geology, Swedish Museum of Natural History, Stockholm. Detailed analytical procedures have been described by Whitehouse et al. (1997). From past studies, it was found that instrumental mass fractionation due to the sputtering process was negligible, so no mass fractionation correction has been applied. Correction for in -situ common lead has been made by measuring the amount of $^{204}Pb$ present and using a Stacey and Kramers (1975) estimation of terrestrial Pb isotope composition. All age errors reported herein are 95% confidence level ($2\sigma$).

## 4.4. Results

#### 4.4.1. Geochemical characteristics

The major and trace element concentration data are reported in Table 1.

According to the discriminant function empirically derived by Shaw (1972), the quartzo-feldspathic gneisses at the Bixiling Complex can be separated into two groups: (1) two paragneisses ($DF < 0$; CF 96-21b and c), and (2) three orthogneisses ($DF > 0$; BJ 95-08, CF 96-21a and d). On one hand, the orthogneisses are of trondhjemitic composition. Their Primitive Mantle-normalized spidergram patterns present negative Ta and/or Nb, Sr, $P_2O_5$ and $TiO_2$ anomalies which are common features of granitic rocks and the upper continental crust as shown in Fig. II-33a. Their Rb, Y, Nb, Yb and Ta concentrations suggest a volcanic arc setting for their formation according to Pearce et al. (1984). On the other hand, the paragneisses have a greywacke composition (Pettijohn et al. 1972). They Primitive Mantle-normalized spidergram patterns are characterized by negative Ta, Nb, $P_2O_5$ and $TiO_2$ anomalies (Fig. II-33a).

All gneisses which constitute the UHPM slab of Shuanghe present positive DF values indicating an igneous origin. They are of trondhjemitic composition. Their Primitive Mantle-normalized spidergram patterns present negative Ta and/or Nb, Sr, $P_2O_5$ and $TiO_2$ anomalies which are common features of granitic and upper continental crust (Fig. II-33b).

Table II-4: Sm-Nd results on whole rocks and mineral separates from the Bixiling locality and the UHPM slab of Shuanghe. Nd model ages are calculated according to Goldstein et al. (1984) and Nägler and Kramers (1998).

| Locality | Sample | Type | Sm | Nd | 143Nd/144Nd | 2σ | 147Sm/144Nd | ε(0) | ε(800) | TDM* | TDM** | f(Sm/Nd) |
|---|---|---|---|---|---|---|---|---|---|---|---|---|
| BIXILING | CF 96-21a | WR | 4.73 | 22.65 | 0.512316 | 0.000005 | 0.1264 | -6.28 | 0.91 | 1.45 | 1.36 | -0.357 |
| | CF 96-21b | WR | 5.93 | 26.27 | 0.512355 | 0.000005 | 0.1364 | -5.52 | 0.65 | 1.56 | 1.45 | -0.307 |
| | CF 96-21c | WR | 6.36 | 26.62 | 0.512382 | 0.000005 | 0.1443 | -4.99 | 0.37 | 1.68 | 1.54 | -0.266 |
| | CF 96-21d | WR | 4.46 | 20 | 0.512332 | 0.000005 | 0.1346 | -5.97 | 0.39 | 1.57 | 1.46 | -0.316 |
| | BJ 95-08 | WR | 4.68 | 22.33 | 0.512323 | 0.000003 | 0.1267 | -6.14 | 1.02 | 1.45 | 1.35 | -0.356 |
| SHUANGHE | CF 96-36 | WR | 5.61 | 36.18 | 0.511454 | 0.000006 | 0.0937 | -23.10 | -12.58 | 2.15 | 2.03 | -0.524 |
| | CF 96-37 | WR | 3.02 | 15.33 | 0.51117 | 0.000003 | 0.1191 | -28.64 | -20.74 | 3.17 | 3 | -0.395 |
| | CF 96-38 | WR | 2.01 | 9.76 | 0.511522 | 0.000006 | 0.1243 | -21.77 | -14.39 | 2.76 | 2.58 | -0.368 |
| | CF 96-39 | Grt | 1.35 | 0.5 | 0.513869 | 0.000028 | 1.6295 | 24.01 | - | - | - | 7.284 |
| | CF 96-39 | Kya | 3.46 | 17.05 | 0.511611 | 0.000017 | 0.1225 | -20.03 | - | - | - | -0.377 |
| | CF 96-39 | WR | 2.68 | 14.86 | 0.51156 | 0.000004 | 0.1091 | -21.03 | -12.09 | 2.31 | 2.17 | -0.445 |
| | CF 96-39* | WR | 2.68 | 14.29 | 0.511547 | 0.000007 | 0.1133 | -21.28 | -12.77 | 2.42 | 2.27 | -0.424 |

*: Nd model ages calculated according to the linear evolution of the Depleted Mantle (Goldstein et al., 1984)
**: Nd model ages calculated according to the polynomial evolution of the Depleted Mantle (Nägler and Kramers, 1998)

Table II-5: Rb-Sr results on whole rocks and mineral separates from the Bixiling locality and the UHPM slab of Shuanghe.

| Locality | Sample | Type | Sr | Rb | 87Sr/86Sr | 2σ | 87Rb/86Sr | 87Sr/86Sr(220) |
|---|---|---|---|---|---|---|---|---|
| BIXILING | CF 96-21a | WR | 261.21 | 59.5 | 0.712263 | 0.000007 | 0.658 | 0.710204 |
| | " | Bt | 29.36 | 372.81 | 0.799911 | 0.000007 | 37.01 | - |
| | " | Ms | 43.52 | 275.99 | 0.761477 | 0.000007 | 18.407 | - |
| | " | Ap | 667.23 | 0.96 | 0.71048 | 0.000007 | 0.004 | - |
| | " | Zo | 988.42 | 3.32 | 0.710541 | 0.000007 | 0.01 | - |
| | CF 96-21b | WR | 362.23 | 101.2 | 0.710636 | 0.000007 | 0.807 | 0.708111 |
| | " | Zo | 6312.7 | 23.79 | 0.708389 | 0.000007 | 0.011 | - |
| | " | Ms | 155.57 | 239.8 | 0.720663 | 0.000007 | 4.458 | - |
| | " | Ap | 719.16 | 0.97 | 0.708412 | 0.000006 | 0.004 | - |
| | CF 96-21c | WR | 430.77 | 105.17 | 0.71032 | 0.000007 | 0.705 | 0.708114 |
| | " | Ms | 144.06 | 225.73 | 0.721102 | 0.000006 | 4.53 | - |
| | " | Zo | 6682.6 | 32.04 | 0.708382 | 0.000009 | 0.014 | - |
| | " | Ap | 1455.08 | 1.61 | 0.708412 | 0.000007 | 0.003 | - |
| | CF 96-21d | WR | 235.1 | 47.86 | 0.711787 | 0.000007 | 0.588 | 0.709947 |
| | " | Bt | 17.75 | 399.92 | 0.886098 | 0.000007 | 66.22 | - |
| | " | Ms | 21.39 | 264.22 | 0.809292 | 0.000007 | 36.035 | - |
| | " | Ap | 767.98 | 0.93 | 0.71009 | 0.000007 | 0.003 | - |
| | " | Zo | 1957.8 | 3.19 | 0.710159 | 0.000006 | 0.005 | - |
| | BJ 95-08 | WR | 248.56 | 45.92 | 0.712129 | 0.000007 | 0.534 | 0.710458 |
| | " | Bt | 26.35 | 355.36 | 0.811665 | 0.000006 | 39.36 | - |
| | " | Ms | 14.97 | 272.95 | 0.860651 | 0.000016 | 53.471 | - |
| | " | Ap | 1120.5 | 0.86 | 0.710558 | 0.000007 | 0.002 | - |
| | " | Zo | 1434.3 | 3.83 | 0.710761 | 0.000008 | 0.008 | - |
| SHUANGHE | CF 96-36 | WR | 997.04 | 50.66 | 0.713618 | 0.000007 | 0.147 | 0.713158 |
| | CF 96-37 | WR | 248.32 | 80.76 | 0.721318 | 0.000007 | 0.941 | 0.718374 |
| | CF 96-38 | WR | 80.67 | 65.86 | 0.720494 | 0.000007 | 2.362 | 0.713104 |
| | CF 96-39 | WR | 397.09 | 35.39 | 0.714358 | 0.000007 | 0.258 | 0.713551 |
| | CF 96-39* | WR | 387.15 | 34.68 | 0.714413 | 0.000006 | 0.259 | 0.713603 |

Figure II-33: Primitive Mantle (PM)-normalized spidergram for gneisses of Bixiling in a) and of Shuanghe in b). Gneisses are characterized by negative Nb, $P_2O_5$, $TiO_2$ anomalies. PM values are those of Hofmann (1988).

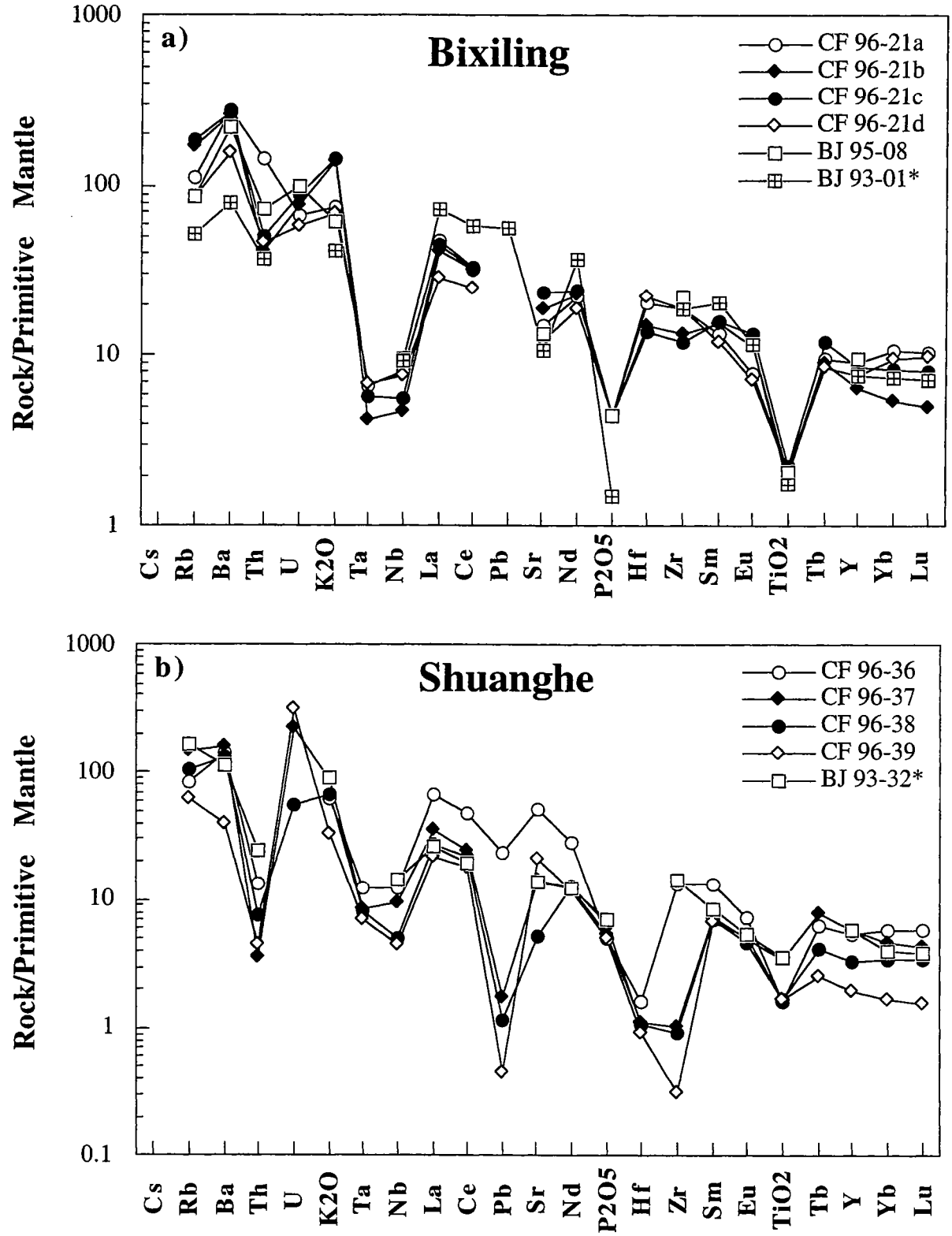

### 4.4.2. Whole rock isotopic data

Granitoids at the Bixiling Complex and the UHPM slab of Shuanghe also present contrasting Sr and Nd isotopic features (Table II-4 and II-5). Paragneisses and orthogneisses of the Bixiling Complex are characterized by (1) $^{87}Sr/^{86}Sr$ isotopic compositions between 0.710 and 0.712, (2) slightly negative $\varepsilon_{Nd}(0)$ values of -4.3 to -3.5, and (3) Nd model ages ($T_{DM}$) ranging from 1.35 to 1.54 Ga. These results indicate late Proterozoic formation. All samples from the UHPM rocks of Shuanghe represent very old rocks as $\varepsilon_{Nd}(0)$ values are significantly negative from -21 to -28 corresponding to $T_{DM}$ ages of 2 to 3 Ga, and very high $^{87}Sr/^{86}Sr$ isotopic compositions (0.714 to 0.721).

### 4.4.3. Geochronology

*U-Pb SIMS zircon results*

Zircon fractions were separated magnetically and gravimetrically from other minerals on sample CF 96-21a (Bixiling) and CF 96-39 (Shuanghe). They were analyzed for U-Pb isotopes by SIMS analyses and the results are reported in Table II-6. Sketchs of zircons are shown in Fig. II-34a. All zircons present a complicated internal structure where several overgrowths around a rounded to subeuhedral core may be observed. U-Pb analyses on zircon CF 96-21a yield: two data points with reverse discordance and three data points which suggest possibly an upper intercept at ~700 Ma and a lower intercept at ~230 Ma. No clear result may be reached due to large errors vis à vis straight concordia in grazzy angle (Fig. II-34b). All zircons from sample CF 96-39 yield discordant data points in the concordia diagram (Fig. II-34c), suggesting several crystal growths. The best regression line gives an upper concordia intercept at 2458 ± 76 Ma and a lower concordia intercept at 233 ± 21 Ma. ~230 Ma is in line with nearly two concordant data points in the Tera-Wasserburg diagram (Fig. II-34d).

*Sm-Nd isotope results*

One garnet and one kyanite fractions were separated from CF 96-39 for Sm-Nd analyses and the results are reported in Table 2. Garnet-Kyanite-WR isochron give an age of 231 ± 35 Ma (MSWD = 2.89) with an εNd(t) of -18.2 (Fig. II-35).

*Rb-Sr isotope results*

Biotite and/or Phengite, Apatite and Zoisite were separated from the host gneisses of the Bixiling Complex for Rb-Sr analyses. The results are given in Table II-5. The two paragneisses present identical phengite-whole rock isochron ages at 198 ± 4 Ma whereas the three orthogneisses provide small range phengite-whole rock ages from 193 ± 4 Ma to 197 ± 4

Table II-6: U-Pb SIMS results on zircon from gneisses of the Bixiling.locality and the UHPM slab of Shuanghe.

| sample | U ppm | Pb ppm | Th/U | 207Pb/206Pb | ±σ % | 206Pb/238U | ±σ % | 207Pb/235U | ±σ % | ρ | 206Pb/204Pb | age (Ma) 207Pb/206Pb | ±σ (Ma) | age (Ma) 206Pb/238U | ±σ (Ma) | age (Ma) 207Pb/235U | ±σ (Ma) |
|---|---|---|---|---|---|---|---|---|---|---|---|---|---|---|---|---|---|
| CF 96-21a | | | | | | | | | | | | | | | | | |
| | 109 | 13 | 0.783 | 0.05999 | 3.34 | 0.0879 | 2.95 | 0.7271 | 3.4 | 0.87 | 1540 | 603 | 72 | 543 | 15 | 555 | 15 |
| | 261 | 49 | 1.711 | 0.06306 | 1.33 | 0.11816 | 3.81 | 1.0274 | 3.95 | 0.97 | 3900 | 710 | 28 | 720 | 26 | 718 | 20 |
| | 347 | 55 | 0.904 | 0.06249 | 2.77 | 0.11049 | 2.16 | 0.952 | 2.3 | 0.94 | 630 | 691 | 59 | 676 | 14 | 679 | 11 |
| | 120 | 12 | 1.246 | 0.05133 | 8.6 | 0.07109 | 3 | 0.5032 | 3.81 | 0.79 | 360 | 256 | 199 | 443 | 13 | 414 | 13 |
| | 85 | 8 | 0.491 | 0.06024 | 3.05 | 0.07673 | 2.86 | 0.6373 | 3.34 | 0.86 | 2230 | 612 | 66 | 477 | 13 | 501 | 13 |
| CF 96-39 | | | | | | | | | | | | | | | | | |
| | 69 | 3 | 0.021 | 0.05682 | 4.26 | 0.03521 | 4.82 | 0.2759 | 6.43 | 0.75 | 290 | 485 | 94 | 223 | 11 | 247 | 14 |
| | 100 | 4 | 0.02 | 0.05317 | 3.13 | 0.03649 | 4.13 | 0.2675 | 5.18 | 0.8 | 530 | 336 | 71 | 231 | 9 | 241 | 11 |
| | 211 | 9 | 0.048 | 0.06403 | 1.42 | 0.04063 | 1.63 | 0.3587 | 2.17 | 0.75 | 1000000 | 743 | 30 | 257 | 4 | 311 | 6 |
| | 52 | 3 | 0.032 | 0.09532 | 9.28 | 0.04182 | 3.17 | 0.5496 | 9.8 | 0.32 | 40 | 1534 | 199 | 264 | 8 | 445 | 35 |
| | 90 | 6 | 0.01 | 0.07641 | 2.81 | 0.05908 | 3.69 | 0.6224 | 4.05 | 0.91 | 1760 | 1106 | 56 | 370 | 13 | 491 | 16 |
| | 90 | 7 | 0.126 | 0.09144 | 1.66 | 0.06388 | 2.23 | 0.8054 | 2.71 | 0.82 | 13760 | 1456 | 32 | 399 | 9 | 600 | 12 |
| | 209 | 21 | 0.227 | 0.11797 | 1.27 | 0.08104 | 2.32 | 1.3181 | 2.59 | 0.89 | 10070 | 1926 | 23 | 502 | 11 | 854 | 15 |
| | 747 | 109 | 0.015 | 0.10147 | 0.46 | 0.13113 | 1.42 | 1.8345 | 1.48 | 0.96 | 25890 | 1651 | 9 | 794 | 11 | 1058 | 10 |
| | 109 | 18 | 0.199 | 0.12787 | 1.07 | 0.13757 | 4.26 | 2.4254 | 4.39 | 0.97 | 21000 | 2069 | 19 | 831 | 33 | 1250 | 32 |
| | 785 | 128 | 0.01 | 0.12653 | 0.48 | 0.1438 | 4.16 | 2.5087 | 4.19 | 0.99 | 28120 | 2050 | 9 | 866 | 34 | 1275 | 30 |
| | 74 | 14 | 0.208 | 0.14106 | 1.01 | 0.14947 | 2.28 | 2.9071 | 2.48 | 0.92 | 11350 | 2240 | 18 | 898 | 19 | 1384 | 19 |
| | 87 | 19 | 0.252 | 0.14541 | 1.29 | 0.1707 | 5.81 | 3.4223 | 5.92 | 0.98 | 5900 | 2293 | 22 | 1016 | 55 | 1510 | 47 |
| | 163 | 46 | 0.203 | 0.15168 | 0.52 | 0.23145 | 1.57 | 4.8405 | 1.65 | 0.95 | 24620 | 2365 | 9 | 1342 | 19 | 1792 | 14 |
| | 64 | 26 | 0.375 | 0.16098 | 0.74 | 0.31847 | 2.65 | 7.0685 | 2.75 | 0.96 | 56430 | 2466 | 13 | 1782 | 41 | 2120 | 25 |
| | 32 | 14 | 0.411 | 0.15235 | 1.97 | 0.34043 | 20.66 | 7.1509 | 20.73 | 1 | 3700 | 2372 | 34 | 1889 | 339 | 2130 | 187 |

Figure II-34: a) Sketch of zircons used for U-Pb isotopes by SIMS.Analyzed area are surrounded by a circle. b) U-Pb data on CF 96-21a, c) U-Pb data on CF 96-39 d) Tera-Wasserburg diagram for U-Pb data on Cf 96-39

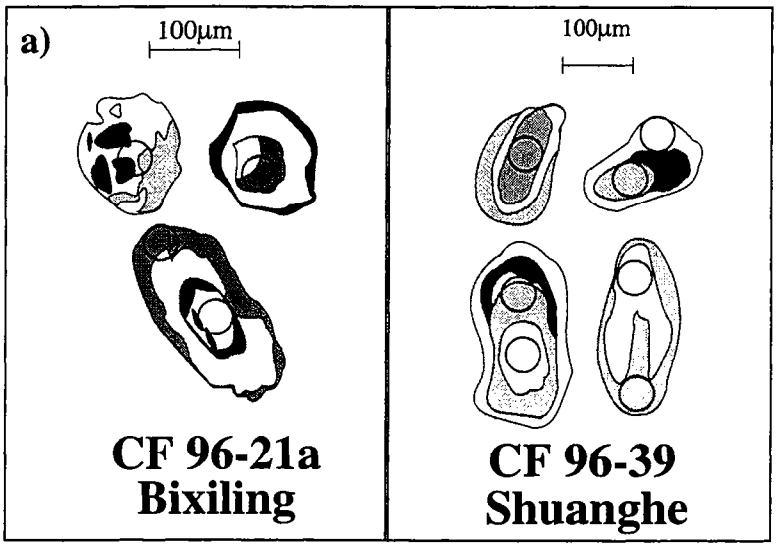


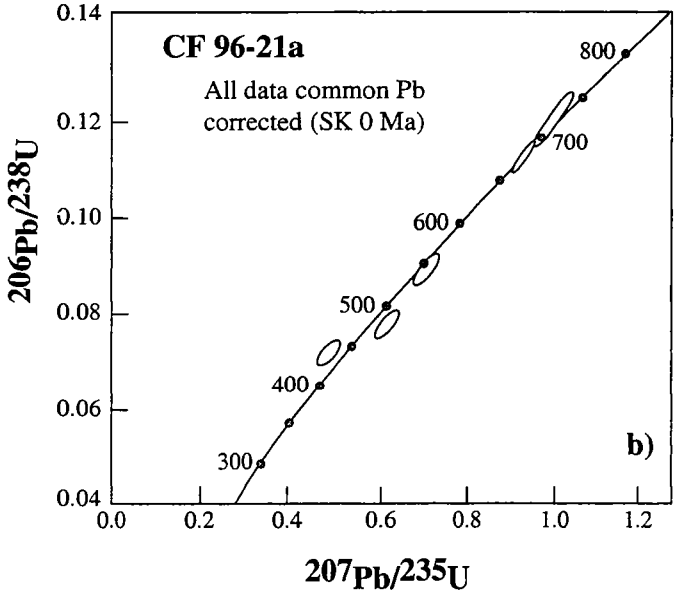


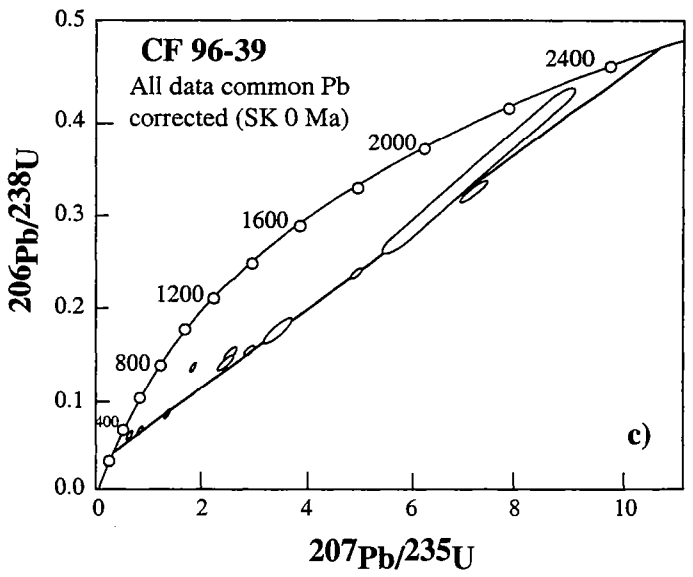


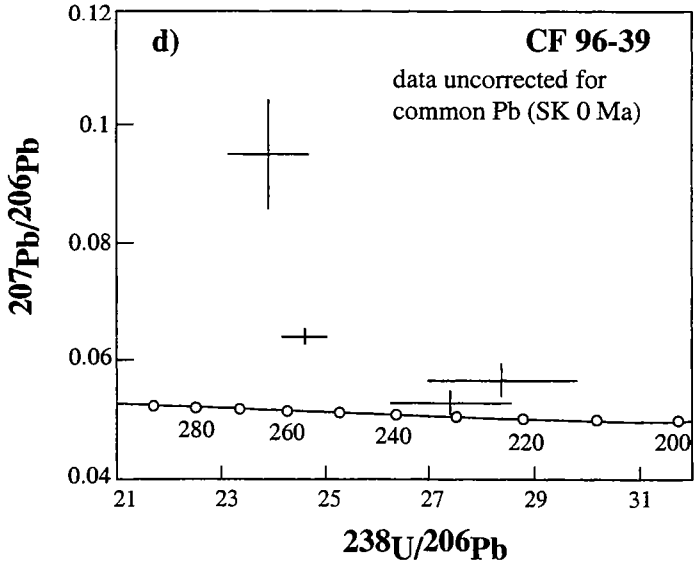

Figure II-35: Sm-Nd garnet-kyanite-whole rock isochron gives an age of 231 ± 35 Ma (MSWD = 2.89; sample CF 96-39).

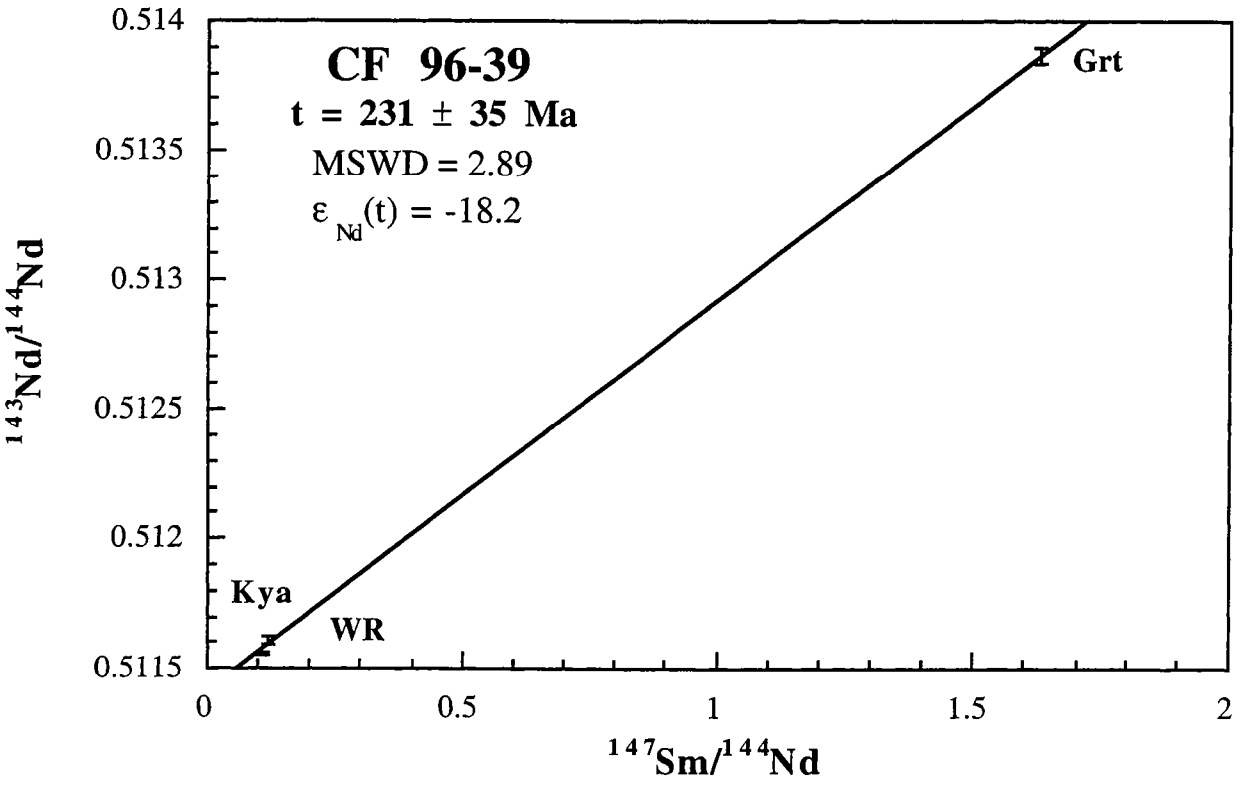

Figure II-36: Rb-Sr mineral isochrons for three orthogneisses (a, d, e) and two paragneisses (b, c).

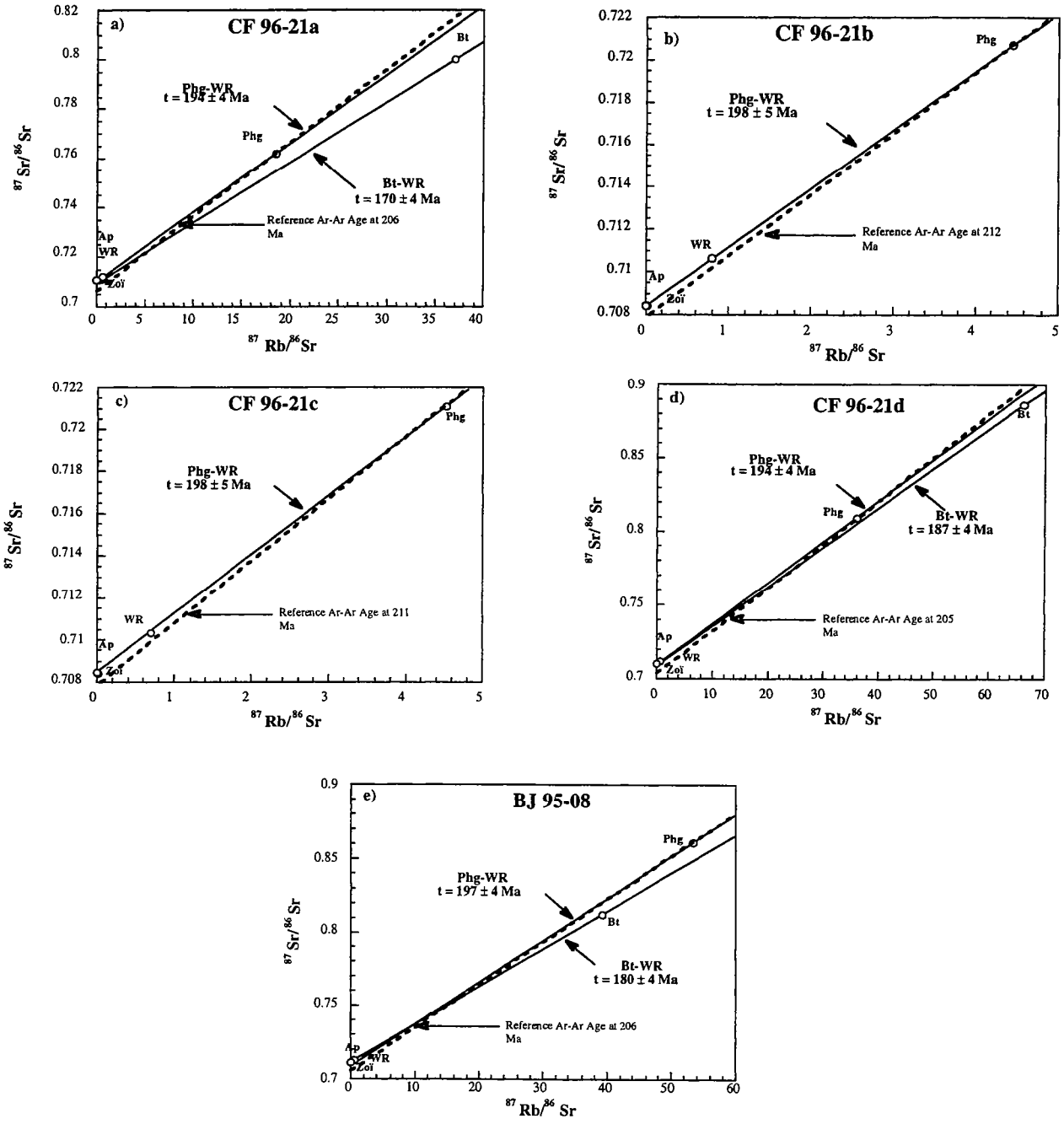

Ma (Fig. II-36a to II-36e). Younger Rb-Sr ages were obtained by three biotite-whole rock isochrons between 170 ± 3 Ma and 187 ± 4 Ma (Fig. II-36a, II-36d, and II-36e).

*Ar-Ar isotope results*

For the country rocks of the Bixiling Complex, 5 to 10 mg of phengite and biotite separates purified for Rb-Sr analyses, were used for Ar-Ar isotope analyses and the results are listed in Table II-7 and Table II-8. The age spectra on phengites from orthogneisses and paragneisses (CF 96-21b and c) are reported in Fig. II-37 and Fig. II-38 respectively. The low and very high temperature steps correspond to very low gas release (below 5%). The other steps for the two phengite fractions on paragneisses define plateau ages of 212-211 ± 2 Ma related to constant Cl/K ratios (~0.0005) in constrast to highly variable Ca/K ratios (0.002 to 0.5). The principal steps of the three phengite fractions on orthogneisses define nearly flat age spectra at about 205 Ma. Nevertheless, these step ages oscillate within a narrow range between 204 and 209 Ma. In addition, this narrow spread in age is also related to constant Cl/K ratios (~0.0006) and highly variable Ca/K ratios (0.002 to 0.5) for the three cases. Electron microprobe analyses were performed on phengites to decipher whether the retrograde metamorphism have influenced the mineral chemical composition. The celadonite content of dated phengite defines a linear trend corresponding to the tschermak exchange (Fe, Mg, Mn) Si = $Al^{IV}$ $Al^{VI}$ as shown in Fig. II-39a. The tschermak content within single phengite is highly variable (3.77 to 3.96). In the $X_{Mg}$ versus Si p.f.u. content diagram (Fig. II-39b), mineral fraction composition define (1) a linear trend where Si p.f.u. content increases with $X_{Mg}$, (2) higher $X_{Mg}$ values for phengite of paragneisses than for phengite of orthogneisses, (3) two distinctive groups of which one presents high Si p.f.u and $X_{Mg}$ values and the other one low Si p.f.u and $X_{Mg}$ values. All Ar-Ar age spectra on phengites give slightly older age than the corresponding Rb-Sr phengite-WR isochron ages. The age spectra on biotite from orthogneisses (CF 96-21a and d, and BJ 95-08) are reported in Fig. II-37. They are hump-shaped and the step ages range between 190 and 210 Ma. In the same manner as phengite, biotite present highly variable Ca/K ratios (0.01 to 0.5) for constant Cl/K ratios (~0.003), which are not related systematically related to older ages. In addition, all Ar-Ar age spectra on biotite are significantly older than the respective Rb-Sr biotite-WR isochron ages.

## 4.5. Discussion

### 4.5.1. Ages of protolith and metamorphism

Our U-Pb SIMS zircon data on samples CF 96-21a indicate that the orthogneisses which surround the Bixiling Complex have late Proterozoic protolith emplacement age (Fig. II-34b). These age are in agreement with the previous U-Pb zircon concordia upper intercept dates at ~800 Ma on gneisses (Ames et al. 1995, Xue et al. 1997). The geochemical characteristics of

Table II-7: Ar-Ar analytical data on phengite and biotite from orthogneisses of the Bixiling locality.

**CF 96-21a Biotite**

| Step | Temperature (°C) | Ar 40 tot. | σ40 | Ar 40 * | Ar 39 | σ39 | 39Ar% | Ar 38 | σ38 | Ar 37 | σ37 | Ar 36 | σ36 | Ca / K | Cl/K | Age (Ma) | σ |
|---|---|---|---|---|---|---|---|---|---|---|---|---|---|---|---|---|---|
| 1 | 450 | 3.17E-08 | 8.70E-12 | 1.51E-08 | 1.21E-09 | 1.20E-12 | 10.78 | 4.65E-11 | 1.90E-13 | 9.20E-11 | 3.00E-02 | 5.62E-11 | 2.90E-13 | 0.1517 | 0.0041 | 142.21 | 0.79 |
| 2 | 508 | 1.17E-08 | 2.30E-12 | 9.84E-09 | 5.66E-10 | 5.80E-13 | 5.03 | 1.42E-11 | 1.90E-13 | 1.78E-11 | 2.40E-02 | 6.18E-12 | 2.40E-13 | 0.0629 | 0.0026 | 194.96 | 1.30 |
| 3 | 564 | 1.90E-08 | 5.80E-12 | 1.75E-08 | 9.83E-10 | 1.00E-12 | 8.73 | 2.40E-11 | 2.50E-13 | 2.41E-11 | 2.30E-02 | 5.17E-12 | 2.80E-13 | 0.0491 | 0.0027 | 199.50 | 0.90 |
| 4 | 597 | 2.20E-08 | 5.70E-12 | 2.13E-08 | 1.16E-09 | 1.10E-12 | 10.31 | 2.70E-11 | 2.10E-13 | 2.38E-11 | 2.10E-02 | 2.25E-12 | 1.90E-13 | 0.0410 | 0.0026 | 205.38 | 0.54 |
| 5 | 627 | 2.20E-08 | 8.50E-12 | 2.15E-08 | 1.17E-09 | 1.20E-12 | 10.43 | 2.67E-11 | 2.40E-13 | 1.14E-11 | 3.00E-02 | 1.53E-12 | 2.40E-13 | 0.0195 | 0.0025 | 205.00 | 0.67 |
| 6 | 669 | 1.94E-08 | 5.20E-12 | 1.84E-08 | 1.01E-09 | 9.60E-13 | 8.96 | 2.22E-11 | 2.00E-13 | 7.74E-12 | 1.70E-02 | 3.32E-12 | 2.40E-13 | 0.0153 | 0.0022 | 204.19 | 0.77 |
| 7 | 690 | 8.28E-09 | 3.40E-12 | 6.90E-09 | 4.05E-10 | 4.50E-13 | 3.59 | 9.02E-12 | 2.10E-13 | 2.67E-12 | 2.40E-02 | 4.68E-12 | 2.30E-13 | 0.0132 | 0.0019 | 191.54 | 1.80 |
| 8 | 721 | 6.87E-09 | 2.50E-12 | 5.99E-09 | 3.31E-10 | 4.20E-13 | 2.94 | 7.44E-12 | 1.80E-13 | 1.36E-11 | 3.10E-02 | 2.96E-12 | 3.70E-13 | 0.0823 | 0.0021 | 203.01 | 3.50 |
| 9 | 747 | 5.92E-09 | 1.80E-12 | 5.41E-09 | 2.92E-10 | 3.30E-13 | 2.59 | 5.69E-12 | 2.00E-13 | 1.14E-11 | 2.60E-02 | 1.75E-12 | 2.90E-13 | 0.0778 | 0.0015 | 207.07 | 3.10 |
| 10 | 778 | 4.00E-09 | 1.40E-12 | 3.57E-09 | 2.05E-10 | 2.80E-13 | 1.82 | 4.72E-12 | 1.60E-13 | 4.88E-12 | 2.70E-02 | 1.44E-12 | 2.00E-13 | 0.0477 | 0.0023 | 195.68 | 3.10 |
| 11 | 822 | 5.14E-09 | 2.30E-12 | 4.35E-09 | 2.60E-10 | 2.80E-13 | 2.31 | 8.73E-12 | 2.20E-13 | 2.35E-11 | 2.40E-02 | 2.70E-12 | 2.40E-13 | 0.1806 | 0.0046 | 187.69 | 3.00 |
| 12 | 880 | 1.03E-08 | 4.90E-12 | 9.75E-09 | 5.43E-10 | 5.90E-13 | 4.83 | 1.10E-11 | 1.90E-13 | 6.03E-11 | 1.60E-02 | 1.76E-12 | 2.20E-13 | 0.2221 | 0.0018 | 201.12 | 1.30 |
| 13 | 987 | 3.41E-08 | 7.50E-12 | 3.35E-08 | 1.86E-09 | 1.70E-12 | 16.51 | 4.06E-11 | 3.00E-13 | 7.99E-11 | 1.60E-02 | 2.04E-12 | 2.20E-13 | 0.0860 | 0.0023 | 201.97 | 0.41 |
| 14 | 1078 | 1.84E-08 | 6.90E-12 | 1.78E-08 | 9.88E-10 | 9.00E-13 | 8.77 | 2.18E-11 | 1.90E-13 | 1.82E-10 | 3.60E-02 | 2.05E-12 | 2.70E-13 | 0.3678 | 0.0023 | 201.66 | 0.85 |
| 15 | 1161 | 3.47E-09 | 1.40E-12 | 3.32E-09 | 1.74E-10 | 2.40E-13 | 1.54 | 4.05E-12 | 2.20E-13 | 1.06E-10 | 2.80E-02 | 5.35E-13 | 2.30E-13 | 1.2188 | 0.0025 | 213.25 | 4.00 |
| 16 | 1392 | 2.08E-09 | 9.00E-13 | 1.68E-09 | 9.61E-11 | 1.60E-13 | 0.85 | 3.38E-12 | 2.20E-13 | 9.07E-11 | 2.80E-02 | 1.36E-12 | 2.20E-13 | 1.8884 | 0.0048 | 196.26 | 7.00 |
| | | | | | | | | | | | | | | | **age** | **195.32** | |

**CF 96-21a Phengite**

| Step | Temperature (°C) | Ar 40 tot. | σ40 | Ar 40 * | Ar 39 | σ39 | 39Ar% | Ar 38 | σ38 | Ar 37 | σ37 | Ar 36 | σ36 | Ca / K | Cl/K | Age (Ma) | σ |
|---|---|---|---|---|---|---|---|---|---|---|---|---|---|---|---|---|---|
| 1 | 556 | 2.16E-08 | 6.10E-12 | 1.43E-08 | 7.57E-10 | 7.40E-13 | 1.44 | 2.69E-11 | 1.50E-13 | 1.91E-11 | 3.20E-02 | 2.48E-11 | 2.20E-13 | 0.0504 | 0.0040 | 210.48 | 0.94 |
| 2 | 637 | 1.41E-08 | 8.50E-12 | 1.17E-08 | 6.42E-10 | 7.70E-13 | 1.22 | 1.44E-11 | 2.40E-13 | 1.71E-11 | 2.70E-02 | 8.18E-12 | 2.00E-13 | 0.0533 | 0.0019 | 203.24 | 1.00 |
| 3 | 687 | 6.17E-08 | 6.10E-11 | 5.67E-08 | 3.11E-09 | 4.00E-12 | 5.94 | 4.93E-11 | 2.40E-13 | 2.02E-11 | 3.00E-02 | 1.69E-11 | 2.40E-13 | 0.0130 | 0.0007 | 203.94 | 0.39 |
| 4 | 711 | 1.89E-07 | 1.10E-10 | 1.81E-07 | 9.93E-09 | 9.80E-12 | 18.94 | 1.51E-10 | 3.50E-13 | 2.74E-11 | 2.90E-02 | 2.76E-11 | 2.30E-13 | 0.0055 | 0.0007 | 204.03 | 0.23 |
| 5 | 736 | 1.68E-07 | 1.30E-10 | 1.63E-07 | 8.86E-09 | 9.60E-12 | 16.90 | 1.36E-10 | 4.00E-13 | 2.84E-11 | 3.40E-02 | 1.55E-11 | 2.10E-13 | 0.0064 | 0.0007 | 205.90 | 0.27 |
| 6 | 758 | 1.18E-07 | 5.60E-11 | 1.15E-07 | 6.25E-09 | 6.10E-12 | 11.91 | 9.55E-11 | 3.00E-13 | 3.09E-11 | 3.40E-02 | 8.91E-12 | 2.20E-13 | 0.0099 | 0.0008 | 206.58 | 0.24 |
| 7 | 784 | 1.49E-07 | 9.10E-11 | 1.47E-07 | 7.91E-09 | 7.70E-12 | 15.09 | 1.20E-10 | 3.60E-13 | 4.01E-11 | 3.00E-02 | 8.65E-12 | 2.40E-13 | 0.0101 | 0.0007 | 207.64 | 0.24 |
| 8 | 807 | 3.83E-08 | 1.20E-11 | 3.73E-08 | 2.01E-09 | 1.90E-12 | 3.83 | 3.16E-11 | 2.20E-13 | 1.45E-11 | 2.80E-02 | 3.23E-12 | 2.80E-13 | 0.0144 | 0.0008 | 207.69 | 0.48 |
| 9 | 842 | 4.15E-08 | 1.40E-11 | 4.02E-08 | 2.19E-09 | 2.00E-12 | 4.17 | 3.39E-11 | 2.70E-13 | 2.87E-11 | 2.20E-02 | 4.21E-12 | 2.70E-13 | 0.0262 | 0.0008 | 206.10 | 0.43 |
| 10 | 868 | 4.87E-08 | 1.40E-11 | 4.75E-08 | 2.58E-09 | 2.50E-12 | 4.92 | 3.98E-11 | 2.20E-13 | 3.20E-11 | 2.60E-02 | 3.84E-12 | 2.50E-13 | 0.0248 | 0.0008 | 206.15 | 0.36 |
| 11 | 899 | 4.85E-08 | 1.40E-11 | 4.75E-08 | 2.59E-09 | 2.30E-12 | 4.94 | 4.01E-11 | 1.40E-13 | 2.23E-11 | 2.10E-02 | 3.60E-12 | 2.40E-13 | 0.0172 | 0.0008 | 205.26 | 0.34 |
| 12 | 963 | 4.51E-08 | 1.90E-11 | 4.44E-08 | 2.41E-09 | 2.30E-12 | 4.60 | 3.45E-11 | 1.60E-13 | 2.57E-11 | 2.90E-02 | 2.25E-12 | 2.20E-13 | 0.0213 | 0.0005 | 206.14 | 0.35 |
| 13 | 1021 | 2.72E-08 | 5.50E-12 | 2.61E-08 | 1.43E-09 | 1.30E-12 | 2.72 | 1.97E-11 | 1.60E-13 | 3.44E-11 | 2.70E-02 | 3.71E-12 | 2.20E-13 | 0.0482 | 0.0004 | 204.48 | 0.51 |
| 14 | 1073 | 1.62E-08 | 5.90E-12 | 1.56E-08 | 8.36E-10 | 8.20E-13 | 1.59 | 1.40E-11 | 1.90E-13 | 2.08E-11 | 2.50E-02 | 2.08E-12 | 1.90E-13 | 0.0499 | 0.0010 | 209.09 | 0.75 |
| 15 | 1140 | 1.05E-08 | 1.80E-12 | 9.71E-09 | 5.24E-10 | 5.30E-13 | 1.00 | 9.99E-12 | 1.50E-13 | 1.12E-11 | 2.60E-02 | 2.55E-12 | 2.00E-13 | 0.0429 | 0.0015 | 207.18 | 1.20 |
| 16 | 1225 | 5.29E-09 | 7.40E-13 | 4.42E-09 | 2.44E-10 | 3.00E-13 | 0.47 | 5.37E-12 | 9.10E-14 | 1.51E-11 | 3.50E-02 | 2.96E-12 | 2.40E-13 | 0.1236 | 0.0018 | 202.94 | 3.10 |
| 17 | 1336 | 3.39E-09 | 1.20E-12 | 2.45E-09 | 1.38E-10 | 1.50E-13 | 0.26 | 1.83E-12 | 1.50E-13 | 1.45E-11 | 2.60E-02 | 3.16E-12 | 2.10E-13 | 0.2100 | ###### | 198.97 | 4.80 |
| 18 | 1381 | 1.28E-09 | 5.90E-13 | 3.04E-10 | 2.97E-11 | 1.90E-13 | 0.06 | 2.00E-13 | 1.50E-13 | 4.00E-12 | 2.10E-02 | 3.32E-12 | 2.20E-13 | 0.2691 | ###### | 117.38 | 24.00 |
| | | | | | | | | | | | | | | | **age** | **205.82** | |

**CF 96-21d Phengite**

| Step | Temperature (°C) | Ar 40 tot. | σ40 | Ar 40 * | Ar 39 | σ39 | 39Ar% | Ar 38 | σ38 | Ar 37 | σ37 | Ar 36 | σ36 | Ca / K | Cl/K | Age (Ma) | σ |
|---|---|---|---|---|---|---|---|---|---|---|---|---|---|---|---|---|---|
| 1 | 611 | 6.06E-09 | 7.50E-12 | 3.77E-09 | 2.15E-10 | 3.90E-13 | 2.83 | 2.60E-11 | 1.40E-13 | 9.25E-12 | 4.00E-02 | 7.73E-12 | 2.40E-13 | 0.0862 | 0.0236 | 197.29 | 3.50 |
| 2 | 687 | 1.46E-08 | 9.80E-12 | 1.33E-08 | 7.41E-10 | 9.50E-13 | 9.77 | 1.09E-11 | 1.40E-13 | 7.75E-12 | 3.00E-02 | 4.55E-12 | 2.00E-13 | 0.0209 | 0.0004 | 200.78 | 0.90 |
| 3 | 712 | 3.77E-08 | 4.70E-11 | 3.62E-08 | 1.97E-09 | 2.70E-12 | 26.00 | 2.88E-11 | 1.70E-13 | 5.16E-12 | 3.80E-02 | 5.22E-12 | 2.60E-13 | 0.0052 | 0.0005 | 205.23 | 0.54 |
| 4 | 761 | 3.07E-08 | 5.50E-11 | 3.00E-08 | 1.62E-09 | 3.70E-12 | 21.39 | 2.31E-11 | 1.90E-13 | 1.38E-11 | 1.90E-02 | 2.46E-12 | 2.80E-13 | 0.0170 | 0.0005 | 206.69 | 0.77 |
| 5 | 812 | 2.01E-08 | 8.00E-12 | 1.94E-08 | 1.06E-09 | 1.20E-12 | 14.01 | 1.65E-11 | 1.90E-13 | 5.83E-12 | 2.00E-02 | 2.56E-12 | 2.10E-13 | 0.0110 | 0.0008 | 203.98 | 0.65 |
| 6 | 881 | 1.51E-08 | 7.10E-12 | 1.44E-08 | 7.96E-10 | 9.10E-13 | 10.50 | 1.15E-11 | 1.20E-13 | 7.62E-12 | 2.60E-02 | 2.51E-12 | 2.60E-13 | 0.0192 | 0.0005 | 202.57 | 1.10 |
| 7 | 981 | 1.19E-08 | 5.20E-12 | 1.14E-08 | 6.26E-10 | 7.60E-13 | 8.25 | 1.03E-11 | 2.10E-13 | 1.12E-11 | 3.70E-02 | 1.59E-12 | 2.10E-13 | 0.0357 | 0.0010 | 203.87 | 1.10 |
| 8 | 1158 | 8.87E-09 | 6.80E-12 | 8.69E-09 | 4.65E-10 | 5.20E-13 | 6.14 | 6.70E-12 | 1.30E-13 | 2.08E-11 | 2.20E-02 | 6.12E-13 | 2.50E-13 | 0.0895 | 0.0006 | 208.76 | 1.70 |
| 9 | 1287 | 1.49E-09 | 8.00E-13 | 1.39E-09 | 7.30E-11 | 1.20E-13 | 0.96 | 1.30E-12 | 1.70E-13 | 6.68E-12 | 1.40E-02 | 3.34E-13 | 2.30E-13 | 0.1832 | 0.0012 | 213.13 | 9.70 |
| 10 | 1384 | 3.68E-10 | 6.60E-14 | 3.86E-10 | 1.20E-11 | 3.50E-14 | 0.16 | 4.45E-13 | 1.90E-13 | 1.69E-12 | 3.10E-02 | ######## | ######## | 0.2827 | 0.0061 | 346.44 | 54.00 |
| | | | | | | | | | | | | | | | **age** | **204.84** | |

**CF 96-21d Biotite**

| Step | Temperature (°C) | Ar 40 tot. | σ40 | Ar 40 * | Ar 39 | σ39 | 39Ar% | Ar 38 | σ38 | Ar 37 | σ37 | Ar 36 | σ36 | Ca / K | Cl/K | Age (Ma) | σ |
|---|---|---|---|---|---|---|---|---|---|---|---|---|---|---|---|---|---|
| 1 | 449 | 1.6121E-08 | 5.40E-12 | 8.19E-09 | 5.86E-10 | 5.60E-13 | 4.30 | 4.66E-11 | 3.20E-13 | 6.32E-11 | 3.10E-02 | 2.69E-11 | 2.90E-13 | 0.2138 | 0.0136 | 158.56 | 1.60 |
| 2 | 514 | 8.2055E-09 | 2.90E-12 | 7.01E-09 | 4.07E-10 | 4.10E-13 | 2.98 | 1.95E-11 | 1.60E-13 | 2.00E-11 | 3.20E-02 | 4.04E-12 | 2.40E-13 | 0.0984 | 0.0079 | 193.57 | 1.80 |
| 3 | 569 | 1.6533E-08 | 5.50E-12 | 1.57E-08 | 8.45E-10 | 8.10E-13 | 6.20 | 3.59E-11 | 1.80E-13 | 1.17E-11 | 3.20E-02 | 2.98E-12 | 2.40E-13 | 0.0276 | 0.0069 | 207.31 | 0.92 |
| 4 | 599 | 2.3026E-08 | 8.00E-12 | 2.25E-08 | 1.19E-09 | 1.30E-12 | 8.76 | 4.96E-11 | 2.10E-13 | 1.03E-11 | 2.90E-02 | 1.65E-12 | 2.10E-13 | 0.0172 | 0.0068 | 210.93 | 0.60 |
| 5 | 631 | 2.5317E-08 | 8.70E-12 | 2.51E-08 | 1.33E-09 | 1.30E-12 | 9.76 | 5.36E-11 | 1.80E-13 | 1.34E-11 | 3.00E-02 | 8.44E-13 | 2.30E-13 | 0.0201 | 0.0065 | 210.48 | 0.58 |
| 6 | 708 | 3.2037E-08 | 7.60E-12 | 3.13E-08 | 1.67E-09 | 1.60E-12 | 12.23 | 6.77E-11 | 1.90E-13 | 2.42E-11 | 3.40E-02 | 2.34E-12 | 2.50E-13 | 0.0290 | 0.0066 | 210.13 | 0.51 |
| 7 | 746 | 1.4804E-08 | 3.70E-12 | 1.43E-08 | 7.64E-10 | 7.80E-13 | 5.61 | 3.09E-11 | 1.90E-13 | 2.13E-11 | 2.80E-02 | 1.74E-12 | 2.10E-13 | 0.0558 | 0.0065 | 209.06 | 0.87 |
| 8 | 820 | 1.4116E-08 | 4.90E-12 | 1.35E-08 | 7.23E-10 | 7.00E-13 | 5.30 | 3.05E-11 | 1.60E-13 | 2.50E-11 | 1.50E-02 | 2.26E-12 | 2.50E-13 | 0.0691 | 0.0069 | 208.06 | 1.10 |
| 9 | 878 | 2.3492E-08 | 8.30E-12 | 2.31E-08 | 1.21E-09 | 1.10E-12 | 8.89 | 4.90E-11 | 1.90E-13 | 6.46E-11 | 1.90E-02 | 1.44E-12 | 2.20E-13 | 0.1066 | 0.0065 | 212.61 | 0.59 |
| 10 | 982 | 6.3717E-08 | 1.70E-11 | 6.32E-08 | 3.37E-09 | 3.10E-12 | 24.74 | 1.36E-10 | 3.30E-13 | 1.05E-10 | 2.90E-02 | 1.90E-12 | 2.20E-13 | 0.0625 | 0.0066 | 209.40 | 0.27 |
| 11 | 1074 | 2.2889E-08 | 4.90E-12 | 2.25E-08 | 1.21E-09 | 1.10E-12 | 8.86 | 4.79E-11 | 2.20E-13 | 1.83E-10 | 4.30E-02 | 1.34E-12 | 2.20E-13 | 0.3031 | 0.0064 | 208.33 | 0.58 |
| 12 | 1152 | 4.7624E-09 | 5.50E-13 | 4.67E-09 | 2.47E-10 | 2.70E-13 | 1.81 | 9.46E-12 | 1.30E-13 | 7.26E-11 | 2.50E-02 | 3.27E-13 | 2.80E-13 | 0.5891 | 0.0061 | 211.62 | 3.30 |
| 13 | 1389 | 1.6468E-09 | 5.40E-13 | 1.48E-09 | 7.78E-11 | 2.40E-13 | 0.57 | 2.71E-12 | 1.80E-13 | 6.53E-11 | 2.40E-02 | 5.66E-13 | 2.10E-13 | 1.6790 | 0.0050 | 213.15 | 8.10 |
| | | | | | | | | | | | | | | | **age** | **207.13** | |

**BJ 95-08 Phengite**

| Step | Temperature (°C) | Ar 40 tot. | σ40 | Ar 40 * | Ar 39 | σ39 | 39Ar% | Ar 38 | σ38 | Ar 37 | σ37 | Ar 36 | σ36 | Ca / K | Cl/K | Age (Ma) | σ |
|---|---|---|---|---|---|---|---|---|---|---|---|---|---|---|---|---|---|
| 1 | 613 | 1.70E-08 | 1.10E-11 | 1.20E-08 | 6.88E-10 | 7.30E-13 | 3.82 | 2.04E-11 | 1.80E-13 | 1.53E-11 | 1.20E-02 | 1.69E-11 | 2.10E-13 | 0.0445 | 0.0031 | 196.38 | 0.97 |
| 2 | 692 | 4.32E-08 | 1.80E-11 | 4.17E-08 | 2.32E-09 | 2.30E-12 | 12.89 | 3.25E-11 | 1.90E-13 | 5.45E-12 | 1.50E-02 | 4.82E-12 | 1.80E-13 | 0.0047 | 0.0004 | 201.24 | 0.32 |
| 3 | 715 | 7.72E-08 | 4.20E-11 | 7.64E-08 | 4.17E-09 | 4.40E-12 | 23.15 | 6.05E-11 | 2.40E-13 | 5.77E-12 | 1.90E-02 | 2.73E-12 | 2.10E-13 | 0.0028 | 0.0006 | 204.95 | 0.28 |
| 4 | 741 | 4.66E-08 | 2.20E-11 | 4.64E-08 | 2.52E-09 | 3.00E-12 | 13.99 | 3.57E-11 | 1.30E-13 | 3.91E-12 | 1.90E-02 | 6.85E-13 | 1.80E-13 | 0.0031 | 0.0005 | 206.10 | 0.34 |
| 5 | 764 | 3.90E-08 | 2.00E-11 | 3.89E-08 | 2.11E-09 | 2.10E-12 | 11.73 | 2.91E-11 | 1.40E-13 | 2.26E-12 | 1.50E-02 | 2.81E-13 | 2.00E-13 | 0.0021 | 0.0005 | 206.12 | 0.37 |
| 6 | 789 | 2.76E-08 | 1.50E-11 | 2.71E-08 | 1.49E-09 | 1.50E-12 | 8.28 | 2.10E-11 | 2.10E-13 | -1.14E-12 | ######## | 1.68E-12 | 1.70E-13 | -0.0015 | 0.0005 | 203.48 | 0.43 |
| 7 | 815 | 1.98E-08 | 9.80E-12 | 1.94E-08 | 1.07E-09 | 1.10E-12 | 5.93 | 1.54E-11 | 1.90E-13 | 6.86E-12 | 4.30E-02 | 1.38E-12 | 2.10E-13 | 0.0128 | 0.0006 | 203.07 | 0.66 |
| 8 | 846 | 1.59E-08 | 5.90E-12 | 1.57E-08 | 8.51E-10 | 9.00E-13 | 4.72 | 1.34E-11 | 1.20E-13 | 4.46E-12 | 3.50E-02 | 8.16E-13 | 2.50E-13 | 0.0105 | 0.0009 | 205.93 | 0.93 |
| 9 | 870 | 1.43E-08 | 6.70E-12 | 1.40E-08 | 7.62E-10 | 8.00E-13 | 4.23 | 1.03E-11 | 1.70E-13 | -2.12E-12 | ######## | 8.75E-13 | 2.50E-13 | -0.0056 | 0.0004 | 205.73 | 1.00 |
| 10 | 900 | 1.15E-08 | 5.80E-12 | 1.15E-08 | 6.17E-10 | 6.60E-13 | 3.43 | 9.04E-12 | 2.00E-13 | 4.16E-13 | 2.00E-02 | 5.27E-14 | 2.20E-13 | 0.0013 | 0.0007 | 208.89 | 1.20 |
| 11 | 964 | 7.72E-09 | 3.00E-12 | 7.74E-09 | 4.13E-10 | 4.00E-13 | 2.29 | 5.30E-12 | 1.50E-13 | -1.05E-12 | ######## | ######## | ######## | -0.0051 | 0.0003 | 209.52 | 1.60 |
| 12 | 1022 | 5.23E-09 | 3.90E-12 | 5.13E-09 | 2.81E-10 | 2.80E-13 | 1.56 | 4.13E-12 | 9.90E-14 | 7.76E-12 | 2.30E-02 | 3.26E-13 | 2.20E-13 | 0.0553 | 0.0006 | 204.75 | 2.40 |
| 13 | 1073 | 5.86E-09 | 3.00E-12 | 5.84E-09 | 3.16E-10 | 3.30E-13 | 1.75 | 4.41E-12 | 1.70E-13 | 4.43E-12 | 2.70E-02 | 5.40E-14 | 2.40E-13 | 0.0280 | 0.0005 | 207.02 | 2.30 |
| 14 | 1135 | 4.27E-09 | 3.60E-12 | 4.08E-09 | 2.27E-10 | 3.70E-13 | 1.26 | 3.55E-12 | 1.90E-13 | 1.22E-11 | 1.30E-02 | 6.34E-13 | 2.50E-13 | 0.1077 | 0.0008 | 201.72 | 3.50 |
| 15 | 1220 | 2.18E-09 | 2.00E-12 | 2.30E-09 | 1.11E-10 | 1.50E-13 | 0.61 | 2.25E-12 | 2.20E-13 | 2.34E-12 | 3.70E-02 | ######## | ######## | 0.0423 | 0.0021 | 230.94 | 7.40 |
| 16 | 1335 | 1.41E-09 | 1.40E-12 | 1.30E-09 | 6.52E-11 | 1.30E-13 | 0.36 | 3.84E-13 | 2.10E-13 | 3.83E-12 | 2.30E-02 | 3.68E-13 | 2.50E-13 | 0.1174 | ###### | 221.48 | 12.00 |
| 17 | 1380 | 7.81E-11 | 1.70E-13 | 2.23E-10 | 5.67E-13 | 2.20E-13 | 0.00 | 2.15E-12 | 3.90E-13 | -1.18E-14 | ######## | ######## | ######## | -0.0416 | 0.9056 | 2301.93 | 620.00 |
| | | | | | | | | | | | | | | | **age** | **204.87** | |

**BJ 95-08 Biotite**

| Step | Temperature (°C) | Ar 40 tot. | σ40 | Ar 40 * | Ar 39 | σ39 | 39Ar% | Ar 38 | σ38 | Ar 37 | σ37 | Ar 36 | σ36 | Ca / K | Cl/K | Age (Ma) | σ |
|---|---|---|---|---|---|---|---|---|---|---|---|---|---|---|---|---|---|
| 1 | 459 | 2.51E-08 | 1.70E-10 | 7.47E-09 | 6.72E-10 | 4.60E-12 | 5.09 | 5.96E-11 | 1.10E-12 | 1.23E-10 | 1.30E-02 | 5.99E-11 | 4.20E-13 | 0.3655 | 0.0139 | 127.16 | 2.40 |
| 2 | 528 | 1.66E-08 | 2.00E-11 | 1.07E-08 | 6.74E-10 | 1.10E-12 | 5.11 | 2.99E-11 | 3.00E-13 | 4.94E-11 | 2.10E-02 | 1.99E-11 | 2.50E-13 | 0.1465 | 0.0062 | 178.93 | 1.20 |
| 3 | 586 | 2.16E-08 | 2.10E-11 | 1.96E-08 | 1.12E-09 | 1.50E-12 | 8.50 | 2.99E-11 | 1.70E-13 | 2.91E-11 | 1.50E-02 | 6.78E-12 | 2.30E-13 | 0.0518 | 0.0032 | 195.70 | 0.72 |
| 4 | 610 | 2.15E-08 | 2.40E-11 | 2.07E-08 | 1.16E-09 | 1.60E-12 | 8.78 | 3.36E-11 | 2.20E-13 | 1.27E-11 | 2.30E-02 | 2.72E-12 | 2.00E-13 | 0.0219 | 0.0039 | 200.00 | 0.63 |
| 5 | 637 | 1.77E-08 | 1.90E-11 | 1.70E-08 | 9.44E-10 | 1.10E-12 | 7.15 | 2.49E-11 | 1.60E-13 | 7.92E-12 | 2.50E-02 | 2.34E-12 | 1.70E-13 | 0.0168 | 0.0033 | 201.77 | 0.63 |
| 6 | 713 | 2.19E-08 | 1.60E-11 | 2.05E-08 | 1.14E-09 | 1.40E-12 | 8.61 | 2.87E-11 | 2.40E-13 | 2.23E-11 | 1.10E-02 | 4.75E-12 | 2.20E-13 | 0.0393 | 0.0029 | 202.06 | 0.67 |
| 7 | 747 | 1.42E-08 | 1.80E-12 | 1.29E-08 | 7.26E-10 | 7.50E-13 | 5.50 | 1.77E-11 | 8.60E-14 | 1.95E-11 | 2.00E-02 | 4.48E-12 | 2.10E-13 | 0.0538 | 0.0026 | 199.05 | 0.93 |
| 8 | 809 | 1.34E-08 | 3.40E-12 | 1.23E-08 | 6.86E-10 | 6.60E-13 | 5.20 | 1.82E-11 | 1.90E-13 | 3.41E-11 | 1.90E-02 | 3.48E-12 | 1.80E-13 | 0.0995 | 0.0032 | 201.58 | 0.84 |
| 9 | 857 | 1.40E-08 | 2.70E-12 | 1.33E-08 | 7.21E-10 | 7.50E-13 | 5.46 | 1.89E-11 | 1.20E-13 | 2.99E-11 | 1.90E-02 | 2.39E-12 | 2.20E-13 | 0.0829 | 0.0032 | 206.23 | 0.98 |
| 10 | 922 | 2.63E-08 | 7.80E-12 | 2.57E-08 | 1.41E-09 | 1.40E-12 | 10.66 | 3.38E-11 | 1.20E-13 | 1.34E-10 | 2.70E-02 | 2.08E-12 | 1.90E-13 | 0.1902 | 0.0028 | 204.81 | 0.47 |
| 11 | 983 | 3.87E-08 | 2.30E-11 | 3.86E-08 | 2.12E-09 | 2.20E-12 | 16.02 | 4.99E-11 | 1.90E-13 | 1.31E-10 | 2.60E-02 | 4.84E-13 | 2.50E-13 | 0.1238 | 0.0027 | 204.25 | 0.42 |
| 12 | 1072 | 2.29E-08 | 4.80E-12 | 2.27E-08 | 1.27E-09 | 1.20E-12 | 9.61 | 2.88E-11 | 1.50E-13 | 3.54E-10 | 4.90E-02 | 1.05E-12 | 2.10E-13 | 0.5587 | 0.0025 | 200.28 | 0.52 |
| 13 | 1153 | 6.09E-09 | 1.70E-12 | 5.76E-09 | 3.44E-10 | 3.70E-13 | 2.61 | 6.88E-12 | 1.70E-13 | 2.40E-10 | 3.30E-02 | 1.16E-12 | 2.50E-13 | 1.3943 | 0.0018 | 188.29 | 2.20 |
| 14 | 1392 | 4.20E-09 | 2.30E-12 | 3.83E-09 | 2.25E-10 | 2.80E-13 | 1.70 | 6.18E-12 | 1.30E-13 | 2.10E-10 | 3.50E-02 | 1.29E-12 | 2.00E-13 | 1.8663 | 0.0034 | 191.63 | 2.80 |
| | | | | | | | | | | | | | | | **age** | **196.37** | |

Table II-8: Ar-Ar analytical data on phengite from paragneisses of the Bixiling Complex.

**CF 96-21b Phengite**

| Step | Temperature (°C) | Ar 40 tot. | σ40 | Ar 40 * | Ar 39 | σ39 | 39Ar% | Ar 38 | σ38 | Ar 37 | σ37 | Ar 36 | σ36 | Ca / K | Cl/K | Age (Ma) | σ |
|---|---|---|---|---|---|---|---|---|---|---|---|---|---|---|---|---|---|
| 1 | 554 | 2.29E-08 | 7.00E-12 | 1.35E-08 | 6.43E-10 | 6.90E-13 | 1.65 | 8.01E-11 | 2.30E-13 | 3.80E-11 | 2.40E-02 | 3.18E-11 | 2.60E-13 | 0.1184 | 0.0238 | 233.86 | 1.30 |
| 2 | 642 | 1.06E-08 | 2.80E-12 | 8.03E-09 | 4.41E-10 | 4.70E-13 | 1.13 | 1.40E-11 | 2.10E-13 | 2.83E-11 | 3.00E-02 | 8.71E-12 | 2.40E-13 | 0.1282 | 0.0037 | 203.88 | 1.70 |
| 3 | 691 | 2.64E-08 | 8.90E-12 | 2.39E-08 | 1.29E-09 | 1.30E-12 | 3.32 | 2.10E-11 | 1.40E-13 | 1.79E-11 | 1.50E-02 | 8.41E-12 | 1.80E-13 | 0.0278 | 0.0008 | 206.91 | 0.47 |
| 4 | 714 | 9.85E-08 | 5.30E-11 | 9.29E-08 | 4.99E-09 | 5.50E-12 | 12.83 | 7.36E-11 | 2.30E-13 | 3.77E-11 | 2.00E-02 | 1.89E-11 | 2.50E-13 | 0.0151 | 0.0005 | 208.15 | 0.29 |
| 5 | 738 | 1.27E-07 | 1.10E-10 | 1.24E-07 | 6.52E-09 | 6.30E-12 | 16.75 | 9.20E-11 | 3.00E-13 | 5.16E-11 | 3.30E-02 | 1.27E-11 | 2.40E-13 | 0.0158 | 0.0005 | 211.87 | 0.29 |
| 6 | 763 | 9.42E-08 | 1.00E-10 | 9.17E-08 | 4.83E-09 | 6.30E-12 | 12.41 | 6.96E-11 | 2.00E-13 | 8.59E-11 | 2.50E-02 | 8.61E-12 | 2.30E-13 | 0.0356 | 0.0005 | 212.12 | 0.37 |
| 7 | 787 | 7.85E-08 | 5.40E-11 | 7.63E-08 | 4.02E-09 | 4.90E-12 | 10.34 | 5.81E-11 | 3.00E-13 | 1.47E-10 | 2.10E-02 | 7.43E-12 | 2.00E-13 | 0.0730 | 0.0005 | 212.00 | 0.32 |
| 8 | 811 | 6.01E-08 | 1.80E-11 | 5.84E-08 | 3.08E-09 | 2.80E-12 | 7.92 | 4.47E-11 | 2.30E-13 | 1.89E-10 | 3.20E-02 | 5.85E-12 | 2.20E-13 | 0.1229 | 0.0006 | 211.74 | 0.30 |
| 9 | 845 | 4.67E-08 | 1.20E-11 | 4.50E-08 | 2.37E-09 | 2.30E-12 | 6.09 | 3.47E-11 | 2.40E-13 | 2.94E-10 | 3.40E-02 | 5.79E-12 | 2.70E-13 | 0.2478 | 0.0006 | 211.97 | 0.40 |
| 10 | 869 | 5.24E-08 | 1.60E-11 | 5.07E-08 | 2.67E-09 | 2.70E-12 | 6.86 | 3.87E-11 | 1.40E-13 | 4.31E-10 | 4.70E-02 | 6.00E-12 | 2.20E-13 | 0.3231 | 0.0005 | 211.95 | 0.33 |
| 11 | 901 | 4.69E-08 | 1.10E-11 | 4.59E-08 | 2.42E-09 | 2.30E-12 | 6.23 | 3.60E-11 | 2.10E-13 | 2.68E-10 | 4.50E-02 | 3.38E-12 | 2.40E-13 | 0.2214 | 0.0007 | 211.76 | 0.36 |
| 12 | 963 | 5.10E-08 | 3.50E-11 | 4.97E-08 | 2.63E-09 | 2.80E-12 | 6.76 | 3.81E-11 | 3.10E-13 | 2.09E-10 | 4.60E-02 | 4.58E-12 | 1.80E-13 | 0.1588 | 0.0006 | 211.12 | 0.33 |
| 13 | 1022 | 2.55E-08 | 9.20E-12 | 2.44E-08 | 1.27E-09 | 1.30E-12 | 3.28 | 1.87E-11 | 2.80E-13 | 4.35E-10 | 7.20E-02 | 3.84E-12 | 2.20E-13 | 0.6830 | 0.0006 | 213.39 | 0.57 |
| 14 | 1075 | 1.79E-08 | 4.90E-12 | 1.68E-08 | 8.69E-10 | 8.30E-13 | 2.23 | 1.38E-11 | 1.50E-13 | 1.72E-10 | 3.10E-02 | 3.86E-12 | 1.90E-13 | 0.3955 | 0.0008 | 215.42 | 0.70 |
| 15 | 1141 | 1.27E-08 | 3.70E-12 | 1.06E-08 | 5.50E-10 | 5.50E-13 | 1.41 | 8.94E-12 | 2.20E-13 | 9.81E-11 | 2.60E-02 | 7.05E-12 | 2.10E-13 | 0.3567 | 0.0005 | 215.95 | 1.20 |
| 16 | 1288 | 7.21E-09 | 2.80E-12 | 5.88E-09 | 2.61E-10 | 2.80E-13 | 0.67 | 4.67E-12 | 1.70E-13 | 9.87E-11 | 4.10E-02 | 4.53E-12 | 1.80E-13 | 0.7570 | 0.0007 | 249.05 | 2.10 |
| 17 | 1369 | 2.34E-09 | 1.00E-12 | 1.20E-09 | 4.66E-11 | 2.50E-13 | 0.12 | 2.90E-12 | 8.70E-14 | 8.99E-11 | 2.20E-02 | 3.87E-12 | 2.10E-13 | 3.8636 | 0.0081 | 282.20 | 13.00 |
| | | | | | | | | | | | | | | | age | **212.01** | |

**CF 96-21c Phengite**

| Step | Temperature (°C) | Ar 40 tot. | σ40 | Ar 40 * | Ar 39 | σ39 | 39Ar% | Ar 38 | σ38 | Ar 37 | σ37 | Ar 36 | σ36 | Ca / K | Cl/K | Age (Ma) | σ |
|---|---|---|---|---|---|---|---|---|---|---|---|---|---|---|---|---|---|
| 1 | 539 | 2.43E-08 | 1.20E-11 | 1.54E-08 | 7.12E-10 | 7.90E-13 | 1.64 | 5.89E-11 | 2.00E-13 | 3.95E-11 | 2.90E-02 | 3.02E-11 | 2.90E-13 | 0.1109 | 0.0145 | 239.55 | 1.30 |
| 2 | 634 | 1.29E-08 | 8.00E-12 | 9.48E-09 | 5.54E-10 | 6.60E-13 | 1.28 | 1.29E-11 | 2.40E-13 | 2.14E-11 | 2.10E-02 | 1.14E-11 | 2.70E-13 | 0.0773 | 0.0018 | 192.29 | 1.60 |
| 3 | 685 | 3.70E-08 | 2.00E-11 | 3.42E-08 | 1.89E-09 | 2.40E-12 | 4.37 | 2.86E-11 | 2.90E-13 | 2.05E-11 | 2.00E-02 | 9.46E-12 | 2.40E-13 | 0.0216 | 0.0006 | 202.27 | 0.48 |
| 4 | 711 | 1.41E-07 | 8.20E-11 | 1.34E-07 | 7.18E-09 | 8.10E-12 | 16.59 | 1.04E-10 | 2.50E-13 | 4.58E-11 | 3.30E-02 | 2.19E-11 | 1.90E-13 | 0.0128 | 0.0005 | 208.68 | 0.26 |
| 5 | 737 | 1.24E-07 | 9.30E-11 | 1.19E-07 | 6.33E-09 | 8.20E-12 | 14.61 | 9.17E-11 | 2.70E-13 | 6.43E-11 | 3.00E-02 | 1.43E-11 | 1.90E-13 | 0.0203 | 0.0005 | 210.91 | 0.31 |
| 6 | 760 | 8.16E-08 | 6.30E-11 | 7.87E-08 | 4.16E-09 | 6.30E-12 | 9.60 | 5.98E-11 | 2.40E-13 | 9.49E-11 | 3.40E-02 | 9.85E-12 | 2.00E-13 | 0.0456 | 0.0005 | 211.47 | 0.37 |
| 7 | 786 | 7.36E-08 | 2.10E-11 | 7.11E-08 | 3.74E-09 | 4.50E-12 | 8.64 | 5.55E-11 | 3.40E-13 | 1.08E-10 | 1.90E-02 | 8.39E-12 | 2.60E-13 | 0.0575 | 0.0006 | 212.38 | 0.33 |
| 8 | 811 | 5.97E-08 | 1.50E-11 | 5.75E-08 | 3.04E-09 | 3.60E-12 | 7.03 | 4.62E-11 | 2.20E-13 | 1.13E-10 | 2.60E-02 | 7.45E-12 | 2.40E-13 | 0.0740 | 0.0007 | 211.07 | 0.34 |
| 9 | 845 | 5.15E-08 | 2.00E-11 | 4.99E-08 | 2.60E-09 | 3.60E-12 | 6.01 | 3.72E-11 | 1.40E-13 | 1.21E-10 | 1.80E-02 | 5.24E-12 | 2.20E-13 | 0.0929 | 0.0005 | 214.16 | 0.39 |
| 10 | 871 | 5.64E-08 | 3.20E-11 | 5.43E-08 | 2.84E-09 | 2.80E-12 | 6.57 | 4.25E-11 | 2.40E-13 | 3.94E-10 | 4.50E-02 | 7.29E-12 | 2.60E-13 | 0.2774 | 0.0006 | 213.27 | 0.36 |
| 11 | 903 | 5.80E-08 | 5.50E-11 | 5.63E-08 | 2.98E-09 | 4.30E-12 | 6.87 | 4.35E-11 | 2.60E-13 | 2.55E-10 | 3.10E-02 | 6.03E-12 | 2.50E-13 | 0.1713 | 0.0006 | 211.26 | 0.43 |
| 12 | 969 | 6.95E-08 | 1.80E-11 | 6.78E-08 | 3.62E-09 | 3.90E-12 | 8.36 | 5.19E-11 | 2.10E-13 | 1.40E-10 | 4.00E-02 | 5.79E-12 | 2.40E-13 | 0.0775 | 0.0005 | 209.33 | 0.30 |
| 13 | 1027 | 3.49E-08 | 2.40E-11 | 3.33E-08 | 1.78E-09 | 2.10E-12 | 4.11 | 2.61E-11 | 2.00E-13 | 3.24E-10 | 4.80E-02 | 5.49E-12 | 2.00E-13 | 0.3641 | 0.0005 | 208.91 | 0.44 |
| 14 | 1080 | 2.04E-08 | 7.70E-12 | 1.80E-08 | 9.62E-10 | 9.00E-13 | 2.22 | 1.68E-11 | 2.30E-13 | 1.96E-10 | 5.20E-02 | 8.17E-12 | 2.30E-13 | 0.4078 | 0.0010 | 209.28 | 0.75 |
| 15 | 1148 | 1.45E-08 | 3.90E-12 | 1.23E-08 | 6.28E-10 | 6.80E-13 | 1.45 | 1.16E-11 | 1.60E-13 | 8.84E-11 | 1.30E-02 | 7.42E-12 | 2.30E-13 | 0.2817 | 0.0010 | 218.46 | 1.20 |
| 16 | 1292 | 8.27E-09 | 4.70E-12 | 6.30E-09 | 2.77E-10 | 3.00E-13 | 0.64 | 6.52E-12 | 1.90E-13 | 7.70E-11 | 2.00E-02 | 6.71E-12 | 2.10E-13 | 0.5551 | 0.0017 | 250.87 | 2.30 |
| | | | | | | | | | | | | | | | age | **211.08** | |

Figure II-37: Ar-Ar age spectra of phengite and biotite from the three orthogneisses.

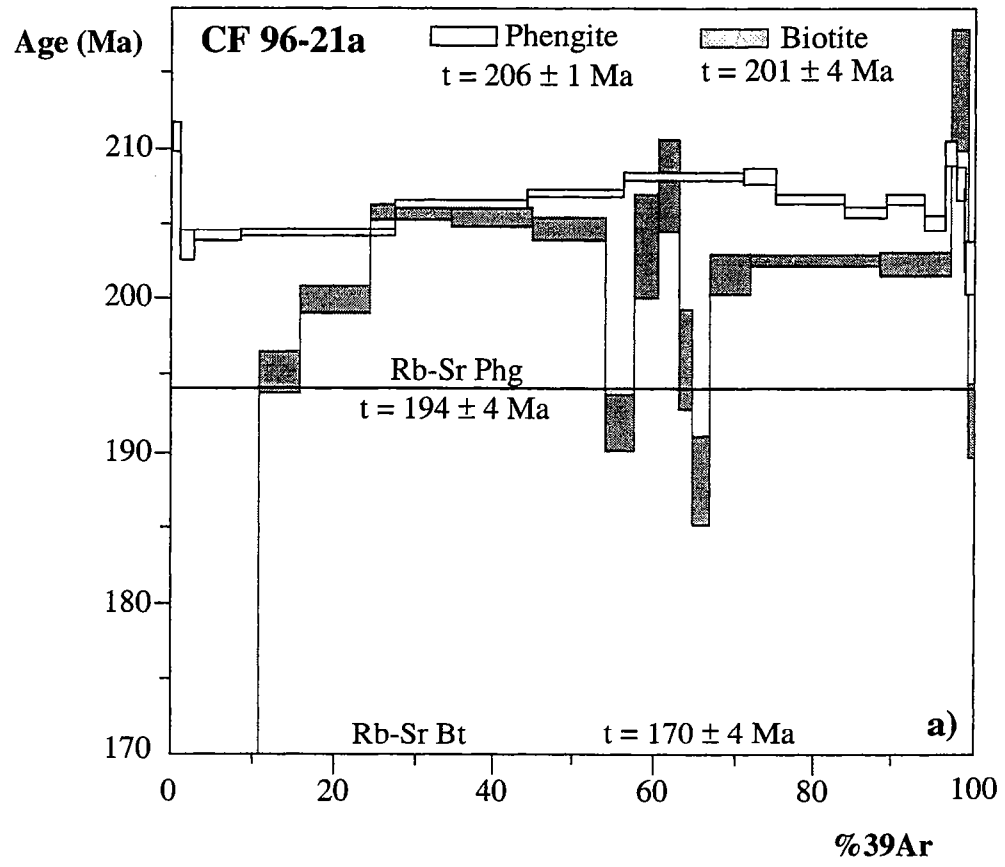


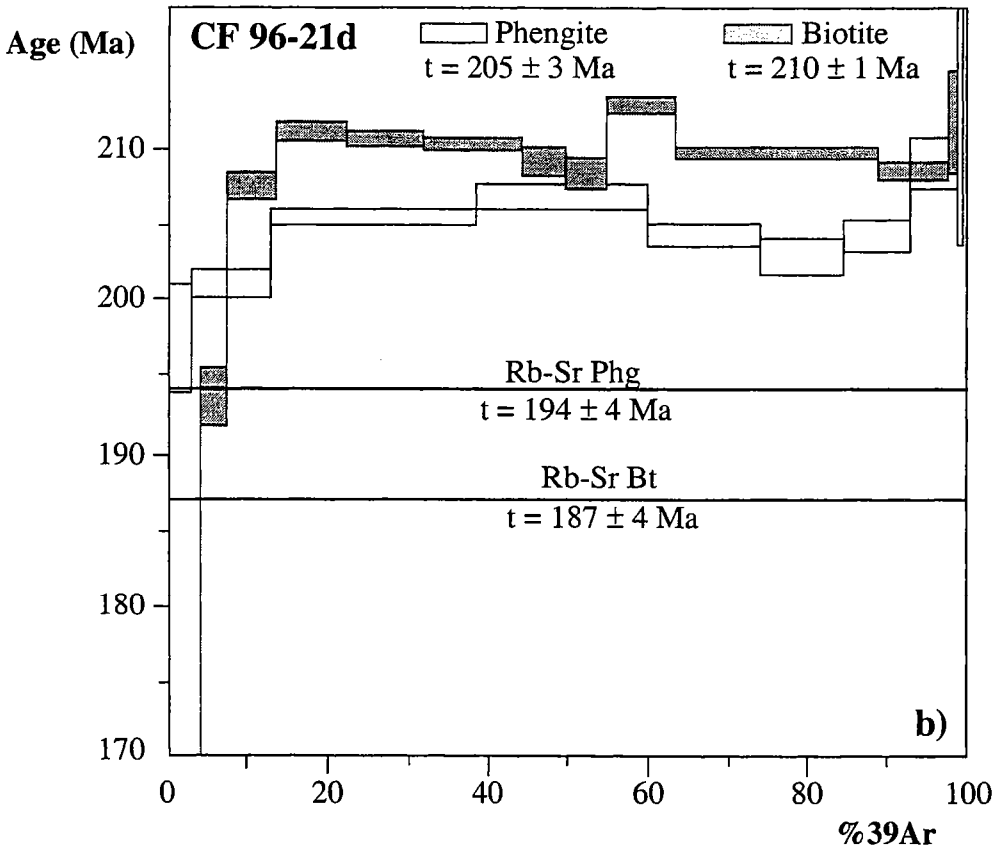

Figure II-37: Continued.

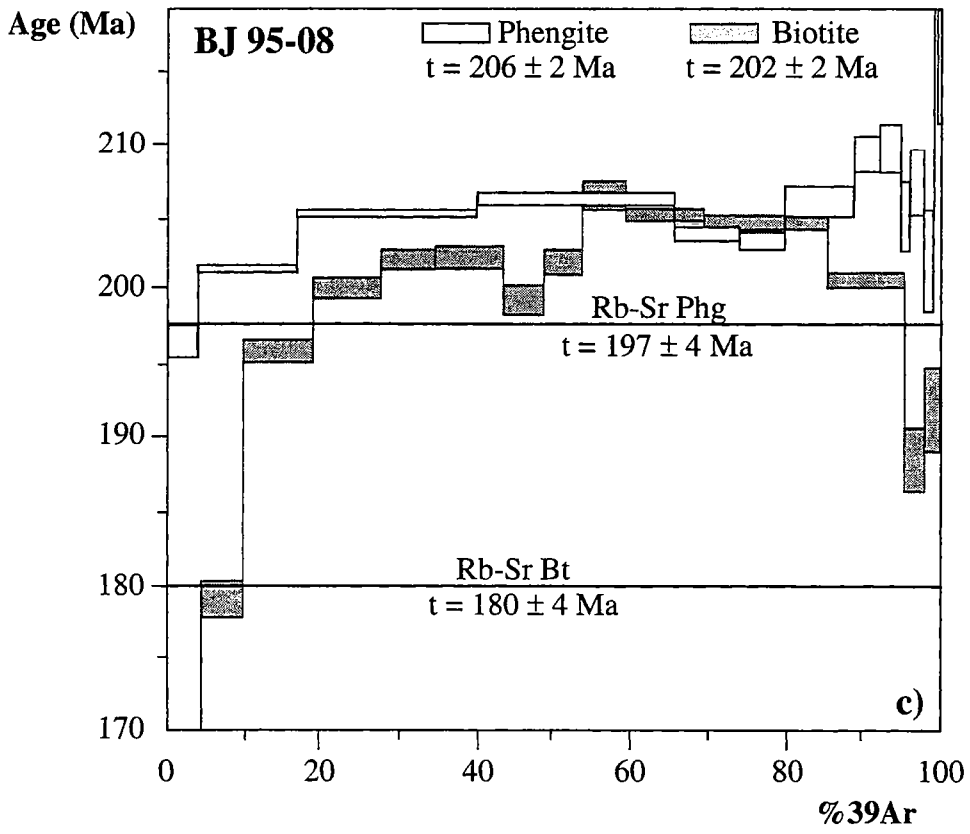

Figure II-38: Ar-Ar age spectra of phengite from the two paragneisses from the Bixiling locality.

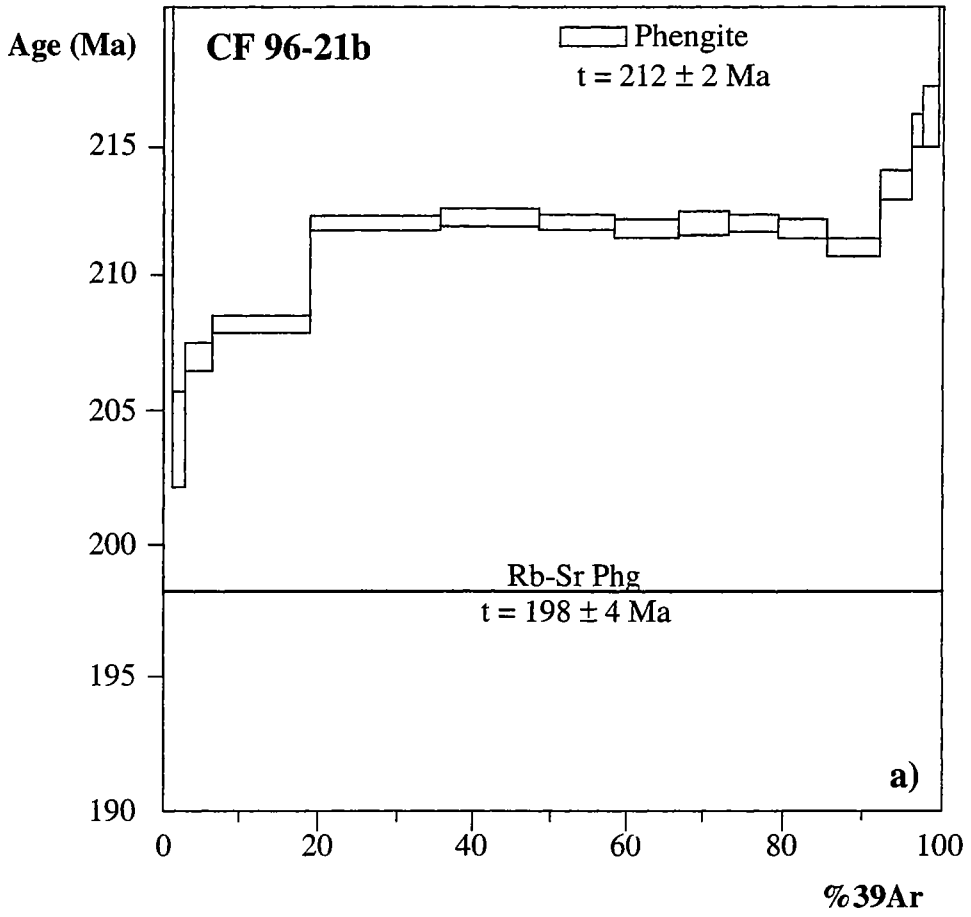


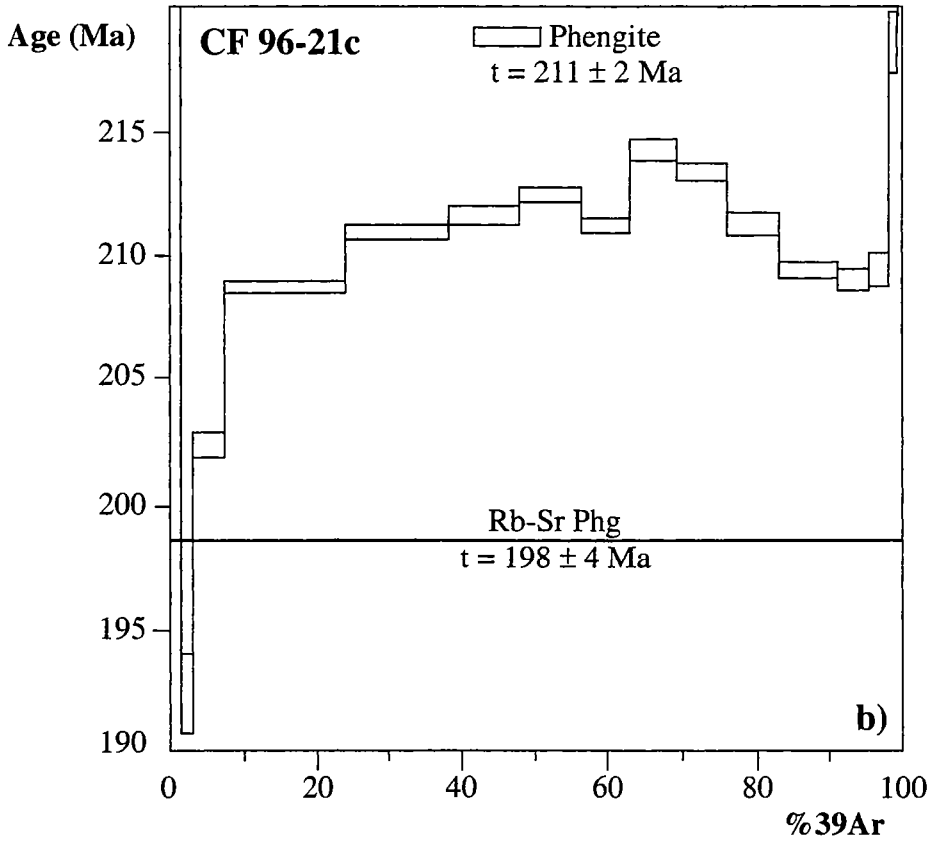

Figure II-39: Microprobe phengite analyses are reported in the Si + Fe + Mg + Mn vs AlVI + AlIV diagram in a) to highlight the extend of Tshermark substitution and in the XMg vs Si p.f.u. diagram in b to decipher different phengite generation.

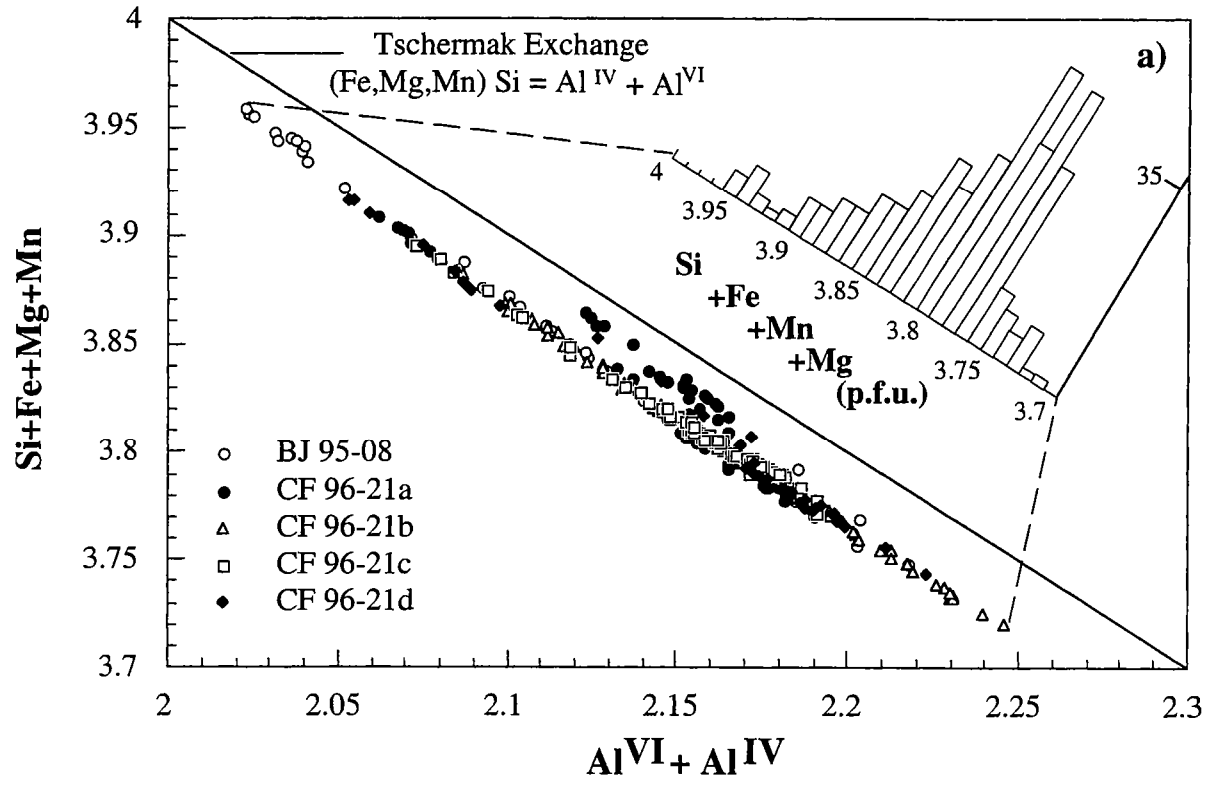


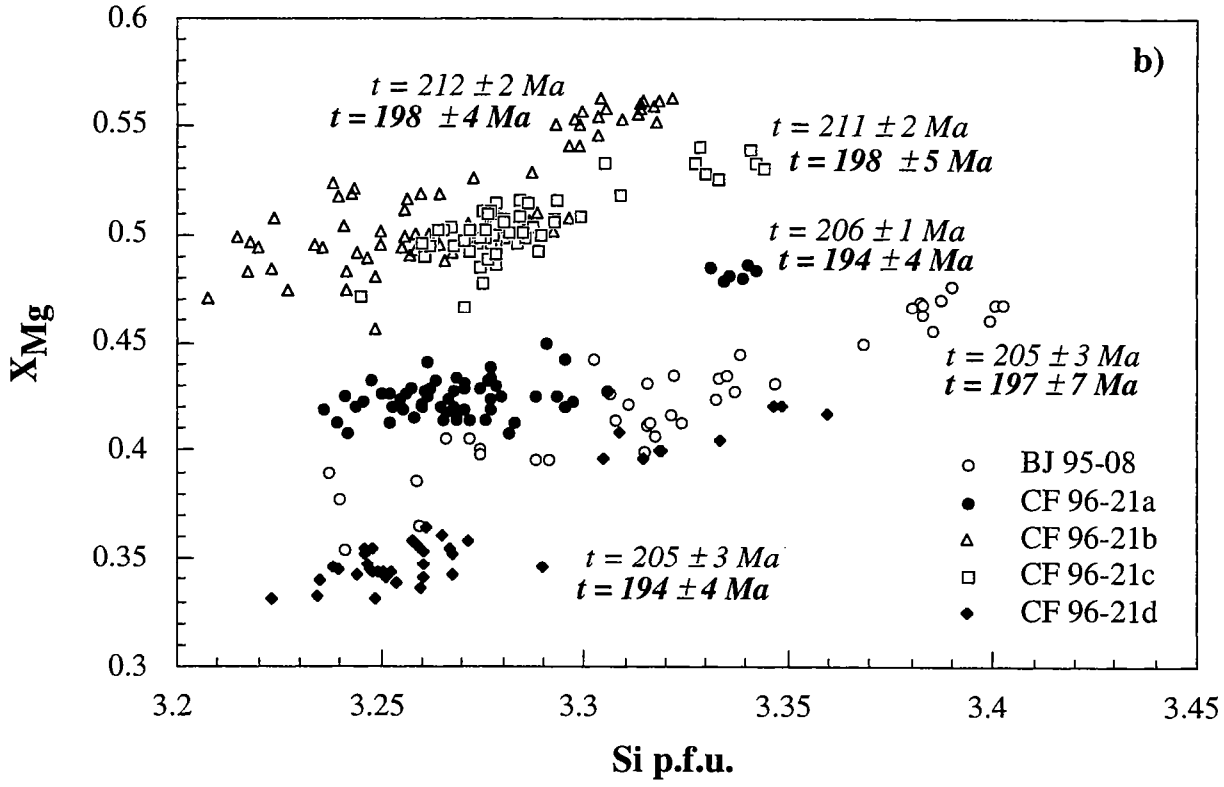

the orthogneisses indicate a volcanic-arc setting for their formation suggesting that they represent either the product of crustal anatexis or a mantle-derived magma. The Bixiling gneisses have $T_{DM}$ ages ranging from 1.35 to 1.54 Ga (Table II-4) and $\varepsilon_{Nd}$(800 Ma) equal to 0.4 to 1. Consequently, the Sm-Nd isotopic features argue that the gneisses were formed by anatexis of an older basement. On the contrary, the coesite-bearing eclogites of the Bixiling Complex derive from a basaltic protolith which had had a short crustal history (Chavagnac and Jahn 1996). They present Nb and Ta negative anomalies which provide evidences for crustal contamination during magma differentiation (Liu et al. 1995, Chavagnac and Jahn 1996). In addition, the intrusion age of the protolith of the Bixiling Complex estimated at about 300 Ma before the UHPM event is in line with the U-Pb zircon data on the host gneisses.

One of the most disputed question is the tectonic relationship between the coesite-bearing eclogites and its country rocks during the UHPM event. The UHPM event was previously dated at 210-220 Ma by Sm-Nd garnet-omphacite-WR isochrons on coesite-bearing eclogites (Chavagnac and Jahn 1996). The U-Pb SIMS data on the country rocks do not show any evidence for 210-220 Ma event. However, U-Pb zircon SIMS ages were obtained on coesite-bearing eclogites from the Bixiling Complex (Chavagnac and Jahn unpubl. data). Their light colored anhedral zircons gave $^{207}Pb/^{206}Pb$ ages at ~700 Ma whereas their dark colored rounded zircons gave a lower intercept in the Tera-Wasserburg diagram at 215 ± 22 Ma. The lack of rounded zircon occurrence within the country rocks is probably due either to an inappropriated chemical whole rock composition to permit crystallization of zircon, or to an artefact of sampling. However, Rb-Sr and Ar-Ar ages on phengite (194 ± 4 to 212 ± 2 Ma) suggest that the country rocks suffered a Triassic metamorphic event after their initial crystallization. The small spread in age overlap the previous Rb-Sr phengite ages on coesite-bearing eclogites of the Bixiling Complex at 198 ± 4 Ma to 223 ± 13 Ma (Chavagnac and Jahn 1996). The mineral paragenesis of the host gneisses at the Bixiling Complex correspond to the retrograde metamorphism under albite-epidote amphibolite facies. Moreover, the geochronological data indicate that they record a coeval metamorphic history as the eclogites suggesting an "in-situ" origin for the eclogites.

The protolith age of Shuanghe gneisses sample CF 96-39 is poorly constrained as the U-Pb SIMS data points are discordant in the concordia diagram. Nonetheless, the regression line yielded an upper intercept of about 2.5 Ga (Fig. II-34c). This is in agreement with early Proterozoic to late Archean $T_{DM}$ ages (> 2 Ga; Table II-4). The lower concordia intercept at 233 ± 21 Ma is in line with two concordant data points in the Tera-Wasserburg diagram at 226 ± 10 Ma (Fig. II-34d). In addition, a Sm-Nd garnet-kyanite-WR isochron provides an age of 231 ± 35 Ma (MSWD = 2.89; $\varepsilon_{Nd}(0)$ = -18.2; Fig. II-35). Multichronometric approach on CF 96-39 argue for a metamorphic event at about 230 Ma in line with the results of the previous U-Pb zircon and Sm-Nd garnet dating performed on

various rock types within the Dabie Mountains (Li et al. 1994, Ames et al. 1995, Chavagnac and Jahn 1996, Rowley et al. 1997). It has been shown from tectono-metamorphic studies that coesite-bearing eclogites and their associated retrograde rocks as well as coesite-bearing jadeite quartzite which present concordant contact, shared the same metamorphic evolution following a clockwise P-T path (Zhang et al. 1995, Cong et al. 1995, Liou et al. 1997). Consequently, the peak metamorphism under eclogite facies at Shuanghe is dated at 230 Ma. It still remains the problem of tectonic relationship between UHPM rocks and their host gneisses. $T_{DM}$ ages and also $\varepsilon_{Nd}(0) = -18.2$ indicate an Early Precambrian origin for the rocks forming the UHPM rocks of Shuanghe. They are difficult to interpret as the host gneisses which have a thrust contact with the UHPM rocks are Proterozoic in age (Jahn et al. 1994) and that only one small massif of granitic gneisses located in the Yangtze Craton are Archean (Zheng et al. 1991). Smith (1988) and Cong et al. (1995) argued that the UHPM rocks have an "exotic/tectonic" emplacement with the low-pressure quartzo-feldspathic gneisses. The host gneisses of the entire UHPM rocks of Shuanghe present clearly discordant foliation compared to UHPM rocks and may favoured an exotic origin of the eclogite. To provide further information on that issue, Rb-Sr and Ar-Ar dating are the appropriate approach to perform on the host gneisses as no high-grade mineralogic assemblage may be observed. Until further works, the "in-situ" and "foreign" model remains a topic of discussion at the Shuanghe locality.

### 4.5.2. Constrasted Ar-Ar and Rb-Sr mineral ages

At the Bixiling locality, Ar-Ar phengite and biotite ages vary between 198 and 212 Ma and overlap the Sm-Nd and Rb-Sr ages obtained on the coesite-bearing eclogites (Chavagnac and Jahn 1996). But, Ar-Ar phengite and biotite age spectra are up to 15 Ma older than their respective Rb-Sr phengite and biotite ages. It was argued that dating of UHP and HP metamorphic rocks can be difficult due to complex geological histories leading to possible incomplete isotope equilibration and also to open/closed system during prograde and retrograde metamorphism, i.e. providing mineral age data which are internally fickle. Several studies from the Dora Maira massif, the Himalaya or the Dabie Shan indicated that Ar-Ar dating on phengites gave ages geologically meaningless due to the effect of Ar excess (Tilton et al. 1991, Mattauer et al. 1991, Scaillet et al. 1992, Tonarini et al. 1993, Li et al. 1994, Hacker and Wang 1995, Arnaud and Kelley 1995). The difference of 15 Ma between Ar-Ar and Rb-Sr minerals ages may be interpreted as well as the consequences of Ar excess. However, spread in ages may also be the results of either several mineral generation growths, or Sr and/Ar inherited components or incomplete resetting of Ar and Sr clocks.

The clue explanation resides in the notion that hydrated minerals released Ar and minerals were isotopically equilibrated with the matrix. Therefore, mineral paragenesis observations and phengite chemistry have been investigated in detail in order to check

differences between samples and zonation within grains. The host lithology may promote or prevente the full Ar/Sr isotope exhange of phengite and biotite with the matrix (Scaillet et al. 1992, Jenkin 1997). The lack of biotite within paragneisses may induce different $X_{Mg}$ value in phengite compared to those within orthogneisses, and subsequently a dependence of Ar retention in phengite as suggested by Dahl (1996). The celadonite content of phengite is shown in terms of Tschermak substitution (Mg,Si = $Al^{IV}$,$Al^{VI}$) in Fig. II-39a illustrating variability in composition from sample to sample but also within grains. This emphasizes (1) the association of a HP phengite (high $X_{Mg}$ and Si p.f.u. contents) and a second generation of phengite, (2) the celadonitic re-equilibration of the second phengite generation during retrograde metamorphism under the albite-epidote amphibolite facies, (3) the higher $X_{Mg}$ content for phengites of paragneisses (Fig. II-39b). These observations indicate that the samples share the coeval process of a HP phengitic phase as well as the partial chemical re-equilibration toward lower P-T conditions. In addition, the phengite fractions present variable Ca/K ratios emphazing the incomplete separation of Ca-bearing phase from phengite one (Table II-7 and II-8). The mineral paragenesis observed are related to albite-epidote amphibolite facies and under these conditions the stable Ca-mineral is zoisite (Nagasaki and Enami 1998). The high Ca/K ratios is related to low and high heating steps without any systematics towards lower or higher ages. This suggests the influence of minute admixture of zoisite on the Ar gas release at low and high temperature steps (Villa et al. 1996). Moreover, the flat portion of the age spectra exhibit probably the constant degas rate between the two generations of phengite whereas the hump-shaped spectra correspond to proportional Ar gas release from the two phengites (Villa et al. 1997). Considering the Rb-Sr system, the occurrences of minute zoisite within phengite combined with the chemical variations within phengite could also disturbed the Sr isotopic equilibrium. Jenkin (1997) modeled the Sr isotope exchange between muscovite, biotite and plagioclase. He showed that Rb-Sr phengite ages may be significantly scattered (up to 15 Ma) due to the amounts of each minerals in the rock. In our case study, the main carrier of Sr is not the plagioclase but the zoisite. Therefore, the older Rb-Sr phengite ages on paragneisses could resulted from the Sr isotope exchange between only two main minerals (phengite and zoisite) whereas for orthogneisses, it is the consequences of Sr isotope exchange between three minerals (phengite, biotite and zoisite). It arises that full trace element equilibrium between phengite and the matrix may not be reached demonstrating that Rb-Sr phengite ages should be taken with caution. The Rb-Sr and or Ar-Ar biotite ages may be interpreted in the same manner as biotite chemical compositions present highly variable Ca/K ratios (Fig. II-36 and II-37, Table II-7).

Furthermore, retrograde metamorphism is also related to fluid circulation as highlighted by the transformation of eclogite into amphibolite along fractures, and also by the strong alteration of biotite into chlorite within Bixiling's host gneisses. However, the preservation of oxygen isotope equilibrium between minerals in eclogites and gneisses avoided

a regional scale infiltration of fluid during exhumation (Backer et al. 1997). As long as oxygen isotope measurements are not performed on minerals from the quartzo-feldspathic gneisses at the Bixiling locality, the effect of fluid activity at lower P-T conditions cannot be rulled out as process for incomplete Ar/Sr isotopic equilibrium.

An additional factor which may control the behaviour of radiogenic isotopes during the metamorphism is the ionic porosity ($Z_i$; Dahl 1996). The $Z_i$ value corresponds to the % of the interlayer unit cell volume which is not occupied by ions (Dahl 1996) and it is inversely porportional with the K-O bond strength. Biotite fractions which were analyzed for Ar-Ar and Rb-Sr dating, present a K content close to 4-5 wt% which is significantly below the expected K concentrations of 9-10 wt% into "clean" biotite. It appears that the K-O bonds within biotite were extensively broken during the retrograde metamorphism. Consequently, the ionic porosity within biotite may have influence the Ar/Sr isotopic equilibrium towards lower P-T conditions. In such circumstances, the incorporation of another Ar source into micas may have taken place suggesting that the older Ar-Ar phengite and biotite ages can be related to an Ar excess. Nonetheless, it seems unlikely that the Ar excess is distributed homogeneously within mica grains by volume diffusion during retrograde metamorphism.

To conclude, the Ar-Ar and Rb-Sr phengite and biotite ages overlap the previous Sm-Nd garnet and Rb-Sr phengite ages obtained on the coesite-bearing eclogite from the Bixiling Complex (Chavagnac and Jahn 1996). The host gneisses undergone an event coeval to the UHP event recorded by the coesite-bearing eclogites. However, the discrepancy between older Ar-Ar phengite and biotite ages and the respective younger Rb-Sr phengite and biotite ages can be explained by either the association of two generations of phengites, or minute admixtures of zoisite within micas disturbing the Ar/Sr isotopic equilibrium, or the Ar excess. We cannot exclude that several mechanisms may have taken place during the retrograde metamorphism.

### 4.5.3. Implications on cooling rates

The occurrence of coesite and its quartz pseudomorph as inclusions within silicate mineral of eclogites indicate that crustal and oceanic material may be burried to mantle depth and further brought back to the surface. Tectonic model aimed at the understanding of the exhumation of "mantle-depth" metamorphic rocks need crucial information regarding the exhumation and cooling rates. Consequently, Ar-Ar and Rb-Sr mineral ages are frequently used to estimate the cooling paths of metamorphic belts and igneous rocks in terms of thermochronology. In such investigations, it is implicity assumed that the isotope transfert is due to pure diffusion, leading to "blocking temperature".

Table I-9: Summarized geochronological data obtained on felsic gneisses from the Bixiling locality and the UHPM slab of Shuanghe.

| | | CF 96-21a | CF 96-21b | CF 96-21c BIXILING | CF 96-21d | BJ 95-08 | CF 96-39 SHUANGHE |
|---|---|---|---|---|---|---|---|
| U-Pb SIMS | zircon | 400 to 700Ma concordant concordia data | - | - | - | - | 2 500 Ma upper intercept 233 Ma lower intercept |
| Sm-Nd | garnet | - | - | - | - | - | 231 ± 35 Ma |
| Rb-Sr | phengite | 194 ± 4 Ma | 198 ± 5 Ma | 198 ± 5 Ma | 194 ± 4 Ma | 197 ± 7 Ma | - |
| Rb-Sr | biotite | 170 ± 4 Ma | - | - | 187 ± 4 Ma | 180 ± 4 Ma | - |
| Ar-Ar | phengite | 206 ±1 Ma | 212 ± 2 Ma | 211 ± 2 Ma | 205 ± 3 Ma | 206 ± 2 Ma | - |
| Ar-Ar | biotite | 201 ± 4 Ma | - | - | 210 ± 1 Ma | 202 ± 2 Ma | - |

Figure II-40: Cooling paths obtained by combining the assumed blocking temperature of isotopic system and the age determined in this study. Cooling rate estimation are also reported.

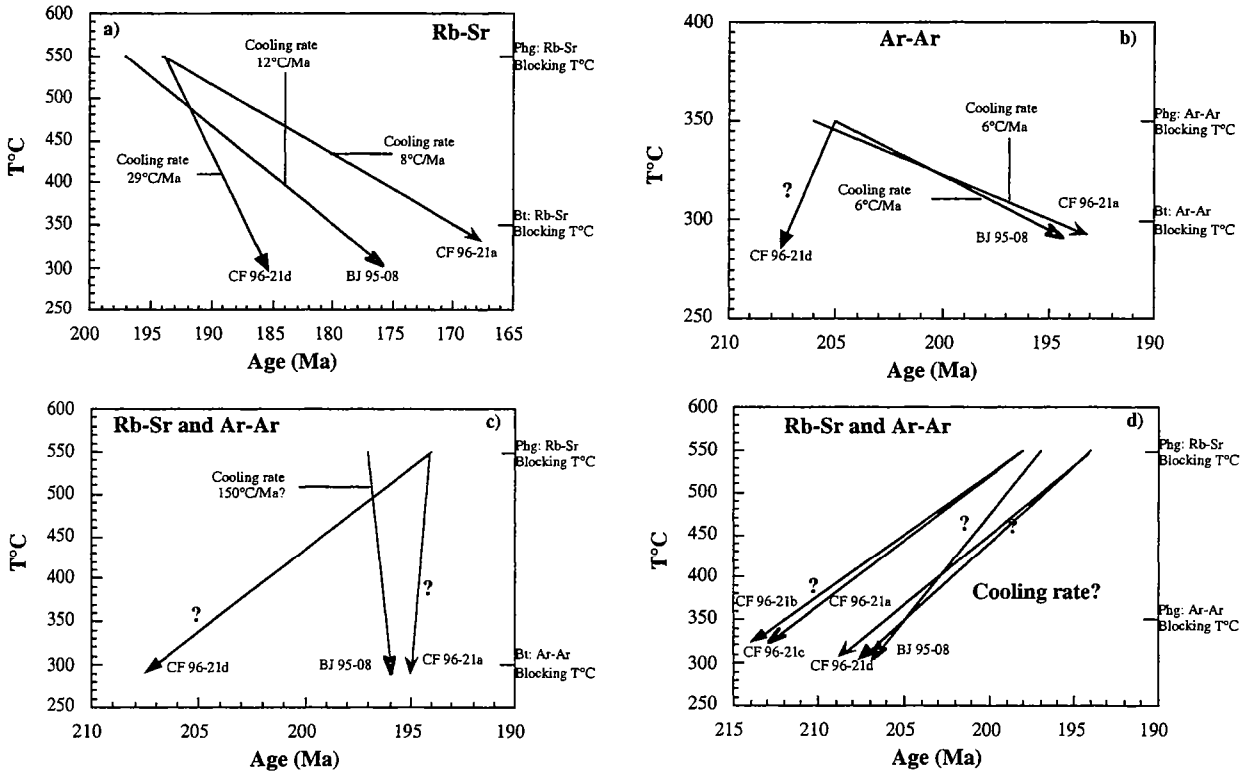

If we consider that diffusion was the only active process for the isotope movement during metamorphism, several "cooling paths" on the UHPM rocks at the Bixiling locality may be constructed by combining either Rb-Sr phengite and biotite ages, or Ar-Ar phengite and biotite ages, or Rb-Sr and Ar-Ar phengite ages, or even Rb-Sr phengite ages and Ar-Ar biotite ages. These hypothetical paths are reported in Fig. II-40 with the respective ages obtained on phengite and biotite fractions from the same sample. Firstly, if Rb-Sr or Ar-Ar phengite and biotite ages are considered (Fig. II-40a and II-40b), cooling rate estimations on samples CF 96-21a and BJ 95-08 vary within a narrow range between 6°C/Ma and 12°C/Ma. These first results are consistent with a cooling rate of ~7°C/Ma obtained on the coesite-bearing eclogites (Chavagnac and Jahn 1996). Consequently, if these two samples were only considered, a "cooling rate" of ~6-12°C/Ma would have been determined. However, a totally different cooling path would have been established if geochonological investigations were concentrated on sample CF 96-21d. The combination of Rb-Sr phengite and biotite ages suggests a cooling rate 3 times higher than the previous estimation (29°C/Ma) whereas the association of Ar-Ar ages cannot provide any cooling rate as the Ar-Ar biotite age is older than that one on phengite (Fig. II-40c and II-40d). Furthermore, any cooling rate can be determined by the combination of Rb-Sr and Ar-Ar ages as all Ar-Ar mineral ages are older than Rb-Sr mineral ages (Fig. II-40d).

Two main explainations can be proposed: (1) the "blocking temperature" for the Ar and Sr clocks should be higher than the temperature considered, and (2) pure diffusion is not the main process for isotope exchange during metamorphism arguing the inconsistency for the use of "blocking temperature". The previous section (§5.2) showed that microprobe analysis provide information on the chemical homogeneity of minerals analysed (Villa et al. 1996, 1997) and the mineral paragenesis may induce incomplete isotope exhange (Jenkins et al. 1995, Jenkins 1997). It appears that several processes such as mineral composition, mineral paragenesis, fluid circulation but also diffusion may prevente or promote the isotopic equilibration of the mineral considered with the matrix. Consequently, the "blocking temperatures" as related to pure diffusion are unreliable parameters to constrain temporally and spatially the tectono-metamorphic evolution of an orogenic belts. In addition, the overlapping of Sm-Nd, Ar-Ar and Rb-Sr mineral ages do not mean that all isotopic systems have the same blocking temperature but merely that the metamorphic event is recorded by various isotopic systems.

We conclude that further geochronological investigation must take into account the chemical re-equilibration during retrograde metamorphic path and the combination of various processes as agents of isotope exchange in order to avoid misunderstanding of geological history on metamorphic orogenic belts.

## 4.6. Conclusions

In this study, the multi-chronometry approach is used to tackle the problem of eclogite-gneiss tectonic relationship during the UHPM event and to determine the cooling paths of the eclogite host gneisses. We showed:

(1) The protolith ages of orthogneisses are late Proterozoic at Bixiling ~700 Ma and late Archean to Early Proterozoic at Shuanghe by U-Pb zircon data. These ages are in line with Nd model ages. The geochemical characteristics of gneisses indicate a volcanic arc setting for their formation.

(2) On Shuanghe's gneisses, the UHPM event is dated at ~230 Ma by U-Pb zircon data in agreement with a Sm-Nd garnet-kyanite-whole rock isochron age at 231 ± 35 Ma. At the Bixiling's locality, Rb-Sr and Ar-Ar phengite dating yield a narrow age range of 198 to 212 Ma overlapping the 190-220 Ma age given by Sm-Nd and Rb-Sr mineral isochron ages on coesite-bearing eclogites (Chavagnac and Jahn 1996). Consequently, the country rocks of coesite-bearing eclogites at Shuanghe and Bixiling underwent a metamorphic event coeval with the eclogites arguing for the "In-situ" tectonic relationship.

(3) Electron microprobe analyses on phengites dated by Ar-Ar and Rb-Sr methods suggest two generations: the first is probably related to the peak metamorphism and the other one crystallized during the retrograde metamorphism under albite-epidote amphibolite facies. The older Ar-Ar phengite and biotite age spectra may be the results of chemical re-equilbration, fluid circulation, and Ar excess.

(4) Pure diffusion cannot be considered as the main process for isotope exchange during retrograde metamorphism and therefore, the use of "blocking temperature" in order to provide cooling rates are unreliable.

# 5. Conclusions

Sm-Nd garnet analyses have been performed on coesite-bearing eclogites and gneisses which belong to the UHPM DabieShan terrane (Central China) in order to examine the consistency between Sm-Nd garnet ages and U-Pb zircons ages.

The coesite-bearing eclogite of the Bixiling Complex (1.5 $km^2$) is a layered mafic-ultramafic intrusion surrounded by quartzo-feldspathic gneisses. Geochemical and Sr-Nd isotopic compositions argued for a mantle-derived magma which was contaminated by variable amounts of the lower continental crust during its crystallization. The Sm-Nd garnet-omphacite-whole rock isochron ages obtained on seven eclogites varied within a narrow range between 210 ± 9 Ma and 218 ± 4 Ma which were interpreted as the age of garnet crystallization during the UHPM event. These ages are in agreement with the 218.5 ± 1.8 Ma and 218.4 ± 2.5 Ma given by the U-Pb zircon ages (Ames et al., 1995). In addition, the primary intrusive age was constrained from a Sm-Nd garnet only isochron which provided an age as well as an initial epsilon Nd value similar to those on Sm-Nd mineral isochrons. These geochronological features emphasized the reproducibility and the consistency in the age and also suggested a mantle-derivation age for the Bixiling Complex shortly before the UHPM event, approximately ~300 Ma. The association of Sm-Nd garnet ages and Rb-Sr phengites ages used in terms of thermochronology suggested a very high initial cooling rate of ~40°C/Ma and a rapid initial uplift of ~10mm/yr.

The host gneisses of the Bixiling Complex are strongly foliated quartzo-feldspathic gneisses which present a mineralogical association related to the albite-epidote amphibolite facies, i.e. a mineral paragenesis displaying no obvious evidence of UHPM features. A multichronometric approach was used to tackle the issue of tectonic relationship between the eclogite and the host gneisses. The U-Pb zircon ages indicated an upper intercept at ~700 Ma for the formation age and a lower intercept loosely constrained at about 250 Ma. Rb-Sr and Ar-Ar phengite dating yielded a narrow age range of 198 to 212 Ma overlapping the 198-223 Ma age given by the Sm-Nd and Rb-Sr mineral isochron ages on coesite-bearing eclogites. It appears that both coesite-bearing eclogite and host gneisses underwent a metamorphic event in the early Trias arguing for an 'in-situ tectonic relationship between these two contrasted lithologies. However, electron microprobe data on phengites indicated two generations leading to the conclusions that incomplete Ar/Sr isotope equilibration may have took place during the retrograde metamorphism. Finally, the use of geochronological data in terms of thermochronology should be considered with caution in order to avoid misunderstanding of geological history of metamorphic orogenic belts.

The UHPM rocks of Shuanghe is exposed as an elongated tectonically bounded thrust slab within foliated orthogneisses. It is composed of an apparent layering of massive eclogite, retrogressed eclogite, and metasedimentary lithologies. All U-Pb zircon data are clearly discordant suggesting an upper intercept of about 2.5 Ga and a lower intercept at 233 ± 21 Ma which is in line with two nearly concordant data points in the Tera-Waserburg diagram. Sm-Nd garnet-kyanite-whole rock isochron yielded an age at 231 ± 35 Ma which is in line with the U-Pb zircon data.

In general, all Sm-Nd garnet ages are very similar to those given by U-Pb zircon ages emphazing that full Nd isotope exchange during UHPM event may be considered to have taken place.

# *PART III*
# *The NdO+ Emission*

# 1. Introduction

Ultramafic rocks and some silicate minerals have Nd concentration below 0.1 ppm which complicates the conventional isotopic analyses as Nd + even on a multicollector mass spectrometer. Run - internal precision result in errors of about ± 0.000050 (2 standard error). These precisions too high for studies aimed at the constraint of Sm-Nd isotope characteristics of lunar, terrestrial, and meteorite evolution. Such studies rely on a precise determination of the age as well as the initial $^{143}Nd/^{144}Nd$ ratios. To achieve this, substantially better ion efficienties are required. It has been shown that ionization of Nd as $NdO^+$ is much more efficient than as $Nd^+$ ionisation. The early analyses as $NdO^+$ ion were performed using single collector mass spectrometers but the development of multi-collector mass spectrometers improved the analytical precision, mainly by using faraday-cup efficiencies and by reducing the analysis time.

This chapter documents the procedure for $NdO^+$ analyses established at the University of Bern as well as some experiments performed at Vrije Universiteit (Amsterdam) in collaboration with Mélanie Griselin and Gareth R. Davies. The first paragraph explains the loading procedure followed in both laboratories. That procedure was used to analyse standards, $^{150}Nd$ spike (determination of the oxygen isotopic composition) and samples. The mass interference corrections are especially critical for $NdO^+$ measurements and are described in the third paragraph. The procedure for $NdO^+$ analysis is described in the fourth paragraph. The last paragraph combines the results obtained on different standards usually measured at Bern. The conclusions on $NdO^+$ emission give crucial factors which should be considered for running Nd samples as $NdO^+$.

# 2. Loading Technique

At the Universität Bern, several kinds of experiments have been completed in order to obtain a stable and high ion beam. During all experiments, the sample was loaded on a Re filament (14 mm; 20 μm Cross; Fig. III-1).

To avoid any problem with organic matter (inhibiter of $NdO^+$ emission), the filament is washed in TOLUOL during 1 minute. ACETONE is used to wash away the TOLUOL. The filament is then dried under light. Subsequently, the filament is outgassed in vacuum at 3.5 A during 30 minutes. In order to optimize the loading procedure, I loaded Nd standards on the filament in different manners.

Figure III-1: Schematic sletch showing the filament conditioning before Nd loading.

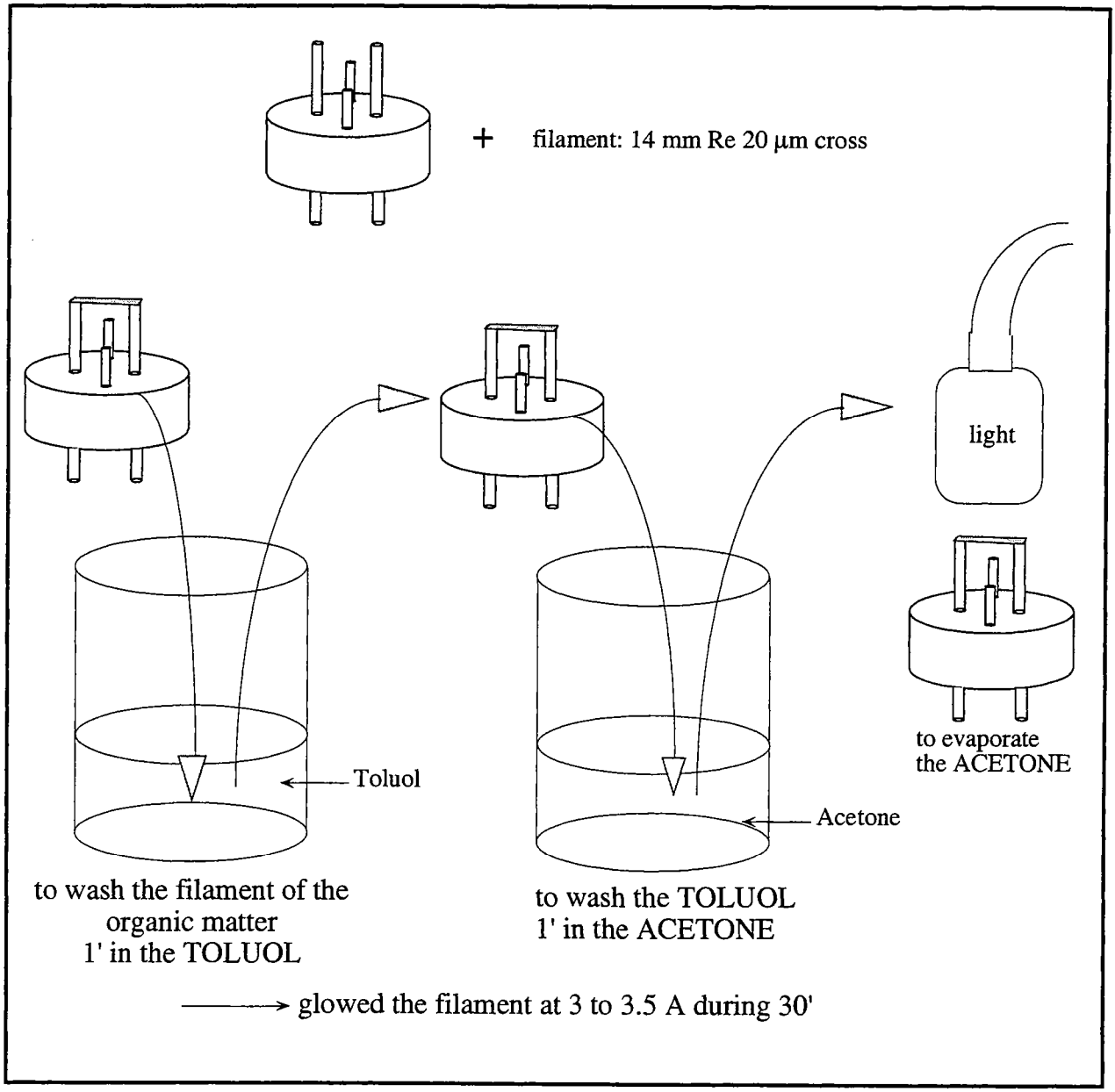

The first set of experiments were carried out on a modified Pb loading procedure. The sample was collected from the beaker with HCl or $HNO_3$ instead of $H_2PO_4$ due to the higher solubility of Nd into these acids. The sample was loaded on the filament and evaporated at 0.5 A preventing its sprawl on the filament. Subsequently, the filament was heated three times to 1.5 A (red filament). To examine the different reagents on the stability and intensity of the ion beam, we changed: (1) the type of acid used to collect the sample from the beaker (HCl or $HNO_3$); (2) the quantity of silicagel and phosphoric acid added to the sample; (3) we tried with and without a flow of $O_2$ into the source of the mas spectrometer. Several conclusions resulted:

1) When the sample is loaded with $HNO_3$, the quantity of silicagel and phosphoric acid should be higher than the quantity of nitric acid.

2) When the sample is loaded with HCl, the quantity of silicagel and phosphoric acid should be equal to the quantity of chlorhydric acid.

3) In both case, the $NdO^+$ beam is quite instable yielding a huge error on the Nd isotopic composition ($3.5\ 10^{-4}$ = 1 standard deviation) in single cup mode. Multi-cup measurements are far less affected by instable beams.

4) The $NdO^+$ emission is much more efficient with $HNO_3$ than with HCl.

5) The $NdO^+$ emission is also much more efficient with a flow of $O_2$ into the souce.

From the first set of experiments, we decided to load the sample on the filament with $HNO_3$ but without silicagel and phosphoric acid. A flow of $O_2$ into the source of the mass spectrometer is defenitively essential to increase the beam intensity of $NdO^+$.

The aims of the second set of $NdO^+$ experiments were two folds: (1) to adjust the normality of nitric acid used for loading; (2) to determine the optimum filament current to run the sample with respects to the stability and intensity of the beam. The observations gave:

1) The beam intensity is smaller (~600 mV) than that obtained by a mixture of silicagel, phosphoric acid and nitric acid but the beam is more stable yielding a lower one standard deviation on the Nd isotopic composition.

2) When the sample is loaded with a very diluted nitric acid (0.25 N), the beam is stable, increasing slightly and homogeneously.

3) When the sample is loaded with 4 N $HNO_3$, the beam increases too fast and therefore dies down very quickly .

4) The current on the filament during the $NdO^+$ emission should be below 1.7 A in order to maintain a stable and increasing beam.

A further point to check is if the oxydation of Nd on the filament during the loading can be increased. To do so, we heated the filament to 1.5 A and led glow light red during 10 secondes instead of glowing 3 times. Several runs confirmed the higher efficiency of Nd oxydation providing a beam intensity above 1 V as well as a stable beam.

In summary, the loading procedure at the Universität Bern is performed into steps: (1) washing the filament with TOLUOL and acetone; (2) outgassing the filament at 3.0-3.5 A during 30 minutes; (3) collecting the sample with 0.25 N $HNO_3$; (4) evaporating the sample at 0.5 A on the filament; (5) glowing 10 secondes (red filament: 1.5 A) after the dryness.

The oxydation of the Nd fraction during the loading will largely determine the intensity and the stability of the ion beam, and therefore it seems really important to convert all Nd to $Nd_2O_3$. The chemical purification of Sm and Nd are completed through a column packed with Teflon coated with HDEPH, conditioned and eluded with dilute HCl. The evaporation of the Nd-bearing solution is done under a light to maintain the Nd as $NdCl_3$ and to suppress $Nd_2O_3$ formation commonly obtained after evaporation on a hot plate. This procedure is essential for further $NdO^+$ analysis as a very diluted acid is used to collect Nd from the beaker. The sample is collected from the beaker with 0.25 N $HNO_3$. Evaporation on the filament (0.5 A) initially leds to the formation of $Nd(NO_3)_3*6H_2O$ (Nd nitrate) and some $NdCl_3$ may be still present. The oxygen which is combined with Nd comes from the nitric acid and from the surrounding air. To complete the oxydation of Nd ($Nd_2O_3$ solid state), the filament is heated to 1.5 A and left at that current during 10 secondes. Finally, in the mass spectrometer the evaporation and ionization of $Nd_2O_3$ provides the formation of $NdO^+$ and $O_2$ gas. With a single collector mass spectrometer, it is important to reach a stable beam. The organic matter which may still be present on the filament should be destroyed.

Figure III-2: Nd loading procedure at the Ubiversität Bern

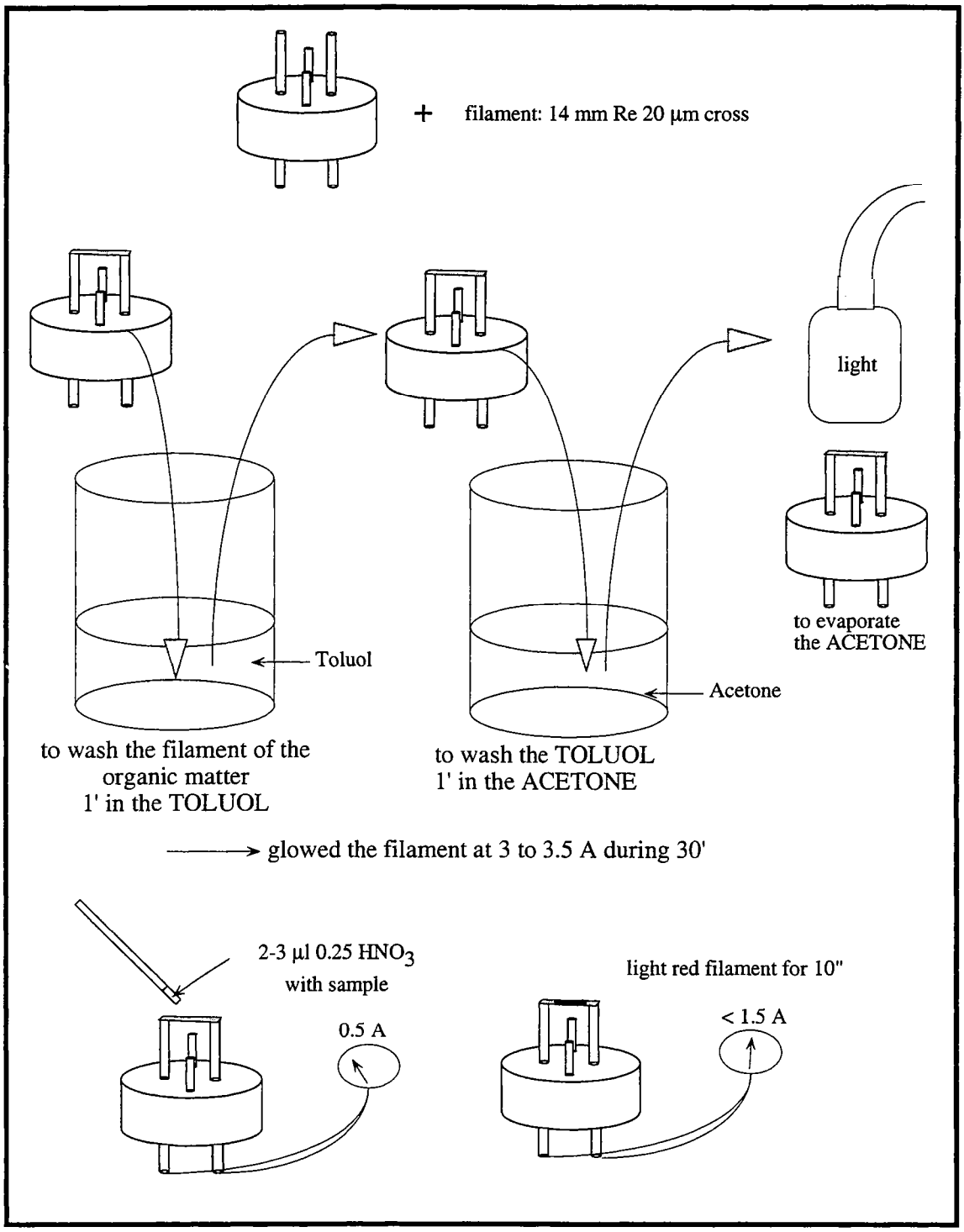

Figure III-3: Mechanical assemblage on the mass spectrometer is drawn in broad outline.

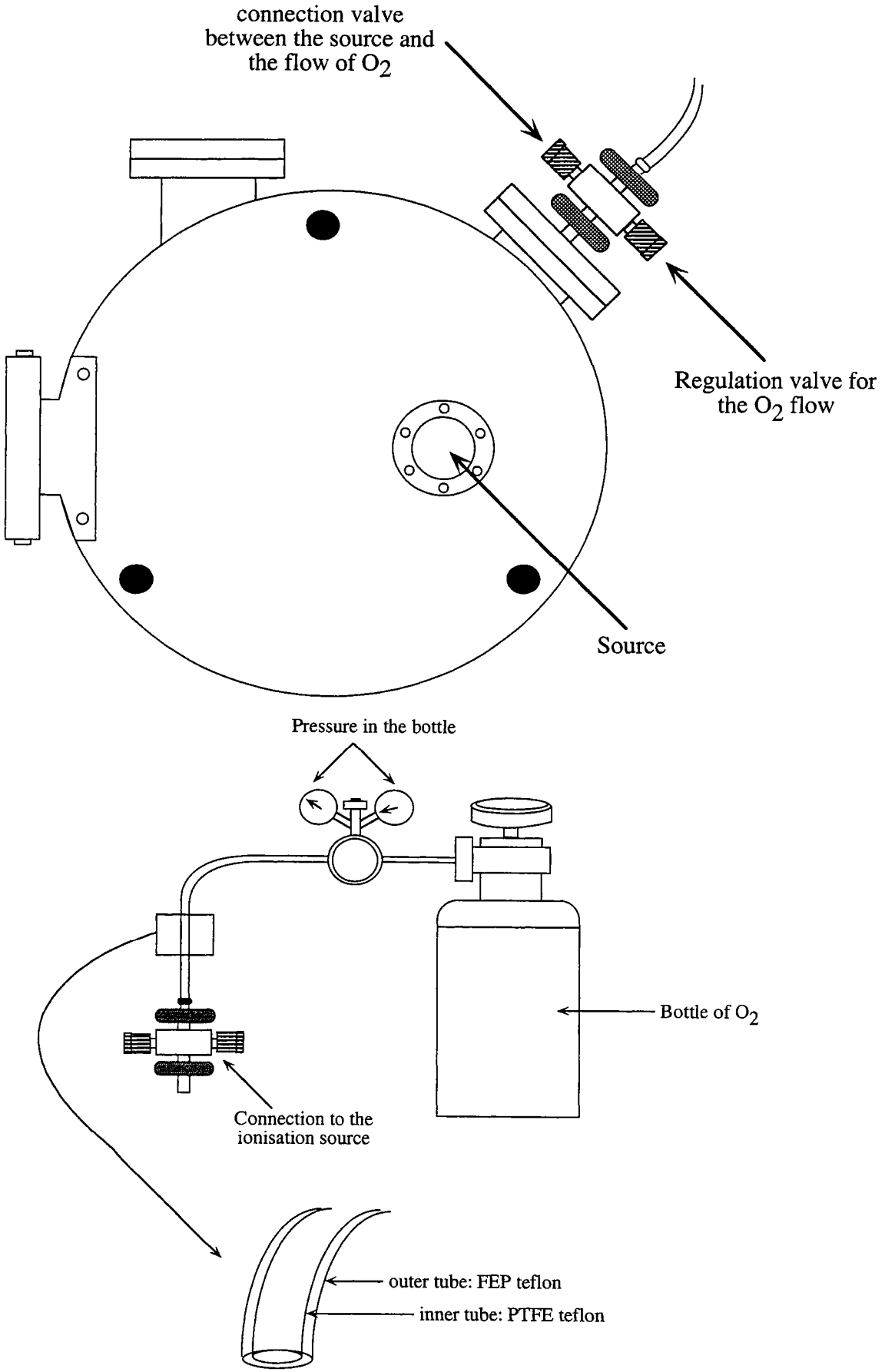

# 3. Mass spectrometer

On a single collector mass spectrometer, it is essential to obtain a stable beam. Thus, Nd is loaded on the filament without phosphoric acid and silicagel and therefore, a device for a flow of oxygen into the source of the mass spectrometer was installed on the VG Sector. The mechanical assemblage is drawn in broad outline in the Fig. III-3. The valve connected the source and the oxygen bottle may be opened when desired for $NdO^+$ analysis. The advantage of an oxygen flow is to reduce the inhibiter effect of organic matter on the $NdO^+$ emission. A single collector mass spectrometer needs 4 hours per analyse.

# 4. Oxygen isotopic composition

Oxygen has three isotopes and Nier (1950) gave the following percentage abundances (gas mass spectrometer): $^{16}O$ = 99.759%, $^{17}O$ = 0.0374% and $^{18}O$ = 0.2039%. A large variability of oxygen isotopic ratios is found in nature and therefore the oxygen isotopic composition determined in one laboratory may not necessarily apply to mass spectrometers on other laboraties. As a result, the oxygen isotopic composition should be accurately measured in order to correct for $REEO^+$ interferences in each laboratory (Wasserburg et al., 1981). Several possibilities have been proposed for the determination of the oxygen isotopic composition. For example, Niederer et al. (1981) obtained the oxygen isotope ratios by measuring $TiO^+$ and $ScO^+$ with the sample loaded on a heavily oxidized Ta filament and intimately mixed with a slurry of $Ta_2O_5$. The ratios obtained were totally different and lower than those obtained by Wasserburg et al (1981). Therefore, two main possibilities have been proposed: (1) $^{141}PrO^+$ and (2) $^{150}NdO^+$. The first way was performed at Amsterdam whereas the second at Bern.

## 4.1. At Vrije Universiteit

The oxygen isotopic compositions were measured on a multi-collector Finigan MAT 262 using a solution of Pr pure at 99%. The main advantage of this solution is the occurrence of only one isotope $^{141}Pr$ and the measurement was done by measuring the ratios $^{141}Pr^{17}O/^{141}Pr^{16}O$ and $^{141}Pr^{18}O/^{141}Pr^{16}O$. However, this solution has several disadvantages. Firstly, even if the Pr is a rare earth like Nd, it may not behave in the same manner as Nd especially when oxydized during the loading. Therefore the oxygen isotopic composition may not be necessarely be appropriate for the oxygen correction on a $NdO^+$ isotopic composition. Secondly, the solution of Pr is pur at 99% of $^{141}Pr$ but it contains a small amount of La and Ce. Consequentely, the occurrence of such elements implies a further correction for these

isobaric interferences on the $PrO^+$ isotope analysis. The only way to correct is to assume already a value for the oxygen isotopic composition. The corrections done on the oxygen isotope ratios may be totally different according to the value of the oxygen isotopic composition considered.

The determined oxygen isotopic compositions are plotted in a $^{17}O/^{16}O$ versus $^{18}O/^{16}O$ diagram (Fig. III-4). The results are very scattered and surprisingly, the higher variability is obtained on the $^{18}O/^{16}O$ ratio. As the $^{150}Nd$ spike solution used for the determination of the oxygen isotopic composition at Bern do not imply further correction for the isobaric interferences on the NdO+ isotope analysis, Vrije Universiteit decided finally to determine their own oxygen isotopic composition with this solution. Oxygen isotope ratios are: $^{17}O/^{16}O = 3.89\ 10^{-4}$ and $^{18}O/^{16}O = 2.064\ 10^{-3}$. All results concerning these kinds of analysis are explained in the Ph.D. of Mélanie Griselin (in prep).

## 4.2. At the Universität Bern

The oxygen isotopic composition is determined on a VG Sector in single collector mode using a solution of $^{150}Nd$ spike. This solution is composed of 97.78% of $^{150}Nd$ and 2.22% of other Nd isotopes. Only few traces of Sm and no La and/or Ce were seen on the mass spectrometer (around 200 cps). Therefore, no mass interferences corrections were done on the oxygen isotopic compositions obtained after a run. The measurement was done by measuring the ratios $^{150}Nd^{18}O/^{150}Nd^{16}O$ and $^{150}Nd^{17}O/^{150}Nd^{16}O$. During the run, the ion beams were generally above 3V on mass 166, 6 to 7 mV on mass 168 and 1 to 1.5 mV on mass 167.

The average of each run of oxygen isotopic ratios determination are compiled and classified according to the acid used for loading in Table III-1. The evolution of these ratios through runs are reported in a $^{150}Nd^{17}O/^{150}Nd^{16}O$ versus $^{150}Nd^{18}O/^{150}Nd^{16}O$ diagram (Fig. III-5) only with 0.25 N $HNO_3$. The average of the oxygen isotope ratios wer done on 2 runs of which $^{150}Nd$ was glowed 3 times red filament and 5 runs of which $^{150}Nd$ solution was glowed red fiolament during 10 secondes.

The average oxygen isotopic composition is (Table III-1):

$$\left(\frac{^{18}O}{^{16}O}\right) = 2.074\,10^{-3} \pm 1.16\,10^{-5}\,(1\sigma_D)\ 2122\ ratios$$

$$\left(\frac{^{17}O}{^{16}O}\right) = 3.86\,10^{-4} \pm 1.32\,10^{-5}\,(1\sigma_D)\ 2079\ ratios$$

Figure III-4: Compilation of the oxygen isotopic composition at Vrije Universiteit.

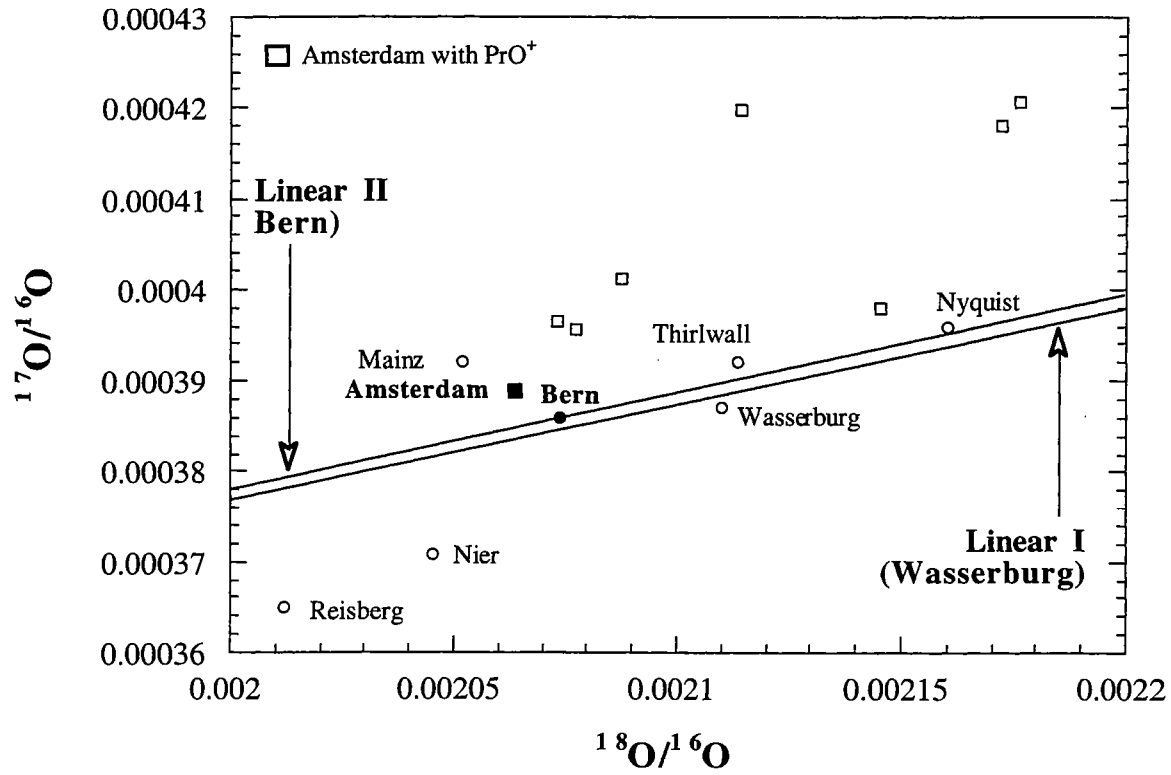


Table III-1: Compilation of the oxygen isotopic composition at Universität Bern according to the acid used for the Nd loading.

| 2.5N HCl | | | | | | |
|---|---|---|---|---|---|---|
| **blocks** | **18O/16O** | **+/- 1SD** | **ratios** | **17O/16O** | **+/- 1SD** | **ratios** |
| 25 | 2.028E-03 | 0.000012 | 234 | 3.847E-04 | 0.000012 | 241 |
| 35 | 1.999E-03 | 0.000023 | 360 | 3.802E-04 | 0.000024 | 358 |
| 30 | 2.050E-03 | 0.000014 | 299 | 3.860E-04 | 0.000013 | 290 |
| | **average values** | 18O/16O | 2.026E-03 | 0.000025 | 893 | |
| | | 17O/16O | 3.84E-04 | 0.000003 | 889 | |

| 0.25N HNO3 | | | | | | |
|---|---|---|---|---|---|---|
| **blocks** | **18O/16O** | **+/- 1SD** | **ratios** | **17O/16O** | **+/- 1SD** | **ratios** |
| 30 | 2.063E-03 | 0.000018 | 308 | 3.668E-04 | 0.000030 | 314 |
| 30 | 2.067E-03 | 0.000014 | 308 | 3.820E-04 | 0.000014 | 285 |
| 30 | 2.089E-03 | 0.000012 | 286 | 3.920E-04 | 0.000011 | 282 |
| 30 | 2.081E-03 | 0.000007 | 299 | 3.922E-04 | 0.000008 | 304 |
| 30 | 2.084E-03 | 0.000012 | 303 | 3.898E-04 | 0.000014 | 306 |
| 30 | 2.077E-03 | 0.000010 | 313 | 3.891E-04 | 0.000007 | 283 |
| 30 | 2.059E-03 | 0.000008 | 305 | 3.878E-04 | 0.000008 | 302 |
| | **average values** | 18O/16O | 2.074E-03 | 0.000011 | 2122 | |
| | | 17O/16O | 3.86E-04 | 0.000009 | 2076 | |

| 0.25N HNO3 plus parafilm during the loading | | | | | | |
|---|---|---|---|---|---|---|
| **blocks** | **18O/16O** | **+/- 1SD** | **ratios** | **17O/16O** | **+/- 1SD** | **ratios** |
| 30 | 2.070E-03 | 0.000008 | 283 | 3.885E-04 | 0.000007 | 297 |
| 30 | 2.055E-03 | 0.000016 | 303 | 3.871E-04 | 0.000017 | 309 |
| 24 | 2.059E-03 | 0.000014 | 230 | 3.852E-04 | 0.000013 | 247 |
| | **average values** | 18O/16O | 2.061E-03 | 0.000007 | 816 | |
| | | 17O/16O | 3.87E-04 | 0.000002 | 853 | |

Figure III-5: Evolution of the oxygen isotopic composition through runs.

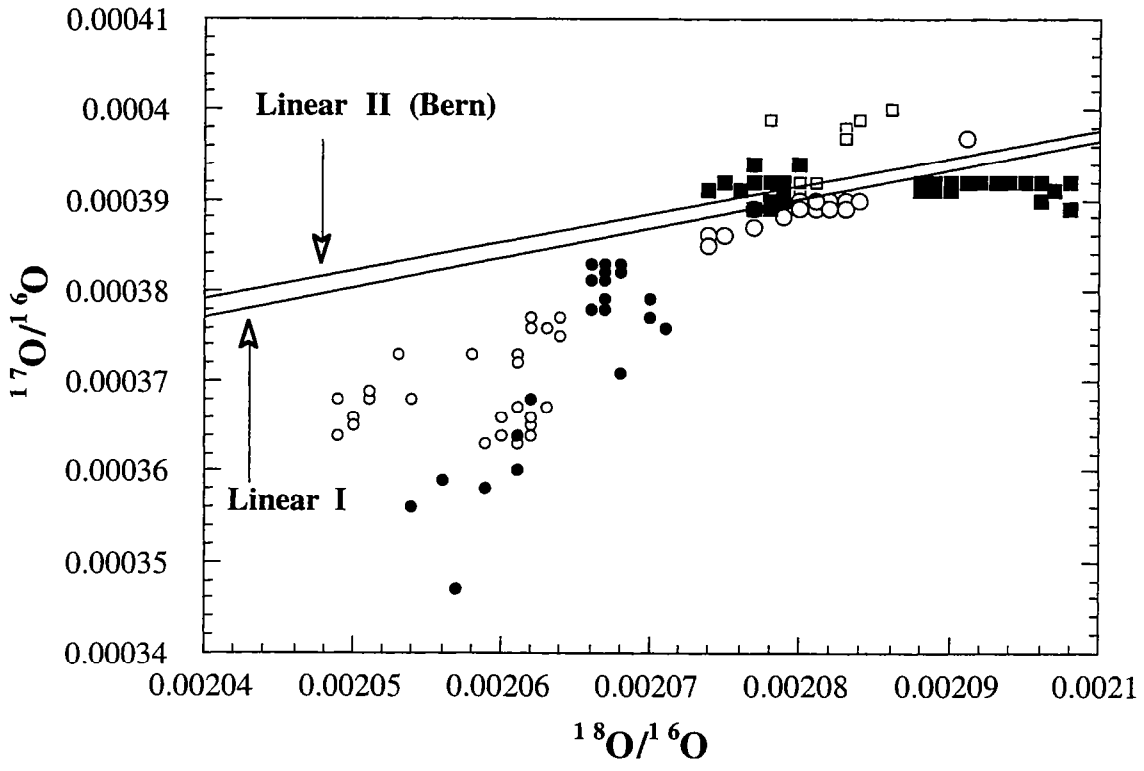

When the $^{150}Nd$ spike was glowed three times red filament, the oxygen isotopic compositions were lower than those obtained when the $^{150}Nd$ spike was glowed light red filament during 10 secondes. Within a single run that showed the largest variation, the lowest average value was $^{150}Nd^{18}O/^{150}Nd^{16}O = 2.049\ 10^{-3}$ and the highest $^{150}Nd^{18}O/^{150}Nd^{16}O = 2.063\ 10^{-3}$. The data obtained on these two runs were used for the calculation of the average value of the oxygen isotopic composition as the ion beam was stable and increasing homogeneously. When the $^{150}Nd$ spike was glowed light red filament during 10 secondes, the oxygen isotopic compositions were closed to each other. Generally, the $^{150}Nd^{17}O/^{150}Nd^{16}O$ and $^{150}Nd^{18}O/^{150}Nd^{16}O$ ratios may be measured with a precision of 0.02 % and 0.15 % respectively. The low ion beam on mass 167 cannot yield a precision on the $^{150}Nd^{17}O/^{150}Nd^{16}O$ ratio in the same order as the precision on the $^{150}Nd^{18}O/^{150}Nd^{16}O$ ratio. Moreover, three external test have been realized with a $^{150}Nd$ spike loaded on a parafilm-free zone of the filament. During these complementary experiments, the $NdO^+$ emission was not so efficient. The ion beam didn't increase homogeneously and was around 2V on mass 166. In addition, the filament current needed to obtain a good beam was higher at 1.85 A. It seems that the parafilm brought organic matter on the filament and therefore the $NdO^+$ emission were reduced. These runs were not included to the calculation of the average oxygen isotopic composition even if the average oxygen isotope ratios obtained were closed to that we determined.

The data follow a mass fractionation trend decribed by:

$$\left(\frac{^{17}O}{^{16}O}\right) = 0.093057 * \left(\frac{^{18}O}{^{16}O}\right) + 0.000193$$

and this trend is very closed to that determined by Wasserburg et al. (1981):

$$\left(\frac{^{17}O}{^{16}O}\right) = 0.09171 * \left(\frac{^{18}O}{^{16}O}\right) + 0.0001935$$

## 4.3. Discussion

The published values of the oxygen isotopic compositions are compiled in Table III-2.

As a large variability of oxygen isotope ratios is evident, each laboratory should determine their own oxygen isotopic composition. The difference between the values can be due to mass fractionation occurring during the loading. The oxygen which was combined with $^{150}Nd$ or $^{141}Pr$ may come from the surrounding air and the chemicals used. Several hypothesis may be proposed:

Table III-2: Published values of the oxygen isotopic compositions.

| References | 18O/16O | 17O/16O | Remarks |
|---|---|---|---|
| Bern Universität | 2.074E-03 | 3.860E-04 | single collector, flow of oxygen into the source |
| Vrije Universiteit (pers. com.) | 2.064E-03 | 3.890E-04 | multi-collector, silicagel |
| Nier (1950) | 2.045E-03 | 3.708E-04 | gas spectrometer |
| Wasserburg et al. (1981) | 2.110E-03 | 3.870E-04 | single collector, flow of oxygen into the source |
| Thirlwall (1991) | 2.114E-03 | 4.011E-04 | multi-collector, silicagel |
| Reisberg and Zindler (1987) | 2.012E-03 | 3.650E-04 | single collector?, flow of oxygen into the source |
| Nyquist (pers. com.) | 2.160E-03 | 3.960E-04 | single collector?, flow of oxygen into the source |
| Mainz University (pers. com.) | 2.052E-03 | 3.920E-04 | multi-collector, silicagel |

1) As noted by Wasserburg et al. (1981), the oxydation of Nd on the Re filament might not be complete.

2) Organic matter is an inhibiter of $NdO^+$ emission as its occurence on the filament will reduce $NdO^+$ to NdO or $PrO^+$ to PrO.

3) The oxydation behaviour of Nd during loading and measurement is not well constrained.

Taking into account these hypothesis, I propose that (1) the oxygen isotope ratios should be determined when the $^{150}Nd$ was glowed light red filament during 10 secondes providing good measurement reproducibility; (2) the $O_2$ leak in the source of the mass spectrometer favours $NdO^+$ emission and it avoids the reduction of $NdO^+$ as NdO.

A single difference in the loading procedure or a change of the element used for the oxygen isotopic measurement may cause several percent of variation in the $^{18}O/^{16}O$ ratio. The oxygen mass fractionation per mass unit is defined in percent by:

$$\alpha = \left[\left(\frac{\left(\frac{^{18}O}{^{16}O}\right)_{Nier}}{\left(\frac{^{18}O}{^{16}O}\right)_{meas}}\right) - 1\right] * \left(\frac{100}{\left(m_{^{18}O} - m_{^{16}O}\right)}\right)$$

$$\alpha = \left[\left(\frac{\left(\frac{^{17}O}{^{16}O}\right)_{Nier}}{\left(\frac{^{17}O}{^{16}O}\right)_{meas}}\right) - 1\right] * \left(\frac{100}{\left(m_{^{17}O} - m_{^{16}O}\right)}\right)$$

Our results are 0.7% and 4.1% respectively. The mass fractionation per mass unit in percent on the $^{17}O/^{16}O$ ratio is high due to the difficulty to measure the small ion beam on mass 167.

# 5. Mass interferences

In order to minimisize the isobaric interferences on the NdO+ beam, the chemical purification of Nd from La, Ce, Pr and Sm must be optimized. It is completed through a column packed with 2 ml Teflon coated with HDEPH, conditioned and eluded with dilute HCl according to the following elution profile.

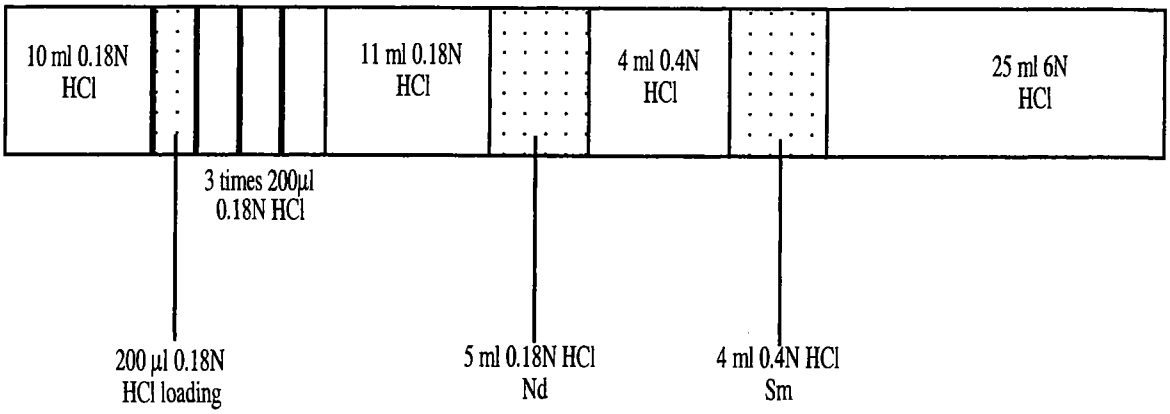


All La, Ce and Pr elements should be contained in the 11 ml 0.18 N HCl eluded solution. However, trace amounts of these usually remain after Nd chemical separation.

Masses measured cover the range 156 to 166 to permit corrections for the isobaric interferences. Masses 156 ($^{139}La^{17}O + {}^{140}Ce^{16}O$), 157 ($^{141}Pr^{16}O + {}^{140}Ce^{17}O$), 158 ($^{141}Pr^{17}O + {}^{140}Ce^{18}O + {}^{142}Ce^{16}O$) and 163 ($^{147}Sm^{16}O$) are not incorporated in the sequence of cycle. These interferences have relatively small effects on the meausred Nd ratios and they are measured outside of the sequnce at the beginning and at the end of each block of 12 cycles.

The Nd isotopic composition are calculated from the following linear equations:

$$R_{17} = \frac{^{17}O}{^{16}O}$$

$$R_{18} = \frac{^{18}O}{^{16}O}$$

$$^{142}Nd = {}^{158}NdO - {}^{140}CeR_{18} - {}^{158}CeO - {}^{141}PrR_{17}$$

$$^{143}Nd = {}^{159}NdO - {}^{142}CeR_{17} - {}^{142}NdR_{17} - {}^{141}PrR_{18}$$

$$^{144}Nd = {}^{160}NdO - {}^{142}CeR_{18} - {}^{142}NdR_{18} - {}^{142}NdR_{18} - {}^{143}NdR_{17}$$

$$^{145}Nd = {}^{161}NdO - {}^{144}NdR_{17} - {}^{143}NdR_{18}$$

$$^{146}Nd = {}^{162}NdO - {}^{145}NdR_{17} - {}^{144}NdR_{18}$$

$$^{148}Nd = {}^{164}NdO - {}^{146}NdR_{18}$$

$$^{150}Nd = {}^{166}NdO - {}^{148}NdR_{18}$$

Figure III-6: Beam intensity on mass 160 versus time. The current on the filament is also indicated.

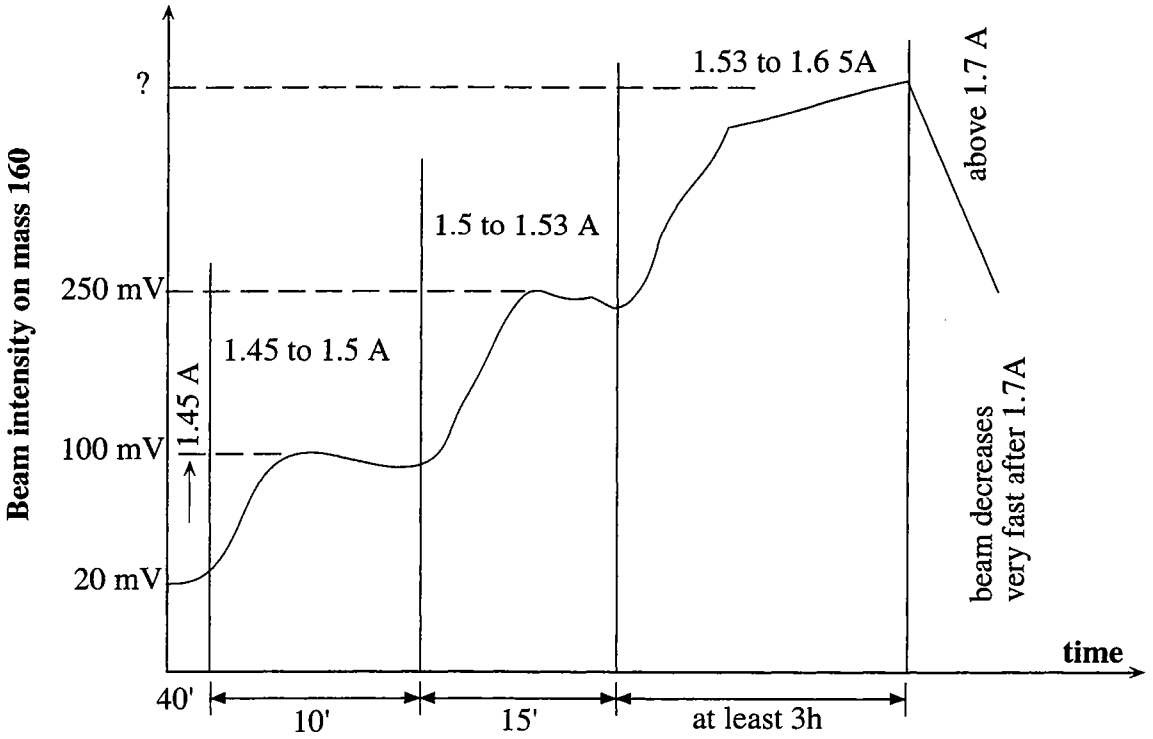


Figure III-7 and 8: Examples of La Jolla and Nd common run using NdO+ emission.

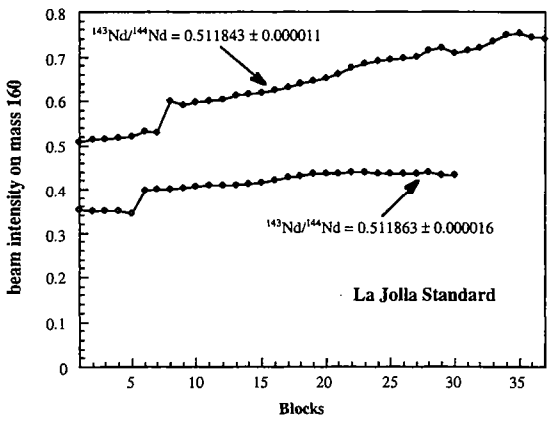


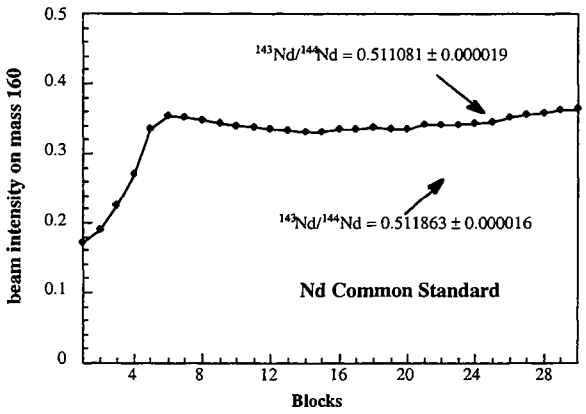

# 6. Results

## 6.1. Generalities

The Nd sample were loaded according to the procedure described in the paragraph 2. For the evaporation and the ionization of the $Nd_2O_3$, the loaded filament was heated into three steps: (1) 1 A in 10 minutes; (2) 1.3 A in 10 minutes and (3) 1.45 A in 10 minutes. At this filament current associated with the flow of oxygen into the source of the mass spectrometer, the ion beam was about 20 mV. The filament was further heated until the beam reached the value of 200 to 250 mV as drawn in broad outline in Fig. III-6.

## 6.2. Standards

Two Nd standards are available at the Universität Bern in order to control the measurement of Nd isotopic composition: (1) the international La jolla Standard ($^{143}Nd/^{144}Nd = 0.511860$); (2) the interne laboratory Nd Common standard ($^{143}Nd/^{144}Nd = 0.511070$). Between 150ng and 300ng of Nd were analyzed. Two examples of La Jolla Standard and one Nd Common standard runs are reported in Fig. III-7 and Fig. III-8 respectively.

In all three cases, the beam intensity was increasing slightly and the ion beam was stable. During these measurements, the mass fractionation percentage was between 0.2 to 0.3% and did not vary. Several runs of each standard have been performed between september 1997 and April 1998, and the results are reported in Table III-3 and Table III-4 respectively and plotted in Fig. III-9 and Fig. III-10 respectively.

The Nd isotopic composition of both standards fluctuated around 0.511860 for La Jolla and 0.511070 for the interne laboratory standard. Neverthelesss, the Nd isotopic composition of all measurements fall between an external reproducibility of ± 0.000030. This ± 0.000030 external reproducibility is as espected for a single collector mass spectrometer compared to ± 0.000015 for a multi-collector mass spectrometer.

Special care was taken to get purest Nd fractions, in other words the chemical separation of REE from major elements was adapted compared with the chemical composition of the sample or the mineral desired for Nd analysis. For example, garnet which has very low Nd concentration, has to be very clean, especially from Fe, Mg and Ca, to perform a good Nd run. I was able to run about 70 ng Nd on a garnet from metapelitic

Table III-3: Nd isotopic compositions of the La Jolla standard using NdO+ emission, between september 1997 and april 1998 .

| date | quantity | blocks | 159Nd/160Nd | ±2sE | ratios | ΔNd | 161Nd/160Nd | ±2sE | ratios |
|---|---|---|---|---|---|---|---|---|---|
| 9/09/97 | 1 µl | 27 | 0.511870 | 0.000026 | 281 | 10 | 0.348385 | 0.000017 | 258 |
| 13/9/97 | 1 µl | 29 | 0.511871 | 0.000019 | 286 | 11 | 0.348384 | 0.000009 | 291 |
| 14/9/97 | 3 µl | 30 | 0.511841 | 0.000018 | 291 | -15 | 0.348382 | 0.000011 | 298 |
| 15/9/97 | 4 µl | 30 | 0.511883 | 0.000026 | 273 | 23 | 0.348385 | 0.000018 | 313 |
| 10/03/97 | 1 µl | 30 | 0.511867 | 0.000023 | 306 | 7 | 0.348382 | 0.000012 | 308 |
| 10/10/97 | 1 µl | 30 | 0.511841 | 0.000016 | 292 | -19 | 0.348377 | 0.000011 | 302 |
| 30/10/97 | 1 µl | 36 | 0.511885 | 0.000024 | 366 | 25 | 0.348385 | 0.000015 | 364 |
| 31/10/97 | 1 µl | 30 | 0.511837 | 0.000022 | 305 | -23 | 0.348381 | 0.000012 | 307 |
| 3/07/98 | 1.5 µl | 37 | 0.511855 | 0.00001 | 367 | -5 | 0.348387 | 0.000008 | 378 |
| 27/3/98 | 1.5 µl | 30 | 0.511854 | 0.00007 | 294 | -6 | 0.348387 | 0.000013 | 283 |
| 23/4/98 | 1µl | 30 | 0.511843 | 0.000013 | 304 | -17 | 0.348402 | 0.000007 | 300 |
| 23/4/98 | 1µl | 37 | 0.511843 | 0.000011 | 359 | -17 | 0.348381 | 0.000005 | 358 |
| 24/4/98 | 1µl | 30 | 0.511863 | 0.000016 | 284 | 3 | 0.348391 | 0.000007 | 279 |
| 26/4/98 | 1µl | 30 | 0.511875 | 0.000014 | 300 | 15 | 0.348394 | 0.000008 | 301 |

Table III-4: Nd isotopic compositions of the Nd Common standard using NdO+ emission, between september 1997 and april 1998 .

| date | quantity | blocks | 159Nd/160Nd | ±2sE | ratios | ΔNd | 161Nd/160Nd | ±2sE | ratios |
|---|---|---|---|---|---|---|---|---|---|
| 26/9/97 | 150ng | 30 | 0.511060 | 0.000025 | 300 | -10 | 0.348364 | 0.000015 | 310 |
| 29/9/97 | 150ng | 30 | 0.511090 | 0.000018 | 297 | 20 | 0.348381 | 0.000012 | 307 |
| 29/9/97 | 150ng | 30 | 0.511088 | 0.000018 | 290 | 18 | 0.348399 | 0.000008 | 287 |
| 10/05/97 | 150ng | 30 | 0.511070 | 0.000018 | 310 | 0 | 0.348372 | 0.000013 | 308 |
| 10/06/97 | 150ng | 30 | 0.511088 | 0.000022 | 291 | 18 | 0.348396 | 0.000011 | 287 |
| 10/10/97 | 150ng | 30 | 0.511058 | 0.000041 | 284 | -12 | 0.348382 | 0.000021 | 303 |
| 10/12/97 | 150ng | 30 | 0.511073 | 0.000018 | 304 | 3 | 0.348385 | 0.000008 | 294 |
| 13/10/97 | 150ng | 30 | 0.511105 | 0.000019 | 303 | 35 | 0.348399 | 0.00001 | 301 |
| 16/10/97 | 150ng | 30 | 0.511100 | 0.000016 | 270 | 30 | 0.348389 | 0.000013 | 308 |
| 20/10/97 | 150ng | 30 | 0.511081 | 0.000019 | 312 | 11 | 0.348395 | 0.000009 | 300 |
| 25/10/97 | 150ng | 34 | 0.511096 | 0.000012 | 342 | 26 | 0.348389 | 0.000008 | 344 |
| 12/07/97 | 1.5 µl | 30 | 0.511079 | 0.000019 | 304 | 9 | 0.34834 | 0.000012 | 306 |
| 12/09/97 | 1 µl | 22 | 0.511069 | 0.00002 | 223 | -1 | 0.348384 | 0.000011 | 224 |

Figure III-9: Evolution of the Nd isotopic compositions of the La Jolla standard between september 1997 and april 1998.

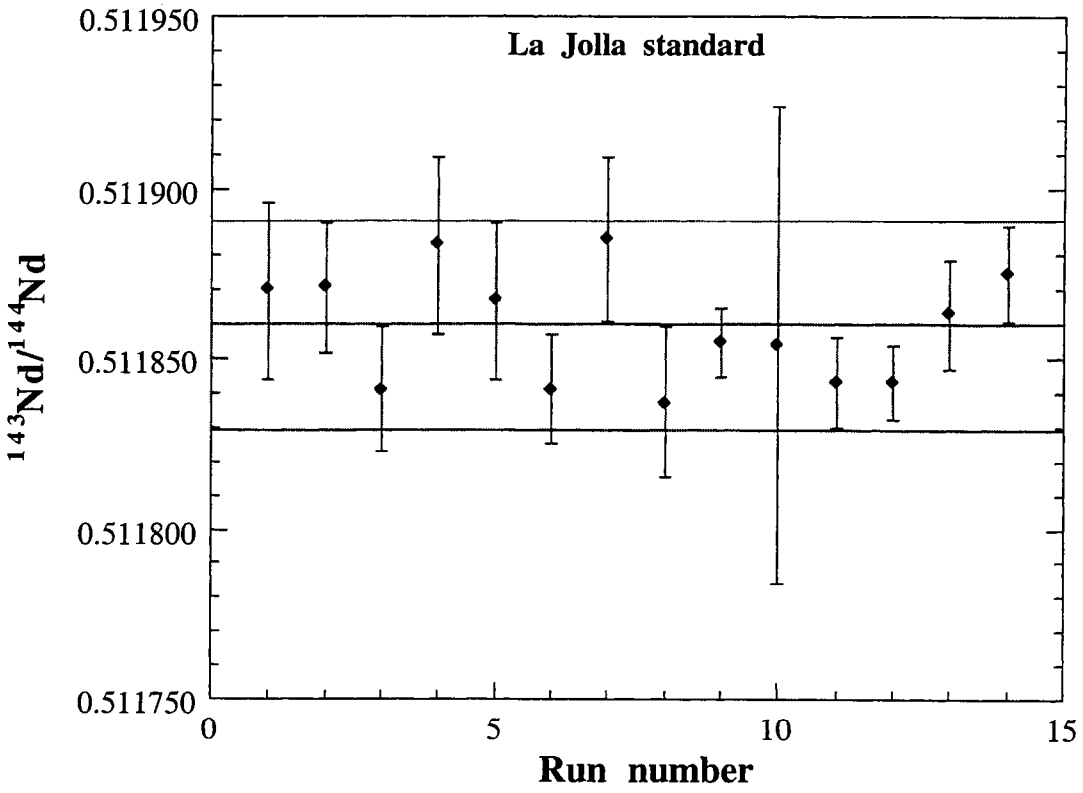


Figure III-10: Evolution of the Nd isotopic compositions of the Nd Common standard between september 1997 and april 1998.

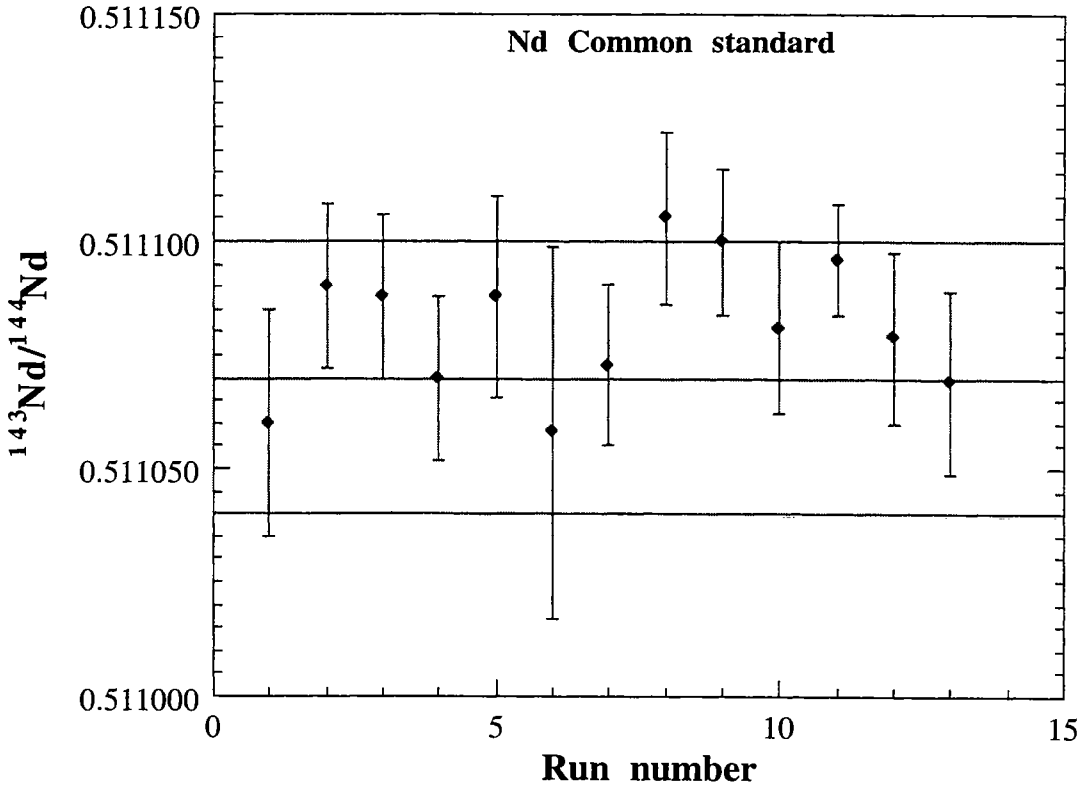

eclogite (de Sigoyer et al., submitted; see appendix B). More than 20ng of Nd should be on the filament for good Nd isotope determination.

# 7. Conclusions

$NdO^+$ emission is a powerful tool to run very low amounts of Nd. Special care should be taken on the oxygen isotopic composition as its ratios are highly variable depending on the element used for O isotope ratio determination as well as on the available mass spectrometer. Whatever the mass spectrometer is, organic matter has to be destroyed on the filament before running any Nd sample as it inhibits $NdO^+$ emission. The oxydation of the Nd fraction during the loading will largely determine the intensity and the stability of the ion beam, and therefore it seems really important to convert all Nd to $Nd_2O_3$. Therefore, I suggest that Nd sample should be loaded on the filament with nitric acid without additional mixture such as silicagel or phosphoric acid (implying $NdO^+$ emission instability), and to use a flow of oxygen into the source of the mass spectrometer, preventing the conversion of $NdO^+$ to NdO. Furthermore, parafilm which may be used for a ponctual Nd loading on the filament should not be used as it adds organic matter.

Two main issues have been addressed during this work regarding the behaviour of the Sm-Nd system during metamorphism.

***(1) Can we still trust in Nd model ages on Proterozoic high grade metamorphic rocks?***

Sm/Nd and $^{143}Nd/^{144}Nd$ ratios are used to calculate Nd model ages which are assumed to be representative of average age of the respective crustal segments. However, it was demonstrated in this study that the fractionation of the Sm/Nd ratios in intracrustal processes may be significant. Therefore, the use of Nd model ages as indicator of crustal history should be considered with caution.

Derivation of granitoid magma is chiefly associated with lower crustal anatexis. Partial melting on « fertile » lithologies (paragneisses) following the Bt dehydration reaction did lead to different behaviour of Sm-Nd systematic in different situations. Major minerals such as garnet or accessory minerals e.g. monazite were not isotopically equilibrated with the other rock-forming minerals at the time of the metamorphic event. Garnet is characterized by high Sm/Nd ratio and Nd radiogenic isotopic compositions. Its incorporation in the partial melt may dominate the chemical and isotopic compositions of leucosomes, raising their Nd isotopic composition. Consequently, the Nd model ages tend to be younger compared to those of the paleosomes. On the contrary, monazite presents low Sm/Nd ratio and unradiogenic Nd isotopic composition and its entrainment or its dissolution in partial melt reduced the Nd isotopic compositon of the melt. Therefore, the Nd model ages are older than those obtained on paleosomes. It appears that minerals may also fractionate the Sm/Nd ratio during intracrustal processes. In the case where migmatites are formed by metamorphic segregation under subsolidus conditions, no Nd isotope exchange takes place between the migmatitic components. Therefore, Nd model ages on paleosome, leucosome and melanosome are geologically meaningless. Nonetheless, the geochemical features combined with REE modeling may provide arguments for closed system behaviour at the whole rock scale. The isotopic compositions of the protolith obtained via mass balance calculations can be used to constrain crustal evolution.

The detailed isotopic studies performed on migmatitic rocks of the Limpopo Belt give a framework for the interpretation of Nd model ages in terms of crustal history in southern Africa. The crustal evolution of the Limpopo Central Zone can be summarized into three main periods: (1) 3.2-2.9 Ga, (2) ~2.6 Ga, and (3) ~2.0 Ga. The two first periods are mainly characterized by magmatitic activity leading to the formation of TTG such as the Sand River Gneisses or the Bulai

Granite intrusion whereas the Early Proterozoic event took place under high-grade metamorphic conditions during which partial melting on older lithologies formed large amount of granitic melt. This is somewhat different from the previous studies who argued for two periods of important continental crust growth at 3.5 Ga and 1.5 Ga (Dia et al., 1990) or at 2.0 and 1.0 Ga (Harris et al., 1987) in southern Africa.

### *(2) A comparison of Sm-Nd garnet ages with U-Pb zircon ages on high-pressure metamorphic rocks?*

Sm-Nd garnet and U-Pb zircon analyses have been performed on coesite-bearing eclogites and gneisses which belong to the UHPM DabieShan terrane (Central China). All Sm-Nd garnet ages are very similar to U-Pb zircon ages emphazing that full Nd isotope exchange may be considered to have taken place during UHPM event.

Sm-Nd garnet-omphacite-whole rock isochron ages obtained on seven eclogites yielded ages ranging from 210 ± 9 Ma to 218 ± 4 Ma. Ages are interpreted as garnet crystallization during the UHPM event. They are in agreement with the 218.5 ± 1.8 Ma and 218.4 ± 2.5 Ma given by U-Pb zircon ages (Ames et al., 1995). In addition, the primary intrusive age was constrained from a Sm-Nd garnet only isochron which provided an age as well as an initial epsilon Nd value similar to those on Sm-Nd mineral isochrons. These geochronological features emphasized the reproducibility and the consistency in the age and also suggested a mantle-derivation age for the Bixiling Complex shortly before the UHPM event, approximately ~300 Ma. The Sm-Nd garnet ages represent reliable ages as (1) the protolith was mantle-derived, (2) the protolith intruded the continental crust shortly before the metamorphic event avoiding a long crustal history, and (3) seven Sm-Nd mineral isochrons yielded ages overlapping each other.

Deux problématiques majeures ont été abordée sau cours de ce travail concernant le comportement du système istopique Sm-Nd durant le métamorphisme.

**(1) Les âges modèles en Nd sur des roches métamorphiques de haut grade sont-ils fiables ?**

Les rapports Sm-Nd et les compositions isotopiques en Nd sont utilisés pour le calcul des âges modèle qui sont considérés comme représentatifs de l'âge auquel le protolithe se sépare de sa source mantellique. Cependant il a été démontré durant ce travail que le fractionnement du rapport Sm-Nd durant les processus intracrustaux peut être très significatif. Les âges modèles en Nd comme indicateurs de l'évolution crustale doivent donc être utilisés avec précaution.

La formation de magmas granitoïdes est principalement reliée à la fusion partielle de la croûte continentale inférieure. La fusion partielle des lithologies « fertiles » (paragneiss) selon la réaction de déshydratation de la biotite met en exergue différent comportement du système Sm-Nd dans différentes conditions. Les minéraux métamorphiques principaux tels que le grenat ou encore les minéraux accessoires comme la monazite ne sont pas nécessairement équilibrés isotopiquement avec les autres minéraux à l'âge du métamorphisme. Le grenat est caractérisé par de forts rapports Sm/Nd ainsi que des compositions isotopiques en Nd très radiogéniques. La présence de ce minéral dans les liquides de fusion partielle peut dominée la composition chimique et isotopique des leucosomes augmentant ainsi leur composition isotopique en Nd. De ce fait les âges modèles ont tendance à être plus jeunes par rapport à ceux des paléosomes. Au contraire la monazite présente de faibles rapports Sm/Nd ainsi qu'une composition isotopique en Nd non radiogénique. Son entrainement ou sa dissolution dans les leucosomes tend à modifier la composition isotopique en Nd des leucosomes vers de plus faibles valeurs. Par conséquent les âges modèles obtenus sont plus vieux que ceux des paléosomes. Ceci met en évidence que les minéraux du métamorphisme peuvent fractionner le rapport Sm/Nd durant le processus de fusion partielle. Dans le cas où les migmatites sont formées par différenciation métamorphique à des conditions subsolidus, aucun échange isotopique en Nd ne se produit entre les différents composants migmatitiques. Ainsi les âges modèles sur les paléosomes, leucosomes et mélanosomes n'ont aucune signification géologique. Néanmoins les caractéristiques géochimiques associée à une modélisation de la distribution des REE peuvent indiquer que le système est resté clos à l'échelle de la roche totale. Les compositions isotopiques en Nd du protolithe peuvent donc être obtenues par l'équation de conservation de masse et peuvent être utilisées pour interpréter l'évolution crustale.

Ces études isotopiques détaillées sur les roches migmatitiques du Limpopo Belt en Afrique du Sud donne une trame pour l'interprétation des âges modèles en Nd en terme d'évolution crustale. Trois périodes majeures caractérisent l'évolution crsutale de la Zone Centrale du Limpopo Belt : (1) 3.2 - 2.9 Ga, (2) ~.2.6 Ga, (3) ~ 2.0 Ga. L'activité magmatique domine essentiellement les deux premières périodes donnant ainsi naissance aux suites de TTG telles que les Sand River Gneisses ou l'intrusion granitique du Bulai. L'événement au début du protérozoïque est relié à un métamorphisme de haut grade durant lequel des liquides granitiques se forment par fusion partielle. Ceci diffère des études précédentes qui ont argumenté en faveur de deux périodes majeures pour la formation de croûte continentale en Afrique du Sudsoit à 3.5 Ga et 1.5 Ga (Dia et al., 1990) ou soit à 2 Ga et 1Ga (Harris et al., 1987).

**(2) Comparaison entre les âges Sm-Nd sur grenat et U-Pb sur zircon sur des roches métamorphiques de haute pression.**

Des analyses en Sm-Nd sur grenat et U-Pb sur Zircon ont été effectuées sur des éclogites à coésite et leur encaissant situés dans la zone métamorphique de ultra haute pression du Dabieshan (Chine centrale). Tous les âges Sm-Nd sur grenat sont similaires aux âges U-Pb sur zircon mettant en évidence que l'échange des isotopes du Nd entre les minéraux peut être considéré comme total.

Les âges isochrones en Sm-Nd sur grenat-omphacite-roche totale varient entre 210 ± 9 Ma et 218 ± 4 Ma. Ces âges sont interprétés comme l'âge de cristallisation du grenat au cours du métamorphisme UHP. Ceci est en accord avec les âges U-Pb sur zircon à 218.4 ± 2.5 et 218.5 ±1.8 Ma. De plus l'âge d'intrusion du massif de Bixiling a été déterminé par une isochrone en Sm-Nd sur grenats qui donne un âge ainsi qu'une valeur initiale de l'épsilon Nd très similaires à ceux des isochrones Sm-Nd sur minéraux. Les caractéristiques géochronologiques mettent en évidence la reproductibilité et la fiabilité de l'âge. Le massif de Bixiling est d'origine mantellique et intrude la croûte continentale peu de temps avant le métamorphisme UHP. Les âges Sm-Nd sur grenat sont donc fiables dans la mesure où le protolithe est mantellique, que le temps de résidence crustal a été court et que cette isochrone en Sm-Nd sur grenat donne des âges similaires.

# *References*

Albarède F. and Brouxel M. (1987) The Sm/Nd secular evolution of the continental crust and the depleted mantle. *Earth Planet. Sci. Lett.* **82**, 25-35.

Allègre C.J. and Ben Othman D. (1980) Nd-Sr isotopic relationship in granitoid rocks and continental crust development: a chemical approach to orogenesis. *Nature* **286**, 335-342.

Allègre C.J., Hart S.R., and Minster J-F. (1983) Chemical structure and evolution of the mantle and continents determined by inversion of Nd and Sr isotopic data. II. Numerical experiments and discussion. *Earth Planet. Sci. Lett.* **66**, 191-213.

Anders E. (1977) Chemical composition of the moon, earth, and eucrite parent body. *Philos. Trans. R. Soc. London, A Math. Phys. Sci.* **285**, 23-40.

Arndt N.T. and Goldstein S.L. (1987) Use and abuse of crust-formation ages. *Geology* **15**, 893-895.

Arndt N.T. and Goldstein S.L. (1989) An open boundary between lower continental crust and mantle : its role in crust formation and crustal recycling. *Tectonophysics* **161**, 201-212.

Bernard-Griffiths J., Peucat J.J., and Ménot R.P. (1991) Isotopic (Rb-Sr, U-Pb and Sm-Nd) and trace element geochemistry of eclogites from the pan-African Belt : A case study of REE fractionation during high-grade metamorphism. *Lithos* **27**, 43-57.

Bowtell S.A., Cliff R.A., and Barnicoat A.C. (1994) Sm-Nd isotopic evidence on the age of eclogitization in the Zermatt-Saas ophiolite. *J. Metam. Geol.* **12**, 187-196.

Cliff R.A., Barnicoat A.C., and Inger S;. (1998) Early Tertiary eclogite facies metamorphism in the Monviso Ophiolite. *J. Metam. Geol.* **16**, 447-455.

DePaolo D.J. (1981) Neodynium isotopes in the Colorado Front Range and crust-mantle evolution in the Proterozoic. *Nature* **291**, 193-196.

DePaolo D.J. (1988) *Neodynium Isotope Geochemistry. An introduction.*

DePaolo D.J. and Wasserburg G.J. (1976a) Nd isotopic variations and petrogenetic models. *Geophys. Res. Lett.* **3**, 249-252.

Drake M.J. (1976) Evolution of major mineral compositions and trace element abundances during fractional crystallization of a model lunar composition. *Geochim. Cosmochim. Acta* **40**, 401-411.

Eugster O., Tera F., Burnett D.S., and Wasserburg G.J. (1970) The isotopic composition of gadolinium and neutron capture effects on some meteorites. *J. Geophys. Res.* **75**, 2753-2768.

Ganapathy R.M. and E. A. (1974) Bulk composition of the moon and earth estimated from meteorites. *Proc. Lunar Planet. Sci. Conf. 5th*, 1181-1206.

Goldstein S.L., O'Nions R.K., and Hamilton P.J. (1984) A Sm-Nd isotopic study of atmospheric dusts and particulates from major river systems. *Earth Planet. Sci. Lett.* **70**, 221-236.

Gruau G., Rosing M., Bridgwater D., and Gill R.C.O. (1996) Resetting of Sm-Nd systematics during metamorphism of the >3.7 Ga rocks: implications for isotopic models of early Earth differentiation. *Chem. Geol.* **133**, 225-240.

Hamilton P.J., O'Nions R.K., Evensen N.M., Bridgewater D., and Allart J.H. (1978) Sm-Nd isotopic investigations of Isua supracrustals and implications for mantle evolution. *Nature* **272**, 41-43.

Haskin L.A., Frey F.A., Schmitt R.A., and Smith R.H. (1966) Meteoritic, solar, and terrestrial rare earth distributions. *Phys. Chem. Earth* **7**, 167-321.

Hedge C.E. (1966) Variations in radiogenic strontium found in volcanic rock. *J. Geophys. Res.* **71**, 6119-6126.

Hensen B.J. and Zhou B. (1995) Retention of isotopic memory in garnets partially broken down during an overprinting granulite-facies metamorphism : implications for the Sm-Nd closure temperature. *Geology* **23**, 225-228.

Hofmann A.W. (1988) Chemical differenciation of the Earth : the relationship between mantle, continental crust, and oceanic crust. *Earth Planet. Sci. Lett.* **90**, 297-314.

Jagoutz E. (1988) Nd and Sr systematics in an eclogite xenolith from Tanzania : Evidence for frozen mineral equilibria in the continental lithosphere. *Geochim. Cosmochim. Acta* **52**, 1285-1293.

Lugmair G.W. (1974) Sm-Nd ages: a new dating method. *Meteoritics* **9**, 369.

Lugmair G.W., Scheinin N.B., and Marti K. (1975a) Sm-Nd age of Apollo 17 basalt 75075: evidence for early differentiation of the lunear exterior. *Proc. Lunar Planet. Sci. Conf. 6th*, 1419-1429.

McCulloch M.T. and Wasserburg G.J. (1978) Sm-Nd and Rb-Sr chronology of continental crust formation. **200**, 1 003-1 011.

Michard A., Gurriet P., Soudant M., and Albarède F. (1985) Nd isotopes in French Phanerozoic shales: external vs. internal aspects of crustal evolution. *Geochim. Cosmochim. Acta* **49**, 601-610.

Moorbath S., Whitehouse M.J., and Kamber B.S. (1997) Extreme Nd-isotope heterogeneity in the early Archean- fact or fiction? Case histories from northern Canada and West Greenland. **135**, 213-231.

Nägler Th.F. and Kramers J.D. (1998) Nd isotopic evolution of the upper mantle during the Precambrian: model, data and the uncertainty of both. *Precam. Res.* **in press**.

Patchett P.J. (1992) Isotopic studies of proterozoic crustal growth and evolution. In *Proterozoic crustal evolution* (ed. Condie K.C.), pp. 537. Elsevier.

Peppard D.F. (1961) Separation of the rare earths by liquid-liquid extraction. In *The Rare Earth* (ed. Spedding F.H. and Daane A.H.), pp. 38-54.

Peucat J.J., Vidal Ph., Bernard Griffiths J., and Condie K.C. (1988) Sr, Nd, and Pb isotopic systematics in the Archean low- and high-grade transition zone of Southern India: syn accretion vs. post accretion granulites. *J. Geol.* **97**, 537-550.

Powell J.E. (1961) Separation of the Rare Earths by ion exchange. In *The Rare Earth* (ed. Spedding F.H. and Daane A.H.), pp. 55-73.

Rosing M.T. (1990) The theoritical effect of metasomatism on Sm-Nd isotopic systems. **54**, 1 337-1 341.

Taylor S.R. and McLennan S.M. (1985) *The continental crust : its composition and evolution.* Blackwell scientific Publications.

Thöni M. and Jagoutz E. (1992) Some new aspects of dating eclogites in orogenic belts : Sm-Nd, Rb-Sr, and Pb-Pb isotopic results from the Austroalpine Saualpe and Koralpe type-locality (Carinthia/Styria, southeastern Austria). *Geochim. Cosmochim. Acta* **56**, 347-368.

Tourpin S., Gruau G., Blais S., and Fourcade S. (1991) Resetting of REE, and Nd and Sr isotopes during carbonitization of a komatiite flow from Finland. *Chem. Geol.* **90**, 15-29.

Wasserburg G.J., Papanastassiou D.A., Nenow E.V., and Bauman C.A. (1969) A programmable magnetic field mass spectrometer with on-line data processing. *Rev. Sci. Instrum.* **40**, 288-295.

Whitehouse M.J., Fowler M.B., and Friend C.R.L. (1996) Conflicting mineral and whole rock isochron ages from the Late-Archean Lewisian Complex of northwestern Scotland : implications for geochronology in polymetamorphic high-grade terrains. *Geochim. Cosmochim. Acta* **61**, 3 085-3 102.

Albarède F. (1995) *Introduction to geochemical modeling.* Cambridge University press.

Allègre C.J. and Minster J.F. (1978) Quantitative models of trace element behaviour in magmatic processes. *Earth Planet. Sci. Lett.* **38**, 1-25.

Anderson D.L. (1994) Superplumes or supercontinents. *Geology* **22**, 39-42.

Aranovich Y.L. and Newton R.C. (1966) $H_2O$ activity in concentrated NaCl solutions at high pressures and temperatures measured by the Brucite-Periclase equilibrium. *Contrib. Mineral. Petrol.* **125**, 200-212.

Aranovich Y.L., Shmulovich K.I., and Fedkin V.V. (1987) The $H_2O$ and $CO_2$ regime in regional metamorphism. *Int. Geol. Rev.* **29**, 1379-1401.

Armstrong R.A., Compston W., Retief E.A., Williams I.S., and Welke H.J. (1991) Zircon ion microprobe studies bearing on the age and evolution of the Witwatersrand triad. *Precam. Res.* **53**, 243-266.

Arndt N.T. and Goldstein S.L. (1987) Use and abuse of crust-formation ages. *Geology* **15**, 893-895.

Arndt N.T., Teixeira N.A., and White W.M. (1989) Bizarre geochemistry of komatiites from the Crixas greenstone belt, Brazil. *Contrib. Mineral. Petrol.* **101**, 187-197.

Arndt N.T. (1998) Pollo con arroz blanco y aceite de palma. In *Brazil Cooking* (ed. Chauvel C.), pp. 27-28. Square Etienne Eusèbe Huard Publication.

Arth J.G. and Hanson G.N. (1975) Geochemistry and origin of the early Precambrian crust of northeastern Minnesota. *Geochim. Cosmochim. Acta* **39**, 325-362.

Ashworth J.R. (1976) Petrogenesis of migmatites in the Huntly-Portsoy area, north-east scotland. In *Mineralogical Magazine*, Vol. 40, pp. 661-682.

Ashworth J.R. (1985) Introduction. In *Migmatites* (ed. Ashworth J.R.), pp. 1-35. Chapman & Hall.

Ashworth J.R. and McLennan E.L. (1985) Textures. In *Migmatites* (ed. A. J.R.), pp. 180-203. Chapman & Hall.

Ayres M. and Harris N.B.W. (1997) REE fractionaton and Nd-isotope disequilibrium during crustal anatexis: constraints from Himalayan leucogranites. *Chem. Geol.* **139**, 249-269.

Ayres M. and Vance D. (1997) A comparative study of diffusion profiles in Hymalayan and Dalradian garnets: Constraints on diffusion data and the relative duration of the metamorphic events. *Contrib. Mineral. Petrol.* **in press.**

Babcock R.S. and Misch P. (1989) Origin of the Skagit migmatites, North Cascades Range, Washington State. *Contrib. Mineral. Petrol.* **101**, 485-495.

Barbey P., Bertrand J.M., Angoua S., and Dautel D. (1989) Petrology and U-Pb geochronology of the Telohat migmatites, Aleksod, Central Hoggar, Algeria. *Contrib. Mineral Petrol.* **101**, 207-219.

Barbey P., Macaudiere J., and Nzenti J.P. (1990) High-pressure dehydration melting of metapelites evidence from the migmatites of Yaoundé (cameroon). *J. Petrol.* **31**, 401-427.

Barton J.M. (1983) Our understanding of the Limpopo Belt - a summary with proposals for future research. In *The Limpopo Belt*, Vol. 8 (ed. Van Biljon W.J. and Legg J.H.), pp. 191-203. *Spec. Publ. Geol. Soc. S. Afr.*

Barton J.M. (1983) Pb.isotopic evidence for the age of the Messina Layered Intrusion, central zone, Limpopo Mobile Belt. *Spec.Publ. Geol. Soc. S. Afr.* **8**, 39-41.

Barton J.M. (1990) Geochronological and isotopic constraints. In *The Limpopo Belt: a fieldworkshop on granulites and deep crustal tectonics.* (ed. van Reenen D.D. and Roering C.), pp. 28-30.

Barton J.M. (1996) The Messina Layered Intrusion, Limpopo Belt, South Africa : an example of in-situ contamination of an Archaean anorthosite complex by continental crust. *Precam. Res.* **78**, 139-150.

Barton J.M., Barton E.S., and Smith C.B. (1996) Petrography, age and origin of the Schiel alkaline complex, northern Transvaal, South Africa. *J. Afr. Earth Sci.* **22**(2), 133-145.

Barton J.M. and Doig R. (1993) Partial melting of various lithologies within the central zone of the Limpopo Belt near Messina, South Africa, and its constraint on the nature of the Limpopo Orogeny. *16th Colloqium of African Geology*, 25-26.

Barton J.M., Doig R., Smit C.B., Bohlender F., and van Reenen D.D. (1992) Isotopic and REE characteristics of the intrusive charno-enderbite and enderbite geographically associated with the Matok Pluton, Limpopo Belt, southern Africa. *Precam. Res.* **55**, 451-467.

Barton J.M., Fripp R.E.P., Horrocks P., and McLean N. (1979) The geology, age and tectonic setting of the Messina Layered Intrusion, Limpopo Mobile Belt, southern Africa. *Am. J. Sci* **279**, 1108-1134.

Barton J.M., Fripp R.E.P., and Horrocks P.C. (1983) Rb-Sr ages and chemical composition of some deformed Archean mafic dykes, central zone, Limpopo Mobile Belt, southern Africa. *Spec. Publ. Geol. Soc. S. Afr.* **8**, 27-37.

Barton J.M., Fripp R.E.P., and Ryan B. (1977) Rb/Sr ages and geochronological setting of ancient dykes in the Sand River area, Limpopo Mobile Belt, South Africa. *Nature* **267**, 487-490.

Barton J.M., Holzer L., Kamber B., Doig R., Kramers J.D., and Nyfeler D. (1994) Discrete metamorphic events in the Limpopo Belt, Southern Africa : implications for the application of P-T paths in complex metamorphic terrains. *Geology* **22**, 1035-1038.

Barton J.M. and Key R.M. (1983) Rb-Sr ages and geological setting of certain rock units from the Central Zone of the Limpopo Mobile Belt, near Zanzibar, eastern Botswana. *Spec. Publ. Geol. Soc. S. Afr.* **8**, 19-25.

Barton J.M. and van Reenen D.D. (1992) When was the Limpopo Orogeny? *Precam. Res.* **55**, 7-11.

Barton J.M., van Reenen D.D., and Roering C.A. (1990) The significance of 3000 ma granulite facies mafic dykes in the central zone of the Limpopo Belt, southern Africa. *Precam. Res.* **48**, 299-308.

Bau M. (1996) Controls on the fractionation of isovalent trace elements in magmatic and aqueous systems: evidence from Y/Ho, Zr/Hf, and lanthanide tetrad effect. *Contrib. Mineral. Petrol.* **123**, 323-333.

Bau M. and Dulski P. (1995) Comparative study of yttrium and rare-earth element behaviours in fluorine-rich hydrothermal fluids. *Contrib. Mineral. Petrol.* **119**, 213-223.

Baumgartner L.P. and Olsen S.N. (1995) A least-squares approach to mass transport calculations using isocon method. *Econ. Geol.* **90**, 1 261-1 270.

Bea F. (1989) A method for modeling mass balance in partial melting and anatectic leucosome segregation. *J. Metam. Geol.* **7**, 619-628.

Bea F. (1996) Residence of REE, Y, Th and U in granites and crustal protoliths; implications for the chemistry of crustal melts. *J. Petrol.* **37**(3), 521-552.

Bea F., Pereira M.D., and Stroh A. (1994) Mineral/leucosome trace-element partitioning in a peraluminous migmatite (a laser ablation-ICP-MS study). *Chem. Geol.* **117**, 291-312.

Berger M. (1995) Petrogenesis of Northern Marginal Zone of Limpopo Belt, Zimbabwe, Soutern Africa. Phil. Nat Ph.D. Thesis, University of Bern.

Berger M., Kramers J.D., and Nägler Th.F. (1995) Geochemistry and geochronology of charnoenderbites in the Northern Marginal Zone of the Limpopo Belt, Southern Africa, and genetic models. *Schweiz. Mineral. Petrogr. Mitt.* **75**, 17-42.

Berman R.G. (1991) Thermobarometry using multi-equilibrium calculations : a new technique, with petrological applications. *Can. Mineral.* **29**, 833-855.

Bernard-Griffiths J., Peucat J.J., and Ménot R.P. (1991) Isotopic (Rb-Sr, U-Pb and Sm-Nd) and trace element geochemistry of eclogites from the pan-African Belt : A case study of REE fractionation during high-grade metamorphism. *Lithos* **27**, 43-57.

Bhatia M.R. and Cook K.A.W. (1986) Trace element characteristics of greywackes and their tectonic discrimination of sedimentary basins. *Contrib. Mineral. Petrol.* **92**, 181-193.

Bloom K.A. (1988) Subsolidus migmatization in high-grade meta-stuffs (Kurkijärvi, southwest Finland). *Lithos* **21**, 263-278.

Bock B., McLennan S.M., and Hanson G.N. (1994) Rare earth elements redistribution and its effects on the neodynium isotope system in the Austin Glen Member of the Normanskill Formation, New York, USA. *Geochim. Cosmochim. Acta* **58**(23), 5 245-5 253.

Bowring S.A. and Housh T. (1995) The Earth's early evolution. *Science* **269**, 1 535-1 540.

Bowring S.A., Housh T.B., and Isachsen C.E. (1990) The Acasta Gneisses: Remnant of Earth's early crust. In *Origin of the Earth* (ed. Newsom H.E. and Jones J.H.), pp. 319-343. Oxford Univ. Press.

Brandl G. and Kröner A. (1993) Preliminary results of single zricon studies from various Archean rocks of the northeastern Transvaal. *16th Colloquium of African Geology*, 54-56.

Brown M. (1973) The definition of metatexis, diatexis and migmatite. *Proc. Geol. Ass.* **84**, 371-382.

Brown M. (1997) Migmatites and melt migration. *Proc. 30th Int. Geol Cong.* **17**(II), 187-202.

Brown M., Averkin Y.A., and McLellan E.L. (1995) Melt segregation in migmatites. *J. Geophys. Res.* **100**(B8), 15 655-15 679.

Brown M. and Fyfe W.S. (1970) The production of granitic melts during ultrametamorphism. *Contrib. Mineral. Petrol.* **28**, 310-318.

Brown M. and Rushmer T. (1997) The role of deformation in the movement of granitic melt: views from the laboratory and the field. In *Deformation-enhanced fluid transport in the Earth's Crust and Mantle.*, Vol. 8 (ed. Holness M.B.), pp. 111-144. Chapman & Hall.

Burke K., Kidd W.S.F., and Kusky T.M. (1985) Is the Ventersdorp Rift System of southern Africa related to a continental collision between the Kaapvaal and Zimbabwe cratons at 2.64 Ga ago? *Tectonophysics* **115**, 1-24.

Burke K., Kidd W.S.F., and Kusky T.M. (1986) Archean foreland basin tectonics in the Witwatersrand, South Africa. *Tectonics* **5**, 439-456.

Burton K.W. and O'Nions R.K. (1990) The timescale and mechanism of granulite formation at Kurunegala, Sri Lanka. *Geochim. Cosmochim. Acta* **106**, 66-89.

Byron C. and Barton J.M. (1990) The setting of mineralization in a portion of the Eersteling goldfield, Pietersburg granite-greenstone terrane. *S. Afr. J. Geol* **93**, 463-472.

Carney J.N., Aldiss D.T., and Lock N.P. (1994) The Geology of Botswana. Geological Survey Department.

Carrington D.P. and Harley S.L. (1995) Partial melting and phase relations in high-grade metapelites : an experimental petrogenetic grid in the KFMASH system. *Contrib. Mineral. Petrol.* **120**, 270-291.

Catherall D.M. (1973) The Shabani younger granite, Shabani, Rhodesia. *Spec. Publ. Geol. Soc. S Afr.* **3**, 197-200.

Chapman D.S. (1986) Thermal gradients in the continental crust. In *The Nature of the Lower continental crust*, Vol. 24 (ed. Dawson J.B., Carswell D.A., Hall J., and Wedepohl K.H.), pp. 63-70. Blackwell Scientific Publications.

Chauvel C., Dupré B., Todt W., Arndt N.T., and Hofmann A.W. (1983) Pb and Nd isotopic correlation in Archean and Proterozoic greenstone belts. *EOS* **64**, 330.

Chavagnac V. (1998) Behaviour of the Sm-Nd system during metamorphism: Examples from the HT-LP metamorphic terrane (The Limpopo Belt, South Africa) and the UHP metamorphic terrane (The Dabie Shan, China)., PhD thesis, University of Rennes 1.

Chavagnac V., Kramers J.D., Holzer L., Nägler Th.F., and Paya B.K. (submitted.) Migmatization at 2.0 Ga in the Mahalapye Complex, Limpopo Belt, Botswana: Implications on Nd model ages. *Contrib. Mineral. Petrol.*

Chavagnac V., Nägler Th. F., and Kramers J.D. (submitted) Metamorphic segregation at subsolidus conditions as igmatization process: Implications on Pb-Nd isotope exchange. *Lithos.*

Chinner G.A. and Sweatman T.R. (1968) A former association of enstatite and kyanite. In *Mineral Mag.*, Vol. 36, pp. 1052-1060.

Choukroune P., Bouhallier H., and Arndt N.T. (1995) Soft lithosphere during periods of Archean crustal growth or crustal reworking. In *Early Precambrian Processes*, Vol. 95 (ed. Coward M.P. and Ries A.C.), pp. 67-86.

Clemens J.D. (1990) The granulite-granite connection. In *Granulites and crustal evolution.*, Vol. 311 (ed. Vielzeuf D. and Vidal Ph.), pp. 25-36. Kluwer.

Clemens J.D., Droop G.T.R., and Stevens G. (1997) High-grade metamorphism, dehydration and crustal melting: a reinvestigation based on new experiments in the silica-saturated portion of the system $KAlO_2$-MgO-$SiO_2$-$H_2O$-$CO_2$ at $P \leq 1.5$ GPa. *Contrib. Mineral. Petrol.***129**, 308-325.

Clemens J.D. and Vielzeuf D. (1987) Constraints on melting and magma production in the crust. *Earth Planet. Sci. Lett.* **86**, 287-306.

Coertze F., Button A., du Plessis M.D., Eriksson K.A., Jansen H., Malherbe S.J., Smit P.J., Visser J.N.J., and Walraven F. (1980) Transvaal Sequence. In *Stratigraphy of South Africa.*, Vol. Handbook, Part I (ed. Kent L.E.), pp. 187-210.

Condie K.C. (1993) Chemical composition and evolution of the upper continental crust : contrasting results from surface samples and shales. *Chem. Geol.* **104**, 1-37.

Corner B., Durrheim R.J., and Nicolayen L.O. (1990) Relationships between the Vredefort structure and the Wiwatersrand basin within the tectonic framework of the Kaapvaal craton as interpreted from regional gravity and aeromagnetic data. *Tectonophysics.* **171**, 49-61.

Corward M.P. and Fairhead J.D. (1980) Gravity and structural evidence for the deep structure of the Limpopo Belt, southern Africa. *Tectonophysics.* **68**, 31-43.

Cox K.G., Johnson R.L., Monkman C.J., Stilman C.J., Vail J.R., and Wood D.N. (1965) The geology of the Nuanetsi Igneous Province. *Phil. Trans. R.Soc. London* **4257**, 71-218.

Crow C. and Condie K.C. (1988) Geochemistry and origin of late Archean volcanics from the Vendersdorp Supergroup, South Africa. *Precam. Res.* **42**, 19-37.

Cuney M. and Barvey P. (1982) Mise en évidence de phénomènes de cristallisation fractionnée dans les migmatites. *C. R. Acad. Sc. Paris* **295**, 37-42.

Dahl P.S. (1996) The effects of composition on retentivity of argon and oxygen in hornblende and related amphiboles: A field-tested empirical model. *Geochim. Cosmochim. Acta* **60**(19), 3 687- 3 700.

Dahl P.S. (1997) An "ionic porosity" approach to modeling compositional effects on diffusivity and retentivity of Ar and O in hornblende and related amphiboles. *Earth Planet. Sci. Lett.* **150**, 277-290.

de Beer J.H. and Stettler E.H. (1992) The deep structure of the Limpopo Belt. *Precam. Res.* **55**, 163-186.

de Ronde C.E.J. and de Wit M.J. (1994) Tectonic history of the Barberton greenstone belt, South Africa : 490 Ma of Archean crustal evolution. *Tectonics* **13**(4), 983-1005.

De Wit M.J. (1991) Archean greenstone belt tectonism and basin development: some insights from the Barberton and Pietersburg greenstone belts, Kaapvaal craton, South Africa. *J. Afr. Earth Sci.* **13**, 553-562.

de Wit M.J. and et al. (1992) Formation of an Archean Continent. *Nature* **357**, 553-562.

Dougan T.W. (1979) Compositional and modal relationships and melting reactions in some migmatitic metapelites from New Hamsphire and Maine. *Am. J. Sci.* **279**, 897-935.

Droop G.T.R. (1989) Reaction history of garnet-sapphirine granulites and conditions of Archaean high-pressure granulite-facies metamorphism in the Central Limpopo Mobile Belt, Zimbabwe. *J. Metam. Geol.* **7**, 383-403.

du Toit M.C., van Reenen D.D., and Roering C. (1983) Some aspects of the geology structure and metamorphism of the Southern Marginal Zone of the Limpopo metamorphic complex. *Spec. Geol. Soc. S. Afr.* **8**, 121-142.

Eriksson K.A., Turner B.R., and Vos R.G. (1981) Evidence of tidal processes from the lower part of the Witwatersrand Supergroup, South Africa. *Sediment. Geol.* **29**, 309-325.

Eriksson P.G. and Clendenin C.W. (1990) A review of the Transvaal Sequence, South Africa. *J. Afr. Earth Sci.* **10**, 101-116.

Erisson K.A., Kidd W.S., and Krapez B. (1988) Basin analysis in regionally metamorphosed and deformed early Archean terrain: examples from southern Africa and western Australia. In *Frontiers in Sedimentary Geology, New perspectives in Basin Analysis.* (ed. Kleinspehn K.L. and Paola C.), pp. 371-404.

Ermanovics I. (1980) The geology of the Mokgware Hills area. Bulletin of Geological Survey of Botswana.

Fleet M.E. and Pan Y. (1995) Crystal chemistry of Rare Earth elements in fluorapatite and some calc-silicates. *Eur. J. Mineral.* **7**, 591-605.

Fountain D.M. and Salisbury M.H. (1981) Exposed cross-sections through the continental crust: Implications for crustal structure, petrology, and evolution. *Earth Planet. Sci. Lett.* **56**, 263-277.

Fourcade S., Martin H., and de Brémond d'Ars J. (1992) Chemical exchange in migmatites during cooling. *Lithos* **28**, 43-53.

Frei R. and Kamber B.S. (1995) Single mineral Pb-Pb dating. *Earth Planet. Sci. Lett.*.

Fripp R.E.P. (1981) The ancient Sand River Gneisses, Limpopo Mobile Belt, South Africa. *Geol. Soc. Aus.* **7**, 329-335.

Fyfe W.S. (1973) The granulite facies, partial melting and the Archean crust. *Philos. Trans. R.Soc. London* **A273**, 457-461.

Gardien V., Thompson A.B., Grujic D., and Ulmer P. (1995) Experimenatl melting of biotite + plagioclase + quartz ± muscovite assemblages and implications for crustal melting. *J. Geophy. Res.* **100**(B8), 15 581-15 591.

Geological Surveys of Botswana S. A. a. Z. (1981) Provisional Geological map of The Limpopo Belt and environs.

Grant J.A. (1985) Phase equilibria in partial melting of pelitic rocks. In *Migmatites* (ed. Ashworth J.R.), pp. 86-144. Chapman & Hall.

Grant J.A. (1986) The Isocon diagram- A simple solution to Gresens' equation for metasomatic alteration. *Econ. Geol.* **81**, 1976-1982.

Grauch R.I. (1989) Rare Earth elements in metamorphic rocks. In *Rare Earth Elements*, Vol. 21 (ed. Lipin B.R. and McKay G.A.), pp. 147-167. Mineralogical Society of America.

Green T.H. and Watson E.B. (1982) Crystallization of apatite in natural magma under high pressure, hydrous conditions, with particular reference to "orogenic" rock series. *Contrib. Mineral. Petrol.* **79**, 96-105.

Gresens R.L. (1967) Composition-volume relationships of metasomatism. *Chem. Geol.* **2**, 47-65.

Gromet L.P. and Silver L.T. (1983) Rare earth elements distributions among minerals in a granodiorite and their petrogenetic implications. *Geochim. Cosmochim. Acta.* **47**, 925-939.

Gruau G., Rosing M., Bridgwater D., and Gill R.C.O. (1996) Metamorphism and Sm-Nd remobilization in the >3,7 Ga Isua Supracrustal Belt of West Greenland : implications for isotopic models of early earth differentiation. *Chem. Geol.* **133**, 225-240.

Gruau G., Rosing M., Bridgwater D., and Gill R.C.O. (1996) Resetting of Sm-Nd systematics during metamorphism of the >3.7 Ga rocks: implications for isotopic models of early Earth differentiation. *Chem. Geol.* **133**, 225-240.

Gwavava O., Swain C.J., Podmore F., and Fairhead J.D. (1992) Evidence of crustal thinning beneath the Limpopo Belt and Lebombo monocline of southern Africa based upon regional gravity studies and implications for the reconstruction of Gondwana. *Tectonophysics* **212**, 1-20.

Hall J. (1986) The physical properties of layered rocks in deep continental crust. In *The nature of the lower continental crust* (ed. J. B. Dawson, D. A. Carswell, J. Hall, and K. H. Wedepohl), pp. 51-62. Blackwell scientific publications.

Hamilton P.J. (1977) Sr isotope and trace element studies of the Great Dyke and Bushweld mafic phase and their relation to Early Proterozoic magma genesis in southern Africa. *J. Petrol.* **18**, 24-52.

Hanson G.N. (1980) Rare earth elements in petrogenetic studies of igneous systems. *Ann. Rev. Earth Planet. Sci.* **8**, 371-406.

Hanson G.N. (1989) An approach to trace element modeling using a simple igneous system as an example. In *Rare Earth Elements*, Vol. 21 (ed. Lipin B.R. and McKay G.A.), pp. 79-97. Mineralogical Society of America.

Hanson G.N. and Langmuir C.H. (1978) Modeling of major and trace elements in mantle-melt systems using trace element approaches. *Geochim. Cosmochim. Acta* **42**, 725-741.

Harley S.L. (1989) The origins of granulites : a metamorphic perspective. *Geol. Mag.* **126**(3), 215-247.

Harris N.B.W., Hawkesworth C.J., Van Clusteren P., and McDermott F. (1987) Evolution of continental crust in southern Africa. *Earth and Planet. Sci. Lett.* **83**, 85-93.

Harris N.B.W. and Holland T.J.B. (1984) The significance of cordierite-hypersthene assemblages from the Beitbridge region of the Central Limpopo Belt ; evidence for rapid decompression in the Archaean? *Am. Min.* **69**, 1 036-1 049.

Harris N.B.W. and Inger S. (1992) Trace element modeling of pelite-derived granites. *Contrib. Mineral. Petrol.* **110**, 46-56.

Harrison T.M. and Watson E.B. (1983) Kinetics of zircon dissolution and zirconium diffusion in granitic melts of variable water content. *Contrib. Mineral. Petrol.* **84**, 66-72.

Hawkesworth C.J., Bickle M.J., Gledhill A.R., Wilson J.F., and Orpen J.L. (1979) A 2.9 Ga event in the Rhodesian Archean. *Earth Planet. Sci. Lett.* **43**, 285-297.

Hawkesworth C.J., Moorbath S., O'Nions R.K., and Wilson J.F. (1975) Age relationships between greenstone belts and "granites" in the Rhodesian Archean Craton. *Earth Planet. Sci. Lett.* **25**, 251-262.

Hegner E., Kröner A., and Hofmann A.W. (1984) Age and Isotope geochemistry of the Archean Pongola and Usushwana suites in Swaziland, southern Africa: a case for crustal contamination of mantle-derived magma. *Earth Planet. Sci. Lett.* **70**, 267-279.

Heinrichs H., Schulz-Dbrick B., and Wedepohl K.H. (1980) Terrestrial geochemistry of Cd, Bi, Tl,Pb, Zn, and Rb. *Geochim. Cosmochim. Acta* **44**, 1519-1523.

Herron M.M. (1988) Geochemical classification of terrigeneous sands and shales from core or log data. *J. Sed. Petrol.* **58**, 820-829.

Hickman M.H. (1974) 3500 Ma-old granite in southern Africa. *Nature* **251**, 295-296.

Hickman M.H. (1978) Isotopic evidence for crustal reworking in the Rhodesian Archean craton, southern Africa. *Geology* **6**, 214-216.

Higushi H. and Nagasawa H. (1969) Partition of trace elements betwenn rock forming minerals and the host volcanic rocks. *Erath Planet. Sci. Lett.* **7**, 281-287.

Hisada K. and Paya B.K. (submitted) Partial melting of quartz-depleted pelitic rocks in the Mahalapye Plutonic block, the Botswanan Limpopo Central Zone: Implications for melt-segregation process. .

Holmes A. and Cahen L. (1957) Géochronologie africaine 1956, résultats acquis au 1er Juillet 1956. *Mem. Acad. R.Sci. Colon. Belg.*, 1-169.

Holmquist P.J. (1921) Typen und nomenklatur der Adergesteine. *Geol. Fören. Stockholm Förth.* **43**, 613-631.

Holness M.B. (1995) The effect of feldspar on quartz-H2O-CO2 dihedral angles at 4 kbar, with consequences for the behaviour of aqueous fluids in migmatites. *Contrib. Mineral. Petrol.* **118**, 356-364.

Holzer L. (1995) The magmatic petrology of the Bulai Pluton and the tectono-metamorphic overprint at 2.0 Ga in the central zone of the Limpopo Belt (Messina-Beitbridge area, southern Africa9:. Diplomarbeit, University of Bern.

Holzer L. (1998) The transpressive orogeny at 2.0 Ga in the Limpopo Belt, Southern Africa. Phil. Nat. Ph.D. thesis, University of Bern.

Holzer L., Barton J.M., Paya B.K., and Kramers J.D. (1998) Tectonothermal history in the western part of the Limpopo Belt: Test of tectonic models and new perspectives. *J. Afr. Earth Sci.* **in press**.

Holzer L., Frei R., Barton J.M., and Kramers J.D. (1998) Unraveling the record of successive high-grade events in the Central Zone of the Limpopo Belt using Pb single phase dating of metamorphic minerals. *Precam. Res.* **87**, 87-115.

Holzer L., Kamber B.S., Kramers J.D., and Frei R. (1996) The tectono-metamorphic event at 2.0 Ga in the Limpopo Belt and the resetting behaviour of chronometers at high temperature. *Spec. Publ. Geol. Surv. Namibia.* **1**, 127-138.

Holzer L., Kramers J.D., and Blenkinsop T.G. (1997) Granulite facies metamorphism in the Limpopo Central Zone (Southern Africa): Evidence for a Proterozoic continental collision between the Kaapvaal and Zimbabwe Cratons. *EUG9*, 365.

Hor A.K., Hutt D.K., Smith J.V., Wakefield J., and Windley B.F. (1975) Petrochemistry and mineralogy of early Precambrian anorthositic rocks of the Limpopo Mobile Belt, southern Africa. *Lithos* **8**, 297-310.

Hutton L.G., Key R.M., and Hutton S.M. (1974) Chemical analyses of rocks, ores and minerals of Botswana. Geological Survey of Botswana.

Inger S. and Harris N. (1993) Geochemical constraints on leucogranite magmatism in the Langtang Valley, Nepal Himalaya. *J. Petrol.* **34**, 345-368.

Jaeckel P., Kröner A., Kamo S.L., Brandl G., and Wendt J.J. (1997) Late Archean to Early Proterozoic granitoid magmatism and high-grade metamorphism in the central Limpopo Belt, South Africa. *J. Geol. Soc. London* **154**(25-44).

Jahn B.M. and Condie K.C. (1976) On the age of the Rhdesian Greenstone Belts. *Contrib. Mineral Petrol.* **57**, 317-330.

James P.R. (1975) A deformation study across the northern margin of the Limpopo Belt, Rhodesia. unpublished Ph.D. thesis, University of Leeds.

Janardhan A.S., Newton R.C., and Hansen E.C. (1982) The transformation of amphibolite facies gneiss to charnockite in southern Karnataka and northern Tamil Nadu, India. *Contrib. Mineral. Petrol.* **79**, 130-149.

Jaupart C. (1983) Horizontal heat transfer due to radioactivity contrasts: Causesand consequences of the linear heat flow relation. *Geophys. J. R. Astron. Soc.* **75**, 411-435.

Jelsma H.A. (1993) Granites and greenstones in Northern Zimbabwe: Tectono-thermal evolution and source regions. Unpublished Ph.D. Thesis, Vrije Universiteit.

Johannes W. (1985) The significance of experimental studies for the formation of migmatites. In *Migmatites* (ed. Ashworth J.R.), pp. 36-85. Blackie.

Johannes W. and Gupta L.N. (1982) Origin and evolution of a migmatite. *Contrib. Mineral Petrol.* **79**, 114-123.

Johannes W. and Holtz F. (1990) Formation and composition of $H_2O$-undersaturated granitic melts. In *High-temperature metamorphism and crustal anatexis.*, pp. 87-104.

Johannes W., Holtz F., and Möller P. (1995) REE distribution in some layered migmatites constraints on their petrogenesis. *Lithos* **35**, 139-152.

Kamber B.S. (1995) . PhD, University of Bern.

Kamber B.S. and Biino G.G. (1995) The evolution of high T-low P granulites in the Northern Marginal Zone sensu-stricto, Limpopo Belt, Zimbabwe - the case for petrograpgy. *Schweiz. Mineral. Petrogr. Mitt.* **75**, 427-454.

Kamber B.S., Biino G.G., Wiljrans J.R., Davies G.R., and Villa I.M. (1996) Archean granulites of the Limpopo Belt, Zimbabwe: one slow exhumation or two rapid events? *Tectonics* **15**(6), 1 414-1 430.

Kamber B.S., Blenkinsop T.G., Villa I.M., and Dahl P.S. (1995) Proterozoic transpressive deformation in the Northern Marginal Zone, Limpopo Belt, Zimbabwe. *J. Geol.* **103**, 493-508.

Kamber B.S., Kramers J.D., Napier R., Cliff R.A., and Rollinson H.R. (1994) The triangle shearzone, Zimbabwe, revisited : new data document an important event at 2.0 Ga in the Limpopo Belt. *Precam. Res.* **70**, 191-213.

Kamo S.L. and Davis D. W. (1994) Reassessment of Archean crustal development in the Barberton Mountain Land, South Africa, based on U-Pb dating. *Tectonics* **13**(1), 167-192.

Key R.M. (1979b) The geology of the country around Machaneng and Chadibe. Geological Survey of Botswana.

Kramers J.D., Chavagnac V., Holzer L., Nägler Th. F., and Villa I.M. (1998) Trace element partitioning can explain an apparent paradox of mineral chronometer memory. *88 Jahrestagung der Geologischen Vereinigung e.V.*, 58.

Kramers J.D. and Ridley J.R. (1989) Can Archean granulites be direct crystallizytion products from a sialic magma layer? *Geology* **17**, 442-445.

Kreissig K. (in prep) The Limpopo Belt Southern Marginal Zone-Kaapvaal craton transition: implications from geochronological, isotope and trace element study. Phil. Nat. Ph.D. thesis, University of Bern.

Kreissig K. and Holzer L. (1997) The Kaapvaal Craton - Southern Marginal Zone (limpopo Belt) connection; implications from geochronological data, Pb isotopes and REE patterns. *EUG9*, 364.

Kreissig K., Nägler Th.F., and Kramers J.D. (in prep) Isotope and trace element geochemical study of Archean juxtaposed provinces in southern Africa. .

Kretz R. (1983) Symbols for rock-forming minerals. *Am. Mineral.* **68**, 277-279.

Lamb W.M. and Valley J.M. (1984) Metamorphism of reduced granulites in low-$CO_2$ vapour-free environment. *Nature* **312**, 56-58.

Le Breton N. and Thompson A.B. (1988) Fluid-absent (dehydration) melting of biotite in metapelites in the early stages of crustal anatexis. *Contrib. Mineral. Petrol.* **99**, 226-237.

Le Fort P. (1981) Manaslu leucogranite: a collision signature of the Himalaya, a model for its genesis and emplacement. *J. Geophys. Res.* **86**, 10545-10568.

Light M.P.R. (1982) The Limpopo Mobile Belt: A result of continental collision. *Tectonics* **1**, 325-342.

Lindh A. and Wahlgren C-H. (1985) Migmatite formation at subsolidus conditions-an alternative to anatexis. *J. Metam. Geol.* **3**, 1-12.

Maaløe S. (1992) Melting and diffusion processes in closed-system migmatization. *J. Metam. Geol.* **10**, 503-516.

MacRae N.D. and Nesbitt H.W. (1980) Partial melting of common metasedimentary rocks: a mass balance approach. *Contrib. Mineral. Petrol.* **75**, 21-26.

Martin A. (1978) The geology of the Belingwe-Shabani schist belt. *Bull. Geol. Surv. Rhodesia.*

Martin A. (1983) The geology of the northern part of the Belingwe greenstone belt and surrounding granitoids. unpublished Ph.D. thesis, University of Zimbabwe.

Martin A. (1991) A geological summary of the Belingwe Greenstone Belt. IGCP.

Mason R. (1973) The Limpopo Mobile Belt, southern Africa. *Phil. Trans. R. Soc. London* **A273**, 463-485.

Masuda A., Nakamura N., and Tanaka T. (1973) Fine structures of mutually normalized rare earth patterns of chrondrites. *Geochim. Cosmochim. Acta* **37**, 239-248.

McCourt S. (1995) The crustal architecture of the Kaapvaal crustal block South Africa, between 3.5 and 2.0 Ga. *Mineral. Deposita* **30**, 89-97.

McCourt S. and van Reenen D.D. (1992) Structural geology and tectonic setting of the Sutherland greenstone belt, Kaapvaal Craton, South Africa. *Precam. Res.* **55**, 93-110.

McCourt S. and Vearncombe J.R. (1987) Shear zones bounding the central zone of Limpopo Mobile belt, southern Africa. *J. Struct. Geol.* **9**, 127-137.

McCourt S. and Vearncombe J.R. (1992) Shear zones of the Limpopo Belt and adjacent granitoid-greenstone terranes: Implications for Late Archean collision tectonics in southern Africa. *Precam. Res.* **55**, 553-570.

McCulloch M.T. and Bennett V.C. (1994) Progressive growth of the Earth's continental crust and depleted mantle : geochemical constraints. *Geochim. Cosmochim. Acta* **58**, 4.717-4.738.

McCulloch M.T. and Wasserburg G.J. (1978) Sm-Nd and Rb-Sr chronology of continental crust formation. *Science* **200**, 1 003-1 011.

McGregor A.M. (1953) Precambrian formations of tropical southern Africa. *Int. Geol. Cong.*, 39-50.

McLellan E.L. (1983) Contrasting textures in metamorphic and anatectic migmatites: an example from the Scottish Caledonides. *J. Metam. Geol.* **1**, 241-262.

Mehnert K.R. (1968) *Migmatites and the Origin of Granitic Rocks.* Elsevier.

Miller C.F. and Mittlefehldt D.W. (1982) Depletion of light rare-earth elements in felsic magmas. *Geology* **10**, 129-133.

Misch P. (1968) Plagioclase composition and non-anatectic origin of migmatitic gneisses in Northern Cascade Mountains of Washington State:. *Contrib. Mineral. Petrol.* **17**, 1-70.

Mkwelli S., Kamber B., and Berger M. (1995) Westward continuation of the Craton Limpopo Belt tectonic break in Zimbabwe Nd new age constraints on the timing of the thrusting. *J. Geol. Soc. London* **152**, 77-83.

Montel J.M. (1993) A model for monazite/melt equilibrium and application to the generation of granitic magmas. *Chem. Geol.* **110**, 127-146.

Moorbath S. (1977) Ages, isotopes and evolution of precambrian continental crust. *Chem, Geol.* **20**, 151-187.

Moorbath S. (1978) Ages and isotopes evidence for evolution of the continental crust. *Philos. Trans. R. Soc. London* **288**, 410-413.

Moorbath S. and Taylor P.N. (1986) Geochronology and related isotope geochemistry of high-grade metamorphic rocks from the lower continental crust. In *The nature of the lower continental crust*, Vol. 24 (ed. Dawson J.B., Carswell D.A., Hall J., and Wedepohl K.H.), pp. 211-220. Blackwell scientific publications.

Moorbath S., Whitehouse M.J., and Kamber B.S. (1997) Extreme Nd-isotope heterogeneity in the early Archean- fact or fiction? Case histories from northern Canada and West Greenland. *Chem. Geol.* **135**, 213-231.

Moorbath S., Wilson J.F., and Cotterill P. (1976) Early Archean age for the Sebakwean Group at Selukwe, Rhodesia. *Nature* **264**, 536-538.

Moorbath S., Wilson J.F., Goodwin R., and Humm M. (1977) Further Rb-Sr age and isotope data on early and late Archean rocks from the Rhdesian craton. *Precam. Res.* **5**, 229-239.

Myers R.E. and et al. (1989) Geochemical stratigraphy of the Klipriviersberg Group volcanics. Univ. Witwatersrand, Johannesburg, South Africa.

Nabelek P.I. and Glascock M.D. (1995) REE-depleted leucogranites, Black Hills, South Dakota: a consequence of disequilibrium melting of monazite-bearing schists. *J. Petrol.* **36**(4), 1 055-1 071.

Nägler Th.F. and Kramers J.D. (1998) Nd isotopic evolution of the upper mantle during the Precambrian: model, data and the uncertainty of both. *Precam. Res.* **in press.**

Nesbitt H.W. (1980) Genesis of the New Quebec and Andirondack granulites : evidence for their production by partial melting. *Contib. Mineral. Petrol.* **72**, 303-310.

Newton R.C. and Hensen E.C. (1986) South India-Sri Lanka high grade terrane as a possible deep crust section. In *The nature of the lower continental crust*, Vol. 24 (ed. J.B. Dawson, D. A. Carswell, J. Hall, and K. H. Wedepohl), pp. 297-307. Blackwell scientific publications.

Newton R.C., Smith J.V., and Windley B.F. (1980) Carbonic metamorphism, granulites and crustal growth. *Nature* **288**, 45-50.

Nier A.O. (1950) A redetermination of the relative abundance of the isotopes of carbon, nitrogen, oxygen, argon, and potassium. *Phys. Res.* **77**, 789-793.

Nisbet E.G., Bickle M.J., and Martin A. (1977) The mafic and ultramafic lavas of the Belingwe greenstone belt, Rhodesia. *J. Petrol.* **18**, 521-566.

Odell J. (1975) The geology of the country around Bangala dam. *Geol. Surv. Rhodesia.*

Olsen S.N. (1982) Open- and closed-system migmatites in the Front Range, Colorado. *Am. J. Sci.* **282**, 1596-1622.

Olsen S.N. (1984) Mass-balance and mass-transfer in migmatites from the Colorado Front Range. *Contrib. Mineral. Petrol.* **85**, 30-44.

Olsen S.N. (1985) Mass-balance in migmatites. In *Migmatites* (ed. Ashworth J.R.), pp. 145-179. Blackwell scientific publications.

Olsen S.N. and Grant J.A. (1991) Isocon analysis of migmatization in the Front Range, Colorado, USA. *J. Metam. Geol.* **9**, 151-164.

Orpen J.L. (1978) Geology of the Bend area, Belingwe, Greenstone Belt, Rhodesia., University of Rhodesia, Zimbabwe.

Pan Y. and Fleet M.E. (1996) Rare earth elements mobility during prograde granulite facies metamorphism : significance of fluorine. *Contrib. Mineral. Petrol.* **123**, 251-262.

Patiño Douce A.E. and Beard J.S. (1995) Dehydration-melting of biotite gneiss and quartz amphibolite from 3 to 15 kbar. *J. Petrol.* **36**(3), 707-738.

Patiño Douce A.E. and Beard J.S. (1996) Effects of P, $f(O_2)$ and Mg/Fe ratio on dehydration melting of model metagreywackes. *J. Petrol.* **37**(5), 999-1024.

Patiño Douce A.E. and Johnston A.D. (1991) Phase equilibria and melt productivity in the pelitic system : implications for the origin of peraluminous granitoids and aluminous granulites. *Contrib. Mineral. Petrol.* **107**, 202-218.

Paya B.K. (1996) The geology of the Bobonong area. Geological Survey of Botswana.

Percival J.A. and Card K.D. (1983) Archean crust as revealed in the Kapuskassing uplift Superior Province, Canada. *Geology* **11**, 323-326.

Peterson J.W., Chacko T., and Kuehner S.M. (1991) The effects of fluorine on the vapour-absent melting of phlogopite + quartz: implications for deep-crustal processes. *Am. Mineral.* **76**, 470-476.

Pettijohn F.J., Potter P.E., and Siever R. (1972) *Sand and sandstones.* Springer-Verlag.

Pichavant M., Montel J-M., and Richard L.R. (1992) Apatite solutbility in peraluminous liquids: experimental data and an extension of the Harrison-Watson model. *Geochim. Cosmochim. Acta* **56**, 3 855-3 861.

Pineau F., Javoy M., Behar F., and Touret J. (1981) La géochimie isotopique du facies granulite du Bamble (Norvège) et l'origine des fluides carbonés de la croûte profonde. *Bull. Mineral.* **104**, 630-641.

Poldevaart A. (1955) Chemistry of the Earth's crust. In *Crust of the Earth*, Vol. 62 (ed. Poldevaart A.), pp. 119-144. *Geol.Soc.Am. Spec. Paper.*

Prinzhofer A. and Allègre C.J. (1985) Residual peridotites and the mechanisms of partial melting. *Earth Planet. Sci. Lett.* **74**, 251-265.

Rapp R.P., Ryerson F.J., and Miller C.F. (1987) Experimental evidence bearing on the stability of manazite during crustal anatexis. *Geophys. Res. Lett.* **14**(3), 307-310.

Rapp R.P. and Watson E.B. (1986) Monazite solubility and dissolution kinetics: implications for the thorium and light rare earth chemistry of felsic magmas. *Contrib. Mineral. Petrol.* **94**, 304-316.

Retief E.A., Compston W., Armstrong R.A., and Williams I.S. (1990) Characteristics and prelininary U-Pb ages from Limpopo Belt lithologies. In *The Limpopo Belt: a field workshop on granulites and deep crustal tectonics.* (ed. Barton J.M.), pp. 95-99. Rand Afrikaans University.

Ridley J. (1992) On the origins and tectonic signficance of the charnockite suite of the Archean Limpopo Belt, Northern Marginal Zone, Zimbabwe. *Precam. Res.* **55**, 407-427.

Robb L.R., Davies D.W., and Kamo S.L. (1990) U-Pb ages on single detrital zircon grains from the Witwatersrand Basin: constraints on the age of sedimentation and on the evolution of granites adjacent to the basin. *J. Geol.* **98**, 311-328.

Robb L.R., Davies D.W., and Kamo S.L. (1991) Chronological framework for the Witwatersrand basin and environs: towards a time-constrained depositional model. *S. Afr. J. Geol* **94**, 86-95.

Robertson I.D.M. (1973a) The geology of the country Mount Towla, Gwanda district. Rhod. Geol. Surv. Bull.

Robertson I.D.M. (1973b) Potash granites of the southern edge of the Rhodesian craton and the Northern Granulite Zone of the Limpopo Mobile Belt. *Symposium on granites, gneisses and related rocks.*

Robewrtson I.D.M. and du Toit M.C. (1981) Mobile Belts, A Limpopo Belt. In *The Precambrian of the Southern Hemisphere.* (ed. Hunter D.R.), pp. 641-671. Elsevier.

Robin P-Y. F. (1978) Pressure solution at grain-to-grain contacts. *Geochim. Cosmochim. Acta* **42**, 1383-1389.

Robin P-Y. F. (1979) Theory of metamorphic segregation and related processes. *Geochim. Cosmochim. Acta* **43**, 1 587-1 600.

Roering C., Barton J.M., and de la Winter H.R. (1990) The Vredefort structure: a perspective with regard to new tectonic data from adjoining terranes. *Tectono.* **171**, 7-22.

Roering C., van Reenen D.D., Smit C.A., Barton J.M., De Beer J.H., De Wit M.J., Stettler E.H., van Schalkwyk J.F., Stevens G., and Pretorius S. (1992) Tectonic model for the evolution of the Limpopo belt. *Precam. Res.* **55**, 539-552.

Rollinson H.R. (1989) Garnet-orthopyroxene thermobarometry of granulites from the northern marginal zone of the Limpopo Belt, Zimbabwe. In *Evolution of metamorphic belts*, Vol. 42 (ed. Daley J.S., Cliff R.A., and Yardley B.W.D.), pp. 331-335. Spec. Publ. Geol. Soc. London.

Rollinson H.R. (1993) A terrane interpretation of the Archean Limpopo Belt. *Geol. Mag.* **130**(6), 755-765.

Rollinson H.R. and Blenkinsop T. (1995) The magmatic, metamorphic and tectonic evolution of The Northern Marginal Zone of The Limpopo Belt in Zimbabwe. **152**, 65-75.

Rollinson H.R. and Lowry D. (1992) Early basic magmatism in the evolution of the Northern Marginal Zone of the Archean Limpopo belt. *Precam. Res* **55**(1), 33-45.

Rosing M.T. (1990) The theoritical effect of metasomatism on Sm-Nd isotopic systems. *Geochim. Cosmochim. Acta* **54**, 1 337-1 341.

Roy R.F., Blackwell D.D., and Birch F. (1968) Heat generation of plutonic rocks and continental heat flow provinces. *Earth Planet. Sci. Lett.* **5**, 1-12.

Rudnick R.L. (1992) Restites, Eu anomalies, and the lower continental crust. *Geochim. Cosmochim. Acta* **56**, 963-970.

Rudnick R.L. and Fountain D.M. (1995) Nature and composition of the continental crust : a lower crustal perspective. *Rew. Geophys.* **33**(3), 267-309.

Rudnick R.L. and Presper T. (1990) Geochemistry of intermediate to high-pressure granulites. In *Granulites and crustal evolution.* (ed. V. D. a. V. Ph.), pp. 523-550. Kluwer Academic Publishers.

Sawyer E.W. (1987) The role of partial melting and fractional crystallization in determining discordant migmatite leucosome compositions. *J. Petrol.* **28**(3), 445-473.

Sawyer E.W. (1991) Disequilibrium melting and rate of melt-residuum seperation during migmatization of mafic rocks from the Grenville Front, Quebec. *J. Petrol.* **32**, 701-738.

Sawyer E.W. and Robin P-Y.F. (1986) The subsolidus segregation of layer-parallel quartz-feldspar veins in greenschist to upper amphibolite facies metasediments. *J. Metam. Geol.* **4**, 237-260.

Schaller M., Steiner O., Studer I., Holzer L., Herwegh M., Villa I.M., and Kramers J.D. (in press) The Palala Shear Zone, Transvaal: Exhumation of Limpopo Central Zone granulites and continent-scale transcurrent movement at 2.0 Ga. *J. Afr Earth Sci.*

Schaller M., Steiner O., Studer I., Holzer L., and Kramers J.D. (1997) Evidence for a 2.0 Ga exhumation in the granulite-facies Central Zone along the Palala shear zone, Limpopo Belt, southern Africa. *EUG9.*

Schilling J-G. (1966) Rare earth fractionation in Hawaiian volcanic rocks. Unplubl. Ph.D. Thesis, Massachusetts Institute of Technology, Cambridge, MA.

Schönberg R., Kruger F.J., and Kramers J.D. (1998) The formation of the PGE gearing Bushveld chromitites and the Merensky Reef by magma mixing; a combined Re-Os and Rb-Sr study. *The 8th V.M. Goldschmidt Conference.*

Schreurs J. (1985) Prograde metamorphism of metapelites, garnet-biotite thermometers and prograde changes of biotite chemistry in high-grade rocks of West Uusimaa, southwest Finland. *Lithos* **1**, 69-80.

Sederholm J.J. (1907) On granite and Gneiss. *Bull. Comm. Geol. Finl.* **23**, 1-110.

Sederholm J.J. (1913) Die Enstehung der migmatischen Gesteine. *Geol. Rundsch.* **4**, 174-195.

Sederholm J.J. (1934) On migmatites and associated Precambrian rocks of South western Finland. *Bull. Comm. Geol. Finl.* **107**, 1-68.

Sevigny J.H. (1993) Monazite controlled Sm/Nd fractionation in leucogranites: An ion microprobe study of garnet phenocrysts. *Geochim. Cosmochim. Acta* **57**, 4 095-4 102.

Skinner A.C. (1978a) The geology of the Mahalapye area. Geological Survey of Botswana.

Smit C.A., Roering C., and van Reenen D.D. (1992) The structural framework of the southern margin of the Limpopo Belt, South Africa. *Precam. Res.* **55**, 51-67.

Spear F.S. (1992) Thermobarometry and P-T paths from granulite facies rocks : an introduction. *Precam. Res.* **55**, 201-207.

Spear F.S. and Kohn M.J. (1996) Trace element zoning in garnet as a monitor of crustal melting. **24**(12), 1 099-1 102.

Stacey J.S. and Kramers J.D. (1975) Approximation of terrestrial lead isotope geochemistry of a two-stage model. *Earth Planet. Sci. Lett.* **26**, 207-221.

Stanistreet I.G. and McCarthy T.S. (1991) Changing tectonosedimentary scenarios relevant to the development of the Late Archean Witwatersrand basin. *J. Afr. Earth Sci.* **13**, 65-82.

Stevens G., Clemens J.D., and Droop G.T.R. (1997) Melt production during granulite-facies anatexis: experimental data from primitive metasedimentary protoliths. *Contrib. Mineral. Petrol.* **128**, 352-370.

Stevens G. and van Reenen D.D. (1992) Constraints on the form of the P-T loop in the Southern Marginal Zone of the Limpopo Belt, South Africa. **55**, 279-296.

Stowe C.W. (1984) The early Archean Selukwe nappe, Zimbabwe. In *Precambrian Tectonics illustrated* (ed. Kröner A. and Greiling R.), pp. 41-56. Schweizerbar'sche Verlagsbuchhandlung.

Streckeisen A. (1976) To each plutonic rock its proper name. *Earth Sci. Rev.* **12**, 1-33.

Stuart G.W. and Zengeni T.G. (1987) Seismic crustal structure of the Limpopo Mobile Belt, Zimbabwe. *Tectonophysics* **144**, 323-335.

Sylvester P.J., Campbell I.H., and Bowyer D.A. (1997) Niobium/Uranium evidence for Early formation of the continental crust. *Science* **275**, 521-523.

Tankard A.J., Jackson M.P.A., Eriksson K.A., Hobday D.K. H. D. R., and Minter W.E.L. (1982) *Crustal evolution of southern Africa. 3.8 Ga of Earth history.* Springer.

Taylor P.N., Jones N.W., and Moorbath S. (1984) Isotopic assessement of relative contributions from crust and mantle sources to the magma genesis of Precambrian granitoid rocks. *Phil. Trans. R. Soc. London* **A310**, 605-625.

Taylor P.N., Kramers J.D., Moorbath S., Wilson J.F., Orpen J.L., and Martin A. (1991) Pb/Pb, Sm-Nd and Rb-Sr geochronology in the Archean Craton of Zimbabwe. *Chem. Geol.* **87**, 175-196.

Taylor S.R. and McLennan S.M. (1981) The composition and evolution of continental crust: Rare Earth elements from sedimentary rocks. *Philos. Trans. R.Soc. London* **301**, 381-399.

Taylor S.R. and McLennan S.M. (1985) *The continental crust : its composition and evolution.* Blackwell scientific Publications.

Taylor S.R. and McLennan S.M. (1995) The geochemical evolution of the continental crust. *Rev. Geophys.* **33**(2), 241-265.

Thompson A.B. (1990) Heat, fluid and melting in the granulite facies. In *Granulites and crustal differentiation* (ed. D. Vielzeuf and Vidal Ph.), pp. 37-58. Kluwer.

Touret J. (1969) Le socle Précambrien de la Norvège méridionale. PhD, Université de Nancy.

Touret J. (1971) Le faciès granulite en Norvège méridionale II : les inclusions fluides. *Lithos* **4**, 423-435.

Touret J. (1985) Fluid regime in southern Norway: the record of fluid in inclusions. In *The deep Proterozoic crust in the North Atlantic provinces.* (ed. Tobi A.C. and Touret J.), pp. 517-49. Kluwer Academic publishers.

Tourpin S., Gruau G., Blais S., and Fourcade S. (1991) Resetting of REE, and Nd and Sr isotopes during carbonitization of a komatiite flow from Finland. *Chem. Geol.* **90**, 15-29.

Treloar P.J. and Blenkinsop T.G. (1995) Archean deformation patterns in Zimbabwe: True indicators of the Tibetan style crustal extrusion or not? In *Early Precambrian processes*, Vol. 95 (ed. Coward P.P. and Ries A.C.), pp. 87-108. *Geol. Soc.Spec. Publ. London.*

Treloar P.J., Coward M.P., and Harris N.B.W. (1992) Himalayan-Tibetan analogies from the evolution of the Zimbabwe Craton and Limpopo Belt. *Precam. Res.* **55**, 571-587.

Tsomondo J.M., Wilson J.F., and Blenkinsop T.G. (1992) Reassessment of the structure and stratigraphy of the early Archean Selukwe Nappe, Zimbabwe. In *The Archean: terrains,*

*processes and metallogeny.*, Vol. 22 (ed. Glover J.E. and Ho S.E.), pp. 123-135. Geol. Depart. (Key Centre) and Univ. Ext., University of Western Australia.

Tsunogae T., Hisada K., Miyano T., Yurimoto H., and Paya B.K. (submitted) New SIMS ages of zircons from the Mahalapye area, the Limpopo Central Zone, eastern Botswana. .

Tsunogae T., Miyano T., and Mahcacha T.P. (1989) Retrograde orthoamphiboles in metapelites near Maratele, southwest Selebi-Phikwe, Botswana. University of Tsukuba.

Tsunogae T., Miyano T., and Ridley J. (1992) Metamorphic P-T profiles from the Zimbabwe Carton to the Limpopo Belt, Zimbabwe. *Precam. Res.* **55**, 259-277.

Tuttle O.F. and Bowen N.L. (1958) Origin of granite in the light of experimental studies in the system $NaAlSi_3O_8$-$KAlSi_3O_8$-$SiO_2$-$H_2O$. *Geol. Soc. Am. Mem.* **74**.

Valley J.W. (1992) Granulite formation is driven by magmatic processes in the deep crust. *Earth-Sci. Rev.* **32**, 145-146.

Valley J.W., Bohlen S.R., Essene E.J., and Lamb W.M. (1990) Metamorphism in the Adirondacks.II. The role of fluids. *J. Petrol.* **31**, 555-596.

Van Breemen O. and Dodson M.H. (1972) Metamorphic chronology of the Limpopo Belt, southern Africa. *Geol. Soc. Am. Bull.* **83**, 2 005-2 018.

van Breemen O., Dodson M.H., and Vail J.R. (1966) Isotopic age measurements on the Limpopo Orogenic Belt, southern Africa. *Earth Planet. Sci. Lett.* **1**, 401-406.

van Breemen O. and Hawkesworth C.J. (1980) Sm-Nd isotopic studies of garnets and their metamorphic host rocks. *Trans. R. Soc. Edinburgh Earth Sci.* **71**, 97-102.

van der Auwera J. (1993) Diffusion controlled growth of pyroxene-bearing margins on amphibolite bands in the granulite facies of Rogaland (SouthWest Norway): implications for granulite formation. *Contrib. Mineral. Petrol.* **114**, 203-220.

van der Molen I. (1985) Interlayer material transport during layer-normal shortening, II, boudinage, pinch-and-swell and migmatite at Søndre Strømfjord Airport, west Greenland. *Tectonophysics* **115**, 275-295.

van Reenen D.D. (1983) Cordierite+garnet+hypersthene+biotite-bearing assemblages as a function of changing metamorphic conditions in the Southern Marginal Zone of the Limpopo metamorphic complex. *Spec. Publ. Geol Soc. S. Afr.* **8**, 143-167.

van Reenen D.D., Barton J.M., Roering C., Smit C.A., and van Schalkwiyk J.F. (1990) The granulite facies rocks of the Limpopo Belt, southern Africa. In *Granulites and crustal evolution.* (ed. Vielzeuf D. and Vidal Ph.), pp. 257-289. Kluwer.

van Reenen D.D., Barton J.M., Roering C., Smith C.A., and van Schalkwyk J.F. (1987) Deep crustal response to continental collision: the Limpopo Belt of Southern Africa. **15**, 11-14.

van Reenen D.D., Roering C., Ashwal L.D., and de Wit M.J. (1992) Regional geological setting of the Limpopo Belt. *Precam. Res.* **55**, 1-5.

Vearncombe J.R. (1986) Structure of veins in a gold-pyrite deposit in banded iron formation, Amalia greenstone belt, South Africa. In *Geol.Mag.*, Vol. 123, pp. 600-609.

Vearncombe J.R. (1988) Structure and metamorphism of the Archean Murchison belt, Kaapvaal Craton, South Africa. *Tectonics* **7**, 761-774.

Vernon R.H. and Collins W.J. (1988) Igneous microstructures in migmatites. *Geology* **16**, 1 126-1 129.

Vielzeuf D., Clemens J.D., Moinet E., and Montel J-M. (1990) Experimental determination of the fluid-absent melting reactions in Al-metagreywackes. *Thrid International Symposium on Experimental Mineralogy, Petrology and Geochemistry.*

Vielzeuf D. and Holloway J.R. (1988) Experimental determination of the fluid-absent melting relations in the pelitic system. *Contrib. Mineral. Petrol.* **98**, 257-276.

Vielzeuf D. and Montel J.M. (1994) Partial melting of metagreywackes. Part 1. Fluid-absent experiments and phase relationships. *Contrib. Mineral. Petrol.* **117**, 375-393.

Walraven F., Frick C., and Lubala R.T. (1992) Pb-isotope geochronology of the Shield Complex, Northern Transvaal, South Africa. *J. Afr. Earth. Sc.* **15**, 103-110.

Wasserburg G.J., Jacobsen S.B., De Paolo D.J., McCulloch M.T., and Wen J. (1981) Precise determination of Sm/Nd ratios, Sm and Nd isotopic abundances in standard solutions. *Geochim. Cosmochim. Acta* **45**, 2 311-2 323.

Watkeys M.K. (1983) A retrospective view of Central Zone of Limpopo Belt, Zimbabwe. *Spec. Publ. Geol. Soc. S. Afr.* **8**, 65-80.

Watson E.B. and Harrison T.M. (1983) Zircon saturation revisited: temperature and composition effects in a variety of crustal magma types. *Earth Planet. Sci. Lett.* **64**, 294-304.

Watson E.B., Vicenzi E.P., and Rapp R.P. (1989) Inclusion/host relations involving accessory minerals in high-grade metamorphic and anatectic rocks. *Contrib. Mineral Petrol.* **101**, 220-231.

Watt G.R., Burns I.M., and Graham G.A. (1996) Chemical characteristics of migmatites : accessory phase distribution and evidence for fast melt segregation rates. *Contrib. Mineral Petrol.* **125**, 100-111.

Watt G.R. and Harley S.L. (1993) Accessory phase controls on the geochemistry of crustal melts and restites produced during water-undersaturated partial melting. *Contrib. Mineral. Petrol.* **114**, 550-566.

Weber C. and Barbey P. (1986) The role of water, mixing processes and metamorphic fabric in the genesis of the Baume migmatites (Ardèche, France). *Contrib. Mineral. Petrol.* **92**, 481-491.

Wedepohl K.H. (1969-1978) *Handbook of Geochemistry*. Springer and Verlag.

Wedepohl K.H. (1995) The composition of the continental crust. *Geochim. Cosmochim. Acta* **59**, 1217-1232.

Whitehouse M.J., Fowler M.B., and Friend C.R.L. (1996) Conflicting mineral and whole rock isochron ages from the Late-Archean Lewisian Complex of northwestern Scotland :

implications for geochronology in polymetamorphic high-grade terrains. *Geochim. Cosmochim. Acta* **61**, 3 085-3 102.

Whitney D.L. and Irving A.J. (1994) Origin of K-poor leucosomes in a metasedimentary migmatite complex by ultrametamorphism, syn-metamorphic magmatism and subsolidus processes. *Lithos* **32**, 173-192.

Wickham S.M. (1987) The segregation and emplacement of granitic magmas. *J. Geol. Soc. London* **144**, 281-297.

Wilson J.F., Jones D.L., and Kramers J.D. (1987) Mafic dyke swarms in Zimbabwe. In *Mafic dyke swarms*, Vol. 34 (ed. Halls H.C. and Fahrig W.F.), pp. 433-444. Geol. Assoc. Canada Spec.

Wilson J.T. (1968) Static or mobile belt: The current scientific evolution. *Am. Philos. Soc. Proc.* **112**, 309-320.

Windley B.F. (1993) Uniformitarianism today: plate tectonics is the key to the past. *J. Geol. Soc.* **150**, 7-19.

Windley B.F., Ackermand D., and Herd R.K. (1984) Sapphirine/kornuperine-bearing rocks and crustal uplift history of the Limpopo Belt, South Africa. *Contrib. Mineral. Petrol.* **86**, 342-358.

Winkler H.G.F. (1961) Die Genese von Graniten und Migmatiten auf Grund neuer Experimente. *Geol. Rundsch.* **61**, 347-364.

Wolf M.B. and London D. (1994) Apatite dissolution into peraluminous haplogranitic melts: an experimental study of solubilities and mechanisms. *Geochim. Cosmochim. Acta* **58**(19), 4 127-4 145.

Wolf M.B. and Wyllie P.J. (1994) Dehydration-melting of amphibolite at 10 kbars: the effects of temperature and time. *Contrib. Mineral. Petrol.* **115**, 369-383.

Worst B.G. (1962) The geology of the Buhwa iron ore deposits and adjoining country. *S. Rhod. Geol. Surv. Bull.*

Zhu C. and Sverjensky D.A. (1992) F-Cl-OH partitioning between biotite and apatite. *Geochim. Cosmochim. Acta* **56**, 3435-3467.

Ames L. (1995) Geochronology and Isotopic character of ultrahigh-pressure metamorphism with implications for collision of the Sino-Korean and Yangtze Cratons, Central China. Geological Sciences, California, Santa Barbara.

Ames L., Tilton G.R., and Zhou G. (1993) Timing of collision of the Sino-Korean and Yangtze Cratons: U-Pb zircon dating of coesite-bearing eclogites. *Geology* **21**, 339-342.

Andersen T.B., Jamtveit B., Dewey J.F., and Swensonn E. (1991) Subduction and eduction of continental crust : major mechanisms during continent-continent collision and orogenic extensional collapse, a model based on the south Norwegian Caledonides. *Terra Nova* **3**, 303-310.

Arnaud N.O. and Kelley S.P. (1994) Dating of high pressure metamorphism with a new high resolution ultra-violet laser ablation microprobe 40Ar/39Ar technique: Dora Maira, western Alps, Italy. *ICOG 8*, 11.

Arnaud N.O. and Kelley S.P. (1995) Evidence for excess argon during high pressure metamorphism in the Dora Maira Massif (western Alps, Italy), using an ultra-violet laser ablation microrpobe $^{40}Ar$-$^{39}Ar$ technique. *Contrib. Mineral. Petrol.***121**, 1-11.

Baker J., Mattews A., Mattey D., Rowley D., and Xue F. (1997) Fluid-rock interactions during ultrahigh pressure metamorphism, Dabies Shan, China. *Geochim. Cosmochim. Acta* **61**(8), 1 685-1 696.

Bohlen S.R. and Boettcher A.L. (1982) The quartz-coesite transformation: A pressure determination and the effects of other components. *J. Geophys. Res.* **87**, 7073-7078.

Burton K.W., Kohn M.J., Cohen A.S., and O`Nions R.K. (1995) The relative diffusion of Pb, Nd, Sr and O in garnet. *Earth Planet.Sci. Lett.* **133**, 199-211.

Cao R.L. and Zhu S.H. (1995) U-Pb and $^{40}Ar/^{39}Ar$ geochronology of coesite-bearing eclogites from the Bixiling complex, Anhui. .

Carswell D.A. (1990) *Eclogite facies rocks.*

Carswell D.A., Wilson R.H., Cong B., Zhai M., and Zhao Z. (1993) Areal extend of the ultrahigh-pressure metamorphism of eclogites and gneisses in Dabieshan, cetral China. *Terra* **5**, 5.

Chavagnac V. and Jahn B-m. (1996) Coesite-bearing eclogites from the Bixiline Complex, Dabie Mountains, China: Sm-Nd ages, geochemical characteristics and tectonic implications. *Chem. Geol.* **133**, 29-51.

Chen J.F., Xie Z., Liu S.S., Li X.M., and Foland K.A. (1995) Cooling age of the Dabie orogen, China, determined by $^{40}Ar/^{39}Ar$ and fission track techniques. *Sci. China* **38**, 749-757.

Chopin C. (1984) Coesite and pure pyrope in high grade blueschists of the Western Alps: A first record and some consequences. *Contrib. Mineral. Petrol.* **86**, 107-118.

Chopin C., Henry C., and Michard A. (1991) Geology and petrology of the coesite-bearing terrain, Dora Maira massif, Western Alps. *Eur. J. Mineral.* **3**, 263-291.

Cliff R.A. (1993) Isotopic dating of metamorphism and cooling. *School Earth and PLanetary Sciences* **7**, 131-140.

Cloos M. (1982) Flow melanges: numerical modelling and geologic constraints on their origin in the Franciscan subduction complex. *Bull. geol. Soc. Am.* **93**, 330-345.

Coleman R.G. and Wang X. (1995) Overview of the geology and tectonics of UHPM. In *UltraHigh-pressure metamorphism* (ed. Coleman R.G. and Wang X.), pp. 1-32. Cambridge University press.

Cong B., Zhai M., Carswell D.A., Wilson R.N., Wang Q., Zhao Z., and Windley B.F. (1995) Petrogenesis of ultrahigh-pressure rocks and their country rocks at Shuanghe in Dabieshan, Central China. *Eur. J. Mineral.* **7**, 119-138.

Cowan D.S. and Silling R.M. (1978) A dynamic model of accretion at trenches and its implications for the tectonic evolution of the subduction complexes. *J. Geophys. Res.* **28**, 177-186.

Cuthbert S.J. and Carswell D.A. (1990) Vormation and exhumation of medium-temperature eclogites in the Scandinavian Caledonides. In *Eclogite Facies Rocks* (ed. Carswell D.A.), pp. 180-203. Blackie.

Dahl P.S. (1996) The crystal-chemical basis for Ar retention in micas:; ineferences from interlayer partitioning and implications for geochronology. *Contrib. Mineral. Petrol.* **123**, 22-39.

Davies J.H. and Von Blanckenburg F. (1995) Slab breakoff : a model of lithosphere detachment and its test in the magmatism and deformation of coolisional orogens. *Earth Planet. Sci. Lett.* **129**, 85-102.

Davy Ph. and Gillet P. (1986) The stacking of thrust slices in collision zones and its thermal consequences. *Tectonophysics.* **5**, 913-929.

Dewey J.F. (1988) Extensional collapse orogens. *Tectonophysics.* **7**(6), 1 123-1 139.

Eide R.J., Liou J.G., and McWilliams M.O. (1994) 40Ar/39Ar constraints on high and ultrahigh pressure metamorphism, Hubei province, China. *Geology* **22**, 601-604.

Enami M., Wang S., Zhang Q., and Hiraiwa I. (1986) Eclogites from the Donghai district, Jinagsu province, east CVhina. *Nagoya University Museum Bulletin* **2**, 55-70.

Enami M. and Zang Q. (1988) Magnesian staurolite in garnet-corundum rocks and eclogite from Donghai district, Jiangsu province, East China. *Am. Mineral.t* **73**, 48-56.

Enami M., Zang Q., and Yin Y. (1993) High-Pressure eclogites in northern Jiangsu-sourthern Shandong province, eastern China. *J. Metam Geol.* **11**, 589-603.

Enami M. and Zhang Q. (1990) Quartz pseudomorphs after coesite in eclogites from Shandong province, east China. *Am. Mineral* **75**, 381-386.

England P.C. and Holland T.J.B. (1979) Archimedes and the Tauern eclogites: the role of buoyancy in the preservation of exotic eclogite blocks. *Earth Planet. Sci. Lett.* **44**, 287-294.

England P.C. and Molnar P. (1990) Surface uplift, uplift of rocks, and exhumation of rocks. *Geology* **18**, 1173-1177.

England P.C. and Thompson A.B. (1984) Pressure-temperature-time paths of regional metamorphism. Heat transfert during the evolutions of regions of thickened continental crust. *J. Petrol.* **25**, 894-928.

Enkin R.J., Yang Z., Chen Y., and Courtillot V. (1992) Paleomagnetic contraints on the geodynamic history of the major blocks of China from the Permian to the present. *J. Geophys. Res.* **97**, 13 953-13 989.

Erlank A.J., Waters F.G., Hawkesworth C.J., Haggerty S.E., Allsop H.L., Rickard R.S., and Menzies M. (1987) Evidence for mantle metasomatism in peridotite noduls from the kimberley pipes, South Africa. In *Mantle Metasomatism* (ed. Menzies M.A. and Hawkesworth C.J.), pp. 211-311. Academic Press.

Ernst W.G. (1988) Tectonic history of subduction zones inferred from retrograde blueschist P-T paths. *Geology* **16**, 1 081-1 084.

Ernst W.G. and Liou J.G. (1995) Contrasting plate-tectonic styles of the Qinling-Dabie-Sulu and Franscican metamorphic belts. *Geology* **23**, 353-356.

Eskola P. (1921) *The mineral facies of rocks.*

Gao S., Zhang B.R., Gu X.M., Xie Q.L., Gao C.L., and Guo X.M. (1995) Silurian-Devonian provenance changes of South Qinling basins: Implications for accretion of the Yangtze (South China) to the North China cratons. *Tectonophysics.*

Gillet P., Choukroune P., Ballèvre M., and Davy Ph. (1986) Thickening history of the western Alps. *Earth Planet. Sci. Lett.* **78**, 44-52.

Gillet P., Ingrin J., and Chopin C. (1984) Coesite in subducted continental crust : P-T history deduced from an elastic model. *Earth Planet. Sci. Lett* **70**, 426-436.

Goldstein S.L., O'Nions R.K., and Hamilton P.J. (1984) A Sm-Nd isotopic study of atmospheric dusts and particulates from major river systems. *Earth Planet. Sci. Lett.* **70**, 221-236.

Griffin W.L., Austrheim A., Brastad K., Bryhni I., Krill A.G., Mörk M.B.E., and Qvale H. (1985) High-pressure metamorphism in the Scandinavian Caledonides. In *The Caledonide Orogen - Scandinavia and related Areas.* (ed. Gee D.G. and Sturt B.A.), pp. 783-801. Wiley J.,.

Hacker B.R. and Peacock S.M. (1997) Creation, Preservation, and exhumation of UHPM rocks. In *The Tectonics of Asia* (ed. Yin A. and Harrison T.M.), pp. 159-181.

Hacker B.R., Ratschbacher L., Webb L., and Shuwen D. (1995) What brought them up ? Exhumation of the Dabie Shan ultrahigh-pressure rocks. *Geology* **23**(8), 743-746.

Hacker B.R. and Wang Q.C. (1995) Ar/Ar geochronology of Ultrahigh-Pressure metamorphism in central China. *Tectonics* **14**, 994-1006.

Hacker B.R. and Wang Q.C. (1995) Cooling history of the ultrahigh-pressure rocks, Dabie Mountains, China. *Tectonics* **14**, 994-1006.

Hacker B.R., Wang X., Eide E.A., and Ratschbacher L. (1995) Qinling-Dabie Ultrahigh-Pressure collisional orogen. In *Tectonics of Asia*, Vol. 9 (ed. Yin A. and Harrison T.M.). Cambridge University press.

Harley S.L. and Carswell D.A. (1995) Ultradeep crustal metamorphism : a prospective view. . *J. Geophys. Res.* **100**(B5), 8 367-8 380.

Hensen B.J. and Zhou B. (1995) Retention of isotopic memory in garnets partially broken down during an overprinting granulite-facies metamorphism : implications for the Sm-Nd closure temperature. *Geology* **23**, 225-228.

Hirajima T., Ishiwatari A., Cong B., Zhang R., Banno S., and Nozaka T. (1990) Coesite from Mengzhong eclogite at Donghai country, northeastern Jiangsu province, China. In *Mineral. Mag.*, Vol. 54, pp. 579-583.

Hofmann A.W. (1988) Chemical differenciation of the Earth : the relationship between mantle, continental crust, and oceanic crust. *Earth Planet.Sci. Lett.* **90**, 297-314.

Houseman G.A. and England P.C. (1986) Finite strain calculations of continental deformation. I. Method and general results for convergent zones. *J. Geophys. Res.* **91**, 3651-3663.

Hsü K.J., Wang Q.C., Li J.L., Zhou D., and Sun S. (1987) Tectonic evolution of Qinling Mountains, China. *Eclogae Geol. Helv.* **71**, 611-635.

Humphries F.J. and Cliff R.A. (1982) Sm-Nd dating and cooling history of Scourian granulites, Sutherland. *Nature* **295**, 515-517.

Ishiwatari A., Hirajima T., Nozaka T., and Banno S. (1990b) An eclogite survey mission to Shandong and Jiangsu province, East China. *J. Geol.* **99**, 382-387.

Jagoutz E. (1988) Nd and Sr systematics in an eclogite xenolith from Tanzania : Evidence for frozen mineral equilibria in the continental lithosphere. *Geochim. Cosmochim. Acta* **52**, 1285-1293.

Jagoutz E., Shatsky V.S., and Sobolev N.V. (1990) Sr-Nd-Pb isotopic study of ultrahigh PT rocks from Kotchetav massif. *EOS Trans. AGU* **71**, 1707.

Jahn B.M. (1998) Geochemical and isotopic characteristics of UHP eclogites and ultramafic rocks of the Dabie orogen: Implications for continental subduction and collisional tectonics. In *When continents collide: Geodynamics and Geochemistry of ultrahigh pressure rocks* (ed. Hacker B. and Liou J.G.). Chapman and Hall.

Jahn B.M., Cornichet J., Cong B., and Yui T.F. (1996) Ultra-high eNd eclogites from an ultra-high pressure metamorphic terrane of China. *Chem. Geol.*

Jahn B.M., Cornichet J., and Cong B.L. (1995a) Crustal evolution of the Qinling-Dabie Orogen: isotopic and geochemical constraints from coesite-bearing eclogites of the Su-Lu and Dabie Terranes, China. *Chinese Sci. Bull.* **40**, 116-119.

Jahn B.M., Cornichet J., Henin O., Le Coz Bouhnik M., and Cong B.L. (1994) Geochemical and isotopic investigation of ultrahigh pressure (UHP) metamorphic terranes in China: Su-Lu and Dabie complexes. *Stanford Workshop on "Ultrahigh-P metamorphism and tectonics"*, A71-A74.

Jenkin G.R.T. (1997) Do cooling paths derived from mica Rb-Sr data reflect true cooling paths? *Geology* **25**(10), 907-910.

Jenkin G.R.T., Rogers G., Fallick A.E., and Farrow C.M. (1995) Rb-Sr closure temperatures in bi-mineralistic rocks: a mode effect and test for different diffusion models. *Chem.Geol.* **122**, 227-240.

Krogh E.J. (1977) Evidence of Precambrian continent-continent collision in western Norway. *Nature* **267**, 17-19.

Kröner A., Compston W., Zhang G.W., Guo A.L., and Todt W. (1988) Age and tectonic setting of late Archean greenstone-gneiss terrane in Henan province, China, as revealed by single-grain zircon dating. *Geology* **16**, 211-215.

Kröner A., Compston W., Zhang G.W., Guo A.L., and Todt W. (1993) Granulites in the Tongbai area, Qinling Belt, China: geochemistry, petrology, single zircon geochronology, and implications for the tectonic evolution of estern Asia. *Tectonics* **12**, 245-255.

Le Maitre R.W., Bateman P., Dubek A., Keller J., Lameyre J., La Bas M.J., Sabine P.A., Schmid R., Sorensen H., Streckeisen A., Wooley A.R., and Zanettin B. (1989) A classification of igneous rocks and glossary of terms. Blackwell.

Li S., Hart S.R., Zheng G., and Guo A. (1989) Timing collision between the north and the couth China blocks- the Sm-Nd isotopic age evidence. *Science in China* **32**, 1 391-1400.

Li S., Wang Y.C., Liu D., Zhou H., and Zhang Z. (1994) Excess argon in phengite from eclogite : evidence from dating of eclogite minerals by Sm-Nd, Rb-Sr and $^{40}Ar/^{39}Ar$ methods. *Chem.Geol.***112**, 343-350.

Li S., Xiao Y., Liou D., and Chen Y. ... (1993) Collision of the North China and Yangtze blocks and formation of coesite-bearing eclogites : timing and processes *Chem.Geol* **109**, 89-111.

Lin J.L., Fuller M., and Zhang W.Y. (1985) Preliminary Phanerozoic polar wander paths for the North and South China Blocks. *Nature* **313**, 444-449.

Liou J.G., Banno S., and Ernst W.G. (1995) Ultrahigh-pressure metamorphism and tectonics. *The Island Arc* **4**, 233-239.

Liou J.G., Wang Q., Zhai M., Zhang R.Y., and Cong B. (1995) Ultrahigh-pressure metamorphic rocks and their associated lithologies from the Dabie Mountains, central China: a field trip guide to the 3rd International Eclogite Field symposium., pp. 71.

Liou J.G. and Zhang R.Y. (1995) Significance of ultrahigh-pressure talc-bearing eclogitic assemblages. *Mineral. Mag.***59**, 93-102.

Liou J.G., Zhang R.Y., and Ernst W.G. (1995) Occurences of hydrous and carbonate phases in ultrahigh-pressure rocks from east-central China : implications for the role of volatiles deep in cold subduction zones. *The Island Arc* **4**, 362-375.

Liou J.G., Zhang R.Y., and Jahn B-m. (1997) Petrology, geochemistry and isotope data on a ultrahigh pressure jadeiite quartzite from Shuanghe, Dabie Mountains, East-Central China. .

Liu R., Fan Q., Zhang Q., Zhao D., and Ma B. (1995) The nature of protolith of Bixiling garnet peridotite-eclogite massif in Dabie Mountains and the implication of its isotopic geochronology. *Acta Petrol. Sinica* **11**, 243-256.

Liu X. and Hao J. (1989) Structure and tectonic evolution of the Tongbai-Dabié range in the East Qinling collisional belt, China. *Tectonics* **8**, 637-645.

Liu X., Nutman A.P., Compston W., Wu J.S., and Shen Q.H. (1992) Remnants of 3800 Ma crust in the Chinese part of the Sino-Korean craton. *Geology* **20**, 339-342.

Ludwig K.R. (1990) ISOPLOT: A plotting and regression program for radioganic isotope data, for IBM-PC compatible computers. USGS Open file report.

Maruyama S., Nutman A.P., Morikawa T., and Liou J.G. (1995) SHRIMP U-Pb geochronology of ultrahigh-pressure metamorphic rocks of the Dabie Mountains, Central China. *Island Arc* **in press**.

Mattauer M., Matte P., Maluski H., Zhiqin X;, Zhang Q.W., and Wang Y.M. (1991) La limite Chine du Nord-Chine du Sud au Paléozoïque et au Trias. Nouvelles données structurales et radiométriques dans le massif de Dabié-Shan (Chaîne de Qinling). *Comptes Rendus de l'Académie des Sciences, Paris* **312**, 1 227-1 233.

Mattauer M., Matte Ph., Malavielle J., Tapponnier P., Maluski H., Qin X.Z., Lun L.Y., and Qin T.Y. (1985) Tectonics of Qinling Belt : build-up and evolution of eastern Asia. *Nature* **317**, 496-500.

McDonough W.F. and Frey F.A. (1989) Rare Earth Elements in upper Mantle rocks. In *Reviews in Mineralogy* (ed. Lipin B.R. and McKay G.A.), pp. 99-145.

Mezger K., Essene E.J., and Halliday A.N. (1992) Closure temperature of Sm-Nd system in metamorphic garnets. *Earth and Planetary Science Letters* **113**, 397-409.

Miyashiro A. (1961) Evolution of metamorphic belt. *J. Petrol.y***2**, 277-311.

Molnar P. and Taponnier P. (1978) Active tectonics of Tibet. *J. Geophys. Res.* **83**, 5361-5375.

Monié P. and Chopin C. (1991) 40Ar/39Ar dating in coesite-bearing and associated units of the Dora Maira massif, western Alps. *Eur. J. Mineral.* **3**, 239-262.

Nagasaki A. and Enami M. (1998) Sr-bearing zoisite and epidote in ultrahigh pressure (UHP) metamorphic rocks from the Su-Lu province, eastern China: An important Sr reservoir under UHP conditions. *Am. Mineral.* **83**, 240-247.

Nägler Th.F. and Kramers J.D. (1998) Nd isotopic evolution of the upper mantle during the Precambrian: model, data and the uncertainty of both. *Precam. Res.* **91**, 233-252.

Okay A.I. (1993) Petrology of diamond and coesite-bearing metamorphic terrain : Dabie-Shan, China. *Eur. J. Mineral* **5**, 659-675.

Okay A.I., Celal Sengör A.M., and Satir M. (1993) Tectonics of an ultrahigh-pressure metamorphic terrane : the Dabié Shan:Tongbai Shan orogen, China. *Tectonics* **12**, 1.320-1.334.

Okay A.I. and Sengör A.M.C. (1992) Evidence for intracontinental thrust-related exhumation of the ultra-high-pressure rocks in China. *Geology* **20**, 411-414.

Palvis T.L. and Bruhn R.L. (1983) Deep seated flow as mechanism for the uplift of broad forearc ridges and its role in the exposure of high P/T metamorphic terranes. *Tectonophysics.* **2**, 473-497.

Peacock S.M. (1990) Fluid processes in subduction zones. *Science* **248**, 329-337.

Peacock S.M. (1993) Metamorphism. dehydration, and the importance of the blueschist-eclogite transition in subducting oceanic crust. *Geol. Soc. Amer. Bul.* **105**, 684-694.

Pearce J.A., Harris N.B.W., and Tindle A.G. (1984) Trace element discrimination diagrams for the tectonic interpretation of granitic rocks. *J. Petrol.* **25**(4), 956-983.

Pettijohn F.J., Potter P.E., and Siever R. (1972) *Sand and Sandstone.*

Platt J.P. (1986) Dynamics of orogenic wedges and the uplift of high-pressure metamorphic rocks. *Geol. Soc. Am. Bull.* **97**, 1 037-1 053.

Platt J.P. (1987) The uplift of high-pressure-low-temperature metamorphic rocks. *Philos. Trans. R. Soc. London* **A321**, 87-103.

Platt J.P. (1993) Exhumation of high-pressure rocks: a review of concepts and proceses. *Terra Nova* **5**, 119-133.

Pollack H.N. and Chapman D.S. (1977) On the regional variation of heat flow, geotherms and the lithospheric thickness. *Tectonophysics.* **38**, 279-296.

R.G.S. Henan. (1989) Regional Geology of Henan Province.

Reinecke T. (1991) Very-high-pressure metamorphism and uplift of coesite-bearing metasediments from the Zermatt-Saas zone, western Alps. *Eur. J. Mineral.* **3**, 7-17.

Rowley D.B., Xue F., Tucker R.D., Peng Z.X., Baker J., and Davis A. (1997) Ages of ultrahigh pressure metamorphism and protolith orthogneisses from the eastern Dabie Shan: U/Pb zircon gechronology. *Earth Planet. Sci. Lett.* **151**, 191-203.

Rubie D.C. (1984) A thermal-tectonic model for high-pressure metamorphism and deformation in the Sesia zone. western Alps. *J. Geol.* **92**, 21-36.

Scaillet S., Féraud G., Ballèvre M., and Amouric M. (1992) Mg/Fe and [(Mg,Fe)Si-Al2] compositional control on argon behaviour in high-pressure white micas: a $^{40}Ar/^{39}Ar$ continuous laser-probe study from the Dora Maira nappe of the internal western Alps, Italy. *Geochim. Cosmochim. Acta* **56**, 2 851-2 872.

Schertl H.P., Schreyer W., and Chopin C. (1991) The pyrope-coesite rocks and their country rocks at Parigi, Dora Maira massif, western Alps: Detailed petrography, mineral chemistry and P-T path. *Contrib. Mineral. Petrol.* **108**, 1-21.

Schreyer W. (1995) Ultradeep metamorphic rocks : the retrospective viewpoint. *J. Geophys.Res.***100**(B5), 8 353-8 366.

Sharp Z.D., Essene E.J., and Hunziker J.C. (1993) Stable isotope geochemistry and phase equilibria of coesite-bearing whiteschists, Dora Maira massif, Western Alps. *Contrib. Mineral. Petrol.* **114**, 1-12.

Shaw D.M. (1972) The origin of the Apsley gneiss, Ontario. *Can. J. Earth Sci.*. **9**, 18-35.

Smith D.C. (1984) Coesite in clinopyroxene in the Caledonides and its implications for geodynamics. *Nature* **310**, 641-644.

Smith D.C. (1988) A review of the peculiar mineralogy of the 'Norwegian coesite-eclogite province', with crystal-chemical, petrological, geochemical and geodynamical notes and an extensive bibliography. In *Eclogites and eclogite-facies Rocks: developments in petrology.*, Vol. 12 (ed. S. D.C.), pp. 1-206.

Stacey J.S. and Kramers J.D. (1975) Approximation of terrestrial lead isotope evolution by a two-stage model. *Earth Planet. Sci. Lett.* **26**, 207-221.

Sun S.S. and McDonough W.F. (1989) Chemical and isotopic systematics of oceanic basalts implications for mantle composition and processes. In *%agmatism in the Ocean Basains*, Vol. 42 (ed. S. A. D. N. M.J.), pp. 313-345. Geolocical Society Special Publication.

Thirlwall M.F. (1991) High-precision multicollector isotopic analysis of low levels of Nd as oxide. *Chem. Geol* **94**, 13-22.

Thöni M. and Jagoutz E. (1992) Some new aspects of dating eclogites in orogenic belts : Sm-Nd, Rb-Sr, and Pb-Pb isotopic results from the Austroalpine Saualpe and Koralpe type-locality (Carinthia/Styria, southeastern Austria). *Geochim. Cosmochim. Acta* **56**, 347-368.

Tilton G.R., Schreyer W., and Schertl H.P. (1989) Pb-Sr-Nd behavior of deeply subducted crustal crust rocks from the Dora Maira Massif, western Alps, Italy *Geochim. Cosmochim. Acta* **53**, 1.391-1.400.

Tilton G.R., Schreyer W., and Schertl H.P. (1991) Pb-Sr-Nd isotopic behavior of deeply subducted crustal rocks from the Dora Maira Massif, western Alps, Italy-II : what is the age of the ultrahigh-pressure metamorphism? *Contrib. Mineral. Petrol.* **108**, 22-33.

Tonarini S., Villa I.M., Oberli F., Meier M., Spencer D.A., Pognante U., and Ramsay J.G. (1993) Eocene age of eclogite metamorphism in Pakistan Himalaya : implications for India-Eurasia collision. *Terra Nova* **5**, 13-20.

Van den Beukel J. (1992) Some thermomechanical aspects of the subduction of continental lithosphere. *Tectonophysics.* **11**(2), 316-329.

van der Moolen L. and van Roermund H.L.M. (1986) The pressure path of solid inclusions in minerals: The retention of coesite inclusions during uplift. *Lithos* **19**, 317-324.

Vidal P. and Hunzicker J.C. (1985) Systematics and problems in isotope work on eclogites. *Chem. Geol.* **52**, 129-141.

Villa I.M., Grobéty B., Kelley S.P., Trigila R., and Wieler R. (1996) Assessing Ar transport paths and mechanisms in the McClure Mountains hornblende. *Contrib. Mineral. Petrol.* **126**, 67-80.

Villa I.M., Ruggieri G., and Puxeddu M. (1997) Petrological and geochronological discrimination of two white-mica generations in a granite cored from Larderello-Travale geothermal field (Italy). *Eur. J. Mineral.* **9**, 563-568.

Von Blanckenburg F. and Davies J.H. (1995) Slab breakoff : a model for syncollisional magmatism and tectonics in the Alps. *Tectonics* **14**, 120-131.

Wang X. and Liou J.G. (1991) Regional ultrahigh-pressure coesite-bearing eclogitic terrane in central China : evidence from country rocks, gneiss, marble, and metapelites. *Geology* **19**, 933-936.

Wang X. and Liou J.G. (1993) Coesite-bearing eclogites from the Dabie Mountains in central China. *Geology* **17**, 1 085-1 088.

Wang X., Liou J.G., and Mao H.K. (1989) Coesite-bearing eclogite from the Dabie Mountains in central China. *Geology* **17**, 1 085-1 088.

Wang X., Liou J.G., and Maruyama S. (1992) Coesite-bearing eclogite from the Dabie montains, Central China : petrogenesis, P-T paths and implications for regional tectonics. *J. Geol.***100**, 231-250.

Wang X., Zhang R.Y., and Liou J.G. (1995) Ultra-High Pressure metamorphic terrane in eastern central China. In *Ultra-High Pressure Metamorphism* (ed. C. U. Press), pp. 356-390.

Wasserburg G.J., Jacobsen S.B., De Paolo D.J., McCulloch M.T., and Wen J. (1981) Precise determination of Sm/Nd ratios, Sm and Nd isotopic abundances in standard solutions. *Geochim. Cosmochim. Acta* **45**, 2 311-2 323.

Watson E.B. and Harrison T.M. (1983) Zircon saturation revisited: temperature and composition effects in a variety of crustal magma types. *Earth Planet. Sci. Lett.* **64**, 294-304.

Whitehouse M.J., Claesson S., Sunde T., and Vestin J. (1997) Ion microprobe U-Pb zircon geochronology and correlation of Archean gneisses from the Lewisian Complex of Guinard Bay, northwestern Scotland. *Geochim. Cosmochim. Acta* **61**(20), 4 429-4 438.

Xu J., Zhu G., Tong W., Cui K., and Liu Q. (1987) Formation and evolution of the Tancheng-Lujiang wrench fault system : a major shear system to the northwest of the Pacific Ocean. *Tectonophysics* **134**, 273-310.

Xu S., Liu Y., Jiang L., Su W., and Ji S. (1994) *Tectonic regime and evolution of Dabie Mountains.*

Xu S., Okay A.I., Shouyuan J., Sengör M.C., Wen S., Yican L., and Laili J. (1992) Diamond from the Dabie Shan metamorphic rocks and its implication for tectonic setting. *Science* **256**, 80-83.

Xue F., Rowley D.B., Tucker R.D., and Peng Z.H. (1997) U-Pb zircon ages of granitoid rocks in the North Dabie Complex, Eastern Dabie Shan, China. *J. Geol* **105**, 744-753.

Yang J. and Smith D.C. (1989) Evidence for a former sanidine-coesite-eclogite- at Lanshantou, east China, and the recogntion of the chinese 'Su-Lu coesite eclogite province'. *Third International Eclogite Conference.*

Yang Z., Courtillot V. B. J., Ma X., Xing L. X. S., and Zhang J. (1992) Jurassic paleomagnetic constraints on the collision of the North and South China Blocks. *Geophys. Res. Lett.* **19**, 577-580.

Yang Z., Ma X., Besse J., Courtillot V., Xing L., Zhang J., and Xu S. (1991) Paleomagnetic results from the Triassic sections in the Ordos basin, North China. *Earth Planet. Sci. Lett.* **104**, 258-277.

Yin A. and Nie S. (1993) An identation model for the north and south China collision and the development of the Tan-Lu and Homan fault systems, Eastern China. *Tectonics* **12**, 801-813.

You Z., Han Y., Suo S., Chen N., and Zhong Z. (1993) Metamorphic history and tectonic evolution of the Qinling-Dabie complex, eastern Qinling Mountains, China. *J. Metam. Geol.***11**, 549-560.

You Z., Han Y., Zhang Z., Day H.W., and Zhai M. (1995) Paleozoic dates from the Dabie Mountains, central China: Implications for ultra-high pressure metamorphism in the Qinling orogenic belt. *AGU Fall Meetint*, F712.

Zhang G., Xiang L., and Meng Q. (1995) The Qinling orogen and intracontinental orogen mechanisms. In *Episode*, Vol. 18, pp. 36-39.

Zhang R. (1992) Petrogenesis of high pressure metamorphic rocks in the Su-Lu and Dianxi regions, China.

Zhang R.Y. and Liou J.G. (1994) Coesite-bearing eclogite in Henan Province, central China : detailed petrography, glaucophane stability and P-T path. *Eur. J. Mineral.* **6**, 217-233.

Zhang R.Y. and Liou J.G. (1996) Coesite inclusions on dolomite from eclogite in the southern Dabie Mountains, China : the significance of carbonate minerals in UHPM rocks. *Am. Mineral.* **81**, 181-186.

Zhang R.Y. and Liou J.G. (1997) Partial transformation of gabbro to coesite-bearing eclogite from Yankou, the Su-Lu terrane, eastern China. . *J. Metam. Geol* **15**, 183-202.

Zhang R.Y., Liou J.G., and Cong B. (1994) Petrogenesis of garnet-bearing ultramafic rocks and associated eclogites in the Su-Lu ultrahigh-P metamorphic terrane, eastern China. . *J. Metam. Geol* **12**, 168-186.

Zhang R.Y., Liou J.G., and Cong B.L. (1995) Talc, Magnesite and Ti-clinohumite-bearing UHP meta-mafic and ultramafic complex in the Dabie mountains, China. *J. Petrol.*, submitted.

Zhang R.Y., Liou J.G., and Cong B.L. (1995) Talc-, magnetite- and Ti-clinohumite-bearing UltraHigh-Pressure meta-mafic and ultramafic complex in the Dabie Mountains, China. *J. Petrol.*, **36**, 1 011-1 037.

Zhang R.Y., Liou J.G., and Ernst W.G. (1995) Ultrahigh-pressure metamorphism and decompressional P-T paths of eclogites and country rocks from Weihai, estern China. *The Island Arc*(4), 293-309.

Zhang R.Y., Liou J.G., and Tsai C.H. (1996) Petrogenesis of high-pressure metamorphic terrane : a new tectonic interpretation for the north Dabieshan, central China. *J. Metamorphic Geol.* **14**, 319-333.

Zhang R.Y., Liou J.G., Wang X., Wang Q., and Liu X. (1993) Discovery of coesite eclogites in Henan province, central China and its tectonic implication. *Acta Petrologica Sinica* **9**, 181-184.

Zhang Y.Q., Vergely P., and Mercier J. (1995) Active faulting an and along the Qinling Range (China) inferred from SPOT imagery analysis and extrusion tectonics of South China. *Tectonophysics* **243**, 69-95.

Zhang Z., You Z., Han Y., and Sang L. (1996) Petrology, metamorphic process and genesis of the Dabie-SuLu eclogite belt, Eastern-Central China. *Acta Geologica Sinica* **9**, 134-156.

Zhang Zh. M. and Liou J.G. (1987) The high P/T metamorphic rocks in China. In *Terrane Accretion and Orogenic Belts*, Vol. 19 (ed. Leitch E.C. and Scheibner E.), pp. 235-247. American Geophysical Union.

Zhao X. and Coe R.S. (1987) Paleomagnetic constraints on the collision and rotation of North and South China. *Nature* **327**, 141-144.

Zheng W.Z., Liu G.L., and Wang X.W. (1991) New information on the Archean eon from the Konloing Group in northern Huangling anticline, Hubei. Bull. Yichang Inst. Geol. Min. Res., CAGS.

Zhou B. and Hensen B.J. (1995) Inherited Sm/Nd isotope components preserved in monazite inclusions within garnets in leucogneiss from East Antactica and implications for closure temperature studies. *Chem.Geol.***121**, 317-326.

de Sigoyer J., Chavagnac V., Villa I.M., Guillot S., and Mascle G. (Submitted) Geochronologic evidences for Upper Paleocene subduction of the Idian continental margin below Asia. *Geology*.

Griselin M. (in prep.) Geochemical study of mantle peridotite: Xigaze and Luobusa ophiolitic massifs, Yarlung-Zangbo suture zone, Tibet. Implication for mantle melting. Ph D., Vrije Universiteit Amsterdam.

Niederer F.R., Papanastassiou D.A., and Wasserburg G.J. (1981) The isotopic composition of Titanum in the Allende & Leoville meteorites. *Geochim. Cosmochim. Acta* **45**, 1017-1031.

Nier A.O. (1950) A redetermination of the relative abundance of the isotopes of carbon, nitrogen, oxygen, argon, and potassium. *Phys. Res.* **77**, 789-793.

Wasserburg G.J., Jacobsen S.B., De Paolo D.J., McCulloch M.T., and Wen J. (1981) Precise determination of Sm/Nd ratios, Sm and Nd isotopic abundances in standard solutions. *Geochim. Cosmochim. Acta* **45**, 2 311-2 323.

# *Appendix A Photographs*

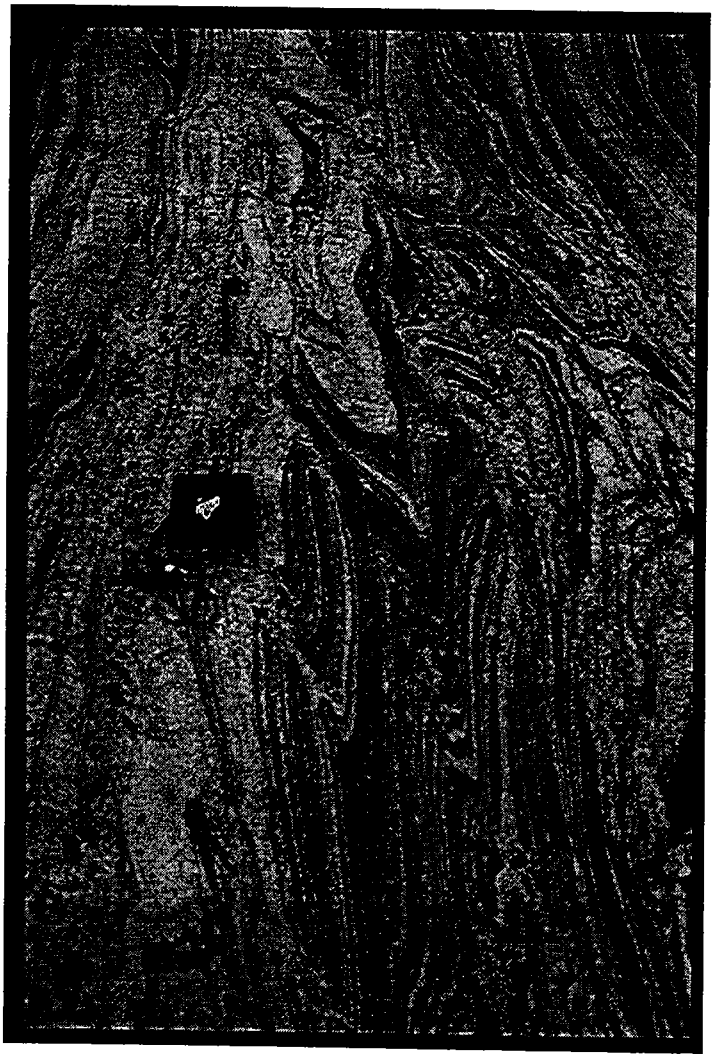

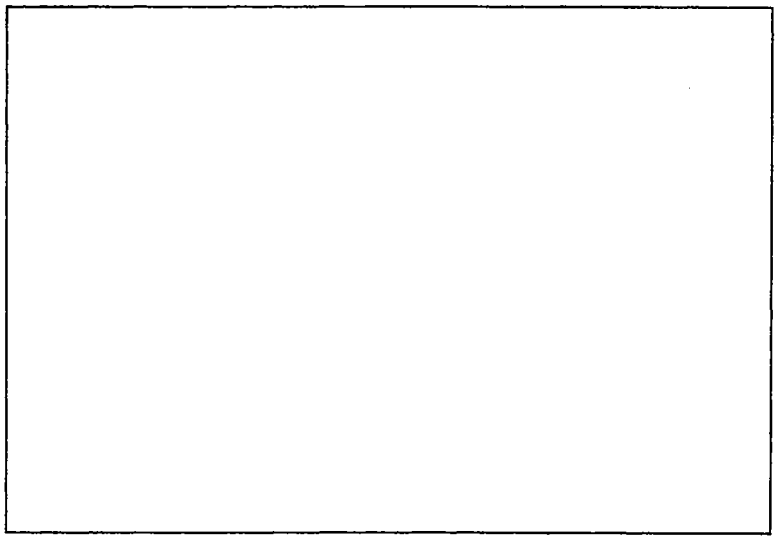

Photo A-1:Sand River Gneisses at the Causeway locality. Typical migmatitic facies showing the folded interlayering of leucocratic veins and mafic-rich layers. This outcrop is well known for the pectacular sheet folds. Migmatite has an igneous origin and were formed during the first high-grade metamorphic event in the Limpopo Central Zone (~3.2-3.0 Ga).

Photo A-2: Sand River Gneiss at the Causeway locality. Folded stromatic migmatite represents the second facies that we can observe in the Sand River Gneisses. Contact between leucocratic and mafic-rich layers are sharp. Melts are parallel to the axial planes of folds. Partial melt associated with folds may concentrate in the hinge zone and may occur in greater abundance in antiformal rather than synformal hinges. No garnet as a product of migmatization was observed.

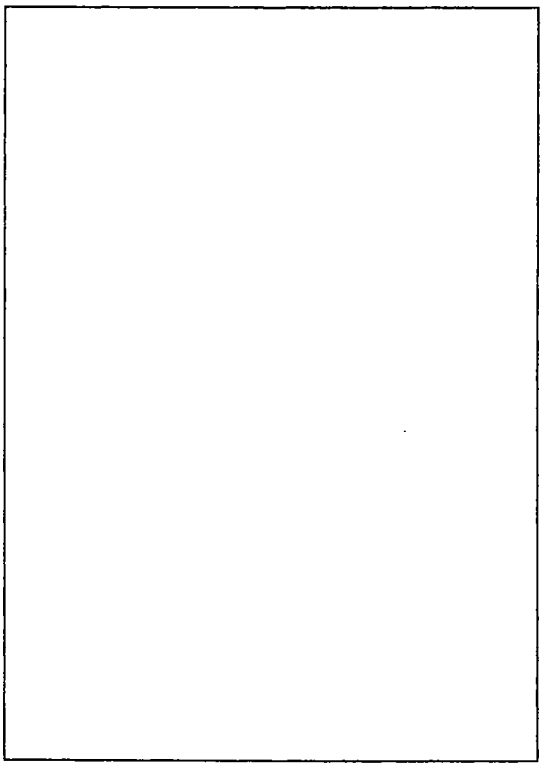

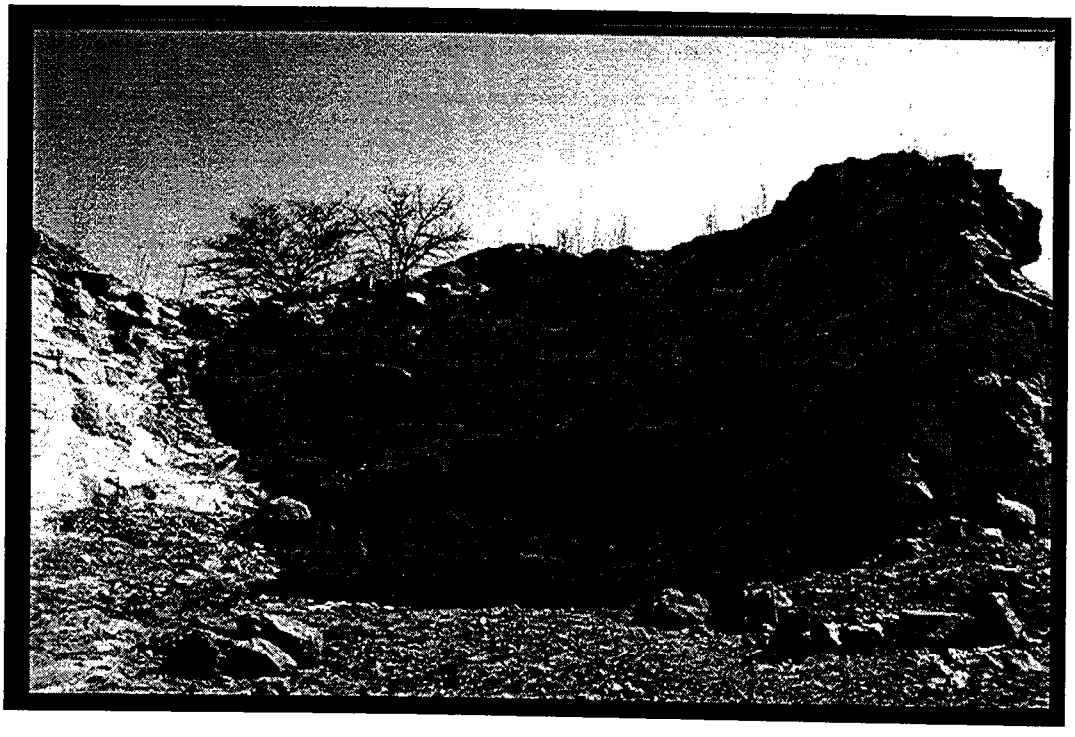

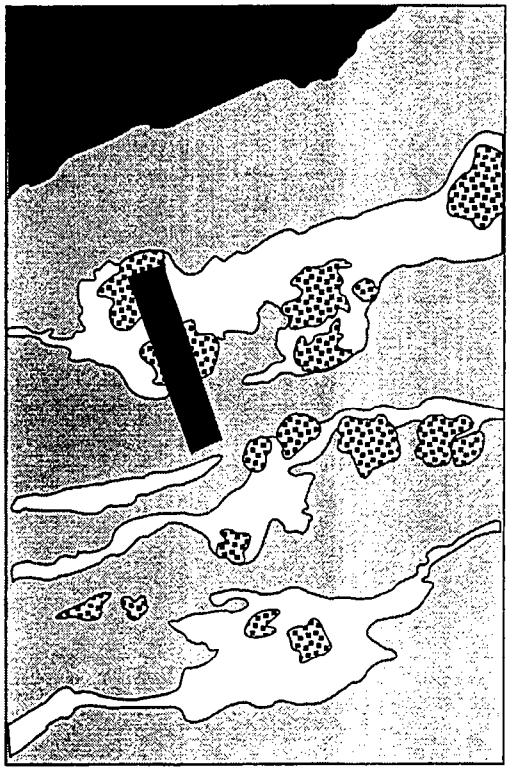

Photo A-3: Example of spatial relationship between garnet-bearing leucocratic layer (in white) and paleosome (in gray). Garnet elongated porphyroblasts are formed via fluid-absent melting reaction which is one process of partial melt production during migmatization. Leucosome layers are concordant to the plastically deformed metamorphic rock. Scale bar = 5 cm.

Photo A-4:Lose Quarry outcrop in the Mahalapye Complex at the southwestern margin of the Limpopo Central Zone. Migmatite presents stromatic to nebulitic texture. The granitic melt was formed via biotite breakdown on a metagreywacke lithology. Paragneisses are recognized as fertile lihtology for partial melt production during migmatization.

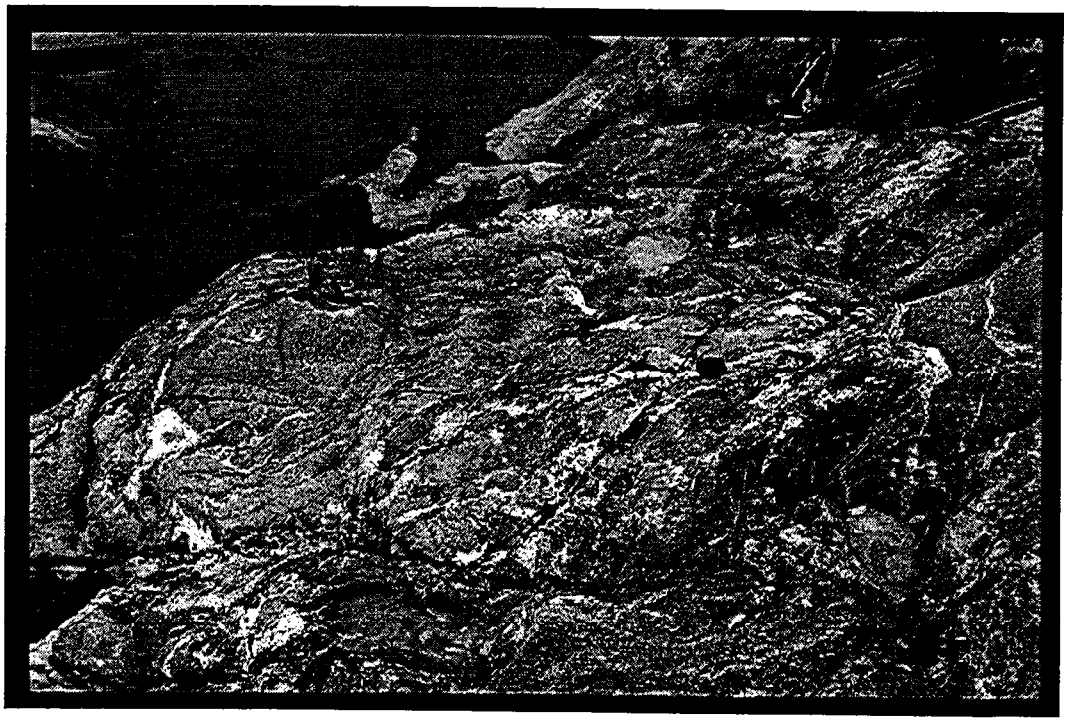

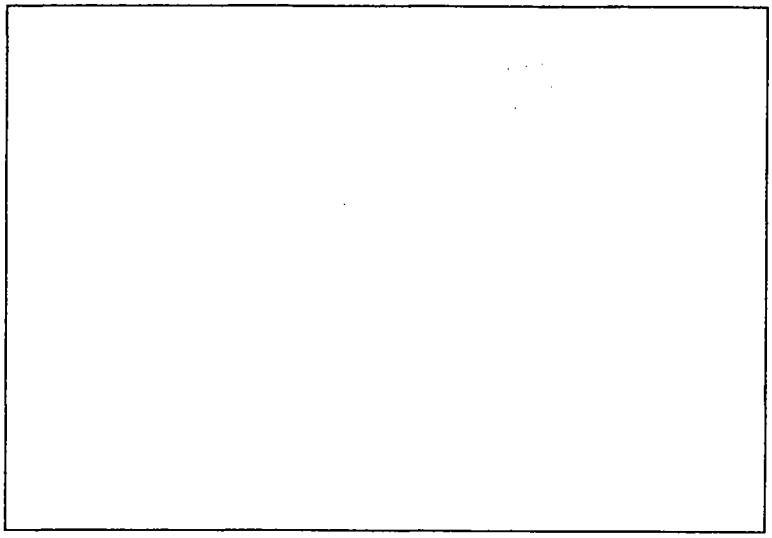

Photo A-5: Outcrop of eclogite in a gneiss host rock in the Su-Lu UHPM province. Note the retrograde reactional zone around eclogite boudins enclosed in the quartzo-feldspathic gneiss.

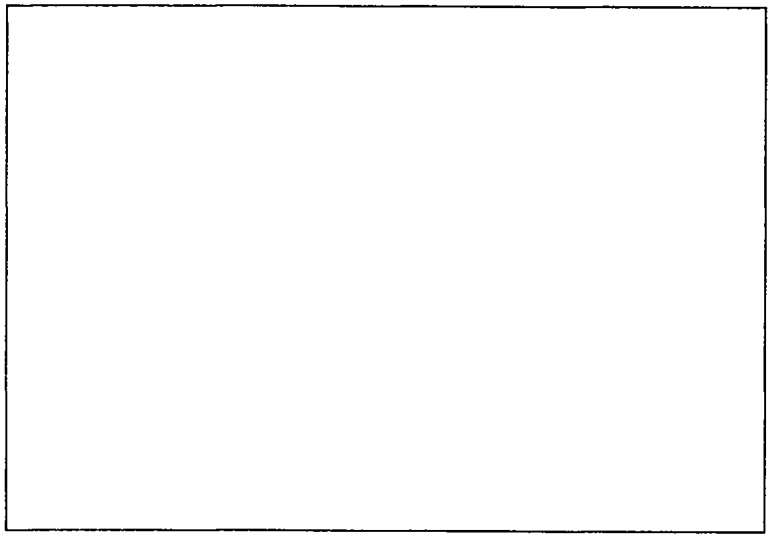

Photo A-6: Outcrop, in a river bed, of eclogite enclosed in a paragneiss host rock at the Shina locality. Note the retrogation of eclogite into amphibolite at the outer rims of eclogitic boudins.

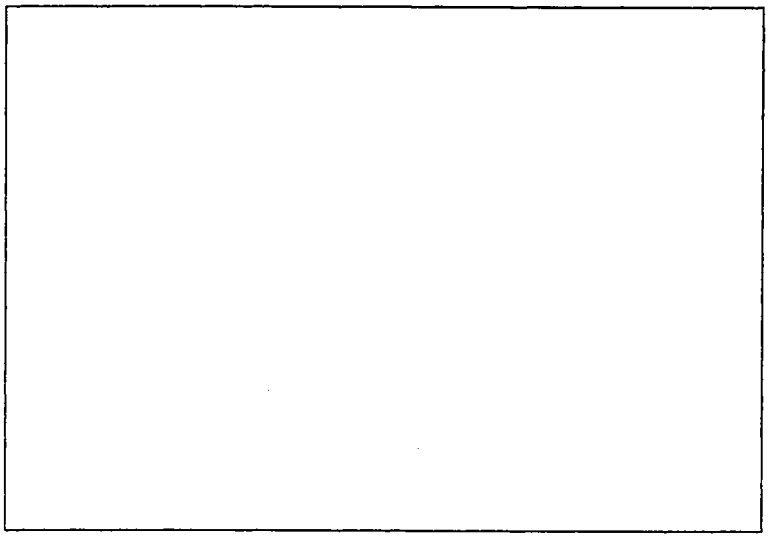

Photo A-7: Beautiful outcrop of disrupted eclogite blocks in a marble host rock at the Shuanghe locality. In the UHPM slab of Shuanghe, eclogites occurr also as lenses enclosed in biotite-garnet gneisses. Scale bar = 50 cm.

# APPENDIX B

## Abstracts

*The Third International Eclogite Field Symposium. Extended Abstact. Chinese Science Bulletin, 1995, Vol. 40: 126-127. Oral.*

# Sm-Nd Isotopic Ages and Geochemical Characteristics of the Bixiling Complex, Dabie Mountains, China

Valérie Chavagnac and Bor-ming Jahn
(Géosciences Rennes, Université de Rennes 1, 35042 Rennes, France)

## Introduction

Sm-Nd isotopic disequilibrium between coexisting garnet and clinopyroxene in eclogites has been documented in many cases (Thöni and Jagoutz, 1992; Jagoutz, 1994, 1995). Thsi casts doubt in the interpretation of garnet-cpx or garnet-WR isochron ages as the true time of eclogite facies metamorphism. On the contrary, we would argue that in many other cases, Sm-Nd isotopic equilibrium between these minerals has been reached and their isochrons have provided significant age information. We have chosen the Bixiling Complex to demonstrate this point.

The Bixling mafic-ultramafic Complex occurs as a relatively large (~1.5 km2) tectonic block within biotite gneisses in the eastern part of the Dabie UHPM terrane. The occurrence of this complex is in quite contrast to most other eclogite bodies, which are commonly present as small disrupted blocks, layers or nodules in eclogite gneisses. The Complex consists mainly of banded eclogites with many layers of ultramafic rocks (garnet peridotite, garnet pyroxenite and wherlite; Zhang et al., 1995). The protoliths most probably represents a layered intrusion which has undergone UHP metamorphism as a consequence of deep subduction of continental mass. Except for common eclogitic phases ( garnet, omphacite, kyanite, phengite, zoisite, and rutile), the Bixiling Complex also contains diagnostic phases of UHPM origin, such as coesite and talc in eclogite, and magnesite and ti-clinohumite in metaultramafic rock (Zhang et al., 1995). Coesite relicts and their pseudomorphs occur as inclusions in garnet, omphacite, kyanite and zoisite in certain eclogite bands.

According to Zhang et al. (1995), the peak eclogite metamorphism took place at 610-700°C and P>27 kbar, whereas the retrograde amphibolite facies is characterized by symplectites of plagioclase and hornblende after omphacite, and replacement of tremolite after talc formed at T<600°C, and P = 6-15 kbar. The metaultramafic assemblages (olivine, enstatite, diopside, garnet; Ti-clinohumite, diopside, enstatite, garnet, magnesite and ± olivine) indicate their formation at 700-800°C and P = 47-67 kbar. Thus the ultramafic rocks appear to have recorded higher P and possibly higher T conditions than the associated mafic rocks. The discrepancy of P-T estimates may suggest 1) some uncertainties in the different geothermobarometers used, 2) neglect of ferric Fe in P-T calculations for the metaultramafic rocks, and 3) possible compositional changes in mafic (eclogite) and ultramafic rocks during decompression (Zhang et al., 1995).

The primary intrusive and metamorphic ages of the Bixiling Complex have not been determined before, although a range of 200-240 Ma has been considered as the best estimate for the continental collision and the UHP metamorphism in the Dabie terrane (Li et al., 1993; Ames et al., 1993, 1995). U-Pb zircon ages of 2210, 907, 492, 418 Ma have been obtained by Liu R.X. et al. (1994). These ages are inconclusive and their significance is uncertain.

The purpose of our study are : 1) to date the UHP metamorphic event using the Sm-Nd mineral isochron technique. Unlike the other isotopic eclogite blocks in the Dabie terrane, the different types of trhe layered complex are assumed comagmatic and have shared the same metamorphic event. Therefore, they should yield the same garnet-omphacite isochron ages if

Nd isotopic equilibrium in all rocks has been reached, 2) to use Sr-Nd isotopic data to examine the nature of the mantle source and the possible crustal contamination during differentiation in the magma chamber, and 3) to use geochemical data to trace the genetic relationship between different rock types and to purpose a petrogenetic model for the layered complex.

## Results and discussion

*Whole rock data:* When compared with all the eclogites from the Dabie and Su-Lu terranes, the Bixiling eclogite and ultramafic rocks (garnet peridotite and garnet pyroxenite) have arrow ranges of εNd(0) values (-0.7 to -2.7) and $^{147}Sm/^{144}Nd$ ratios (0.16-0.19). This is in strong contrast with the majority of eclogites from Su-Lu and Dabie which have low εNd(0) values (-6 to -20), the lowest among the world's known eclogite occurrences (see Jahn et al., 1994, this volume). In an εNd vs $^{87}Sr/^{86}Sr$ diagram, the Bixiling rocks fall just beneath the "mantle array" in the third quadrangle. This suggests that the original magma was probably contaminated by a small amount of depleted granulites in the differentiation and evolution of this layered complex. For comparison, the Nd-Sr isotopic data of garnet pyroxenites from the Rizhao area (Su-Lu terrane) fall in the "mantle array". Such a feature is consistent with that these ultramafic bodies represent mantle xenoliths of tectonic origin. Their Sr and Nd isotopic compositions could be representative of the lithospheric mantle characteristics in the Su-Lu and Dabie region.

*Mineral data:* Garnet, omphacite, and other accessory minerals (phengite, kyanite, rutile, etc..) were separated from 6 eclogites and 1 garnet peridotite for Sm-Nd and Rb-Sr isotopic analyses. All garnet-omphacite or garnet-omphacite-WR isochrons give very coherent and tight age range from 210-218 Ma ($2\sigma$ from 3 to 9 Ma) with only one exception of 231 ± 4 Ma which will be double-checked by duplicated analyses. All isochrons hqve near chondritic εNd(T) values of -0.1 to -1.8, but with errors of about ±0.5. In addition, all garnet data points are well aligned to form similar "isochron" age of 225 ± 7 Ma ( εNd(T) = -2.5 ± 1.1). These results lead to several important conclusions: 1) The coherent mineral Sm-Ns ages obtained for different rock types from the same pluton indicate the attainment of isotopic equilibrium during the UHP metamorphism (T = 700-800°C, P > 30 kbar, from the combined P-T information of eclogite and ultramafic rocks cited above). 2) The Sm-Nd mineral ages are identical within error limits with the zircon U-Pb ages of 212 ± 11 Ma from nearby eclogites (Ames et al., 1993, 1995). Thus, the age of 210-220 Ma is probably the best estimate for the time of the UHP metamorphism and the continental collision. 3) The comparable zircon U-Pb and garnet Sm-Nd ages suggest that the blocking temperature of garnet is more likely of 700°C, not 600°C as claimed by Mezger et al. (1992). 4) The fact that the garnet data alone also give a similar (or slightly older) age and initial εNd(T) value as the other garnet-omphacite pairs strongly suggest that the Bixiling Complex was intruded not long ago before the UHP metamorphism. If it was intruded in the Proterozoic, it would be extremely fortituous to have the all garnet age similar to the other mineral isochron ages. The available whole rock Sm-Nd data are too scattered to define an isochron, but their disposition is consistent with a young Paleozoic intrusive age.

## Conclusions

1. Unlike most of the eclogites from the Su-Lu and Dabie terranes, the eclogites and ultramafic rocks of the Bixiling Complex have distinct Sr and Nd isotopic compositions. A mantle origin and a small amount of lower crustal contamination is suggested in the petrogenesis and evolution of the Layered Complex.
2. The garnet-omphacite (or garnet-omphacite-whole rock) data of five eclogites and one garnet peridotite yield very coherent ages of about 210-218 Ma, which is identical within

error limits with the zircon U-Pb ages for the neighboring eclogites (Ames et al., 1993, 1995). The age range of 210-220 Ma represents the best estimate for the UHP metamorphism and the collision between the Yangtze and Sino-Korean cratons.

3. The garnet only isochron of comparable age and εNd(T) value suggests that the Bixiling Complex was intruded shortly before the UHP metamorphism. It is definitely not of Proterozoic age as the majority of other eclogites from the Su-Lu and Dabie terranes.
4. The possibility of the Bixiling as part of a layered intrusive sequence within the subducted Tethys oceanic lithosphere cannot be excluded. However, it is difficult to reconcile with isotopic data which require its intrusion to the lower continental crust. Besides, the breakoff of the Tethys oceanic slab during the continental collision was hypothesized to explain the general lack of N-MORB signature in the eclogites analyzed so far (Jahn et al., this volume).

**References**

Ames et al., 1993, Geology, 21:3 39-342.
Ames et al., 1995, Tectonics (submitted).
Jahn, 1994, Stanford Workshop on UHP metamorphism/tectonics, A71-A74.
Jahn et al, this volume.
Li et al., 1993, Chem. Geol., 109: 89-111.
Mezger et al., 1992, EPSL, 113: 397-409.
Thöni and Jagoutz, 1992, GCA, 56: 347-368.
Zhang et al., 1995, J. Petrology (submitted).

*Bochumer Geologische und Geotechnische Arbeiten. Extended Abstract. 1995. Oral.*

# Isotopic Ages (Sm-Nd and Rb-Sr) and Geochemical characteristics of the Bixiling Complex from the Dabie Mountains, China

Valérie Chavagnac and Bor-ming Jahn
(Géosciences Rennes, Université de Rennes 1, 35042 Rennes, France)

## Introduction

Sm-Nd isotopic disequilibrium between coexisting garnet and clinopyroxene in eclogites has been documented in many cases (Thöni and Jagoutz, 1992; Jagoutz, 1994, 1995). Thsi casts doubt in the interpretation of garnet-cpx or garnet-WR isochron ages as the true time of eclogite facies metamorphism. On the contrary, we would argue that in many other cases, Sm-Nd isotopic equilibrium between these minerals has been reached and their isochrons have provided significant age information. We have chosen the Bixiling Complex to demonstrate this point.

The Bixling mafic-ultramafic Complex occurs as a relatively large (~1.5 km2) tectonic block within biotite gneisses in the eastern part of the Dabie UHPM terrane. The occurrence of this complex is in quite contrast to most other eclogite bodies, which are commonly present as small disrupted blocks, layers or nodules in eclogite gneisses. The Complex consists mainly of banded eclogites with many layers of ultramafic rocks (garnet peridotite, garnet pyroxenite and wherlite; Zhang et al., 1995). The protoliths most probably represents a layered intrusion which has undergone UHP metamorphism as a consequence of deep subduction of continental mass. Except for common eclogitic phases ( garnet, omphacite, kyanite, phengite, zoisite, and rutile), the Bixiling Complex also contains diagnostic phases of UHPM origin, such as coesite and talc in eclogite, and magnesite and ti-clinohumite in metaultramafic rock (Zhang et al., 1995). Coesite relicts and their pseudomorphs occur as inclusions in garnet, omphacite, kyanite and zoisite in certain eclogite bands.

According to Zhang et al. (1995), the peak eclogite metamorphism took place at 610-700°C and P>27 kbar, whereas the retrograde amphibolite facies is characterized by symplectites of plagioclase and hornblende after omphacite, and replacement of tremolite after talc formed at T<600°C, and P = 6-15 kbar. The metaultramafic assemblages (olivine, enstatite, diopside, garnet; Ti-clinohumite, diopside, enstatite, garnet, magnesite and ± olivine) indicate their formation at 700-800°C and P = 47-67 kbar. Thus the ultramafic rocks appear to have recorded higher P and possibly higher T conditions than the associated mafic rocks. The discrepancy of P-T estimates may suggest 1) some uncertainties in the different geothermobarometers used, 2) neglect of ferric Fe in P-T calculations for the metaultramafic rocks, and 3) possible compositional changes in mafic (eclogite) and ultramafic rocks during decompression (Zhang et al., 1995).

The primary intrusive and metamorphic ages of the Bixiling Complex have not been determined before, although a range of 200-240 Ma has been considered as the best estimate for the continental collision and the UHP metamorphism in the Dabie terrane (Li et al., 1993; Ames et al., 1993, 1995). U-Pb zircon ages of 2210, 907, 492, 418 Ma have been obtained by Liu R.X. et al. (1994). These ages are inconclusive and their significance is uncertain.

The purpose of our study are : 1) to date the UHP metamorphic event using the Sm-Nd mineral isochron technique. Unlike the other isotopic eclogite blocks in the Dabie terrane, the different types of trhe layered complex are assumed comagmatic and have shared the same metamorphic event. Therefore, they should yield the same garnet-omphacite isochron ages if Nd isotopic equilibrium in all rocks has been reached, 2) to use Sr-Nd isotopic data to

examine the nature of the mantle source and the possible crustal contamination during differentiation in the magma chamber, and 3) to use geochemical data to trace the genetic relationship between different rock types and to purpose a petrogenetic model for the layered complex.

## Results and discussion

*Whole rock data:* When compared with all the eclogites from the Dabie and Su-Lu terranes, the Bixiling eclogite and ultramafic rocks (garnet peridotite and garnet pyroxenite) have arrow ranges of εNd(0) values (-0.7 to -2.7) and $^{147}Sm/^{144}Nd$ ratios (0.16-0.19). This is in strong contrast with the majority of eclogites from Su-Lu and Dabie which have low εNd(0) values (-6 to -20), the lowest among the world's known eclogite occurrences (see Jahn et al., 1994, this volume). In an εNd vs $^{87}Sr/^{86}Sr$ diagram, the Bixiling rocks fall just beneath the "mantle array" in the third quadrangle. This suggests that the original magma was probably contaminated by a small amount of depleted granulites in the differentiation and evolution of this layered complex. For comparison, the Nd-Sr isotopic data of garnet pyroxenites from the Rizhao area (Su-Lu terrane) fall in the "mantle array". Such a feature is consistent with that these ultramafic bodies represent mantle xenoliths of tectonic origin. Their Sr and Nd isotopic compositions could be representative of the lithospheric mantle characteristics in the Su-Lu and Dabie region.

*Mineral data:* Garnet, omphacite, and other accessory minerals (phengite, kyanite, rutile, etc..) were separated from 6 eclogites and 1 garnet peridotite for Sm-Nd and Rb-Sr isotopic analyses. All garnet-omphacite or garnet-omphacite-WR isochrons give very coherent and tight age range from 210-218 Ma ($2\sigma$ from 3 to 9 Ma) with only one exception of 231 ± 4 Ma which will be double-checked by duplicated analyses. All isochrons hqve near chondritic εNd(T) values of -0.1 to -1.8, but with errors of about ±0.5. In addition, all garnet data points are well aligned to form similar "isochron" age of 225 ± 7 Ma ( εNd(T) = -2.5 ± 1.1). These results lead to several important conclusions: 1) The coherent mineral Sm-Ns ages obtained for different rock types from the same pluton indicate the attainment of isotopic equilibrium during the UHP metamorphism (T = 700-800°C, P > 30 kbar, from the combined P-T information of eclogite and ultramafic rocks cited above). 2) The Sm-Nd mineral ages are identical within error limits with the zircon U-Pb ages of 212 ± 11 Ma from nearby eclogites (Ames et al., 1993, 1995). Thus, the age of 210-220 Ma is probably the best estimate for the time of the UHP metamorphism and the continental collision. 3) The comparable zircon U-Pb and garnet Sm-Nd ages suggest that the blocking temperature of garnet is more likely of 700°C, not 600°C as claimed by Mezger et al. (1992). 4) The fact that the garnet data alone also give a similar (or slightly older) age and initial εNd(T) value as the other garnet-omphacite pairs strongly suggest that the Bixiling Complex was intruded not long ago before the UHP metamorphism. If it was intruded in the Proterozoic, it would be extremely fortituous to have the all garnet age similar to the other mineral isochron ages. The available whole rock Sm-Nd data are too scattered to define an isochron, but their disposition is consistent with a young Paleozoic intrusive age.

## Conclusions

1. Unlike most of the eclogites from the Su-Lu and Dabie terranes, the eclogites and ultramafic rocks of the Bixiling Complex have distinct Sr and Nd isotopic compositions. A mantle origin and a small amount of lower crustal contamination is suggested in the petrogenesis and evolution of the Layered Complex.
2. The garnet-omphacite (or garnet-omphacite-whole rock) data of five eclogites and one garnet peridotite yield very coherent ages of about 210-218 Ma, which is identical within error limits with the zircon U-Pb ages for the neighboring eclogites (Ames et al., 1993, 1995).

The age range of 210-220 Ma represents the best estimate for the UHP metamorphism and the collision between the Yangtze and Sino-Korean cratons.

3. The garnet only isochron of comparable age and εNd(T) value suggests that the Bixiling Complex was intruded shortly before the UHP metamorphism. It is definitely not of Proterozoic age as the majority of other eclogites from the Su-Lu and Dabie terranes.
4. The possibility of the Bixiling as part of a layered intrusive sequence within the subducted Tethys oceanic lithosphere cannot be excluded. However, it is difficult to reconcile with isotopic data which require its intrusion to the lower continental crust. Besides, the breakoff of the Tethys oceanic slab during the continental collision was hypothesized to explain the general lack of N-MORB signature in the eclogites analyzed so far (Jahn et al., this volume).

**References**

Ames et al., 1993, Geology, 21:3 39-342.
Ames et al., 1995, Tectonics (submitted).
Cao et al., 1995, 3rd International Eclogite Field Symposium. Poster.
Jahn et al, 1995, Chinese Science Bulletin, Vol. 40: 116-119.
Jahn et al., 1995, this volume.
Li et al., 1993, Chem. Geol., 109: 89-111.
Liu et al., 1993, Acta Petrologica Sinica, 11: 243-256.
Mezger et al., 1992, EPSL, 113: 397-409.
Thöni and Jagoutz, 1992, GCA, 56: 347-368.
Zhang et al., 1995, J. Petrology (submitted).

*V.M. Goldschmidt Conference, 1996, Heidelberg, Germany. Vol. 1, 103. Oral.*

# Coesite-bearing eclogites from the Bixiling Complex, Dabie Mountains, China: Sm-Nd ages, geochemical characteristics and tectonic implications.

Valérie Chavagnac[1,2] and Bor-ming Jahn[1]
1: Géosciences Rennes, Université de Rennes 1, 35042 Rennes, France
2: Universität Bern, Gruppe isotopengeologie, 3012 Bern, Switzerland

## Introduction

The Bixiling mafic-ultramafic complex occurs as a relatively large (≈ 1.5 $km^2$) tectonic block within biotite gneisses in eastern part of the Dabie ultrahigh-pressure metamorphic (UHPM) terrane. The complex consists mainly of banded eclogites with many lenses of ultramafic rocks. The protoliths most probably represent a layered intrusion undergone UHP metamorphism as a result of deep subduction of continental mass. Geochemical and isotopic (Rb-Sr and Sm-Nd) analyses on whole-rock and mineral constituents yield many interesting results concerning the age of metamorphism, the age and nature of protoliths, and the high rates of initial cooling and uplift of the Complex, and probably much of the Dabie UHPM terrane.

## Results and Discussion

The Bixiling eclogites and ultramafic rocks have narrow ranges of near-chondritic Nd isotopic compositions ($\varepsilon_{Nd}(0)$ = -0.6 to -2.7) and $^{147}Sm/^{144}Nd$ ratios (≈ 0.16 to 0.19). This feature is in strong contrast with the majority of eclogites from the Su-Lu and Dabie terranes which have low $\varepsilon_{Nd}(0)$ values (-6 to -20) and smaller $^{147}Sm/^{144}Nd$ ratios (≈ 0.1 to 0.15). Trace element and Sr-Nd isotopic characteristics suggest that the original magma was derived from the upper mantle and intruded in the lower crust where the magma was probably contaminated by variable amounts of lower crustal rocks (granulites) during the differentiation of this layered complex.

Sm-Nd isotopic analyses on garnet and omphacite from 6 eclogites and 1 garnet peridotite give very coherent isochron ages ranging from 210 to 218 Ma with only one exception of 231 ± 4 Ma. All isochrons have near-chondritic $\varepsilon_{Nd}(T)$ values (-0.1 to -1.8). In addition, all garnet data points are well aligned to form a similar "isochron" age of 225 ± 7 Ma with $\varepsilon_{Nd}(T)$ = -2.5 ± 1.1. Similarly, Rb-Sr isotopic analyses on phengite and other minerals yield almost the same age results; and the phengite-only data also define a similar isochron age of about 210 Ma.

## Conclusions

The above results lead to several important conclusions: (1) The coherent mineral Sm-Nd ages obtained for both mafic and ultramafic rocks from the same intrusion indicate attainment of isotopic equilibrium during the UHP metamorphism. (2) The Sm-Nd mineral ages are identical within error limits with the zircon U-Pb ages of ≈ 220 Ma (Ames et al., 1993, 1995) from nearby eclogites. Thus, the age of 210-220 Ma is probably the best estimate for the time of the UHP metamorphism and the continental collision, a conclusion reached earlier by Li et al. (1993). (3) The fact that the garnet data points alone also give a similar (or

slightly older) age and a slightly lower initial εNd(T) value as the other garnet-omphacite pairs strongly suggests that the Bixiling complex was intruded shortly before the UHP metamorphism. The same conclusion can be drawn from the phengite-only Rb-Sr isochron argument. The available whole-rock Sm-Nd data are too scattered to define an isochron, but their disposition is consistent with a young (late Paleozoic to early Mesozoic) intrusive age. The recently reported Archean age of ≈ 2.8 Ga (Cao and Zhu, 1995) and an early Proterozoic age of ≈ 2.2 Ga (Liu et al., 1995) could be interpreted as the ages of zircons from the lower crust contaminant. The interpretation of the Bixiling complex as the oldest (late Archean) UHP metamorphic terrane is considered fallacious.

Using the known P-T conditions and probable blocking temperatures for Sm-Nd and Rb-Sr sytems in garnet, phengite and biotite, very high rates of initial cooling (≈ 50°/Ma) and early stage of uplift (≈ 10 mm/yr) were calculated for the Bixiling Complex. This is in strong contrast with the Weihai eclogites from the Su-Lu terrane in which slow cooling and slow uplift (≈ 1 mm/yr) rates were estimated (Jahn et al., 1995). Evidently, the exhumation of UHPM rocks was not of the same style everywhere in the Dabie and Su-Lu terranes.

## References

Ames, L., Tilton, G.R., Zhou, G., 1993. Geology, 21: 339-342.
Ames, L., Zhou, G., Xiong, B., 1995 Tectonics (in press).
Cao, R.L., Zhu, S.H., 1995, Geochimica, 24: 152-160.
Jahn, B.M., Cornichet, J., Cong, B.L., Yui, T.F., 1995. Chemical Geology (in press).
Liu, R., Fan, Q., Li, H., Zhang, Q., Zhao, D., Ma, B., 1995. Acta Petrol. Sinica, 11: 243-256.

*EUG 9, Strasbourg, 1997. Terra Nova, Vol. 9: 366. Poster.*

# Nd systematics in migmatites: Examples for "too old" leucosomes from the Limpopo Belt

Valérie Chavagnac, Thomas F. Nägler and Jan D. Kramers
Universität Bern, Gruppe isotopengeologie, 3012 Bern, Switzerland

We present new geochemical data and Nd model ages on The Mahalapye Complex, Botswana, a part of the Limpopo Belt. This complex is composed of granite and granodioritic to adamellitic gneisses in the central part, and of migmatites along the margins. All rocks studied came from the Lose Quarry which belongs to the migmatitic area. From one Grt-bearing metagreywacke the whole rock and a separated Grt-bearing leucosome were analysed in order to test for Nd isotopic equilibrium. Incongruent melting of Bt under granulite facies metamorphism produces Grt according to the dehydration reaction Bt + Plg + Qtz => Grt + melt (Vielzeuf and Montel, 1994). From this reaction, Grt-bearing leucosome therefore should picture the melt fraction. However, the REE pattern of leucosome is inconsistent with a dehydration melting as it is LREE depleted with a slight negative Eu anomaly. The whole rock is characterized by a HREE depleted pattern with a weak positive Eu anomaly. The behavior of HREE would thus be consistent with fractionation of Grt. The whole rock sample gave a Late Archean Nd model ages (2.7 Ga). The WR - leucosome pair indicates that the migmatization took place around 2 Ga. This age is further constrained by U-Pb on monazites, Pb-stepwise-leaching Grt and Sm-Nd WR-apatites ages. Further a total of 3 WR samples plot on a Sm-Nd isochron of 2041±120 Ma (MSWD=0.153) in accord with Nd isotopic equilibrium between different samples at that age. However, the leucosomes show an errorchrone of 2.5 Ga as well as old and variable Nd model ages (2.8 to 3.2 Ga). Thus, the Sm-Nd system of the leucosomes can not be used to trace the source- or migmatitic age. Further, the leucosome data are in opposition to Nd isotopic equilibration at 2 Ga. The WR isochron may therefore be accidental or represent a correlation that was already present in the protholiths.

As a consequence the meaning of Nd model ages of migmatites as well as gneisses highly depend on wether the sample is rearly representative of the protolith and not dominated by either the leucosome or melanosome. This should be taken into consideration in Nd WR studies in high-grade terrains.

## Reference

Vielzeuf, D., and Montel, J-M., 1994, Contrib. Mineral. Petrol., 117, 375-393.

*MAEGS-10, Carlsbad, 1997, Journal of the Czech Geological Society, Vol. 42: 33.*

# Isotopic equilibrium/disequilibrium in migmatization: An example from the Limpopo Belt, Botswana

Valérie Chavagnac and Jan D. Kramers
Universität Bern, Gruppe Isotopengeologie, 3012 Bern, Switzerland

Since the eighties, several obvious cases of disturbance of the Sm-Nd system during intracrustal processes such as metamorphism and partial melting have been found implying that Sm-Nd model ages are often not meaningfull as protolith ages. Therefore, it is important to understand what controls Nd isotopic equilibrium on a centimeter scale during such processes. From this perspective we present geochemical as well as Nd and Pb isotopes data on a migmatitic sample from the Central Zone of the Limpopo Belt, Botswana. This sample was cut into 4 pieces of several centimeter size. In order to test the Nd and Pb isotopic equilibrium, we took one piece representing very well interlayered leucosome, melanosome and paleosome. It would be expected that the leucosome should portray the partial melt. However, the REE pattern of leucosome is LREE depleted compared to the REE patterns of melanosome and paleosome. These unexpected REE patterns may be explained by the behaviour of accessory minerals such as apatite, monazite or zircon which mainly control the REE as well as Th and U budget of a rock. Thus their partial or total dissolution during a high-grade metamorphic event will strongly affect the REE contents of each migmatitic components. If Nd isotopic equilibrium was reached during migmatization, the leucosomes would yield too old $T_{DM}$ ages, and those of melanosomes would be too young. However, in addition the Nd isotopic compositions indicate that no Nd isotopic equilibrium is attained in migmatization. Epsilon Nd values at 2.0 Ga (the age of the high-grade event) differ by more than 1 epsilon between these parts. Moreover, the U-Pb isotopic compositions on the same fragments yield a Pb-Pb isochron of 1998 ± 68 Ma (MSWD = 0.65; 6 points) indicating that Pb isotopic equilibrium was reached. All migmatitic components are well above the Stacey and Kramers curve which suggests a long crustal history prior to 2.0 Ga.

*88th Annual Meeting: Geologische Vereinigung, Bern, 1998, Terra Nostra, Vol. 1: 43. Poster.*

# Effets on Sm-Nd systematics during migmatization and their bearing on crustal growth studies

Valérie Chavagnac, Thomas F. Nägler and Jan D. Kramers
Universität Bern, Gruppe Isotopengeologie, 3012 Bern, Switzerland

Initial $\varepsilon_{Nd}$ values and Nd model ages have been extensively used to study the growth of the continental crust through Earth's history. However, recent cases of obvious disturbance of the Sm-Nd system during intracrustal processes put many wide ranging conclusions from crustal Sm-Nd works into question.

Migmatites give the opportunity to study the chemical fractionation and Nd isotope exchange during high grade metamorphic conditions. We carried out major and trace elements as well as Nd isotopic analyses on two outcrops of migmatites within the Limpopo Belt, Botswana. The Mahalapye Migmatites are formed by biotite breakdown under fluid-absent melting. In contrast, the Phikwe migmatites are formed by metamorphic differentiation at subsolidus conditions. Results show in both cases, that chemical equilibrium and full Nd isotope exchange were not attained between the migmatitic components during migmatization. Leucosomes from the Mahalapye Migmatites exhibit apparent Nd model ages on average 250 Ma older than those of the melanosomes. This is due to accessory monazite entering the leucosome in preference to apatite. It is impossible to define a crustal residence age for the protolith as an average of the various $T_{DM}$ ages derived from a migmatite outcrop. The true spread in mantle derivation ages for the sediment source region probably exceeds the range of $T_{DM}$ ages found in the outcrop.

In the Phikwe case, the major and trace element distributions of leucosomes and paleosomes indicate that mineral phases did not reach chemical equilibrium with their respective migmatitic component. However, the results clearly indicate that whole rocks remained closed systems during migmatization, allowing the calculation of chemical and Nd isotope compositions of the protolith. The obtained composite Nd model ages (2.8 Ga) are consistent with a Sm-Nd whole rock isochron age. In this case the Sm-Nd systematics can yield clear indications for the study of the evolution of the Southern African continental crust.

*88th Annual Meeting: Geologische Vereinigung, Bern, 1998, Terra Nostra, Vol. 1: 58 Poster.*

# Trace element partitioning can explain an apparent paradox of mineral chronometer memory

Jan D. Kramers, Valérie Chavagnac, Lorenz Holzer, Thomas F. Nägler and Igor M. Villa
Universität Bern, Gruppe Isotopengeologie, 3012 Bern, Switzerland

The 'closure and opening' characteristics of dateable minerals is usually regarded as a function of the diffusivity of radiogenic isotopes in their mineral lattice. This diffusivity may be reasonably well predicted by ionic porosity calculations (Dahl, 1996, 1997). For instance, biotite is predicted to be unretentive for Sr and Ar, apatite intermediate for Nd and Sr, and monazite retentive for Nd and Pb. However, apatite may retain old isotopic memories even in high grade metamorphism, apparently contradicting such predictions and causing confusion in efforts to constrain the dynamics of orogens.

It is generally assumed that trace element transport outside the mineral grain, (in melt, fluid or mineral), is not rate limiting. However, this assumption is not universally valid. Fluids may be buffered at low activities by mineral reactions, especially when melting occurs nearby, and diffusion in minerals surrounding the dated grains may then be important. A dependence of 'closure behaviour' on equilibrium partitioning between minerals is readily shown by an argumentation using Fick's law. The rate of diffusion is given by $F = -D\partial C/\partial x$, where C is the concentration of a trace species, and F is its rate of transport through a unit area perpendicular to x. D is the diffusion coefficient. If a grain of mineral A is embedded in a medium B, e.g. another mineral, then equilibrium exists for a trace element i if ${}^iC_A/{}^iC_B = {}^iK$, where ${}^iK$ is the equilibrium partition coefficient for all isotopes of i between the two phases. In equilibrium, $\partial C/\partial x=0$ adjacent to the interface in both phases, and there is no net diffusion. If a radiogenic isotope of i has been produced in A over time, incipient diffusion during a thermal event will set up concentration gradients in A and B for that isotope only. Close to the interface these are related by $\partial C_A/\partial x = {}^iK\partial C_B/\partial x$. If element i is strongly compatible in phase A (${}^iK>>1$), then exchange is impeded by phase B unless the diffusion coefficient for i in phase B is much greater. If ${}^iK<1$, diffusivity in the surrounding medium B will rarely be a limiting factor.

Sr in biotite is generally a case of ${}^iK<1$, a further reason why this system is so readily reset. In contrast, ${}^iK>>1$ for Nd and Sr in apatite (explaining the apparent paradox of a retentivity greater than predicted by theory) and for Nd in monazite, where it combines with an already small intrinsic diffusivity to ensure isotopic inheritance.

## References

Dahl, P., Earth Planet. Sci. Lett. 150 (1997): 277-290.
Dahl, P., Contrib. Min. Petr., 60 (1996):3687-3700.

*88th Annual Meeting: Geologische Vereinigung, Bern, 1998, Terra Nostra, Vol. 1: 17. Oral.*

# The Limpopo Belt of Southern Africa: Perspective from an ancient orogen on "modern" ones

Lorenz Holzer, Katharina Kreissig, Valérie Chavagnac, Mirjam Schaller and Jan D. Kramers
Universität Bern, Gruppe Isotopengeologie, 3012 Bern, Switzerland

The Limpopo Belt is a complex high grade province situated between the Kaapvaal and Zimbabwe Craton in Southern Africa. It strikes WSW-ENE, is 200 km wide and contains several tectonic lineaments of lithospheric scale. Until recently the high grade metamorphism and all structural features were interpreted as a product of a single late Archean continental collision between the Kaapvaal and Zimbabwe Cratons. Combined geochronological, structural and petrographic studies have now invalided such models. Although several Archean magmatic and metamorphic episodes are in evidence, studies of the major tectonic lineaments have shown that the final juxtaposition of the adjacent cratons occured in a transpressive orogen at 2.0 Ga. The perception of a 2 Ga tectonic event in the Limpopo Belt puts a new perspective on mid Proterozoic geological framework. The 2 Ga event in the Limpopo Belt can be linked with contemporaneous fold belts at the western edges of the Kaapvaal and Zombabwe Cratons (Kheis and Magondi) and between the Kongo and Tanzania Cratons, which also include the oldest known eclogites (in the Usagaran belt, Tanzania).

There are clear analogies between the Proterozoic belts in southern Africa and "modern" orogens. The Proterozoic high grade provinces can thus be considered as equivalents to the roots of alpine type orogens and offer insight into tectono-metamorphic processes at 30 to 40 km depths. The following points are of particular interest: a) the internal structure of deep seated cristalline units can hardly be monitored by means of seismic investigations. Weak density contrasts may be one reason, - complex, polyphase fold structures may be an another. b) the kinematics within the suture zones bounding the different cristalline blocks at deep crustal levels may be different from that in the upper crust, because of different rheology and decoupling processes. The exhumed lower crustal structures in the Limpopo Belt are characterized by large width (up to 50 km) and important horizontal strike slip displacements. c) the timing of (tectono-) metamorphic processes in the Limpopo Central Zone determined by combined petrological and geochronological studies reveal periods with fast cooling- and decompression rates (up to 10 mm/yr, 14°C/Ma) shortly after peak metamorphism (2020 Ma), followed by slower processes (0.7 mm/yr, 8°C/Ma) during the retrograde path. These rates are comparable with cooloing-, uplift-, exhumation-, an sedimentation rates from alpine type orogens.

*17ème Réunion des Sciences de la Terre, Brest, 1998, p 92. Oral.*

# Evolution crustale de l'Archéen au Protérozoique en Afrique du Sud: Quand s'effectue la juxtaposition finale des Cratons Kaapvaal and Zimbabwe?

Valérie Chavagnac, Lorenz Holzer, Katharina Kreissig,
Jan D. Kramers, and Thomas F. Nägler
Universität Bern, Gruppe Isotopengeologie, 3012 Bern, Switzerland

Le Limpopo Belt (LB) représente un terrain métamorphique de haut grade séparant deux provinces archéennes de bas grade, les cratons Kaapvaal et Zimbabwe. Cette chaîne montre une géométrie générale à double déversement archéen. Le LB se compose d'une zone centrale (ZC) et de deux zones marginales (SMZ et NMZ) qui sont séparées par des zones de cisaillement dextre. Le métamorphisme granulitique dans les 3 zones a été interprété comme le résultat de la collision continentale à 2.6 Ga entre les deux cratons (Van Reenen et al., 1992). Cependant, les différentes études ont mis en évidence un événement tectono-métamorphique à 2.0 Ga qui ressemble à une collision transpressive. L'activité magmatique dans le craton Kaapvaal cesse vers 2.65 Ga alors qu'elle se poursuit jusqu'à 2.55 Ga dans le craton Zimbabwe. Les compositions isotopiques en Pb confirment que les deux cratons ont une évolution crustale différente au cours de l'Archéen. Par ailleurs, la SMZ et la NMZ ont des caractéristiques géochimiques similaires à leur craton adjacent, suggérant une origine proche mais aucun résultat tend à prouver leur coalescence durant l'Archéen. Trois périodes majeures de l'Archéen au début Protérozoïque régissent l'évolution crustale en Afrique du Sud: 1) La période comprise entre 3.5-2.9 Ga se caractérise par une intense activité magmatique dans la ZC du LB et dans les deux cratons; 2) Vers 2.6 Ga, la formation des granulites de BP dans le LB s'accompagne d'une accrétion magmatique marquée par d'importantes intrusions granitiques et charnockitiques. Ces corps plutoniques ont cristallisé en milieu de croûte continentale sous le faciès granulitique pour la SMZ et la NMZ et sous le faciès amphibolitique pour les cratons. Ils sont interprétés comme le produit de la fusion du manteau sous continental ou de la refusion/fusion d'enderbites et/ou de sédiments. Les évolutions métamorphiques de SMZ et NMZ sont diachroniques et différentes (horaire et anti horaire respectivement); 3) L'événement à 2.0 Ga implique un métamorphisme de haut grade, un fort recyclage crustal, l'activation de deux zones de cisaillement dextre dans le LB ainsi que la formation de deux zones orogéniques aux frontières ouest des deux cratons. L'évolution crustale distincte des deux cratons et du LB à l'Archéen tend à proposer une juxtaposition finale de ces unités à 2.0 Ga.

*17ème Réunion des Sciences de la Terre, Brest, 1998, p 100. Oral.*

# Datation des éclogites éocenes du Tso Morari et héritage isotopique

Julia de Sigoyer[1], Igor M. Villa[2], Valérie Chavagnac[2], Stéphane Guillot[1], George Mascle[3]
1: CNRS, Université Claude Bernard-ENS Lyon, France
2:Universität Bern, Gruppe Isotopengeologie, 3012 Bern, Switzerland
3: CNRS, Université Joseph Fourier, Grenoble, France

Les éclogites du Tso Morari (Est Ladakh), marqueur de la subduction de la marge continentale Indienne, sont associées à des roches fortement rétromorphosées ou non déformées. Pour contraindre lévolution de l'unité HP, diverses méthodes géochronologiques ont été testées. Deux isochrones internes Sm/Nd ont été obtenues sur Ap-Grt-RT pour un granite non déformé (Ch 216e) et pour un métagreywacke rétromorphosé (Ch 223d). Pour les deux échantillons les âges modèles $T_{DM}$ > 2 Ga suggèrent une origine ancienne. Les minéraux analysés sont à l'équilibre isotopique (MSWD = 0.5). Le granite a un âge Ordovicien de 458 ± 14 Ma, il n'a pas été rééquilibré isotopiquement lors de l'orogenèse himalayenne, alors que la métagreywacke a recristallisé probablement au Tertiaire (17 ± 56 Ma). L'âge du granite confirme sa parenté avec les orthogneiss de la marge Indienne et valide les arguments stratigraphiques, qui attribuent le Tso Morari à cette marge. Pour une métapélite éclogitisée (Ch 157a) (20 ± 3 kbar, 580°C ± 50 °C) l'isochrone Sm/Nd sur (Grt-RT) donne un âge de 53 ± 8 Ma. Cet âge apparent est peu etre vieilli par un héritâge de Nd, du fait de l'âge $T_{DM}$ > 2 Ga de cette roche. Cependant si cet âge est vrai, il date l'éclogitisation et la subduction de la marge Indienne à l'éocène inférieur, confirmant les données paléomagnétiques et stratigraphiques. Une isochrone interne Rb/Sr a été obtenue pour la métagreywacke (Ch 223d) sur Ms-Ap-RT et donne un âge réaliste de 45 ± 4 Ma (MSWD = 0.02). Pour la métapélite (Ch 157a) l'isochrone Rb/Sr sur Ms-RT donne un âge apparent de 93 ± 4 Ma, trop vieux pour avoir une signification géologique.

Les données 39Ar/40Ar sur les phengites de la métapélite (Ch 157a), et deux éclogites (Ch 165d, Ch 266a), montrent également des âges apparents crétacés, géologiquement irréalistes dans ce contexte. L'ensemble des données montrent une large hétérogénéité due au fait que le protolith indien, constitué d'orthogneiss ordoviciens et de sédiments paléozoïques, a subit une équilibration isotopique partielle lors de l'éclogitisation à L'éocène inférieur. l'héritâge isotopique est contrôlé par la proportion de minéraux néoformés, plutôt que pard des excès d'Ar et de Sr dans les phengites ou par les températures de fermeture (car les âges sur Grt seraient plus anciens que les âges sur Ms).

*HKT Conference, Pakistan., 1998, Extended abstract. Oral.*

# Multichronometry of the Tso Morari Eclogites: From Ordovician plutonism to Lower Eocene eclogitization

Julia de Sigoyer[1], Igor M. Villa[2], Valérie Chavagnac[2], Stéphane Guillot[1], George Mascle[3]
1: CNRS, Université Claude Bernard-ENS Lyon, France
2:Universität Bern, Gruppe Isotopengeologie, 3012 Bern, Switzerland
3: CNRS, Université Joseph Fourier, Grenoble, France

The occurrence of eclogites in the Tso Morari unit (East Ladakh) has been atributed to the subduction of Indian continental margin (de Sigoyer et al., 1997). Some of these rocks were retrogressed in amphibolite facies, while others apparently totally escaped eclogitization. As dating eclogitic rocks exposes numerous difficulties, we applied a variety of geochronological methods in order to obtain a consistency check.

**Sm-Nd** internal isochrons were obtained on the undeformed Polokonkala granite (Ch 216e), on a metagreywacke of intermediate metamorphic grade (Ch 223d) and on an eclogitized metapelite (Ch 157a) (20 + 2 kbar, 550°C ± 50°C). Two Ap-Grt-WR isochrons on the formed two samples show low MSWD = 0.5, meaning that Grt (± inclusions) is in isotopic equilibrium with WR and Ap. Both whole rocks give very high Nd model ages ($T_{DM}$ > 2 Ga) implying recycling of cratonic material. The granite has an Ordovician age of 458 + 14 Ma; it is unaffected by Himalayan overprint, while the metagreywacke was reset probably in the Tertiary (17 ± 56 Ma). The Ordovician age for the undeformed Polokonkala granite is consistent with the 487 ± 25 Ma Rb-Sr isochrone age (Trivedi et al., 1986) on the same granite, and confirms the relationship between the Polokonkala granite and the Ordovician orthogneiss recognized all over the Rupshu and Nyimaling area (Stutz, 1988). The occurrence of these Ordovician granites, typical of the Indian continental margin (Le Fort, 1988), confirms the stratigraphical evidences of Colchen et al. (1994) which related the Tso Morari unit to the Indian subcontinent. Fir Ch 157a we obtained a two point Grt-WR age of 53 ± 8 Ma, which can be explained by three possibilities. (i) The "age" is too old, as it suffers from Nd inheritance; as this rock also has a $T_{DM}$ > 2 Ga, a small modal percentage of old relicts would have a large influence. (ii) The "age" is a true age, and it dates the eclogitization and the early subduction of the Indian margin at the Lower Eocene. (iii) The "age" is too young, as it is possible that the Sm/Nd system did not achieve initial isotopic equilibrium in eclogite-facies metamorphism (Thöni and Jagoutz, 1992). Whatever the uncertainty, this result confirms the Himalayan origin of the Tso Morari eclogites and this Lower Eocene age is consistent with the paleomagnetic data (Patriat and Adache, 1984) and the stratigraphic observations (Garzanti et al., 1985) which suggested that the onset of the Indian continental subduction started between 57 and 53 Ma (Paleocene to Ypresien). Note that an age of 44 ± 3 Ma was obtained for the Kaghan eclogites (Tonarini et al., 1993; Spencer and Gebauer, 1996).

**Rb-Sr** internal isochrons were obtained on the metagreywacke, Ch 223d, and the metapelite, Ch 157a. For the latter, a two point Ms-WR line gives a 93 ± 4 Ma apparent bulk age; for Ch 223d, Ms-Ap-WR define an siochron with MSWD = 0.02 and T = 45 ± 4 Ma. These contradictory results on arguably contemporaneous metamorphic rocks suggest again that the isotopic inheritance plays a substantial role in the Tso Morari eclogites. We can compare the present results with those by Linner et al. (1997), whoc reported a 26 ± 0.5 Ma two point Ms-WR line on eclogite and two Ms-WR ages around 50 Ma on a mylonitic gneiss.

**$^{39}Ar/^{40}Ar$** data from three HP-LT white micas (metapelite Ch 157a and two metabasalts, Ch 165d and Ch 266a) all have Cretaceous apparent ages but show clear

evidence of mixed generations. The $^{39}Ar/^{40}Ar$ "age" is too old, as the Indian crust that was to become an eclogite, still was south of the Equator in Mid-Cretaceous. The coincidence for the Rb-Sr and $^{39}Ar/^{40}Ar$ ages for Ch 157a strongly argues that Ar and Sr are partly inherited; this also implies that the general use of "excess Ar" to explain the old Ar ages of HP micas is unjustified.

**Dicussion**

Our data apparently show a large heterogeneity. However, the pattern of the samples so far analyzed can be explained by a comparatively simple interpretation. The Indian protolith (Ordovician orthogneisses with a Proterozoic prehistory; Upper Paleozoic sediments of older provenance) underwent very extensive, but not complete, isotopic equilibration during the Early Tertiary eclogitization. The degree of isotopic inheritance varies for the different isotopic chronometers (e.g. Ch 157a). Note that inheritance is not controlled by a "closure temperature" (which would be higher for Grt than for Ms) but rather by the extent of mineral neoformation.

**References**

de Sigoyer et al. 1997, Eur. J.. Mineral., 9: 1 073-1 083.
Trivedi et al. 1986, Terra Cognita, 6: 144.
Stutz 1988, Mémoire de Géologie (Lausanne), 3, pp 149.
Le Fort 1988, Phil. Trans. R. Soc. London, 326: 281-299.
Colchen et al 1994, J. Nepal Geol. Soc., 10: 23.
Thöni and Jagoutz 1992, Geochim. Cosmochim. Acta, 56: 347-368.
Patriat and Adache 1984, Nature, 311: 615-621.
Garzanti et al. 1987, Geodinamica Acta, 1: 297-312.
Tonarini et al. 1993, Terra Nova, 5: 13-20.
Spencer and Gebauer 1996, 11th H.K.T. Workshop, p147.
Linner et al. 1997, 12th H.K.T. Workshop, p 175-176.

*AGU Spring Meeting, Boston. 1998*

# Sm-Nd and U-Pb systematics on migmatites and their effects on crustal growth studies

Valérie Chavagnac, Thomas F. Nägler, and Jan D. Kramers
Universität Bern, Gruppe Isotopengeologie, 3012 Bern, Switzerland

Since the early eighties, many isotopic systems are used to constrain crustal evolution. However, even the "robust" Sm-Nd system can show obvious disturbances during intracrustal processes, which puts wide ranging conclusions from Sm-Nd crustal studies into question.

Migmatites are ideal rocks to study the chemical and isotopic fractionation which may occur during high grade metamorphic events. From this perspective we carried out major and trace element as well as Sm-Nd and U-Pb analyses on three outcrops of migmatites (Limpopo Belt, Botswana and South Africa). Mahalapye and Palala migmatites (metagreywacke and metapelite respectively) are formed by Bt breakdown under fluid-absent melting. However, the same formation process did not result in the same behaviour of major and trace elements and isotopic systems. In the first case, chemical equilibrium and full Nd isotope exchange were not attained between melt and paleosome and Mnz preferentially entered the leucosome, causing their apparent Nd model ages to be on average 250 Ma older than those of the paleosomes. The true spread in mantle derivation ages probably exceeds the range of Nd model ages found in the outcrop. In contrast, Palala migmatites show chemical equilibrium and nearly full Nd-Pb isotope exchange between all migmatitic components. The Nd model ages on both leucosomes and paleosomes are in the same order (3.0-3.2 Ga). In the third case (Phikwe), migmatites are formed by metamorphic segregation at subsolidus conditions. Here, the major and trace element distribution as well as the Nd isotopic compositions in each migmatitic component are related only to the proportional amounts of the minerals. Therefore, chemical equilibrium and full Nd isotope exchange are not attained. Nevertheless, the results clearly indicate a closed system during migmatization allowing the calculation of chemical and Nd features of the protolith. Composite Nd model ages are the same for two samples (2.8 Ga). In contrast to Nd, Pb isotopes show complete inter-mineral exchange during 2.0 Ga amphibolite facies metamorphism.

This discrepancy between the Sm-Nd and Pb behaviour may be explained by the very high concentration of Nd in Ap, Mnz or Hbl to ensure isotopic inheritance, by the grain size of the protolith, also by the quantity of fluid which may be generated by dehydration reactions.

*AGU Spring Meeting, Boston. 1998*

# Multichronometry of Tso Morari eclogites, Eocene age and inheritance in Himalaya

Julia de Sigoyer[1], Igor M. Villa[2], Valérie Chavagnac[2], Stéphane Guillot[1]
1: CNRS, Université Claude Bernard-ENS Lyon, France
2:Universität Bern, Gruppe Isotopengeologie, 3012 Bern, Switzerland

The Hp-LT rocks (20 kbar, 580°C) of the Tso Morari (East Ladakh), associated with amphibolitic retrogressed, and undeformed rocks, are related to the subduction of the Indian margin. Several geochronological methods are tested to constrain the HP unit evolution. Two internal Rb-Sr isochrons (Ap-Grt-WR) for an undeformed garnite (G1), and a retrogressed metagreywacke (M2), with a low MSWD (0.5) show that the minerals are in isotopic equilibrium. Both WR give high Nd model ages ($T_{DM}$ > 2 Ga), implying recycling of cratonic material. The granite has an Ordovician age of 458 ± 14 Ma. it is unaffected by Himalayan overprint, while the metagreywacke was reset probably in the Tertiary (17 ± 56 Ma). The Ordovician age of the granite has a typical Indian continental signature, confirming the stratigraphical evidences which related the Tso Morari unit to the Indian subcontinent. For an eclogitized metapelite (P3) a Sm-Nd age of 53 ± 8 Ma is obtained on Grt-WR. This apparent age could be grown old by Nd inherirance; as this rock has also a $T_{DM}$ > 2 Ga. However, this age is consistent with the paleomagnetic and stratigraphical data suggesting that the early subduction of the Indian margin occurred during Lower Eocene. Rb-Sr internal isochron obtained on Ms-Ap-WR for the metagreywacke (M2) gives a confident age of 45 ± 4 Ma (MSWD = 0.02). For the metapelite, (P3) the Ms-WR line gives a 93 ± 4 Ma apparent bulk age, too old to have a geological significance. $^{39}Ar/^{40}Ar$ data on three phengitic mineral fractions of the metapelite (P3) and two eclogites have Cretaceous apparent ages, without any geological significance in this context. The large heterogeneity of ous geochronological data is explained by uncomplete isotopic equilibration during the Lower Eocene eclogitization of the Indian Ordovician protolith. The degree of isotopic inheritance varies for the different isotopic chronometers (e.g. P3). It seems not controlled by a "closure temperature" (which would be higher for Grt than for Ms), neither by excess Ar in HP micas, but rather by the extend of mineral neoformation.

*8th annual V.M. Goldschmidt Conference, Toulouse, France, 1998, Extended abstract*

# Behaviour of Sm-Nd and U-Pb systematics during migmatization and its effects on crustal growth studies

Valérie Chavagnac, Jan D. Kramers, and Thomas F. Nägler
Universität Bern, Gruppe Isotopengeologie, 3012 Bern, Switzerland

In Sm-Nd studies aimed at constraining crustal growth history, Sm-Nd systematics are normally considered to be undisturbed at the whole rock scale during intracrustal processes such as alteration, metamorphism or even partial melting. However, if Sm-Nd systematics are disturbed during intracrustal processes, this could put wide ranging conclusions from Sm-Nd crustal studies into question.

Migmatites are ideal rocks to study the chemical and isotopic fractionation which may occur during high grade metamorphic events. From this perspective, we carried out Sm-Nd, U-Pb work associated with major and trace element analyses on three outcrops of migmatites generated during the 2.0 Ga orogeny in the Central Zone of the Limpopo Belt (Botswana and South Africa). The Central Zone which is mainly composed of orthogneisses and paragneisses underwent granulite facies metamorphism followed by decompression metamorphic consitions (clockwise P-T loop) at 2.0 Ga. Partial melting following the Bt breakdown reaction in high temperature, low pressure rocks did lead to different behaviour of Sm-Nd systematics for metagreywacke and metapelite. In the first case, chemical equilibrium and full Nd isotope exchange were not reached due to the effect of accessory minerals (monazite and apatite) on the compositions of the partial melt. Monazite entered the melt in preference to apatite, either by dissolution or by entrainment and its unradiogenic Nd isotope signature dominates the leucosome. As a consequence, the Nd model ages on partial melt are up to 400 Ma older than those on paleosomes. The Nd model ages of these rocks cannot be used to constrain the evolution of the Southern African continental crust and in view of this, Nd model ages on any leucocratic crustally derived rocks in this region are suspect.

In constrast, partial melts obtained by the same metamorphic reaction on metapelite exhibit chemical equilibrium with paleosomes as well as nearly full Nd isotope echange while Pb-Pb systematics are not fully reset and reflect an errorchron of c. 2300 Ma. The same accessory minerals are present in both paleosome and leucosome but they were either newly formed, or recrystallized during the metamorphic event. In other words, the accessory minerals were chemically and isotopically equilibrated with the partial melt and the paleosomes. The Nd model ages on leucosomes and paleosomes therefore coincide and they can be used to constrain the crustal growth in the region.

In migmatites formed by metamorphic differentiation at subsolidus conditions, chemical equilibrium and Nd isotope exchange were not reached during migmatization. The distributions of the elements are related, in that case, to the proportional amounts of each mineral in the migmatitic components, which resulted from reorganization according to rheological competency under stress. However, full Pb isotope exchange is reached as hightlighted by a Pb-Pb WR isochron yielding 2.0 Ga, the age of the metamorphic event. Lack of isotope exchange reflects in the main 1) the presence of pre-metamorphic, magmatic hornblende, and 2) accessory minerals such as apatite or monazite, with very high concentrations of unradiogenic Nd and remained preferentially in the paleosome, lowering the Nd isotopic composition of that migmatitic component. However, even if chemical equilibrium and full Nd isotope exchange were not reached, the geochemical characteristics combined with REE modelling provided arguments for closed system behaviour of the whole rock during migmatization. Therefore, the chemical and isotopic compositions of the protolith

may be obtained via mass balance calculations and can be used as marker for the crustal evolution.

The discrepancy between the Sm-Nd and U-Pb systems during migmatization cannot be explained in an unique manner. It is clear that, in the absence of chemical equilibrium, full isotope exchange of Nd or Pb (full "resetting" of the Sm-Nd and U-Pb isotope systems) cannot be assumed to have taken place. On the one hand, apatite, monazite, xenotime, titanite, allanite and zircon mainly control the REE as well as Th and U budget of a rock, and equilibration of nascent melt with these accessory minerals could be poor (Sawyer, 1991; Watt and Harley, 1993) whereby armoring within residual phases would be an important, but not necessary, contributing factor. This could have a particularly strong effect if combined with rapid melt extraction (Watt et al., 1996). On the other hand, the protolith lithologies with regard to their grain size (metagreywacke and metapelite) and their quantity of fluid available during metamorphism, may be an important factor for the redistribution of trace elements and for isotope exchange. Presence of a mobile fluid will enable the resetting of Pb-Pb systematics (subsolidus segregation) but not of Sm-Nd; once a melt is formed, fluid is dissolved in it and therefore less mobile. Whether a Nd model ages can be reconstructed for a migmatized rock further depends on whether the total sample is really representative of the protolith and not dominated by either the leucosome or melanosome. This should be taken into consideration in Nd WR studies in high and medium grade terrains.

*8th annual V.M. Goldschmidt Conference, Toulouse, France, 1998, Extended abstract*

# Geochronological evidence for the "in situ" tectonic relationship in the Dabie UHP metamorphic terrane, Central China

Valérie Chavagnac[1,2] and Bor-ming Jahn[1]
1: Géosciences Rennes, Université Rennes, 35042 Rennes, France
2:Universität Bern, Gruppe Isotopengeologie, 3012 Bern, Switzerland

The Dabie Mountains and the Su-Lu region in central China are known to contain the largest distribution of ultrahigh pressure metamorphic (UHPM) rocks in the world. They are parts of the Qinling-Dabie orogen formed by collision between the Sino-Korean and Yangtse cratons. The preservation of UHP minerals has inspired different models to explain the deep subduction of continental crust and the mechanisms for subsequent unroofing of the UHPM rocks. In the absence of good constraints from geochemical, isotopic and age data for different lithotectonic units, numerous tectonic models have been proposed. It appears that the greatest controversy to date concerns the primary age and the nature of eclogite protoliths, their tectonic relation with the associated ultramafic rocks and enclosing granitic gneisses ("in-situ" vs "foreign" hypothesis), the areal extent of the UHPM rocks, and their mode of exhumation.

Here we report new geochemical and Sr-Nd for the host gneisses of the largest coesite-bearing eclogite body in this terranne - the Bixiling Complex. These data will be used to tackle the problem of eclogite-gneiss tectonic relationship. The Bixiling Complex has well preserved its UHP paragenesis of which coesite and quartz pseudomorph occur as inclusions within garnet or omphacite. In contrast, the host gneisses exhibit a typical phase assemblage of the albite-epidote amphibolite facies (plagioclase + biotite + zoisite + K-feldspar + quartz + muscovite + apatite) corresponding to the retrograde metamorphism of the Bixiling Complex. However, the presence of garnet, though very minor in amount, may suggest a previous higher metamorphic condition. Geochemically, the host gneisses are of TTG composition (tonalite-trondhjemite-granodiorite) and are characterized by negative Ti, P, Ta and Nb anomalies in their spidergrams, hence suggesting their protolith formation in ancient arc environments. Much of the protoliths of the gneisses from the Dabie UHP terrane was probably formed in late Proterozoic (750-800 Ma; Ames et al., 1996; Rowley et al., 1997; Hacker et al., 1998). However, there is indication of older protoliths from Sm-Nd model age ($T_{DM}$) data for gneisses from Shuanhe (Chen and Jahn, 1998). The Bixiling gneisses have $T_{DM}$ of 1.3 to 1.5 Ga, and $\varepsilon Nd(800\ Ma) = +4.2$ - , indicating their late Proterozoic formation and juvenile character.

Geochronological constraints are obviously essential for understanding the gneiss-eclogite tectonic relationship. Rb-Sr isotope analyses of whole-rock and constituent phases for five gneisses yielded a tight range of Ms-WR-Zo isochron ages from 194 to 198 Ma, and Bt-WR-Zo isochron ages from 174 to 188 Ma (Fig. 1 and 2). On face values, the Ms Rb-Sr ages are only slightly younger than the Phg-WR Rb-Sr ages obtained on the coesite-bearing eclogite from the Bixling Complex (Fig. 3; 198 to 223 Ma; Chavagnac and Jahn, 1996). Moreover, the Bt Rb-Sr ages are also in agreement with that of an amphibolite near the Bixiling Complex. Thus, when combined the new age information with the published zircon age data (Ames et al., 1996; Rowley et al., 1997; Hacker et al., 1998), the eclogites and their host gneisses appear to have undergone a similar metamorphic history. Further age dating by Ar-Ar on Bt and Ms and fission tracks on Ap from the same samples are being carried out. The exhumation and cooling rates of the gneisses and enclosed Bixiling eclogite complex will be better evaluated by the combination of different isotopic ages.

## References

Rowley et al., 1997, *Earth Planet. Sci. Lett.*, **151**, 191-203.
Hacker et al., submitted, *Earth Planet. Sci. Lett.*
Ames L., Zhou G., and Xiong B., 1996, *Tectonics*, **15**, 472-489.
Chavagnac V. and Jahn B-m, 1996, *Chem. Geol.*, **133**, 29-51.

# APPENDIX C

## Geochronologic evidence for Upper Paleocene subduction of the Indian continental margin below Asia

# Geochronologic evidences for Upper Paleocene subduction of the Indian continental margin below Asia

Julia de Sigoyer[1], Valérie Chavagnac[2], Igor M. Villa[2],
Stéphane Guillot[1], Georges Mascle[3]

[1]UFR Sciences Terre., UCB -ENS Lyon, CNRS, Bat 402, F-69622 Villeurbanne.
[2]Isotopengeologie, Universität Bern, Erlachstrasse 9a,CH-3012 Bern
[3]Institut Dolomieu, CNRS, rue Gignoux, F-38100 Grenoble.

**submitted to Geology**

The multichronometric study of the LT eclogitic Tso Morari unit (Ladakh, India) precises the early evolution of the NW-Himalayan belt. Sm-Nd ages confirme the affiliation of this unit to the Indian plate, and date its eclogitisation, i.e. the subduction of the Indian margin during the Upper Paleocene. We show that the exhumation of the HP unit began rapidly at 55 ± 7 Ma in a subductional context, across the mantle wedge, and continued slower during the Himalayan collision across the continental crust, allowing a temperature increase and a partial recrystallization dated at 45 ± 4 Ma by Rb-Sr method.

The collision between India and Asia has not only modified the motion of lithospheric plates, but has also created changes in sedimentation, climate, oceanic circulation and faunal distribution (1-3). Precise timing of the first contact between the two continents is critical to understand its more widespread consequences. Extensive discussions deal with the age of the onset of collision. In the western part of Himalaya the proposed ages range from 65 to 45 Ma (4, 5). The discrepancies between the ages result not only from the use of different indirect approaches, but also from the confusion made between the time of the first India-Asia contact and the age of the true collision. On the basis of similar terrestrial fauna found in India and Asia, the first contact between the two landmasses was placed at 65 Ma (3, 6). Paleomagnetic data reflecting variations in the direction and in the velocity of the Indian plate motion, also date this contact as early Paleocene (7). In the same way, the continental contamination described in the magmatism of the south Asian margin (8) is related to the subducted Indian margin at about 60 Ma in Ladakh, and chemical arguments suggest that continental subduction was still active up to the lower Eocene (ibid.). On stratigraphical arguments, the obduction of the accretionary prism onto the Indian plate is situated between 66 and 55.5 Ma in Pakistan (5), whereas in Zanskar the shoaling sedimentation interpreted as flexural consequences of this obduction are dated during the Upper Paleocene (57 Ma) (9). All these indirect approaches, argue for a Paleocene contact between India and Asia before the true collision, i.e., the closure of epicontinental marine domain associated with a strong decrease in the convergence velocity (from 18 down to 10 cm/yr) dated at Lower Eocene time by paleomagnetic arguments (2,4,7). On a biostratigraphical point of view the true collision is dated at about 54-52 Ma, by the onlap of volcanic arenites derived from Asia onto the Indian continental terraces (9, 10).

To avoid the problem of the interpretation of ages, we propose to directly date the subduction of India below Asia by dating the continental subduction-related rocks, i.e., eclogites presumed to derive from the Indian margin. Such eclogites have so far been described in two localities of the Himalayan belt, the Kaghan valley (north Pakistan) (11), and the Tso Morari dome (eastern Ladakh) (12). The Sm-Nd age of 49 ± 6 Ma obtained on Kaghan

metadolerites (13), is younger than the robust stratigraphical results obtained in Zanskar (9). However the Kaghan eclogites underwent temperature condition of about 650 °C (11) suggesting that the age obtained could be cooling ages or retrogressed ages, rather than eclogitic crystallization ages. The eclogites of the Tso Morari, on the other hand, have preserved low temperature eclogitic conditions (14). Furthermore, eclogitic paragenese is not only preserved in the metabasic lenses but also in the metapelites and metagreywackes (15). The choice of the samples and of the isotopic system is crucial to investigate the timing of the tectono-metamorphic evolution of the Tso Morari dome. Sm-Nd and Rb-Sr analyses were performed on specific samples representing different stages of the dome evolution. We dated with Sm-Nd system, the protolith, to clarify the affiliation of the dome with the Indian plate; the eclogitic event, in order to constrain the age of the subduction of the Indian margin below the Asian margin, that immediately preceded the India-Asia collision and finally we obtained a Rb-Sr age for the retrogression which precises the end of the exhumation of the Tso Morari unit. These new results are discussed, pointing out their implications for the early evolution of the Himalayan orogenesis.

The Tso Morari dome is located in eastern Ladakh, between the Indus suture zone to the North and the Zanskar sedimentary unit to the South (Fig. 1). It has been described as a distal block of the thinned Indian continental margin (12, 16, 17). It consists of a gneissic basement overlaid by a Permo-Triassic cover of metapelites, metabasalts and metagreywackes. Petrological studies on this dome show that all the lithologies underwent HP-LT metamorphism (20 ± 3 kbar; 550 ± 50°C), due to the continental subduction of the Indian margin below Asia (14, 15). In order to precise the origin and the age of the Tso Morari protolith, an undeformed alkaline granite (Ch216e) was sampled close to the Polokongka La pass, in the central part of the dome (Fig. 1). This (Ch216e) granite is scarcely deformed and metamorphosed, it still presents magmatic textures and minerals, such as quartz, potassic feldspar, muscovite, biotite, garnet, zoisite, apatite and tourmaline. Sm-Nd analysis were performed on this granite.

To date the LT eclogitic event, the geochronological investigations show that Sm-Nd system give better results than the Rb-Sr, especially when it is applied on metapelitic rocks rather than on the metabasites (18). Therefore, we selected a well preserved HP-LT metapelite (Ch157a) sampled in the north-western limb of the Tso Morari dome (Fig. 1). The studied HP metapelite is Fe-rich and could correspond to the Triassic Lilang formation (19). The precise petrological description of the Fe-rich metapelite is found in (15). The metapelite contains garnet, jadeite, chloritoid, paragonite, glaucophane, phengite, zoisite, chlorite ± biotite. Zoned garnets are helicitic, and mainly composed of almandine (Xalm = 63-79 %). The inclusions of pure jadeite and chloritoid rimmed by paragonite within garnet core, are characteristic for eclogitic conditions (20 ± 3 kbar, 550 ± 50°C) (15). The garnet rims, contain fewer inclusions,

and are in equilibrium with the blue amphiboles which compose the foliation associated with phengite and paragonite. Microprobe analyses show that amphiboles are mainly ferro-glaucophanes. Jadeite is never observed in the matrix, nor associated with glaucophanes. (15) argues that glaucophane was developed at the expense of jadeite according to the reaction

jadeite + chloritoid = glaucophane + paragonite + garnet

which occurred at the onset of decompression from 20 ± 1 kbar, without temperature change (Fig. 2). Garnet grew at and after the pressure peak, while glaucophane only grew during the quasi-isothermal decompression from 20 to 11 kbar (Fig. 2) (15).

During the next step of the decompression, a slight increase of temperature took place, some rocks recorded a more extensive recrystallization and deformation than others. A retrogressed metapelite (Ch223d), collected in the north eastern part of the Tso Morari dome, north-east of the Polokongka La pass (Fig. 1), is associated in the field with strongly retrogressed eclogites. This metapelite (Ch223d) is composed of quartz, white mica with low Si (3.1-3.3 p.f.u.), garnet, apatite, zoisite ± biotite, and is stable under amphibolitic conditions, at about (11 ± 2 kbar, 610 ± 70°C) (14). Rb-Sr analysis were performed on this sample to date the retrogression, and to constrain the Tso Morari exhumation.

The dating of the Tso Morari rocks is done according to field observations and to their tectono-metamorphic evolution. Therefore, in order to obtain the protolith age, we separated garnet and apatite from the (Ch216e) granite and dated it by Sm-Nd. The occurrence of garnet with glaucophane in the HP metapelite (Ch157a), allows Sm-Nd dating. For the retrogressed metapelite (Ch223d), Muscovite and apatite were analyzed by Rb-Sr.

All the minerals were separated by magnetic field, density contrast and hand-picked under binocular. Analytical techniques used in this study follow (21) for the Rb/Sr analyses, and (22) for Sm-Nd analyses. The uncertainty on Sm/Nd ratios is less than ± 0.3%. Chemical procedural blanks are Sm 50 pg, Nd 180 pg. Sm-Nd model ages were calculated relative to depleted mantle evolution. The Nd evolution of the Depleted Mantle is approximated by a third order polynomial fit (23):

$$\varepsilon_{Nd}(T) \text{ sample} = 0.164T^3 - 0.566T^2 - 2.79T + 10.4$$

Sm-Nd and Rb-Sr results are listed in Table. 1. The regression line used for age determination are done with ISOPLOT (24) and the uncertainties used are ± 0.3% for Sm, ± 0.005% for Nd, ± 2% for Rb and ± 0.05% for Sr.

For the Polokongka La granite (Ch216e), the Sm-Nd analyses on garnet, apatite and whole rock gave an age of 458 ± 14 Ma (2s) (Fig. 3A), with a low MSWD = 0.48. This result is interpreted as the age of garnet and apatite crystallization, it is consistent with a previous Rb-Sr age at 487 ± 25 Ma on the Polokongka La granite (25). Moreover the $\varepsilon_{Nd,i}$ = -9 and $T_{DM}$ = 3 Ga are typical for the old granites of Indian craton (16, 26), confirming the affiliation of Tso Morari dome to the Indian plate.

For HP metapelite (Ch157a) garnet, glaucophane and whole rock define an isochron age of 55 ± 7 Ma (2s) (Fig. 3B). The large negative initial epsilon value ($\varepsilon_{Nd,i}$ = -17.3) and the $T_{DM}$ = 3 Ga suggest an old continental origin for the metapelite protolith. The 55 Ma isochron is dominated by the garnet. The low MSWD (= 1.59), means that garnet, glaucophane and the whole rock were in isotopic equilibrium at the time of their crystallization. The latter took place at 550 ± 50°C (15), under the garnet and glaucophane Sm-Nd blocking temperature estimated at about 650°C (18), which ensures that we date the crystallisation of garnet and glaucophane during the early stage of the metapelite decompression. We conclude that the HP-LT Tso Morari unit started to be exhumed during the Upper Paleocene. The subduction of the distal part of the Indian continent that was to become the Tso Morari HP unit occurred therefore just before 55 ± 7 Ma. According to the paleomagnetic data, the convergence velocity of India relative to Asia was about 18 cm/yr before 50 Ma (2). At such convergence rate the Tso Morari unit subducted down to 70 km in only 1 ± 0,5 Ma, (for a Benioff plane dip angle of 15-30°) suggesting that the onset of the subduction of the Indian continental margin may have begun during the Upper Paleocene. Such a suggestion is consistent with palaeontological, biostratigraphical, paleomagnetic and magmatic evidences for the first India-Asia contact during Paleocene (3, 7-9) (see discussion above). We also note that the exhumation of the HP Tso Morari unit started during the Upper Paleocene (55 ± 7 Ma) before the Lower Eocene collision (1, 2, 9, 10). This new result and the low temperature conditions recorded by the Tso Morari eclogitic rocks suggest that the exhumation of this unit, occurred quickly after its burial, when the continental subduction was still active, and probably within the mantle wedge from 70 km depth up to lower crustal level 40 km (27). As this first step of exhumation is isothermal and by analogy with the Alpine eclogites, a rapid exhumation rate is expected (28), what is coherent with the high convergence rate recorded before 50 Ma between the Indian and the Asian plates (2).

The time constrain on the progress of exhumation is given by Rb-Sr muscovite, apatite, whole rock isochron on the (Ch223d) metapelite, at 45 ± 4 Ma (2s) (MSWD = 0.2) (Fig. 3C). This metapelite had partly recrystallized under amphibolitic conditions during a temperature increase up to 610 ± 70°C, when the Tso Morari reached crustal depth of 40 ± 7 km, leading to the recrystallization of phengites into muscovites with $Si^{4+}$ < 3.3 p.f.u.. We

therefore interpret the 45 Ma age as the age of the amphibolitic facies recrystallization, near the temperature peak. At this time, most of the epicontinental sea basins had disappeared, the true India-Asia collision had already begun (4, 7, 9, 10), it is associated with a strong decrease in the convergence rate between the two plates (2), leading to a temperature increase of the metamorphic rocks (29). Then, we propose to relate the second step of the Tso Morari exhumation, dated at 45 ± 4 Ma, and associated with a temperature increase under crustal conditions, to a decrease of the exhumation rate in collisional context.

With this multichronometric study we confirm the Indian continental origin for the Tso Morari dome, by a Sm-Nd age of 458 ± 14 Ma obtained on an undeformed granite. The Sm-Nd age of 55 ± 7 Ma on a HP-LT metapelite of the Tso Morari dome argues for an upper Paleocene subduction of the Indian continental margin below Asia. This age also implies that the Tso Morari HP unit began its exhumation during the Upper Paleocene when the continental subduction was still active (Fig. 4A). The quasi-isothermal decompression of HP-LT Tso Morari rocks from 70 km up to crustal level, must have quickly followed the subduction and suggests rapid exhumation rate, probably within the mantle wedge. Since crustal depth of about 40 km, the rate of the Tso Morari exhumation across the continental crust decreased, allowing the thermal relaxation that led to the amphibolite facies recrystallization dated by Rb-Sr at 45 ± 4 Ma (Fig. 4B). The end of the Tso Morari rocks exhumation is then contemporaneous to the Himalayan collisional event. Our results suggest that the exhumation of HP-LT Tso Morari eclogitic massif was a discontinuous process. It began early in the Himalayan orogenesis, it was probably rapid when the continental subduction was still active and continued slower, during the collision .

## REFERENCES AND NOTES

1. J. P. Bassoulet, et al., *Compte Rendu Académie Sciences* **290**; 961-964 (1980).

2. P. Patriat and J. Achache, *Nature* **311**, 615-621 (1984).

3. J. J. Jaeger, V. Courtillot, P. Tapponier, *Geology* **17**, 316-319 (1989).

4. J. F. Dewey, S. Cande, W. C. Pitman, *Eclogae Geologica Helvetica* **82**, 717-734 (1989).

5. R. A. Beck, et al., *Nature* **373**, 55-58 (1995).

6. J. C. Rage, et al., *idid.* **375**, 286 (1995).

7. C. T. Klootwijk, J. S. Gee, J. W. Peirce, G. M. Smith, P. L. McFadden, *Geology* **20**, 395-398 (1992).

8. M. P. Searle, et al., *Geol. Soc. Am. Bull.* **98**, 678-701 (1987).

9. E. Garzanti, A. Baud, G. Mascle, *Geodinamica Acta* **1**, 297-312 (1987).

10. D. B. Rowley, *Earth Planet. Sci. Lett.* **145**, 1-13 (1996).

11. U. Pognante and D. A. Spencer, *Europ. J. Mineral.* **3/3**, 613-618 (1991).

12. A. Berthelsen, *Medd. fra Dansk Geol. Forening. Kobenhavn* **12**, 350-415 (1953).

13. S. Tonarini, et al., *Terra Nova* **5**, 13-20 (1993).

14. J. de Sigoyer, S. Guillot, J. M. Lardeaux, G. Mascle, *Europ. J. Mineral.* **9**, 1073-1083 (1997).

15 S. Guillot, J. de Sigoyer, J. M. Lardeaux, G. Mascle, *Contrib. Mineral. Petrol.* **128**, 197-212 (1997).

16. V. C. Thakur, *Wadia Institute of Himalaya Geology (Dehra Dun)*, 1-8 (1983).

17. G. Fuchs and M. Linner, *Jaherbuch der geologischen bundesanstalt* **138**, 655-685 (1995).

18. M. Thöni and E. Jagoutz, *Geochimi. Cosmochim. Acta.* **56**, 347-368 (1992).

19. M. Colchen, G. Mascle, G. Delaygue, *J. Nepal Geol. Soc.* **10**, 23 (1994).

20. R. Kretz, *Am. mineral.* **68**, 277-279 (1983).

21. T. Pettke and L. W. Diamond, *Geochimi. Cosmochim. Acta* **59**, 4009-4027 (1995).

22. G. J. Wasserburg, S. B. Jacobsen , D. J. De Paolo , M. T. McCullough, J. Wen, *Geochim. Cosmochim. Acta.* **45**, 2311-2323 (1981).

23. T. F. Nägler and J. D. Kramers, *Precamb. Research* in press.

24. K. R. Ludwig, *U.S. Geol. Survey* , 91-445 (1990).

25. J. R. Trivedi, K. Kewal, Sharma, K. Gopalan, *Terra Cognita* **6**, 144 (1986).

26. P. Le Fort, in *Collision Tectonics.* M. P.Cowards and A. C. Ries Eds. (Geol. Soc. London Special Publ., 19, London, 1986), pp. 159-172.

27. S. Guillot, K. Hatori, J. de Sigoyer, *Special Issue Geological Bull. Peshwar, Pakistan* . **31**, 72-73 (1998).

28. S. Duchêne et al., *Nature* **387**, 586-589 (1997).

29. U. Pognante, *Geodinamica Acta,* **6**, 5-17 (1993).

30. This work was supported by the CNRS-INSU program IDYL-HIMALAYA.

## Captions

**Fig. 1.** Geological map of the Tso Morari area, (East Ladakh) showing the sample localization.

**Fig. 2.** P-T path of the Tso Morari eclogitic metapelites in a petrogenetic grid for the NFMASH multisystem, from (17). It shows the first decompression step involving the crystallization of garnet and glaucophane since 20 kbar down to 11 Kbar. Mineral abbreviations are from (22).

**Fig. 3.** (**A**) Three point Sm-Nd isochron (Grt, Ap, and Whole Rock) for the Ch216e granite. (**B**) Sm-Nd isochron for the HP metapelite (Ch157a) on (Grt, Gln and Whole Rock) giving a crystallization age of 55 ± 7 Ma. (**C**) Rb-Sr isochron on (Ap, Mu, Whole rock) giving an age of 45 ± 4 Ma. Mineral abbreviations are from (22).

**Table 1.** Sm-Nd and Rb-Sr analyses on whole rocks and minerals separates from the Tso Morari dome. (a) Ch216e granite, (b) Ch157a HP metapelite, (c) Ch223d retrogressed metapelite. Mineral abbreviations are (22). See text for the discussion.

**Table 1:** Sm-Nd and Rb-Sr analyses on whole rocks and minerals separates from the Tso Morari Dome, Ch216e granite, Ch157a HP metapelite, Ch223d retrogressed metapelite. Mineral abbreviations are from (22).

| sample | type | Sm (ppm) | Nd (ppm) | 147Sm/144Nd | 143Nd/144Nd | 2σE | eNd(0) | TDM | f(Sm/Nd) |
|---|---|---|---|---|---|---|---|---|---|
| CH 216e | WR | 4.91 | 18.34 | 0.1618 | 0.512070 | 18 | -11.08 | 2.83 | -0.178 |
| | Grt | 15.37 | 16.76 | 0.5543 | 0.513247 | 31 | 11.88 | - | 1.818 |
| | Ap | 271.69 | 475.63 | 0.3458 | 0.512611 | 15 | -0.53 | - | 0.758 |
| CH 157a | WR | 4.15 | 17 | 0.1475 | 0.511731 | 0.000017 | -17.69 | 3.01 | -0.250 |
| | Gln | 92.94 | 518.85 | 0.1083 | 0.511694 | 0.000027 | -18.41 | - | -0.449 |
| | Grt | 3.83 | 2.76 | 0.8384 | 0.511969 | 0.000021 | -13.05 | - | 3.262 |
| sample | type | Rb (ppm) | Sr (ppm) | 87Rb/86Sr | 87Sr/86Sr | 2σE | | | |
| CH 223d | WR | 131.33 | 257.99 | 1.476 | 0.72917 | 6.21E-04 | | | |
| | Phe | 402.66 | 151.00 | 7.734 | 0.73332 | 1.22E-04 | | | |
| | Ap | 1.12 | 2412.33 | 0.001 | 0.72838 | 1.48E-04 | | | |

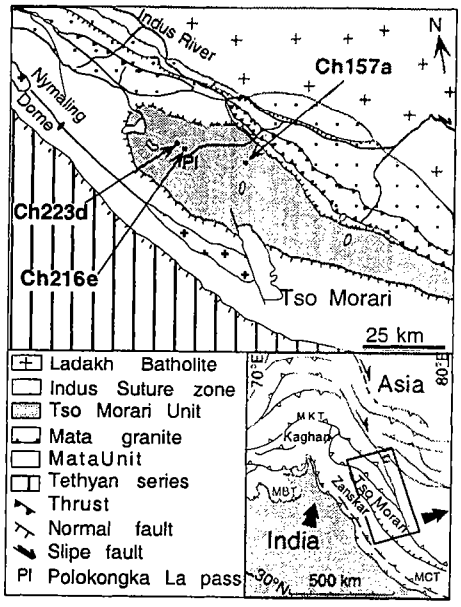


Figure 1

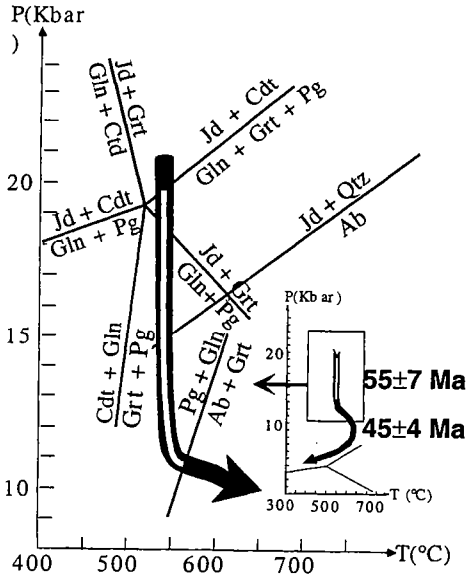


Figure 2

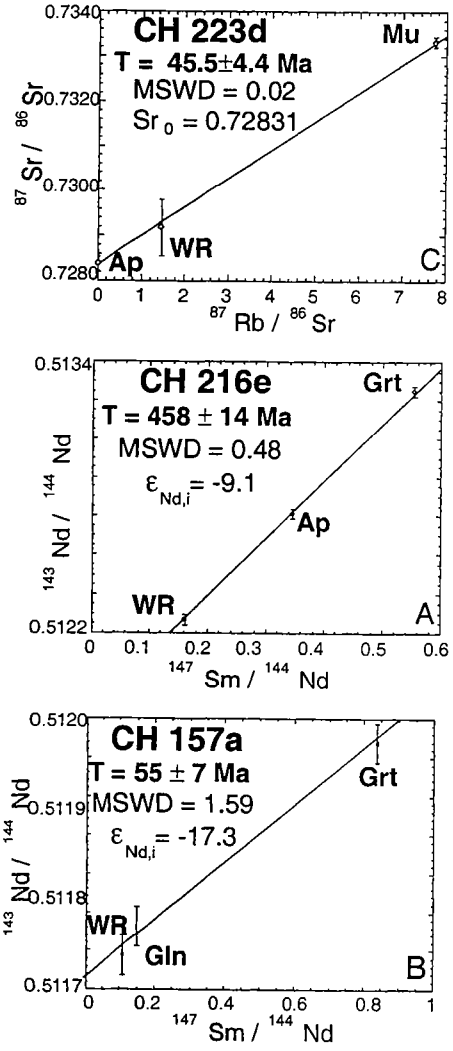


Figure 3

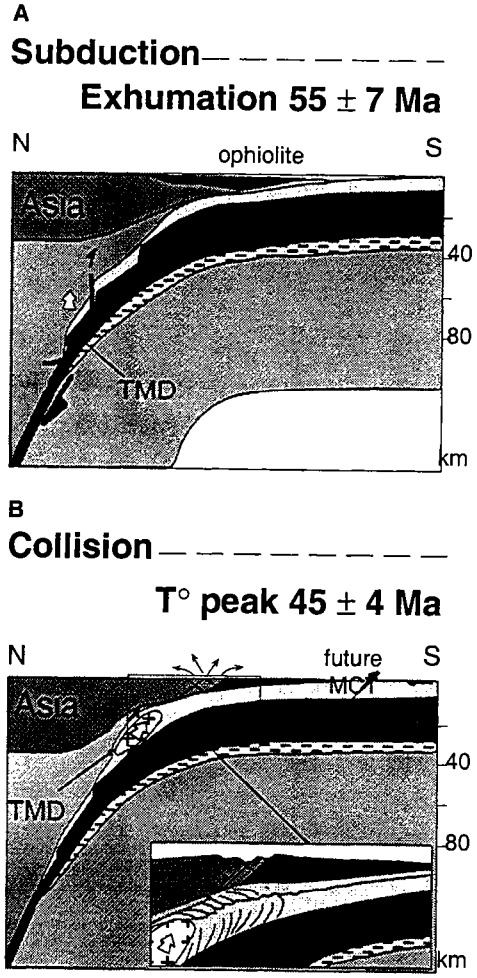


Figure 4

**MEMOIRES DE GEOSCIENCES-RENNES**
**Université de Rennes I - Campus de Beaulieu**
**35042 - RENNES Cedex .**
**Tel : 02- 99.28.60.80**
**Fax : 02-99-28-26-02**

**Dans la même collection :**

N°1 - **H. MARTIN** - Nature, origine et évolution d'un segment de croûte continentale archéenne : contraintes chimiques et isotopiques. Exemple de la Finlande orientale. **392 p., 183 fig., 51 tabl., 4 pl. (1985).** **Epuisé**

N°2 - **G. QUERRE** - Palingénèse de la croûte continentale à l'Archéen : Les granitoïdes tardifs (2,5-2,4 Ga) de Finlande Orientale. Pétrologie et géochimie. **226 p., 74 fig., 41 tabl., 3 pl. (1985).** **Epuisé**

N°3 - **J. DURAND** - Le Grès Armoricain. Sédimentologie. Traces fossiles. Milieux de depôt. **150 p., 76 fig., 9 tabl., 19 pl. (1985).** **Epuisé**

N°4 - **D. PRIOUR** - Genèse des zones de cisaillement : Application de la méthode des éléments finis à la simulation numérique de la déformation des roches. **157 p., 106 fig., 7 tabl. (1985).** **55F.**

N°5 - **V. NGAKO** - Evolution métamorphique et structurale de la bordure sud-ouest de la "série de Poli", segment camerounais de la chaîne panafricaine. **185 p., 76 fig., 16 tabl., 12 pl. (1986).** **70F.**

N°6 - **J. DE POULPIQUET** - Etude géophysique d'un marqueur magnétique situé sur la marge continentale sud-armoricaine. **159 p., 121 fig., 5 tabl. (1986)** **55F.**

N°7 - **P. BARBEY** - Signification géodynamique des domaines granulitiques. La ceinture des granulites de Laponie : une suture de collision continentale d'âge protérozoique inférieur (1.9-2.4 Ga). **324 p., 89 fig., 46 tabl., 11 pl. (1986).** **115F.**

N°8 - **Ph. DAVY** - Modélisation thermo-mécanique de la collision continentale. **233 p., 72 fig., 2 tabl. (1986).** **95F.**

N°9 - **Y. GEORGET** - Nature et origine des granites peralumineux à cordiérite et des roches associées. Exemple des granitoïdes du Massif Armoricain (France) : Pétrologie et géochimie. **250 p., 140 fig., 67 tabl. (1986).** **Epuisé**

N°10 - **D. MARQUER** - Transfert de matière et déformation progressive des granitoides. Exemple des massifs de l'Aar et du Gothard (Alpes Centrales Suisses). **287 p., 134 fig., 52 tabl., 5 cartes hors-texte (1987).** **Epuisé.**

N°11 - **J.S. SALIS** -Variation séculaire du champ magnétique terrestre. Direction et Paléointensité sur la période 7.000-70.000 BP dans la Chaîne des Puys. **190 p., 73 fig., 28 tabl., I carte hors-texte (1987).** **90F.**

N°12 - **Y. GERARD** - Etude expérimentale des interactions entre déformation et transformation de phase. Exemple de la transition calcite-aragonite. **126 p., 42 fig., 3 tabl., 10 pl. (1987).** **75F.**

N°13 - **H. TATTEVIN** - Déformation et transformation de phases induites par ondes de choc dans les silicates. Caractérisation par la microscopie électronique en transmission. **150 p., 50 fig., I tabl., 13 pl. (1987).** **95F.**

N°14 - **J.L. PAQUETTE** - Comportement des systèmes isotopiques U-Pb et Sm-Nd dans le métamorphisme éclogitique. Chaîne Hercynienne et Chaîne Alpine. **190 p., 88 fig., 39 tab., 2 pl. (1987).** **95F.**

N°15 - **B. VENDEVILLE** - Champs de failles et tectonique en extension; modélisation experimentale. **392 p., 181 fig., I tabl., 82 pl. (1987).** **Epuisé**

N°16 - **E. TAILLEBOIS** - Cadre géologique des indices sulfurés à Zn, Pb, Cu, Fe du secteur de Gouézec-St-Thois : Dévono-Carbonifère du flanc Sud du Bassin de Châteaulin (Finistère). **195 p., 64 fig., 41 tabl., 8 pl. photo., 8 pl. h.texte. (1987).** **110F**

N°17 - **J.P. COGNE** - Contribution a l'étude paléomagnétique des roches déformées. **204 p., 86 fig., 17 tabl. (1987).** **90F.**

N°18 - **E. DENIS** - Les sédiments briovériens (Protérozoïque supérieur) de Bretagne septentrionale et occidentale : Nature, mise en place et évolution. **263 p., 148 fig., 26 tab., 8 pl. (1988).** **140F.**

N°19 - **M. BALLEVRE** - Collision continentale et chemins P-T : l'Unité pennique du Grand Paradis (Alpes Occidentales). **340 p., 146 fig., 10 tabl., (1988).** **Epuisé**

N°20 - **J.P. GRATIER** - L'équilibrage des coupes géologiques. Buts, méthodes et applications. Atelier du Groupe d'Etudes Tectoniques le 8 Avril 1987 à Rennes. **165 p., 82 fig., 2 tabl. (1988).** **85F.**

N°21 - **R.P. MENOT** - Magmatismes paléozoïques et structuration carbonifère du Massif de Belledonne (Alpes Francaises). Contraintes nouvelles pour les schémas d'évolution de la chaine varisque ouest-européenne. **465 p., 101 fig., 31 tab., 6 pl., (1988).** **Epuisé**

N°22 - **S. BLAIS** - Les ceintures de roches vertes archéennes de Finlande Orientale : Géologie, pétrologie, géochimie et évolution géodynamique. **312 p., 107 fig., 98 tab., 11pl. photo, I pl. h.texte, (1989). 160F**

N°23 - **A. CHAUVIN** - Intensité du champ magnétique terrestre en période stable de transition, enregistrée par des séquences de coulées volcaniques du Quaternaire. **217 p., 100 fig., 13 tab. (1989). 100F.**

N°24 - **J.P. VUICHARD** - La marge austroalpine durant la collision alpine; évolution tectonométamorphique de la zone de Sesia-Lanzo. **307 p., 143 fig., 26 tab., 6 pl. hors-texte. (1989). 170F.**

N°25 - **C. GUERROT** - Archéen et Protérozoïque dans la chaîne hercynienne ouest-européenne : géochimie isotopique (Sr-Nd-Pb) et géochronologie U-Pb sur zircons. **180 p., 68 fig., 29 tab., I pl. (1989) 90F.**

N°26 - **J.L. LAGARDE** - Granites tardi-carbonifères et déformation crustale. L'exemple de la Méseta marocaine. **353 p., 244 fig., 15pl. (1989) 210F.**

N°27 - **Ph. BARDY** - L'orogène cadomien dans le Nord-Est du Massif Armoricain et en Manche Occidentale. Etude tectonométamorphique et géophysique. **395 p., 142 fig., 7 tab., I pl. hors-texte. (1989). 175F.**

N°28 - **D. GAPAIS** - Les Orthogneiss : Structures, mécanismes de déformation et analyse cinématique. **377 p., 184 fig., 3 tab. (1989). 275F.**

N°29 - **E. LE GOFF** - Conditions pression-température de la déformation dans les orthogneiss : Modèle thermodynamique et exemples naturels. **321 p., 146 fig., 42 tab. (1989). 150F.**

N°30 - **D. KHATTACH** - Paléomagnétisme de formations paléozoiques du Maroc. **220 p., 97 fig., 35 tab., (1989). 100F.**

N°31 - **A. HAIDER** - Géologie de la formation ferrifère précambrienne et du complexe granulitique encaissant de Buur (Sud de la Somalie). Implications sur l'évolution crustale du socle de Buur. **215 p., 18 fig., 42 tab., 7 pl. (1989). 130 F.**

N°32 - **T. DANIEL** - Traitement numérique d'image appliqué à l'analyse texturale de roches déformées. **186 p., 121 fig., 4 tab. (1989). 210 F.**

N°33 - **C. LECUYER** - Hydrothermalisme fossile dans une paléocroûte océanique associée à un centre d'expansion lent : Le complexe ophiolitique de Trinity (N. Californie, U.S.A). **342 p., 109 fig., 73 tab. (1989). 200 F.**

N°34 - **P. RICHARD** - Champs de failles au dessus d'un décrochement de socle: modélisation expérimentale. **382 p., 137 fig. (1989).** **400 F.**

N°35 - **J. de BREMOND d'ARS** - Estimation des propriétés rhéologiques des magmas par l'étude des instabilités gravitaires. Pétrologie du complexe plutonique lité de Guernesey. **370 p., 128 fig., 64 tabl. (1989).** **180 F.**

N°36 - **A. LE CLEAC'H** - Contribution à l'étude des propriétés physiques des minéraux à haute pression : Spectroscopie et calcul des grandeurs thermodynamiques de la lawsonite, des épidotes et des polymorphes de $SiO_2$. **190 p., 72 fig., 37 tabl. (1989).** **100 F.**

N°37 - **0. MERLE** - Cinématique des nappes superficielles et profondes dans une chaîne de collision. **280 p., 165 fig., 3 tabl. (1990).** **160F.**

N°38 - **P. ALLEMAND** - Approche expérimentale de la mécanique du rifting continental. **205 p., 106 fig., 13 tabl. (1990).** **160F.**

N°39 - **Ch. BASILE** - Analyse structurale et modélisation analogique d'une marge transformante : l'exemple de la marge de Côte-d'Ivoire - Ghana. **230 p., 161 fig., 7 tabl. ( 1990 ) .** **Epuisé**

N°40 - **M. AUDIBERT** - Déformation discontinue et rotations de blocs. Méthodes numériques de restauration. Application à la Galilée. **250 p., 80 fig., 5 tabl., (1991).** **150F.**

N°41 - **G. RUFFET** - Paléomagnétisme et 40Ar/39Ar : étude combinée sur des intrusions précambriennes et paléozoïques du Trégor (Massif Armoricain) . **261 p., 80 fig., 19 tabl. (1991).** **120F.**

N°42 - **P. SUZANNE** - Extrusion latérale de l'Anatolie : Géométrie et mécanisme de la fracturation. **262 p., 100 fig., 12 pl., 5 tabl. (1991).** **210F.**

N°43 - **G. FIQUET** - Propriétés thermodynamiques de minéraux du manteau supérieur. Calorimétrie à haute température et spectroscopie Raman à haute pression et haute température. **274 p., 101 fig., 53 tabl. (1991).** **130F.**

N°44 - **J. MARTINOD** - Instabilités périodiques de la lithosphère (Flambage, Boudinage en compression et en extension). **283 p., 117 fig., 3 tabl., 2 pl. couleur. (1991).** **170F.**

N°45 - **M.O. BESLIER** - Formation des marges passives et remontée du manteau: Modélisation expérimentale et exemple de la marge de la Galice. **257 p., 86 fig., 5 tab., 2 pl. noir/blanc, 2 Pl. couleur. (1991).** **180F.**

N°46 - **J.B.L. FRANCOLIN** - Analyse structurale du Bassin du Rio Do Peixe. (Brésil) : **250 p., 83 fig., 3 tab., 9 pl. couleur. (1992).** **300F.**

N° 47 - **S. TOURPIN** - Perte des mémoires isotopiques (Nd, Sr, O) et géochimiques (REE) primaires des komatiites au cours du métamorphisme : exemple de la Finlande Orientale. **185 p., 53 fig., 23 tabl. (1992).** **100F.**

N° 48 - **J.A. BARRAT** - Genèse des magmas associés à l'ouverture d'un domaine océanique : Géochimie des laves du Nord-Est de l'Afrique (Mer Rouge - Afar) et d'Arabie. **175 p., 47 fig., 23 tab. (1992).** **100F.**

N° 49 - **E. HALLOT** - Injection dans les réservoirs magmatiques. Contraintes pétrologiques (Massifs de Fort La Latte et de Saint Brieuc, Bretagne Nord) et modélisation analogique. **331 p., 101 fig., 30 tabl. (1993).** **180F.**

N°50 - **T. SOURIOT** - Cinématique de l'extension post-pliocène en Afar. Imagerie SPOT et modélisation analogique. **225 p., 2 pl. coul., I tabl., 91 fig., 16 pl. photo., I carte H.Texte. (1993).** **I90F.**

N° 51 - **T. EUZEN** - Pétrogenèse des granites de collision post- épaississement. Le cas des granites crustaux et mantelliques du Complexe de Pontivy-Rostrenen (Massif Armoricain, France). **350 p., 2 pl. coul., 34 tabl. en annexe, (1993).** **I90F.**

N° 52 - **J. LE GALL** - Reconstitution des dynamismes éruptifs d'une province paléovolcanique : l'exemple du graben cambrien du Maine (Est du Massif Armoricain). Pétrogenèse des magmas andésitiques et ignimbritiques et leur signification dans l'évolution géodynamique cadomienne. **370 p., 30pl. photo., I pl. coul. (1993).** **350 F.**

N° 53 - **J. C. THOMAS** - Cinématique tertiaire et rotations de blocs dans l'ouest de l'Asie Centrale (Tien Shan Kirghiz et dépression Tadjik). Etude structurale et paléomagnétique. **330 p., 107 fig., 2 pl. coul., 18 tabl., 1 carte, annexes. (1993).** **220 F.**

N°54 - **F. LAFONT** - Influences relatives de la subsidence et de l'eustatisme sur la localisation et la géométrie des réservoirs d'un système deltaïque. Exemple de l'Eocène du bassin de Jaca, Pyrénées Orientales., **270 p., 115 fig., dont 17 pl. couleur. (1994).** **150 F.**

N° 55 - **C. BIELLMANN** - Stabilité et réactivité des carbonates à très hautes pression et température. Implications pour le stockage du Carbone dans le manteau terrestre., **230 p., 74 fig., 11 tabl., 1 pl. couleur (1993).** **175 F.**

N°56 - **A. POTREL** - Evolution tectono-métamorphique d'un segment de croûte continentale archéenne. Exemple de l'Amsaga (R.I. Mauritanie), dorsale Réguibat (Craton Ouest Africain). **400 p., (dont annexes) 125 fig., 21 tabl., 1 pl. couleur, 43 pl. photo (1994).** **270 F.**

N° 57 - **M. KUNTZ** - Approche expérimentale de la déformation dans les systèmes préfracturés : Contribution à l'étude de l'inversion tectonique des bassins sédimentaires. **220 p., 19 pl., 87 fig., 3 tabl. (1994).** **155 F.**

N° 58 - **D. ROUBY** - Restauration en carte des domaines faillés en extension. Méthode et applications. **266 p., 98 fig. dont annexes (1994).** **180 F.**

N° 59 - **J.J. TONDJI-BIYO** - Chevauchements et bassins compressifs. Influence de l'érosion et de la sédimentation. Modélisation analogique et exemples naturels. **426 p., 141 fig., 4 pl. couleur, 21 tableaux, dont annexes (1995).** **270 F.**

N° 60 - **H. BOUHALLIER** - Evolution structurale et métamorphique de la croûte continentale archéenne (Craton de Dharwar, Inde du Sud). **277 p., 100 fig., dont 5 pl. coul., 7 tab., dont annexes (1995).** **150 F.**

N° 61 - **P. GAUTIER** - Géométrie crustale et cinématique de l'extension tardi-orogénique dans la domaine centre-égéen (îles des Cyclades et d'Eubée, Grèce). **430 p., 89 fig., dont 4 pl. coul., 1 tabl., dont annexes (1995).** **220F.**

N° 62 - **M.T. ROMAN BERDIEL** - Mécanismes d'intrusion des granites supracrustaux. Modèles analogiques et exemples naturels. **270 p., 75 fig., 5 pl. laser, 9 tabl. (1995).** **160F.**

N° 63 - **M. JULLIEN** - Polytypisme, ordre d'empilement et interstratification dans la cookéite et les phyllosilicates non micacés du métamorphisme. Influence de la pression. **226 p., 61 fig., 8 tabl. (1995).** **150 F.**

N° 64 - **Y. LAHAYE** - L'altération des komatiites. **224 p., 70 fig., 29 tabl., + annexes (1995).** **150 F.**

N° 65 - **A. CRAVE** - Quantification de l'Organisation des réseaux hydrographiques. **210 p., 68 fig., dont annexe (1995).** **120 F.**

N° 66 - **A. ESSAIFI** - Relations entre magmatisme-déformation et altération hydrothermale : L'exemple des Jebilet centrales (Hercynien, Maroc). **331 p., 248 fig., 4 tabl., dont annexes (1995).** **170 F.**

N° 67 - **M. LE RAVALEC** - Vitesses et perméabilité des roches : modélisation du rôle des fluides et des fissures. **276 p., 119 fig. 3 pl. couleur, 5 tabl., dont annexe (1995).** **140 F.**

n° 68 - **A. SEMIANI** - Métallogénie de la zone de cisaillement aurifère est-ouzzalienne : structure, pétrologie et géochimie des gisements d'or de Tirek-Amesmessa (Hoggar occidental, Algérie). **262 p.,72 fig., 36 tabl., 4 pl. couleur + annexes, (1995).** **130 F.**

N° 69 - **F. MOREAU** - Méthodes de traitement de données géophysiques par transformée en ondelettes. **177 p., 57 fig., + annexes. (1995).** **100 F.**

N° 70 - **B. TOURNERIE** - Imagerie de réflecteurs électromagnétiques en régime diffusif : Méthode et applications en Géophysique. **165 p., 45 fig., 8 tabl., + annexes, (1995).** **100 F.**

N° 71 - **T. NALPAS** - Inversion des grabens du Sud de la Mer du Nord. Données de sub-surface et modélisation analogique. **245 p., 110 fig., dont 10 pl. coul., (1994).** **120 F.**

N° 72 - **M. URREIZTIETA** - Tectonique néogène et bassins transpressifs en bordure méridionale de l'Altiplano-Puna (27°S), Nord-Ouest argentin. **311 p., 111 fig., 5 tabl., 6 pl. couleur, dont annexe. (1995).** **200 F.**

N° 73 - **A.N. KOUAMELAN** - Géochronologie et Géochimie des Formations Archéennes et Protérozoïques de la Dorsale de Man en Côte d'Ivoire. Implications pour la Transition Archéen-Protéorozoïque. **290 p., 99 fig., 23 tabl., 2 pl. couleur, dont annexe (1996).** **120 F.**

N° 74 - **Y. GARCIA** - Variation de l'intensité du champ magnétique en France durant les deux derniers millénaires. **331 p., 122 fig., 35 tab., dont annexe. (1996).** **150 F.**

N° 75 - **M. A. SANTOS PINTO** - Le recyclage de la croûte continentale archéenne : Exemple du bloc du Gavião- Bahia, Brésil. **193 p., 102 fig., 51 tab. (1996).** **100 F.**

N° 76 - **D. CHARDON** - Les déformations continentales archéennes : Exemples naturels et modélisation thermomécanique. **300 p., 127 fig., 6 tabl., 4 pl. photo; dont annexes. (1997).** **130 F.**

N° 77 - **C. ROBIN** - Mesure stratigraphique de la déformation : Application à l'évolution jurassique du Bassin de Paris. **293 p., 129 fig., 9 pl. couleur, dont annexes. (1997).** **180 F.**

N° 78 - **D. GRANJEON** - Modélisation stratigraphique déterministe : Conception et applications d'un modèle diffusif 3D multilithologique. **197 p., 56 fig., 22 tabl., 8 pl. couleur. (1997).** **100 F.**

**Hors Série - P. DAVY, F. GUILLOCHEAU, B. HAMELIN (Coordinateurs) -** Géomorphologie : Processus et modélisation. Ecole thématique du CNRS, **146 p., 69 fig., 2 tab., Lumigny, Juillet (1996) .** **50 F**

**N° 79 - A. JAFFREZIC -** Géochimie des éléments métalliques, des nitrates et du carbone organique dissous dans les eaux et les sols hydromorphes. Agriculture intensive et qualité des eaux dans les zones humides en Bretagne. **296 p., 143 fig., 46 tabl., 1 pl. coul., dont annexes (1997).** **130 F.**

**N° 80 - O. BOUR -** Transferts de fluides dans les milieux fracturés : Effets d'échelle. **272 p., 100 fig., 1 tabl., (1997).** **100 F.**

**n° 81 - E. BONNET -** La localisation de la déformation dans les milieux fragile-ductile : Approche expérimentale et application à la lithosphère continentale. **183 p., 85 fig., 4 tabl., (1997).** **85 F.**

**N° 82 - S. GESSA -** Le genre *Nowakia* (Dacryoconarides) dans le Praguien de la République Tchèque : Biométrie, systématique, phylogénie, paléoenvironnements. **256 p., 132 fig., 8 pl., + annexes. (1997).** **125 F.**

**N° 83 - T. MAUDUIT -** Déformation gravitaire synsédimentaire sur une marge passive. Modélisation analogique et applications du Golfe de Guinée, **260 p., 96 fig., dont 12 pl. coul., (1998)** **100 F.**

**N° 84 - G. QUEREL -** Cristallochimie des éléments traces dans les phases du manteau terrestre : Applications de la spectroscopie de luminescence à haute pression et haute température. **241 p., 101 fig., 23 tabl., (1998).** **95 F.**

**N° 85 - M. DIRAISON** - Evolution cénozoïque du Bassin de Magellan et Tectonique des andes australes. **333 p., 119 fig., dont 6 pl. coul., 2 pl. hors-texte, 7 tabl., (1998) .** **130 F.**

**N° 86 - S. BONNET -** Tectonique et dynamique du relief : le socle armoricain au Pleistocène. **352 p., 144 fig.,dont 7 pl. coul., + 1 pl. couleur et 7 transparents en annexe. (1998).** **115 F.**

**N° 87 - F. TOUCHARD -** Caractérisation hydrogéologique d'un aquifère en socle fracturé : Site de Ploemeur (Morbihan). **271 p., 103 fig., dont 5 coul., 37 tabl., annexe. (1999).** **115 F.**

**N° 88 - T.V. LE -** Stratigraphie sismique et modélisation stratigraphique : application à l'évolution tectonique oligo-miocène du Bassin du Fleuve Rouge (Vietman). **229 p.,131 fig., dont 16 pl. couleur + annexe. (1999).** **110 F.**

N° 89 - **V. CHAVAGNAC** - Behaviour of the Sm-Nd isotopic system during metamorphism : Examples from the HT-LP metamorphic terrane of the Limpopo Belt, South Africa and the UHP metamorphic terrane of Dabieshan, Central China. **405 p., 126 fig., 34 tabl. (1999).** **150 F.**

# MEMOIRES DE GEOSCIENCES

à retourner à :

Arlette FALAISE
Géosciences - Rennes I
Université de Rennes
35042 - RENNES Cédex (France)
Tél 02.99.28.60.80 Fax : 02.99.28.60.80

accompagné : soit de votre BON DE COMMANDE
ou bien de votre règlement (chèque libellé à l'ordre de) :
Madame l'Agent Comptable du CNRS

## BON DE COMMANDE

NOM : .....

ORGANISME .....

ADRESSE .....

Veuillez me faire parvenir les ouvrages suivants :

| N° | Auteur | Nb | P.U. | TOTAL |
|---|---|---|---|---|
| | | | | |
| | | | | |
| | | | | |
| | | | | |
| | | | | |
| | | | | |
| | | | | |

| | |
|---|---|
| Frais d'envoi : 20,00 F pour le 1er volume<br>par volume supplémentaire : 5,00 F TOTAL | |
| TOTAL DE LA COMMANDE | |

**Imprimé à l'Université de Rennes I**

**Dépôt Légal**

**1er Trimestre 1999**

## Résumé

Les buts de cette thèse sont (1) de déterminer si les âges modèles en Nd obtenus sur des terrains protérozoïques migmatisés correspondent réellement à l'âge d'extraction du magma de sa source mantellique (exemple du Limpopo Belt en Afrique du Sud) et (2) de comparer les âges Sm-Nd sur grenat et les âges U-Pb sur zircon déterminés sur des éclogites (exemple du Dabieshan en Chine Centrale).

La Zone Centrale du Limpopo Belt est constituée principalement d'orthogneiss et de paragneiss. Elle a subi un métamorphisme granulitique suivi par des conditions métamorphiques de décompression à 2.0 Ga (trajectoire pression et température dans le sens horaire). Nous avons effectué des analyses isotopiques en Sm-Nd et U-Pb combinées aux analyses en éléments majeurs et traces sur trois examples de migmatites formées à 2.0 Ga afin d'étudier le fractionnement chimique et isotopique qui pourrait avoir lieu au cours de la migmatisation. La fusion partielle selon la réaction de déhydratation de la biotite met en exergue des comportements différents du système isotopique Sm-Nd dans les métagreywackes et dans les métapélites. Dans le premier cas, l'équilibre chimique et l'homogénéisation isotopique en Nd n'ont pas été achevés à cause de la fusion incongruente du plagioclase et de l'influence des minéraux accessoires sur la composition chimique des liquides. Il est démontré que la monazite est préférentiellement entraînée dans les leucosomes plutôt que l'apatite, provoquant ainsi la domination de la composition chimique de la monazite sur celles des liquides. De plus, la composition isotopique en Nd non-radiogénique de ce minéral accessoire domine celle du leucosome. Ainsi, les âges modèles en Nd des leucosomes sont jusqu'à 400 Ma plus vieux que ceux obtenus sur les paléosomes. Les âges modèles en Nd obtenus sur ces roches ne peuvent donc pas être utilisés comme âge de formation de la croûte continentale en Afrique du Sud. Dans le cas des métapelites, la fusion incongruente du plagioclase a influencé la distribution des éléments majeurs, des Larges Ion Lithophile Element ainsi que des Rare Earth Element entre les paléosomes et les leucosomes. L'échange isotopique en Nd entre les différents composants migmatitiques a été pratiquement atteint, au contraire des isotopes du Pb qui ne montrent qu'une homogénéisation partielle. Cependant, deux leucosomes à grenat présentent des compositions isotopiques en Sm-Nd et U-Pb supérieures aux autres composants migmatitiques. Ceci suggère qu'en règle générale les minéraux accessoires ont été chimiquement et isotopiquement équilibrés avec les leucosomes et les paléosomes. De ce fait, les âges modèles en Nd calculés sur les paléosomes et les leucosomes représentent des âges significatifs pour la formation de la croûte continentale dans la Zone Centrale du Limpopo Belt. Le dernier exemple est un orthogneiss migmatitique qui s'est formé par ségrégation métamorphique à des conditions subsolidus. La distribution des éléments majeurs et traces est directement proportionnelle à la quantité de chaque minéraux formant les composants migmatitiques. L'échange isotopique en Pb a été achevé comme le montre l'isochrone en Pb-Pb sur les roches totales à 2.0 Ga. De plus, les caractéristiques géochimiques associées à une modélisation de la distribution des REE indiquent que le système est resté clos à l'échelle de la roche totale durant le processus de migmatisation.. Ainsi, la composition isotopique en Nd du protolithe a pu être déterminée grâce à l'équation de conservation de masse et peut être utilisée pour définir l'âge de la formation de la croûte continentale.

Le terrain Métamorphique de Ultra-Haute Pression (UHPM) du Dabieshan est caractérisé par la présence de coésite et de quartz pseudomorphe dans les éclogites de composition basaltique mais aussi dans les roches d'origine sédimentaire. Les isochrones en Sm-Nd sur grenat-omphacite-roche totale des éclogites à coésite du Massif de Bixiling donnent des âges variant entre 210 ± 9 Ma et 218 ± 4 Ma, très similaires aux âges U-Pb sur zircon à 218.4 ± 1.8 Ma et 218.4 ± 2.5 Ma (Ames et al., 1995). De plus, une isochrone Sm-Nd sur grenat-disthène-roche totale d'une éclogite rétromorphosée donne un âge à 231 ± 35 Ma en accord avec un âge à 233 ± 21 Ma (intercepte bas dans le diagramme concordia). Nous avons effectué des datations par les méthodes Rb-Sr et Ar-Ar sur des phengites et des biotites de l'encaissant des éclogites à coésite de Bixiling. Les âges varient entre 198 ± 4 Ma et 212 ± 2 Ma recouvrant les âges précedemment obtenus par Sm-Nd sur les éclogites à coésite. Par conséquent, les âges Sm-Nd sur grenat sont en accord avec les âges U-Pb sur zircon et montrent que les gneiss quartzo-feldspathiques ont subi un événement métamorphique à ~210 Ma comme les éclogites. L'homogénéisation isotopique en Nd entre les différents minéraux semblent être atteinte à l'âge du métamorphisme.



Editions de GEOSCIENCES RENNES

Université de Rennes I

F - 35042 - RENNES Cédex